THE PHYSICAL REVIEW

VOLUME 85 NUMBER

JANUARY 1,

Published for the

AMERICAN PHYSICAL SOCIETY

by the

Information for Contributors

Manuscripts

Send manuscripts to R. [illegible] Goudsmit, Brookhaven National Laboratory, Upton, Long Island, New York.

Each article submitted will in general consist of (a) textual material, i.e., all material which is to be set in type, and (b) drawings or photographs from which zinc etchings or copper halftones will be made. Textual material will consist of an abstract, the body of the paper, tabular material, references, and figure captions. All of this material must be in English, typewritten (except mathematical expressions) double spaced with wide margins (for editorial instructions to the printer) on a durable, white paper, preferably letter size. The original copy, not the carbon, should be submitted.

For general style, spelling, abbreviations, and form, recent issues of this journal should be consulted.

The prime requisite is that the copy shall be clear to the typesetter, who is neither a physicist nor a mathematician.

Abstracts

An abstract must accompany each article. It should be adequate as an index and as a summary. As an index, it should give all subjects, major and minor, concerning which new information is presented. As a summary it should give the conclusions of the article and all numerical results of general interest.

Mathematical Expressions

All but the simplest mathematical expressions should be carefully printed in by hand. Be sure to distinguish between capital and small letters. Indicate clearly superscripts and subscripts by inverted carets and carets, respectively. Avoid complicated superscripts and subscripts. Avoid repetition of a complicated expression by representing it by some convenient symbol. Identify in the margin Greek letters and unusual symbols. Use fractional exponents instead of root signs. Use the solidus (/) for fractions wherever its use will save vertical space.

References

References should appear as footnotes, numbered consecutively, and arranged thus:

[1] A. E. Smith, Phys. Rev. [illegible] (1932).
[2] H. Lamb, *Hydrodynamics* (Cambridge University Press, Teddington, England, 1940), sixth edition, pp. 573, 645.

Tables

All but the simplest tabular material should be organized in tabular form rather than as a part of the running text. Tables may be typewritten on sheets separate from the running text with indications in the margin of the running text where the table is to be inserted. Each table must have a caption which will make the data in the table intelligible without reference to the text. Avoid complicated column headings; if necessary, use symbols which are explained in the table caption.

Figures

Wherever possible figures should be planned for the width of a column of the *Physical Review* (3 inches). A convenient reduction ratio is about 2:1 or 3:1. The original drawings or photographs should therefore be in general about 6 to 9 inches wide and the lettering and symbols should be large enough on the original that when reduced they shall not be less than about $\frac{1}{16}$ in. (~1.5 mm). If the reduction is 3:1, the original lettering should be not less than $\frac{1}{8}$ in. high.

The process of making zinc etchings or copper halftones is a black and white photographic one. Therefore line drawings must be in *india ink* on white paper or tracing cloth. Coordinate paper is not desirable but if used must be blue lined and the coordinate lines which are to show must be inked over.

Photographs should have maximum black and white contrast.

Plan figures to use space efficiently. Avoid wasting space, particularly at the top or bottom.

Identify on the back or other suitable place each original drawing or photograph with the author's name and the figure number. Figures should be numbered consecutively and their approximate position indicated in the margin of the running text. Figure captions should be typed and included with the manuscript (not as part of the figure).

Avoid round and oval photographs.

Alterations

Take great care that each manuscript is typographically accurate. A limited number of alterations in proof are unavoidable, but the cost of making extensive alterations after the article has been set in type will be charged to the author.

Proof and all correspondence concerning papers in the process of publication should be addressed to the Publication Manager, American Institute of Physics, 57 East 55 Street, New York 22, New York.

THE PHYSICAL REVIEW

A journal of experimental and theoretical physics established by E. L. Nichols in 1893

VOLUME 85

Second Series

JANUARY 1–MARCH 15, 1952

Published for the

AMERICAN PHYSICAL SOCIETY

by the

AMERICAN INSTITUTE OF PHYSICS
Incorporated

THE PHYSICAL REVIEW

A journal of experimental and theoretical physics established by E. L. Nichols in 1893

Published by the American Institute of Physics for the

AMERICAN PHYSICAL SOCIETY

Officers

President

C. C. LAURITSEN
California Institute of Technology
Pasadena, California

Vice-President

J. H. VAN VLECK
Harvard University
Cambridge, Massachusetts

Secretary

K. K. DARROW
Bell Telephone Laboratories
Office:
Columbia University
New York 27, New York

Treasurer

G. B. PEGRAM
Columbia University
New York 27, New York

Local Secretary for the Pacific Coast

J. KAPLAN
University of California at Los Angeles
Los Angeles, California

Managing Editor

S. A. GOUDSMIT
Brookhaven National Laboratory
Upton, Long Island
New York

BOARD OF EDITORS

Editor

S. A. GOUDSMIT

Assistant Editor

S. PASTERNACK

Associate Editors

J. BARDEEN — HARVEY BROOKS — M. GOLDHABER
T. BONNER — R. F. CHRISTY — R. HOFSTADTER
R. G. HERB — C. L. CRITCHFIELD — A. W. LAWSON
W. E. LAMB, JR. — M. DEUTSCH — A. PAIS
A. J. F. SIEGERT — T. H. JOHNSON — R. SERBER
W. E. STEPHENS — BRUNO ROSSI — C. H. TOWNES

Manuscripts for publication should be submitted to S. A. GOUDSMIT, Brookhaven National Laboratory, Upton, Long Island, New York. The authors' institutions are requested to pay a publication charge of $8 per page which, if honored, entitles them to 100 free reprints. Instructions will be sent with galley proofs.

Proof and all correspondence concerning papers in the process of publication should be addressed to the Publication Manager, American Institute of Physics, 57 East 55 Street, New York 22, New York.

Subscription Price

United States and Canada $25.00
Elsewhere $27.00

Back Numbers [1]

Yearly back number rate when complete year is available:
Prior to 1949: $20.00
Thereafter: $27.00
Single copies: $2.00 each, prior to July, 1929;
$1.00 each, July, 1929–December, 1941;
$2.00 each, January, 1942–December, 1946;
$1.00 each, January, 1947–December, 1948;
$1.25 each, thereafter.
General index, 1893–1920: $4.00.

Subscriptions, renewals, and orders for back numbers should be addressed to the American Institute of Physics, 57 East 55 Street, New York 22, New York.

Changes of address in the case of members of the American Physical Society should be addressed to the Treasurer; in the case of other subscribers to the American Institute of Physics.

[1] For Series 1 inquire of Physics Department, Cornell University, Ithaca, New York.

The Physical Review is published semi-monthly at Prince and Lemon Streets, Lancaster, Pennsylvania.

Entered as second-class matter March 6, 1947, at the Post Office at Lancaster, Pennsylvania, under the Act of March 3, 1879.

Acceptance for mailing at special rate of postage provided for in paragraph (d-2), section 34.40, P. L. & R. of 1948, authorized January 27, 1933.

THE
PHYSICAL REVIEW

A journal of experimental and theoretical physics established by E. L. Nichols in 1893

SECOND SERIES, VOL. 85, NO. 1 JANUARY 1, 1952

Adiabatic Thermal Changes in Barium Titanate Ceramic at Low Temperatures*

ROLAND W. SCHMITT†
Rice Institute, Houston, Texas
(Received September 19, 1951)

The adiabatic thermal changes at 4°K in barium titanate ceramic show a heating effect whether the the electric field is applied or removed. An interpretation of these results is that the polarization process is thermodynamically irreversible. The large temperature dependence of the dielectric constant at 4°K may be understood as a result of the thermodynamically irreversible polarization. Quantitative results are given as to the temperature rise as a function of electric field strength and as a function of temperature.

INTRODUCTION

BARIUM titanate in ceramic form has a dielectric constant of about one hundred at a temperature of 4°K and within the liquid helium temperature range the dielectric constant exhibits a large temperature dependence.[1,2] This temperature dependence suggests that one might be able to detect sizeable temperature changes in the material if its state of polarization were changed adiabatically, and in the experiment reported here such temperature changes are measured. By these measurements one can distinguish between thermodynamically reversible and irreversible polarization mechanisms. With reversible mechanisms, an increase in field strength will cause a temperature change opposite in sign to that caused by a decrease in field strength. With irreversible polarization mechanisms, however, any change in field strength causes an increase in entropy which manifests itself in adiabatic processes as an increase in temperature. The results presented in this paper point to irreversible processes as predominating in $BaTiO_3$ ceramic at low temperatures because all of the temperature changes represent heating. An interpretation of the large temperature dependence of the dielectric constant that is consistent with these results and also with those of Merz[3] is also given.

EXPERIMENTAL APPARATUS AND TECHNIQUE

To measure the adiabatic thermal changes in a dielectric at low temperatures one must be able to (1) cool the specimen to liquid helium temperatures, (2) thermally isolate it from the surroundings, (3) apply or remove high voltages, and (4) measure the resulting temperature changes. The cryostat used to accomplish these steps is shown in Fig. 1. Around the liquid helium Dewar, 0, is another Dewar flask, not shown, which contains liquid nitrogen. Temperatures below 4.2°K are attained by pumping on the liquid helium bath through the tube, *M*, and are measured by measuring the pressure above the bath with a mercury manometer (not shown). A constant bath temperature is maintained by the familiar technique of regulating the pumping speed and monitoring through use of a differential oil manometer.

The specimens are ceramic disks of $BaTiO_3$ 3.28 cm in diameter and 0.221 cm thick, kindly furnished by the Bell Telephone Laboratories. On one side of the specimen a circular disk of silver paste (No. 50, Hanovia Chemical Company) 2.54 cm in diameter is painted and fired. A flat silver strip to serve as a lead is attached to this condenser plate with additional silver paste. The opposite face of the specimen also has a condenser plate made with silver paste, but it has two areas separated by 2 mm. This side of the specimen is shown in Fig. 2. Each of the silver areas shown in the figure has a silver strip attached to it and to each silver strip is soldered a No. 40 copper wire lead. The carbon thermometer is made by painting a colloidal suspension of carbon in an alcoholic base (Dag Dispersion No. 154, Acheson Colloids Corporation) on the specimen to cover the 2-mm gap between the two silver patches. Upon drying, the colloidal suspension leaves a thin, hard layer of carbon that is in good thermal contact with the specimen and which, in addition to serving as the thermometer, serves

* The research was supported by the ONR.
† Now with General Electric Research Laboratory, the Knolls, Schenectady, New York.
[1] B. Wul, J. Phys. U.S.S.R. **10**, 64 (1946).
[2] R. F. Blunt and W. F. Love, Phys. Rev. **76**, 1202 (1949).
[3] W. J. Merz, Phys. Rev. **81**, 1064 (1951).

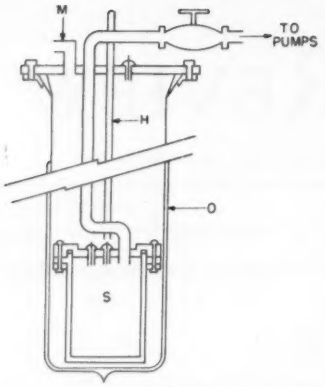

FIG. 1. The cryostat used for adiabatic application of electric field.

also to complete the condenser plate on the one face of the specimen.

The specimen is hung in the vacuum space, S of Fig. 1, into which exchange gas is introduced to establish good thermal contact between the specimen and the bath. The carbon thermometer is calibrated against the bath temperature with this exchange gas surrounding it. The specimen can then be partially isolated from the bath by pumping the gas out of S; however, the electrical leads still constitute a sizeable heat leak between the bath and specimen.

The value of the carbon resistance is measured with an ordinary Wheatstone bridge. A compensating resistance is placed in series with the unknown in order that all arms of the bridge always contain the same amount of resistance. In this way the current through the carbon thermometer is maintained approximately constant at 0.2 milliampere and gives only a small heat dissipation. A diagram of the bridge and high voltage circuits is shown in Fig. 3. The two circuits have one point in common and that is the point, A, (Figs. 2 and 3). From this point a No. 40 copper wire is taken to the

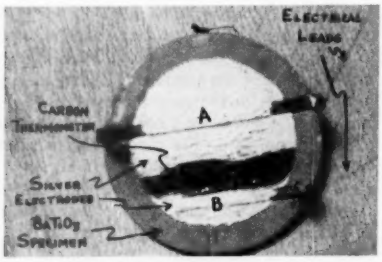

FIG. 2. The specimen of ceramic barium titanate showing electrodes and carbon thermometer.

wall of the vacuum jacket and soldered, thus allowing the pumping line and metallic frame of the apparatus to be used as the grounded lead of the high voltage circuit. Because of this, the two carbon thermometer leads emanating from A and B must everywhere be isolated electrically from the frame in order to prevent thermal emf's from being set up in the bridge circuit. These two leads are, therefore, taken out of the vacuum jacket through two Kovar seals, through the helium bath and then through two more Kovar seals in the top plate of the cryostat. The switch S_2 may be used to check that no thermal emf's are present and S_3 to obtain the zero position of the galvanometer.

The high voltage lead, C, is also taken out of the vacuum jacket through a Kovar seal and then into a glass tube, H of Fig. 1, which extends through the top plate of the cryostat. The glass tube is to prevent arcing in the helium gas above the liquid bath, particularly at pressures below atmospheric. The switch, S_1, is used to apply or remove voltage from the specimen. During either of these processes the charges that flow onto or off of the condenser plate, AB, can flow through both

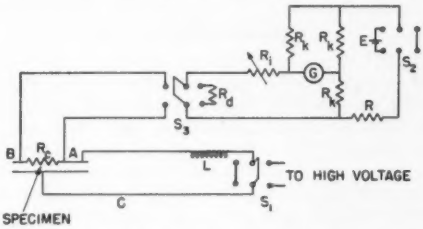

FIG. 3. The schematic of the electric circuit used in these experiments.

R_c and other parts of the bridge circuit, causing the galvanometer to suffer spurious deflections. The inductance, L, of ten henries is inserted in the charging circuit to minimize these. The spurious deflections can be measured by removing the battery from the bridge circuit with S_2 and noting the galvanometer deflections that occur when the specimen is charged or discharged. For the smallest temperature change observed these deflections were less than 10 percent of the deflections caused by thermometer changes.

After the exchange gas is pumped out of the vacuum jacket and equilibrium between the heat leaks and the power dissipated in the carbon resistor established, the bridge is set near balance and voltages applied to and removed from the specimen. During these processes the galvanometer deflection is followed as a function of time without changing the bridge settings. Thus the bridge is usually slightly off balance but the deviation from balance is never more than 0.1 percent.

The change in voltage across the specimen and hence the change in temperature of the specimen take place very rapidly compared to the rate at which heat leaks

out of the specimen into the bath. Furthermore, the time constant of response of the bridge galvanometer is made long compared to either of these processes. Therefore, to compute the initial temperature change, $(\Delta T)_0$, it is a sufficiently good approximation to assume that the temperature changes instantaneously upon application or removal of the voltage and then decays according to the law $\Delta T=(\Delta T)_0 e^{-wt}$. The deflection of the bridge galvanometer is governed by the equation

$$(dx/dt)+\beta x=\beta GA(\Delta T)_0 e^{-wt} \text{ for } t>0,$$

where $\gamma=1/\beta$ is the time constant of the bridge circuit, G is its sensitivity to changes of resistance in mm deflection per ohm change, A is the sensitivity of the carbon thermometer in ohms per millidegree temperature change, and x is the galvanometer deflection from its initial value. Since β, G, and A are measured directly,

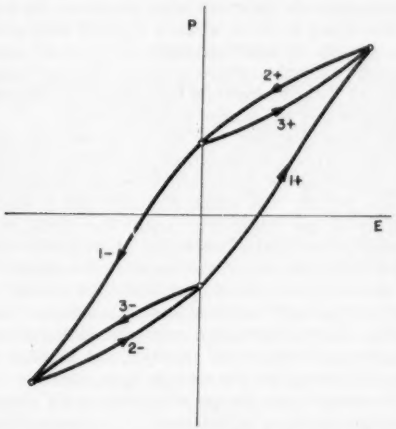

FIG. 4. Polarization processes for which the temperature rise is given in Table I.

it is necessary to measure only the peak value of the galvanometer deflection and the time at which it occurs in order to calculate w and $(\Delta T)_0$.

In the present experiment the major error in computing $(\Delta T)_0$ arises from the error in measuring the time at which the maximum deflection occurs. This error can be greatly reduced by a moderate reduction in the heat leaks. However, in view of the results obtained on barium titanate ceramic it is unlikely that more precise measurements would yield significant information not obtained from the present measurements. Hence no refinement of the measurements on this material is contemplated.

In view of the fact that barium titanate is ferroelectric the application and removal of voltages is always done in a definite sequence so as to be certain of the portion of the hysteresis loop over which the change is taking place. The various paths traversed in the measurements are shown in Fig. 4, where the small circles indicate the end states of a particular process and the arrows designate the direction in which the change takes place. The various processes are numbered for convenience in referring to them in Table I.

TABLE I. Adiabatic thermal changes in $BaTiO_3$.

ΔE volts/cm	ΔT in millidegrees 2.75°K	4.3°K	Process (see Fig. 4)
4520	+55±13	+22±6	1+
	51±13	19±6	1−
	44±12	19±6	2+
	46±14	23±6	2−
	41±13	15±5	3+
		14±5	3−
6790	+178±28	+67±13	1+
	187±35	66±13	1−
	123±28	45±10	2+
	121±27	49±12	2−
	88±20	35±12	3+
	94±20	35±12	3−
9040	+638±100	+266±58	1+
	235±45	110±25	2+
	207±37		3+

EXPERIMENTAL RESULTS

Measurements of the adiabatic thermal changes in barium titanate ceramic have been made at temperatures of 2.75°K and 4.3°K. The results are shown by Table I in which the first column gives the applied electric field, the second and third columns give the rise in temperature in millidegrees for the specimen at 2.75°K and 4.3°K respectively, and the fourth column gives the path designation for the state of polarization described by Fig. 4.

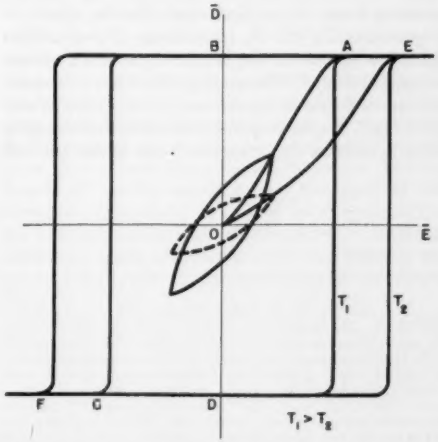

FIG. 5. The effect of temperature on the polarization of ceramic barium titanate.

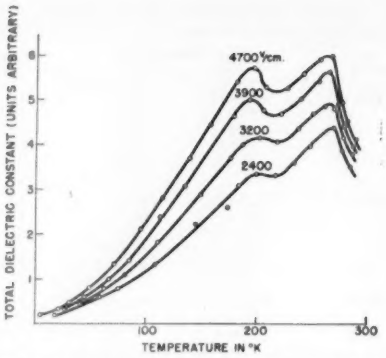

FIG. 6. Relative change of the total dielectric constant of ceramic barium titanate with temperature and with applied electric field.

The ratio of the ΔT at 2.75°K to that for the corresponding proces at 4.3°K is always close to $(4.3/2.75)^2$. If the heating per unit volume remained constant one would expect the ΔT-ratio to be close to the cube of the temperature ratio provided the specific heat decreases as T^3. The heating per unit volume, therefore, seems to decrease with decreasing temperature.

DISCUSSION

The results given in Table I suggest that the mechanisms which give rise to the macroscopic polarization when an electric field is applied to $BaTiO_3$ ceramic at low temperatures are almost entirely thermodynamically irreversible ones. The way that these can lead to a large temperature variation of dielectric constant is shown in Fig. 5, where the loops *ABCD* and *EBFD* represent hysteresis loops for an ideal single domain crystal at temperatures T_1 and T_2 respectively $(T_1 > T_2)$. This figure is a plot of the displacement vector, *D*, against the applied field, *E*. The virgin curves of a multidomain specimen will then be represented by the curves *OA* and *OE* in Fig. 5. If measurements are made at field strengths below saturation the hysteresis loops traced out will have their tips near points on the virgin curves. Hence for low field strengths the total dielectric constant, defined as the ratio D/E, will become smaller as the temperature decreases. This comes about not because of a change in the spontaneous polarization (thermodynamically reversible) but because an increase in coercivity makes it more difficult to change the domain structure (thermodynamically irreversible). This view is consistent with the results of Merz[3] who has shown that at low temperatures the coercivity of the material increases with decreasing temperature while the spontaneous polarization remains constant.

It should be noted that if the process described in the preceding paragraph and by Fig. 5 plays a significant part in determining the temperature variation of the dielectric constant, then one could expect this temperature variation of the total dielectric constant to increase with increasing field strengths as long as the measurements are made well below saturation. Such an effect is shown in Fig. 6, which is a plot of data taken from pictures of hysteresis loops, the pictures being obtained by a method similar to that of Mueller.[4] Below about 180°K the temperature variation of the dielectric constant is seen to be larger at higher fields.

The views described here are, of course, not contradictory to previous theoretical views[5,6] which attempt only to account for the occurrence of the ferroelectric state in $BaTiO_3$. The notion expressed here is simply that, given the ferroelectric state, the spontaneous polarization has attained essentially its saturation value at low temperatures and the temperature variation of the dielectric constant is most likely due entirely to thermodynamically irreversible domain effects. Thus, the third law of thermodynamics will not require the temperature variation of the dielectric constant to approach zero as the temperature approaches zero.

The author acknowledges with pleasure the encouragement and advice of Professor C. F. Squire and for a fellowship granted by the Magnolia Petroleum Company during the course of this work.

[4] H. Mueller, Phys. Rev. **47**, 175 (1935).
[5] J. C. Slater, Phys. Rev. **78**, 748 (1950).
[6] A. F. Devonshire, Phil. Mag. **40**, 1040 (1949).

Internal Conversion Angular Correlations*

M. E. Rose, L. C. Biedenharn, and G. B. Arfken
Oak Ridge National Laboratory, Oak Ridge, Tennessee
(Received September 26, 1951)

It is shown that the angular correlation between a conversion electron and any other radiation emitted in a double nuclear cascade can be obtained immediately if the corresponding correlation with a γ-ray replacing the conversion electron is known. This latter is known for all cases of practical interest. Specifically, if the correlation function for γ-rays and a radiation x is expanded in Legendre polynomials, the correlation function with a conversion electron replacing the γ-ray is obtained by multiplying the coefficients of each polynomial P_ν by a parameter b_ν. The case of conversion-conversion correlation, in all practical cases, is obtained from the $\gamma-\gamma$ correlation by inserting two factors b_ν, one for each conversion electron. The coefficients b_ν are calculated relativistically and numerical results are presented for K-shell conversion for 12 values of Z in the range $10 \leqslant Z \leqslant 96$ and transition energies from 0.3 mc^2 to 5.0 mc^2 for ten multipoles (5 electric and 5 magnetic). It is pointed out that the present results apply in γ-electron correlation if the γ is a mixed multipole but the case in which the conversion transition is mixed is not computed. The angular distribution functions for electrons in a coulomb field undergoing any type of transition are obtained in terms of the relevant matrix elements by the use of the Green function for the Dirac electron in a coulomb field. It is also shown that the angular distribution function is obtained from matrix elements based on, not the scattered wave, but on the time-space reversed scattered wave.

I. INTRODUCTION

In the investigation of the angular correlation between two radiations emitted by an excited nucleus in two successive transitions, the directional correlation involving emission of internal conversion electrons becomes important whenever either or both transitions correspond to large conversion coefficients. Thus, the effect is of primary interest in heavy nuclei,[1] low energy transitions and/or high order multipoles.[2] An essential restriction does enter from both the experimental and theoretical points of view in that it is desirable to avoid cases in which the intermediate state is long-lived.[3] However, this restriction applies only to the second transition so that, perhaps more often than not, the first transition may correspond to large internal conversion. These remarks apply, of course, only to the practical application of the results given below. So far as content of this paper is concerned, application of the results to correlations between conversion electrons and any other radiation (including another conversion electron transition) may be made and, for different radiations, the distinction between the cases in which the conversion electron is emitted first or second is trivial. We do make the assumption that the intermediate state is sufficiently short-lived so that hfs and other perturbing couplings may be ignored.[3,4]

Although a number of experimental studies of conversion correlation have been reported in the literature,[1] there had been no adequate theoretical treatment of the problem whereby the results of the experiments could be interpreted and used for the purpose of identifying the transitions involved. Previous work is confined largely to two papers by Gardner.[5] In the first of these Gardner discussed the nonrelativistic treatment of the conversion-conversion correlation. This was necessarily confined to electric multipoles and omitted the contribution to final states involving spin flip. The restriction was also made to ejection of s-electrons only but this restriction is not essential to the nonrelativistic limit. In the second paper an extension is made to the conversion-conversion correlation in which one of the transitions is a pure magnetic, the other a pure electric multipole and again the initial electronic states are s-states. In the v^2/c^2 approximation considered in this reference both final states (with and without spin flip) enter but essential interference terms between them do not appear. In any case numerical results are not given. It is of importance to note that while the error introduced by the nonrelativistic treatment of the correlation problem is, in general, much smaller than that arising in the calculation of the absolute conversion coefficients (since only ratios of matrix elements are involved in the former) the dependence of the correla-

* This paper is based on work performed for the AEC at the Oak Ridge National Laboratory.

[1] The restriction to heavy nuclei is not very stringent. Conversion correlation has been experimentally investigated in elements as light as Br, L. I. Rusenov and Ye. I. Chuykin, Doklady Akad. Nauk. U.S.S.R. **68**, 1029 (1949); also in Sm, C. M. Fowler (private communication); Hf^{181}, A. H. Ward and D. Walker, Nature **163**, 168 (1949) and A. Lundly, Phys. Rev. **76**, 993 (1949); Hg^{197}, Walter, Huber, and Zunti, Helv. Phys. Acta **23**, 697 (1950) and O. Huber and F. Humbel, Helv. Phys. Acta. **24**, 127 (1951).

[2] Rose, Goertzel, Spinrad, Harr, and Strong, Phys. Rev. **83**, 79 (1951). References to equations of this paper will be denoted with the suffix 1.

[3] H. Frauenfelder, Phys. Rev. **82**, 549 (1951); Aeppli, Bishop, Frauenfelder, Walter, and Zunti, Phys. Rev. **82**, 550 (1951).

[4] Compare, G. Goertzel, Phys. Rev. **70**, 897 (1946).

[5] J. W. Gardner, Proc. Phys. Soc. (London) **A62**, 763 (1949); **64**, 238 (1951). The result for electric multipoles, namely that the $F_L^M(\vartheta)$ functions (see Eq. (2) below) are proportional to $|Y_L^M|^2$, where (for the case considered by Gardner) L and M are the angular momentum quantum numbers of the electron, is also obtained if the spin is treated in Pauli approximation and a sum over spins is performed. The essential point here is that the orbital angular momentum of the electrons corresponds to a good quantum number. An outline of the formal aspects of the theory was discussed by M. Fierz, Helv. Phys. Acta **22**, 489 (1949).

tion functions on the multipole index L is also much less sensitive for the former (for essentially the same reason). Hence a greater accuracy is required in the correlation calculation.

A relativistic treatment of the formal aspect of the problem was given by Ling.[6] However, the pertinent matrix elements were calculated using the scattered wave function instead of the time-space reversed scattered wave function and, as the following shows (Sec. III), the latter is the correct procedure. This part of the problem was treated correctly by Lloyd.[7]

In the following we give a completely relativistic treatment of the conversion correlation problem. Since the pertinent matrix elements (Eqs. (41) and (43) below) are exactly those which arise in the conversion coefficient calculation[2] the numerical results are given for just those cases previously considered. In particular, we consider conversion from the K-shell only (without screening) although the extension to other shells is almost immediate once numerical values for the matrix elements become available. It is planned to make this extension in the near future. The form in which the numerical results are given is as follows: If the correlation between a γ-ray and any other radiation x is known and is expressed as an expansion in Legendre polynomials, the correlation with a conversion electron replacing the γ-ray is obtained by multiplying the coefficients of each Legendre polynomial $P_\nu(\cos\vartheta)$ by a coefficient $b_\nu(Z, k, \pi, L)$ (Eqs. (46) and (48)) where Z, k are as in reference 2, $\pi = e$, m refers to the parity (electric, magnetic respectively) and the multipole is a (pure) 2^L pole. For conversion-conversion correlation (Sec. V(c)) we multiply the coefficients in the $\gamma-\gamma$ correlation function[8] by $b_\nu(Z, k_1, \pi_1, L_1)b_\nu(Z, k_2, \pi_2, L_2)$. The prescription just given also applies when the x-transition is a mixed one [Sec. V(e)] involving superposition of different angular momenta. Corresponding results for the case in which the conversion transition is mixed[7] could also be obtained from the formalism given below but we do not give any numerical results for this case.

As indicated, and as would be expected, the conversion correlation is not only parity dependent but is also dependent on the physical parameters Z, k. This is in contrast to the $\gamma-\gamma$ correlation, for example, and so far as physical parameter dependence is concerned, it is in contrast to the nonrelativistic electric multipole conversion correlation.[5,6] The dependence on physical parameters enters here because of the presence of more than one final state (there are two for initial electron angular momentum $j=\frac{1}{2}$) and the fact that these final states are physically different (linearly independent radial functions). The dependence on physical parameters, and on parity as well, is a property of the angular distribution functions $F_L{}^M(\vartheta)$ [Eqs. (2) and (25)] which describe a Dirac electron undergoing a transition in a (coulomb) field between specified states and corresponding to a prescribed direction of motion at large distances. Up to a certain point [Eqs. (25) and (26)], the formal treatment given below applies as well to the angular distribution function for a number of other problems: emission of β-particles with coulomb effects included, ejection of photoelectrons, pair formation, etc.

II. GENERAL FORMALISM

We consider a double cascade in which a nucleus makes a transition from a state of angular momentum J_1 to an intermediate state J emitting radiation 1 of angular momentum L_1 and then emits radiation 2 of angular momentum L_2 in going to a final state J_2. This cascade is designated by $J_1(L_1)J(L_2)J_2$. The components of J_1, L_1, J, L_2, J_2 on an arbitrary quantization axis are m_1, M_1, m, M_2, m_2 respectively with the usual conservation rules applying. Selecting the direction of the second radiation as the quantization axis, and with ϑ denoting the angle between radiations, the angular correlation function can be written in the form[9]

$$W(\vartheta)=\sum_{m_1M_1mM}[C_{m_1M_1}{}^{J_1L_1J}]^2F_{L_1}{}^{M_1}(\vartheta)\times[C_{mM_2}{}^{JL_2J_2}]^2F_{L_1}{}^{M_2}(0), \quad (1)$$

where $C_{m_1M_1}{}^{J_1L_1J}$ is the vector addition coefficient[10] and $F_{L_i}{}^{M_i}(\vartheta)$ is the angular distribution function for radiation i. It will be noted that the dependence on J_1, J, J_2 is entirely contained in the C-coefficients. Since we are interested only in the angular dependence of W, multiplicative factors in the $F_L{}^M$ independent of the magnetic quantum numbers are irrelevant and will be discarded, from time to time, in the sequel.

For an electron in a final state described by a wave function $\Psi(\mathbf{r}, t)$ the $F_L{}^M$ is obtained from the radial Dirac current per unit solid angle:

$$F_L{}^M(\vartheta)=r^2J_r=-r^2(\Psi^\dagger\alpha_r\Psi) \quad (2)$$

with $r\to\infty$, and with a summation over final spins and an average over initial spins implied. The dagger in Eq. (2) means hermitian conjugate. For a transition induced by a time-dependent perturbation $\mathcal{H}_1e^{-ikt}+\mathcal{H}_1{}^*e^{ikt}$ we have[11]

$$(\mathcal{H}_0+\mathcal{H}_1e^{-ikt})\Psi=i\partial\Psi/\partial t \quad (3)$$

wherein $\mathcal{H}_0$ is the Dirac hamiltonian for an electron in a coulomb field and we have emitted the conjugate term, as usual, since it will make no final contribution. The current in (2) is then calculated from the perturbation solution of (3).

[6] D. S. Ling, Ph.D. dissertation (University of Michigan, 1948).
[7] S. P. Lloyd, private communication.
[8] D. R. Hamilton, Phys. Rev. **58**, 122 (1940). See also D. S. Ling and D. L. Falkoff, Phys. Rev. **76**, 1639 (1949); W. Arnold, Phys. Rev. **80**, 34 (1950).
[9] D. L. Falkoff and G. E. Uhlenbeck, Phys. Rev. **79**, 323 (1950).
[10] E. U. Condon and G. H. Shortley, *Theory of Atomic Spectra* (Cambridge University Press, London, 1935), Chapter III. There denoted by $(J_1L_1m_1M_1|J_1L_1Jm)$. See Appendix C.
[11] Throughout we use relativistic units: $\hbar=m=c=1$. In the following kmc^2 will be the energy released in the nuclear transition.

An alternative, and completely equivalent procedure is the following: We introduce the fourier transform $\psi(E, \mathbf{r})$ according to

$$\Psi(\mathbf{r}, t)=\int_{-\infty}^{\infty} \psi(E, \mathbf{r})e^{-iEt}dE \tag{4}$$

then (3) becomes

$$(\mathcal{H}_0-E)\psi(E, \mathbf{r})=-\mathcal{H}_1\psi(E-k, \mathbf{r})\rightarrow-\mathcal{H}_1\psi_i(E_i, \mathbf{r}) \tag{3a}$$

where the replacement indicated by the arrow introduces the initial state wave function ψ_i with total energy E_i, consistent with the perturbation solution to solution to first order in $\mathcal{H}_1$. Then if the Green function solution of (3a) is used to obtain the current, the result is the same as given by Eq. (2).[12] That is,

$$F_L{}^M(\vartheta)=-r^2(\psi^\dagger\alpha_r\psi) \tag{2a}$$

with $r\rightarrow\infty$.

A. The Green Function[13]

We wish to solve Eq. (3a), that is

$$(E-V+\boldsymbol{\alpha}\cdot\mathbf{p}+\beta)\psi=\mathcal{H}_1\psi_i, \tag{5}$$

where V is a central field ($V=-\alpha Z/r$) and the initial state ψ_i is specified, by the use of the Green function for the operator on the left-hand side of (5). The most convenient procedure is to obtain the free-particle Green function and then make the appropriate modifications in the radial functions. With

$$(E+\boldsymbol{\alpha}\cdot\mathbf{p}+\beta)G^{(0)}(\mathbf{r}, \mathbf{r}')=\delta(\mathbf{r}-\mathbf{r}')I,$$

where I is the (4×4) unit matrix, we have

$$G^{(0)}(\mathbf{r}, \mathbf{r}')=-(E-\beta+i\boldsymbol{\alpha}\cdot\nabla)\frac{e^{ip|\mathbf{r}-\mathbf{r}'|}}{4\pi|\mathbf{r}-\mathbf{r}'|}. \tag{6}$$

In (6) the ∇ operator acts on $\mathbf{r}$ and $p=(E^2-1)^{\frac{1}{2}}$. In (6) we use the familiar expansion

$$\frac{e^{ip|\mathbf{r}-\mathbf{r}'|}}{4\pi|\mathbf{r}-\mathbf{r}'|}=ip\sum_{lm} h_l(pr_>)j_l(pr_<)Y_l{}^m(\mathbf{r})Y_l{}^{m*}(\mathbf{r}'), \tag{7}$$

where the order of the arguments in spherical harmonics is immaterial, and h_l, j_l are the spherical hankel functions of the first kind and spherical bessel function respectively.

$$\boldsymbol{\alpha}\cdot\nabla=\rho_1\sigma_r\left(\frac{\partial}{\partial r}+\frac{1}{r}\right)+\rho_1\boldsymbol{\sigma}_r\rho_3K/r \tag{8}$$

and ρ_1, ρ_3 are the matrices operating in Dirac (ρ) space,

$$\rho_1=\begin{pmatrix}0 & 1\\ 1 & 0\end{pmatrix},\quad \rho_3=\beta=\begin{pmatrix}1 & 0\\ 0 & -1\end{pmatrix}$$

while $\boldsymbol{\sigma}$-matrices operate in Pauli space. Of course, products of ρ- and $\boldsymbol{\sigma}$-operators imply direct products. In (8)

$$K=-\rho_3(\boldsymbol{\sigma}\cdot\mathbf{L}+1),\quad \mathbf{L}=-i\mathbf{r}\times\nabla. \tag{9}$$

Noting that we can write the unit matrix in $\boldsymbol{\sigma}$-space in the form (Appendix A),

$$I_\sigma=\sum_\tau \chi_\mathfrak{l}{}^\tau\chi_\mathfrak{l}{}^{\tau\dagger} \tag{10}$$

we have the result

$$\sum_m Y_l{}^m(\mathbf{r})Y_l{}^{m*}(\mathbf{r}')I_\sigma=\sum_{\kappa\mu}\chi_\kappa{}^\mu(\mathbf{r})\chi_\kappa{}^{\mu\dagger}(\mathbf{r}') \tag{11}$$

where $\chi_\kappa{}^\mu$ is the Pauli central field spinor (Appendix A) and the sum over κ includes only l, $-l-1$. From (6), (7), (11), and (A11) we obtain for $r>r'$:

$$\begin{aligned}G_{11}{}^{(0)}/(E-1)&=-ip\sum_{\kappa\mu}h_{l(\kappa)}(pr)j_{l(\kappa)}(pr')\chi_\kappa{}^\mu(\mathbf{r})\chi_\kappa{}^{\mu\dagger}(\mathbf{r}')\\ &=G_{22}{}^{(0)}/(E+1)\\ G_{12}{}^{(0)}=G_{21}{}^{(0)}&=-p^2\sum_{\kappa\mu}S(\kappa)h_{l(-\kappa)}(pr)\\ &\quad\times j_{l(\kappa)}(pr')\chi_{-\kappa}{}^\mu(\mathbf{r})\chi_\kappa{}^{\mu\dagger}(\mathbf{r}').\end{aligned} \tag{12}$$

It is very convenient to write Eq. (12) in a form such that each term (κ, μ) is expressed in terms of field-free Dirac eigenfunctions in the angular momentum representation. These are

$$\phi_\kappa{}^\mu(\mathbf{r})=\begin{pmatrix}-iS(\kappa)(E-1/E+1)^{\frac{1}{2}}z_{l(-\kappa)}(pr)\chi_{-\kappa}{}^\mu(\mathbf{r})\\ z_{l(\kappa)}(pr)\chi_\kappa{}^\mu(\mathbf{r})\end{pmatrix}. \tag{13}$$

Retaining the notation $\phi_\kappa{}^\mu$ for standing waves (spherical cylinder function $z_l=j_l$) and using $\bar{\phi}_\kappa{}^\mu$ for outgoing waves ($z_l=h_l$) we find by changing κ to $-\kappa$ in the first column of $G^{(0)}$, thus simply reordering the terms, the result for $r>r'$

$$G^{(0)}(r, r')=-ip(E+1)\sum_{\kappa\mu}\bar{\phi}_\kappa{}^\mu(\mathbf{r})\phi_\kappa{}^{\mu\dagger}(\mathbf{r}'). \tag{14}$$

To obtain the Green function for the coulomb field, we replace $\bar{\phi}_\kappa{}^\mu$ and $\phi_\kappa{}^\mu$ by coulomb field solutions which differ from (13) only in that z_l is replaced by Dirac radial functions with exactly the same normalization.[14,15] It is convenient for comparison purposes and later identification of radial matrix elements to use the same radial functions used before.[2,15] These latter differ by a factor $-S(\kappa)(p(E+1)/\pi)^{\frac{1}{2}}$ from the former. Thus, we write, in accord with previous notation,

$$\Phi_\kappa{}^\mu(\mathbf{r})=\begin{pmatrix}-if_\kappa\chi_{-\kappa}{}^\mu\\ g_\kappa\chi_\kappa{}^\mu\end{pmatrix} \tag{15a}$$

for the standing wave solution of the Dirac coulomb

[12] The proof of this equivalence in the nonrelativistic case is given by H. A. Bethe, Ann. Physik **4**, 443 (1930). The generalization to the relativistic case is almost immediate. See E. Greuling and M. L. Meeks, Phys. Rev. **82**, 531 (1951).

[13] Appendix A contains a discussion of the sign convention and representation used throughout this and subsequent sections.

[14] M. E. Rose, Phys. Rev. **82**, 389 (1951).

[15] M. E. Rose, Phys. Rev. **51**, 484 (1937).

field and

$$\bar{\Phi}_\kappa{}^\mu(\mathbf{r})=\begin{pmatrix} -i\bar{f}_\kappa\chi_{-\kappa}{}^\mu \\ \bar{g}_\kappa\chi_\kappa{}^\mu \end{pmatrix} \tag{15b}$$

for the outgoing wave solution. Specifically, the normalization is such that $r\to\infty$

$$\begin{aligned} f_\kappa(\infty)&=-\left(\frac{p(E-1)}{\pi}\right)^{\frac{1}{2}}\lim_{r\to\infty} j_{l(-\kappa)}(pr+\Delta_\kappa), \\ g_\kappa(\infty)&=-\left(\frac{p(E+1)}{\pi}\right)^{\frac{1}{2}} S(\kappa)\lim_{r\to\infty} j_{l(\kappa)}(pr+\Delta_\kappa), \end{aligned} \tag{16}$$

where

$$\Delta_\kappa=\delta_\kappa(Z)-\delta_\kappa(Z=0) \tag{16a}$$

and $\delta_\kappa(Z)$ is the phase defined in reference 15. The irregular coulomb field solutions are defined so that $\bar{f}_\kappa$ and $\bar{g}_\kappa$ have the asymptotic behavior (16) with $j_{l(\pm\kappa)}$ replaced by $h_{l(\pm\kappa)}$. The definition of Δ_κ is unchanged.

Finally, the desired Green function is, for $r>r'$

$$G(\mathbf{r},\mathbf{r}')=-\pi i\sum_{\kappa\mu}\bar{\Phi}_\kappa{}^\mu(\mathbf{r})\Phi_\kappa{}^{\mu\dagger}(\mathbf{r}'). \tag{17}$$

The Green function for $r<r'$ is

$$G(\mathbf{r},\mathbf{r}')=-\pi i\sum_{\kappa\mu}\Phi_\kappa{}^\mu(\mathbf{r})\bar{\Phi}_\kappa{}^{\mu\dagger}(\mathbf{r}') \tag{18}$$

but the hermitian conjugate operation applies only to the spin-angular spinors $\chi_{\pm\kappa}{}^\mu$.

B. The Angular Distribution

The solution of (5) which has the required asymptotic behavior, that of an outgoing wave, is

$$\psi(\mathbf{r})=\int d\mathbf{r}'\bar{G}(\mathbf{r},\mathbf{r}')\mathcal{H}_1(\mathbf{r}')\psi_i(\mathbf{r}'). \tag{19}$$

Using Eq. (17) the asymptotic form of ψ is

$$\psi_\infty=-\pi i\sum_{\kappa\mu}\bar{\Phi}_\kappa{}^\mu(\mathbf{r})\langle\Phi_\kappa{}^\mu(\mathbf{r}')|\mathcal{H}_1|\psi_i\rangle. \tag{20}$$

Here, and in the following angular brackets designate scalar product formation over spin and configuration space. More explicitly, Eq. (20) may be written in the form

$$\psi_\infty=i\pi^{\frac{1}{2}}\frac{e^{ipr}}{r}\sum_{\kappa\mu}e^{i\Delta_\kappa}S(\kappa)\langle\Phi_\kappa{}^\mu(\mathbf{r}')|\mathcal{H}_1|\psi_i\rangle \times\begin{pmatrix} -iS(\kappa)(E-1)^{\frac{1}{2}}p^{-\frac{1}{2}}\chi_{-\kappa}{}^\mu\exp[-\frac{1}{2}\pi i(l(-\kappa)+1)] \\ (E+1)^{\frac{1}{2}}p^{-\frac{1}{2}}\chi_\kappa{}^\mu\exp[-\frac{1}{2}\pi i(l(\kappa)+1)] \end{pmatrix}. \tag{21}$$

The angular distribution function, which is the current per unit solid angle in the radially outward direction for a specific initial state and for large r, is

$$\begin{aligned} F_L{}^M(\vartheta)&=-r^2(\psi|\rho_1\sigma_r|\psi) \\ &=i\sum_{\kappa\kappa'}\sum_{\mu\mu'}e^{i(\Delta_\kappa-\Delta_{\kappa'})}S(\kappa)S(\kappa') \\ &\times\langle\kappa'\mu'|\mathcal{H}_1|\psi_i\rangle^*\langle\kappa\mu|\mathcal{H}_1|\psi_i\rangle \\ &\times\{S(\kappa)\exp\{\tfrac{1}{2}\pi i[l(\kappa')-l(-\kappa)]\} \\ &\times(\chi_{\kappa'}{}^{\mu'}|\sigma_r|\chi_{-\kappa}{}^\mu) \\ &-S(\kappa')\exp\{\tfrac{1}{2}\pi i[l(-\kappa')-l(\kappa)]\} \\ &\times(\chi_{-\kappa'}{}^{\mu'}|\sigma_r|\chi_\kappa{}^\mu)\}. \end{aligned} \tag{22}$$

This represents the angular distribution function for an initial state of specific magnetic quantum number, τ, say. What is eventually required is the average of (22) over τ. However, in order to avoid confusion of notation we retain the symbol $F_L{}^M$ for both angular distribution functions and rely on the context to make the meaning clear. Also, in Eq. (22) and in the following, the logarithmic term in the phases Δ_κ and δ_κ can be dropped since it is clear that it cancels out in the expression for $F_L{}^M$.

From Appendix A we find

$$\begin{aligned} (\chi_{-\kappa'}{}^{\mu'}|\sigma_r|\chi_\kappa{}^\mu)&=-(\chi_{-\kappa'}{}^{\mu'}|\chi_{-\kappa}{}^\mu) \\ &=-(\chi_{\kappa'}{}^{\mu'}|\chi_\kappa{}^\mu)=(\chi_{\kappa'}{}^{\mu'}|\sigma_r|\chi_{-\kappa}{}^\mu) \end{aligned} \tag{23}$$

and we note that

$$\begin{aligned} S(\kappa')\exp\{\tfrac{1}{2}\pi i[l(-\kappa')-l(\kappa)]\}& \\ =-S(\kappa)\exp\{\tfrac{1}{2}\pi i[l(\kappa')-l(-\kappa)]\}&. \end{aligned} \tag{24}$$

Further, we consider a definite magnetic quantum number, τ, for the initial state ψ_i so that $\mu=\mu'=M+\tau$. Then, averaging over τ,

$$\begin{aligned} F_L{}^M(\vartheta)&=-i\sum_{\kappa\kappa'\tau}e^{i(\Delta_\kappa-\Delta_{\kappa'})}S(\kappa) \\ &\times\exp\{\tfrac{1}{2}\pi i[l(-\kappa')-l(\kappa)]\langle\kappa',M+\tau|\mathcal{H}_1|\psi_i\rangle^* \\ &\times\langle\kappa,M+\tau|\mathcal{H}_1|\psi_i\rangle(\chi_{\kappa'}{}^{M+\tau}|\chi_\kappa{}^{M+\tau}). \end{aligned} \tag{25}$$

Using the definition (A5), (A1), and Appendix B we find

$$\begin{aligned} (\chi_{\kappa'}{}^\mu|\chi_\kappa{}^\mu)&=\sum_\nu[(2l(\kappa)+1)(2l(\kappa')+1)|\kappa\kappa'|/\pi(2\nu+1)]^{\frac{1}{2}} \\ &\times C_0{}^{l(\kappa)}{}_0{}^{l(\kappa')}{}_\nu C_{\mu}{}^{j}{}_{-\mu}{}^{j'}{}_\nu(-)^{\nu+\frac{1}{2}-\mu+\kappa+\kappa'} \\ &\times W(l(\kappa),l(\kappa'),j,j';\nu\tfrac{1}{2})Y_\nu{}^0(\cos\vartheta), \end{aligned} \tag{26}$$

where $j=|\kappa|-\frac{1}{2}$, $j'=|\kappa'|-\frac{1}{2}$, and W is a Racah coefficient.[16]

Combining the results (25) and (26) one obtains the starting point for calculating the angular distribution functions $F_L{}^M$ for any interaction involving an electron in a coulomb field with the direction of motion specified

[16] G. Racah, Phys. Rev. **62**, 438 (1942); **63**, 367 (1943).

asymptotically with reference to an arbitrary axis of quantization.

III. RELATION TO SCATTERED WAVE

The result (21) for the wave function describing the outgoing wave has a rather interesting physical interpretation. In fact, we show in this section that the radial current, summed over spins of initial and final states, can be calculated from the square modulus of matrix elements of the perturbation $\mathcal{H}_1$ between the initial state and a "final" state ψ_f where ψ_f is *not* the scattered wave but is the time and space reversed scattered wave. Thus, ψ_f has the asymptotic behavior of a plane wave plus an *incoming* wave rather than a plane wave plus an outgoing wave.[17] This is the point which was overlooked in previous work.[6,18]

In order to demonstrate the result just stated we carry out the sum over μ in Eq. (21). Since, as the Green function (17) shows, the sum in question is of the form $\sum_\mu \chi_\kappa{}^\mu(\mathbf{r})\chi_\kappa{}^{\mu\dagger}(\mathbf{r}')$, which is invariant under rotations in spin and configuration space, we can choose the direction of $\mathbf{r}$ as the quantization axis for the present purpose. Then since

$$\begin{aligned}\chi_\kappa{}^\mu(0)&=(|\kappa|/4\pi)^{\frac{1}{2}}[-S(\kappa)]^{\mu+\frac{1}{2}}\chi_{\frac{1}{2}}{}^\mu; \quad \mu=\pm\tfrac{1}{2}\\ &=0; \qquad\qquad\qquad\quad \mu\neq\pm\tfrac{1}{2}\end{aligned} \tag{27}$$

we obtain from (21)

$$\psi_\infty=\frac{ie^{ipr}}{r}\sum_\kappa(|\kappa|/4\pi)^{\frac{1}{2}}e^{i\Delta_\kappa} \times\{\langle\Phi_\kappa{}^{\frac{1}{2}}|\mathcal{H}_1|\psi_i\rangle\Lambda_+ +\langle\Phi_\kappa{}^{-\frac{1}{2}}|\mathcal{H}_1|\psi_i\rangle\Lambda_-\}, \tag{28}$$

where the spinors $\Lambda_\pm$ are

$$\Lambda_+=\begin{pmatrix}-\dfrac{ip}{E+1}\chi_{\frac{1}{2}}{}^{\frac{1}{2}}\exp[-\frac{1}{2}\pi i(l(-\kappa)+1)]\\ -\chi_{\frac{1}{2}}{}^{\frac{1}{2}}S(\kappa)\exp[-\frac{1}{2}\pi i(l(\kappa)+1)]\end{pmatrix}, \tag{29}$$

and Λ_- is obtained by changing $\chi_{\frac{1}{2}}{}^{\frac{1}{2}}$ to $\chi_{\frac{1}{2}}{}^{-\frac{1}{2}}$ and multiplying by $S(\kappa)\rho_3$. Since

$$-i\exp[-\tfrac{1}{2}\pi i(l(-\kappa)+1]=S(\kappa)\exp[-\tfrac{1}{2}\pi i/2(l(\kappa)+1)],$$

and $l(\kappa)=l(-\kappa)+S(\kappa)$, we can write (28) in the form $\psi_\infty=\psi_+ +\psi_-$

$$\psi_+=\frac{ie^{ipr}}{4\pi r}\sum_\kappa(4\pi|\kappa|)^{\frac{1}{2}}e^{i\Delta_\kappa}\exp[-\tfrac{1}{2}\pi il(-\kappa)] \times\langle\Phi_\kappa{}^{\frac{1}{2}}|\mathcal{H}_1|\psi_i\rangle D_+, \tag{30}$$

$$\psi_-=\frac{ie^{ipr}}{4\pi r}\sum_\kappa(4\pi|\kappa|)^{\frac{1}{2}}e^{i\Delta_\kappa}\exp[-\tfrac{1}{2}\pi i(l(\kappa)+1)] \times\langle\Phi_\kappa{}^{-\frac{1}{2}}|\mathcal{H}_1|\psi_i\rangle D_-$$

and $D_\pm$ are the Dirac plane wave spinors for the momentum along the quantization axis with $+$ and $-$ corresponding to spin "up," spin "down," respectively:

$$D_+=\begin{pmatrix}-p/(E+1)\\0\\1\\0\end{pmatrix} \qquad D_-=\begin{pmatrix}0\\p/(E+1)\\0\\1\end{pmatrix}. \tag{31}$$

If in (30) we write the sum of matrix elements as a single matrix element, that is

$$\psi_\pm=\langle\Phi_\pm|\mathcal{H}_1|\psi_i\rangle\frac{e^{ipr}}{4\pi r}D_\pm \tag{32}$$

then

$$\begin{aligned}\Phi_+&=-i\sum_\kappa(4\pi|\kappa|)^{\frac{1}{2}}e^{-i\Delta_\kappa}\exp[\tfrac{1}{2}\pi il(-\kappa)]\Phi_\kappa{}^{\frac{1}{2}},\\ \Phi_-&=-i\sum_\kappa(4\pi|\kappa|)^{\frac{1}{2}}e^{-i\Delta_\kappa}\exp[\tfrac{1}{2}\pi i(l(\kappa)+1)]\Phi_\kappa{}^{-\frac{1}{2}}.\end{aligned} \tag{33}$$

We now compare with the scattered wave which has the asymptotic behavior: plane wave plus outgoing spherical wave. For a fixed spin direction specified by σ

$$\psi_{sc}{}^\sigma=\sum_\kappa(4\pi|\kappa|)^{\frac{1}{2}}e^{i\Delta_\kappa} \times\exp[\tfrac{1}{2}\pi i(l(\kappa)-(\sigma+\tfrac{1}{2})(1+S(\kappa))]\Phi_\kappa{}^\sigma, \quad \sigma=\pm\tfrac{1}{2}. \tag{34}$$

To this we apply the space and time reversal operators I_S (β times space inversion) and I_T ($i\sigma_2$ times complex conjugation). Then

$$I_TI_S\Phi_\kappa{}^\sigma=(-)^{\sigma+\frac{1}{2}-\kappa}\Phi_\kappa{}^{-\sigma}.$$

Noting that $|\kappa|=l(\kappa)-\frac{1}{2}(S(\kappa)-1)$ we obtain

$$I_TI_S\psi_{sc}{}^{\frac{1}{2}}=\sum_\kappa(4\pi|\kappa|)^{\frac{1}{2}}e^{-i\Delta_\kappa}\exp[\tfrac{1}{2}\pi il(\kappa)]\Phi_\kappa{}^{-\frac{1}{2}}, \tag{35a}$$

$$I_TI_S\psi_{sc}{}^{-\frac{1}{2}}=\sum_\kappa(4\pi|\kappa|)^{\frac{1}{2}}e^{-i\Delta_\kappa} \times\exp[\tfrac{1}{2}\pi i(l(-\kappa)+1)]\Phi_\kappa{}^{\frac{1}{2}}. \tag{35b}$$

Comparing with (33) we see that

$$\Phi_+=-I_TI_S\psi_{sc}{}^{-\frac{1}{2}}, \quad \Phi_-=I_TI_S\psi_{sc}{}^{\frac{1}{2}}. \tag{36}$$

Thus, except for a spin reversal, the wave functions $\psi_f(\equiv\Phi_\pm)$ which are used in calculating the current are the time and space reversed scattered wave. For the current summed over final spins the spin reversal is irrelevant. However, the effect of time and space reversal is to change the sign of the coulomb phase shifts δ_κ (Eq. 16(a)) in the final results and this is not an irrelevant change.

IV. APPLICATION TO *K*-SHELL INTERNAL CONVERSION

For the K-shell (or L_I shell, for example) we have $\psi_i\equiv\psi_{-1}{}^\tau$ and $\tau=\pm\frac{1}{2}$. The radiation fields in a convenient gauge have been given elsewhere.[2] Discarding an irrelevant multiplicative factor ($[2/\pi L(L+1)]$) throughout, we discuss the magnetic and electric conversion separately.

[17] This result is well known for the nonrelativistic problem (see N. F. Mott and H. S. W. Massey, *The Theory of Atomic Collisions* (Oxford University Press, New York, 1933), p. 258). For noncentral potentials a proof is given by W. Rarita and J. Schwinger, Phys. Rev. **59**, 556 (1941).

[18] M. Fuchs, Ph.D. dissertation (University of Michigan, 1951).

(A) Magnetic Conversion

For a magnetic 2^L pole we have

$$\langle\kappa\mu|\mathcal{H}_1^m|-1\tau\rangle=\langle\kappa\mu|\rho_1(\boldsymbol{\sigma}\cdot\mathbf{L}Y_L{}^M)|-1\tau\rangle$$
$$=i[R_3'\langle\chi_{-\kappa}{}^\mu|\boldsymbol{\sigma}\cdot\mathbf{L}Y_L{}^M|\chi_{-1}{}^\tau\rangle$$
$$-R_4'\langle\chi_\kappa{}^\mu|\boldsymbol{\sigma}\cdot\mathbf{L}Y_L{}^M|\chi_1{}^\tau\rangle]_\kappa \quad (37)$$

where in the notation of reference 2, Eq. (17_1), has been introduced for the radial matrix elements and the final state in the R' integrals is described by the single index κ. In (37) $\mathbf{L}$ acts on $Y_L{}^M$ only. This latter fact enables us to conclude that

$$\langle\chi_\kappa{}^\mu|\boldsymbol{\sigma}\cdot\mathbf{L}Y_L{}^M|\chi_1{}^\tau\rangle=-\langle\chi_{-\kappa}{}^\mu|\boldsymbol{\sigma}\cdot\mathbf{L}Y_L{}^M|\chi_{-1}{}^\tau\rangle. \quad (38)$$

Equation (38) together with (A.9) yields

$$\langle\chi_{-\kappa}{}^\mu|\boldsymbol{\sigma}\cdot\mathbf{L}Y_L{}^M|\chi_1{}^\tau\rangle=(\kappa-1)\langle\chi_\kappa{}^\mu|Y_L{}^M\chi_{-1}{}^\tau\rangle. \quad (39)$$

However,

$$Y_L{}^M\chi_{-1}{}^\tau=(4\pi)^{-\frac{1}{2}}Y_L{}^M\chi_1{}^\tau=(4\pi)^{-\frac{1}{2}}\sum_{\bar\kappa}C_{M\tau}{}^{L\frac{1}{2}j}\chi_\kappa{}^{M+\tau}, \quad (40)$$

where $\bar\kappa=L$, $-L-1$, and $j=|\bar\kappa|-\frac{1}{2}$. Finally,

$$\langle\kappa\mu|\mathcal{H}_1^m|-1\tau\rangle=i(4\pi)^{-\frac{1}{2}}C_{M\tau}{}^{L\frac{1}{2}j}(\kappa-1)$$
$$\times(R_3'+R_4')_\kappa(\delta_{\kappa,-L}+\delta_{\kappa,L+1})$$
$$\equiv C_{M\tau}{}^{L\frac{1}{2}j}Q'(\kappa,L,m), \quad (41)$$

where the last factor in the first equality, contains Kronecker deltas.

(B) Electric Conversion

Here we evaluate the matrix element

$$\langle\kappa\mu|\mathcal{H}_1^e|-1\tau\rangle=\langle\kappa\mu|\rho_1h_{L-1}(r\boldsymbol{\sigma}\cdot\nabla+L\sigma_r)Y_L{}^M$$
$$+iLY_L{}^Mh_L|-1\tau\rangle \quad (42)$$

and the spherical hankel functions, which appear explicitly, have argument kr. Using

$$r\boldsymbol{\sigma}\cdot\nabla=\sigma_r(\mathbf{r}\cdot\nabla+i\boldsymbol{\sigma}\cdot\mathbf{r}\times\nabla)=\sigma_r(\partial/\partial r-\boldsymbol{\sigma}\cdot\mathbf{L})$$

Eq. (42) becomes

$$\langle\kappa\mu|\mathcal{H}_1^e|-1\tau\rangle$$
$$=iL[R_1+R_2-R_3+R_4]_\kappa\langle\chi_\kappa{}^\mu|Y_L{}^M|\chi_{-1}{}^\tau\rangle$$
$$-i(\kappa+1)(R_2+R_4)_\kappa\langle\chi_\kappa{}^\mu|Y_L{}^M|\chi_{-1}{}^\tau\rangle$$
$$=i(4\pi)^{-\frac{1}{2}}C_{M\tau}{}^{L\frac{1}{2}j}[L(R_1+R_2-R_3+R_4)$$
$$-(\kappa+1)(R_3+R_4)]_\kappa(\delta_{\kappa,L}+\delta_{\kappa,-L-1})$$
$$\equiv C_{M\tau}{}^{L\frac{1}{2}j}Q(\kappa,L,e), \quad (43)$$

where the notation (13_1) has been introduced.

(C) The Angular Distribution for *K*-Shell Conversion

In terms of the Q-coefficients defined by (41) and (43) the $F_L{}^M$ may be written formally for either parity. From (25) and (26)

$$F_L{}^M(\vartheta)=-i\sum_{\kappa\kappa'\tau\nu}(-)^{\nu+\frac{1}{2}-M-\tau+\kappa+\kappa'}S(\kappa)$$
$$\times e^{i(\Delta_\kappa-\Delta_{\kappa'})}\exp\{\tfrac{1}{2}\pi i[l(-\kappa')-l(\kappa)]\}$$
$$\times[(2l(\kappa)+1)(2l(\kappa')+1)|\kappa\kappa'|/\pi(2\nu+1)]^{\frac{1}{2}}$$
$$\times C_{M\tau}{}^{L\frac{1}{2}j}C_{M\tau}{}^{L\frac{1}{2}j'}C_0{}^{l(\kappa)}{}_0{}^{l(\kappa')\nu}$$
$$\times W(l(\kappa)l(\kappa')jj';\nu\tfrac{1}{2})Q^*(\kappa',L,\pi)$$
$$\times Q(\kappa,L,\pi)Y_\nu{}^0(\cos\vartheta). \quad (44)$$

Using (B.3) the sum over τ may be performed and with $\delta_\kappa(Z=0)=\frac{1}{2}\pi[\frac{1}{2}(1+S(\kappa))-|\kappa|]$ we obtain for electric multipoles

$$F_L{}^M(\vartheta)=\sum_{\nu=0}^{2L}(-)^MC_{1-1}{}^{LL\nu}C_{M-M}{}^{LL\nu}$$
$$\times(4\pi(2\nu+1))^{-\frac{1}{2}}b_\nu'Y_\nu{}^0(\cos\vartheta) \quad (45)$$

where ν takes on only even values ($C_{00}{}^{LL\nu}=0$ for ν odd) and

$$\frac{\nu(\nu+1)-2L(L+1)}{2L(L+1)(2L+1)}b_\nu'$$
$$=L^2|Q(L,L,e)|^2W^2(L,L,L-\tfrac{1}{2},L-\tfrac{1}{2};\nu\tfrac{1}{2})$$
$$+(L+1)^2|Q(-L-1,L,e)|^2$$
$$\times W^2(L,L,L+\tfrac{1}{2},L+\tfrac{1}{2};\nu\tfrac{1}{2})$$
$$-2L(L+1)Re[(e^{i\Delta_L}Q(L,L,e))^*e^{i\Delta_{-L-1}}$$
$$\times Q(-L-1,L,e)]W^2(L,L,L+\tfrac{1}{2},L-\tfrac{1}{2};\nu\tfrac{1}{2}). \quad (45a)$$

The angular distribution function given by (45) differs from that for emission of electromagnetic radiation[8,19] only in the factor $b_\nu'(e)$ and the two become identical (aside from a trivial normalization factor) when $b_\nu'=1$. We normalize to $b_0'(e)=1$ and using (B.6–8) we obtain for $b_\nu(e)=b_\nu'(e)/b_0'(e)$

$$b_\nu(e)=1+\frac{\nu(\nu+1)}{2L(L+1)-\nu(\nu+1)}$$
$$\times\frac{L}{2L+1}\frac{|L+1+T_e|^2}{L(L+1)+|T_e|^2}, \quad (46)$$

where

$$T_e=\frac{e^{i\delta_L}}{e^{i\delta_{-L-1}}}\frac{[L(R_1+R_2)-(2L+1)R_3-R_4]_{\kappa=L}}{[R_1+R_2+2R_4]_{\kappa=-L-1}}. \quad (46a)$$

[19] Biedenharn, Arfken, and Rose, Phys. Rev. **83**, 586 (1951).

For magnetic multipoles the allowed κ-values are $-L$, $L+1$. Using (B.4, 5) we find

$$F_L{}^M(\vartheta)=\sum_0^{2L}(-)^M C_{1-1}{}^{LL\nu}C_{M-M}{}^{LL\nu}\times(4\pi(2\nu+1))^{-1}b_\nu(m)Y_\nu{}^0(\cos\vartheta) \quad (47)$$

and for the b_ν normalized to $b_0=1$ we have

$$b_\nu(m)=1+\frac{\nu(\nu+1)}{2L(L+1)-\nu(\nu+1)}\times\frac{L(L+1)}{2L+1}\frac{|1-T_m|^2}{L+1+L|T_m|^2}, \quad (48)$$

where

$$T_m=\frac{e^{i\delta_{L+1}}}{e^{i\delta_{-L}}}\frac{(R_3'+R_4')_{\kappa=-L+1}}{(R_3'+R_4')_{\kappa=-L}}. \quad (48a)$$

It is of interest to recognize that for γ-rays, spin $\frac{1}{2}$ particles and for spinless particles as well, the M-dependence of the angular distribution functions, when expanded in Legendre polynomials, is entirely contained in the vector addition coefficient $(-)^M C_{M-M}{}^{LL\nu}$. It is for this reason that the simple parametrization given by (45) and (47) is possible. This would not have been possible if any other expansion, powers of $\cos^2\vartheta$ say, had been employed. It is evident, Sec. V, that these remarks also apply to the angular correlation function $W(\vartheta)$.[20]

V. THE ANGULAR CORRELATION

A. Special Cases of Conversion Correlation

It is clear from the foregoing that the prescription given in Sec. I applies; namely, if the Legendre polynomial expansion of the correlation between a γ-ray and a radiation x is

$$W_{\gamma-x}(\vartheta)=\sum_{\nu=0}^{\nu_m}A_\nu(\gamma-x)P_\nu(\cos\vartheta) \quad (49a)$$

then the correlation function for a conversion electron and radiation x is [see (*c*) below],

$$W_{e-x}(\vartheta)=\sum_{\nu=0}^{\nu_m}b_\nu A_\nu(\gamma-x)P_\nu(\cos\vartheta). \quad (49b)$$

In (49) $\frac{1}{2}\nu_m$ is the smallest integer of the set L_1, L_2, J (or $J-\frac{1}{2}$) if J is integer (or half-integer). The order in which the transitions occur is contained solely in the coefficients A_ν and we observe that the correlation $J_1(L_1)J(L_2)J_2$ is the same as the correlation $J_2(L_2)J(L_1)J_1$. In (49a, b) it is to be understood that the γ-ray is a pure 2^L multipole. Then b_ν is obtained from (46) for electric or from (48) for magnetic conversion transitions. See, however, (*e*) below.

[20] This result is implicitly contained in S. P. Lloyd, Ph.D. dissertation (University of Illinois, 1951).

We consider the following correlations:

(*a*) *Conversion-Gamma Correlation*

Then in (49b) $A_\nu(\gamma-x)\equiv A_\nu(\gamma-\gamma)$. The $\gamma-\gamma$ correlation has been quite extensively studied. For the most practical case that the γ-rays are emitted with the lowest angular momentum allowed by angular momentum selection rules, that is

$$L_i=|J-J_i| \quad (J_i\neq J); \quad L_i=1 \quad (J_i=J) \quad (50)$$

Lloyd[21] has given a tabulation of $A_\nu(\gamma-\gamma)$ for all transitions up to 2^4 pole–2^4 pole. In Lloyd's tabulation the normalization is $A_0=1$. For cases not covered by (50) the $A_\nu(\gamma-\gamma)$ may be obtained for $L_1\leqslant 2$, $L_2\leqslant 2$ from the tabulation of Falkoff and Uhlenbeck[9] and of Hamilton.[6] A useful form for $W_{\gamma\gamma}$ is (see Appendix B and reference 19)

$$W_{\gamma-\gamma}(\vartheta)=N\sum_{\nu=0}^{\nu_m}C_{1-1}{}^{L_1L_1\nu}C_{1-1}{}^{L_2L_2\nu}\times W(JJL_1L_1;\nu J_1)W(JJL_2L_2;\nu J_2)P_\nu(\cos\vartheta) \quad (51)$$

where, with the normalization factor

$$N=(-)^{J_1-J_2}(2L_1+1)(2L_2+1)(2J+1),$$

the coefficient of P_0 is equal to unity. The tabulation of the coefficients A_ν for cases not covered by (50) can then be extended considerably using Racah function tabulation of Biedenharn.[22]

(*b*) *β-Conversion Correlation*

The coefficients $A_\nu(\beta-\gamma)$ have been given[23] for the five pure β-invariants up through second forbidden transitions in the approximation $Z=0$. The case $Z\neq 0$ has been considered in the approximation $Z/137v\ll 1$ by Fuchs.[18] A calculation without this approximation could be carried out using the results of Sec. II but this has not yet been done.

(*c*) *Conversion-Conversion Correlation*

After the first conversion transition has taken place the half-empty K-shell will be filled very rapidly by x-ray emission or emission of Auger electrons. In fact the measured widths of x-ray lines shows that this filling-up time is much smaller than the intermediate state lifetime in any practical correlation experiment.[24]

[21] S. P. Lloyd, Phys. Rev. **83**, 716 (1951).

[22] L. C. Biedenharn and M. E. Rose, Oak Ridge National Laboratory Report No. 1098 (1951).

[23] D. L. Falkoff and G. E. Uhlenbeck, Phys. Rev. **79**, 334 (1950).

[24] A. H. Compton and S. K. Allison, *X-Rays in Theory and Experiment* (D. Van Nostrand Company, Inc., New York, 1935); also R. M. Steffen, Helv. Phys. Acta **22**, 167 (1949). If this were not so the initial electronic states would be different for the first and second conversion transitions and the probability amplitude for the double transition would be composed of two parts corresponding to two choices for the order of emission of the K-electrons. Then (reference 6) there would be a cross term between the two modes by which the cascade could take place. The evidence cited shows that this cross term is exceedingly negligible.

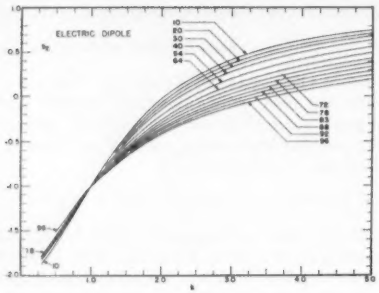

FIG. 1. b_ν coefficients for electric 2^l-pole transitions *versus* k (transition energy in mc^2 units). The attached numbers refer to the value of Z.

Also, the filling-up time is much shorter than the precession period corresponding to the hfs interaction of the nucleus and a single K-electron. Therefore it follows that the conversion-conversion correlation function is

$$W_{e-e}(\vartheta)=\sum_{\nu=0}^{\nu_m} b_\nu(1)b_\nu(2)A_\nu(\gamma-\gamma)P_\nu(\cos\vartheta) \quad (52)$$

where $b_\nu(1)$ refers to the first conversion electron emitted, etc.

(d) *Conversion-Alpha Correlation*

Such a cascade would be of interest in the case of a few heavy elements. The correlation function is

$$W_{e-\alpha}(\vartheta)=\sum_{\nu=0}^{\nu_m} b_\nu(e)b_\nu(\alpha)A_\nu(\gamma-\gamma)P_\nu(\cos\vartheta), \quad (53)$$

where

$$b_\nu(\alpha)=-C_{00}{}^{LL\nu}/C_{1-1}{}^{LL\nu}$$
$$=2L(L+1)/[2L(L+1)-\nu(\nu+1)]. \quad (53a)$$

This applies when the α-particles are emitted with essentially a single orbital angular momentum.

(e) *Mixed Transitions*

The case in which the conversion electron transition is not pure could be calculated along exactly the same lines as the pure transitions discussed, (Sec. IV). These would involve new coefficients, different from the b_ν. However, if the nonconversion transition is a mixed one, the conversion transition pure, then (49b) still applies. However the $A_\nu(\gamma-\gamma)$ must take into account the fact that a superposition of different angular momenta are emitted in one of the transitions. For correlation with both transitions mixed the coefficients have been given by Lloyd[21] to first order in ϵ, where ϵ^2 is the ratio of intensities of electric 2^{L+1} pole to magnetic 2^L pole. For one pure γ and one mixed γ the coefficients (with no neglections) are given by Ling and Falkoff[3] for a mixture of electric quadrupole and magnetic dipole and a pure dipole or quadrupole. For a correlation with a pure conversion transition of multipole index L_1 and either parity and a mixed γ-transition in which the radiation field is electric 2^{L_2+1} and magnetic 2^{L_2} the correlation function is

$$W_{e-\gamma}(\vartheta)=1+(1+\epsilon^2)^{-1}\sum_{\nu=2}^{\nu_m} b_\nu(L_1,\pi)\{\epsilon^2 A_\nu{}^{(e)}(\gamma-\gamma)$$
$$+A_\nu{}^{(m)}(\gamma-\gamma)\pm\epsilon x y_\nu(L_2)A_\nu{}^{(m)}\}P_\nu(\cos\vartheta). \quad (54)$$

The choice of $\pm$ sign in the cross term depends on whether the mixed transition occurs first or second[21] but note that, in the absence of a reliable nuclear model, the sign of ϵ is undetermined. However ϵ is real.[26] The $A_\nu{}^{(e,m)}$ are the coefficients for the pure 2^{L_2+1} electric,

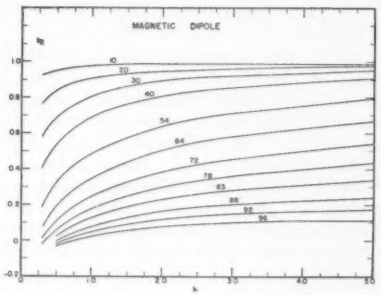

FIG. 2. Same as Fig. 1 for magnetic 2^l-pole transitions.

2^{L_2} magnetic radiations correlated with a pure $\gamma-2^{L_1}$ pole. The normalization is always $A_0=1$. Of course, for pure radiations the A_ν are parity independent and the indices e or m merely serve to indicate whether one uses L_2+1 or L_2 (respectively) for the multipole index for one transition along with L_1 for the other. The quantities x and $y_\nu(L)$ are defined by Lloyd.[21] The coefficients $A_\nu{}^{(m)}$ are given in Lloyd's tables[21] but $A_\nu{}^{(e)}$ corresponds to the correlation $J_1(L_1)J(L_2+1)J\pm L_2$ and these are not included in reference 21. The required coefficients $(A_\nu{}^{(e)}(\gamma-\gamma))$ can readily be obtained from the tabulated ones. In the transition to $J+L_2$

$$A_2=[J(L_2-2)-3(L_2+1)]A_2'/J(L_2+1). \quad (55a)$$

The superscript e has been dropped and A_2' refers to the correlation involving $J_2=J+L_2+1$ as given in reference 21. For the transition to $J-L_2$

$$A_2=[J(L_2-2)+4L_2+1]A_2''/(J+1)(L_2+1) \quad (55b)$$

with A_2'' referring to a transition to $J-L_2-1$. If $L_2=1$, (dipole-quadrupole mixture),

$$A_4=-2(2J+5)A_4'/J; \quad J_2=J+1 \quad (55c)$$

or

$$A_4=-2(2J-3)A_4''/J; \quad J_2=J-1. \quad (55d)$$

[26] S. P. Lloyd, Phys. Rev. **81**, 161 (1951).

The above correction factors cover the vast majority of experimentally realized cases.[26] For correction factors for correlations involving quadrupole-octupole mixtures or higher multipoles in cascade with quadrupoles or higher ($L_1 \geq 2$), reference should be made to the Racah function tables.[22]

(f) *Triple Correlations*

For a triple cascade[19] in which three radiations are emitted successively the procedure for converting from a standard correlation, say $\gamma-\gamma-\gamma$, to one in which one or more γ-rays are replaced by conversion electrons is just the same. One inserts a factor b_ν for each conversion electron. Consider, for example, a triple cascade in which the correlation between only the first and third radiations is observed. The correlation function with conversion electrons replacing either the first or third or both first and third γ-rays is obtained by inserting $b_\nu(1)$ or $b_\nu(3)$ or $b_\nu(1)b_\nu(3)$, respectively, in the $\gamma_1-\gamma_3$ correlation:

$$W_{\gamma_1-\gamma_3}(\vartheta)=\sum_{\nu=0}^{\nu_m}\bar{A}_\nu P_\nu(\cos\vartheta).$$

Designating the cascade by $J_1(L_1)J(L_2)J'(L_3)J_2$, where L_2 refers to a pure 2^{L_2} pole γ-ray, we have $\frac{1}{2}\nu_m=$ minimum of $[L_1, L_3, J$ (or $J-\frac{1}{2}$), J' (or $J'-\frac{1}{2})]$. The coefficients $\bar{A}_\nu$ are given elsewhere.[27]

B. Results

From Eqs. (46) and (48) it is obvious that for both electric and magnetic transitions all the coefficients

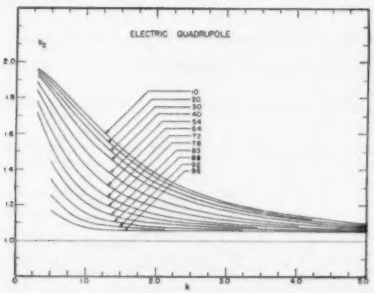

FIG. 3. Same as Fig. 1 for electric 2^3-pole transitions.

b_ν ($\nu>2$) are readily obtained from b_2 by

$$b_\nu(\pi)-1=\frac{\nu(\nu+1)[L(L+1)-3]}{3[2L(L+1)-\nu(\nu+1)]}(b_2(\pi)-1) \quad (56)$$

[26] According to M. Goldhaber and A. W. Sunyar, Phys. Rev. **83**, 906 (1951), multipole mixtures should occur only for $L_2=1$ (i.e., magnetic-dipole plus electric quadrupole). If $L_1=1$ and/or $J=1$ or $3/2$, $\nu_m=2$ and only the coefficient A_2 enters so that (55a, b) give the complete correction factor to Lloyd's tables in this case.

[27] Arfken, Biedenharn, and Rose, Oak Ridge National Laboratory Report No. 1103 (1951).

($\pi=e$ or m), so that only b_2 need be tabulated for each multipole.

In Figs. 1–10 the coefficients b_2 are given as functions of k for 12 values of Z in the range 10–96 for ten multipoles: $L=1-5$ electric and $L=1-5$ magnetic.[28] Figures 5, 7, and 9 give the b_2 coefficients for electric 2^3, 2^4, and 2^5 poles for the smaller Z-values and these coefficients for the same multipoles and for the larger Z-values are given in Figs. 5a, 7a, and 9a on an enlarged scale. The lowest k-value for which computations could be made is $k=0.3(Z\leq 78)$ and $k=0.5(Z>78)$.

For smaller k values, in the electric case, extrapolation toward the threshold can be made with the aid of the nonrelativistic limit:

$$b_2(e)=L(L+1)/[L(L+1)-3], \quad (\alpha Z\ll 1, k\ll 1). \quad (57)$$

For the magnetic transitions the "nonrelativistic" limit is Z, k dependent.[5] Experience with the corresponding limits for the conversion coefficients[2] indicates that this limit may be somewhat less reliable in the magnetic case. As an additional guide in extrapolation we can use the fact that $W(\vartheta)\geq 0$ by definition. From this it is possible to conclude that for both electric and magnetic transitions

$$\begin{aligned} -2\leq b_2\leq 1; \quad & L=1 \\ 1\leq b_2\leq b_2(\alpha); \quad & L>1. \end{aligned} \quad (57a)$$

Compare Eqs. (46) and (48). The fact that the nonrelativistic limit (for electric multipole) is an upper ($L>1$) or a lower ($L=1$) bound is a more useful extrapolation aid for the electric than for the magnetic transitions.

The high energy limit can be obtained by using the Casimir approximation[8] (asymptotic forms of the radial Dirac functions are used). Then one finds immediately that $b_2(\pi)=1(\pi=e$ or $m)$ and thus all $b_\nu(\pi)=1$. This implies that at high energies the conversion electrons give the same correlation function as the corresponding cascade with a photon replacing the conversion electron. The fact that the two limits, nonrelativistic and high

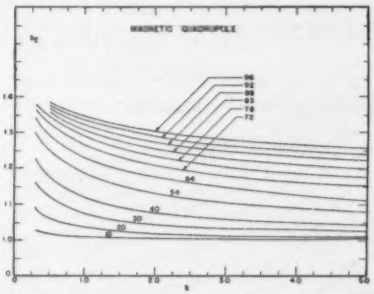

FIG. 4. Same as Fig. 1 for magnetic 2^3-pole transitions.

[28] The numerical results from which the curves of Fig. 1–10 were obtained are given in Rose, Biedenharn, and Arfken, Oak Ridge National Laboratory Report No. 1097 (1951).

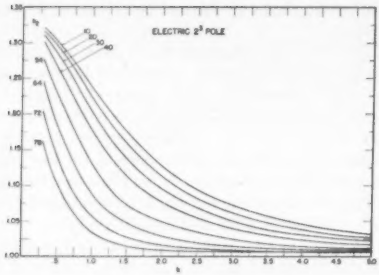

FIG. 5. Same as Fig. 1 for electric 2^3-pole transitions. Only lower Z values shown.

energy approach a common value with increasing L is clearly evident from the results which show a decreasing sensitivity, so far as energy dependence is concerned, with increasing L. The limit $Z=0$, for magnetic multipoles only, also gives a photon correlation; that is, $b_\nu(m)=1$ for all ν. The electric multipoles have the

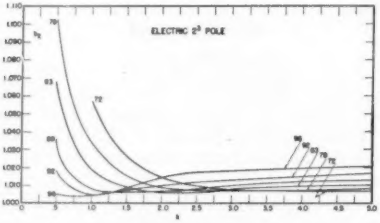

FIG. 5a. Same as Fig. 5 for the higher Z values and on an enlarged scale.

opposite Z-dependence; that is, they increase with decreasing Z (except for $L=1$ and $k\leqslant 1$) and for $L\geqslant 2$ the values of the b_2 coefficients as given lie between unity and the $Z=0$ limit:

$$b_2(Z=0)=1+\frac{12L}{[L(L+1)-3][(L+1)k^2+4L]}.$$

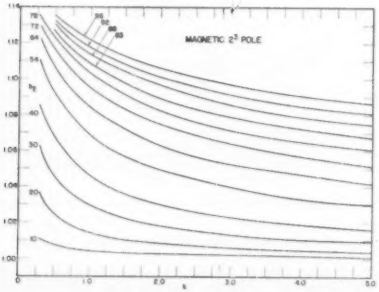

FIG. 6. Same as Fig. 1 for magnetic 2^3-pole transitions.

It will be noted that for cascades in which $\nu_m=2$ the sign of the anisotropy, $W(\vartheta)-1$, is reversed as compared to the γ-ray case for the low energy electric dipole conversion electrons but is the same for other cases.

The authors are indebted to Dr. C. L. Perry, Mr. Carl Perhacs, and Mrs. N. Dismuke of the Mathematics Panel, Oak Ridge National Laboratory, for performing the computations.

APPENDIX A. SIGN CONVENTIONS, PROPERTIES OF THE SPINORS

Throughout we use the Condon-Shortley[10] definition of the spherical harmonics Y_l^m. This differs by a phase

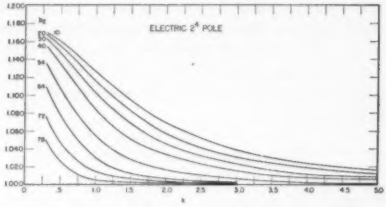

FIG. 7. Same as Fig. 5 for electric 2^4-pole transitions.

$(-)^m$ from the definition adopted in reference 15. We also use the well-known result that

$$Y_L{}^M Y_{L'}{}^{M'}=\sum_{\nu=|L-L'|}^{L+L'}[(2L+1)(2L'+1)/4\pi(2\nu+1)]^{\frac{1}{2}}\times C_{00}{}^{LL'\nu}C_{M-M'}{}^{LL'\nu}Y_\nu{}^{M+M'}. \quad \text{(A.1)}$$

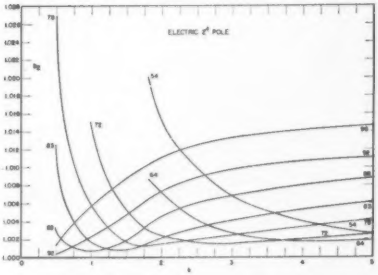

FIG. 7a. Same as Fig. 5a for electric 2^4-pole transitions.

The representation of the Dirac matrices is defined by (5) and $\boldsymbol{\alpha}=\rho_1\boldsymbol{\sigma}$ where

$$\boldsymbol{\sigma}=\begin{pmatrix}\mathbf{k} & \mathbf{i}-i\mathbf{j}\\ \mathbf{i}+i\mathbf{j} & -\mathbf{k}\end{pmatrix}$$

in terms of the cartesian unit vectors $\mathbf{i}$, $\mathbf{j}$, $\mathbf{k}$. The Pauli spinors introduced in (10) are such that

$$\sigma_\kappa\chi_\mathfrak{j}{}^\tau=2\tau\chi_\mathfrak{j}{}^\tau. \quad \text{(A.2)}$$

The discussion of the Dirac spinors (types (*a*) and (*b*)[15]) is unified by the introduction of κ the eigenvalue of K [Eq. (9)]:

$$j=|\kappa|-\tfrac{1}{2}, \tag{A.3}$$

$$\begin{aligned} l(\kappa)&=\kappa, && \kappa>0\\ &=|\kappa|-1, && \kappa<0 \end{aligned} \tag{A.4}$$

so that κ, which is a nonvanishing integer, specifies both j and l. Then the Pauli central field spinors are

$$\chi_\kappa{}^\mu=\sum_\tau C_{\mu-\tau\,\tau}{}^{l(\kappa)\frac{1}{2}j}\chi_{\frac{1}{2}}{}^\tau Y_{l(\kappa)}{}^{\mu-\tau} \tag{A.5}$$

with the properties (capital letters in (A.6–10) designate operators)

$$\mathbf{J}^2\chi_\kappa{}^\mu=(|\kappa|-\tfrac{1}{2})(|\kappa|+\tfrac{1}{2})\chi_\kappa{}^\mu, \tag{A.6}$$

$$J_z\chi_\kappa{}^\mu=\mu\chi_\kappa{}^\mu, \tag{A.7}$$

$$\mathbf{L}^2\chi_\kappa{}^\mu=l(\kappa)(l(\kappa)+1)\chi_\kappa{}^\mu=\kappa(\kappa+1)\chi_\kappa{}^\mu, \tag{A.8}$$

$$(\boldsymbol{\sigma}\cdot\mathbf{L}+1)\chi_\kappa{}^\mu=-\kappa\chi_\kappa{}^\mu, \tag{A.9}$$

$$(\mathbf{r}/r)\cdot\boldsymbol{\sigma}\chi_\kappa{}^\mu\equiv\sigma_r\chi_\kappa{}^\mu=-\chi_{-\kappa}{}^\mu. \tag{A.10}$$

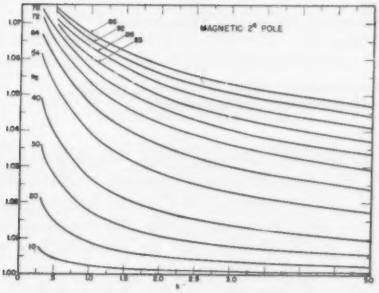

FIG. 8. Same as Fig. 1 for magnetic 2^4-pole transitions.

The relation between $\chi_\kappa{}^\mu$ and the $\Omega_{lj}{}^\mu$ introduced in Eq. (4_1) is

$$\chi_\kappa{}^\mu=(-)^{\mu-\frac{1}{2}}S(-\kappa)\Omega_{lj}{}^\mu,$$

where $S(x)\equiv$ sign of x.

For the spherical cylinder functions (Eq. (7)),

$$\left(\frac{d}{dr}+\frac{1+\kappa}{r}\right)Z_{l(\kappa)}(pr)=pS(\kappa)Z_{l(-\kappa)}(pr). \tag{A.11}$$

APPENDIX B. SOME PROPERTIES OF THE VECTOR ADDITION AND RACAH COEFFICIENTS[16]

Repeated use is made in Sec. II and III of various symmetry relations for the vector addition and Racah coefficients. For convenience these are listed below. We consider the vector addition coefficient $C_{m_1m_2m_3}{}^{j_1j_2j_3}$. In the notation used we omit m_3 (the z-component of j_3) or, in general, the third subscript since in all cases it is the sum of the first two. Then,

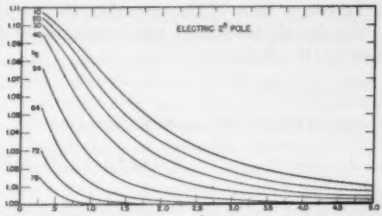

FIG. 9. Same as Fig. 5 for electric 2^5-pole transitions.

$$\begin{aligned} C_{m_1m_2}{}^{j_1j_2j_3}&=(-)^{j_1+j_2-j_3}C_{-m_1-m_2}{}^{j_1j_2j_3}\\ &=(-)^{j_1+j_2-j_3}C_{m_2m_1}{}^{j_2j_1j_3}\\ &=(-)^{j_1-m_1}[(2j_3+1)/(2j_2+1)]^{\frac{1}{2}}C_{m_1-m_3}{}^{j_1j_3j_2}\\ &=(-)^{j_2+m_2}[(2j_3+1)/(2j_1+1)]^{\frac{1}{2}}C_{-m_3m_2}{}^{j_3j_2j_1}\\ &=(-)^{j_1-j_2+m_3}[(2j_3+1)/(2j_1+1)]^{\frac{1}{2}}C_{m_2-m_3}{}^{j_2j_3j_1}. \end{aligned} \tag{B.1}$$

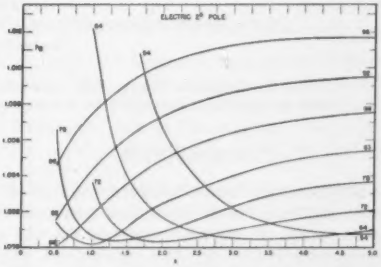

FIG. 9a. Same as Fig. 5a for electric 2^5-pole transitions.

The Racah coefficients obey the following symmetry relations:

$$\begin{aligned} W(abcd;ef)&=W(badc;ef)=W(cdab;ef)\\ &=W(acbd;fe)=(-)^{e+f-a-d}W(ebcf;ad)\\ &=(-)^{e+f-b-c}W(aefd;bc) \end{aligned} \tag{B.2}$$

and all the other relations which can be obtained by

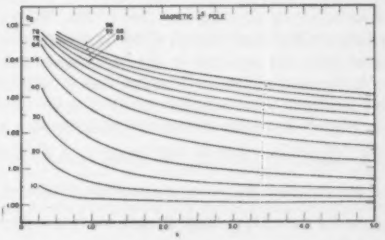

FIG. 10. Same as Fig. 1 for magnetic 2^5-pole transitions.

combining two or more of the operations indicated in (B.2). The Racah coefficients are introduced in the foregoing by the following:

$$C_{m_1m_2}{}^{j_1j_2j}C_{m_1+m_2m_3}{}^{jj_3j_4}$$
$$=\sum_J(2J+1)^{\frac{1}{2}}(2j+1)^{\frac{1}{2}}C_{m_2m_3}{}^{j_2j_3J}C_{m_1m_2+m_3}{}^{j_1Jj_4}$$
$$\times W(j_1j_2j_4j_3;jJ). \quad \text{(B.3)}$$

We also use

$$(2L+1)C_{00}{}^{LL\nu}W(LLL-\tfrac{1}{2}L-\tfrac{1}{2};\nu\tfrac{1}{2})$$
$$=(2L-1)C_0{}^{L-1}{}_0{}^{L-1\nu}$$
$$\times W(L-1\,L-1\,L-\tfrac{1}{2}\,L-\tfrac{1}{2};\nu\tfrac{1}{2}), \quad \text{(B.4)}$$

$$(2L+1)C_{00}{}^{LL\nu}W(LLL-\tfrac{1}{2}\,L+\tfrac{1}{2};\nu\tfrac{1}{2})$$
$$=[(2L-1)(2L+3)]^{\frac{1}{2}}C_0{}^{L-1}{}_0{}^{L+1\nu}$$
$$\times W(L-1\,L+1\,L-\tfrac{1}{2}\,L+\tfrac{1}{2};\nu\tfrac{1}{2}) \quad \text{(B.5)}$$

and

$$W^2(LLL-\tfrac{1}{2}\,L-\tfrac{1}{2};\nu\tfrac{1}{2})=\frac{(2L-\nu)(2L+\nu+1)}{4L^2(2L+1)^2}, \quad \text{(B.6)}$$

$$W^2(LLL+\tfrac{1}{2}\,L+\tfrac{1}{2};\nu\tfrac{1}{2})=\frac{(2L+1-\nu)(2L+2+\nu)}{4(L+1)^2(2L+1)^2}, \quad \text{(B.7)}$$

$$W^2(LLL+\tfrac{1}{2}\,L-\tfrac{1}{2};\nu\tfrac{1}{2})=\frac{\nu(\nu+1)}{4L(L+1)(2L+1)^2}. \quad \text{(B.8)}$$

PHYSICAL REVIEW VOLUME 85, NUMBER 1 JANUARY 1, 1952

A Note on the Adiabatic Thermomagnetic Effects

HERBERT B. CALLEN
Randal Morgan Laboratory of Physics, University of Pennsylvania, Philadelphia, Pennsylvania
(Received September 25, 1951)

The thermodynamic theory of the transverse adiabatic thermomagnetic effects is extended; and the final complete set of thermodynamic relations among all thermomagnetic effects is summarized.

1. INTRODUCTION

In a previous paper[1] various thermomagnetic[2] effects were analyzed by the methods of irreversible thermodynamics, which provides a framework whereby any thermomagnetic coefficient, when once defined, may be expressed in terms of a set of six independent constants of the material, called the "kinetic coefficients." It was shown that, in addition to the Bridgeman relation, there exist further relations among the thermomagnetic coefficients. Because of the complexity of the formulas for the thermomagnetic coefficients in terms of the kinetic coefficients, these predicted relations could only be given implicitly in (I), and only the limiting forms for small fields were given explicitly. In a recent paper,[3] however, Mazur and Prigogine have shown that a particular inversion of the fundamental equations greatly simplifies the resultant formulas and allows the new relations to be obtained in explicit form. Moreover, the adiabatic Hall and Nernst effects were specifically excluded from the analysis in (I) because, as will be seen, the analysis of these effects requires an extension of the methods there employed. Here again Mazur and Prigogine[3] have considered the problem and have given a treatment of these effects, which is valid for metals. The general theory of these effects will be given, and the final complete set of thermodynamic relations among all thermomagnetic effects will be summarized.

I wish to acknowledge here my conversations with Dr. Mazur and Professor Prigogine, in which the clarification of these problems was jointly evolved.

2. THE DEFINITION OF THE ADIABATIC EFFECTS

For definiteness we shall first consider the adiabatic Hall effect. This effect concerns the appearance of a transverse potential gradient when a longitudinal electric current flows perpendicularly to a magnetic field. The appropriate boundary conditions are that no longitudinal temperature gradient nor any transverse currents of either heat or electricity may exist. The adiabatic Hall coefficient R_a is then

$$R_a=(\text{potential gradient})_y/H_z(eJ_x), \quad (2.1)$$

with the conditions that

$$dT/dX=Q_y=J_y=0. \quad (2.2)$$

Here H_z is the magnetic field, taken in the Z-direction; eJ_x is the longitudinal electric current (e being the electronic charge); eJ_y is the transverse electric current; Q_y is the transverse heat current, and T is the temperature.

Although Eqs. (2.1) and (2.2) seem at first to provide a quantitative definition of the adiabatic Hall coeffi-

[1] H. B. Callen, Phys. Rev. **73**, 1349 (1948), hereafter referred to as (I).

[2] We abandon here the rather cumbersome division of the effects into thermomagnetic and galvanomagnetic effects, and we simply use the first term to imply all such effects in a magnetic field.

[3] P. Mazur and I. Prigogine, J. phys. et radium **12**, 616 (1951).

cient, the subtlety lies in the meaning of the ambiguous term "potential gradient." This term might perhaps be taken as implying either the purely electrical potential gradient, or the purely chemical potential gradient, or the sum of these—the "electrochemical" potential gradient. However, the choice among these possibilities is not a matter of pure unfettered freedom of theoretical definition, for this effect has long been measured experimentally, and the theoretical definition must of course be chosen so as to be experimentally significant. We wish to show that the choice of the total electrochemical potential gradient may be adopted with complete consistency with experimental practice. The choice of the electrical potential gradient, proposed by Gerlach[4] and adopted by Mazur and Prigogine, will be shown to be experimentally acceptable only when applied to a metal. In order to demonstrate these facts we first show that the total electrochemical potential gradient, which is determined by the basic equations, cannot be uniquely dissociated into electrical and chemical components by thermodynamic means, but that such a resolution depends upon detailed models. Secondly, we show that the Hall coefficient, if defined in terms of the total electrochemical potential gradient, can indeed be measured by standard experimental methods.

3. RESOLUTION INTO ELECTRICAL AND CHEMICAL POTENTIALS

We suppose that the transverse temperature gradient $\nabla_y T$ and the transverse electrochemical potential gradient $\nabla_y \mu$ in a sample are given (these quantities being determined by the basic thermodynamic equations), and we inquire into the possibility of a thermodynamic calculation of the electrical potential gradient $\nabla_y \mu_e$. The electrochemical potential is composed of the sum of electrical and chemical components, so that

$$\nabla_y \mu = \nabla_y \mu_e + \nabla_y \mu_c. \tag{3.1}$$

Expressing the chemical potential as a function of the pressure, temperature, and the concentration of the electrons we find[5]

$$\nabla_y \mu = \nabla_y \mu_e + v \nabla_y P - s \nabla_y T + (\partial \mu_c / \partial n) \nabla_y n, \tag{3.2}$$

where v is the partial specific volume of the electrons, s is the partial specific entropy of the electrons, and n is the electron concentration. The boundary condition on all thermomagnetic experiments is $\nabla P = 0$, so that

$$\nabla_y \mu + s \nabla_y T = \nabla_y \mu_e + (\partial \mu_c / \partial n) \nabla_y n, \tag{3.3}$$

and the two quantities on the left are each known. Our problem then is the resolution of the right member, which is known *in toto*, into the two terms $\nabla_y \mu_e$ and $(\partial \mu_c / \partial n) \nabla_y n$. It is immediately clear that such a resolution is, in general, impossible, because $\nabla_y \mu_e$ and $\nabla_y n$ are independent variables, and the simple knowledge of the sum cannot suffice to determine each of the two separate variables. Or, to view the problem more physically, we may note that such a happenstance as the existence of surface states in the sample will completely alter the division of the right member of (3.3) into electrical and concentration terms. If there are enough surface states on the lateral edges of the sample, the required electrochemical potential gradient may be contributed completely by the electric field without any necessity for a concentration gradient, whereas the absence of surface states would require the development of a transverse concentration gradient.

There is one particular case in which the resolution desired can be unambiguously made. That is, if $\partial \mu_c / \partial n = 0$. In this case the second term in (3.3) vanishes, and $\nabla_y \mu_e$ is completely determined. This is precisely the condition valid for a metal. For the shift in Fermi level with electron concentration is inversely proportional to the density of electronic energy levels in the vicinity of the Fermi level,

$$\partial \mu_c / \partial n \sim (\text{density of levels near Fermi level})^{-1}, \tag{3.4}$$

and in metals the density of levels at the Fermi level is extremely high, so that $\partial \mu_c / \partial n$ is negligibly small. However, it should be noted that in semiconductors the Fermi level falls in the forbidden band where the density of levels is extremely small, so that $\partial \mu_c / \partial n$ may be very large.

We thus conclude that the knowledge of $\nabla_y \mu$ and of $\nabla_y T$ does not suffice to determine $\nabla_y \mu_e$ except if $\partial \mu_c / \partial n = 0$, a condition valid only in metals.

4. MEASUREMENT OF THE ADIABATIC EFFECTS

Having seen that the only definition of the adiabatic thermomagnetic effects which is amenable to thermodynamic analysis is that involving the gradient of the total electrochemical potential gradient, we now consider a typical experiment and show that such a definition is satisfactory from the experimental viewpoint. In a measurement of the adiabatic Hall effect the transverse potential gradient may be sensed by two metallic probes leading from the lateral edges of the sample to, say, a quadrant electrometer. The quadrant electrometer then senses the difference in electrical potential between the two metallic probes. The condition of thermodynamic equilibrium between the probes and the lateral surfaces of the sample requires that the difference in the total electrochemical potential between the two probes shall be equal to the change in electrochemical potential across the sample. It is thus the difference of electrochemical potential $\Delta \mu$ between the two probes that we desire to measure. But since the probes are metallic, we have simply

$$\Delta \mu = \Delta \mu_e - s \Delta T, \tag{4.1}$$

with both the pressure and concentration terms of Eq.

[4] W. Gerlach, *Handbuch der Physik* (Verlag. Julius Springer, Berlin, 1928), Vol. 13, Chapter 6.

[5] S. R. DeGroot, *Thermodynamics of Irreversible Processes* (North-Holland Publishing Company, Amsterdam, Netherlands, 1951).

(3.2) vanishing. The quadrant electrometer measures $\Delta\mu_e$, and ΔT is easily measured, whereas s, the partial specific entropy of the electrons in the metal probe, is a thermodynamic property of the metal which may be assumed to be known. Thus the measurement serves to determine $\Delta\mu$ in a satisfactory manner.

It should be noted, that, from the point of view of thermodynamics, the partial specific entropy s is undetermined within an additive constant, and only the difference in s for two materials is uniquely determined. The absolute values of the adiabatic thermomagnetic coefficients thus also depend upon the choice of a zero for entropy. The addition of a constant s_0 to the specific entropy changes $\Delta\mu$ to $\Delta\mu+s_0\Delta T$ and, as we shall see later, adds s_0/e times the Ettingshausen coefficient to the adiabatic Hall coefficient. The standard convention[6] that $s=0$ at $T=0$ renders the adiabatic coefficients unique and is particularly convenient if the measurement of thermomagnetic coefficients is to be combined with analysis of simple models to yield information on the electronic structure. We wish in fact to stress that the arbitrariness in s_0 in no way detracts from the practical usefulness of the adiabatic coefficients. For the ultimate purpose of the measurement of these coefficients is to yield atomistic information by comparison with solid-state theory, in which case the unique choice $s=0$ at $T=0$ is demanded by basic quantum-mechanical principles. We shall accordingly assume hereafter that all quantities are made unique by this convention.

5. QUANTITATIVE ANALYSIS OF THE EFFECTS

In (I) the analysis of the thermomagnetic effects was based upon the equations

$$\begin{aligned}
-J_x&=L_{11}(1/T)\nabla_x\mu+L_{12}\nabla_x(1/T)\\
&\quad+L_{13}(1/T)\nabla_y\mu+L_{14}\nabla_y(1/T),\\
Q_x&=L_{12}(1/T)\nabla_x\mu+L_{22}\nabla_x(1/T)\\
&\quad+L_{14}(1/T)\nabla_y\mu+L_{24}\nabla_y(1/T),\\
-J_y&=-L_{13}(1/T)\nabla_x\mu-L_{14}\nabla_x(1/T)\\
&\quad+L_{11}(1/T)\nabla_y\mu+L_{12}\nabla_y(1/T),\\
Q_y&=-L_{14}(1/T)\nabla_x\mu-L_{24}\nabla_x(1/T)\\
&\quad+L_{12}(1/T)\nabla_y\mu+L_{22}\nabla_y(1/T),
\end{aligned}\tag{5.1}$$

where the symmetry of the coefficients follows from the assumed isotropy of the material and from the application of the Onsager reciprocal relations. The quantities J_x and J_y denote particle currents densities (so that eJ denotes an electric current density), and Q_x is a "heat current density" defined by the difference between the total energy current density W_x and the potential energy current density μJ_x. The simplifying technique of Mazur and Prigogine is to invert these equations so that the independent variables are the electric currents and temperature gradients, which are the quantities directly controlled by the experimenter. In particular, Eqs. (5.1) are equivalent to the set

$$\begin{aligned}
-(1/e)\nabla_x\mu&=\mathfrak{L}_{11}eJ_x+\mathfrak{L}_{12}eJ_y-\mathfrak{L}_{13}\nabla_xT-\mathfrak{L}_{14}\nabla_yT,\\
-(1/e)\nabla_y\mu&=-\mathfrak{L}_{12}eJ_x+\mathfrak{L}_{11}eJ_y+\mathfrak{L}_{14}\nabla_xT-\mathfrak{L}_{13}\nabla_yT,\\
Q_x&=-T\mathfrak{L}_{13}eJ_x-T\mathfrak{L}_{14}eJ_y-\mathfrak{L}_{33}\nabla_xT-\mathfrak{L}_{34}\nabla_yT,\\
Q_y&=T\mathfrak{L}_{14}eJ_x-T\mathfrak{L}_{13}eJ_y+\mathfrak{L}_{34}\nabla_xT-\mathfrak{L}_{33}\nabla_yT,
\end{aligned}\tag{5.2}$$

where factors of e and T have been absorbed into the kinetic coefficients for convenience. The quantities eJ are now electric current densities, and the quantities $(1/e)\mu$ have the dimensions of energy per unit charge rather than of energy per particle. The coefficients $\mathfrak{L}_{11}$, $\mathfrak{L}_{13}$, and $\mathfrak{L}_{33}$ are even functions of the magnetic field, whereas $\mathfrak{L}_{12}$, $\mathfrak{L}_{14}$, and $\mathfrak{L}_{34}$ are odd functions of the magnetic field. We now retabulate the definitions and the values of the various thermomagnetic coefficients in terms of these kinetic coefficients, including the adiabatic Hall and Nernst effects in accordance with our definitions thereof.

(a) The Isothermal Electric Conductivity

$$\sigma_i\equiv -eJ_x/e^{-1}\nabla_x\mu \quad\text{with}\quad \nabla_xT=\nabla_yT=J_y=0, \tag{5.3}$$

whence

$$\sigma_i=\mathfrak{L}_{11}^{-1}. \tag{5.4}$$

(b) The Adiabatic Electric Conductivity

$$\sigma_a\equiv -eJ_x/e^{-1}\nabla_x\mu \quad\text{with}\quad \nabla_xT=Q_y=J_y=0, \tag{5.5}$$

whence

$$\sigma_a=(\mathfrak{L}_{11}-T\mathfrak{L}_{14}^2\mathfrak{L}_{33}^{-1})^{-1}. \tag{5.6}$$

(c) The Isothermal Heat Conductivity

$$\kappa_i\equiv -Q_x/\nabla_xT \quad\text{with}\quad J_x=J_y=\nabla_yT=0, \tag{5.7}$$

whence

$$\kappa_i=\mathfrak{L}_{33}. \tag{5.8}$$

(d) The Adiabatic Heat Conductivity

$$\kappa_a\equiv -Q_x/\nabla_xT \quad\text{with}\quad J_x=J_y=Q_y=0, \tag{5.9}$$

whence

$$\kappa_a=(\mathfrak{L}_{33}^2+\mathfrak{L}_{34}^2)/\mathfrak{L}_{33}. \tag{5.10}$$

(e) The Isothermal Hall Effect

$$R_i\equiv(1/e)\nabla_y\mu/HeJ_x \quad\text{with}\quad J_y=\nabla_yT=\nabla_xT=0, \tag{5.11}$$

whence

$$R_i=\mathfrak{L}_{12}/H. \tag{5.12}$$

(f) The Adiabatic Hall Effect

$$R_a\equiv(1/e)\nabla_y\mu/HeJ_x \quad\text{with}\quad \nabla_xT=Q_y=J_y=0, \tag{5.13}$$

whence

$$R_a=(\mathfrak{L}_{12}+\mathfrak{L}_{13}\mathfrak{L}_{33}^{-1}\mathfrak{L}_{14}T)/H. \tag{5.14}$$

[6] The Nernst theorem, or the "third law of thermodynamics," does not require that $s=0$ at $T=0$ but only demands that the entropy difference for two materials should vanish at $T=0$.

(g) The Isothermal Nernst Effect

$$\eta_i \equiv -(1/e)\nabla_y\mu/H\nabla_x T \quad \text{with} \quad J_x = J_y = \nabla_y T = 0, \tag{5.15}$$

whence

$$\eta_i = \mathfrak{L}_{14}/H. \tag{5.16}$$

(h) The Adiabatic Nernst Effect

$$\eta_a \equiv -(1/e)\nabla_y\mu/H\nabla_x T \quad \text{with} \quad J_x = J_y = Q_y = 0, \tag{5.17}$$

whence

$$\eta_a = (\mathfrak{L}_{14} - \mathfrak{L}_{13}\mathfrak{L}_{33}^{-1}\mathfrak{L}_{34})/H. \tag{5.18}$$

(i) The Ettingshausen Effect

$$(\text{Ett}) \equiv \nabla_y T/HeJ_x \quad \text{with} \quad J_y = Q_y = \nabla_x T = 0, \tag{5.19}$$

whence

$$(\text{Ett}) = (T\mathfrak{L}_{14})/(H\mathfrak{L}_{33}). \tag{5.20}$$

(j) The Leduc-Righi Effect

$$(\text{Leduc}) \equiv \nabla_y T/H\nabla_x T \quad \text{with} \quad J_x = J_y = Q_y = 0, \tag{5.21}$$

whence

$$(\text{Leduc}) = (\mathfrak{L}_{34})/(H\mathfrak{L}_{33}). \tag{5.22}$$

Examination of these relations shows that each of the kinetic coefficients, except $\mathfrak{L}_{13}$, is related in a simple and direct way to a standard thermomagnetic coefficient. The coefficient $\mathfrak{L}_{13}$ appears only in the two adiabatic coefficients. This calls our attention to the fact that $\mathfrak{L}_{13}$ is itself not uniquely determined except to the additive constant s_0/e. This fact may be seen by recalling that the "heat current density" Q_x is arbitrary to the additive transfer heat Ts_0J_x. From the third of Eqs. (5.2) we then see that this implies that $\mathfrak{L}_{13}$ is indeed arbitrary to the additive constant s_0/e. Addition of a constant s_0/e to $\mathfrak{L}_{13}$ adds $e^{-1}s_0$(Ett) to R_a and adds $e^{-1}s_0$(Leduc) to η_a, as can be seen from Eqs. (5.14) and (5.20), and from (5.18) and (5.22). This is just the arbitrariness which appeared from Eq. (4.1) in our discussion of the method of measurement of the adiabatic effects. The arbitrariness is completely eliminated by the convention that $s=0$ at $T=0$.

The coefficient $\mathfrak{L}_{13}$ may be given a physical interpretation by recalling its relation to the absolute thermoelectric power ϵ.[1] Essentially the thermoelectric power is the $\nabla_x\mu$ induced by a parallel gradient of temperature.

(k) Absolute Thermoelectric Power

$$\epsilon = (1/e)\nabla_x\mu/\nabla_x T \quad \text{with} \quad J_x = J_y = \nabla_y T = 0, \tag{5.23}$$

whence

$$\epsilon = \mathfrak{L}_{13}. \tag{5.24}$$

The absolute thermoelectric power is thus also undetermined within the additive constant s_0/e, but the difference of thermoelectric powers for two substances is uniquely determined and represents the thermoelectric power of the appropriate thermocouple. A similar effect to (5.23), but defined in terms of a purely electric potential gradient, is referred to by Mazur and Prigogine as the "isothermal longitudinal Ettingshausen-Nernst effect," and these authors also define an associated adiabatic effect with the condition $Q_y=0$ replacing the condition $\nabla_y T=0$.

The fundamental set of kinetic equations can now be written in the matrix form

$$\begin{bmatrix} -(1/e)\nabla_x\mu \\ -(1/e)\nabla_y\mu \\ Q_x \\ Q_y \end{bmatrix} = \begin{bmatrix} \sigma_i^{-1} & HR_i & -\epsilon & -H\eta_i \\ -HR_i & \sigma_i^{-1} & H\eta_i & -\epsilon \\ -T\epsilon & -TH\eta_i & -\kappa_i & -H\kappa_i(\text{Leduc}) \\ TH\eta_i & -T\epsilon & H\kappa_i(\text{Leduc}) & -\kappa_i \end{bmatrix} \cdot \begin{bmatrix} eJ_x \\ eJ_y \\ \nabla_x T \\ \nabla_y T \end{bmatrix}, \tag{5.25}$$

and we further find the relations

$$\kappa_i(\text{Ett}) = T\eta_i, \tag{5.26}$$

$$\kappa_a - \kappa_i = H^2\kappa_i(\text{Leduc}),^2 \tag{5.27}$$

$$\sigma_i^{-1} - \sigma_a^{-1} = H^2\eta_i(\text{Ett}), \tag{5.28}$$

$$R_a - R_i = \epsilon(\text{Ett}), \tag{5.29}$$

$$\eta_i - \eta_a = \epsilon(\text{Leduc}). \tag{5.30}$$

The Eqs. (5.25) allow any situation to be analyzed in a simple and direct way, and automatically relate the effect of interest to the six fundamental thermomagnetic coefficients σ_i, R_i, ϵ, η_i, κ_i and (Leduc). It should also be noted that the Eqs. (5.26) and (5.30) among the thermomagnetic coefficients, being purely thermodynamic in character, remain valid independently of the choice of the constant s_0.

Range Straggling of a Nonrelativistic Charged Particle

H. W. LEWIS*
Institute for Advanced Study, Princeton, New Jersey
(Received June 14, 1951)

The validity of the gaussian approximation for the range straggling, due to ionization and excitation, of a nonrelativistic charged heavy particle is investigated. Exact solutions are obtained which show that, in comparison with the usual theory: (a) the mean range of a particle is slightly increased; (b) the range distribution has a tail in the direction of shorter-than-average range; (c) the most probable range is slightly longer than the mean range. First a fictitious problem is solved, and then the transition to the real world is made.

I. INTRODUCTION

IT is well known that any physical effect which involves the accumulation of the effects of repeated chance events of the same or similar character leads to a straggling or dispersion in the final result, which depends in its form on the nature of the fundamental law involved. (Thus, the expected range in matter of a particle of a given energy is not a precise quantity, but exhibits a dispersion around the mean.) In the case, however, in which a very large number of individual events are combined, and they are sufficiently similar to insure that no one will be the source of a significant fraction of the straggling, one can show that, otherwise independently of the fundamental law, the distribution of the stochastic variable involved will be gaussian, with a variance equal to the sum of the contributions from the separate events. This is the central limit theorem of statistics, and served as the basis for the original work of Bohr[1] on the titled subject.

Now, however, that quite precise experiments[2] on the range distributions of particles are feasible in the energy region in which ionization and excitation of atoms are the only significant phenomena, it has seemed worthwhile to look into the question of the applicability of the central limit theorem to this problem, and to study the departure of the range distribution from the gaussian form. A very rough treatment is adequate for orientation, and is the subject of the next section.

II. ORIENTATION

The probability per unit length for an encounter between a charged particle and an atom, in which the incident particle loses an energy between T and $T+\Delta T$, is given very closely, in nonrelativistic approximation, by

$$P(T)=k\Delta T/2ET^2 \tag{1}$$

where $k=2\pi NZz^2Me^4/m$, M, E, and ze are the mass, energy, and charge of the incident particle, N the number of atoms of atomic number Z per unit volume, and e and m the charge and mass of the electron. It is assumed that the velocity of the incident particle is much larger than that of the K-electrons of the atom—when this is not true, correction terms appear.[3] One can easily show that the maximum energy loss that can occur is ϵE, where $\epsilon=4m/[M(1+m/M)^2]$, and, according to Bloch,[4] one can schematize the behavior at small T by supposing that there is a minimum energy loss that can occur, given by $I^2/\epsilon E$, where I is a sort of mean ionization energy for the atom, and is approximately proportional to Z. Thus

$$-\left\langle\frac{dE}{dx}\right\rangle=\frac{k}{2E}\ln\frac{T_{\max}}{T_{\min}}=\frac{k}{E}\ln\frac{\epsilon E}{I} \tag{2}$$

which is sufficiently close for our purposes.

Since the straggling is small, one can get an estimate of it by remarking that the collisions are independent, so that the number in a short distance Δx is distributed according to the Poisson law, with

$$\langle\Delta N^2\rangle=\langle N\rangle=k\Delta T\Delta x/2ET^2 \tag{3}$$

as given by (1). Thus

$$\langle\Delta E^2\rangle=T^2\langle\Delta N^2\rangle=k\Delta T\Delta x/2E \tag{4}$$

which gives the dispersion in energy produced by collisions in Δx which result in energy losses in ΔT. Integration over T, and neglect of the small lower limit, yields

$$\langle\Delta E^2\rangle=\tfrac{1}{2}k\epsilon\Delta x. \tag{4'}$$

Now we can use the smallness of the straggling to write the dispersion in the range R

$$\langle\Delta R^2\rangle=\left(\frac{dE}{dx}\right)^{-2}\langle\Delta E^2\rangle=\tfrac{1}{2}k\epsilon\Delta x\left(\frac{dE}{dx}\right)^{-2}$$
$$=\tfrac{1}{2}k\epsilon\left(-\frac{dE}{dx}\right)^{-3}\Delta E. \tag{5}$$

This can now be integrated to yield the total range-

* On leave from the University of California, Berkeley, California, where this work was begun.

[1] N. Bohr, Phil. Mag. **30**, 581 (1915).

[2] C. J. Bakker and E. Segrè, Phys. Rev. **81**, 489 (1951).

[3] M. L. Livingston and H. Bethe, Revs. Modern Phys. **9**, 245 (1937).

[4] F. Bloch, Z. Physik **81**, 363 (1938).

straggling

$$\langle \Delta R^2 \rangle = \tfrac{1}{2} k\epsilon \int_0^{E_0} dE \left(\frac{dE}{dx}\right)^{-3} \tag{5'}$$

which is the well-known Bohr formula.[1] It is adequate for the moment to use some mean value of $\ln(\epsilon E/I)$, call it L, so that

$$\langle \Delta R^2 \rangle = \frac{\epsilon}{2L} \langle R \rangle^2 \tag{6}$$

and

$$\langle R \rangle = E_0^2/2kL. \tag{6'}$$

The average number of collisions required to stop the particle is

$$N_{\text{total}} \cong \epsilon E_0^2/4LI^2 \tag{7}$$

which, for a typical case of a 100-Mev proton in aluminum, is of the order of 10^7, which one might consider large enough to justify the gaussian approximation.

To see that this is not the case, we need only to invert the order of the integrations, and consider only energy losses larger than some $T_0 > T_{\min}$. One finds then, for the fraction f of the total range straggling provided by energy losses greater than T_0,

$$f = 1 - \frac{4}{3}\frac{T_0}{\epsilon E_0} + \frac{1}{3}\left(\frac{T_0}{\epsilon E_0}\right)^4 \tag{8}$$

and for the corresponding mean number of collisions

$$\langle N \rangle = \frac{1}{2\epsilon L}\left[\frac{\epsilon E_0}{T_0} - 1 - \ln\frac{\epsilon E_0}{T_0}\right]. \tag{9}$$

Thus, for $T_0 = \epsilon E_0/2$, we have 35 percent of the range straggling, and the number of collisions involved, for a proton and $L=7$ (corresponding to 100 Mev in aluminum), is nine. This is not a large number, and can, in fact, be reduced further by taking an oblique rather than horizontal cut out of the energy loss spectrum.

For a meson the situation is even more striking, since, corresponding to the above situation, one single collision produces 35 percent of the straggling for a 10-Mev μ-meson.

III. THE SIMPLIFIED PROBLEM

If we define a quantity $\delta = T_{\min}/E = I^2/\epsilon E^2$, corresponding to $\epsilon = T_{\max}/E = 4m/M(1+m/M)^2$, then the Boltzmann equation for the energy distribution function $f(E, x)$ at a point x can be written, according to (1)

$$\frac{\partial f(E,x)}{\partial x} = \frac{k}{2}\int_{E/1-\delta}^{E/1-\epsilon} \frac{f(E',x)dE'}{E'(E'-E)^2} - \frac{k}{2E} f(E,x) \int_{E(1-\epsilon)}^{E(1-\delta)} \frac{dE'}{(E-E')^2}$$

$$= \frac{k}{2E^2}\int_{1+\delta}^{1/1-\epsilon} \frac{dy}{(y-1)^2}\left[\frac{f(Ey,x)}{y} - f(E,x)\right]. \tag{10}$$

if we neglect δ^2, and therefore the difference between $\delta(E)$ and $\delta(E')$. For the case of a 100-Mev proton in aluminum, $\delta \sim 10^{-3}$, so that this is an excellent approximation. Now define $Eg(E,x) = f(E,x)$, so that

$$\frac{\partial g(E,x)}{\partial x} = \frac{k}{2E^2}\int_{\delta(E)}^{\epsilon_1} \frac{d\eta}{\eta^2}[g(E(1+\eta),x) - g(E,x)] \tag{11}$$

with $\epsilon_1 = \epsilon/1-\epsilon$. The simplicity of (11) is destroyed by the dependence of δ on E, so that we will now, in order to homogenize the equation, regard δ as a constant, and will call this the simplified problem. We will see, in the next section, how we can then take its energy dependence into account.

With a constant δ, the number of particles absorbed per unit length is

$$-\frac{dN}{dx} = -\frac{d}{dx}\int_0^\infty Eg(E,x)dE$$

$$= -\frac{k}{2}\int_\delta^{\epsilon_1} \frac{d\eta}{\eta^2}\int_0^\infty \frac{dE}{E}[g(E(1+\eta),x) - g(E,x)]. \tag{12}$$

The second of these integrals is equal to zero, provided that each of the terms in the square bracket leads to a convergent integral, the condition for which is: $g(0,x) = 0$. Thus, no particles will be absorbed if the distribution function $f(E,x)$ goes to zero at $E=0$ more strongly than linearly. In a real case, therefore, $f(E,x)$ will be at most linear, and we can, in fact, show that all that interests us is the coefficient of the linear term. Since, if we consider N_Δ, the number of particles with an energy greater than Δ,

$$-\frac{dN_\Delta}{dx} = -\frac{k}{2}\int_\delta^{\epsilon_1} \frac{d\eta}{\eta^2}\int_\Delta^\infty \frac{dE}{E}[g(E(1+\eta),x) - g(E,x)]$$

$$= -\frac{k}{2}\int_\delta^{\epsilon_1} \frac{d\eta}{\eta^2}\left[\int_{\Delta(1+\eta)}^\infty - \int_\Delta^\infty\right] g(E,x)\frac{dE}{E}$$

$$= \frac{k}{2}\int_\delta^{\epsilon_1} \frac{d\eta}{\eta^2}\int^{\Delta(1+\eta)} g(E,x)\frac{dE}{E}$$

and

$$-\frac{dN}{dx} = -\lim_{\Delta\to 0}\frac{dN_\Delta}{dx} = \frac{k}{2}g(0,x)\int_\delta^{\epsilon_1} \frac{d\eta}{\eta^2}\ln(1+\eta)$$

$$= kA_0 g(0,x) \tag{13}$$

where we call the last integral $2A_0$. In this way our problem is made simpler, since we don't have to find the energy distribution at every point, in order to find the rate of absorption.

We might note, parenthetically, that (11) admits of an infinite set of polynomial solutions, which are extremely simple to construct, but which cannot be combined into a convergent representation of a real

case. This is a consequence of the essential singularity at $E=\infty$.

To solve (11), with constant δ, we first carry out a laplace transformation in x, setting

$$kA_0 g(0,x)=-\frac{dN}{dx}=\frac{1}{2\pi i}\int_C G(\lambda)\exp(\lambda x)d\lambda \quad (14)$$

and

$$\int_0^\infty E^{2n+1}g(E,x)dE=\frac{1}{2\pi i}\int_C M_n(\lambda)\exp(\lambda x)d\lambda \quad (15)$$

which, for $n=0$, gives the transformation of $N(x)$. Now (11) becomes

$$\lambda M_n(\lambda)=-kA_nM_{n-1}(\lambda) \quad (16)$$

defining

$$A_n\equiv\frac{1}{2}\int_\delta^{\epsilon_1}\frac{d\eta}{\eta^2}[1-(1+\eta)^{-2n}]$$

for $n\geqslant 1$. We also have $-\lambda M_0=G(\lambda)$, so that

$$M_n(\lambda)=-\left(-\frac{k}{\lambda}\right)^n\frac{G(\lambda)}{\lambda}\prod_{\nu=1}^{n}A_\nu. \quad (17)$$

The initial condition that there is, at $x=0$, one particle with an energy E_0, can now be used to fix $G(\lambda)$, since

$$\frac{1}{2\pi i}\int_C M_n(\lambda)d\lambda = E_0^{2n}=-(-k)^n\cdot\prod_{\nu=1}^{n}A_\nu\cdot\frac{1}{2\pi i}\int_C d\lambda G(\lambda)\lambda^{-n-1}$$

or

$$\frac{1}{2\pi i}\int_C G(\lambda)\lambda^{-n-1}d\lambda=-(-E_0^2/k)^n\left[\prod_{\nu=1}^{n}A_\nu\right]^{-1} \quad (18)$$

where the product must be replaced by unity for $n=0$.

One can now easily find the moments of the range distribution by remarking that, since it takes only a finite number of collisions to stop a particle, dN/dx must decrease exponentially for large enough x. Consequently $G(\lambda)$ must be well-behaved not only in the entire right half-plane, but also in the left neighborhood of the imaginary axis. Therefore the contour C can be taken parallel to the imaginary axis, and some small but finite distance to the left of it. Then

$$\langle x^n\rangle=\int_0^\infty x^n dx\cdot\frac{1}{2\pi i}\int_C G(\lambda)\exp(\lambda x)d\lambda = \frac{(-)^{n+1}n!}{2\pi i}\int_C G(\lambda)\lambda^{-n-1}d\lambda$$

since, along C, the real part of λ is everywhere negative. Consequently

$$\langle x^n\rangle=(E_0^2/k)^n n!\Big/\prod_{\nu=1}^{n}A_\nu \quad (19)$$

which is exact.

IV. THE MORE REALISTIC PROBLEM

The procedure for taking into account, in (19), the dependence of δ on E, can be easily illustrated in the case of the mean range. This is given by (19) with $n=1$; $\langle x\rangle=E^2/kA_1$ for a particle of energy E. If we consider now a particle of energy $E+dE$, its mean range is $(E+dE)^2/kA_1$. But the mean residual range, after the particle is degraded to an energy E, is independent of what has happened before, so that the mean distance traveled in dropping from $E+dE$ to E is $dR=2EdE/kA_1$, where, now, $\delta(E)$ is evaluated at the energy E. Thus, since the contributions to the range of a particle, from all decrements of energy dE, are rigorously independent, the mean range in the real problem is

$$\langle R\rangle=k^{-1}\int_{0+}^{E_0}2EdE/A_1. \quad (20)$$

If we evaluate A_1 approximately, $A_1\approx 2\ln(\epsilon_1 E/I)-3\epsilon_1/2$, which closely relates (20) to (2). The difference is real, and represents the difference between the mean length traversed per unit energy, and the inverse of the mean energy lost per unit length.

The lower limit 0+ in the integral means that we must go down to an energy for which ϵ_1 remains larger than δ. This is the characteristic ambiguity in the meaning of the "end of the range," and occurs at a sufficiently low energy that we needn't worry about it —for example, around 50 kev for a proton in aluminum, where all our other approximations have long since broken down.

Our problem is, for the higher moments, to find functions, like $\langle x\rangle$, whose contributions from the various energy decrements are independent. The next such is well known to be $\langle x^2\rangle-\langle x\rangle^2$, for which

$$d[\langle x^2\rangle-\langle x\rangle^2]=4E^3dE[2/A_1A_2-1/A_1^2]/k^2$$

so that

$$\langle R^2\rangle-\langle R\rangle^2=\frac{4}{k^2}\int_{0+}^{E_0}E^3dE\left[\frac{2}{A_1A_2}-\frac{1}{A_1^2}\right]. \quad (21)$$

However, $\langle R\rangle$ can be obtained from (20), so that (21) yields $\langle R^2\rangle$.

The hierarchy of functions which have this property of additivity from one interval to the next is well known in statistics, and is called the set of semi-invariants of Thiele.[5] They can be defined in the following manner: consider the set of moments α_n (corresponding to $\langle x^n\rangle$), and construct the function

$$f(t)=1+\sum_1^\infty d_\nu t^\nu/\nu!.$$

[5] Thiele, *Theory of Observations* (London, 1903).

Then the coefficient of $t^n/n!$ in the series expansion of $\ln f(t)$ is β_n, the nth semi-invariant. One can easily construct them, and the first few are given by

$$\begin{aligned}
&\beta_1=\alpha_1\\
&\beta_2=\alpha_2-\alpha_1^2\\
&\beta_3=\alpha_3-3\alpha_1\alpha_2+2\alpha_1^3\\
&\beta_4=\alpha_4-4\alpha_1\alpha_3-3\alpha_2^2+12\alpha_1^2\alpha_2-6\alpha_1^4, \text{ etc.}\cdots.
\end{aligned} \tag{22}$$

These expressions are simpler if one centers the distribution so that $\alpha_1=0$. The gaussian distribution has the property that $\beta_n=0$ for $n\geqslant 3$.

The direct procedure is, then, to construct from (22) the expressions corresponding to (20) and (21), and carry out the requisite numerical integrations.

It is more convenient in most cases, however, to expand the integrals A_n in powers of ϵ_1, and then construct the β_n. One finds, for the β_n in the simplified problem, all within an accuracy corresponding to the lowest order in ϵ_1 (2 percent for a μ-meson, 0.2 percent for a proton), denoting $r_0^2=\epsilon_1 E_0^4/k^2A_1^3$, and $\beta_0^2=\epsilon_1 A_1$,

$$\begin{aligned}
&\beta_2=r_0^2\\
&\beta_3=-2\beta_0/3\cdot(1-6/A_1)\cdot r_0^3\\
&\beta_4=2\beta_0^2/3\cdot(1-15/A_1+45/A_1^2)\cdot r_0^4\\
&\beta_5=-4\beta_0^3/5(1-30/A_1+230/A_1^2-420/A_1^3)\cdot r_0^5.
\end{aligned} \tag{23}$$

Thus the expressions to which we will have to apply the procedures described above will all be of the form E_0^{2n}/A_1^m, which is, within the accuracy mentioned, a standard exponential-integral form. It is, in fact, adequate to make an asymptotic expansion of these integrals in inverse powers of A_1, so that the transition from the simplified to the real problem is described by carrying out in (23) the transformation

$$\frac{E_0^{2n}}{A_1^m}\to 2n\int_{0+}^{E_0}\frac{E^{2n-1}dE}{A_1^m(E)}\to \frac{E_0^{2n}}{A^n}\left[1+\overset{\text{asymptotic}}{\sum_{\sigma=1}}\frac{m(m+1)\cdots(m+\sigma-1)}{(nA)^\sigma}\right]$$

where we have called $A_1(E_0)=A$. Then, calling $\beta^2=\epsilon_1 A$, and $r^2=\epsilon_1 E_0^4/k^2A^3$, (23) becomes, for the real problem,

$$\begin{aligned}
&\beta_2=\left(1+\frac{3}{2A}+\frac{3}{A^2}+\frac{15}{2A^3}+\cdots\right)\cdot r^2\\
&\beta_3=-\frac{2}{3}\beta\cdot\left(1-\frac{14}{3A}-\frac{70}{9A^2}-\frac{140}{9A^3}\cdots\right)\cdot r^3\\
&\beta_4=\frac{2}{3}\beta^2\cdot\left(1-\frac{55}{4A}+\frac{195}{8A^2}+\frac{1365}{32A^3}\cdots\right)\cdot r^4\\
&\beta_5=-\frac{4}{5}\beta^3\cdot\left(1-\frac{144}{5A}+\frac{4742}{25A^2}-\frac{14564}{125A^3}\cdots\right)\cdot r^5.
\end{aligned} \tag{23'}$$

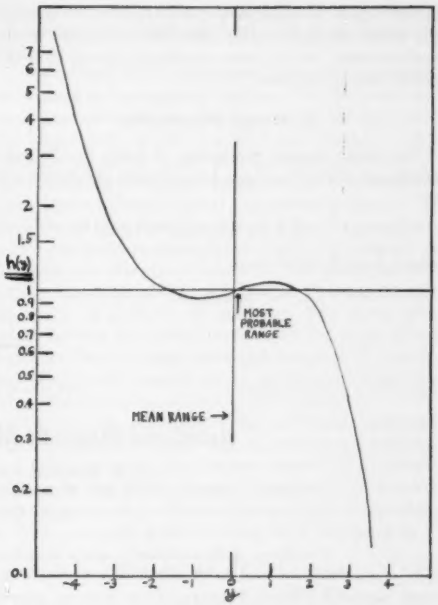

FIG. 1. $h(y)$ *vs* y for a 13-Mev μ-meson. $h(y)$ is the factor by which the normal gaussian distribution must be multiplied to obtain the correct range distribution, and is equal to unity for a normal distribution.

We can now construct the range distribution function, from the β_n, as a series of corrections to a gaussian distribution with the correct variance. If we define $\gamma_\nu=\beta_\nu/\nu!\beta_2^{\nu/2}$, and call the range distribution around the mean $h(y)\exp[-y^2/2]$, where $y=(x-\langle x\rangle)/\beta_2^{\frac{1}{2}}$, then the Edgeworth series [6] for $h(y)$ is

$$\begin{aligned}
h(y)=&[1]+[\gamma_3H_3(y)]+[\gamma_4H_4(y)+\tfrac{1}{2}\gamma_3^2H_6(y)]\\
&+[\gamma_5H_5(y)+\gamma_3\gamma_4H_7(y)+\tfrac{1}{6}\gamma_3^3H_9(y)]+\cdots
\end{aligned} \tag{24}$$

where the $H_n(y)$ are the hermite polynomials, and terms in the same square bracket are of the same order in β. For a typical case of a 13.5-Mev μ-meson in aluminum, we have $\gamma_3=-0.0336$, $\gamma_4=0.00136$, and $\gamma_5=-0.000162$, so that the convergence is indeed quite rapid. For this case, the function $h(y)$ is plotted in Fig. 1.

V. SUMMARY OF RESULTS

A. Mean Range

The mean range of a particle is given by (20), which differs from the usual expression by the appearance of A_1 in the denominator of the integrand, rather than $2\ln(\epsilon_1 E/I)$. Thus, the mean range is lengthened by a

[6] See H. Cramér, *Mathematical Methods of Statistics* (Princeton University Press, Princeton, 1946).

factor which is essentially $1+3\epsilon_1/2A+\cdots$, through the effect mentioned after (20). This is a small effect, and amounts, in the case mentioned above, to a 0.2 percent range increase.

B. Range Distribution

The mean square straggling is given by the old expression of Bohr, and can be expressed asymptotically by

$$\beta_2=\langle\Delta R^2\rangle=r^2[1+3/2A+3/A^2+15/2A^3+\cdots]$$

where $r^2=\epsilon_1E_0^4/k^2A^2$, and

$$A=A_1(E_0)\approx 2\ln(\epsilon_1E_0/I)-3\epsilon_1/2+\cdots.$$

If we define $y=(x-\langle x\rangle)/\beta_2^{\frac{1}{2}}$, and $\gamma_\nu=\beta_\nu/\nu!\beta_2^{\nu/2}$, with the β_ν given by (23[1]), then the range distribution is $h(y)\exp[-y^2/2]$, with $h(y)$ given as an expansion in hermite polynomials by (24). This function has a pronounced tail toward shorter-than-average range.

C. Most Probable Range

The most probable range is somewhat longer than the mean range, to compensate for the short range tail. One can estimate from the above that the displacement is

$$R_{\text{prob}}-R_{\text{mean}}\sim-3\gamma_3\beta_2^{\frac{1}{2}}=-\beta_2/2\beta_2$$

which is about 0.1 unit in Fig. 1, and is indicated there.

PHYSICAL REVIEW VOLUME 85, NUMBER 1 JANUARY 1, 1952

Rotational Magnetic Moments of $^1\Sigma$ Molecules*†

J. R. ESHBACH‡ AND M. W. P. STRANDBERG
Research Laboratory of Electronics, Massachusetts Institute of Technology, Cambridge, Massachusetts

(Received September 11, 1951)

The theory of the rotational magnetic moment in $^1\Sigma$ molecules is presented. This theory is applied in particular to describe experiments on the Zeeman effect for a linear rotor, OCS, and a symmetric top, NH_3.

1. THEORY

THE recent development of experimental techniques for observing low energy quantum transitions in the microwave and radiofrequency parts of the spectrum permits the study of molecular interactions which were previously not observable. These include internal molecular interactions, as well as the interaction of molecules and their component particles with externally applied fields. This report is concerned in particular with the magnetic moment generated by a molecule due to its free rotation, and the interaction of this moment with an external magnetic field, the Zeeman effect.

The measurements reported in Part 2 were made on molecular absorption lines in the microwave region. Other methods are available for making somewhat similar Zeeman measurements, notably the very precise molecular-beam technique.[1,2] These other experiments will not be discussed here except to point out that the various methods complement each other, since each has its own experimental difficulties, with the result that some types of molecules and interactions can be effectively studied by one method and not by another. In some instances the various methods may serve as a check on each other.

The molecules to which the following discussion applies are those with $^1\Sigma$ electronic ground states, that is, those with zero total orbital and zero total spin angular momenta. Such molecules include by far the majority of the known cases, since the pairing of electrons with oppositely directed spins and the filling of electronic shells are so important to the formation of a chemical bond. The oxygen and nitric oxide molecules are important exceptions, each possessing a magnetic moment about equal to a Bohr magnetron since the electronic angular momenta are not zero in the ground state. For the $^1\Sigma$ molecules the rotational magnetic moment is much smaller and can be pictured as the result of electric currents due to the circulation of the charged nuclei and electrons. The nuclei can be considered to rotate as a semirigid framework, but, as will be seen, it is too naive to assume that the electronic contribution will be that of the electronic charge cloud frozen and rotating with the nuclear framework. Rather, the molecular rotation perturbs the electronic motion, due to the noncentral nature of the potential within a molecule, and internal electric currents are set up even though the electronic charge density distribution remains essentially unchanged from that of the fictitious nonrotating molecule.

* Preliminary presentation of this work was made in Phys. Rev. 82, 327(A) (1951).

† This work has been supported in part by the Signal Corps, the Air Materiel Command, and ONR.

‡ Now with General Electric Research Laboratory, Schenectady, New York.

[1] Rabi, Millman, Kusch, and Zacharias, Phys. Rev. **55**, 526 (1939).

[2] Kellogg, Rabi, Ramsey, and Zacharias, Phys. Rev. **56**, 728 (1939).

The theory of the Zeeman effect on the energy levels of a system involving a given magnetic moment or interacting moments is well known, and examples are provided in the experiments described later. But to interpret properly these experimental results it is also necessary to investigate how the rotational molecular moment actually arises and, in particular, its dependence on the rotational state of the molecule, and the molecular structural constants. This theory is implicit in Van Vleck's classic work on susceptibilities[3,4] and has been carried out by others for some cases of specific symmetry. Condon,[5] using wave mechanics, calculated the Zeeman effect for a symmetric top due to a point charge rigidly fixed on the top. This calculation, of course, includes the linear rotor as a special case and represents quite well the nuclear contribution to these moments. Wick[6–8] was first to calculate the electronic contribution to the rotational moment in the case of a diatomic molecule with two equivalent nuclei. Ramsey[9] has extended his theory to the case of a diatomic molecule with isotopic nuclei. Wick's immediate purpose was to explain the results of experiments by Frisch and Stern[10] and Estermann and Stern[11] on the hydrogen molecule. These experiments represent the initial measurements of such moments aside from susceptibility determinations. The measured moment of hydrogen indicated that the electronic contribution was much smaller than that of a rigid charge cloud, but Wick showed that it was indeed of the order of magnitude that one would expect on a more realistic picture of the electronic motion. Wick's considerations in one of his earlier papers[6] on the diatomic molecule are quite simple and instructive and are repeated here to preface the derivation given later for the general rotating molecule.

As shown by Van Vleck,[3] two terms are of importance for the susceptibility theory of $^1\Sigma$ molecules. One is a diamagnetic term resulting from the Larmor precession of the electrons in a magnetic field and the other is an induced electronic paramagnetism due to the non-central potential for electronic motion which hinders the pure Larmor precession. These terms are given in Eq. (1).

$$\bar{\chi}_{\text{molecule}} = -\frac{e^2}{4mc^2}\sum_i \langle X_i^2+Y_i^2\rangle_{Av} + \frac{e^2}{2m^2c^2}\sum_n{}' \frac{\langle|(0|L_Z|n)|^2\rangle_{Av}}{E_n-E_0} \quad (1)$$

where $\bar{\chi}_{\text{molecule}}$ is the average susceptibility per molecule and the magnetic field is assumed to be along the space-fixed Z-axis.

The first term is the diamagnetic term and represents the average of the squared distance of an electron from the Z-axis summed over the electrons of the molecule. The second term gives a positive contribution to the susceptibility and is a sum over the electronic states of terms involving the matrix elements of the Z-component of the total electronic orbital angular momentum. Van Vleck shows that the right side of Eq. (1) is invariant to changes in the position of the Z-axis with respect to the molecule. For convenience in the following discussion the Z-axis will here be taken to pass through the center of mass of the molecule. Van Vleck also points out that the second term is zero for atoms if the Z-axis is taken through the atomic nucleus, that is to say, the Larmor precession is unhindered since the potential function is spherically symmetric.

Now consider, following Wick,[6] a diatomic molecule rotating about the Z-axis with an angular velocity ω_Z in a field-free space, the nuclear axis of the molecule rotating in the $X-Y$ plane. If the electrons rotated with the molecule as a frozen charge cloud, they would produce a magnetic moment along the Z-axis equal to

$$-(e/2c)\omega_Z\sum_i\langle X_i^2+Y_i^2\rangle_{Av}. \quad (2)$$

It may be seen, by inverting Larmor's theorem, that the motion of the electrons due to the molecular rotation will be the same to a first approximation as that which would have been produced by a magnetic field

$$H_Z = -2mc\omega_Z/e. \quad (3)$$

By multiplying this field by the molecular susceptibility, Eq. (1), the magnetic moment due to rotation-induced electronic currents is obtained. This result is added to Eq. (2), leaving only the paramagnetic term with a negative sign, since the diamagnetic circulation just cancels the moment due to the rotation of the electronic charge. Thus

$$m_{Z\,\text{elec}} = -\frac{e}{mc}\omega_Z\sum_n{}'\frac{|(0|L_Z|n)|^2}{E_n-E_0}. \quad (4)$$

With $\hbar\omega_Z = 2BJ_Z$, where B is the rotational constant, $\hbar^2/2I$, I is the moment of inertia, and J_Z is the rotational quantum number, Wick's result is

$$m_{Z\,\text{elec}} = -4B\sum_n{}'\frac{|(0|L_Z|n)|^2}{E_n-E_0} \quad (5)$$

Bohr magnetrons per rotational quantum number. This derivation shows the origin of the electronic contribution to the rotational moment. As Wick points out, this moment is of the same sign as that of a rigid electronic rotation but may be entirely different in magnitude. In another paper,[7] Wick derives this same result more rigorously.

[3] J. H. Van Vleck, *The Theory of Electric and Magnetic Susceptibilities* (Clarendon Press, Oxford, 1932).
[4] J. H. Van Vleck, Phys. Rev. **29**, 727 (1927); Phys. Rev. **30**, 31 (1927); Phys. Rev. **31**, 587 (1928).
[5] E. U. Condon, Phys. Rev. **30**, 781 (1927).
[6] G. C. Wick, Z. Physik **85**, 25 (1933).
[7] G. C. Wick, Nuovo cimento **10**, 118 (1933).
[8] G. C. Wick, Phys. Rev. **73**, 51 (1948).
[9] N. F. Ramsey, Jr., Phys. Rev. **58**, 226 (1940).
[10] R. Frisch and O. Stern, Z. Physik **85**, 4 (1933).
[11] I. Estermann and O. Stern, Z. Physik **85**, 17 (1933).

From Larmor's theorem for atoms it is seen that the inner shell electrons of atoms bound in a molecule will be permitted more nearly free diamagnetic circulation about their own nucleus than the outer or valence electrons, since the inner electrons are in an almost spherically symmetric potential with respect to their own nucleus. Their contribution to the rotational moment can therefore be described as effectively canceling some of the charge of their own nucleus, since they will precess about their nucleus at a velocity just equal to the rotational velocity. The magnetic moment along the axis of a linear molecule is handled in a fashion similar to that for atoms; since the potential is cylindrically symmetric, completely free diamagnetic circulation is possible and no magnetic moment exists.

Since the present work was undertaken, Jen[12] has derived an expression for the rotational magnetic moment of a symmetric top molecule whose electronic and nuclear charge principal axes are coincident with the principal axes of inertia. The resulting nuclear contribution is the same as in Condon's expression[5] and the electronic contribution involves terms of Wick's type as in Eq. (5). Jen unnecessarily separates the electrons into "firmly bound" (inner shell) and "free," and arrives at an expression containing some terms which are not obviously related to the total molecular wave functions. The concept of "firmly bound" and "free" electrons is useful for qualitative discussion or for the estimation of magnetic moments, but, since the demarcation is not at all sharp, the device has doubtful value in a quantitative expression. Jen's derivation for the symmetric top follows Condon's wave-mechanical analysis, but includes the electrons as mentioned. The wave mechanical analysis for the symmetric top, however, does not indicate a satisfactory approach to the calculation of the rotational moment of a more general molecule.

A more general formulation of the problem has been devised and is presented here. The approach differs from Condon's and Jen's in that the magnetic moment is calculated directly from the defining equation

$$\mathbf{m}=(1/2c)\sum_i e_i(\mathbf{r}_i\times\mathbf{v}_i). \tag{6}$$

Such a starting point proves to yield general expressions more simply than the alternate method of calculating the Zeeman effect for the energy levels and inferring the moment from

$$m_Z(J,\tau)=-\partial W(J,\tau)/\partial H. \tag{7}$$

$W(J,\tau)$ is the energy of the rotational state characterized by the rotational quantum numbers J and τ, and H is the magnetic field. As will be seen, by starting with Eq. (6) one naturally arrives at the complete matrix of $\mathbf{m}$, rather than the diagonal elements referred to a space-fixed axis, as is likely to be the case when Eq. (7) is used. The complete matrix could be obtained from the wave-mechanical approach in certain cases, but with considerably more effort than by the method used here. The off-diagonal elements of the matrix are important for the general Zeeman effect, and add to the understanding of rotational moments. The present general formulation is actually simpler to carry out than the wave-mechanical calculation for the symmetric top since the rotational magnetic moment matrix is developed in terms of the molecular angular momenta and direction cosine matrices which are well known. Thus the rotational magnetic moment problem in the general molecule is solved to about the same degree that the free rotation problem has been solved, and any future simplification in the relevant matrices is immediately applicable to rotational moments through the relations given.

[12] C. K. Jen, Cruft Laboratory Technical Report No. 114, Harvard University, August 22, 1950, and Phys. Rev. **81**, 197 (1951).

Theory of Rotational Magnetic Moments in $^1\Sigma$ Polyatomic Molecules

The magnetic moment of a system of particles is defined by the equation

$$\mathbf{m}=(1/2c)\sum_i e_i(\mathbf{r}_i\times\mathbf{v}_i) \tag{8}$$

where e_i is the charge of the ith particle, $\mathbf{r}_i$ is the position vector of the ith particle from an arbitrary origin, $\mathbf{v}_i$ is the velocity vector of the ith particle, and the sum is over all particles. The magnetic moment due to the free rotation of a $^1\Sigma$ polyatomic molecule will be calculated using this definition, but before doing so it is necessary to derive what are essentially the velocities, $\mathbf{v}_i$, from the rotational problem.

In the conventional fashion, the nuclear system will be taken as a rigid framework. This introduces a tremendous simplification of the analytical problem, and in most cases the error incurred will be well beyond the accuracy of measurements. Vibrational and centrifugal effects on the rotational magnetic moments will be briefly discussed later. With this simplification, the hamiltonian for the molecular system, after the translational part has been separated, may be written

$$H=\tfrac{1}{2}\sum_g N_g^2/I_g+(1/2m)\sum_g\sum_j (p_g)_j^2+V(a,b,c), \tag{9}$$

where N_g is the instantaneous angular momentum of the nuclear system, referred to the principal axes of inertia, $g=a$, b, and c, fixed in the molecule; I_g is a principal moment of inertia of the nuclear system; p_g is an instantaneous linear momentum of the jth electron, referred to the principal inertial axis g; $V(a,b,c)$ is the potential function for electronic motion and involves only the relative coordinates of the particles. The total angular momentum of such a system of particles is a constant of the motion. Let this quantity be $\mathbf{P}$; then instantaneously

$$\mathbf{P}=\mathbf{N}+\mathbf{L} \tag{10}$$

where $\mathbf{N}$ is the angular momentum of the nuclear

system and $\mathbf{L}$ is the total electronic angular momentum. Substituting for $\mathbf{N}$ in Eq. (9), one gets[13]

$$H=\frac{1}{2}\sum_g \frac{P_g^2}{I_g}-\sum_g \frac{P_g L_g}{I_g}+\frac{1}{2}\sum_g \frac{L_g^2}{I_g}+\frac{1}{2m}\sum_g\sum_i (p_g)_i^2+V(a,b,c). \quad (11)$$

For $^1\Sigma$ molecules $\mathbf{L}$ is zero if a nonrotating molecule is imagined and is quite small compared to $\mathbf{P}$ in the rotating molecule. This fact is substantiated by the magnetic moment measurements. The fact that the electron mass is small compared to nuclear masses means that for $^1\Sigma$ molecules the molecular rotation is essentially unchanged whether the presence of the electrons is acknowledged or not. But since the electronic charge is of the same size as nuclear charges, a very small fraction of a quantum of electronic angular momentum can produce a magnetic moment comparable to that of the nuclear system possessing a full quantum. For this reason, the third term of the right-hand side of Eq. (11) will be entirely negligible for the rotational problem, and the second term may be taken as a relevant perturbation term. This perturbation term may be considered to act on the electronic motion alone, since, as explained above, it yields the change in electronic motion which is far more important in giving rise to the existence of an electronic contribution to the molecular magnetic moment than as a small correction to the nuclear motion. This amounts to the separation of the wave function into that of the original rigid rotor wave function and of the new, perturbed, electronic wave function.

The nuclear motion can therefore be specified by P_a^2/I_a, P_b^2/I_b and P_c^2/I_c. The electronic motion can be found by first considering the unperturbed electronic problem, which is seen to be independent of the molecular rotation

$$H^0=\frac{1}{2m}\sum_g\sum_i (p_g)_i^2+V(a,b,c), \quad (12)$$

and then the rotation dependent perturbation

$$H^2=-\sum_g P_g L_g/I_g. \quad (13)$$

Nuclear Contribution

By expanding Eq. (8) and referring all quantities instantaneously to the principal axes of inertia, one has

$$\begin{aligned}(m_a)_{\text{nuc}}&=(1/2c)\textstyle\sum_k e_k[(b_k^2+c_k^2)\omega_a-(a_kb_k)\omega_b-(a_kc_k)\omega_c]\\(m_b)_{\text{nuc}}&=(1/2c)\textstyle\sum_k e_k[-(b_ka_k)\omega_a+(c_k^2+a_k^2)\omega_b-(b_kc_k)\omega_c]\\(m_c)_{\text{nuc}}&=(1/2c)\textstyle\sum_k e_k[-(c_ka_k)\omega_a-(c_kb_k)\omega_b+(a_k^2+b_k^2)\omega_c]\end{aligned} \quad (14)$$

where e_k is the charge of the kth nucleus, a_k, b_k, and c_k are the coordinates of the kth nucleus referred to the principal inertial axes, and ω_a, ω_b, and ω_c are the angular velocities resolved along the inertial axes. But

$$\omega_g=P_g/I_g \quad (15)$$

and thus

$$(m_g)_{\text{nuc}}=\sum_{g'=a,b,c} G_{gg'}P_{g'} \quad (16)$$

where

$$G_{aa}'=(1/2cI_a)\textstyle\sum_k e_k(b_k^2+c_k^2)$$

is a typical diagonal element of the $G_{gg'}$ tensor, and

$$G_{ab}'=-(1/2cI_b)\textstyle\sum_k e_k(a_kb_k)$$

is a typical off-diagonal element.

Because of the initial assumptions, Eq. (16) does not involve the electronic coordinates, but this by no means indicates that the $\mathbf{m}_{\text{nuc}}$ matrix is independent of the electronic state; rather, this result is always to be applied only to $^1\Sigma$ states. The nuclear contribution to the rotational moment matrix will thus depend on the rotational state and is given in terms of constants of the molecule, the $G_{gg'}$, and the matrices of the angular momenta P_g.

Electronic Contribution

Since all of the electrons have the same value for e/m, Eq. (8) reduces to

$$(m_g)_{\text{elec}}=-eL_g/2mc \quad (17)$$

where $\mathbf{L}$ will depend on $\mathbf{P}$ through the perturbation term Eq. (13). If $\mathbf{L}$ is calculated for the electronic ground state of a $^1\Sigma$ molecule using the wave functions of the unperturbed electronic problem Eq. (12), the result is of course zero. That is

$$(0|L_g|0)=0 \quad (18)$$

where the 0's stand for the unperturbed electronic ground states, ψ_0^0. By ordinary perturbation theory, the first-order electronic state is given by

$$\psi_0^1=\psi_0^0+\sum_n{}'\sum_g \frac{P_g}{I_g}\frac{(n|L_g|0)}{E_n-E_0}\psi_n^0. \quad (19)$$

Thus, to the first order, the expectation value of L_g is

$$(0|L_g|0)^1=(0|L_g|0)+\sum_n{}'\sum_{g'}\frac{P_{g'}}{I_{g'}}\times\frac{(0|L_g|n)(n|L_{g'}|0)+(0|L_{g'}|n)(n|L_g|0)}{E_n-E_0}+\text{higher order terms } (g'=a,b,c). \quad (20)$$

Combining Eqs. (20), (18), and (17), the result may be

[13] A similar derivation of this hamiltonian is given by H. B. G. Casimir, *Rotation of a Rigid Body in Quantum Mechanics* (J. B. Walter's Uitgevers-Maatschappj M. V., The Hague, 1931), p. 99.

written

$$(m_g)_{\text{elec}}=\frac{1}{2}\sum_{g'}(G_{gg'}''+G_{gg'}''^{*})P_{g'} \tag{21}$$

where

$$G_{gg'}''=-\frac{e}{mcI_{g'}}\sum_{n}{}'\frac{(0|L_g|n)(n|L_{g'}|0)}{E_n-E_0}$$

and

$$G_{gg'}''^{*}=-\frac{e}{mcI_{g'}}\sum_{n}{}'\frac{(0|L_g|n)(n|L_{g}|0)}{E_n-E_0}.$$

As in the case of the nuclear contribution, the relation Eq. (21) gives the electronic contribution to the rotational magnetic moment matrix as a function of constants of the molecule, $G_{gg'}''$ and the matrices of the angular momenta P_g.

It can easily be shown that the $G_{gg'}'$ and the $G_{gg'}''$ transform in the same way under a rotation of the molecule fixed coordinate system from which they are calculated. Also, it is easily established that $I_{g'}G_{gg'}'$ and $I_{g'}G_{gg'}''$ will have a set of principal axes fixed in the molecule, which, in general will not be the same for each and neither need be the same as the principal axes of inertia. However, in the case of a true symmetric top these tensors possess only diagonal elements, the principal axes being the same as the principal inertial axes of the molecule. Even in the case of many asymmetric tops it is clear that some or all of the off-diagonal elements may be zero. Thus the situation is not quite so hopeless as one might expect on considering the general problem.

The $G_{gg'}'$ and $G_{gg'}''$ may of course be added to form a new tensor, $G_{gg'}$, in terms of which the total rotational moment is expressible as

$$m_g=\tfrac{1}{2}\textstyle\sum_{g'}(G_{gg'}+G_{gg'}^{*})P_{g'} \quad (g \text{ and } g'=a,\,b,\,c) \tag{22}$$

where

$$\begin{aligned}G_{gg'}&=G_{gg'}'+G_{gg'}''\\ G_{gg'}^{*}&=G_{gg'}'+G_{gg'}''^{*}.\end{aligned} \tag{23}$$

With a static magnetic field along a space-fixed axis $F(F=X,\,Y,\,Z)$ we are interested in the expectation of the magnetic moment along the axis. The transformation from molecule-fixed axes $g=a,\,b,\,c$ to the space-fixed axis F is given by the direction cosines as[14]

$$m_F=\textstyle\sum_g \Phi_{Fg}m_g, \tag{24}$$

where Φ_{Fg} is the direction cosine. Using Eq. (22) this relation may be written

$$m_F=\tfrac{1}{2}\textstyle\sum_g \Phi_{Fg}\sum_{g'}(G_{gg'}+G_{gg'}^{*})P_{g'}. \tag{25}$$

Let us consider first the nuclear contribution to the magnetic moment. Since in general $G_{gg'}\neq G_{g'g}'$, the nuclear contribution to the magnetic moment in the molecule-fixed system does not commute with the direction cosine transformation. Thus, in the usual quantum-mechanical fashion we use an average of the product to assure a hermitian matrix for m_F, which differs by only a scalar factor from an energy. Thus, the nuclear contribution is

$$(m_F)_{\text{nuc}}=\tfrac{1}{2}\textstyle\sum\left[(m_g)_{\text{nuc}}\Phi_{Fg}+\Phi_{Fg}(m_g)_{\text{nuc}}\right]$$

or

$$(m_F)_{\text{nuc}}=\tfrac{1}{2}\textstyle\sum_g\sum_{g'}G_{gg'}'(P_{g'}\Phi_{Fg}+\Phi_{Fg}P_{g'}). \tag{26}$$

The electronic contribution to the magnetic moment must, of course, commute with the direction cosine transformation, since it differs only by a scalar factor from the electronic angular momentum. The commutation in this case results from the existence of matrix elements of Φ_{Fg} which are off-diagonal in n, the electronic quantum number. These off-diagonal elements in n are readily evaluated directly, using the wave function of Eq. (19), or, since we are interested in $\langle L_F\rangle$, the quantities $\langle\Phi_{Fg}L_g\rangle$ are more conveniently calculated. The resulting contribution by the electrons to the magnetic moment may be written in terms of the direction cosine matrix elements diagonal in n as

$$(m_F)_{\text{elec}}=\tfrac{1}{2}\textstyle\sum_g\sum_{g'}(G_{gg'}''P_{g'}\Phi_{Fg}+G_{gg'}''^{*}\Phi_{Fg}P_{g'}). \tag{27}$$

The total space-fixed rotational magnetic moment may thus be written conveniently in terms of our previous notation

$$m_F=\tfrac{1}{2}\textstyle\sum_g\sum_{g'}(G_{gg'}P_{g'}\Phi_{Fg}+G_{gg'}^{*}\Phi_{Fg}P_{g'}). \tag{28}$$

In a representation in which P^2, P_z and $M(P_Z)$ are diagonal, the well-known matrix elements of the angular momenta are

$$\begin{aligned}&(J,K,M|P_z|J,K,M)=\hbar K\\ &(J,K,M|P_y|J,K+1,M)\\ &\qquad=\pm i(J,K,M|P_x|J,K+1,M)\\ &\qquad=\tfrac{1}{2}\hbar[J(J+1)-K(K+1)]^{\frac{1}{2}}.\end{aligned} \tag{29}$$

The association of a, b, and c with x, y, and z may be made in any of six different ways in the general polyatomic molecule. It should be apparent that for symmetric rotors, for example, the z-axis should be taken as the symmetry axis of the molecule for simplicity. For linear rotors, similarly, the z-axis would be taken as the internuclear axis. For asymmetric rotors the assignment should be made in the usual fashion, i.e., to minimize the free rotation problem.

The matrix elements for the direction cosines in factored form and in the above representation are given in Table I, which is copied from reference 14. Note that the total element is given as

$$\begin{aligned}(J,K,M|\Phi_{Fg}|J',K',M')&=(J|\Phi_{Fg}|J')\\ &\cdot(J,K|\Phi_{Fg}|J',K')\cdot(J,M|\Phi_{Fg}|J',M').\end{aligned} \tag{30}$$

Simple matrix multiplication of these elements thus gives the desired matrix for m_F for the general polyatomic molecule. A few generally pertinent matrix elements are given in the Appendix.

[14] See Cross, Hainer, and Wing, J. Chem. Phys. **11**, 27 (1943); **12**, 210 (1944), for an exhaustive general discussion of the transformations involved in the following section.

TABLE I. Direction cosine matrix elements.

Matrix element factor	Value of J': $J+1$	J	$J-1$
$(J\|\Phi_{Fg}\|J')$	$[4(J+1)[(2J+1)(2J+3)]^{\frac{1}{2}}]^{-1}$	$[4J(J+1)]^{-1}$	$[4J(4J^2-1)^{\frac{1}{2}}]^{-1}$
$(J,K\|\Phi_{Fg}\|J',K)$	$2[(J+1)^2-K^2]^{\frac{1}{2}}$	$2K$	$-2(J^2-K^2)^{\frac{1}{2}}$
$(J,K\|\Phi_{Fg}\|J',K\pm1)$ $=\mp i(J,K\|\Phi_{Fx}\|J',K\pm1)$	$\mp[(J\pm K+1)(J\pm K+2)]^{\frac{1}{2}}$	$[J(J+1)-K(K\pm1)]^{\frac{1}{2}}$	$\mp[(J\mp K)(J\mp K-1)]^{\frac{1}{2}}$
$(J,M\|\Phi_{Zg}\|J',M)$	$2[(J+1)^2-M^2]^{\frac{1}{2}}$	$2M$	$-2(J^2-M^2)^{\frac{1}{2}}$
$(J,M\|\Phi_{Yg}\|J',M\pm1)$ $=\pm i(J,M\|\Phi_{Xg}\|J',M\pm1)$	$\mp[(J\pm M+1)(J\pm M+2)]^{\frac{1}{2}}$	$[J(J+1)-M(M\pm1)]^{\frac{1}{2}}$	$\mp[(J\mp M)(J\mp M-1)]^{\frac{1}{2}}$

Certain simplifications are possible in the case of linear and symmetric rotors. The matrix elements for these cases are given in the Appendix. No immediate reduction in the number of elements of m_F is possible for the general asymmetric molecule with no symmetry. It should be apparent, however, that in particular cases a charge symmetry axis may exist, e.g., H_2O, PH_2D, and in these cases the symmetry may be exploited to reduce the number of independent elements of m_F.

The magnetic moment matrix derived from the foregoing theory is applied in Part 2 for the case of linear rotors and symmetric top molecules. In these cases the diagonal elements of the magnetic moment m_F yield, by inspection, the "g-factor" associated with the F space-fixed axis. Work in progress in this Laboratory on asymmetric molecules will, when reported, discuss the practical application of the theory to asymmetric molecules. Stated simply, a certain transformation, XT, diagonalizes the free rotational energy matrix of an asymmetric top (since it is not diagonal in the representation of Eq. (27)). The evaluation of XT is given explicitly in reference 14. This same transformation must be applied to m_F, Eq. (25). The diagonal elements of $T'X'm_FXT$ are then used to determine, by inspection, the effective molecular "g-factor" in a particular rotational state, as in the case of linear and symmetric rotors. Off-diagonal elements may be handled in the case of near degeneracy by means of the usual perturbation theory applied to the actual interaction energy of m_F with the external F-axis magnetic field.

Vibrational and Centrifugal Effects

The gyromagnetic tensor elements, $G_{gg'}$, are seen from Eqs. (16) and (21) to be constants for a molecule under the assumption of a rigid nuclear structure. These factors will in general be a function of the vibrational state and will vary with centrifugal distortion in an actual molecule. However, it is to be expected that these effects will be small and the $G_{gg'}$ would only involve the vibrational and rotational quantum numbers if their calculation were carried to a high approximation.

The nuclear contribution, for example, is essentially the ratio of the second moment of charge

$$\sum_k e_k(b_k^2+c_k^2)$$

to the moment of inertia

$$I_a=\sum_k M_k(b_k^2+c_k^2).$$

Therefore, if the ratio e_k/M_k were the same for all nuclei, vibrational and centrifugal effects would indeed be negligible. But it is in fact true that for most nuclei, except that of hydrogen, the ratio of atomic number to mass number is about the same, namely about one-half. Thus, for molecules not involving hydrogen and for those with only hydrogen off the axis concerned, these effects on the nuclear contribution may be neglected.

Isotopic Effects

The application of the above theory to isotopic molecules is straightforward, since it is only necessary to transform the G-tensor, Eq. (22), by translation and rotation in order to correct it to the new center of mass and the new principal inertial axes. Rotation of the G-tensor is straightforward. Translation may be accounted for by relations such as the invariance of expressions of the form of Eq. (1).[15] In fact, when the first moments of the nuclear and electronic charge are identical at a point on the axis along which translation is being performed, i.e., no electric dipole moment exists on that axis, it is evident that the change in G' cancels the change in G''. When the nuclear and electronic charge centers do not coincide on the axis along which translation is being performed a slight correction must be made in terms of the electric dipole moment. Finally, the scale factors such as the I_g's must be revised.

The Zeeman Effect on Rotational Absorption Lines

The Zeeman effect is the splitting of a spectral line into several components accompanying the application of a magnetic field to the emitting or absorbing system. This splitting is of course the result of the removal of the spatial degeneracy of the energy levels concerned

[15] See reference 3, Chapter X, Sec. 68.

and is intimately related to the magnetic moment of the system.

For the molecules under discussion, the perturbation energy due to the magnetic field may be written[16]

$$E_m^1 = -(J, \tau, M|m_Z|J, \tau, M)_H, \tag{31}$$

where $(J, \tau, M|m_Z|J, \tau, M)$ is a diagonal matrix element of Eq. (25) (transformed if necessary for an asymmetric rotor). This matrix element is directly a function of the rotational quantum numbers, J, τ, and M, but may depend slightly on the vibrational state as explained previously. Examples for linear and symmetric top molecules are given in the Appendix. It may be shown in general[17] that Eq. (31) may be rewritten as

$$E_m^1 = -\mu_0 M g H \quad (M = J, J-1, \cdots, -J) \tag{32}$$

where $\mu_0 = eh/2M_p c$, the nuclear magnetron, and g is the splitting factor for the particular level. For symmetric tops g is found from the Appendix to be

$$g(J, K) = g_{xx} + (g_{zz} - g_{xx})K^2/J(J+1), \tag{33}$$

where z refers to the symmetry axis and $g_{xx} = g_{yy}$.[18] Therefore, the total energy may be written

$$E = E^0 + E_m^1 = E^0(J, K) - \mu_0 M g H, \tag{34}$$

where E^0 is the unperturbed energy of the particular vibrational-rotational level.

Dipole selection rules for M are $\Delta M = 0$, which applies when the electric vector of the incident radiation is parallel to the magnetic field (π-transitions), and $\Delta M = +1$, which applies if it is perpendicular to the magnetic field (σ-transitions). Thus the transition frequencies are

$$\begin{aligned} \nu_\pi &= \nu^0 - (\mu_0/h)(g_2 - g_1)HM \\ \nu_\sigma &= \nu_\pi \mp (\mu_0/h)g_2 H \end{aligned} \tag{35}$$

where $\nu^0 = (E_2 - E_1)/h$, the frequency of the unsplit absorption, and the subscripts 1 and 2 refer to the lower and upper levels respectively. From Eq. (35) it is seen that if $g_2 = g_1$, then $\nu_\pi = \nu^0$ and $\nu_\sigma = \nu^0 \mp (\mu_0/h)g_2 H$, which is a normal Zeeman effect; that is, there is no deviation for the π-components, and the σ-components form a symmetrically spaced doublet with respect to the unsplit line. This is the case for linear molecules in the ground bending vibrational states and symmetric top molecules if $K = 0$, since $\Delta K = 0$ for electric dipole transitions. In general, however, the Zeeman pattern is anomalous and may consist of several components for both π- and σ-transitions. In any case, the π-transition measurements give $g_2 - g_1$ directly, and the combination of π- and σ-measurements is necessary to evaluate both g_1 and g_2. It is to be expected that due to centrifugal distortion many "normal" patterns would become anomalous to some degree of resolution.

In some molecules one or more of the nuclei may interact with the molecular rotation because of the nuclear moments in the presence of the internal fields of the molecule. If such an interaction is of sufficient strength, the rotational absorption lines will exhibit a resolvable hyperfine structure. Since molecular rotational magnetic moments are of the same order of magnitude as nuclear magnetic moments, the analysis of the Zeeman effect in terms of these moments becomes more complicated. The theory of the Zeeman effect under these conditions has been adapted to molecular rotational absorptions by Jen[19] and Coester[20] from a similar case in atomic spectra.[21] It should be stressed that the molecular g-factors entering this theory are not constants of the molecule, but depend on the rotational state and the $g_{\alpha\alpha'}$-tensor just developed.

Relation of Rotational Moments to Magnetic Susceptibilities

The magnetic susceptibility for $^1\Sigma$ molecules given by Van Vleck,[3] is

$$\chi_{\text{mole}} = -\frac{Le^2}{6mc^2}\sum_i \langle r_i^2 \rangle_{\text{Av}} + 2L\left(\frac{e}{2mc}\right)^2 \times \sum_n{}' \frac{|(n|L_Z|0)|^2}{E_n - E_0} \tag{36}$$

where L is Avogadro's number and i refers to the ith electron of the molecule. Aside from dimensional factors, the only difference of the second term of Eq. (36) from the diagonal elements of the electronic contribution to the rotational moment tensor, Eq. (21), is that in Eq. (36) the matrix elements are referred to the space-fixed Z-axis, while the diagonal rotational moment tensor elements are referred to the molecule-fixed axes, a, b, and c. However, in averaging over a volume of gas the following replacement may be made

$$\text{Av}|(n|L_Z|0)|^2 = \tfrac{1}{3}\{|(n|L_a|0)|^2 + |(n|L_b|0)|^2 + |(n|L_c|0)|^2\}. \tag{37}$$

Thus, once the diagonal elements g_{aa}'', g_{bb}'', and g_{cc}'' are known, the paramagnetic term in the susceptibility can be calculated.

Zeeman effect measurements on rotational absorptions do not yield the $g_{\alpha\alpha}''$ elements directly, but rather the elements $g_{\alpha\alpha}$, which are the sum of the electronic $g_{\alpha\alpha}''$ and the nuclear $g_{\alpha\alpha}'$. However, since the effective internuclear distances are usually known from analysis

[16] Equation (31) is only true for the first-order Zeeman effect, but is sufficient for the present discussion. Detailed discussion of the Zeeman effect is given in the standard references.

[17] Since XT is diagonal in J and M, see second reference 14, p. 213.

[18] It is convenient to define the dimensionless gyromagnetic tensor elements as $g_{\alpha\alpha'} = (\hbar/\mu_0)G_{\alpha\alpha'}$.

[19] C. K. Jen, Phys. Rev. **74**, 1396 (1948); Phys. Rev. **76**, 1494 (1949).

[20] F. Coester, Phys. Rev. **77**, 454 (1950).

[21] E. Back and S. A. Goudsmit, Z. Physik **47**, 174 (1928).

of the rotational spectrum, the nuclear contribution to the g_{vv} can be easily calculated from Eq. (16), and thus the g_{vv}'' become known from Zeeman measurements.

The diamagnetic term in the susceptibility depends only on the electronic charge density distribution in the electronic ground state of the molecule. This can be estimated fairly well; or, if the susceptibility is also measured, then the diamagnetic term and thus the

$$\sum_i \langle r_i^2 \rangle_{kk}$$

for the electronic ground state becomes known.

The susceptibility expression in terms of the electronic part of the rotational gyromagnetic tensor elements becomes

$$\chi_{\text{mole}} = \frac{Le^2}{6mc^2}\left[-\sum_i \langle r_i^2 \rangle_{kk} + \frac{1}{2M_p} \sum_{v=a,b,c} g_{vv}'' I_v\right]. \quad (38)$$

There would presumably be a temperature-dependent paramagnetic contribution to the susceptibility resulting from the rotational magnetic moments, since these are not field induced. However, such a term would be very small compared with those of Eq. (38).

2. MEASUREMENTS

Carbonyl Sulfide (OCS): A Linear Rotor

The Zeeman effect on the $J=1\rightarrow 2$ rotational transition of $O^{16}C^{12}S^{32}$ in its ground vibrational state was observed. Experiments were performed for both π- and σ-transitions using linearly polarized radiation, and for the σ-transitions using circularly polarized radiation. The method and apparatus are described in a forthcoming report.

Carbonyl sulfide was known to be a linear molecule,[22,23] and therefore, on the basis of the theory of Part I, a normal Zeeman effect was to be expected and was in fact observed.

The π-transitions were observed at about 3000 gauss with a full line width at half-intensity of about 0.10 Mc/sec. No change in line shape or intensity was perceptible from that of the zero field line. The σ-observations resulted in a doublet, the components being of equal intensity. The measured splittings are given in Table II. The value of g for this line represents the g-factor along an axis normal to the nuclear axis, as may be seen from Part I and the Appendix.

The circular polarization experiment was set up for observing $\Delta M=+1$ transitions and again for $\Delta M=-1$ transitions. Both observations indicated that the g-factor was negative. A negative OCS g-factor was also required for consistency in experiments on the hyperfine pattern of the $J=1\rightarrow 2$ transition of $O^{16}C^{12}S^{33}$ reported by Eshbach, Hillger, and Jen[24] and to be described in detail in a separate report.

TABLE II. σ Zeeman component measurements for the $J=1\rightarrow 2$ rotational absorption of $O^{16}C^{12}S^{32}$ at 24,325.92 Mc/sec.

$\Delta\nu$ measured[a] (Mc/sec)	H (gauss)	$g=\Delta\nu/2\mu_0 H$ (nuclear units)
0.175	4929	0.0233
0.198	4664	0.0278
0.163	4496	0.0238
0.167	4280	0.0256
		average $=0.0251\pm0.002$

[a] The measured $\Delta\nu$ represents the total splitting between the two σ-components.

Thus, the rotational moments of OCS in its ground vibrational state are describable by $g_{xx}=g_{yy}=-0.025\pm0.002$ nuclear unit.

Previous g-factor measurements on OCS have been made by Coles[25] and by Jen.[26] Neither of these observers determined the sign of the g-factor, and their results had rather large uncertainties. Since both the sign and magnitude were important for a check on the $O^{16}C^{12}S^{32}$ experiments, these measurements were repeated. Jen's measured value is $|g(\text{OCS})|=0.029\pm0.006$ nuclear unit.

Ammonia ($N^{15}H_3$) A Symmetric Top Molecule

The microwave spectrum of ammonia is unique in several respects. Besides being the first molecular absorption spectrum to have been observed and studied in the microwave region[27,28] and having unusually strong absorptions, this molecule has a large number of lines with quite different rotational quantum numbers in a compact region of the spectrum. The reason that this is possible lies in the unusual nature of the transition involved. Ammonia is a pyramidal, symmetric top molecule, whose microwave spectrum arises from transitions between vibrational inversion levels with the same rotational quantum numbers, J and K. The inversion which takes place is that of the nitrogen through the plane of the hydrogens along the axis of symmetry. There are two stable positions for the nitrogen nucleus, one on either side of this plane, with a rather low potential barrier separating them. The coupling or "tunnel" effect, between the two regions where classical vibrations could occur, splits the ground vibrational level into a closely-spaced doublet, of about 22,000 Mc/sec separation. The height of the barrier depends noticeably on centrifugal effects and therefore on the rotational quantum numbers, J and K. The resulting lines occur over a few thousand megacycles, centering at about 22,000 Mc/sec.[29]

The convenient position of these lines and their high

[22] Strandberg, Wentink, and Kyhl, Phys. Rev. **75**, 270 (1949).
[23] G. Herzberg, *Molecular Spectra and Molecular Structure: II. Infrared and Raman Spectra of Polyatomic Molecules* (D. Van Nostrand Company, Inc., New York, 1945).
[24] Eshbach, Hillger, and Jen, Phys. Rev. **80**, 1106 (1950).
[25] D. K. Coles, *Microwave Spectroscopy, Advances in Electronics* (Academic Press, Inc., New York, 1950), Vol. II.
[26] C. K. Jen, Cruft Laboratory Technical Report No. 116, Harvard, October 5, 1950; also as Phys. Rev. **81**, 197 (1951).
[27] C. E. Cleeton and N. H. Williams, Phys. Rev. **45**, 234 (1934).
[28] B. Bleany and R. P. Penrose, Nature **157**, 339 (1936).
[29] P. Kisliuk and C. H. Townes, J. Research Natl. Bur. Standards, RP 2107, **44**, 611 (1950).

TABLE III. σ component Zeeman measurements for ammonia inversion lines.

		$H=5635$ gauss			
Molecule	Line J, K	Frequency (29) (Mc/sec)	$\Delta\nu^a$ (Mc/sec)	$K^2/J(J+1)$	$g(J, K)$
$N^{15}H_3$	3, 1	21,202.30	4.72	0.083	0.550
	2, 1	22,044.28	4.75	0.167	0.553
	3, 2	21,783.98	4.60	0.333	0.535
	1, 1	22,624.96	4.48	0.500	0.521
	6, 5	21,667.93	4.43	0.595	0.516
	3, 3	22,789.41	4.29	0.750	0.500
	6, 6	23,922.32	4.24	0.859	0.494
$N^{14}H_3$	3, 2	22,834.10	4.60	0.333	0.535

[a] The measured $\Delta\nu$ represents the total splitting between the two components.

absorption coefficients allow one almost free choice of the values of J and K for the purpose of studying the rotational magnetic moment of this symmetric top. The g-factor for a symmetric top was given in Eq. (33). The value of $K^2/J(J+1)$ is just the square of the direction cosine between the total angular momentum vector, **J**, and the symmetry axis z, along which there is a component of the total angular momentum in an amount $K\hbar$. Thus it is seen that for $J=K$ the magnetic moment will be essentially due to g_{zz}, while for $K=0$ it depends only on $g_{zz}=g_{yy}$. Therefore the measurements were made on lines chosen so as to give a wide range of values of $K^2/J(J+1)$.

For these inversion transitions, the selection rules, $\Delta J=0$ and $\Delta K=0$, result in the same g-factor for both the upper and the lower energy levels, since the change in $g(J, K)$ between the two inversion states is probably negligible. It should be noted that this is not the case for symmetric top rotational transitions, where the selection rules, $\Delta J=\pm 1$ and $\Delta K=0$, give rise to an anomalous Zeeman effect.

The measurements were made on the isotopic molecule $N^{15}H_3$, since for the more abundant $N^{14}H_3$ a resolvable interaction between the N^{14} nuclear quadrupole moment and the gradient of the molecular electric field complicates the spectrum. This does not occur for $N^{15}H_3$ and the observed Zeeman effect was normal as expected. The splitting of the σ-component doublets was measured for seven lines with values of $K^2/J(J+0)$ ranging from 0.083 to 0.859 and all measurements were made in a field of 5635 gauss. The measured splittings and resulting $g(J, K)$'s are listed in Table III. Each entry in this table represents an average of from three to six measurements.

Figure 1 shows a plot of these results, with the estimated experimental error ($\sim\pm 1$ percent) indicated by the vertical bars through the plotted points. An additional consistent error of about ± 1 percent in the measurement of the magnetic field is possible. The intercepts at $K^2/J(J+1)=1$ and 0 are g_{zz} and g_{xx}, respectively. Thus, $g_{zz}=g_{yy}=+0.560\pm 0.007$ and $g_{xx}=+0.484\pm 0.007$. The signs of the g-factors were again determined by the circular polarization method.

A measurement on the $N^{14}H_3$ line for $J=3$, $K=2$ was made, since for this particular line there is no hyperfine pattern. Experimentally the $g(3, 2)$ for $N^{14}H_3$ coincides with that for $N^{15}H_3$; however, one would expect that a small difference actually exists. According to the theory of Part I, the g_{zz} should be the same for both molecules and a calculation shows that the $g_{zz}(N^{14}H_3)$ should be about 0.1 percent higher than the $g_{zz}(N^{15}H_3)$. Thus, to the accuracy of the present experiments no measurable difference between $g(3, 2)$ for $N^{14}H_3$ and $N^{15}H_3$ should exist.

Jen[19] has made similar measurements on $N^{15}H_3$ in connection with the Zeeman effect on the $N^{14}H_3$ hyperfine pattern. However, his measurements were only on components of lines for which $J=K$, and for these he of course detected no variation of g with J and K. He reports $g(N^{15}H_3)=0.477\pm 0.03$ and since he used only $J=K$ lines, this is essentially to be compared with g_{zz} above.

Correlation with Susceptibilities

The results of the measurements of the rotational g-factors of OCS and NH_3 may be used in conjunction with the published susceptibilities[20] to yield a value of

$$\sum_i \langle r_i^2 \rangle_{Av}$$

for the ground electronic state of these molecules through Eq. (38). Solving Eq. (38) for

$$\sum_i \langle r_i^2 \rangle_{Av}$$

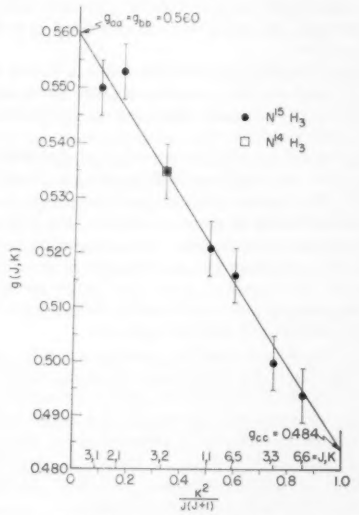

FIG. 1. Ammonia molecular g-factor.

[20] *Handbook of Chemistry and Physics* (Chemical Rubber Publishing Company, Cleveland, Ohio, 1947), thirtieth edition, p. 1991.

and dividing by the total number of electrons yields an expression for $\langle r^2\rangle_{Av}$ which is the sum of a term depending on the susceptibility and a term depending on the g_{vv}''s. Both of these terms are positive for a diamagnetic gas.

The value of $\langle r_i^2\rangle_{Av}$ has been calculated in this way for OCS, NH_3, and H_2 (using Ramsey's data).[9] The magnetic susceptibility of OCS is not listed but that of both CO_2 and CS_2 has been measured.[10] These specific susceptibility values are $\chi(CO_2)=-0.423\times10^{-6}$ and $\chi(CS_2)=-0.54\times10^{-6}$, and since the structures of the three molecules OCS, CO_2 and CS_2 are very similar, it is not unreasonable to take χ(OCS) to be the average of that for the other two. In the following it is therefore taken as $\chi(OCS)=-0.48\times10^{-6}$. Calculations in the case of H_2 are given here for comparison purposes. The g-factor of H_2 is more accurately known than for any other molecule, the most precise measurement having been made by Ramsey[9] using the molecular beam technique.

The calculated values of the $\langle r^2\rangle_{Av}$ for these molecules are given in Table IV, along with the values of the contributions of the susceptibility and g''-factor terms to the $\langle r^2\rangle_{Av}$.

The distance, r, is here taken from the center of gravity of the molecule. In each case, rough calculations show that these results are reasonable numbers, and more precise evaluation would require use of specific wave functions.

The relative magnitudes of the contributing terms, $\langle r^2\rangle_{Av}(\chi)$ and $\langle r^2\rangle_{Av}(g'')$, should be noted. In the case of OCS the larger contribution comes from g'', which is to be expected, since the majority of the electrons are in the almost spherical potential of their own nucleus, that is to say, the inner shell electrons are fairly free to precess about their own nucleus, but $\langle r^2\rangle_{Av}$ is measured from the molecular center of gravity. Thus, in the case of a molecule with nuclei far from the center of gravity, the main contribution will come from $\langle r^2\rangle_{Av}(g'')$, while $\langle r^2\rangle_{Av}(\chi)$ is a measure of the precession about the individual nuclei. The opposite case is demonstrated by the values for H_2, where an almost free precession can take place about the molecular center of gravity itself.

TABLE IV. Calculated values of $\langle r^2\rangle_{Av}$ for electronic ground states.

Molecule	Specific susceptibility (26) (cgs electromagnetic)	$\langle r^2\rangle_{Av}(\chi)$ 10^{-16} cm^2	$\langle r^2\rangle_{Av}(g'')$ 10^{-16} cm^2	$\langle r^2\rangle_{Av}$ 10^{-16} cm^2	$[\langle r^2\rangle_{Av}]^{\frac{1}{2}}$ 10^{-8} cm
OCS	-0.48×10^{-6}[a]	0.34	1.44	1.78	1.34
NH_3	-1.1×10^{-6}	0.66	0.13	0.79	0.88
H_2	-1.97×10^{-6}	0.697	0.016	0.713	0.845

[a] Estimated, see text.

TABLE V. Estimated and measured g-factors.

Molecule	Estimated positive limit $g_{oo}(=g_{bb})$	Estimated positive limit g_{zz}	Measured values $g_{oo}(=g_{bb})$	Measured values g_{zz}
H_2[a]	+1.0	—	+0.878	—
NH_3	+0.60	+0.50	+0.560	+0.484
OCS	+0.045	—	−0.025	—

[a] See reference 9.

Estimation of the Positive Limit of Rotational g-Factors

Following the ideas in these susceptibility considerations, and the discussion of rotational moments given by Wick,[8] it is possible to formulate a means of estimating the rotational g-factors.

As has been pointed out, the nuclear part of the g-factors can be satisfactorily calculated from a knowledge of the effective internuclear distances in a given vibration-rotation state; but the electronic part is in general of comparable magnitude and more difficult to estimate. Thus, in general, the net g-factors become differences of two large numbers. However, following the previous discussion, the main effect of the inner electronic shells in the rotating molecule is a precession which cancels off a comparable amount of charge of their own nucleus as far as the magnetic moments are concerned. Further, from the case of hydrogen, it is seen that the valence electrons can very roughly be said to precess about an average position between the atoms they are binding and at about the rotational velocity. Thus, considering a charge at the position of the nuclei of a magnitude equal to the atomic number minus the number of inner shell electrons, and the valence electrons to be located at their average positions, the elements of the g-factor tensor can be estimated by calculating the second moments of such a charge distribution

$$\sum_i e_i(b_i^2+c_i^2)$$

for example, and dividing by the corresponding moment of inertia.

One of the main errors in this procedure arises from the neglect of polarization effects on inner shells, and for nuclei of large atomic number this could cause a large relative error. However, for molecules containing such nuclei, the g-factors will generally be small and the absolute error will not be serious. It appears that this procedure will at least give the positive limit to the g-factors.

Table V is a comparison of the g-factors estimated in this way with the measured values.

APPENDIX

Rotational magnetic moment matrix elements on the space-fixed $Z(M)$ axis.

1. General Molecule

$$(J,K,M|m_Z|J,K,M)=\mu_0 M\left\{\frac{g_{xx}+g_{yy}}{2}+\frac{K^2}{J(J+1)}\left[g_{zz}-\frac{g_{xx}+g_{yy}}{2}\right]+i\frac{K}{J(J+1)}\left[\frac{g_{yx}-g_{yx}^*}{2}-\frac{g_{xy}-g_{xy}^*}{2}\right]\right\},$$

$$(J,K,M|m_Z|J,K+1,M)=\mu_0 M\frac{[J(J+1)-K(K+1)]^{\frac{1}{2}}}{4J(J+1)}$$
$$\times\{i[K(g_{xx}+g_{zz}^*)+(K+1)(g_{xx}+g_{zz}^*)]+K(g_{xy}+g_{yz}^*)+(K+1)(g_{yz}+g_{xy}^*)\},$$

$$(J,K,M|m_Z|J,K+2,M)=\mu_0 M\frac{\{[J(J+1)-K(K+1)][J(J+1)-(K+1)(K+2)]\}^{\frac{1}{2}}}{8J(J+1)}$$
$$\times\{2(g_{yy}-g_{xx})+i[g_{xy}+g_{xy}^*+g_{yx}+g_{yx}^*]\},$$

$$(J,K,M|m_Z|J+1,K,M)=\frac{1}{2(J+1)}\left\{\frac{[(J+1)^2-K^2][(J+1)^2-M^2]}{(2J+1)(2J+3)}\right\}^{\frac{1}{2}}$$
$$\times\{K(2g_{zz}-g_{xx}-g_{yy})-i[J(g_{xy}-g_{yx})+(J+2)(g_{xy}^*-g_{yx}^*)]\},$$

$$(J,K,M|m_Z|J+1,K\pm1,M)=\frac{1}{2(J+1)}\left\{\frac{(J\pm K+1)(J\pm K+2)[(J+1)^2-M^2]}{(2J+1)(2J+3)}\right\}^{\frac{1}{2}}$$
$$\times\{-K(ig_{xz}\pm g_{yz})-(K\pm1)(ig_{xz}^*\pm g_{yz}^*)$$
$$+(J\pm K)(g_{xy}\pm g_{xx})+(J\pm K+1)(g_{xy}^*\pm ig_{xx}^*\},$$

$$(J,K,M|m_Z|J+1,K\pm2,M)=\frac{1}{4(J+1)}\left\{\frac{(J\pm K)(J\pm K+1)(J\pm K+2)(J\pm K+3)[(J+1)^2-M^2]}{(2J+1)(2J+3)}\right\}^{\frac{1}{2}}$$
$$\times\{\pm(g_{xx}-g_{yy})-\tfrac{1}{2}i(g_{xy}+g_{xy}^*+g_{yx}+g_{yx}^*)\}.$$

2. Special Cases

A. Linear Rotor (ground bending vibrational state): z refers to nuclear axis, thus $g_{xx}=g_{yy}$, $g_{zz}=0$, $(J,M|m_Z|J,M)=\mu_0 M g_{xx}$.

B. Symmetric Rotor: z refers to symmetry axis, thus $g_{xx}=g_{yy}$.

$$(J,K,M|m_Z|J,K,M)=\mu_0 M\{g_{xx}+(g_{zz}-g_{xx})K^2/J(J+1)\}$$

$$(J,K,M|m_Z|J+1,K,M)=\frac{\mu_0(g_{zz}-g_{xx})}{(J+1)}\left\{\frac{[(J+1)^2-K^2][(J+1)^2-M^2]}{(2J+1)(2J+3)}\right\}^{\frac{1}{2}}.$$

Note: The total matrix may be constructed from its hermitian property. The $g_{QQ'}$'s are dimensionless and defined by

$$g_{QQ'}=hG_{QQ'}/\mu_0,$$

where μ_0 is the nuclear magneton, $\mu_0=eh/2M_pc$.

On the Critical State of Normal Fluids

LOUIS GOLDSTEIN
University of California, Los Alamos Scientific Laboratory, Los Alamos, New Mexico
(Received September 24, 1951)

It will be shown, within the framework of the correlation liquid model, that in the space of relative momenta normal liquids have a distribution which leads to a condensation in this momentum space at the approach of their critical state. Other states do not exhibit this condensation process.

I. INTRODUCTION

WE have studied previously a series of analogies between normal fluids undergoing condensation in coordinate space and ideal Bose-Einstein fluids undergoing condensation in momentum space.[1] Also, a more complete investigation was made of the scattering properties of both types of fluids for short and long wave electromagnetic radiation and for de Broglie waves, essentially for slow neutrons.[1,2] The analogies disclosed initially between some of the macroscopic variables of state of these fluids[3] and analyzed later on the molecular level[1] hinted already at the possibility of deriving some additional properties of the remarkable asymptotic state which is the critical state of normal fluids. We should like to give here a result obtained along these lines.

II. RELATIVE MOMENTUM DISTRIBUTIONS IN NORMAL LIQUIDS

We have obtained previously[2] the explicit rigorous coherent scattering structure factor of normal monatomic liquids on the basis of the Ornstein-Zernike static correlation liquid model. This structure factor is the same for electromagnetic radiation and slow neutrons, and has to be generalized somewhat for the latter for atoms with nonzero nuclear spin.[2] It is equally assumed that the neutrons are coupled uniquely to the atomic nuclei. The model defines the local spatial distribution of the atoms around one of them, chosen arbitrarily within the liquid, by

$$dn(r, T)/dv = n(T) + n(T)Q(r, T) = n(T) + g(r, T). \quad (1)$$

Here, $n(T)$ is the mean atomic concentration, $Q(r, T)$ is the correlation function, $g(r, T)$ the correlation concentration or density, and r is the separation of the point in question from the origin occupied by a liquid atom. The coherent scattering structure factor per liquid atom turns out to be[2]

$$F_L^2(k, T) = 1 + \int g(r, T) \cos(\mathbf{k}\cdot\mathbf{r}) dv(r), \quad (2)$$

the integral on the right-hand side being extended over the volume of the liquid. The vector $\mathbf{k}$ is the change of the propagation vector of the incident waves $\mathbf{K}$ in the coherent scattering process, or

$$\mathbf{k} = 2\mathbf{K}\sin\theta = (4\pi\sin\theta)/\lambda, \quad (3)$$

where (2θ) is the scattering angle and λ the wavelength of the incident waves. The correlation structure factor will be defined by

$$G_L(k, T) = \int g(r, T) \cos(\mathbf{k}\cdot\mathbf{r}) dv(r) = F_L^2 - 1. \quad (4)$$

Equations (2) and (3) are entirely rigorous and valid for any $\mathbf{k}$, with the exception of extremely small values where the classical ideal gas structure factor should be included.[1,2] While we shall be mostly concerned here with small k values, we will be interested mainly in the behavior of the correlation structure factor $G_L(k, T)$.

We may look upon Eq. (4), considering $\mathbf{k}$ as some running vector in k-space, as the three-dimensional fourier cosine transform of the correlation density. By Fourier's theorem,

$$g(r, T) = (2\pi)^{-3} \int G_L(k, T) \cos(\mathbf{k}\cdot\mathbf{r}) d\mathbf{k}, \quad (5)$$

$d\mathbf{k}$ being a volume element in k-space centered at the endpoint of the vector $\mathbf{k}$.

The correlation density or concentration $g(r, T)$ is the deviation, positive or negative, of the actual concentration of the fluid from its mean value $n(T)$, as seen from a liquid atom or molecule that is in the space of relative atomic or molecular coordinates. By Eq. (4), $G_L(k, T)$[4] is defined to be a concentration in the space associated with the relative momenta, G_L being the momentum space transform of $g(r, T)$. Or,

$$dg(k, T) = G_L(k, T) d\mathbf{k}, \quad (6)$$

is the number of liquid atoms per unit volume with momentum $(h/2\pi)\mathbf{k}$, between $(h/2\pi)\mathbf{k}$ and $(h/2\pi) \times (\mathbf{k}+d\mathbf{k})$. As $g(r, T)$ may be positive or negative, $G_L(k, T)$ being a deviation of the actual concentration in relative momentum space from its mean, may also be positive or negative. This achieves the physical definition of $G_L(k, T)$.

[1] L. Goldstein, Phys. Rev. **83**, 289 (1951).
[2] L. Goldstein, Phys. Rev. **84**, 466 (1951).
[3] L. Goldstein, J. Chem. Phys. **14**, 276 (1946) and Phys. Rev. **57**, 241 (1940).

[4] In reference 2, the quantity k was denoted throughout by Δk.

III. CONDENSATION IN THE SPACE OF RELATIVE MOMENTA. THE CRITICAL STATE

The structure factor is, explicitly,[2]

$$F_L^2(k, T)=\langle\Delta N^2\rangle_{kl}/N+\sum_1^\infty(-)^n k^{2n} r_G^{2n}/(2n+1)!,$$

$$r_G^0=\int g(r, T)4\pi r^2 dr=G(T); \tag{7}$$

$$r_G^{2n}=\int r^{2n} g(r, T)4\pi r^2 dr,$$

where N is the total number of liquid atoms and the r_G^{2k}'s are the even momenta of the correlation density, $\langle\Delta N^2\rangle_{kl}/N$ is the mean square fluctuation of the number of liquid atoms per atom. A form entirely equivalent to the preceding one was shown to obtain using the direct liquid interaction density function $f(r, T)$, instead of the correlation density. This form is

$$F_L^2(k, T)=[\langle\Delta N^2\rangle_{kl}/N]\Big[1+(\langle\Delta N^2\rangle_{kl}/N) \times\sum_1^\infty(-)^{n+1}k^{2n} r_f^{2n}/(2n+1)!\Big]^{-1}, \tag{8}$$

$$r_f^0=\int f(r, T)4\pi r^2 dr=F(T),$$

$$r_f^{2n}=\int r^{2n} f(r, T)4\pi r^2 dr,$$

where the r_f^{2k}'s are the even momenta of the $f(r, T)$ distribution function. The liquid model establishes a unique relation connecting the distribution $f(r, T)$ and $g(r, T)$, namely,

$$g(r, T)=f(r, T)+\int g(r-r', T)f(r', T)dv(r'), \tag{9}$$

which was discussed previously.[2]

It was further shown[2] that, with what is known generally on these functions and specifically on their zeroth moment, $F(T)$ and $G(T)$, the small momentum change coherent cross-section structure factor behaves differently in two liquid temperature regions. The division of the temperature interval over which the liquid phase exists automatically suggests itself through a temperature T_i such that

$$F(T_i)=G(T_i)=0. \tag{10}$$

At this temperature,

$$\langle\Delta N^2\rangle_{kl}/N=n(T_i)k_B T_i\chi_T=1, \tag{11}$$

i.e., the mean square fluctuation of the liquid atoms per atom, as given by statistical thermodynamics, k_B denoting here Boltzmann's constant and χ_T the isothermal compressibility, reduces to its classical value of unity at this temperature T_i. One of the main differences in the behavior of F_L^2 below and above T_i consists in that it increases and decreases, respectively, at very small k-values, with increasing k. That is,

$$\lim_{k\ \text{small}}\frac{dF_L^2(k, T<T_i)}{dk}>0,$$
$$\lim_{k\ \text{small}}\frac{dF_L^2(k, T>T_i)}{dk}<0. \tag{12}$$

Furthermore, at $T<T_i$,

$$\lim_{k\to 0}\frac{dg(k, T)}{d\mathbf{k}}=\lim_{k\to 0}F_L^2(k, T)-1=G(T) =n(T)k_B T\chi_T-1<0, \tag{13}$$

or the density in the space of relative momenta, at very small momenta, is negative. In this space, there is thus a hole in the distribution at these momenta, i.e., the concentration of liquid atoms in this momentum range is less than some mean concentration, the actual concentration being necessarily positive or zero. As the liquid temperature increases, $(dg(k, T)/d\mathbf{k})$ increases. It vanishes at T_i and continues to increase beyond T_i, where it becomes positive. At $T>T_i$, the small momentum atomic concentration is thus larger than the mean concentration.

Since $F_L^2(k, T)$ depends only on the length $|\mathbf{k}|$ of the relative momenta, the radial distribution in this space is

$$dg(k, T)/dk=4\pi k^2[F_L^2(k, T)-1], \tag{14}$$

and this quantity vanishes strictly in the limit of $k\to 0$, at all temperatures $T<T_c$, T_c denoting the critical temperature. This is seen at once using in (14) either forms, (7) or (8), of $F_L^2(k, T)$.

Consider now the approach toward the critical temperature. One finds here, using Eq. (8),

$$\lim_{T\to T_c}F_L^2(k, T)=\Big[\sum_1^\infty(-)^{n+1}k^{2n} r_f^{2n}/(2n+1)!\Big]^{-1}, \tag{15}$$

because

$$\lim_{T\to T_c}\langle\Delta N^2\rangle_{kl}/N\to\infty. \tag{16}$$

Hence, for very small k-values, for which

$$k^{2n} r_f^{2n}\ll 1, \quad n=1, 2, \cdots, \tag{17}$$

$$\lim_{k\ \text{small}}\frac{dg(k, T_c)}{d\mathbf{k}}=\lim_{k\ \text{small}}F_L^2(k, T_c)-1\gg 1. \tag{18}$$

The density in the space of relative momenta at small momenta increases thus as the critical temperature is being approached from temperatures $T<T_c$, to become very large at the critical temperature. This is a unique

state of the liquid where this density is larger than in any other state. But in order to obtain a clearer idea of the state of affairs at the approach of the critical state, we have to consider anew the radial distributoin in the space of relative momenta. Since $F_L^2(k, T)$ depends only on the magnitude $|\mathbf{k}|$, the distribution in k-space is isotropic. Hence, the radial distribution function in this space, that is the number of atoms per unit volume and per unit relative momentum range, at small momenta, is

$$\lim_{k\to 0}\frac{dg(k, T_c)}{dk}=\lim_{k\to 0}4\pi k^2[F_L^2(k, T_c)-1]$$

$$=\lim_{k\to 0}4\pi k^2 F_L^2(k, T_c)=24\pi/r_F^2, \quad (19)$$

which is finite. But we have just shown, Eq. (14), that in all states $T<T_c$, this quantity vanishes strictly. We thus see that in the space of relative momenta the approach of the critical state, in the limit, is accompanied by an accumulation of atoms in the region of vanishing momenta. This accumulation of atoms in this vanishing momentum state is entirely similar to the Bose-Einstein condensation process in ordinary momentum space of ideal symmetric fluids. On the basis of the rigorous Eq. (19), valid only in the unique limiting critical state of normal fluids, it appears justified to describe this unique state as one of condensation in the space of relative momenta of the fluid atoms. This is the result which we set out to derive.

In concluding we note that the equivalence of these two condensation processes in the behavior of the macroscopic variables of state manifests itself, as pointed out previously,[3] in that the isothermals of these fluids reach the limiting state of condensation with a vanishing slope. Finally, it should be added that while the preceding result has been obtained in the simplest case of monatomic liquids, its extension to molecular liquids presents no difficulties, so that the condensation process in the space of relative momenta at the approach of the critical state is of general validity in liquids, subject only to the applicability of the correlation model.

PHYSICAL REVIEW VOLUME 85, NUMBER 1 JANUARY 1, 1952

Nuclear Magnetic Moment and $j-j$ Coupling Shell Model

MASATAKA MIZUSHIMA AND MINORU UMEZAWA
Physics Department, Faculty of Science, Tokyo University, Tokyo, Japan
(Received June 25, 1951)

It is shown that the magnetic moment of nuclei can be explained by a refined $j-j$ coupling shell model, where neutron and proton shells are treated simultaneously, using the isotopic spin variable. The experimental moments agree well with the calculated ones for those states which have definite isotopic spin multiplicity. It is shown that a nuclear force caused by a neutral or symmetric meson is consistent with our results, but one caused by a charged meson is excluded.

I. INTRODUCTION

THE spin-orbit coupling shell model proposed by Mayer[1] succeeded in explaining nuclear magnetic moments, β-decay and isomerism, etc.[2,3] In such a one-particle approximation, however, the nuclear magnetic moment must lie on the Schmidt line. But, as is well known, the values of nuclear magnetic moments deviate considerably to the inside region between two Schmidt lines, and this deviation has been considered to suggest that the angular momentum of the outer nucleon does not hold. It was first suggested that the nuclear state is a linear combination of two states with $l=j-\frac{1}{2}$ and $l=j+\frac{1}{2}$, which correspond to the two Schmidt limits respectively.[4] But it was soon pointed out that this is not plausible, since these two states have opposite parity and cannot combine. Next, the effect of exchange currents was examined in order to explain this deviation, but this effect was found to be not sufficiently large, and, moreover, the moment can deviate to the outside region as well as to the inside of the two Schmidt limits in that theory.[5]

On the other hand, the nuclear quadrupole moments of some nuclei are too large to be expected from a one-particle shell model, and some types of asymmetric drop model have been proposed to explain it.[6-8] Since the angular momentum of the outer nucleon is not rigorously constant in the asymmetric drop model, the model was also used to explain the deviation of the magnetic

[1] M. G. Mayer, Phys. Rev. **78**, 16 (1950).
[2] Umezawa, Nakamura, Ono, Yamaguchi, and Taketani, Prog. Theor. Phys. **6**, 408 (1951).
[3] E. Feenberg, Phys. Rev. **76**, 1275 (1949).
[4] L. W. Nordheim, Phys. Rev. **75**, 1894 (1949).
[5] R. G. Sachs, Phys. Rev. **74**, 433 (1948); R. K. Osborne and L. L. Foldy, Phys. Rev. **79**, 795 (1950); L. Spruch, Phys. Rev. **80**, 372 (1950).
[6] J. Rainwater, Phys. Rev. **79**, 432 (1950).
[7] A. Bohr, Phys. Rev. **81**, 134 (1951).
[8] L. L. Foldy and F. J. Milford, Phys. Rev. **80**, 751 (1950).

TABLE I. Irreducible representation of $\mathcal{T}(\tau_1, \tau_2, \tau_3)$ in $\mathfrak{S}_3$.

T	
3/2	χ_0
1/2	χ_2

moment from the Schmidt line.[7-9] But it was pointed out that the magnetic moments of B^{10} and N^{14} agree well with the calculated value, although they have a non-vanishing spin of 3 and 1, for which, according to the above model, the deviation from the calculated value is expected. This seems to be a contradiction to the asymmetric drop model.

On the other hand, some evidence for the $j-j$ coupling model has been obtained in the investigation of lower excited states of even-even nuclei. Horie, Yamaguchi, Yoshida, and one of the present authors[10] have shown that the ground, first, and some of the second excited states of even-even nuclei have a spin of 0, 2, and 4, respectively, except for the closed shell nuclei, and this fact can be explained easily by the $j-j$ coupling shell model, while the $L-S$ coupling model fails to explain this fact, since a lower odd spin state is also possible in the latter scheme.

In this paper we propose a refined $j-j$ coupling shell model, and calculate nuclear magnetic moments assuming some features about the hamiltonians of nuclei.[11]

II. REMARK ON THE MAGNETIC MOMENT OF NUCLEI WITH (CLOSED SHELL±ONE) NUCLEONS

It may be worth noting that by the above term, nuclei with (closed shell±one) nucleons, those nuclei are meant which have (closed shell±one) neutrons +(closed shell) protons or *vice versa*. If we neglect the contribution of the closed shells entirely, the theoretical values of the magnetic moment can be obtained straightforwardly.[12]

Comparison of theoretical and experimental values of magnetic moment for this kind of nuclei was made in Table I of our preliminary paper.[11] Among eleven nuclei cited there, disagreement is found only for B^{11}, Al^{27}, and P^{31}.

III. CALCULATION OF THE MAGNETIC MOMENT OF NUCLEI WITH (CLOSED SHELL±THREE) NUCLEONS

The following discussion can easily be extended to cases of more than three nucleons, but since they are relatively unimportant we shall limit our discussion to the case of three nucleons.

The proton and neutron are treated as a nucleon in different states, using the isotopic spin function τ.

We assume that the total wave function of our nucleus can be written as

$$\Psi = \Phi(\text{inner})\mathfrak{R}(r_1, r_2, r_3)\Theta(j_1, j_2, j_3)\mathcal{T}(\tau_1, \tau_2, \tau_3), \quad (1)$$

where Φ(inner) means the wave function of the nucleons in inner closed shell, $\mathfrak{R}(r_1, r_2, r_3)$ is the radial wave function of the three nucleons in the outer shell, $\Theta(j_1, j_2, j_3)$ is their angular wave function in the sense of $j-j$ coupling shell model, and $\mathcal{T}(\tau_1, \tau_2, \tau_3)$ is their isotopic spin eigenfunction, which means an eigenfunction for a definite $|\mathbf{T}| = |\sum_i \boldsymbol{\tau}_i|$. The important assumption in (1) is that the angular part (including ordinary spin) and isotopic spin part can be separated from the other parts.

Since the individual isotopic spin τ is a dichotomic variable, the total spin function $\mathcal{T}(\tau_1, \tau_2, \tau_3)$, which is an irreducible representation of the rotation group in isotopic spin space, is also an irreducible representation of the permutation group of order three. The representation to which each isotopic spin state belongs is shown in Table I, where $T = |\mathbf{T}| = |\sum_i \boldsymbol{\tau}_i|$ and χ_0, χ_1, and χ_2 are the totally symmetric, antisymmetric, and two-dimensional representations of the permutation group $\mathfrak{S}_3$, respectively.

The angular part $\Theta(j_1, j_2, j_3)$ is an irreducible representation of the rotation group. The reduction of the product representation in this group can be done in the usual way; but since the spin function thus reduced is, in general, still a reducible representation of the permutation group, we must further reduce it in the latter group. The results are shown in Table II, where only the results for the case of

$$I = |\sum_i^3 \mathbf{j}_i| = j$$

with $j = 3/2$ and $5/2$ are shown, since they are the only practically important cases.[13]

The total wave function Ψ must be a representation χ_1, according to the well known Pauli principle. Thus, if T is fixed, the symmetric properties of $\Theta(j_1, j_2, j_3)$ are restricted. For a charge quartet state ($T=3/2$) $\Theta(j_1, j_2, j_3)$ must belong to the representation χ_1, and for a charge doublet state ($T=1/2$), it must belong to χ_2, since $\chi_1 \times \chi_0 = \chi_1$, $\chi_2 \times \chi_2 = \chi_0 + \chi_1 + \chi_2$, and no other representation can make Ψ antisymmetric. We can see from Table II that, for Li^7, Be^9, and Cl^{35}, whose configurations are $(2p_{3/2})^3$, $(2p_{3/2})^{-3}$, and $(3d_{3/2})^3$, respectively, and $I = 3/2$, the angular part of the wave func-

TABLE II. Irreducible representations of $\Theta(j_1, j_2, j_3)$ in $\mathfrak{S}_3$.

$I(=\lvert\sum_i j_i\rvert = j)$	
3/2	$\chi_0+\chi_1+\chi_2$
5/2	$\chi_0+\chi_1+2\chi_2$

[9] H. Kopfermann, Naturwiss. **38**, 29 (1951).
[10] Horie, Umezawa, Yamaguchi, and Yoshida, Prog. Theor. Phys. **6**, 254 (1951).
[11] A preliminary paper was published by M. Mizushima and M. Umezawa, Phys. Rev. **83**, 463 (1951).
[12] L. Rosenfeld, *Nuclear Forces* (North-Holland Publishing Company, Amsterdam, 1949), Sec. II, p. 402.
[13] For other cases see, for example, M. Mizushima and T. Ito, J. Chem. Phys. **19**, 739 (1951).

tion is uniquely determined for each charge multiplet state, and for Mg^{25}, whose configuration is $(3d_{5/2})^{-3}$ and spin is 5/2, there are two independent possible angular wave functions.

The magnetic moment can be easily calculated if we know $\Theta(j_1, j_2, j_3)$ and $\Upsilon(\tau_1, \tau_2, \tau_3)$ explicitly, by calculating the average of

$$M_s=\sum_i\{g_p(\tau_{zi}-1)+g_n(\tau_{zi}+1)\}j_{zi}/2$$

for $I_z=I$ state. The results are shown in Table III. In this table we see that for Li^7 and Be^9, the calculated moment for isotopic spin doublet state agrees well with experiment, while in the case of Cl^{35}, the value corresponding to the isotopic spin quartet state agrees with experiment. In the case of Mg^{25}, since there are two independent states for $I=5/2$, $T=1/2$, the calculated magnetic moment can take any value between the two limits, unless some further specification on the hamiltonian is made. It is interesting that the experimental result agrees with the lower limit for this state.

IV. DISCUSSION

Our success with the nuclei of (closed shell±one) nucleons shows that the calculation of magnetic moments on the Mayer shell model is fairly good. At this point it must be noted that our interpretation of (closed shell±one) nucleons is slightly different from hers. Mayer treated the neutron shell and the proton shell separately. Thus, for example, a nucleus with (closed shell±two) protons+(closed shell±one) neutrons is treated in the same way as a nucleus with (closed shell) proton+(closed shell±one) neutrons in Mayer's scheme. But from our standpoint, they are entirely different. The former is a nucleus with (closed shell ±three) nucleons, and is treated in Sec. III.

The good agreement between our result and experiment in the case of (closed shell±three) nucleons shows that the ground states of these nuclei have a definite isotopic spin multiplicity.

In order to be able to assign definite isotopic spin multiplicity to each stationary state, the hamiltonian H of our nuclei must satisfy a commutation relation $[|\mathbf{T}|^2, H]=0$. There are three typical kinds of charge dependence of the internuclear force in the meson theory: the forces corresponding to neutral, symmetrical, and charged mesons. In the neutral meson theory H does not contain any factor which depends on isotopic spin; thus it commutes with $|\mathbf{T}|^2$. In the symmetrical meson theory, the internuclear potential can be expressed as $f(r_{12})\tau_1\tau_2$ where $f(r_{12})$ is a function which depends on relative coordinate, ordinary spin, etc. By a straightforward calculation one can show that $[|\mathbf{T}|^2, \sum f(r_{ij})\tau_i\tau_j]=0$; thus, in this case also, each stationary state has a definite isotopic spin multiplicity. But in the charged meson theory, in which $H=\sum f(r_{ij})(\tau_{xi}\tau_{xj}+\tau_{yi}\tau_{yj})$, $|\mathbf{T}|^2$ does not commute with H. Our result that each stationary state of nuclei has a definite isotopic spin multiplicity is consistent with neutral and symmetrical meson theory, but contradicts charged meson theory.

TABLE III. Magnetic moments of nuclei with (closed shell±3) nucleons.

	I	Configuration	T_z	T	μ_{calc}	μ_{exp}[a]	μ_S[b]
Li^7	3/2	$(2p_{3/2})^3$	1/2	1/2	3.07	3.26	3.79
				3/2	0		
Be^9	3/2	$(2p_{3/2})^{-3}$	1/2	1/2	−1.14	−1.18	−1.91
				3/2	1.9		
Cl^{35}	3/2	$(3d_{3/2})^3$	1/2	1/2	−0.48	0.82	0.12
				3/2	0.80		
Mg^{25}	5/2	$(3d_{5/2})^{-3}$	1/2	1/2	−1.06 to 2.76	−0.96	−1.91
				3/2	2.57		

[a] J. E. Mack, Revs. Modern Phys. 22, 64 (1950).
[b] Value in the Schmidt limit.

It should be remembered that the coulomb potential $H_c=\frac{1}{4}(e^2/r_{ij})(1-\tau_{zi})(1-\tau_{zj})$ does not commute with $|\mathbf{T}|^2$; but this effect is usually not very large, and can be treated as a small perturbation.

That the ground states of these nuclei, except Cl^{35}, are charge doublet states is consistent with the fact that the ground states of their neighboring isobars, in which only the charge quartet state can appear, have much higher energy. Also it can be seen that the theoretical estimate of the energy by means of our wave function yields the same conclusion if an attractive internuclear potential is used. The latter conclusion is valid for both the neutral and the symmetrical meson theories. The details of the energy calculation will be published in another paper.

The reason that the ground state of Cl^{35} is charge quartet is not clear.

Our result for Mg^{25} seems to indicate that the magnetic moment can be diagonalized with H in a space diagonal in I and T. The operator of the z component of the magnetic moment is

$$M_z=\{(g_n+g_p)I_z+(g_n-g_p)\sum\tau_{zi}j_{zi}\}/2$$

since the g-factors are common to nucleons in the same shell. The first term being always commutable with H, we have only to examine the commutability of the second term with H. If the range of the internuclear potential is very small compared to the dimensions of the nucleus, we can approximate it by the delta-function $\delta(r_{ij})$. In this case we can show without much difficulty that the H corresponding to the neutral and symmetrical theories commutes with M_z in our limited space, by using the commutability of $\delta(r_{ij})$ and j_{zi}. If the range of the internuclear potential is larger than the dimensions of the nucleus, we can expand the space-dependent factor of the internuclear potential as $\varphi(r_i)\varphi(r_j)+\varphi'(r_i)\varphi'(r_j)\cos\theta_{ij}+\cdots$, where $\varphi(r_i)$ is a

function which depends only on the radial coordinate of the ith nucleon. Taking the average over $\boldsymbol{r}$, we can neglect the higher terms in the above expansion under the above assumption. Thus our hamiltonian reduces to $a\sum_{i>j}1$ and $a\sum_{i>j}\boldsymbol{\tau}_i\boldsymbol{\tau}_j$ for the neutral and the symmetrical theories, respectively, confirming the commutability of H and $|\mathbf{T}|^2$.[14] Since the range of the internuclear potential is 1.5×10^{-13} cm, and the radius of Mg^{25} is 7×10^{-13} cm, the present situation seems to favor the former approximation.

It should be mentioned that the success in the case of odd-odd nuclei by Feenberg[3] is also preserved as such in our theory.

We wish to thank Professor Muneo Sasaki and Dr. Hisashi Horie for their continued help and encouragement throughout the work. We also owe thanks to Professors S. Nakamura, T. Yamanouchi, and M. Kotani, and Drs. S. Tani and H. Narumi for their discussion.

APPENDIX

The spin function which is a representation of both rotational and permutation groups can be constructed as follows:

We start from an invariant formula,

$$I=\prod_{i>j}(u_1^{(i)}u_2^{(j)}-u_2^{(i)}u_1^{(j)})^{\sigma_{ij}} \times\prod_k(u_1^{(k)}x_1+u_2^{(k)}x_2)^{2s}-g^k, \quad \text{(A1)}$$

where $i, j, k=1, 2, \cdots \nu$, $\sum_{i>j}\sigma_{ij}=\nu s-S$ with individual spin s and total spin S, and the g_k's are so chosen as to make I a function of order $2s$ for every u_1 and u_2. Since, in general, there are n sets of (σ_{ij}, g_k) which satisfy the above condition, we obtain n formulas $I_1, I_2, \cdots I_n$. The representation $D(R)$ of an operator of the permutation group $\mathfrak{S}_\nu$ is then calculated for all R, taking $I_1, \cdots I_n$ as the basis. If $\mathfrak{D}_l(R)$ is an irreducible representation χ_l of the operator R and α is an arbitrary vector of order $n\times m$, where m is the order of $\mathfrak{D}_l(R)$, we can obtain m linear combinations of I_p as:

$$(I_1, \cdots, I_n)(\textstyle\sum_R D(R)\alpha\mathfrak{D}_l(R)^{-1}) =(\sum_p a_p^{(1)}I_p, \cdots, \sum_p a_p^{(m)}I_p). \quad \text{(A2)}$$

Then each linear combination of I_p is expanded, and the coefficient of $x_1^{S+M}x_2^{S-M}$ is calculated as $\Theta_{S,M}^{(1)}$, $\Theta_{S,M}^{(2)}$, $\cdots$, $\Theta_{S,M}^{(m)}$. This set of $\Theta_{S,M}$ is the required spin function which is a representation of the permutation group $\mathfrak{S}_\nu$, if we put the individual spin function $U_\lambda^{(i)}$ as

$$U_\lambda^{(i)}=(u_1^{(i)})^{s+\lambda}(u_2^{(i)})^{s-\lambda}\{(s+\lambda)!(s-\lambda)!\}^{-1/2}, \quad \text{(A3)}$$

where $\lambda=s_z$.

Some of the explicit spin functions thus obtained are as follows: For $\nu=3$, $s=3/2$, $S=3/2$, and the χ_2 representation,

$$\{-(3/2,-3/2,3/2)-(-3/2,3/2,3/2) +(3/2,-1/2,3/2)+(-1/2,3/2,3/2) -(3/2,1/2,-1/2)-(1/2,3/2,-1/2) +2(3/2,3/2,-3/2)\}/10^{1/2},$$

and

$$\{3(3/2,-3/2,3/2)-2(1/2,-1/2,3/2) +2(-1/2,1/2,3/2)-3(-3/2,3/2,3/2) -(3/2,-1/2,1/2)+(-1/2,3/2,1/2) +(3/2,1/2,-1/2)-(1/2,3/2,-1/2)\}/30^{1/2}.$$

For $\nu=3$, $s=5/2$, $S=5/2$ and the χ_2 representation,

$$\{-18(5/2,-5/2,5/2)+10(3/2,-3/2,5/2) -7(1/2,-1/2,5/2)+7(-1/2,1/2,5/2) -10(-3/2,3/2,5/2)+18(-5/2,5/2,5/2) +8(5/2,-3/2,3/2)-12\cdot10^{-1/2}(3/2,-1/2,3/2) +12\cdot10^{-1/2}(-1/2,3/2,3/2)-8(-3/2,5/2,3/2) -5(5/2,-1/2,1/2)+9\cdot5^{-1/2}(3/2,1/2,1/2) -9\cdot5^{-1/2}(1/2,3/2,1/2)+5(-1/2,5/2,1/2) +2(5/2,1/2,-1/2)-2(1/2,5/2,-1/2) -2(5/2,3/2,-3/2)+2(3/2,5/2,-3/2)\} \times(2\cdot3\cdot7\cdot11\cdot13/5)^{-1/2},$$

and

$$\{-6(5/2,-5/2,5/2)+2(3/2,-3/2,5/2) -(1/2,-1/2,5/2)-(-1/2,1/2,5/2) +2(-3/2,3/2,5/2)-6(-5/2,5/2,5/2) +4(5/2,-3/2,3/2)-2(2/5)^{1/2}(3/2,-1/2,3/2) +6\cdot5^{-1/2}(1/2,1/2,3/2)-2(2/5)^{1/2}(-1/2,3/2,3/2) +4(-3/2,5/2,3/2)-3(5/2,-1/2,1/2) -3\cdot5^{-1/2}(3/2,1/2,1/2)-3\cdot5^{-1/2}(1/2,3/2,1/2) -3(-1/2,5/2,1/2)+4(5/2,1/2,-1/2) +4(2/5)^{1/2}(3/2,3/2,-1/2)+4(1/2,5/2,-1/2) -6(5/2,3/2,-3/2)-6(3/2,5/2,-3/2) +12(5/2,5/2,-5/2)\}(2\cdot7\cdot11\cdot13/5)^{-1/2}.$$

The other functions needed in the present calculation can be easily obtained. In the above formulas $(\lambda_1, \lambda_2, \lambda_3)\equiv U_{\lambda_1}^{(1)}U_{\lambda_2}^{(2)}U_{\lambda_3}^{(3)}$.

Note added in proof.—Ross obtained the same results as are given in Table III.[15]

[14] It may be worth noting that in these cases M_z commutes with H in the whole space, in the neutral meson theory.

[15] E. P. Wigner (private communication).

Motion of an Electron in a Perturbed Periodic Potential

E. N. ADAMS, II
Institute for Nuclear Studies, University of Chicago, Chicago, Illinois
(Received August 16, 1951)

Wannier's theorem concerning the motion of an electron in a perturbed periodic potential is generalized so as to take into account transitions between energy bands. The generalized form of the theory is placed on a rigorous quantum-mechanical foundation and the basic approximation of Wannier's form of the theorem elucidated. A compact matrix formulation is developed which permits the multiband character of the formalism to be handled expeditiously. It is shown that corrections to Wannier's approximate equation of motion arising from variations of the potential within a unit cell require a multiband formalism, since these corrections affect the motion primarily by causing transitions between bands. The correction terms are expressed in such a form that they may be conveniently treated as perturbations. A generalized form of Wannier's theorem is presented in which the perturbing potential may depend upon both the coordinate and momentum of the electron. The special case that the perturbative potential is due to slowly varying combined electric and magnetic fields is discussed in detail. Applicability to the problem of the electron-phonon interaction is discussed briefly.

INTRODUCTION

SLATER has recently[1] published a discussion of some applications of a theorem of Wannier's[2] concerning the motion of an electron in a perturbed periodic potential. The theorem states that in a certain approximation the motion of the electron can be found by solving the Schroedinger equation

$$[E^0(p)+V'(r)-i\hbar\partial/\partial t]\Psi(r)=0 \qquad (1)$$

in which $V'(r)$ is the perturbative potential and $E^0(\hbar k)$ is the energy of that state in the unperturbed potential which has "pseudomomentum" $\hbar k$. The solution function $\Psi(r)$ is a probability amplitude in the sense that $|\Psi(r)|^2$ gives essentially the probability for finding the electron in unit cell of the lattice at r. Thus, provided the perturbation does not lead to the existence of eigenstates which are localized within a region of the dimensions of unit cell, the solution of Eq. (1) affords a good approximation to the electron probability distribution.

In this paper Wannier's theorem is obtained in a form which is more general than Eq. (1) and which is applicable to a broader class of problems. In addition certain assumptions made in Slater's proof are made more precise. Slater's derivation of Eq. (1) assumes: (*a*) that the perturbation is sufficiently "weak" so that a given eigenstate in the perturbed potential may be expanded in the eigenstates of the unperturbed hamiltonian belonging to a single band, and (*b*) that the perturbative potential $V'(r)$ is such a slowly varying function of position that its variation across a unit cell may be neglected. The two assumptions are closely related, since the first effect of the variation of $V'(r)$ with position is to admix states of different bands. If, as is commonly the case for metals, two of the unperturbed energy bands overlap, the assumptions of the derivation would not seem to be assured *a priori*, for even a quite small variation of $V'(r)$ with position could lead to a strong mixing of originally degenerate states. In this case the applicability of Eq. (1) would be in doubt.

In order to be able to treat the case that bands are degenerate or nearly degenerate, the formalism must be broadened so as to include the possibility of transitions between bands. Such an extension is established in a quite natural way by a simple generalizing of the treatment given by Slater. The generalized formulation employs a $\Psi(r)$ which is a multicomponent function, having one component for each band. It satisfies an equation similar to Eq. (1) except that there are terms in the hamiltonian which couple its components belonging to different bands. Introduction of the multicomponent Ψ has several advantages. One advantage is that an eigenvalue problem can be written down for which it is the rigorous solution. While this eigenvalue problem is not itself of a mathematically tractable form, it provides a suitable point of departure for arriving at the basic approximation of the Wannier method. A second advantage is that using the multicomponent Ψ one can express the corrections to the hamiltonian due to the nonconstancy of $V'(r)$ as what is effectively a power series in d, where d is the length of unit cell. Such a power series development is quite convenient from the point of view of perturbation theory, because the basic approximation of the theory is expected to be a good one in just those cases for which the power series in d converges rapidly. Another generalization which is made using the multicomponent Ψ is the treatment of a perturbation which depends on the momentum. As a consequence the important problem of the perturbation due to a magnetic field can be fitted into the formalism.

Section I is devoted to a derivation of the rigorous eigenvalue problem for $\Psi(r)$. Section II introduces a convenient matrix notation. In Sec. III the basic approximation of the Wannier method is discussed. It is shown that Eq. (1) may be obtained as the lowest order approximation to a more general equation of motion; it is also shown that corrections to Eq. (1) depending on

[1] J. C. Slater, Phys. Rev. **76**, 1592 (1949).
[2] G. H. Wannier, Phys. Rev. **52**, 191 (1937).

the variation of $V'(r)$ across unit cell can be made in the way suggested by Slater,[2] but that a multiband formalism is required to express them. The motion of an electron in a constant electric field is discussed by way of illustration. In Sec. IV the perturbation due to a magnetic field is discussed, and the part of the perturbation which leads to transitions between bands separated from the part which leads to motion within a band. Several well-known theorems concerning the motion of wave packets in slowly varying electric and magnetic fields are shown to follow from the theory in a formally simple way. In Sec. V it is indicated how the formalism may be applied to the problem of the electron-phonon interaction.

I

The basic functions for expanding solutions of the perturbed problem are the localized one-electron functions which Slater denotes as $a(q-Q_m)$. To avoid subsequent notational confusion these functions will be here denoted as $\varphi_{mn}(r)$, the index n designating to which band of the unperturbed problem the function φ_{mn} belongs. The φ_{mn} are constructed from the Bloch functions

$$\psi_{kn}(r)=[\Delta/(2\pi)^3]^{\frac{1}{2}}e^{ik\cdot r}u_{kn}(r) \tag{2}$$

by the recipe

$$\varphi_{mn}(r)=[\Delta/(2\pi)^3]^{\frac{1}{2}}\int d^3k e^{-ik\cdot r_m}\psi_{kn}(r). \tag{3}$$

The integral d^3k is an integral over the interior of the (reduced) brillouin zone, and Δ is the volume of a unit cell. r_m is a vector from the origin to a standard point in the mth unit cell, and the origin is so chosen that $r_0=0$. Thus the r_m are the translations which carry the lattice into itself, and satisfy the condition

$$e^{iK_L\cdot r_m}=1 \tag{4}$$

for any K_L of the reciprocal lattice. With the $u_{kn}(r)$ normalized over the unit cell the Bloch functions satisfy the orthogonality relation

$$(\psi_{kn},\psi_{k'n'})=\delta_{nn'}\delta(k-k'). \tag{5}$$

From Eqs. (3) and (5) the φ_{mn} are seen to satisfy an orthogonality relation

$$(\varphi_{mn},\varphi_{m'n'})=\delta_{nn'}\delta_{mm'}. \tag{6}$$

Thus the φ_{mn} form an orthonormal set. They also form a complete set since the complete set of functions ψ_{kn} can be expanded as

$$\psi_{kn}(r)=[\Delta/(2\pi)^3]^{\frac{1}{2}}\sum_m e^{ik\cdot r_m}\varphi_{mn}. \tag{7}$$

The hamiltonian of the perturbed problem is given by

$$H=H^0+V'(p^\mu,x^\nu),\quad H^0=p^2/2m+V_L. \tag{8}$$

[2] See appendix to reference 1.

H^0 is the hamiltonian for the electron in the unperturbed periodic potential and V' is a function of p^μ and x^ν subject chiefly to the restriction that it is hermitian. Although it will later be assumed that V' can be developed as a power series in its six arguments, this is a formal step which does not actually restrict the form of V'. A wave function ψ for the electron can be expressed in terms of the φ_{mn} as

$$\psi(r)=\sum_{m,n}\Psi_n(r_m)\varphi_{mn}(r). \tag{9}$$

$\Psi_n(r)$ is a function which is defined only when its argument takes on one of the discrete set of values r_m. Since the function $\varphi_{mn}(r)$ is strongly localized[2] about the point r_m, $|\Psi_n(r_m)|^2$ is essentially the probability that the electron is in the unit cell at r_m and in the nth band.

The object of the following paragraphs is to express certain operations on the wave function ψ in terms of differential operations on the amplitudes $\Psi_n(r_m)$. It is necessary, therefore, to define the function $\Psi_n(r)$ for values of the argument other than the r_m. Since the r_m are isolated points, there are many ways to choose a function $\Psi_n(r)$ which takes on the values prescribed by Eq. (9). Thus the extended function $\Psi_n(r)$ may also be required to satisfy the condition that its derivatives up to an arbitrary finite order shall everywhere exist and be finite. Hereafter, then, it will be assumed that the domain of definition for $\Psi_n(r)$ has been extended so that $\Psi_n(r)$ and its derivatives are defined and exist for all values of r.

It can now be shown that if $\mathcal{O}$ is an operator which satisfies

$$\mathcal{O}\psi_{kn}=\sum_{n'}\psi_{kn'}\mathcal{O}_{n'n}(\hbar k) \tag{10}$$

then for a ψ given by Eq. (9)

$$\mathcal{O}\psi=\sum_{m,n}\varphi_{mn}(r)[\textstyle\sum_{n'}\mathcal{O}_{rn'}(\hbar\nabla_m/i)\Psi_{n'}(r_m)]. \tag{11}$$

According to Eq. (10), $\mathcal{O}$ is an operator which has the selection rule that it connects only states which have the same translational symmetry. The essentials of the proof of Eq. (11) are contained in the appendix of Slater's paper,[1] although he does not consider transitions between bands. The elements of the proof will be reproduced here in order to show how the argument must be modified to permit the discussion of the operator x^ν. The proof of Eq. (11) depends on the fact that $\mathcal{O}_{n'n}(\hbar k)$ is only defined for values of k lying in the reduced brillouin zone. It is, therefore, possible to expand $\mathcal{O}_{n'n}(\hbar k)$ in a multiple fourier series with the period of the reciprocal lattice.[1]

$$\mathcal{O}_{nn'}(\hbar k)=\sum_s\mathcal{O}_{nn'}{}^{(s)}e^{-ik\cdot r_s}. \tag{12}$$

If now Eq. (3) is inserted for φ_{mn} in Eq. (9) and $\mathcal{O}$ is made to operate on ψ, then by Eqs. (10) and (12),

$$\mathcal{O}\psi=\sum_{m,n}\Psi_n(r_m)[\Delta/(2\pi)^3]^{\frac{1}{2}}$$
$$\times\int d^3k e^{-ik\cdot r_m}\textstyle\sum_{n',s}\psi_{kn'}\mathcal{O}_{n'n}{}^{(s)}e^{-ik\cdot r_s}. \tag{13}$$

Equation (13) can be rearranged to read

$$\mathcal{O}\psi=\sum_{m,n}\varphi_{mn}(r)\sum_{n',s}\mathcal{O}_{nn'}^{(s)}\Psi_{n'}(r_m-r_s). \quad (14)$$

The assumed differentiability of $\Psi_n(r)$ permits the use of the displacement operator identity:

$$\Psi_n(r_m-r_s)=\exp(-r_s\cdot\nabla_m)\Psi_n(r_m) \quad (15)$$

and Eq. (14) becomes

$$\mathcal{O}\psi=\sum_{m,n}\varphi_{mn}(r)\sum_{n'}\times[\sum_s \mathcal{O}_{nn'}^{(s)}\exp(-ir_s\cdot\nabla_m/i)]\Psi_{n'}(r_m). \quad (16)$$

Eq. (12) is used to sum the bracketed expression in Eq. (16) and Eq. (11) results.

It is easily verified that if $\mathcal{O}$ and $\mathcal{O}'$ each satisfy Eq. (10) then

$$\mathcal{O}\mathcal{O}'\psi=\sum_{m,n}\varphi_{mn}(r)\sum_{n'}\times[\sum_{n''}\mathcal{O}_{nn''}(h\nabla_m/i)\mathcal{O}_{n''n'}'(h\nabla_m/i)]\Psi_{n'}(r_m). \quad (17)$$

Of particular interest are the operators p^μ and x^ν. p^μ is clearly an example of the operator $\mathcal{O}$ in Eq. (10). In conformity with subsequent notation its matrix elements are written

$$p^\mu\psi_{kn}=\sum_{n'}\psi_{kn'}\pi_{n'n}{}^\mu(hk). \quad (18)$$

All of the matrix elements $\pi_{n'n}{}^\mu$ are finite and well-behaved functions of k, so by Eq. (11)

$$p^\mu\psi=\sum_{m,n}\varphi_{mn}(r)\sum_{n'}\pi_{nn'}{}^\mu(p_m)\Psi_{n'}(r_m) \quad (19)$$

in which $h\nabla_m/i$ has been written simply as p_m.

$x^\nu\psi_{kn}$ cannot be written as a simple expansion like Eq. (10), because the matrix elements $x_{nn'}{}^\nu(hk)$ do not all exist. However, a direct evaluation of $x^\nu\varphi_{mn}$ is possible. Clearly

$$x^\nu\varphi_{mn}=x_m{}^\nu\varphi_{mn}+(x^\nu-x_m{}^\nu)\varphi_{mn}. \quad (20)$$

The second term of Eq. (20) can be written

$$(x^\nu-x_m{}^\nu)\varphi_{mn}=[\Delta/(2\pi)^3]^{\frac{1}{2}}\int d^3k(1/i)\frac{\partial}{\partial k^\nu}[e^{-ik\cdot r_m}\psi_{kn}]+[\Delta/(2\pi)^3]\int d^3k e^{ik\cdot r-r_m}i\frac{\partial u_{kn}}{\partial k^\nu}. \quad (21)$$

In Appendix A it is shown that the first integral is zero provided the brillouin zone structure satisfies certain "connectivity" conditions. Assuming these,

$$(x^\nu-x_m{}^\nu)\varphi_{mn}=[\Delta/(2\pi)^3]\int d^3k e^{ik\cdot r-r_m}i(\partial u_{kn}/\partial k^\nu). \quad (22)$$

u_{kn} is a continuous function of k, so the derivatives $\partial u_{kn}/\partial k^\nu$ will exist everywhere. The existence of the derivatives for values of k at the edge of a brillouin zone may be shown by a suitable specification of the limiting processes used in calculating the derivative. Since the functions $u_{kn'}$ for fixed k form an orthonormal complete set of regular functions which are periodic with the periodicity of the lattice, $i\partial u_{kn}/\partial k^\nu$ may be expressed in terms of the $u_{kn'}$.

$$i\partial u_{kn}/\partial k^\nu=\sum_{n'}u_{kn'}\xi_{n'n}{}^\nu(hk). \quad (23)$$

The coefficients $\xi_{n'n}{}^\nu$ may be determined from the differential equation satisfied by u_{kn}.

$$[(h^2/2m)(k+\nabla/i)^2+V_L-E_n{}^0(hk)]u_{kn}=0. \quad (24)$$

Differentiating Eq. (24) by k^ν gives

$$\left[\frac{h^2}{2m}\left(k+\frac{\nabla}{i}\right)^2+V_L-E_n{}^0(hk)\right]i\frac{\partial u_{kn}}{\partial k^\nu}-\frac{1}{i}\left[\frac{h^2}{m}\left(k^\nu+\frac{1}{i}\frac{\partial}{\partial x^\nu}\right)-\frac{\partial E_n{}^0(hk)}{\partial k^\nu}\right]u_{kn}=0. \quad (25)$$

Inserting the expansion Eq. (23) into Eq. (25), multiplying by $u_{kn'}{}^*$, and integrating, gives

$$\xi_{n'n}{}^\nu(hk)=(h/mi)\pi_{n'n}{}^\nu(hk)/[E_{n'}{}^0(hk)-E_n{}^0(hk)] \quad (n'\neq n). \quad (26)$$

$\xi_{nn}{}^\nu(hk)$ cannot be determined by a procedure such as that used above. In Appendix B it is shown that by a proper choice of the relative phases within each band it can be arranged that[12]

$$\xi_{nn}{}^\nu(hk)=0. \quad (27)$$

With the aid of Eqs. (26) and (27), Eq. (22) may be written

$$(x^\nu-x_m{}^\nu)\varphi_{mn}=\sum_{n'}[\Delta/(2\pi)^3]^{\frac{1}{2}}\int d^3k\times e^{-ik\cdot r_m}\psi_{kn'}\xi_{n'n}{}^\nu(hk). \quad (28)$$

Equations (20) and (28) can now be used to obtain an expression for $x^\nu\psi$.

$$x^\nu\psi=\sum_{m,n}\varphi_{mn}(r)x_m{}^\nu\Psi_n(r_m)+\sum_{m,n}\Psi_n(r_m)[\Delta/(2\pi)^3]^{\frac{1}{2}}\times\int d^3k e^{-ik\cdot r_m}\sum_{n'}\psi_{kn'}\xi_{n'n}{}^\nu(hk). \quad (29)$$

[12] *Note added in proof.*—Cases can arise for which the choice of phases described in Appendix B cannot be made for every band. More precisely, if one makes the choice of phase so that $\xi_{nn}{}^\nu=0$, it will be found that the convergence of the Fourier series Eq. (7) is not uniform, so that it cannot be differentiated term by term as was assumed in the text. The nonuniformity of convergence can be removed by a suitable choice of phases, and the theory developed here requires that such a choice be made. The theoretical developments made here are affected only to the extent that $\xi_{nn}{}^\nu$ is no longer to be taken zero, but is now to be a real function of p. While the principal theoretical result as given by Eq. (47) is not changed, changes are required in details of Eqs. (50) and (68). The only qualitative result which is altered in cases for which $\xi_{nn}{}^\nu\neq 0$ is that there are additional terms in Eqs. (1) and (68) which are linear in the fields and which do not involve transitions between bands. These additional terms follow directly from the generally valid Eq. (47) so they need not be given here.

The first term of Eq. (29) is already in the desired form. The second term is of the same form as the expression Eq. (13). The arguments used in Eqs. (12)–(16) may therefore by applied without change. As a result $x^\nu\psi$ can be written in a form very similar to Eq. (11);

$$x^\nu\psi=\sum_{m,n}\varphi_{mn}(r)[x_m{}^\nu\Psi_n(r_m)+\sum_{n'}\xi_{nn'}{}^\nu(p_m)\Psi_{n'}(r_m)]. \tag{30}$$

It may be readily verified that each of the expressions $x^\nu x^\mu$, $x^\nu p^\mu$, $p^\mu x^\nu$ satisfies Eq. (17) *mutatis mutandis*. If the perturbation $V'(p^\mu, x^\nu)$ of Eq. (8) can be developed as a power series in its arguments, then $V'\psi$ can be expressed in terms of operations on the $\Psi_n(r_m)$, through repeated use of Eqs. (17), (18), and (30). The result of this process will be written for the moment as

$$V'(p^\mu, x^\nu)\psi=\sum_{m,n}\varphi_{mn}(r)\sum_{n'}v_{nn'}{}'(p_m, r_m)\Psi_{n'}(r_m). \tag{31}$$

The operator H_0 is clearly such an operator as $\mathcal{O}$ of Eq. (10). The Schroedinger equation,

$$[H-i\hbar\partial/\partial t]\psi=0 \tag{32}$$

with H given by Eq. (8) can therefore be written

$$\sum_{m,n}\varphi_{mn}(r)[E_n{}^0(p_m)\Psi_n(r_m)$$
$$+\sum_{n'}v_{nn'}{}'(p_m, r_m)\Psi_{n'}(r_m)-i\hbar\partial\Psi_n(r_m)/\partial t]=0. \tag{33}$$

The φ_{mn} are independent functions, so Eq. (33) will hold only if Eq. (34) is satisfied for all r_m.

$$E_n{}^0(p_m)\Psi_n(r_m)+\sum_{n'}v_{nn'}{}'(p_m, r_m)\Psi_{n'}(r_m)$$
$$-i\hbar\partial\Psi_n(r_m)/\partial t=0. \tag{34}$$

Eq. (34) is the generalized form of the Wannier equation.

The differential relation Eq. (34) must be satisfied at each of the points r_m but not necessarily at other points. Even if one specified some kind of boundary conditions, these, together with Eq. (34) would not be sufficient to determine the $\Psi_n(r_m)$. In order to see what kind of additional conditions are necessary, consider the case that $\psi^{(i)}$ is one of the eigenstates of the perturbed hamiltonian. If the "right linear combinations" are made of wave functions belonging to degenerate energy levels, then the $\psi^{(i)}$ will satisfy

$$(\psi^{(i)}, \psi^{(j)})=\delta_{ij} \tag{35}$$

in which the single label i denotes a complete labeling of an energy state. Equation (35) leads to the additional conditions on the $\Psi_n{}^{(i)}(r_m)$

$$\sum_{m,n}\Psi_n{}^{*(i)}(r_m)\Psi_n{}^{(j)}(r_m)=\delta_{ij}. \tag{36}$$

Equation (34) becomes

$$E_n{}^0(p_m)\Psi_n{}^{(i)}(r_m)+\sum_{n'}v_{nn'}{}'(p_m, r_m)\Psi_{n'}{}^{(i)}(r_m)$$
$$-E^{(i)}\Psi_n{}^{(i)}(r_m)=0. \tag{34a}$$

Equations (34a) and Eq. (36) comprise all of the conditions which the $\Psi_n{}^{(i)}(r_m)$ must satisfy, so together they constitute a specification of the eigenvalue problem for the perturbed hamiltonian. In principle Eqs. (34a) and (36) determine the manner in which the $\Psi_n(r)$ must be defined at points other than the r_m. Actually, the condition Eq. (36) is particularly awkward to satisfy, and it is not easy to see how solution which satisfy it can be found in a systematic way. This question will be taken up in a later section, where the fundamental approximation of the Wannier method is discussed.

II

The results of Sec. I can be put into a rather convenient form by the introduction of a simple matrix notation. A multicomponent function $\mathbf{\Psi}(r_m)$ is introduced which has the component $\Psi_n(r_m)$ in the nth band.

$$\mathbf{\Psi}(r_m)=\begin{pmatrix}\Psi_1(r_m)\\ \Psi_2(r_m)\\ \vdots\end{pmatrix}. \tag{37}$$

Operators $\tau_{nn'}$ are defined with matrix elements

$$(\tau_{nn'})_{n''n'''}=\delta_{nn''}\delta_{n'n'''}. \tag{38}$$

According to Eq. (38) $\tau_{nn'}$ is a matrix which has only one nonvanishing matrix element. When applied to $\mathbf{\Psi}(r_m)$ it annihilates all components of $\mathbf{\Psi}(r_m)$ except the component in the n'th band, and transfers this surviving component to the position of the component belonging to the nth band. The algebra of the $\tau_{nn'}$ is contained in the equation,

$$\tau_{nn''}\tau_{n'''n'}=\tau_{nn'}\delta_{n''n'''}. \tag{39}$$

It is convenient to use the terminology that an operator $\mathcal{O}$ which operates on ψ is represented by an operator $\boldsymbol{O}$ which operates on $\mathbf{\Psi}(r_m)$. For example, the operator $\mathcal{O}$ of Eq. (10) would be represented by

$$\boldsymbol{O}(p_m)=\sum_{n,n'}\tau_{nn'}\mathcal{O}_{nn'}(p_m) \tag{40}$$

and Eq. (11) could be expressed as

$$\mathcal{O}\psi\rightarrow\boldsymbol{O}\mathbf{\Psi}(r_m). \tag{41}$$

It is useful to have a separate designation for each of the following operators:

$$\begin{aligned}
&\pi_n{}^\mu\equiv\sum_n\tau_{nn}\pi_{nn}{}^\mu(p_m),\\
&\pi'^\mu\equiv\sum_{n,n'\neq n}\tau_{nn'}\pi_{nn'}{}^\mu(p_m),\\
&\pi^\mu\equiv\pi_n{}^\mu+\pi'^\mu,\\
&\xi'^\nu\equiv\sum_{n,n'}\tau_{nn'}\xi_{nn'}{}^\nu(p_m),\\
&\xi^\nu\equiv x_m{}^\nu+\xi'^\nu,\\
&\mathbf{E}\equiv\sum_n\tau_{nn}E_n{}^0(p_m).
\end{aligned} \tag{42}$$

Each of the terms in the hamiltonian Eq. (8) is repre-

sented in a simple way by means of the operators Eq. (42).

$$\begin{aligned} p^\mu\psi &\rightarrow \pi^\mu\Psi(r_m), \\ x^\nu\psi &\rightarrow \xi^\nu\Psi(r_m), \\ H_0\psi &\rightarrow \mathbf{E}\Psi(r_m), \end{aligned} \tag{43}$$

$$V'(p^\mu, x^\nu)\psi \rightarrow \mathbf{V}'\Psi(r_m) \equiv V'(\pi^\mu, \xi^\nu)\Psi(r_m).$$

The last of the Eqs. (43) shows how the $v_{nn'}'(p_m, r_m)$ of Eq. (31) are to be found. The equation is obtained by simply putting back together the assumed power series development of $V'(p^\mu, x^\nu)$. In terms of the operators defined by Eqs. (42), the generalized Wannier equation Eq. (34) becomes simply

$$[\mathbf{E}+V'(\pi^\mu, \xi^\nu)-i\hbar\partial/\partial t]\Psi(r_m)=0. \tag{44}$$

It is worthwhile to write down several useful relations. One is the set of commutation rules

$$[\pi^\mu, \xi^\nu]=(\hbar/i)\delta_{\mu\nu}\equiv(\hbar/i)\delta_{\mu\nu}\textstyle\sum_n \tau_{nn} \tag{45a}$$

which follows from the fact that $[\pi^\mu, \xi^\nu]$ represents $[p^\mu, x^\nu]$ by Eq. (17). If Eq. (45a) is written out in terms of the $\tau_{nn'}$, it is seen that the equality of coefficients of τ_{nn} is just a statement of the f sum rule in the usual form.

$$\sum_{n'\neq n}\frac{2}{m}\frac{\pi_{nn'^\mu}\pi_{n'n}{}^\mu}{[E_{n'}{}^0-E_n{}^0]}=1-m\frac{\partial^2 E_n{}^0}{\partial p^{\mu 2}}.$$

It may be noted that in this proof of the f sum rule it is unnecessary to employ the device[4] ordinarily used of forming wave packets which are later made infinitely sharp. Other useful commutation rules are

$$(i/\hbar)[\mathbf{E}, \xi^\mu]=(1/m)\pi^\mu, \tag{45b}$$

$$(i/\hbar)[\mathbf{E}, x_m{}^\mu]=\textstyle\sum_n \tau_{nn}[\partial E_n{}^0(p_m)/\partial p_m{}^\mu]=(1/m)\pi_m{}^\mu. \tag{45c}$$

III

In the notation of Sec. II Eqs. (34a) and (36) become

$$[\mathbf{E}(p_m)+V'(\pi^\mu, \xi^\nu)-E^{(i)}]\Psi^{(i)}(r_m)=0, \tag{46a}$$

$$\textstyle\sum_m(\Psi^{(i)}(r_m), \Psi^{(j)}(r_m))=\delta_{ij}. \tag{46b}$$

The solution of Eqs. (46) would provide rigorous solutions of the Schroedinger equation. However, the mathematical structure of the problem presents great difficulty. While it is possible to devise procedures which define $\Psi^{(i)}(r)$ for all values of its argument in such a manner that Eq. (46a) is satisfied at all lattice points, it is not clear that there exists a systematic way of insuring that Eq. (46b) is simultaneously satisfied.

These difficulties can be avoided by making an approximation which, although it places limitations on the perturbations which can be treated, permits the problem to be solved by standard methods. The approximation which effects the simplification is to replace the condition Eq. (46b) by the condition,

$$\int d^3r_m(\Psi^{(i)}(r_m), \Psi^{(j)}(r_m))=\delta_{ij}$$

or, in the usual scalar product notation,

$$(\Psi^{(i)}, \Psi^{(j)})=\delta_{ij}. \tag{46b'}$$

The advantage of the condition Eq. (46b') is that it will be satisfied automatically, provided only that Eq. (46a) is required to hold at every point. Thus the problem is reduced to that of solving the self adjoint coupled differential equations Eq. (46a), which are of a familiar type.

The assumption of Eq. (46b') instead of Eq. (46b) is to be regarded as the basic approximation of the Wannier method. No attempt will be made in this paper to obtain a set of quantitative criteria as to the error made by this approximation. However, a brief investigation makes it seem likely that the approximation is a good one provided that no strongly localized bound states exist. In any particular case the errors can be investigated on the basis of the Eqs. (46) themselves.

The basic approximation is to treat the amplitude $\Psi(r)$ as an actual wave function. Sums over r_m are replaced by integrals, so the subscripts $_m$ are no longer necessary and will be dropped henceforth. The condition Eq. (46b') needs no longer to be written down explicitly, since it will be satisfied automatically, provided that standard boundary conditions are required of Ψ. Thus the problem has now been reduced to that of solving the equation:

$$[\mathbf{E}(p)+V'(\pi^\mu(p), \xi^\nu(p, x))-i\hbar\partial/\partial t]\Psi(r)=0 \tag{47}$$

subject to standard boundary conditions on Ψ.

Equation (47) is to be applied to problems for which the solution functions extend over regions of dimension large compared to the dimension d of a unit cell. It may be expected that in such problems effects due to variation of the potential across a unit cell are small and could be taken into account by perturbation theory. It will now be seen how these variations can be treated as perturbations.

Consider a problem for which

$$V'=\phi(\xi^\nu) \tag{48}$$

and write the arguments of ϕ as

$$\phi(\xi^\nu)=\phi(x^\nu+\xi^\nu). \tag{49a}$$

The operator ξ^ν has eigenvalues which are usually of the order of magnitude d or smaller (the exceptional case arises in the model of very weak interaction for which case ξ^ν may have larger eigenvalues corresponding to states very near the face of the brillouin zone). There-

[4] A. Sommerfeld and H. Bethe, *Handbuch der Physik* (Verlag. Julius Springer, Berlin, 1933), **24**, 2, 376.

fore it is possible to develop $\phi(x^\nu+\xi^\nu)$ in powers of the ξ^ν and to ignore all but the lowest order terms. Henceforth the convention is used that where repeated Greek indices occur a summation is to be understood. With this understanding

$$\phi(\xi^\nu)=\phi(x^\nu)+(1/2)\{\xi^\mu,\ \partial\phi(x^\nu)/\partial x^\mu\}+\cdots. \quad (49b)$$

The curly brackets signify the anticommutator. Anticommutators[5] are necessary to make the linear and higher terms hermitian, since the ξ^ν are functions of the p^μ and do not commute with the x^λ.

In terms of the expansion Eq. (49b) it is possible to make a quantitative criterion as to the approximation involved in the Wannier Eq. (1). If all terms of Eq. (49b) involving the ξ^μ may be neglected with respect to $\phi(x^\nu)$, Eq. (47) becomes

$$[\mathbf{E}(p)+\phi(x^\nu)-i\hbar\partial/\partial t]\mathbf{\Psi}^*=0. \quad (50)$$

The bracketed operator in Eq. (50) has no matrix elements between bands, so Eq. (50) is just Eq. (1) written in the multiband notation. If the term in ξ^μ must be taken into account, the resulting equation cannot conveniently be expressed without the multicomponent $\mathbf{\Psi}^*$, for the linear term $\frac{1}{2}\{\xi^\mu,\ \partial\phi(x^\nu)/\partial x^\mu\}$ has nonvanishing matrix elements only between bands. The nondiagonal character of the linear term has the result that the corrections to Eq. (1) due to transitions between bands affect the equation of motion within a band only in the second order of powers of the ξ^μ. An examination of Eq. (28) of Sec. I shows that the expansion Eq. (49b) in powers of ξ^μ is equivalent to an expansion in powers of $(x^\mu-x_m^\mu)$, which is the natural form for correction terms in the Wannier theory. Since the basic approximation made in Eqs. (46) is expected to be best justified when the expansion converges rapidly, the expansion Eq. (49b) is a particularly convenient one from the standpoint of perturbation theory.

The motion of an electron in a constant electric field will serve to illustrate the application of the ideas of this section. The equation of motion Eq. (50) is

$$[\mathbf{E}(p)+e\mathcal{E}^\mu x^\mu+e\mathcal{E}^\mu\xi^\mu-i\hbar\partial/\partial t]\mathbf{\Psi}^*=0. \quad (51)$$

Suppose that the term $e\mathcal{E}^\mu\xi^\mu$ may be treated as a perturbation, and that initially the electron is in a plane wave state $e^{ik\cdot r}$. A solution to the zero order equation is

$$\Psi_n(r,t)=c_n\exp\left\{i(k-e\mathcal{E}t/\hbar)\cdot r - (i/\hbar)\int_0^t E_n^0(\hbar k-e\mathcal{E}\tau)d\tau\right\} \quad (52)$$

as is easily verified. Equation (52) expresses the well known result[6] that the electron is accelerated so that its "pseudo momentum" satisfies the classical equation for the change of momentum of a free particle in the constant force field. By means of Eqs. (9) and (7) it can be seen that $\mathbf{\Psi}^*$ given by Eq. (52) describes a motion from one Bloch state to another so that the electron moves across the brillouin zone in a direction parallel to the electric field. At the face of a brillouin zone reflection occurs because of the identity of ψ_{kjm} and $\psi_{kj'n}$. (See Appendix A.)

If the linear term of Eq. (51) is taken into account, transitions between bands will result. Assuming that initially the electron is in band n_0, the wave functions may be written in the form

$$\Psi_n(r,t)=c_n(t)\exp\left\{ik(t)\cdot r-(i/\hbar)\int_0^t E_n^0(\hbar k(\tau))d\tau\right\} \quad (53)$$

with

$$k(t)=k-e\mathcal{E}t/\hbar;\quad c_n(0)=\delta_{nn_0}.$$

Inserting (53) in (51), and considering times so short that $|c_n|^2\ll 1$ $(n\neq n_0)$,

$$i\hbar\dot{c}_n(t)=e\mathcal{E}^\mu\xi_{nn_0}^\mu(\hbar k(t)c_{n_0}(t)\times\exp\left\{(i/\hbar)\int_0^t[E_n^0(k(\tau))-E_{n_0}^0(k(\tau))]d\tau\right\}. \quad (54)$$

In the case that transitions are relatively improbable, the electron can make a complete transit of the brillouin zone with small chance of excitation. The time of transit is given by $T=\hbar k_f/e\mathcal{E}$ for motion perpendicular to a face. $c_n(T)$ is given by

$$c_n(T)\doteq\int_0^T dt(e\mathcal{E}^\mu\xi_{nn_0}^\mu(\hbar k(t))/i\hbar)\times\exp\left\{(i/\hbar)\int_0^t[E_n^0(k(\tau))-E_{n_0}^0(k(\tau))]d\tau\right\}. \quad (55)$$

Zener[7] and Houston[8] have evaluated the integral (55) according to the simple model of weak interaction, and interpreted the resulting transition probability per cycle, $|c_n(T)|^2$, in terms of dielectric breakdown in high electric fields.

IV

If the perturbation $\mathbf{V}'$ of Eq. (47) depends on the π^μ, Eq. (1) does not apply. That is to say the Wannier Eq. (1) cannot be used to treat a problem involving a perturbation such as that due to a magnetic field. However, Luttinger[9] has derived a form for Eq. (1) which extends the one band Wannier equation to include the effect of the magnetic field perturbation.

[5] In addition to the anticommutators, the expansion Eq. (49b) contains terms which involve commutators of various powers of the ξ^μ with powers of the x^ν. While some of these commutators arise from the term linear in ξ^μ, they all are terms of higher order, since, e.g., $\partial\xi^\mu/\partial p^\nu\sim O(\xi^\mu\xi^\nu)$. Thus Eq. (49b) displays all of the first order terms.

[6] See reference 1 for a list of published derivations.

[7] C. Zener, Proc. Roy. Soc. (London) **145**, 523 (1934).

[8] W. V. Houston, Phys. Rev. **57**, 184 (1940). Houston's treatment is very similar to the treatment which is most natural from the viewpoint of this paper.

[9] Phys. Rev. **84**, 814 (1951). I am indebted to Dr. Luttinger for pointing out the advantages of the gauge transformation used in this section.

Equation (47) includes the magnetic perturbation as a special case. However, the form of the perturbation does not permit a distinction between effects which lead to transitions between bands and effects which simply lead to motion within a given band. The confusion of effects arises partly from the arbitrariness allowed in the gauging of the vector potential and partly from the peculiar relation between velocity and momentum in the presence of magnetic fields. It is the purpose of this section to describe a unitary transformation which disentangles the two kinds of effect and transforms the Wannier Eq. (47) to a form which is more simply understood. While the simplified form obtained is strictly correct only if the magnetic field is constant, it will be clear how to construct a transformation to a similar form if the variation of the magnetic field with position is not so slow as to be negligible. It will be shown that the transformed Eq. (47) yields Luttinger's form of Eq. (1) as a zero order approximation in which all transitions between bands are neglected.

For the case to be discussed Eq. (47) becomes

$$[\mathbf{E}(p)+(e/2mc)\{\mathbf{A}^\mu, \pi^\mu\}+(e^2/2mc^2)\mathbf{A}^\mu\mathbf{A}^\mu - e\phi(\xi^\nu)-ih\partial/\partial t]\Psi^\nu=0. \quad (56)$$

Beginning with Eq. (56) the convention is made that

$$\mathbf{A}^\mu\equiv A^\mu(\xi^\nu), \quad A^\mu\equiv A^\mu(x^\nu). \quad (57)$$

The anticommutator is written because it is not assumed that $\partial\mathbf{A}^\mu/\partial x^\mu=0$. Both $\mathbf{A}^\mu$ and π^μ have nondiagonal matrix elements, i.e., matrix elements connecting states in different bands. Since the nondiagonal part of π^μ is in general large, the term which is linear in e involves particularly strong coupling of bands wherever $\mathbf{A}^\mu$ is large. At least part of this coupling of bands is only apparent and leads to no admixture of the real energy bands, for the magnitude of the vector potential does not affect the energies of states. The coupling terms are readily altered by means of gauge transformations. The unitary transformation

$$U=\exp(iS/h), \quad S=(e/c)\mathbf{G}\equiv(e/c)G(\xi^\nu) \quad (58)$$

transforms Eq. (56) to

$$\left[\mathbf{E}(p)+\frac{e}{2mc}\left\{\mathbf{A}^\mu-\frac{\partial\mathbf{G}}{\partial x^\mu}, \pi^\mu\right\} +\frac{e^2}{2mc^2}\left(\mathbf{A}^\mu-\frac{\partial\mathbf{G}}{\partial x^\mu}\right)\left(\mathbf{A}^\mu-\frac{\partial\mathbf{G}}{\partial x^\mu}\right) -e\phi(\xi^\nu)-\frac{e}{c}\frac{\partial\mathbf{G}}{\partial t}-ih\frac{\partial}{\partial t}\right]\Psi^\nu=0. \quad (59)$$

Equation (59) may be established with the aid of the commutation rules Eqs. (45) and the expansion

$$u\mathbf{H}u^{-1}=\mathbf{H}+(i/h)[S, \mathbf{H}] +(1/2!)(i/h)[S, [S, \mathbf{H}]]+\cdots. \quad (60)$$

A comparison of Eqs. (56) and (59) shows that the transformation (58) is a gauge transformation

$$A^\mu\rightarrow A^\mu-\partial G/\partial x^\mu, \quad \phi\rightarrow\phi+(1/c)\partial G/\partial t. \quad (61)$$

The first step in reducing the coupling between bands is to make a gauge transformation which removes any superfluous coupling due to the permissible arbitrariness of the vector potential. The gauge transformation is accomplished with the aid of the transformation function

$$S_0=(e/c)\int_0^1 d\lambda\xi^\mu A^\mu(\lambda\xi^\nu). \quad (62a)$$

It can be verified[9] that

$$\partial S_0/\partial x^\mu=(e/c)[\mathbf{A}^\mu-\mathbf{A}_1{}^\mu],$$

$$\mathbf{A}_1{}^\mu\equiv-\int_0^1 d\lambda\lambda[\xi\times\mathfrak{K}(\lambda\xi^\nu)]^\mu. \quad (62b)$$

In subsequent equations the term $(e/c)\partial\mathbf{G}/\partial t$ of Eq. (59) will be omitted for brevity, since its treatment presents no particular problem. Then according to Eq. (59), the unitary transformation Eq. (58) with S_0 given by Eq. (62) transforms the Wannier equation to the form

$$[\mathbf{E}+(e/2mc)\{\mathbf{A}_1{}^\mu, \pi^\mu\}+(e^2/2mc^2)\mathbf{A}_1{}^\mu\mathbf{A}_1{}^\mu - e\phi(\xi^\nu)-ih\partial/\partial t]\Psi^\nu=0. \quad (63)$$

Equation (63) still contains terms which provide strong couplings between bands, inasmuch as $\mathbf{A}_1{}^\mu$ is proportional to the ξ^ν, which become large. This coupling cannot be eliminated by a gauge transformation, since the magnetic field cannot be gauged away. However, on the basis of the considerations discussed at the beginning of the section, it should be possible to transform away all couplings which depend on the magnitude of $A_1{}^\mu$ and leave only couplings proportional to the fields and their derivatives. The required transformation S_1 was not found in a simple closed form. Instead S_1 was developed as a power series in e and the successive terms determined as in perturbation theory. In Appendix C two transformations, S_1 and S_2, are given. The transformation S_1 removes to the second order in e all coupling terms which involve $A_1{}^\mu$. The transformation S_2 removes to the third order in e all coupling terms which involve $A_1{}^\mu$, but not products of $A_1{}^\mu$ by the fields. A comparison of the two transformations illustrates the procedure for finding by trial and error a transformation which eliminates superflous coupling terms to an additional order in e. To eliminate completely the unwanted couplings to third order one would have to add to S_2 terms involving $A_1{}^\mu A_1{}^\nu\partial A_1{}^\lambda/\partial x^\sigma$ and then terms involving $A_1{}^\mu(\partial A_1{}^\nu/\partial x^\sigma)(\partial A_1{}^\lambda/\partial x^\rho)$, choosing the added terms to eliminate the undesired couplings. Thus the transformation is carried to higher order by first transforming away the powers of $A_1{}^\mu$,

and then the products of powers of $A_1{}^\mu$ by increasing powers of the fields.

The unitary transformation with S_1 given by Eq. (C-1) is used to transform Eq. (63). The result, correct to second order in e, is that the transformed Ψ' satisfies

$$[\{\mathbf{E}(p)+(e/2mc)(\partial A_1{}^\nu/\partial x^\mu)(\{\xi^\mu(p),\pi^\nu(p)\}+\{\pi_n{}^\nu(p),\xi^\mu(p)\}-\{\pi_n{}^\mu(p),\xi^\nu(p)\})-e(\partial\phi/\partial x^\mu)\xi^\mu(p)\}^{p\to p+(e/c)A_1}-e\phi(x^\nu)+\mathcal{O}_2(e^2)-ih\partial/\partial t]\Psi'=0. \quad (64)$$

The second-order terms $\mathcal{O}_2(e^2)$ are given in Appendix C. It should be repeated that Eq. (64) was obtained in the approximation that derivatives of the magnetic and electric fields could be neglected. If these derivatives could not be neglected, more terms would have to be added to S_1 and more coupling terms would occur in Eq. (64). Since the additional complications would add nothing to the exposition of the procedure, they were avoided. In Eq. (64) the factors $\partial A_1{}^\nu/\partial x^\mu$ which occur are components of the magnetic field, so the coupling between bands due to the magnetic perturbation has been expressed in terms of the magnetic field. The operators $\mathbf{E}$, π^μ, ξ^ν, which formerly were functions of p are now the same functions of $p+(e/c)A_1$.

As a final step the Wannier function Ψ' is subjected to a unitary transformation generated by

$$S_3=-(e/c)\int_0^1 d\lambda x^\mu A^\mu(\lambda x^\nu). \quad (65)$$

The only effect of the transformation S_3 is to replace

$$p^\mu+eA_1{}^\mu/c\to p^\mu+eA^\mu/c \quad (66)$$

as is seen from Eq. (62).

After the successive transformations Eqs. (62), (C-1), and (65) have been carried out the Wannier function Ψ' is found to satisfy the equation,

$$[\mathbf{E}(p+eA/c)-e\phi(x)-ih\partial/\partial t+\{(e/2mc)(\partial A_1{}^\nu/\partial x^\mu)\times(\{\pi^\nu,\xi^\mu\}+\{\pi_n{}^\nu,\xi^\mu\}-\{\pi_n{}^\mu,\xi^\nu\})-e(\partial\phi/\partial x^\mu)\xi^\mu\}^{p\to p+eA/c}+\mathcal{O}_2(e^2)+\cdots]\Psi'=0. \quad (67)$$

It is worthwhile to remark on the manner in which the transformation S_1 accomplishes the decoupling of states in different bands. The details of the form of the terms in S_1 suggest that what is done is equivalent to a correction to second order of the Bloch functions, which were used to construct the basic φ_{mn}. However, the procedure employed here is considerably simpler than that of modifying the ψ_{kn} to take account of the magnetic perturbation. In the first place, the Wannier formalism avoids any necessity for the elaborate treatment required to handle divergent integrals which arise if the perturbation theory is carried out using Bloch functions as the basic functions. In the second place the perturbation theory is carried out explicitly only to the extent necessary to effect the decoupling of states in different bands, no reference needs to be made to energy states, and the result of the perturbation corrections is expressed simply in terms of a change in the differential equations which the components $\Psi_n(r)$ must satisfy.

Several comments may be made concerning the terms in Eq. (67). In the first place, the powers of the $\partial A_1{}^\nu/\partial x^\mu$ occur together with corresponding powers of ξ^λ. This implies that transitions between bands arise only because of the interplay of various forces on the electron within a unit cell. For ordinary magnetic fields an expansion in powers of $(\partial A_1{}^\nu/\partial x^\mu)\xi^\lambda$ should converge rapidly. The term linear in e can be seen to be simply the nondiagonal matrix element of the orbital angular momentum about the origin of the unit cell together with an electric field term discussed in the previous section. Because of its nondiagonal character, the linear term affects the motion within a band only in second order. The quadratic terms describe various double transition processes. It is interesting that one of the terms contains the products of electric and magnetic field strengths. If all terms involving transitions between bands are dropped from Eq. (67), it reduces to

$$[\mathbf{E}(p+eA/c)-e\phi(x^\nu)-ih\partial/\partial t]\Psi'=0. \quad (68)$$

Equation (68) is Luttinger's form of Eq. (1), expressed in the many band notation. The equation is gauge invariant against gauge transformations with

$$S=(e/c)G(x^\nu).$$

Equation (68) may be used to derive several results which are well known in the theory of periodic potentials.

$$\dot{x}^\mu=(i/h)[\mathbf{H},x^\mu]=(i/h)[\mathbf{E}(p+eA/c)-e\phi,x^\mu]=\partial\mathbf{E}(p+eA/c)/\partial p^\mu=(1/m)\pi_n{}^\mu(p+eA/c), \quad (69a)$$

$$\dot{p}^\mu+\frac{e\dot{A}^\mu}{c}=(i/h)[\mathbf{H},p^\mu+eA^\mu/c]=e\partial\phi/\partial x^\mu-(e/c)[\dot{x}\times\mathfrak{H}]^\mu, \quad (69b)$$

$$\ddot{x}^\mu=(i/mh)[\mathbf{H},\pi_n{}^\mu(p+eA/c)]=e\frac{\partial\phi}{\partial x^\nu}\frac{\partial^2\mathbf{E}(p+eA/c)}{\partial p^\mu\partial p^\nu}+(i/mh)[\mathbf{E}(p+e/cA),\pi_n{}^\mu(p+eA/c)]. \quad (69c)$$

Equation (69b) shows that the "crystal kinetic momentum" is changed by the field according to the Lorentz equation, provided that the "crystal velocity" replaces the velocity in the Lorentz equation. Because of the noncommutability of the components $p^\mu+eA^\mu/c$, there are no eigenstates of $p^\mu+eA^\mu/c$; however, wave packets may be constructed for which $p^\mu+eA^\mu/c$ is nearly sharp, and Eq. (69b) then describes the motion of such a packet. The first term of Eq. (69c), in which $\partial\phi/\partial x^\nu$ has been treated as almost constant, shows that the "acceleration" of the electron by an electric field is the same as for a free particle with the "effective mass"

tensor

$$(1/m_{eff})^{\mu\nu}=\frac{\partial^2\mathbf{E}(p+eA/c)}{\partial p^\mu \partial p^\nu}. \tag{70}$$

An examination of the commutator (69c) shows that an equivalent result holds for the "acceleration" in a magnetic field. Because of the possible dependence of $\pi_n{}^\mu$ on higher powers of $p+eA/c$, no simple form for the second term can be written in general. However, in the case that the energy $\mathbf{E}$ may be approximated as a quadratic function of the "crystal momentum"

$$\mathbf{E}(p+eA/c)=(1/2m_{eff})^{\mu\nu}(p^\mu+eA^\mu/c)(p^\nu+eA^\nu/c) \tag{71}$$

the usual result[10] can be obtained explicitly:

$$\begin{aligned}\dot{x}^\mu&=(1/m_{eff})^{\mu\nu}(p^\nu+eA^\nu/c),\\ \dot{\pi}^\mu&=(1/m_{eff})^{\mu\nu}[e\partial\phi/\partial x^\nu-(e/c)[\dot{x}\times\mathfrak{IC}]^\nu].\end{aligned} \tag{72}$$

Equations (69)–(72) apply to the motion of wave packets in the perturbed periodic potential, and have been previously derived by a number of methods.[11] Equation (67), however, can be used to treat the motion of the electron in a higher approximation than the semiclassical wave packet limit. For example, Eq. (67) can be applied to the problem of finding the energy levels of an electron in a periodic potential perturbed by the vector potential of an external magnetic field, a problem which cannot be discussed using wave packets since the energy of a wave packet is not sharp. For attacking this difficult problem, Eq. (67) would appear to be the most promising weapon hitherto proposed.

V

Slater[1] has discussed a number of problems for which the Wannier equation provides a valuable expository device. With the developments made in the present work the range of applicability of the equation has been broadened. An important problem to which the present form of the theory may be applied is that of the perturbation of the periodic potential by the elastic vibrations of the lattice. It must be admitted that such an application of the theory requires a model of the solid state which is too crude to be considered a good description of the actual physical situation in a solid body. However, even very crude models have provided useful insights into the processes taking place in solids, so it is worthwhile to investigate such a model if there is reason is reason to believe that it incorporates the essential features of the mechanism which is to be investigated.

No detailed application to a problem in which lattice vibrations play a role will be made in this paper. However, it will be pointed out that the form of the Wannier equation developed here can be readily applied to the problem if the "deformable potential" model[12] is assumed for the interaction between electrons and elastic waves. On this model the perturbative potential in the Wannier equation is one which can be expressed in terms of the π^μ, the quantized amplitudes for the vibration field, and plane wave factors, by means of such relations as

$$(\partial V_L/\partial x^\mu)\psi\rightarrow(i/\hbar)[\pi^\mu,\mathbf{E}]\Psi. \tag{73}$$

Using approximation procedures like those of Sec. III it is then possible to separate effects leading to motion within a band and effects which admix states in different bands. *Umklapp* processes can be treated in a straightforward manner. Thus within the limitations of the "deformable potential" model, the main features of the electron-phonon interaction can be studied, taking account of the modification of free electron behavior due to the crystal periodicity. An example of a problem to which the present method seems particularly well adapted is the determination of the perturbing effect of phonon waves on electron states located at or near the face of a brillouin zone.

ACKNOWLEDGMENTS

The writer would like to express his appreciation to Dr. Irving Isenberg for helpful discussions of the work presented here, to Dr. George Parzen, Dr. M. L. Goldberger, Professor G. Wentzel, and Professor Clarence Zener for discussions of particular points, and to Dr. J. M. Luttinger for communicating the results of his work before publication.

APPENDIX A

The integral

$$\int d^3k(1/i)(\partial/\partial k^\nu)[e^{-ik\cdot r}u_{kn}]$$

can be transformed to a surface integral over the faces of the brillouin zone

$$(1/i)\int dS_\nu(k)e^{-ik\cdot r}u_{kn}. \tag{A-1}$$

Consider a face f of the zone, which is associated to a vector K_f of the reciprocal lattice. A point k_f on the face f satisfies

$$(k_f-1/2K_f)\cdot K_f=0. \tag{A-2}$$

For every vector k_f there is a vector k_f' which is "connected" to k_f by K_f

$$k_f'=k_f-K_f. \tag{A-3}$$

It will be shown that

$$u_{k_f'n}=u_{k_fn}. \tag{A-4}$$

Equation (A-4) follows immediately from Eqs. (4) and

[10] F. Seitz, *Modern Theory of Solids* (McGraw-Hill Book Company, Inc., New York, 1940), p. 317. Note that the argument used here tells nothing about the acceleration in a magnetic field, since $v\cdot v\times\mathfrak{IC}=0$.

[11] W. Shockley, *Electrons and Holes in Semiconductors* (D. Van Nostrand Company, Inc., New York, 1950), Sec. 15.6 of this book contains references to a number of the published proofs of these equations. See also the footnotes of reference 1.

[12] See reference 4, p. 506.

(7) for

$$\psi_{kfn}=[\Delta/(2\pi)^3]^{\frac{1}{2}}\sum_m \exp(ik_f\cdot r_m)\varphi_{mn}$$
$$=[\Delta/(2\pi)^3]^{\frac{1}{2}}\sum_m \exp(iK_f\cdot r_m)\exp(ik_f'\cdot r_m)\varphi_{mn}=\psi_{kf'n}.$$

It should be remarked that the formalism of this paper depends just on the fact that ψ_{kfn} is "connected" to a state $\psi_{kf'n}$, that is, a state in the same band. In the three-dimensional case it seems that other connections are possible when the bands overlap. Therefore it will be regarded as one of the assumptions of this paper that even though the bands overlap, states which are "connected" by a reciprocal lattice vector are not degenerate unless they are in the same band. It is only when this condition is fulfilled that the subscript n on the φ_{mn} has an unambiguous meaning.

Consider now the contribution to the integral (A-1) of an area $dS_\nu(k_f)$ on the face f. This contribution is

$$dS_\nu(k_f)\exp(-ik_f\cdot r_m)\psi_{kn}. \tag{A-5a}$$

There is a contribution from the corresponding area $dS_\nu(k_f')$ on the parallel face $-f$, which is associated to the vector $-K_f$.

$$dS_\nu(k_f')\exp(-ik_f'\cdot r_m). \tag{A-5b}$$

By Eq. (4) of the text

$$\exp(ik_f\cdot r_m)=\exp(ik_f'\cdot r_m)$$

while by Eq. (A-4),

$$\psi_{kfn}=\psi_{kf'n}.$$

Since the two faces are parallel, the ν components of their normals are of equal magnitude and opposite sign. Thus the contributions (A-6a) and (A-6b) cancel one another. It follows immediately that the integral (A-1) vanishes.

APPENDIX B

The integral

$$I_{kn}{}^\nu\equiv i\int_\Delta u_{kn}{}^*(\partial u_{kn}/\partial k^\nu)d^3x \tag{B-1}$$

is real, as can be seen by taking its complex conjugate and using the normalization condition

$$\int_\Delta u_{kn}{}^*u_{kn}d^3x=0. \tag{B-2}$$

Define $\tilde{u}_{kn}$ by the choice of phases

$$\tilde{u}_{kn}=\exp[i\eta_n(k)]u_{kn}. \tag{B-3}$$

Then

$$\tilde{I}_{kn}{}^\nu=I_{kn}{}^\nu-\partial\eta_n(k)/\partial k^\nu. \tag{B-4}$$

The phase function $\eta_n(k)$ can be chosen to make $\tilde{I}_{kn}{}^\nu=0$ provided that $I_{kn}{}^\nu$ is the gradient of a function of k. That $I_{kn}{}^\nu$ is a gradient may be established by showing that its curl is zero. Thus

$$\mathrm{curl}_k\mathbf{I}_{kn}=i\int_\Delta(\nabla_k u_{kn}{}^*)\times(\nabla_k u_{kn})d^3x. \tag{B-5}$$

Now $i\nabla_k$ is a hermitian operator all of whose matrix elements exist, so it follows that

$$i\nabla_k u_{kn}=\sum_{n'}u_{kn'}\langle n'|\,i\nabla_k\,|n\rangle. \tag{B-6}$$

Inserting (B-6) in (B-5)

$$\mathrm{curl}_k\mathbf{I}_{kn}=i\sum_{n'}\langle n|\,i\nabla_k\,|n'\rangle\langle n'|\,i\nabla_k\,|n\rangle$$
$$=i\langle n|\,i\nabla_k\times i\nabla_k\,|n\rangle. \tag{B-7}$$

Since the components of $i\nabla_k$ commute, the expression on the right hand side of Eq. (B-7) vanishes. From the vanishing of (B-7) it follows that $I_{kn}{}^\nu$ is the gradient of a function of k; taking this function to be the $\eta_n(k)$ of Eq. (B-4) gives the result that $\tilde{I}_{kn}{}^\nu$ vanishes. If then the basic Bloch functions are defined in terms of the $\tilde{u}_{kn}$ rather than the u_{kn}, the integral (B-1) vanishes. This choice determines all relative phases within a band.

APPENDIX C

The transformation which to second order in e removes all coupling terms in $A_1{}^\mu$ is

$$S_1=(e/2c)\{A_1{}^\mu,\xi^\mu\}+(e^2/8c^2)\{A_1{}^\mu,\{A_1{}^\nu,\partial\xi^\nu/\partial p^\mu\}\}$$
$$-(e^2/8c^2)(\partial A_1{}^\nu/\partial x^\mu)\{A_1{}^\lambda,\{\xi^\nu,\partial\xi^\lambda/\partial p^\mu\}\}. \tag{C-1}$$

The transformation S_2 does the same thing as S_1 and in addition removes coupling terms involving $A_1{}^\mu A_1{}^\nu A_1{}^\lambda$.

$$S_2=S_1+(e^3/48c^3)\{A_1{}^\mu,\{A_1{}^\nu,\{A_1{}^\lambda,\partial^2\xi^\lambda/\partial p^\mu\partial p^\nu\}\}\}$$
$$-(e^3i/96\hbar c^3)\{A_1{}^\mu,\{A_1{}^\nu,\{A_1{}^\lambda,[\xi^\mu,\partial\xi^\lambda/\partial p^\nu]\}\}\}. \tag{C-2}$$

To complete the elimination to third order would require the determination of other terms in S_2 proportional to $A_1{}^\mu A_1{}^\nu\partial A_1{}^\lambda/\partial x^\sigma$ and then

$$A_1{}^\mu(\partial A_1{}^\nu/\partial x^\sigma)(\partial A_1{}^\lambda/\partial x^\rho).$$

The second-order terms which were denoted as $\mathcal{O}_2(e^2)$ in Eq. (64) are

$$\mathcal{O}_2(e^2)=\frac{e^2}{2mc^2}\frac{\partial A_1{}^\nu}{\partial x^\mu}\frac{\partial A_1{}^\nu}{\partial x^\lambda}\xi^\mu\xi^\lambda-\frac{e^2}{2c}\frac{\partial\phi}{\partial x^\mu}\frac{\partial A_1{}^\nu}{\partial x^\lambda}\left\{\xi^\nu,\frac{\partial\xi^\mu}{\partial p^\lambda}\right\}$$
$$+\frac{e^2}{8mc^2}\frac{\partial A_1{}^\nu}{\partial x^\mu}\frac{\partial A_1{}^\lambda}{\partial x^\sigma}\Bigg(3\left[\frac{\partial\pi_n{}^\mu}{\partial p^\lambda},\frac{\partial\xi^\nu}{\partial p^\sigma}\right]$$
$$+\left[\frac{\partial\pi^\lambda}{\partial p^\mu},\frac{\partial\xi^\nu}{\partial p^\sigma}\right]+3\frac{i}{\hbar}\left\{\xi^\lambda,\frac{\partial}{\partial p^\sigma}\{\xi^\nu,\pi_n{}^\mu\}\right\}$$
$$+\frac{i}{\hbar}\left\{\pi_n{}^\sigma,\left\{\xi^\nu,\frac{\partial\xi^\lambda}{\partial p^\mu}\right\}\right\}\Bigg). \tag{C-3}$$

The Cross Section for the Radiative Capture of Protons by C^{13} at 129 kev*

ERIC JOHN WOODBURY AND WILLIAM ALFRED FOWLER
Kellogg Radiation Laboratory, California Institute of Technology, Pasadena, California
(Received September 27, 1951)

The cross section for the capture of protons by C^{13} at 129 kilovolts is

$$\sigma = 5 \pm 1 \times 10^{-30} \text{ cm}^2.$$

This measurement was made possible through the use of a scintillation counter that had an over-all detection efficiency of 8.7 percent, and a pulsed ion source that had a peak proton current capability of one milliampere. A rough analysis of the radiation shows that 80 percent is due to the transition to the ground state of N^{14}, while the exact nature of the remaining 20 percent was not determined.

I. INTRODUCTION

THIRTEEN years ago H. A. Bethe proposed the carbon-nitrogen cycle as a source of solar energy, but the experimental evidence needed to verify or reject his theory was meager.[1] A program to obtain relevant evidence has been carried on for sometime in this laboratory. The excitation curves for the reactions in the cycle have been investigated over a wide range of proton energies, and the alpha-particle, gamma-ray, and positron spectra have been analyzed wherever possible. The cross sections become extremely small at solar energies (~25 kev) making it impossible to measure them directly. It has been considered desirable to make measurements at the lowest possible proton energies in order to reduce the range of the extrapolation required to estimate cross sections at such low energies.

All of the reactions, except the $C^{13}(p,\gamma)N^{14}$ reaction, give ionizing particles as reaction products. Such particles are more easily detected than gamma-radiation, and the cross sections for these reactions were the first to be measured at low energies.[2–4] The Geiger-Müller counter, ordinarily used in the past for detecting gamma-radiation, has two serious defects in low intensity measurements. First it is inefficient in converting gamma-radiation into detectable ionizing radiation since the amount of converting material is limited to the range of the secondary electrons produced. Second, because the pulse from the counter does not depend on the type of initiating radiation, x-rays and cosmic rays created a background that limits the intensity that can be observed. The scintillation counter partially overcomes both of these defects. The transparent crystal used as the phosphor has considerable mass, and will interact with a large part of the radiation passing through it. By placing the crystal close to the source a large solid angle is obtained without a complicated experimental arrangement. In addition, since the scintillation counter is a semiproportional detector, some of the background due to cosmic rays and x-rays can be eliminated.

The C^{13}, N^{14}, and N^{15} cross sections had been measured near 100 kilovolts, and it was considered desirable to measure the C^{13} cross section near this energy if at all possible. Estimates indicated that a proton current of one milliampere would be necessary to give a reaction intensity above the expected background. At the University of California a pulsed ion source has been recently developed that is capable of producing peak currents of this magnitude, but the average current is low, and if the advantage of a large peak current is to be utilized in overcoming background, the counter must be turned on only during the pulse.[5] This has been done without undue complication.

II. EXPERIMENTAL ARRANGEMENT

The accelerating voltage used in this experiment was supplied by a transformer and rectifier, while the accelerating column was a short version of the columns currently being used on the California Institute of Technology 3-Mev electrostatic accelerator. The ion source was a P.I.G. type ion source.[5,6] Figure 1 shows an assembly drawing of the source and focusing arrangement. Figure 2 shows a block diagram of the apparatus. The trigger source creates a 30 cps pulse which is lengthened to 760 microseconds by the counter-gate generator. The integrator anticoincidence circuit blocks this pulse, preventing operation of the ion source and scalers, during discharge of the ten microfarad integrating capacitor. After being passed by the anticoincidence circuit, the pulse starts the sweep of the current monitoring synchroscope, turns on the scalars by means of coincidence circuits, and finally is differentiated and converted into a light pulse. At the ion source this light pulse is reconverted into an electrical pulse that is used to start a single cycle multivibrator whose output pulse determines the duty cycle of the ion source. To provide proper integration the duty cycle of the scalers is made slightly greater than the duty cycle of the ion source.

* This work was assisted by the joint program of the ONR and AEC.
[1] H. A. Bethe, Phys. Rev. **53**, 608 (1938).
[2] R. N. Hall and W. A. Fowler, Phys. Rev. **77**, 197 (1950).
[3] Woodbury, Hall, and Fowler, Phys. Rev. **75**, 462(A) (1949).
[4] Schardt, Woodbury, and Fowler, Phys. Rev. **76**, 587(A) (1949).
[5] J. D. Gow, University of California, Berkeley, California (unpublished).
[6] A. Guthrie and R. Wakerling, *The Characteristics of Electrical Discharges in Magnetic Fields* (McGraw-Hill Book Company, Inc., New York, 1949), Chapter on "The P.I.G. Type Discharge."

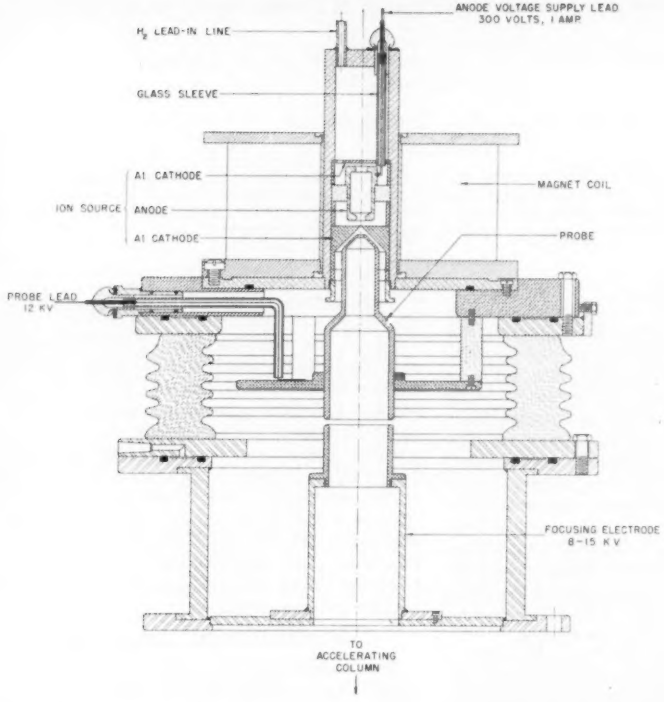

FIG. 1. Philips Ion Gauge (P.I.G.) type discharge ion source, and focusing system used with the accelerator.

The accelerating voltage was determined by measuring the current in a precision resistor column with a Weston microammeter. The actual voltage available for accelerating the protons is lower than the meter reading, for it depends on the current drawn from the voltage supply during the pulse, whereas the meter reading depends on the average current. Because the pulse current amounts to two milliamperes in addition to the average current of one and one-half milliamperes, and because the internal resistance of the supply was purposely made 500,000 ohms in order to limit the current during the occasional breakdowns of the accelerating column, it is necessary to make a one kilovolt correction to the meter reading. In addition to the 0.25 percent

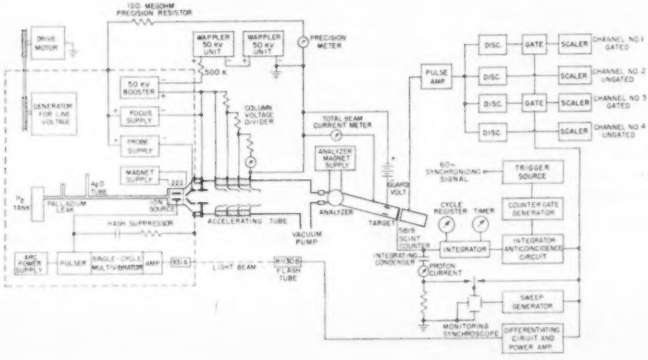

FIG. 2. Block diagram of apparatus used in the 128 kilovolt determination.

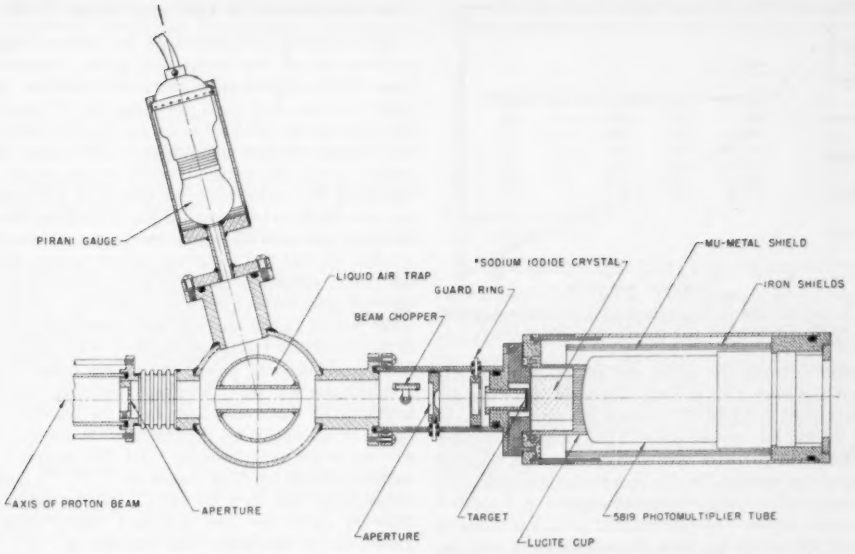

FIG. 3. Scintillation counter and target chamber. The target chamber vacuum was ordinarily 2×10^{-6} mm or better. The Pirani gauge is merely for rough vacuum readings when pumping down after target changes.

error in the voltage measurement an uncertainty of ~1 kilovolt is introduced by the ripple and fluctuations of the accelerating voltage.

III. COUNTER CONSTRUCTION AND CALIBRATION

Figure 3 shows an assembly drawing of the counter and target chamber. The distance between the target surface and the face of the thallium-activated sodium iodide crystal is 0.040 inch. The crystal is a one-inch cube cut from a larger blank supplied by the Harshaw Chemical Company. Because of the hygroscopic nature of sodium iodide, the Lucite cup is filled with sodium-dried mineral oil. A layer of Celvacene grease is formed between the Lucite cup and the photosensitive cathode of the 5819 photomultiplier tube to improve the optical coupling.

Photomultipliers and electronic amplifiers are subject to a certain amount of inherent instability. Figure 4 shows the integral bias curve obtained from a Co^{60} source that could be placed in a standard position near the counter. By finding the intercept of the straight line portion with the ordinate a convenient check of the detection efficiency is made, while the intercept of the straight line with the abscissa is a measure of the amplification of the system. The break at low bias is due to back-scattered radiation from Compton interactions in the surroundings of the crystals. With the amplifier gain reduced, the integral bias curves shown in Fig. 5 were found for gamma-rays of four different energies. Figure 6, showing the relation between the x-intercepts of the straight line portions of these curves and the energy of the respective gamma-rays, demonstrates the semiproportional nature of the scintillation detector. It is possible to obtain gamma-ray energies more accurately through the use of a differential technique, but such a technique is not an efficient way to make weak intensity measurements. Neglecting the radiation scattered into the crystal from the surroundings, the y-intercept of an integral bias curve gives the fraction, that is counted, of the yield of the source into the solid angle subtended by the counter. It can be shown, under reasonable assumptions, and if the points corresponding to less than a few hundred kilovolts of energy are neglected, that the error made by neglecting the scattered radiation is fairly small for the radiation energies considered in this experiment. Furthermore, any such error is partially eliminated if the absolute calibration of the counter is made using a gamma-ray energy comparable to gamma-ray energies in the unknown source.

The absolute calibration of the counter was made using the radiation from the $F^{19}(p,\alpha\gamma)$ reaction at one million volts bombarding energy. The radiation from this reaction consists of a mixture of 6- and 7-Mev gamma-rays, and at this bombarding energy the thick target yield for a thick CaF_2 target in the forward direction is 7.1×10^{-7} gamma-rays per proton.[7] There are also 5-Mev nuclear pairs from this reaction, and the

[7] Chao, Tollestrup, Fowler, and Lauritsen, Phys. Rev. **79**, 108 (1950).

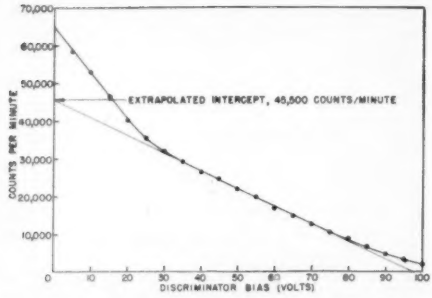

FIG. 4. Integral bias curve obtained using the calibrating Co^{60} source. The amplifier gain is eight times that of Fig. 5.

absorber between the target and crystal was not sufficient to absorb them entirely. The yield of the nuclear pairs is given as 0.10×10^{-7} particle per proton.[8] Therefore, taking into proper account the increased counter efficiency for particles over gamma-rays, the effective yield of the reaction for this counter is determining its detection efficiency for gamma-radiation is 7.4×10^{-7} event per proton. The experimental yield was found to be 422,000 counts for 1.05 microcoulombs of protons. Over a limited range of gamma-ray energies the efficiency of the counter might be expected to be proportional to the total absorption coefficient of sodium iodide. In an experiment to check the validity of this assumption the yield of the 2.3-Mev radiation from $C^{12}(p,\gamma)$ was determined at one million volts bombarding energy using a graphite target. It was found to be 7.2×10^{-10} gamma-ray per proton as compared to the value 7.3×10^{-10} given by other methods.[9,10] This required a 12 percent correction because of the change in the total absorption coefficient in going to the lower energies, and so the close agreement between the yield found and that predicted, justifies the assumption made.

The C^{13} targets used in the low energy work were prepared by cracking enriched methyl iodide on clean tantalum strips. The resulting layer of carbon was thin and hard.[11] The actual percentage of carbon as C^{13}, 61 percent according to the data supplied by Eastman Kodak, was checked by comparative yield measurements with ordinary graphite. Measurements made at the sharp 1.76-Mev resonance in C^{13} indicated that the thickness of the targets for protons was 20 kev at this energy. Because of the increase in the stopping cross section for carbon at lower energies, the thickness for protons at the energy used was great enough to insure a thick target yield.

[8] Streib, Fowler, and Lauritsen, Phys. Rev. **59**, 253 (1941).
[9] Fowler, Lauritsen, and Lauritsen, Revs. Modern Phys. **20**, 236 (1948).
[10] Recently a value of 7.7×10^{-10} has been found by J. D. Seagrave of this laboratory for this yield.
[11] J. D. Seagrave (to be published).

IV. REDUCTION OF THE DATA FROM $C^{13}+H^1$

After shielding the counter with two inches of lead, a good fraction of the background pulses, presumably those due to high energy cosmic-ray particles, were larger than any that could arise from the C^{13} reaction. This information was used to reduce the uncertainty in the background correction. Also it is possible and desirable to utilize the period between proton pulses for measuring the background, for then local fluctuations are more likely to be accounted for. With these ideas in mind the data were taken with four scalers and four discriminators. The first scaler was turned on only during the proton pulse and its discriminator was set to the bias voltage at which a reading was desired. The second scaler was on all the time and its discriminator was set to the same bias voltage as the first. The third scaler was turned on only during the proton pulse and its discriminator was set to a voltage just larger than the largest pulse that could arise from the reaction. The fourth scaler was on all the time and its discriminator was set to the same bias the third. We designate the counts collected by these scalers as C_1, C_2, C_3, and C_4, respectively. The data C_3 and C_4 may be subtracted from C_1 and C_2 for they represent pulses which are known to be too large. The numbers (C_1-C_3) and (C_2-C_4) then form the raw data to be used. We designate these by n_0 and N_0, respectively. The quantity (N_0-n_0) contains only the background for a period proportional to $(1-\tau)$, where τ is the duty cycle. Therefore, B, the background while the counter is on, is

$$B=\tau(N_0-n_0)(1-\tau)^{-1}.$$

The counts, n, corresponding to the C^{13} radiation are therefore given by

$$n=n_0-B=(n_0-\tau N_0)(1-\tau)^{-1}.$$

The statistical error in n is computed by noting that the error in $(N_0-n_0)(1-\tau)^{-1}$ is $0.7(N_0-n_0)^{\frac{1}{2}}(1-\tau)^{-\frac{1}{2}}$, and

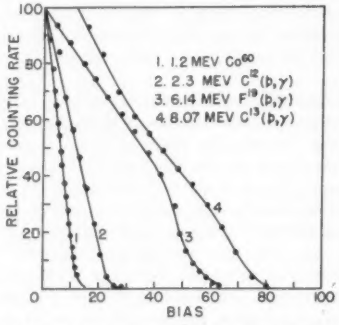

FIG. 5. Integral bias curves with targets of calcium fluoride, graphite, and enriched C^{13}. The break in the C^{13} curve is due to a lower energy component in the radiation. The Co^{60} curve of Fig. 4 is shown replotted to the same scale as that of this figure.

so the error in B can be found by using the differentiation rule and simplifying the resulting expression to yield

$$\epsilon(B)=0.7\tau(1-\tau)^{-\frac{1}{2}}(N_0-n_0)^{\frac{1}{2}}(1+\tau)^{\frac{1}{2}};$$

therefore the statistical error in n is

$$\epsilon(n)=0.7[n_0+\tau(1-\tau)^{-1}(1+\tau)(N_0-n_0)]^{\frac{1}{2}}.$$

If $\tau\ll 1$, and if $n_0<N_0$, as is true in this experiment then the error may be written as

$$\epsilon(n)\approx 0.7(n_0+\tau N_0)^{\frac{1}{2}}.$$

The yield can be determined by using the counter calibration obtained from fluroine, or it can be determined, assuming the yield as known at 700 kev, by comparing the counter yield at the lower voltage with the counter yield at 700 kev. When the yield has been calculated the cross section can be found by using the method of Hall and Fowler.[2] This yields the equation,

$$\sigma=(3Y\epsilon/fE^{\frac{1}{2}})(1+E^{\frac{1}{2}}/Z_0),$$

where f represents the fraction of C^{13} in the target, ϵ the stopping power of carbon, and E the energy of the bombarding protons in Mev. This equation is found by evaluating the following integral assuming that ϵ is constant,

$$Y=\int_0^E \frac{\sigma}{\epsilon}dE.$$

The assumption is good, for ϵ is nearly constant from 90 kilovolts to 130 kilovolts, and σ drops so rapidly with energy that the contribution below 90 kilovolts is relatively unimportant. Hall and Fowler give as an approximate form for σ,

$$\sigma=(a/E)\exp(-0.99Z_0/E^{\frac{1}{2}}).$$

This is derived from the asymptotic form of the penetration factor.

Typical counting data are tabulated in Table I and

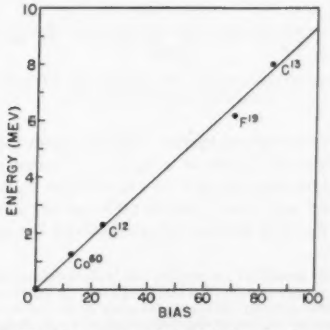

FIG. 6. The bias energy relationship for the data of Fig. 5 using the extrapolated intercepts of the straight line portions with the abscissa as the bias values.

TABLE I. Data obtained from C^{12} at 129 kilovolts.

Bias	C_1	C_2	C_3	C_4	Charge microcoulombs	True counts per 1000 microcoulombs
10	63	5	643	182	26,400	1.84±0.22
15	66	6	484	230	35,200	1.54±0.16
20	65	4	602	303	48,400	1.21±0.13
25	61	5	512	282	46,600	1.09±0.12
30	73	13	745	454	70,400	0.759±.081
40	44	9	456	326	48,400	0.665±0.089
50	21	3	314	228	38,700	0.417±0.084

Voltage 129±1 kilovolts
$\tau=0.0227$

shown graphically in Fig. 7. Making use of the counter efficiency of 8.7 percent, the target enrichment of 61 percent, and the y intercept from Fig. 7 corresponding to the hard radiation, the yield of the hard radiation for a pure target is found to be, 3.7×10^{-15} gamma-ray per proton. Noting that the soft radiation is about 3.5 Mev the yield of soft radiation is 2.8×10^{-15} gamma-ray per proton for a pure target. The corresponding cross sections are

$$\sigma=3.7\times10^{-33}\ \text{cm}^2$$

and

$$\sigma=2.8\times10^{-33}\ \text{cm}^2$$

respectively. Assuming the soft radiation is due to a two-step cascade a total cross section may be written

$$\sigma=5.1\times10^{-33}\ \text{cm}^2$$

or assuming a three-step cascade,

$$\sigma=4.6\times10^{-33}\ \text{cm}^2.$$

In either case we can round off the results to give the cross section as $5\pm1\times10^{-33}$ cm^2 at 129±1 kev.

Figure 8 gives a bias curve made using an ordinary graphite target at a bombarding energy of 700 kilovolts. The soft radiation is mostly from C^{12}. Comparing the yield of the hard radiation from this target at 700 kilovolts with the yield of hard radiation from the enriched target at 129 kilovolts, gives

$$Y_{700}/Y_{129}=2.2\pm0.3\times20^6.$$

The errors have been estimated as follows. In the ratio just given only the counting rates, the values of the charges collected by the integrator, and the enrichment factor enter directly. The integration error is negligible. The statsitical and extrapolation error in the counting rate at 700 kilovolts is not more than a few percent, and at 129 kilovolts it is ten percent. The enrichment factor is known within a few percent. Therefore the probable error has been set at 12 percent.

In determining the absolute cross section other errors arise. The fluorine yield which was used for calibration is uncertain to ten percent, and the stopping cross section which enters into the calculation is not known to better than ten percent. These errors, combined with

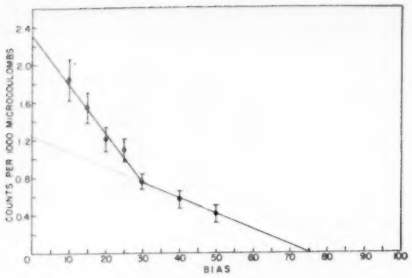

FIG. 7. Integral bias curve at 129 kilovolts for C^{13} using data of Table I.

those already mentioned, produce an uncertainty of twenty percent in the cross section.

The error in the accelerating voltage has been given as ~1 kilovolt. If surface layers were formed on the target, the effective accelerating voltage might be much lower than calculated. Because of the very rapid variation of cross section with energy, a one percent reduction in the voltage would result in an eight percent reduction in the yield. If a surface layer built up on the target, the counting rate would rapidly decrease in each experiment. This was not observed. In addition the targets did not show any discoloration after use.

V. COMPARISON WITH THE RADIATION AT HIGHER ENERGY

It is possible to make some prediction of the cross section to be expected at 129 kilovolts from the nature and yield of the reaction at higher energy. There are many resonances, but only two are of sufficient strength and breadth to contribute to the cross section at 129 kilovolts. These are the well-known resonance at 554 kilovolts, and a broad resonance at 1.25 million volts.

It is not known whether these resonances will interfere at the low energy, and so for comparison with the observed results they will be studied separately. The most useful tool for doing this is the single level Breit-Wigner dispersion formula,

$$\sigma = \pi\lambda^2 \frac{\omega\Gamma_\gamma\Gamma_p}{(E-E_R)^2+\frac{1}{4}\Gamma^2}.$$

λ is the wavelength of the incident proton in the center-of-mass system, $\omega\Gamma_\gamma$ is a small factor nearly independent of energy,[12] E_R is the energy of the bombarding proton at resonance, E is the actual bombarding energy, Γ is $\Gamma_\gamma+\Gamma_p$, and finally Γ_p is given by $P(E)^{\frac{1}{2}}G$ where $P(E)^{\frac{1}{2}}$ is the penetration factor while G is the width at one

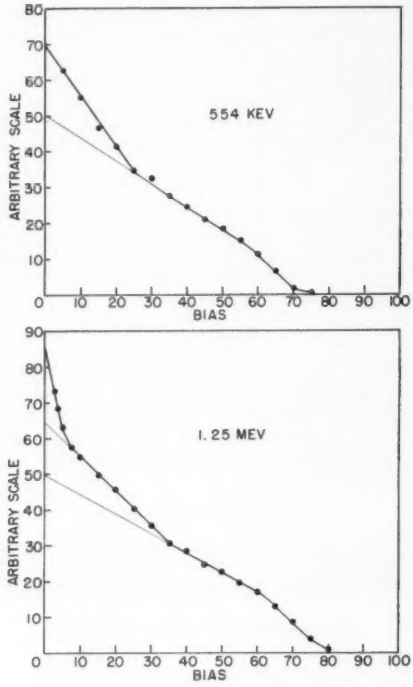

FIG. 9. Integral bias curves at 554 kilovolts and 1.25 million volts using thin enriched C^{13} targets.

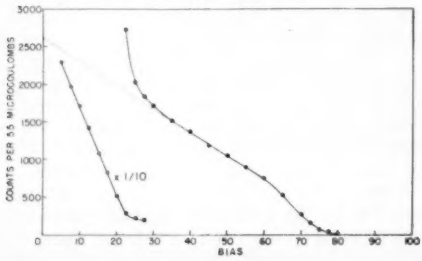

FIG. 8. Integral bias curve at 700 kilovolts for a graphite target.

million volts without barrier. $P(E)^{\frac{1}{2}}$ has been tabulated by Christy and Latter as a function of target nucleus and bombarding energy.[13] At low energies Γ_p becomes very small and thus Γ may be neglected in comparison to $(E-E_R)$. For purposes of extrapolation the equation

[12] Strictly speaking Γ_γ is proportional to E_γ^3 for dipole radiation. For high energy gamma-rays and comparatively small variations in bombarding energy the statement made in the text is true. The error made by neglecting the dependence of Γ_γ on energy is not greater than 10 percent for the worst case.

[13] R. F. Christy and R. Latter, Revs. Modern Phys. **20**, 185 (1948).

may be re-expressed as

$$\sigma=\frac{E_R}{E}\frac{P(E)^{\frac{1}{2}}}{[P(E)^{\frac{1}{2}}]_R}\left[\frac{\Gamma_{pR}}{E-E_R}\right]^2\frac{\sigma_R}{4},$$

where $\pi\lambda^2$ has been given by

$$\pi\hbar^2M/2\mu^2E.$$

Here μ is the reduced mass of the system, and M is the proton mass.

The integral bias curves at 554 kev and also at 1.25 Mev taken with a thin target are given in Fig. 9. Except for the very low energy tail on the higher energy curve, they are of the same nature as the curve at 129 kev. They both show about 35 percent total soft radiation as compared to 43 percent for 129 kev, but the error on the latter figure is sufficient to rule out attaching any importance to the difference. J. D. Seagrave has found the widths of the resonances as 32.5 kev for the lower resonance and 500 kev for the higher resonance. The best values available for σ_R are $\sigma_{554}=1.44\times10^{-27}$ cm^2 and $\sigma_{1.25}=0.062\times10^{-27}$ cm^2. These are calculated from total yields using Geiger tubes.[11] Making use of the extrapolation formula these yield

$$\sigma=2.55\times10^{-33}\text{ cm}^2$$

and

$$\sigma=0.99\times10^{-33}\text{ cm}^2,$$

respectively, at 129 kilovolts. This assumes both resonances are due to s-wave protons. These may be combined to give

$$\sigma=3.54\times10^{-33}\text{ cm}^2$$

assuming no interference. It is seen that this value as well as the bias curves would emphasize the cascade as predominantly a triple one, but the evidence is not strong.

R. G. Thomas has recently proposed an improved method of extrapolation in place of the method used here.[14] His results are difficult to apply except in the case of C^{12} and similar nuclei with spin zero in the ground state, but they indicate that the cross section predicted by the standard method should be too low. In the case of C^{12}, which has been measured by Hall and Fowler, his method indeed predicts the correct value. In this regard it is interesting to note that the ratio of the cross sections for the capture of protons by C^{13} to C^{12} at 129 kilovolts is 4.6, and is the same as that predicted by the extrapolation from higher resonances despite the fact that both cross sections are thirty percent higher than the extrapolated values.

We wish to acknowledge the assistance of J. D. Seagrave and R. B. Day in operating the 3-Mev electrostatic generator for the fluorine calibration and other work done at higher energies. In addition we should like to thank the entire staff of the laboratory for the many suggestions and services that they rendered.

[14] R. G. Thomas, Phys. Rev. **81**, 418(L) (1951).

Polarization of Scattered Quanta

J. I. HOOVER, W. R. FAUST, AND C. F. DOHNE
Nucleonics Division, Naval Research Laboratory, Washington, D. C.
(Received August 27, 1951)

An experimental study of the polarization effect of doubly scattered Co^{60} γ-rays as a function of the angle of scattering has been made using scintillation detectors and coincidence counting. Although there are large statistical deviations from the theoretical values at certain points, a comparison between the experimental and theoretical values indicate no serious disagreement.

I. INTRODUCTION

A RECENT theoretical paper[1] discussed the Compton effect for polarized light, using the results to predict the azimuthal variation in intensity of initially unpolarized light which has undergone two Compton scatterings. Numerous experimental polarization studies[2] have been made in the x-ray region at angles of 90° by means of ionization chambers. An experimental study at angles other than 90° has been made at this laboratory using a cobalt 60 source and scintillation detectors. In this process, Fig. 1, a photon of momentum k_0, is Compton scattered through an angle θ_1. The resulting photon of momentum k_1 is then scattered through an angle θ_2 to produce a photon of momentum k_2 and an electron which is detected. The scattered gamma-ray k_2 is detected by allowing it to be absorbed photoelectrically in a NaI (Tl) crystal. Coincidences between k_1 and k_2 as a function of θ_1, θ_2, and ϕ (azimuthal angle of k_2 about the axis of k_1) were used to determine the degree of polarization of the scattered gamma-ray of momentum k_1.

II. DESCRIPTION OF EXPERIMENT

A collimated beam of Co^{60} γ-rays from a 5-curie source is allowed to fall on a copper scatterer S. The singly scattered radiation is then scattered off a crystal C_1 where the recoil electron is detected. The doubly scattered radiation then falls on a crystal C_2 where it is detected by photoelectric absorption. Coincidences between C_1 and C_2 are then observed. The singly scattered radiation from the copper is prevented from being scattered to crystal C_2 and then to C_1 by a 5-cm lead block interposed between S and C_2. The crystals C_1 and C_2 were clear NaI (Tl) mounted in Nujol on the photocathode of 5819 photomultipliers. The crystals were 2.5-cm×2.5-cm×2- to 4-mm thick, freshly cut from 1-in.×1-in.×½-in. crystals. C_1 and C_2 were mounted on a brass bar which kept their position with respect to each other constant at a distance of 10 cm. C_1 was mounted 10 cm from S and was arranged in such a way as to present a constant area to the scattered radiation K_1 and a constant area to C_2 for all values of ϕ. By moving the brass bar along the periphery of a four foot diameter "C", ϕ could be varied from 0° to 90°.

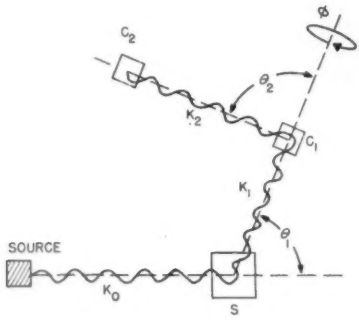

FIG. 1. Successive Compton scatterings.

The output of each photomultiplier was amplified and fed through a trigger circuit to the input of a scaler and a coincidence circuit. Traffic counters, which were operated from a single timer, recorded the data from each photomultiplier and the coincidence circuit hourly. Rather stringent stability requirements were placed on this equipment. Long term constant drifts in the apparatus could be partially compensated for by the proper choice of sequence in taking the data. However, irregular, or short term drifts, which were difficult to detect, could cause serious error, but would not necessarily be reflected in the calculated probable error. Each hourly recording was treated as an observation in the analysis of the data.

Resolving time measurements of the coincidence circuit were made in the conventional manner by observing the accidental counting rate A and computing the resolving time τ from

$$2\tau = A/R_1R_2.$$

Here R_1 and R_2 are the single counting rates (counts/sec) of the counters C_1 and C_2 respectively. Data for the resolving time measurements were taken and analyzed in the same manner as the experimental data. The measured resolving time was $0.147\pm0.01\mu$sec. The resolving time was measured before, during, and at the termination of the experiment. All three sets of data agreed within the experimental error.

[1] A. Wightman, Phys. Rev. **74**, 1813 (1948).
[2] E.g., C. G. Barkla, Proc. Roy. Soc. (London) **77**, 247 (1906); A. H. Compton and C. F. Hagenow, J. Opt. Soc. Am. and Rev. Sci. Instr. **14**, 487 (1924).

TABLE I. Ratio $C_{\phi=0}/C_{\phi=\phi}$.

ϕ	Experimental	Theoretical	Ratio of deviation to statistical probable error
	$\theta_1=83°$		
90°	1.778±0.111	1.76	+0.16
70°	1.342±0.073	1.561	−3.1
50°	1.094±0.045	1.218	−2.75
30°	1.041±0.033	1.085	−1.33
	$\theta_1=50°$		
90°	1.494±0.044	1.445	+1.11
70°	1.534±0.046	1.368	+3.61
50°	1.274±0.039	1.222	+1.33
30°	1.096±0.035	1.081	+0.43

TABLE II. Average counts per hour.

Channel I $\times 10^5$	Channel II $\times 10^4$	Coincidence (corrected for accidentals)
3.35	1.62	29.722
3.11	1.51	27.613
3.18	1.64	30.657

III. DISCUSSION OF RESULTS

Between 100 and 150 observations of the coincidence counting rate were made for each value of ϕ and θ_1, approximately half of which were background readings, i.e., scatterer removed from the beam. The observed coincidence counting rate for each observation was corrected for the accidental coincidence counting rate to obtain the true coincidence counting rate. These data were then analyzed statistically using the Pierce-Chauvenet criterion[3] as a basis upon which to reject observations with abnormally high deviations.

The results are tabulated in Table I where the angle ϕ at which measurements were made is listed in column 1. Columns 2 and 3 are respectively the experimental and theoretical ratio $C_{\phi=0}/C_{\phi=\phi}$, where $C_\phi=0$ is the coincidence counting rate when the crystal C_2 is in the plane of k_0 and k_1, $C_{\phi=\phi}$ is the coincidence counting rate where C_2 is at the angle ϕ to the plane containing k_0 and k_1. Column 4 is the deviations between the experimental and theoretical values in terms of the experimental probable error.

The theoretical ratio* was obtained by integrating Wightman's equation (10)[1] for ΔN over the solid angle subtended by the crystals in the experimental arrangement, and then computing the ratio for the appropriate values of θ_1 and θ_2.

Although large deviations occur at some points, the experimental data, on the average, agree with the theoretical within about 1.5 probable errors. Considering the experimental difficulty and statistical error this agreement is reasonable. The data with few exceptions were consistent; however, it is likely that the probable error is higher than that calculated from the sum of the squares of the deviations because of the extremely low coincidence counting rate. At the maximum (30 counts/hr) the number of coincidence counts per photon striking the copper scatterer was only 8.8×10^{-10}.

The most probable source of error was the potential instability of electronic equipment operating over extended periods. Although periodic checks made on the various components revealed the necessity for major adjustments, drifting and other small irregularities could not be detected in this manner. The effect of the latter is difficult to estimate except from the general consistency of sets of data taken at different times. Table II lists three average sets of data taken at one position approximately 10 days apart.

As can be seen, the agreement between the three sets of data is good; however it could be highly desirable to repeat the experiment using a much stronger source, and shorter counting times.

The authors wish to thank Dr. F. N. D. Kurie, for his continued interest and support, and Dr. M. H. Johnson and Dr. Lewis Slack for a number of beneficial suggestions.

[3] T. B. Crumpler and J. H. Yoe, *Chemical Computations and Errors* (John Wiley & Sons Inc., New York, 1940), p. 190.

* Computed for the average Co^{60} γ-ray 1.25 Mev.

Theory of Molecular Hydrogen and Deuterium in Magnetic Fields*

NORMAN F. RAMSEY
Harvard University, Cambridge, Massachusetts
(Received September 24, 1951)

The hamiltonian of a diatomic homonuclear molecule in a magnetic field is discussed. Included in the hamiltonian are the effects of the nuclear and rotational magnetic moments interacting with the external magnetic field, magnetic shielding, molecular diamagnetism, the spin-spin magnetic interaction of the two nuclei, the interaction of the nuclear magnetic moments with the field due to the rotation of the molecule, and the interaction of nuclear electric quadrupole moments. Perturbation theory expressions for the energy of H_2 and D_2 in the first rotational state are obtained in both strong and weak field limits. The secular equation is numerically solved for intermediate fields. Curves are given showing the theoretical dependence of the energy and the transition frequencies upon the field.

I. INTRODUCTION

IN the original molecular beam studies of hydrogen and deuterium by Kellogg, Rabi, Ramsey, and Zacharias[1-3] that led to the discovery of the deuteron quadrupole moment, the measurements were made only in strong external magnetic fields. Consequently the theory of the energy levels and transition frequencies was limited to a perturbation treatment in which the interactions within the molecule were assumed small in comparison with the interaction of the nuclear moments with the external magnetic field.

However, as a confirmation of the assumed nature of the interaction and as a means of increasing the precision of the measurement of the interaction constants within the molecule, experiments have recently been made by Kolsky, Phipps, Ramsey, and Silsbee[4-6] in the limit of weak and intermediate values of the magnetic field. The present paper contains the theory of the energy levels and transition frequencies relevant to weak, strong, and intermediate field experiments with H_2 and D_2 molecules in the first rotational state. Magnetic shielding effects which were neglected in the earlier discussion are included in the present one.

TABLE I. Nonvanishing matrix elements of $\mathcal{H}$ in $m_I m_J$ representation.

m_I	m_J	m_I'	m_J'	$(m_I m_J\|\ \mathcal{H}\ \|m_I' m_J')/h$
±1	±1	±1	±1	$\mp(1-\sigma_{i1})a\mp(1-\sigma_{J1})b-c+\frac{1}{4}d-\frac{1}{2}f-g$
±1	0	±1	0	$\mp(1-\sigma_{i0})a-d+\frac{3}{4}f-g$
0	±1	0	±1	$\mp(1-\sigma_{J1})b-d-\frac{1}{2}f-g$
±1	∓1	±1	∓1	$\mp(1-\sigma_{i1})a\pm(1-\sigma_{J1})b+c+\frac{1}{4}d-\frac{1}{2}f-g$
0	0	0	0	$2d+\frac{3}{4}f-g$
±1	0	0	±1	$-c+\frac{3}{4}d$
0	±1	±1	0	$-c+\frac{3}{4}d$
0	0	±1	∓1	$-c-\frac{3}{4}d$
±1	∓1	0	0	$-c-\frac{3}{4}d$
∓1	±1	±1	∓1	$3d$

II. THE HAMILTONIAN

The hamiltonian for a homonuclear $^1\Sigma$ diatomic molecule in a magnetic field $\mathbf{H}$ may be taken as

$$\begin{aligned}\mathcal{H}/h=&-[1-\sigma_i(\mathbf{J})]a\mathbf{I}\cdot\mathbf{H}/H\\&-[1-\sigma_J(\mathbf{J})]b\mathbf{J}\cdot\mathbf{H}/H-c\mathbf{I}\cdot\mathbf{J}\\&+\frac{5d}{(2J-1)(2J+3)}\{3(\mathbf{I}\cdot\mathbf{J})^2+\tfrac{3}{2}\mathbf{I}\cdot\mathbf{J}-\mathbf{I}^2\mathbf{J}^2\}\\&-\frac{5f}{3(2J-1)(2J+3)}\cdot\{3(\mathbf{J}\cdot\mathbf{H})^2/H^2-\mathbf{J}^2\}-g \quad (1)\end{aligned}$$

where $\mathbf{I}$ is the resultant spin angular momentum in units of $\hbar$ and $\mathbf{J}$ is the molecular rotational angular momentum in units of $\hbar$.

The first term in (1) corresponds to the interaction of the nuclear magnetic moments with the external magnetic fields and a is defined by

$$a=\mu_i H/ih \quad (2)$$

TABLE II. Nonvanishing matrix elements of $\mathcal{H}$ in Fm representation.

F	m	F'	m'	$(Fm\|\ \mathcal{H}\ \|F'm')/h$
2	±2	2	±2	$\frac{1}{4}d-c\mp a\mp b$
2	±1	2	±1	$\frac{1}{4}d-c\mp\frac{1}{2}a\mp\frac{1}{2}b$
1	±1	1	±1	$-(5/2)d+c\mp\frac{1}{2}a\mp\frac{1}{2}b$
2	0	2	0	$\frac{1}{4}d-c$
1	0	1	0	$-(5/2)d+c$
0	0	0	0	$5d+2c$
1	±1	2	±1	$\frac{1}{2}(a-b)$
2	±1	1	±1	$\frac{1}{2}(a-b)$
2	0	1	0	$(a-b)/3^{\frac{1}{2}}$
1	0	2	0	$(a-b)/3^{\frac{1}{2}}$
0	0	1	0	$(a-b)2^{\frac{1}{2}}/3^{\frac{1}{2}}$
1	0	0	0	$(a-b)2^{\frac{1}{2}}/3^{\frac{1}{2}}$

* This work was partially supported by the joint program of the ONR and AEC.

[1] Kellogg, Rabi, Ramsey, and Zacharias, Phys. Rev. **56**, 728 (1939). In the present paper, these authors are frequently referred to as KRRZ.

[2] Kellogg, Rabi, Ramsey, and Zacharias, Phys. Rev. **57**, 677 (1940). In the present paper, these authors are frequently referred to as KRRZ.

[3] N. F. Ramsey, Phys. Rev. **58**, 226 (1940). The signs of k in the first three tables of this reference are reversed.

[4] Kolsky, Phipps, Ramsey, and Silsbee, Phys. Rev. **79**, 883 (1950).

[5] Kolsky, Phipps, Ramsey, and Silsbee, Phys. Rev. **80**, 483 (1950).

[6] Kolsky, Phipps, Ramsey, and Silsbee, Phys. Rev. **82**, 1061 (1951).

TABLE III. Perturbation theory in strong fields. C_2, C_2', and C_3 are second- and third-order perturbations and are defined by

$$C_2=[(c+\tfrac{1}{2}d)^2+(9/2)d^2]/(a-b)$$
$$C_2'=(c-\tfrac{3}{2}d)^2/(a-b)$$
$$C_3=(c+\tfrac{1}{2}d)^2(c-(9/2)d)/(a-b)^2.$$

The state designation is the same for H_2 and D_2.

State	m_I	m_J	Energy/h	
A/L	∓1	∓1	$\pm(1-\sigma_{i1})a\pm(1-\sigma_{J1})b-c+\frac{1}{2}d-\frac{1}{2}f-g$	
B/K	∓1	0	$\pm(1-\sigma_{i0})a-d+\frac{1}{2}f-g$	$\pm C_2'$
C/G	∓1	±1	$\pm(1-\sigma_{i1})a\mp(1-\sigma_{J1})b+c+\frac{1}{2}d-\frac{1}{2}f-g$	$\pm C_2-C_3$
D/F	0	∓1	$\pm(1-\sigma_{J1})b-d-\frac{1}{2}f-g$	$\mp C_2'$
E	0	0	$2d+\frac{1}{2}f-g$	$+2C_2$

where μ_i is the magnetic moment of one of the nuclei and i the corresponding nuclear spin. The factor $[1-\sigma_i(\mathbf{J})]$ arises from the magnetic shielding of the nucleus by the molecule. As shown by Ramsey[7,8]

$$\sigma_i(\mathbf{J})=\tfrac{2}{3}\sigma_o+\tfrac{1}{3}\sigma_\pi+(\sigma_\pi-\sigma_o)[2/3(2J-1)(2J+3)]\times\{3(\mathbf{J}\cdot\mathbf{H})^2/H^2J^2-\mathbf{J}^2\} \quad (3)$$

where J is the quantum number of the total rotational

TABLE IV. Perturbation theory in weak fields. K_2 and K_2' are second-order perturbations defined by

$$K_2=(a-b)^2/(2c-3d)$$
$$K_2'=2(a-b)^2/3(c+(15/2)d).$$

The third-order perturbations vanish.

H_2 state	D_2 state	F	m	Energy/h
A/L	A/L	2	∓2	$-c+\frac{1}{2}d\pm(a+b)$
B/F	D/K	1	∓1	$c-(5/2)d\pm\frac{1}{2}(a+b)+\frac{1}{4}K_2$
C	C	0	0	$2c+5d \quad +K_2'$
D/K	B/F	2	∓1	$-c+\frac{1}{2}d\pm\frac{1}{2}(a+b)-\frac{1}{4}K_2$
E	G	1	0	$c-(5/2)d \quad +\frac{1}{2}K_2-K_2'$
G	E	2	0	$-c+\frac{1}{2}d \quad -\frac{1}{2}K_2$

angular momentum and σ_o is the magnetic shielding constant for a magnetic field applied perpendicular to the internuclear axis while σ_π is the shielding constant for fields parallel to the internuclear axis. Theoretical expressions for σ_o and σ_π have been given by Ramsey.[8]

The second term in (1) provides for the interaction of the molecular rotational magnetic moment with the external magnetic field and b is defined by

$$b=\mu_J H/Jh \quad (4)$$

TABLE V. Assumed values for constants in secular equations. The constants are given in kilocycles per second.

Constant	H_2	D_2
a	$4.258H$	$0.6536H$
b	$0.6717H$	$0.3368H$
c	113.8	8.783
d	57.68	25.24

[7] N. F. Ramsey, Phys. Rev. **78**, 699 (1950).
[8] N. F. Ramsey, Phys. Rev. **83**, 540, 659 (1951).

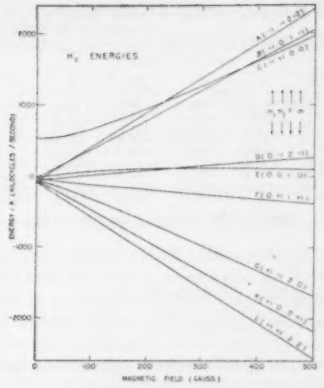

FIG. 1. Energies of H_2 states as functions of magnetic field.

where μ_J is the magnetic moment due to the rotation of the molecule in rotational state J. The third term corresponds to the spin rotational magnetic interaction and c is related to the quantity H' of KRRZ[1,2] by

$$c=\mu_i H'/ih. \quad (5)$$

The fourth term in (1) includes the combination of the spin-spin magnetic interaction of the two nuclei with each other together with the interaction of any nuclear electrical quadrupole moment with the variation of the molecular electric field in the vicinity of the nucleus. That these two separate phenomena combine in this way in homonuclear molecules is shown by KRRZ[1,2] who also show that for computation of matrix elements diagonal in J and in I, the quantum number of the total spin angular momentum, d can be expressed

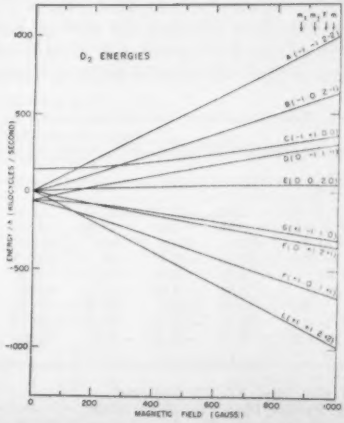

FIG. 2. Energies of D_2 states as functions of magnetic field.

TABLE VI. Numerical solution of secular equation for H_2. The energy divided by h is given in kilocycles per second for the designated state in the indicated magnetic field. Magnetic field (gauss).

State $(m_I m_J F m)$	0	5	10	20	60	100	140	180	220	260	300	400	500
$A(-1-1\ 2-2)$	−84.96	−60.31	−35.66	13.6	210.8	408.0	605.2	802.4	999.6	1197	1394	1887	2380
$B(-1\ 0\ 1-1)$	30.38	−16.62	−0.37	36.69	201.2	370.2	539.9	709.9	880.1	1050	1221	1647	2072
$C(-1+1\ 0\ 0)$	516.0	516.4	517.6	522.2	569.1	653.2	759.3	879.0	1006	1138	1273	1618	1969
$D(0-1\ 2-1)$	−84.96	−74.09	−65.69	−53.45	−20.8	3.71	34.9	62.1	89.2	116.2	143.0	210	278
$E(0\ 0\ 1\ 0)$	−30.54	−28.96	−24.17	−11.63	40.51	65.06	82.84	93.09	99.34	103.3	106.3	109.8	112.1
$F(0+1\ 1+1)$	−30.40	−41.27	−49.69	−61.9	−94.6	−122.8	−150.3	−177.5	−204.5	−231.5	−258.5	−325.5	−393
$G(+1-1\ 2\ 0)$	−84.90	−86.75	−90.84	−106.1	−188.4	−317.5	−441.4	−571.3	−704.8	−840.8	−978	−1326	−1679
$K(+1\ 0\ 2+1)$	−84.96	−98.74	−115.0	−152.0	−316.7	−485.7	−655.3	−825.3	−995	−1166	−1336	−1762	−2187
$L(+1+1\ 2+2)$	−84.96	−109.6	−134.3	−183.6	−380.8	−578.0	−775	−972	−1170	−1367	−1564	−2057	−2550

as

$$dh=\left\langle\frac{\mu_i^2}{i^2r^3}\right\rangle\frac{I(I+1)+4i(i+1)}{5(2I-1)(2I+3)}$$
$$-\frac{eQ\partial^2V^e/\partial z_0^2}{10i(2i-1)}\left[1-\frac{I(I+1)+4i(i+1)}{(2I-1)(2I+3)}\right] \quad (6)$$

where r is the distance between the two nuclei, Q is the deuteron quadrupole moment, V^e is the potential from the charges external to a small sphere surrounding the nucleus and z_0 is along the internuclear axis of the molecule. The quantity $\partial^2V^e/\partial z_0^2$ is related[9] to the quantity q of KRRZ[2] by

$$\partial^2V^e/\partial z_0^2=-eq(2J+3)/J. \quad (7)$$

The last two terms in (1) are for the diamagnetic interaction of the molecule with the external magnetic field. If ξ_σ is the magnetic susceptibility of the molecule for a field perpendicular to internuclear axis and ξ_π is the susceptibility parallel to that axis

$$f=(\xi_\sigma-\xi_\pi)H^2/5h \quad (8)$$

and

$$g=(\tfrac{1}{3}\xi_\sigma+\tfrac{1}{6}\xi_\pi)H^2/h. \quad (9)$$

The form of diamagnetic interaction given in (1), (8), and (9) arises from averaging the $\sin^2\theta$ of Ramsey's paper[10] on diamagnetic interaction in the same manner as in his later paper[9] on magnetic shielding. Theoretical expressions for ξ_σ and ξ_π have been given.[10] The quantity f is related to the quantities $\xi_{\pm1}$, ξ_0, and k previously used by Ramsey[3] by[10]

$$f=H^2(\xi_{\pm1}-\xi_0)/2h=H^2k\mu_J/Jh. \quad (10)$$

In principle, the magnetic shielding which arises in the spin-spin magnetic interaction should also be included.† However, this correction has been negligibly small in all experiments so far and consequently is omitted here. However, when the external magnetic field is so weak that the spin-spin magnetic interaction is comparable to the interaction of either spin with the magnetic field, the diamagnetic correction for the external field is comparably small. Consequently, for consistency in approximations as well as for simplification, all diamagnetic corrections will be omitted in magnetic fields sufficiently low that a perturbation treatment in the high field approximation is not adequate.

The cases of greatest experimental interest[1, 2, 6] are molecular hydrogen and deuterium in the first rotational state for both of which $I=J=1$. In these cases the subscripts H and D can be used to designate hydrogen and deuterium and

$$d_Hh=\langle 4\mu_H^2/5r^3\rangle=(2/5)2\mu_HH_H'' \quad (11)$$

$$d_Dh=\left\langle\frac{2\mu_D^2}{5r^3}\right\rangle+\frac{1}{10}eQ\frac{\partial^2V^e}{\partial z_0^2}$$
$$=(2/5)\mu_D(H''_D+H'''_D)=2\mu_DS_D \quad (12)$$

TABLE VII. Numerical solution of secular equation for D_2. The energy divided by h is given in kilocycles per second for the designated state in the indicated magnetic field. Magnetic field (gauss).

State $(m_I m_J F m)$	0	10	20	50	100	200	300	400	600	800	1000
$A(-1-1\ 2-2)$	3.84	13.74	23.65	53.36	102.9	201.9	301.0	400.0	598.1	796.2	994.2
$B(-1\ 0\ 2\ -1)$	3.84	8.84	13.92	29.66	57.39	116.8	179.0	242.6	371.3	500.9	631.1
$C(-1+1\ 0\ 0)$	143.8	143.8	143.9	144.6	147.2	157.0	172.6	192.7	241.9	297.4	356.0
$D(0-1\ 1-1)$	−54.32	−49.41	−44.59	−30.62	−8.83	30.80	67.60	103.2	172.6	240.9	308.9
$E(0\ 0\ 2\ 0)$	3.84	3.91	4.06	5.21	8.76	18.11	26.66	32.96	40.51	44.31	46.30
$F(0+1\ 2+1)$	3.84	−1.08	−5.90	−19.87	−41.65	−81.28	−118.1	−153.6	−223.0	−291.4	−359.4
$G(+1-1\ 1\ 0)$	−54.33	−54.41	−54.68	−56.54	−62.61	−81.80	−105.9	−132.4	−189.1	−248.4	−309.0
$K(+1\ 0\ 1+1)$	−54.32	−59.32	−64.40	−80.14	−107.9	−167.3	−229.5	−293.0	−421.7	−551.4	−681.6
$L(+1+1\ 2+2)$	3.84	−6.06	−15.97	−45.68	−95.20	−194.2	−293.3	−392.3	−590.4	−788.5	−986.6

[9] B. T. Feld, Phys. Rev. **72**, 1116 (1947).
[10] N. F. Ramsey, Phys. Rev. **78**, 221 (1950).
† *Note added in proof.*—The effect of magnetic shielding on the nuclear spin-spin interaction is discussed in a letter by Ramsey and Purcell now in course of publication in *The Physical Review*.

TABLE VIII. Transition frequencies for allowed transitions in the strong field limit. The transition designation is the same for H_3 and D_3.

Transition	m_I	m_J	m_I'	m_J'	Transition frequency
AD/FL	$-1/0$	∓1	$0/+1$	∓1	$(1-\sigma_{11})a\pm(-c+\frac{1}{2}d)$ $+C_3'$
DG/CF	$0/-1$	∓1	$+1/0$	∓1	$(1-\sigma_{11})a\mp(c+\frac{1}{2}d)$ $+C_3-C_3'$ $\pm C_3$
BE/EK	$-1/0$	0	$0/+1$	0	$(1-\sigma_{10})a\mp3d$ $+C_3'$ $\mp2C_3$
AB/KL	∓1	$-1/0$	∓1	$0/+1$	$(1-\sigma_{J1})b\pm(-c+\frac{1}{2}d)\mp f$ $-C_3'$
BC/GK	∓1	$0/-1$	∓1	$+1/0$	$(1-\sigma_{J1})b\mp(c+\frac{1}{2}d)\pm f$ $-(C_3-C_3')$ $\pm C_3$
DE/EF	0	$-1/0$	0	$0/+1$	$(1-\sigma_{J1})b\mp3d$ $\mp f$ $-C_3'$ $\mp2C_3$

where H'', H''', and S_D are identical with the corresponding quantities used by KRRZ.[1-3]

III. THE ENERGY MATRICES

From (1) the energy matrices can be calculated. This will be done only for $I=J=1$, since this is the case of greatest interest.

The energy matrix will first be written in the m_Im_J representation which is most appropriate to strong external fields. To simplify the writing one can let σ_{i0} be the magnetic shielding of the nucleus when $m_J=0$ and σ_{i1} when $m_J=\pm1$. Then, from (3)

$$\sigma_{i0}=\tfrac{2}{3}\sigma_\sigma+\tfrac{1}{3}\sigma_\pi, \quad \sigma_{i1}=\tfrac{1}{3}\sigma_\sigma+\tfrac{1}{3}\sigma_\pi. \tag{13}$$

The nonvanishing matrix elements of $(m_Im_J|\mathcal{H}|m_i'm_J')$ with the aid of the tables in KRRZ[3] can be shown to have the values given in Table I.

Alternatively one can use the F, m representation which is most appropriate to very weak magnetic fields where F is the total quantum number of the resultant angular momentum $\mathbf{F}$ which equals $\mathbf{I}+\mathbf{J}$ and m is the magnetic quantum number of $\mathbf{F}$. In the weak field limit to which this representation is most appropriate the diamagnetic corrections are very small and indeed are comparable to the diamagnetic correction to the spin-spin magnetic interaction which has already been omitted because of its small size. Therefore, all diamagnetic corrections are omitted in the matrix elements. In the evaluation of some of the matrix elements from (1), the tables of Feld and Lamb[11] are useful. The nonzero matrix elements $(Fm|\mathcal{H}|F'm')$ have the values given in Table II.

IV. PERTURBATION THEORIES

Perturbation theory calculations appropriate to the high field limit have been carried out by KRRZ with the omission of the magnetic shielding and diamagnetic interaction terms. When these are included, one obtains for the energies of the nine states the expressions given in Table III, where perturbations up to third order are included. For the simplification of the correlation of the states in the strong field limit to those in the weak field limit, each state is designated with a capital letter which is used for the same state in the low field limit. The notation A/L, used when plus or minus (±1) signs are employed, indicates that the upper choice of sign goes with state A while the lower goes with state L.

In the weak field limit, the energy levels can be calculated from the energy matrix of Table II. The results to third-order perturbation theory are given in Table IV. Corresponding to the fact that the Fm and m_Im_J quantum numbers are differently correlated to each other in the H_3 and D_3 cases because of the numerically different values of the parameters, the state designations are different in the H_3 and D_3 cases.

V. SOLUTION OF SECULAR EQUATION

For intermediate values of the magnetic field, the secular equation must be solved. For reasons mentioned previously, the magnetic shielding and diamagnetic interaction terms will be omitted in the calculation of the secular equation. From either Table I or II the solutions of the secular equations become

$$W_{A/L}/h=\pm a\pm b-c+\tfrac{1}{4}d \tag{14}$$

TABLE IX. Transition frequencies for allowed transitions in weak field limit. Primes on the designation for the transition indicates a transition with $\Delta m=0$.

Transition H_3	D_3	F	m	F'	m'	Transition frequency	
CB/CF	CD/CK	0	0	1	∓1	$c+(15/2)d\mp\frac{1}{2}(a+b)$	$-\frac{1}{2}K_3+K_3'$
CE'	CG'	0	0	1	0	$c+(15/2)d$	$-\frac{1}{2}K_3+2K_3'$
BA/FL	DA/KL	1	∓1	2	∓2	$2c-3d\mp\frac{1}{2}(a+b)$	$+\frac{1}{2}K_3$
BD'/FK'	DB'/KF'	1	∓1	2	∓1	$2c-3d$	$+\frac{1}{2}K_3$
BG/FG	DE/KE	1	∓1	2	0	$2c-3d\pm\frac{1}{2}(a+b)$	$+(7/12)K_3$
ED/EK	GB/FG	1	0	2	∓1	$2c-3d\mp\frac{1}{2}(a+b)$	$+\frac{1}{2}K_3$
EG'	GE'	1	0	2	0	$2c-3d$	$+\frac{1}{2}K_3-K_3'$
BE/FE	DG/KG	1	∓1	1	0	$\pm\frac{1}{2}(a+b)$	$-(1/12)K_3+K_3'$
AD/LK	AB/LF	2	∓2	2	∓1	$\pm\frac{1}{2}(a+b)$	$+\frac{1}{2}K_3$
DG/KG	BE/FE	2	∓1	2	0	$\pm\frac{1}{2}(a+b)$	$+(1/12)K_3$

[11] B. T. Feld and W. Lamb, Phys. Rev. **67**, 15 (1945).

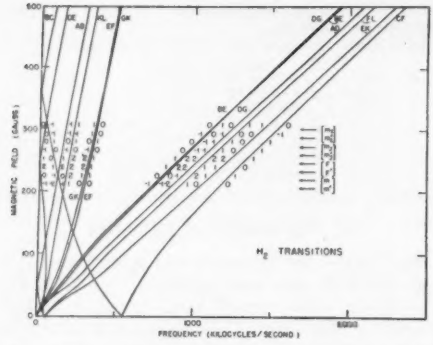

FIG. 3. Frequencies of H_2 transitions that are allowed in the strong field limit. Curves that are dashed along the lower halves indicate forbidden transitions in the weak field limit whereas the full curves indicate allowed transitions in the weak field limit.

$$W_{B/K}/h=\tfrac{1}{2}(\pm a\pm b-2d) \pm\tfrac{1}{2}[(a-b)^2+4(-c+\tfrac{3}{2}d)^2]^{\frac{1}{2}} \quad (15)$$

$$W_{D/F}/h=\tfrac{1}{2}(\pm a\pm b-2d) \mp\tfrac{1}{2}[(a-b)^2+4(-c+\tfrac{3}{2}d)^2]^{\frac{1}{2}} \quad (16)$$

and W_C, W_A, and W_E are the three roots of the cubic equation

$$(W/h)^3-(2c+3d)(W/h)^2 -[(a-b)^2+c^2+45d^2/4+cd](W/h)+2(a-b)^2d -\tfrac{1}{2}(d-2c)(-(5/2)d+c)(5d+2c)=0. \quad (17)$$

W_C is the root which in the high field limit approaches $(a-b)h$ while W_A approaches $(-a+b)h$.

Although, the cubic equation can, in principle, be solved analytically, in practice it is more convenient to leave it in the above form and to solve the cubic numerically. This has been done for H_2 and D_2. The

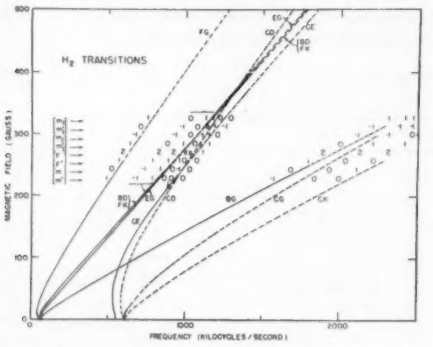

FIG. 4. Frequencies of H_2 transitions that are forbidden in the strong field limit. Curves that are dashed along the lower halves indicate forbidden transitions in the weak field limit whereas the full curves indicate allowed transitions in the weak field limit.

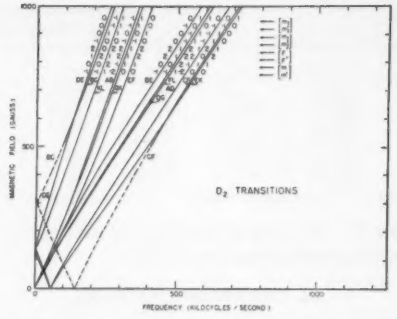

FIG. 5. Frequencies of D_2 transitions that are allowed in the strong field limit. Curves that are dashed along the lower halves indicate forbidden transitions in the weak field limit whereas the full curves indicate allowed transitions in the weak field limit.

constants assumed for a, b, c, and d are given in Table V. These are the best values obtainable from the experiments of Kolsky, Phipps, Ramsey, and Silsbee.[4-6]

The results of these calculations are plotted in Figs. 1 and 2. Since in interpreting the experiments, more accuracy is often needed than that available from the curves, the numerical results obtained are also tabulated in Tables VI and VII.

VI. RESONANCE FREQUENCIES

In the high field limit, expressions for the transition frequencies can be obtained by differencing the energies of Table III. The results are given in Table VIII. Only transitions allowed in strong fields ($\Delta m_I=\pm 1$, $\Delta m_J=0$, or $\Delta m_I=0$, $\Delta m_J=\pm 1$) are listed. The transition from state A to state D is designated as AD.

In the low field limit, expressions for the transition frequencies can be obtained by differencing the energies of Table IV. The results for the allowed transitions

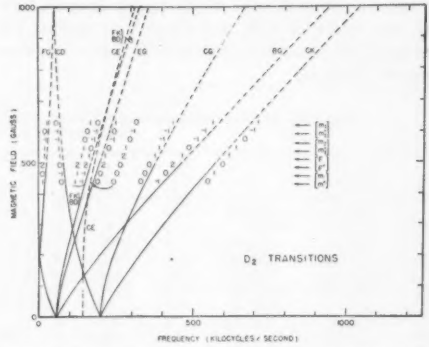

FIG. 6. Frequencies of D_2 transitions that are forbidden in the strong field limit. Curves that are dashed along the lower halves indicate forbidden transitions in the weak field limit whereas the full curves indicate allowed transitions in the weak field limit.

($\Delta F=0, \pm1, \Delta m=0, \pm1$) are given in Table IX. A prime added to the transition designation as CE' indicates a transition for which $\Delta m=0$. The oscillating field inducing such transitions must be parallel to the external field.

In intermediate fields the transition frequencies can be obtained by differencing the values of Tables VI and VII. The results of such a procedure are plotted in Figs. 3, 4, 5, and 6. Lines which are dotted along either their upper or lower halves indicate transitions forbidden in either the strong or weak field limit. The quantum numbers associated with each transition can be obtained by correlating the quantum numbers with the transition designation with the aid of Tables III and IV.

The author wishes to thank Mr. Vaughn Culler for his assistance in calculating the values in Tables VI and VII.

PHYSICAL REVIEW VOLUME 85, NUMBER 1 JANUARY 1, 1952

Superposition of Configurations in the Ground State of He I*

LOUIS C. GREEN AND MARJORIE M. MULDER, *Strawbridge Observatory, Haverford College, Haverford, Pennsylvania*
C. W. UFFORD AND E. SLAYMAKER, *Randall Morgan Laboratory, University of Pennsylvania, Philadelphia, Pennsylvania*
ELEANOR KRAWITZ AND R. T. MERTZ, *Watson Scientific Computing Laboratory, Columbia University, New York, New York*

(Received September 24, 1951)

To obtain some understanding of the role played by various configurations in configuration interaction, the Hylleraas six-term expression for the ground-state wave function of He I has been expanded in series of orthogonal functions. To determine the degree of dependence of the coefficients of the expansion on the specific function used for the ground state, the Hylleraas three-term expression was also expanded. Two sets of orthogonal functions were used. One set consisted of orthogonalized symmetrized product type wave functions where the functions for the individual electrons were found from a Hartree self-consistent field without exchange. The second set consisted of orthogonalized variationally determined analytic wave functions. The results emphasize the large number of configurations which would have to be considered if the Hylleraas wave function were to be represented with high accuracy. After $1s^2$ the largest contributors among the configurations considered were $2p^2$ and $2s^2$.

IT has long been recognized[1] that the method of the self-consistent field involves three principal approximations: (a) the neglect of relativity effects, (b) the neglect of exchange effects, and (c) the neglect of the nonseparability of the wave functions. Relativity effects should be small for the lighter atoms. Exchange effects have been extensively investigated, principally by Hartree using Fock's equations. The inclusion of exchange improves the wave functions considerably and usually improves the energies somewhat. However, something is left to be desired. For example in O, O^+, and O^{++} the average difference between the observed and the calculated energies for the three lowest states are found to be 0.188, 0.088, and 0.114 respectively in units of the ionization energy of hydrogen when self-consistent field wave functions without exchange are used with Slater's integrals.[2] If wave functions with exchange are employed, the values obtained are 0.198, 0.086, and 0.080 with no improvement in the ratio of the multiplet separations.[3] To obtain further improvement one may attempt to remove the approximation involved in the neglect of the nonseparability of the wave functions. This has usually been done by considering the effects of superposition of configurations. A number of calculations of this sort have been made.[4] In general some improvement in multiplet separations has been obtained when superposition was included but in the two most thorough treatments of such effects by self-consistent field methods, the work of Hartree[5] on O, O^+, and O^{++} and the work of Jucys[5] on C, the results were disappointing. Hartree, by the superposition of $1s^22p^{6+2}$ on $1s^22s^22p^6$, obtained for the average difference between the observed and calculated energies for the same lowest states of O, O^+, and O^{++} mentioned above 0.180, 0.108, and 0.090 respectively using wave functions with exchange to determine the effects of the configuration interaction. The ratio of the multiplet separations was considerably improved for O and somewhat improved for O^+ and O^{++}. Jucys, by superposing $1s^22s^22p^2$, $1s^22p^4$, $1s^22s^32p3p$, and $1s^22s2p^23s$ for CI reduced the average difference between the observed

* This work was supported in part by an ONR contract administered by the University of Pennsylvania, and in part by a grant from the Research Corporation.

[1] D. R. Hartree and W. Hartree, Proc. Roy. Soc. (London) **A150**, 9 (1935).

[2] D. R. Hartree and M. M. Black, Proc. Roy. Soc. (London) **A139**, 311 (1933).

[3] Hartree, Hartree, and Swirles, Trans. Roy. Soc. (London) **A238**, 229 (1939).

[4] C. W. Ufford, Phys. Rev. **44**, 732 (1933). R. E. Trees, Phys. Rev. **83**, 756 (1951). A. A. Schweizer, Phys. Rev. **80**, 1080 (1950). E. Trefftz, Z. Astrophys. **26**, 240 (1949) and **28**, 67 (1950). H. H. Marvin, Phys. Rev. **47**, 521 (1935). A. Many, Phys. Rev. **70**, 511 (1946). F. Rohrlich, Phys. Rev. **74**, 1372 (1948). J. N. P. Hume and M. F. Crawford, Phys. Rev. **84**, 486 (1951).

[5] A. Jucys (sometimes transliterated A. Yutsis), J. Exp. Theor. Phys., U.S.S.R. **19**, 565 (1949).

TABLE I. Coefficients for the expansions of Hylleraas functions for the ground state of He I in terms of symmetrized product type functions.

Configurations	Self-consistent field functions: Six-term Ψ_H Non-Or.	Six-term Ψ_H Orthog.	Three-term Ψ_H Non-Or.	Three-term Ψ_H Orthog.	Analytic functions: Three-term Ψ_H Non-Or.	Three-term Ψ_H Orthog.
$1s^2$	+0.9966	+0.9961	+0.9955	+0.9955	+0.9873	+0.9928
$1s2s$	−0.0020	−0.0023	−0.0004	−0.0005	+0.0556	+0.0553
$1s3s$	−0.0018	−0.0018	−0.0012	−0.0012		
$2s^2$	−0.0263	−0.0263				
$2p^2$ [a]	−0.0273	−0.0273	−0.0223	−0.0223		
Sum of squares of coefficients	+0.9947	+0.9936	+0.9915	+0.9915	+0.9779	+0.9887

[a] Spin and angular part chosen with signs as follows: $-6^{-\frac{1}{2}}(\alpha_1\beta_2-\beta_1\alpha_2)\times\{Y(1,1|1)Y(1,-1|2)-Y(1,0|1)Y(1,0|2)+Y(1,-1|1)Y(1,1|2)\}$.

and calculated energies for the three terms of the lowest configuration, $1s^22s^22p^2$, from 0.556 to 0.482 using self-consistent field wave functions without exchange, but the ratio of the multiplet separations became somewhat poorer.

In view of these results it seemed wise to investigate the effects of superposition by considering a relatively simple case in some detail. Consequently it was decided to expand certain of the Hylleraas wave functions for the ground state of He I in terms of sets of functions representing the various configurations.[6]

The six-term Hylleraas wave function gives the energy of the ground state of He I to one part in 6600. This accuracy was thought to be adequate for a preliminary survey. It also seemed wise to expand the Hylleraas three-term function at the same time in order to gain some knowledge of the dependence of the coefficients of the expansion on the specific function used for the ground state. This function reproduces the experimentally determined energy to one part in 2300. The two functions used for the ground state were therefore

$$\Psi_H=N_6e^{-Z_6s}(1+a_1u+a_2t^2+a_3s+a_4s^2+a_5u^2)$$

and

$$\Psi_H=N_3e^{-Z_3s}(1+b_1u+b_2t^2),$$

where $s=\rho_1+\rho_2$, $t=\rho_1-\rho_2$, and $u=\rho_{12}$, and the ρ's are expressed in atomic units. The values which were used for the constants were: $N_6=1.38189$, $Z_6=1.818$, $a_1=0.353$, $a_2=0.128$, $a_3=-0.101$, $a_4=0.033$, $a_5=-0.032$, and $N_3=1.32135$, $Z_3=1.816$, $b_1=0.30$, $b_2=0.13$.

The more critical choice is that of what type of functions to use in the expansion. Since more complicated atoms can be treated with moderate success only in the central field approximation, it seemed wise to test the effect of superposition in the present case by using sets of functions whose individual members were identifiable with particular solutions of the central field problem. The best functions of this type for He I are those for the self-consistent field without exchange given by Wilson and Lindsay.[7] Among the configurations which they give, we have used the following $1s^2$, $1s2s$, $2s^2$, and $2p^2$. To these we have added $1s3s$. Since the coefficients in the expansion depend on the set of functions used, it was thought desirable to see how the coefficients changed when a second set of functions was used. For this purpose analytic functions were chosen. For the $1s^2$ configuration the function $\exp[-1.6875(\rho_1+\rho_2)]$ was used, and for $1s2s$ the variationally determined function given by Morse, Young, and Haurwitz.[8]

The number of configurations which need to be considered in the present case is considerably reduced by the fact that superposition of configurations can only occur between configurations of the same parity.[9] Among the configurations involving electrons with smaller l-values we are thus limited to those of types: *nsms*, *npmp*, *nsmd*, and *ndmd*. Further, in pure Russell-Saunders coupling, only terms with the same L and S interact.[9] In He I the term intervals of the $1s2p\ ^3P$ are of the order 1 cm^{-1} whereas the separation of the ^3P and the ^1P is of the order of 2050 cm^{-1}. The coupling would therefore appear to be almost purely Russell-Saunders in character. Since the ground state is certainly primarily $1s^2\ ^1S$, the configuration *nsmd* can be eliminated. In addition it is only necessary to consider the ^1S terms of the remaining configurations. From the numerical wave functions given by Wilson and Lindsay, symmetrized products were made up and these were the functions used in the expansion. Morse's variational wave function for the $1s2s\ ^1S$ state was already in the symmetrized form.

The results of the present work are collected in Table I. The meaning of the various columns is clear except for the headings of Non-Or. and Orthog. to whose explanation we now turn. If the Hylleraas wave function, Ψ_H, is written

$$\Psi_H=c_1\psi(1s^2)+c_2\psi(1s2s)+\cdots, \qquad (1)$$

where the ψ's are the symmetrized product functions described above, we are at once faced with the fact that these ψ's are not orthogonal except for the $2p^2$ function which is orthogonal to all *nsms* functions. In view of this, two sets of coefficients are given in Table I for each of the expansions which have been made. One set is determined using the non-orthogonal functions. In this case we assume that (for the numerical functions) the five configurations considered, namely $1s^2$, $1s2s$, $1s3s$, $2s^2$, and $2p^2$, are the only ones which make any contribution to the ground state. One can then solve the system of simultaneous linear equations obtained from Eq. (1) by multiplication of both sides by the various ψ's and integration over all space for the different c's.

[6] The possibility of treating configuration interaction in He I in this way was suggested to one of us (L. C. G.) by Dr. G. Breit.

[7] W. S. Wilson and R. B. Lindsay, Phys. Rev. **47**, 681 (1935). We are indebted to these authors for supplying us with more complete tables of their wave functions than were published.

[8] Morse, Young, and Haurwitz, Phys. Rev. **48**, 948 (1935).

[9] E. U. Condon and G. H. Shortley, *The Theory of Atomic Spectra* (Cambridge University Press, London, 1935), p. 366.

It was felt that if the values obtained for the various coefficients did not change appreciably as the series was broken off after three, four, and five terms, considerable confidence could be placed in the values obtained even from this limited expansion. In the worst case, that of $1s^2$, in going from the three to the four term expression the change was only 0.0004 so that some measure of stability seems to have been obtained in the values of these coefficients.

Another possible way of dealing with the fact that our ψ's are not orthogonal is, of course, to build from them by the Schmidt process[10] a new set of functions which are orthogonal. This has also been done and the results are given in Table I. However, such a procedure is open to some criticism, for the different members of the set of self-consistent field functions are not solutions of the same differential equation and of course this is also true of the analytic functions. After orthogonalization the nature of the new functions is somewhat obscure. On the other hand, it is clear from the similarity of the coefficients for the orthogonal and non-orthogonal functions in Table I that the effect of orthogonalization is small, that is, the ψ's were almost orthogonal initially. This would of course account for the stability of the coefficients of the ψ's noted above. As far as the effect of orthogonalization on the functions is concerned, it would therefore seem that the results in Table I can be taken with some confidence.

If now the coefficients in Table I are examined, the importance of the $1s^2$ configuration appears in every column. This is, of course, no surprise in view of the fact that the energy of $1s^2$, as found for example by Wilson[11] differs by only 1.4 percent from the experimentally determined value and the contribution to the ground state energy of this configuration should be roughly proportional to the square of its coefficient in Table I.

Perhaps the second most noticeable point in Table I is the large size of the coefficients for $2s^2$ and $2p^2$. These are so much larger than the coefficients for other excited states considered that it was thought wise, in spite of the agreement of the customary checking computations, to repeat the whole calculation for at least one of them using different numerical methods. The result obtained for $2s^2$ was 0.0266, somewhat larger but less accurate than before. It might appear possible that the large size of this coefficient was the result of not having orthogonalized this function to all the various possible members of the $1sms$ set of functions. An examination of the effect on this coefficient of orthogonalizing $2s^2$ to $1s^2$, $1s2s$, and $1s3s$ shows that the largest effect arises from $1s^2$ but that even here it is necessary to subtract only 0.01648 of $1s^2$ from Wilson and Lindsay's $2s^2$ to obtain a $2s^2$ orthogonal to $1s^2$. It therefore seems unlikely, but not certain, that the coefficient for $2s^2$ would be radically changed by orthogonalization to all members of the $1sms$ set. To check the coefficients of $2p^2$ further, the value of the constants in an arbitrary linear combination of $1s^2\ {}^1S$ and $2p^2\ {}^1S$ using hydrogenic functions with $Z=2$ have been determined by the variational method. The coefficient of the $2p^2\ {}^1S$ proved to be 0.0271 in as good agreement as could be expected with the value given in Table I for the six-term Hylleraas function. Since $2p^2$ is orthogonal to all $nsms$ wave functions and is the lowest member of the $npmp$ set, there is no possibility of any reduction in the size of its coefficient through orthogonalization.

It is also clear from Table I that the values of the coefficients for the configurations making the smaller contribution are sensitive to whether the three or the six term Hylleraas function is used. The indication is, however that the larger coefficients are relatively stable.

Finally it should be noted that if the expansions represented the Hylleraas function accurately, the sum of the squares of the expansion coefficients of the orthogonal functions would be one. Since the coefficients of all configurations considered other than $1s^2$ are small and therefore make a still smaller contribution to the sum of the squares, it is highly probable that it would be necessary when using self-consistent field functions to consider a large number of configurations if the ground-state wave function or energy is desired to high accuracy.

In summary, the present work emphasizes (a) the large contribution of $1s^2$ to the ground state wave function, (b) the surprisingly large size of the $2s^2$ and $2p^2$ contributions, and (c) the very large number of configurations which would have to be considered if a high accuracy wave function or energy were desired.

[10] D. Jackson, *Fourier Series and Orthogonal Polynomials* (Carus Monograph No. 6, the Mathematical Association of America, Oberlin, Ohio, 1941), p. 151.

[11] W. S. Wilson, Phys. Rev. **48**, 536 (1935).

Pressure Effects of Argon and Helium on the Resonance Lines of Silver*

EUGENE D. CLAYTON AND SHANG-YI CH'EN
Physics Department, University of Oregon, Eugene, Oregon

(Received September 25, 1951)

The shift and the broadening of Ag λλ3280 and 3382 produced by argon and helium for pressures up to 83.3 atmospheres at about 950°C were determined. The shift of Pb 2833 was also measured under the same conditions. Argon produces a red shift and a slight red asymmetry, while helium produces a violet shift and a very slight violet asymmetry for all these lines. The $^2P_{\frac{1}{2}}$ component of silver resonance lines is shifted more than the $^2P_{\frac{3}{2}}$ component. The relative difference in the shift is much more pronounced for helium than for argon. For helium the $^2P_{\frac{1}{2}}$ component is shifted about six times greater than the $^2P_{\frac{3}{2}}$ component.

Both the shift and the broadening appear to be linear with the relative density for argon or helium. The $^2P_{\frac{1}{2}}$ component produces a shift of 0.289 cm^{-1} (red) per unit relative density of argon, and of 0.131 cm^{-1} (violet) per unit relative density of helium. The corresponding figures for the $^2P_{\frac{3}{2}}$ component are 0.248 cm^{-1} (red) and 0.023 cm^{-1} (violet) per unit r.d. Shifts for Pb 2833 are respectively 0.388 cm^{-1} (red) and 0.188 cm^{-1} (violet) per unit r.d. for argon and helium.

There is no significant difference between the half-widths of the doublet components of the silver lines for helium. They are broadened 0.466 cm^{-1} per unit r.d. For argon the $^2P_{\frac{3}{2}}$ component is broadened slightly more than the $^2P_{\frac{1}{2}}$ component. The $^2P_{\frac{1}{2}}$ and the $^2P_{\frac{3}{2}}$ components are broadened respectively 0.468 cm^{-1} and 0.560 cm^{-1} per unit r.d. The optical collision diameters as calculated from the half-widths turn out to be 6.50A for He-Ag and 11.3A for A-Ag.

ALTHOUGH experimental observations of the pressure effects of foreign gases on the absorption lines of alkali metals have been made quite extensively, very little is known of other metal lines except Hg. In the present research the resonance lines of silver were found quite convenient for investigation. The shift and broadening of the λ3280 and λ3382 for silver were measured for pressures up to 83.3 atmospheres of helium or argon at about 950°C. The λ2833 of lead appeared in the absorption spectrum as an impurity, and the shift of this line was measured under the same conditions.

TABLE I. Shift of the resonance lines of silver produced by argon and helium.

Plate No.	P atmos	T °K	Relative density	Shift (λ3382) A	Shift (λ3382) cm^{-1}	Shift (λ3280) A	Shift (λ3280) cm^{-1}
			(a) Argon—Red				
29	6.80	1228	1.51	0.069	0.60	0.024	0.23
29	13.61	1238	3.00	0.158	1.38	0.108	1.00
29	20.41	1228	4.54	0.131	1.14	0.062	0.58
29	27.22	1228	6.05	0.138	1.21	0.111	1.03
28	37.43	1193	8.56	0.296	2.58	0.237	2.20
28	50.35	1198	11.47	0.369	3.23	0.281	2.61
31	59.54	1213	13.40	0.461	4.03	0.379	3.52
31	68.05	1213	15.31	0.461	4.03	0.356	3.31
30	74.85	1203	16.99	0.608	5.31	0.480	4.46
30	83.36	1203	18.92	0.621	5.43	0.563	5.23
			(b) Helium—Violet				
26	13.61	1193	3.11	0.049	0.43	0.023	0.21
26	20.41	1198	4.65	0.050	0.43	0.022	0.20
25	27.22	1203	6.18	0.091	0.79	0.006	0.05
25	34.02	1203	7.72	0.109	0.95	0.026	0.24
24	42.19	1248	9.23	0.140	1.23	0.034	0.31
33	47.63	1228	10.59	0.147	1.29	0.032	0.30
33	57.84	1228	12.86	0.201	1.76	0.023	0.21
32	68.05	1228	15.13	0.251	2.20	0.043	0.40
32	83.36	1228	18.53	0.263	2.30	0.036	0.33

* This work was supported by the Frederick Gardner Cottrell grant of the Research Corporation.

EXPERIMENTAL

The construction of the stainless steel pressure tube was essentially the same as before.[1] The pressure windows were made of clear fused quartz plugs held by Nilvar cones, which was kept below 300°C to avoid leakage. The inner absorption tube was 13.3 cm long. Two clear fused quartz rods were inserted in the main pressure tube for the purpose of reducing the convection currents present in the light path. These rods also served as the windows for the inner absorption tube. The tube was heated by means of a nichrome heating coil. With a power of 1600 watts a temperature of about 950°C could be obtained within about 30 minutes.

The Bausch and Lomb large Littrow quartz spectrograph has a dispersion of 5.985A/mm in the region of the 3280A line, 6.518A/mm in the region of the 3382A line. The shift was determined by means of the precision comparator by David W. Mann. Readings could be made directly by 0.001 mm, and estimated to 0.0001

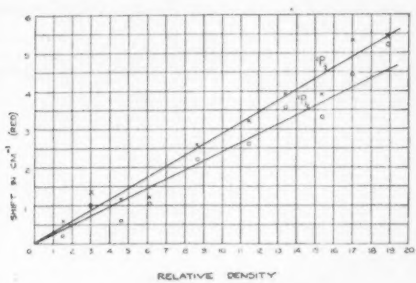

FIG. 1. Shift *vs* relative density of argon.

[1] Shang-yi Ch'en, Phys. Rev. **58**, 1051 (1940).

mm. A number of readings were taken on each line; the plate was then reversed and the readings repeated so as to minimize personal error in determining the line centers.

A hydrogen discharge tube was used as light source. The Eastman type III-0 plates were calibrated by means of five neutral screens and a recording microphotometer. The half-widths as here determined are the widths of the lines at half of their intensity maxima.

The foreign gases were supplied by the Matheson Company. The purity of helium was stated to be 99.8 percent and that of argon, 99.6 percent. The impurities in helium were listed as nitrogen with a small amount of hydrogen, and those in argon as 0.001 percent hydrogen and 0.001 percent oxygen with the balance of nitrogen.

RESULTS

(1) The Shift of Ag Lines

The shift of the silver doublet under different pressures of argon and helium up to 83.3 atmospheres is

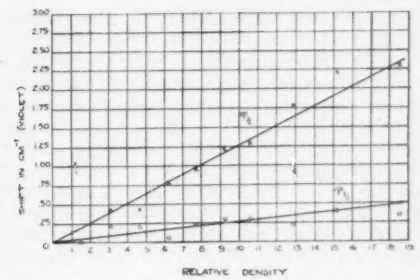

FIG. 2. Shift *vs* relative density of helium.

summarized in Table I and plotted in Figs. 1 and 2. It is to be noted that for argon both lines are displaced towards the red and the $^2P_{\frac{1}{2}}$, or the long wavelength component, is shifted more than the $^2P_{\frac{3}{2}}$ component. For helium both lines are shifted towards the violet. The relative difference in the shift of the two components is much more pronounced for helium. The $^2P_{\frac{3}{2}}$ component is shifted about six times greater than the $^2P_{\frac{1}{2}}$ component.

For both argon and helium the shift is seen to be linear with the relative density. By the method of least squares the slopes of the lines in Figs. 1 and 2 were obtained. The shifts are:

For the $^2P_{\frac{1}{2}}$ component:

0.289 cm^{-1} (red)/unit r.d. of argon
0.131 cm^{-1} (violet)/unit r.d. of helium.

For the $^2P_{\frac{3}{2}}$ component:

0.248 cm^{-1} (red)/unit r.d. of argon
0.023 cm^{-1} (violet)/unit r.d. of helium.

TABLE II. Shift of the λ2833 lead line produced by argon and helium.

Plate No.	P atmos	T °K	Relative density	A	Shift cm^{-1}
			(a) Argon—Red		
29	6.80	1228	1.51	0.043	0.54
29	13.61	1238	3.00	0.122	1.51
29	20.41	1228	4.54	0.097	1.20
29	27.22	1228	6.05	0.128	1.60
28	37.43	1193	8.56	0.323	4.02
			(b) Helium—Violet		
27	6.80	1198	1.55	0.003	0.03
26	13.61	1193	3.11	0.049	0.61
26	20.41	1198	4.65	0.066	0.82
25	27.22	1203	6.18	0.107	1.34
25	34.02	1203	7.72	0.112	1.40
24	42.19	1248	9.23	0.138	1.72

(2) The Shift of the Lead Line λ2833

The shift of Pb 2833 under helium and argon is given in Table II and Fig. 3. Argon produces red shift, while helium produces a violet. The shift resulting from argon is greater than that from helium. The slopes of the lines for argon and helium are respectively 0.388 cm^{-1} and 0.188 cm^{-1} per unit relative density of these gases.

(3) The Broadening of the Silver Lines

Table III and Fig. 4 give the data pertaining to the half-width of the silver doublet under various pressures of helium and argon. For helium there is no significant difference between the half-widths of the doublet components. They are broadened 0.466 cm^{-1} per unit relative density. For argon the $^2P_{\frac{1}{2}}$ component is broadened slightly more than the $^2P_{\frac{3}{2}}$ component. The $^2P_{\frac{1}{2}}$ and the $^2P_{\frac{3}{2}}$ components are broadened respectively 0.468 cm^{-1} and 0.560 cm^{-1} per unit relative density. Argon produces a slight asymmetry towards the red, while helium a very small asymmetry towards the violet. Doppler half-widths were calculated for these components at a temperature of 952°C. They are 0.071 and 0.073 cm^{-1} respectively.

(4) The Optical Collision Diameters

From the measured half-widths, $\Delta\nu_{\frac{1}{2}}$, of the lines it is possible to calculate the optical collision diameters,

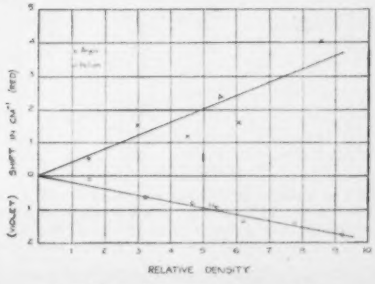

FIG. 3. Shift of Pb 2833 *vs* relative density.

TABLE III. Half-widths of the resonance lines of silver produced by argon and helium.

Plate No.	P atmos	T °K	Relative density	Half-width A (λ3280) cm^{-1}		A (λ3382) cm^{-1}	
			(a) Argon				
20	9.53	1183	2.20	0.377	3.50	0.447	3.91
19	23.14	1203	5.25	0.542	5.04	0.570	4.98
28	37.43	1193	8.56	0.823	7.65	0.735	6.42
28	50.35	1198	11.47	0.867	8.06	0.800	6.99
31	59.54	1213	13.40	1.030	9.57	1.078	9.42
30	74.85	1203	16.99	1.287	11.96	1.090	9.53
30	83.36	1203	18.92	1.708	15.87	1.423	12.43
			(b) Helium				
27	3.40	1193	0.78			0.348	3.04
26	13.61	1193	3.11	0.411	3.82	0.478	4.18
25	27.22	1203	6.18	0.418	3.88	0.433	3.78
25	34.02	1203	7.72	0.578	5.37	0.575	5.02
33	47.63	1228	10.59	0.762	7.08	0.831	7.26
33	57.84	1228	12.86	0.940	8.73	0.932	8.15
32	68.05	1228	15.13	1.076	10.00	1.186	10.36
32	83.36	1228	18.53	1.173	10.90	1.306	11.41

ρ, by the equation:

$$\rho^2=[\pi\Delta\nu_{\frac{1}{2}}/2n(2\pi kT)^{\frac{1}{2}}][mM/(m+M)]^{\frac{1}{2}},$$

where m and M are the masses of the absorbing and of the perturbing atoms, respectively. Taking

$\Delta\nu_{\frac{1}{2}}/n=0.466$ cm^{-1} for helium
$=0.51$ cm^{-1} for argon,
$\rho=6.50$A for He−Ag, and $\rho=11.3$A for A−Ag.

DISCUSSION

It is to be noted that certain experimental observations, such as those for Na D-lines[2] with A, N_2, and H_2 and those for the first doublet of the K principal series[3] with N_2 for small densities (r.d. smaller than, say, 5) confirm the existing theory[4] that the two doublet components should suffer equal pressure effects. The difference in behavior for the doublet components was totally neglected by Füchtbauer and Gossler[5] in their experiments with Cs.

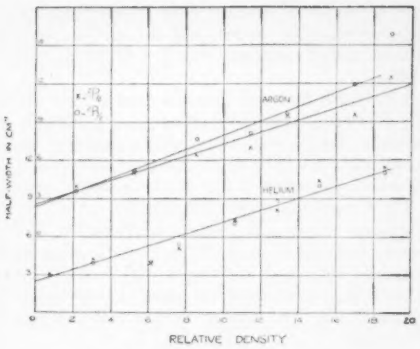

FIG. 4. Half-width vs relative density.

But it has been well established by recent observations[6] that when the relative density is high there is definitely a difference in behavior. So far all results show that (1) the long wavelength component ($^2P_{\frac{1}{2}}$) exhibits a greater shift than the short wavelength component ($^2P_{\frac{1}{2}}$), except for the third member of the K principal series with N_2; and (2) the broadening of the $^2P_{\frac{1}{2}}$ component is greater than that of the $^2P_{\frac{1}{2}}$ component, except for the second member of the Rb principal series with Ne and He. This is to call attention to the fact that the dependence of the perturbing effects of foreign gases upon j values is not yet theoretically predicted.

[2] H. Margenau and W. W. Watson, Phys. Rev. **44**, 92 (1933).
[3] W. W. Watson and H. Margenau, Phys. Rev. **44**, 748 (1933).
[4] H. Margenau, Phys. Rev. **40**, 387 (1932).
[5] C. Füchtbauer and F. Gossler, Z. Physik **87**, 89 (1933).
[6] Such as reference 3 and G. F. Hull, Phys. Rev. **50**, 1148 (1936); T. Z. Ny and S. Y. Ch'en, Phys. Rev. **52**, 1158 (1937); reference 1, and the present article.

The Magnetic Susceptibility of Uranium*

C. J. KRIESSMAN, JR.,† AND T. R. MCGUIRE
U. S. Naval Ordnance Laboratory, White Oak, Maryland
(Received September 18, 1951)

Using a body force method the magnetic susceptibility of uranium has been found to increase from 1.66×10^{-6} emu per gram at -195°C to 2.16×10^{-6} emu per gram at 1120°C. The room temperature value is 1.72×10^{-6} emu per gram. Two abrupt increases in the susceptibility were observed at 698°C and 808°C.

INTRODUCTION

THE magnetic susceptibility of uranium as a function of temperature has been measured by Honda,[1] Owen,[2] Bommer,[3] and Bates and Mallard.[4] The data of Bates and Mallard, which are the most reliable because they were obtained using a high purity sample, differ from the earlier measurements in two respects: (1) the absolute value of the susceptibility is much lower, and (2) the susceptibility increases with increasing temperature. Since the measurements of Bates and Mallard only extend to 350°C, and since it is known that two structure transitions[5-7] occur in uranium at higher temperatures, it seemed desirable to repeat and extend the temperature dependence measurements.

EXPERIMENTAL METHOD

The measurements were made with a body force method[8] using an electrodynamic torsion balance. The sample is suspended from one end of the balance arm by a quartz fiber. The sample and fiber are inside a quartz tube which is situated in a platinum wound furnace[9] that rests between the pole pieces of an electromagnet.

Temperatures are measured using a calibrated platinum-platinum 10 percent rhodium thermocouple. The accurate determination of high temperatures in susceptibility measurements is difficult for several reasons. Because of inequalities of temperature along the furnace, we found that the temperature of the sample could be fixed only within ±10°C. Also, since the thermocouple cannot be placed directly on the sample, the location of the thermocouple is critical. In order to keep it as close as possible to the sample, the thermocouple was wrapped around the quartz tube with the junction at the position of the sample.

The uranium sample[10] was 99.9 percent pure and contained 140 parts per million of iron and 40 parts per million of nickel. The sample contained only 10 parts per million of chromium and no reported amount of molybdenum. This is important because small amounts of chromium and molybdenum are known to depress the temperatures at which the structure transitions occur.[5] The sample was outgassed at 1000°C and a pressure of 10^{-4} mm of Hg to drive off any occluded gases, and was then sealed off in an evacuated quartz vial.

RESULTS

Two sets of temperature dependence measurements were made. In the first measurements shown in Fig. 1(A), the susceptibility increased regularly from 1.72×10^{-6} emu per gram at -195°C to 1.85×10^{-6} emu per gram at 350°C. Between room temperature and 350°C this is the same relative increase as that measured by Bates and Mallard,[4] although their absolute value at room temperature was lower. Above 350°C the susceptibility continues to increase regularly until about 702°C where there is an abrupt increase of about 6 percent. This increase is probably associated with

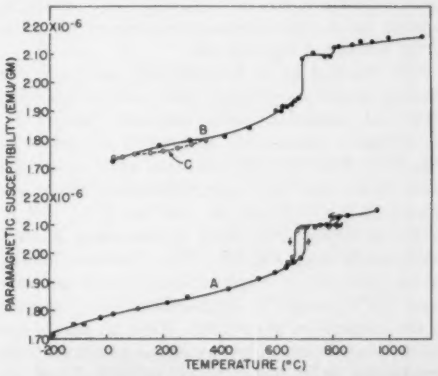

FIG. 1. The magnetic susceptibility of uranium as a function of temperature showing two transitions ($\alpha-\beta$) at 698°C and ($\beta-\gamma$) at 808°C. A, first set of measurements. B, second set of measurements. C, data of Bates and Mallard.

* Supported in part by the ONR.
† Also at Catholic University, Washington, D. C.
[1] K. Honda, Ann. Physik **32**, 1027 (1910).
[2] M. Owen, Ann. Physik **37**, 657 (1912).
[3] H. Bommer, Z. anorg. u. allgem. Chem. **247**, 249 (1941).
[4] L. F. Bates and J. R. Mallard, Proc. Phys. Soc. (London) **63**, 520 (1950).
[5] A. S. Wilson and R. E. Rundle, Acta Cryst. **2**, 126 (1949).
[6] C. W. Tucker, Jr., Knolls Atomic Power Lab., Schenectady, New York, private communication referred to by Kasper, Decker, and Belanger, J. Appl. Phys. **22**, 361 (1951).
[7] J. Thewlis, Nature **168**, 198 (1951).
[8] T. R. McGuire and C. T. Lane, Rev. Sci. Instr. **20**, 489 (1949).
[9] T. R. McGuire and C. J. Kriessman, Jr. (to be published).
[10] Obtained from Johnson, Mathey and Company, Sample No. 1539.

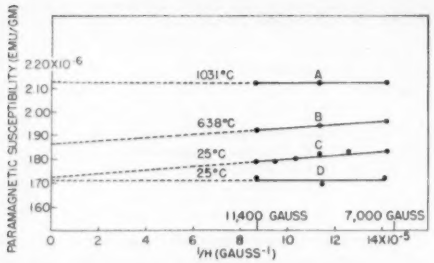

FIG. 2. Field dependence of uranium. A, B, and C, first set of measurements. D, second set of measurements.

the crystal structure change[5-7] orthorhombic to tetragonal ($\alpha-\beta$) which is known to occur at 640°C. Above 702°C the susceptibility remains constant until about 820°C where there is another sudden but smaller increase which is probably connected with the structure change[5,7] tetragonal to cubic ($\beta-\gamma$) which is reported at 760°C. When the temperature was lowered, a small temperature hysteresis was observed in the $\beta-\gamma$ transition region. A larger temperature hysteresis was noted in the $\alpha-\beta$ transition region. The susceptibility transition temperatures reported here are lower than those previously reported by us;[11] the earlier values were in error due to improper location of the thermocouple.

Field dependence measurements were made at various temperatures to determine whether the iron and nickel were acting as ferromagnetic impurities since Bates and Mallard[4] reported that their sample contained no iron in a ferromagnetic form. These measurements, shown in Figs. 2(A), (B), and (C), indicate that a slight ferromagnetic impurity is present at the two lowest temperatures.

After the first set of measurements was made, the uranium sample was removed from the vial, washed in nitric acid, resealed in another evacuated vial, and the susceptibility remeasured. The results are shown in Fig. 1(B). The susceptibility curve again shows the same shape, but the lower temperature values are smaller (1.73×10^{-6} emu per gram at 25°C) and in better agreement with those of Bates and Mallard which are shown in Fig. 1(C). Also, the discontinuities in the susceptibility occur at slightly lower temperatures, 698°C and 808°C. Measurements were not made as the temperature was lowered. When the sample was taken from the vial and remeasured, an even lower room temperature value was recorded: 1.71×10^{-6} emu per gram. Field dependence measurements made at room temperature indicate that the ferromagnetic impurity had disappeared [Fig. 2(D)].

[11] C. J. Kriessman and T. R. McGuire, Phys. Rev. **83**, 870 (1951).

TABLE I. Summary of data on transition temperatures in uranium.

Measurement	$\alpha-\beta$ transition T°C	$\beta-\gamma$ transition T°C
Crystal structure[a]	640	760
Specific heat[b]	661	770
Electrical resistance[c]	667	772
Magnetic susceptibility	698	808

[a] See reference 5.
[b] D. Ginnings and R. J. Corruccini, J. Research Natl. Bur. Standards **39**, 309 (1947).
[c] A. I. Dahl and M. S. Van Dusen, J. Research Natl. Bur. Standards **39**, 53 (1947).

DISCUSSION OF RESULTS

The amount of ferromagnetic impurity in the sample can be determined from the field dependence data by applying the Honda-Owen[1] equation

$$\chi_H=\chi_\infty+\sigma/H,$$

where χ_∞ is the corrected susceptibility extrapolated to infinite field and σ is the saturation magnetization of the impurity. Using the 25°C data of the first set of measurements we find that $\sigma=0.0008$ cgs unit per gram. If this impurity is assumed to be entirely iron, then only 4 parts per million of the sample act ferromagnetically. The remaining 136 parts per million of iron in the sample might be present in the paramagnetic form U_6Fe as suggested by Bates and Mallard. They give the susceptibility of this compound as 2.04×10^{-6} emu per gram, and in the small amount present it would not affect the measured susceptibility.

The field dependence data of Fig. 2(C) gives 1.72×10^{-6} emu per gram as the corrected room temperature value of the susceptibility for the first set of measurements. This value is within 1 percent of that reported by Bates and Mallard. Since the field dependence for the second set of measurements indicates that no ferromagnetic impurity was present, it seems that the heating of the sample to high temperatures either caused the iron, which was present as a ferromagnetic impurity, to be converted to some sort of paramagnetic form or forced the impurity to leave the sample entirely. Some grounds for the hypothesis that the impurity was forced to leave the sample by heating to a high temperature may be found in the work of Dahl and Cleaves[12] on the freezing point of uranium. They found that the longer the sample was heated at high temperatures, the purer it became because the impurities concentrated themselves in a crust on the surface of the sample where they might then be removed by washing in an acid.

The structure transitions in uranium and the specific heat and resistance discontinuities associated with these transitions have been reported at lower temperatures than those at which we have found the susceptibility transitions. Impurities are known to affect transition temperatures in uranium,[5,13] and this may account for the spread of temperatures shown in Table I.

[12] A. I. Dahl and H. E. Cleaves, J. Research Natl. Bur. Standards **43**, 513 (1949).

High Energy Neutron Collisions with Helium*

CLIFFORD SWARTZ†
University of Rochester, Rochester, New York
(Received September 25, 1951)

A cloud-chamber investigation has been made of high energy neutron collisions with helium. 377 elastic recoils and 126 disintegrations have been observed. Two groups are selected from the elastic collisions according to the energy of the incident neutron, estimated from the appearance and delta-ray structure of the recoiling alpha-particle. The scattering by neutrons in the 10- to 30-Mev range appears roughly isotropic in the center of mass, while neutrons with energy greater than 50 Mev are scattered strongly in the forward direction. An absence of evidence for neutrons scattered at very small angles is described. This seems different than that predicted by one theory of neutron-helium collisions.

INTRODUCTION

A CLOUD chamber, filled with helium and water vapor at a pressure of 66 centimeters, has been exposed to the high energy neutron beam from the 130-in. cyclotron at the University of Rochester. Two thousand seven hundred pictures were searched for evidence of helium elastic recoils and disintegrations. The helium events can, with few exceptions, be distinguished from events due to oxygen in the water vapor. The angular distribution of helium recoils (hereafter called α-recoils) has been plotted for two different energy groups of incident neutrons. The modes of disintegration cannot definitely be determined from the present data, although certain possibilities can be ruled out.

EXPERIMENTAL ARRANGEMENT

The cloud chamber is fifteen inches in diameter, five inches deep, with an illuminated depth of three inches. It was necessary to provide extensive radiation shielding for the chamber, not only to block the high energy neutrons and scattered protons, but also to shut out the sea of low energy neutrons which fills the cyclotron room. The final shielding arrangement, shown in Fig. 1, provides tolerable conditions. The water wall inside the blockhouse was found essential for absorbing neutrons in the million volt range which have a large cross section for helium scattering. An indication of the effectiveness of the blockhouse can be obtained by comparing the number of events per unit volume which occur inside the central zone of the cloud chamber defined by the collimated neutron beam to the numer per unit volume which occur outside. This "signal-to-noise" ratio is about 18:1.

The neutron beam is produced by allowing protons with an energy of 235 Mev to strike a beryllium target, $\frac{1}{2}$-in. wide (along the proton orbit) and $\frac{1}{4}$-in. thick (radially). The energy spectrum of the neutrons has been measured in front of the blockhouse by Guernsey, Mott, Nelson, and Roberts[1] using a scintillation crystal telescope to detect neutron-proton scattering. A preliminary result of their work is shown in Fig. 2. It is unlikely that the shape of the final curve will differ from that shown, although the maximum may be shifted by as much as 20 Mev. The absolute number of neutrons has not been measured accurately. Carbon activation experiments and evidence from star production in nuclear emulsions indicate that during the cloud chamber runs the neutron intensity at the cloud chamber was between 2000 and 10,000 per square centimeter per second.

It was not possible to pulse the oscillator or arc of the cyclotron so that the radiation would be emitted during the optimum portion of the sensitive time of the cloud chamber. Instead a mechanical method was used.

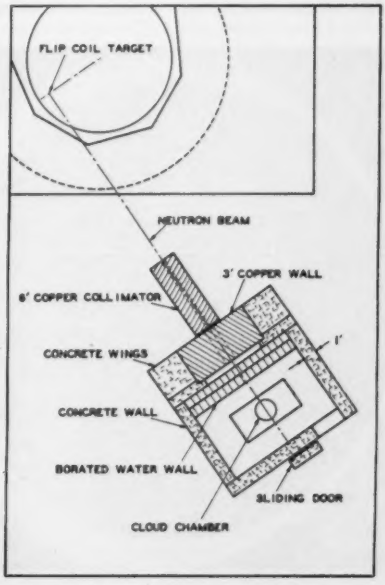

FIG. 1. Floor plan of shielding used in cyclotron building.

* Assisted by the AEC.
† Now at Brookhaven National Laboratory, Upton, Long Island, New York.
[1] Guernsey, Mott, Nelson, and Roberts, private communication.

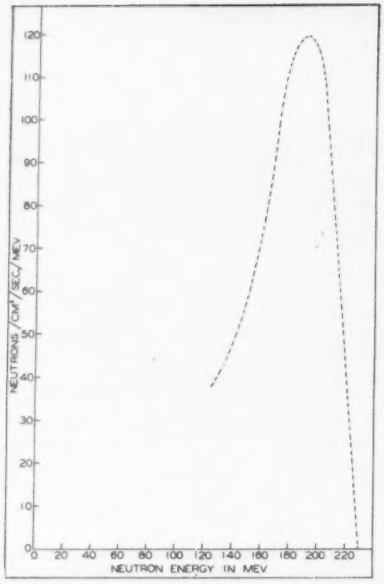

FIG. 2. Preliminary measurement of neutron energy spectrum.

Copper targets mounted on two flip coils at thirteen inches from the center of the cyclotron could be raised by a signal from the cloud chamber. These stopped the protons at the 15-Mev radius, and completely eliminated radiation in the blockhouse. As one target fell, the other rose, allowing a pulse of protons to pass through with a timing precision of about $\frac{1}{10}$ second.

METHODS OF ANALYSIS

Since oxygen was present at all times in the water vapor, a control run of some three hundred pictures was made with only oxygen and water vapor in the chamber. No event was found, which, considering the difference in stopping power of the gases, looked like either of the helium reactions shown in Figs. 3 and 4.

The heavily ionizing track of Fig. 3 starts in a well-illuminated region of the chamber and has all the characteristics of the track of an alpha-particle. Three hundred seventy-seven of these "α-recoils" from elastically scattered neutrons were observed. The angle between the direction of a recoil and the incident neutron was measured with an accuracy of one degree on a three-dimensional analyzing table. Although no magnetic field was available, the energy of the α-recoils could be estimated within wide limits from their visible range, by their appearance, and by the nature of their delta-rays.

It was experimentally determined by two independent methods that the appearance of clearly distinguishable delta-rays on α-recoils requires that the energy of the α-particle be greater than 7 Mev. First, the beginnings of alpha-tracks from polonium (5.3 Mev) do not show delta-rays, and one α-recoil whose energy, determined

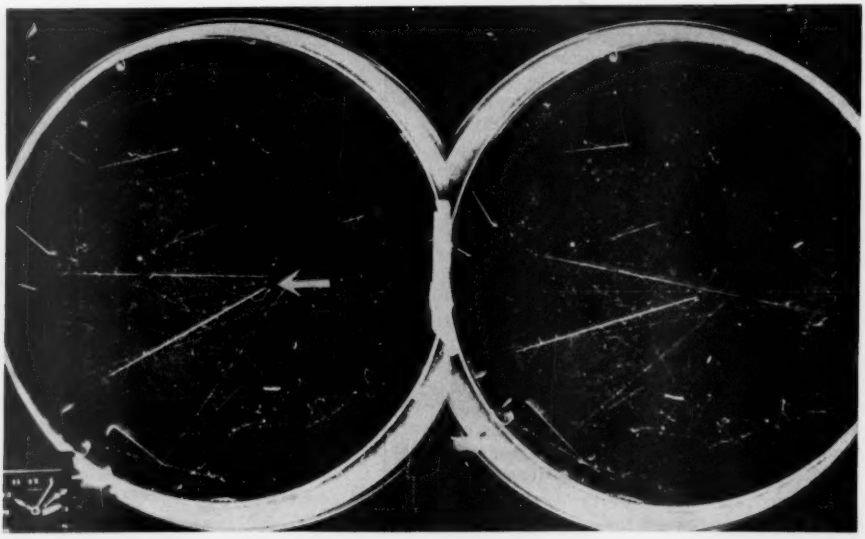

FIG. 3. Elastic collision of neutron with helium. Neutrons pass through chamber in direction shown by arrow.

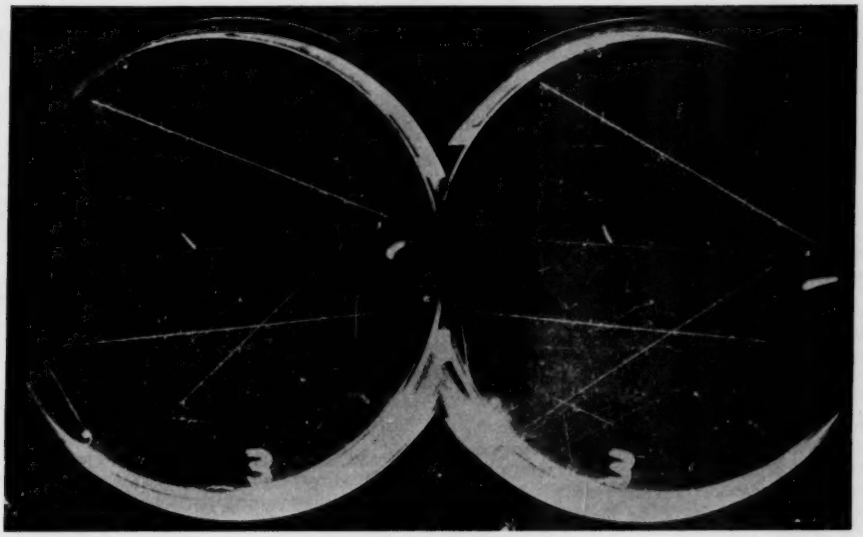

FIG. 4. Neutron induced helium disintegration.

by track length, is 6.5 Mev shows only "pebbles" i.e., the deltas are less than one millimeter in length. Secondly, quite a few α-recoils with tiny deltas were observed which had been emitted at large angles from the incident neutron direction. The dynamics of the collision links the energies of the neutron and α-recoil, and since the neutron cannot have an energy greater than 235 Mev, this determines the maximum energy that the recoil can have. Several such tracks with deltas one or two millimeters long were found whose energy cannot be over 8 Mev. The limit approached by these two methods, and the appearance of tracks near this limit are both consistent with a value of 7 Mev as the boundary where distinguishable delta-rays first appear.

Each recoil, then, is assigned energy limits depending on its appearance. If it ends in the chamber, its range determines its energy exactly. If it leaves the illuminated region and has no definitely distinguishable delta-rays, its energy is under 7 Mev. Its observable length in this case determines a minimum energy. If delta-rays can be seen but are less than four millimeters long, the energy of the α-recoil is listed as being between 7 and 15 Mev. Whenever the length of the deltas can be accurately measured, the α-recoil is assigned an energy such that its velocity is half that of the fastest delta-electron, corresponding to the minimum allowable energy. The neutron energy limits can then be found from the dynamics of the collision.

Figure 4 shows a picture of a typical helium disintegration. There are two lightly ionizing tracks, a type of two-prong star which was never observed in the oxygen bombardment. The oxygen two-prong stars are quite clearly cases where a fast, lightly ionizing particle is emitted from a heavy recoiling particle. The longest recoil observed out of 220 two-prong events in oxygen would have had a track length of only ten centimeters in helium. Such stars are also seen in helium—but only a few more than can be accounted for by assuming that they come from the oxygen present in the water vapor. Of the two-prong stars seen in the helium pictures, 102 are listed as being definitely due to helium, 67 appear to be the same as those seen in oxygen, and 34 are considered borderline cases. While it is not possible to classify an individual star in the borderline group, the fraction of them which are due to helium can be derived. The ratio of two-prong to three-prong stars in the oxygen pictures is 1.8. This agrees well with Berkeley's[2] similar figure of 1.7. But if only the two-prong stars definitely due to oxygen are counted in the helium run, this ratio is 1.5. If all the borderline cases are added, the ratio goes to 2.3. If the intermediate group is split so as to yield the correct two-prong to three-prong ratio, 24 cases should be considered due to helium and the remaining 10 due to the oxygen in the water vapor. It should be emphasized, however, that unless a star is very definitely of the helium type, it is classified as questionable. The questionable group includes many stars which appear to be due to helium

[2] N. Horning and L. Baumhoff, Phys. Rev **75**, 378 (1949).

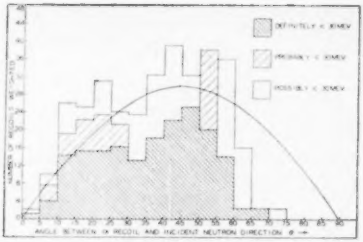

FIG. 5. Angular distribution in laboratory of helium recoils struck by neutrons under 30 Mev. Solid line is curve data should fit if the scattering were isotropic in the center of mass.

but where the illuminated length of one of the prongs is too short to allow it to be positively identified.

ANALYSIS OF THE ELASTIC RECOILS

It is found practical to select two major groups of elastic α-recoils according to the estimated energy of the bombarding neutron. The first group contains all those recoils which have been struck by neutrons definitely under 30 Mev, probably under 30 Mev, and possibly under 30 Mev. The angular distribution of these recoils is plotted as a function of the angle between incident neutron direction and α-recoil direction. Thus, a large angle means that the neutron was scattered nearly forward, and that there was little momentum transfer. Figure 5 shows this distribution for the group struck by neutrons under 30 Mev. The coding shows the contributions of the three sub-groups—definitely, probably, or possibly under 30 Mev. The second main division contains those recoils where the incident neutron was definitely, probably, or possibly *over* 50 Mev. Figure 6 shows the angular distribution of this group, and is coded so that the contributions of the sub-groups can be seen.

These distributions have been corrected for a blindness inherent in the stereoscopic viewing system. Tracks near the vertical are hard to measure and even at angles up to 55° from the vertical are sometimes missed in the survey. The relative number missed for a given angle can be found directly from the data by assuming that there should by an isotropic distribution in the polar angle about the incident neutron direction. The effect of this blindness is to decrease the number of tracks recorded at large angles to the neutron direction.

The general trend toward neutron scattering in the forward direction as the energy increases can be seen by comparing Figs. 5 and 6. The experimental evidence for recoils at angles greater than 65° in Fig. 5 and greater than 85° in Fig. 6 is poor, since these recoils would have such a low energy that they could easily be missed. The solid line in each case is the curve the data should fit if the scattering were isotropic in the center-of-mass system. This curve can be calculated without taking into consideration the velocity of the center of mass, since the relation between scattering angle for the recoiling α-particle in the center-of-mass system and in the lab system is independent of the velocity of the center of mass.

The dotted curve in Fig. 6 shows the angular distribution of recoils in the laboratory predicted by J. Heidmann[3] for neutrons of 90 Mev. In spite of the uncertainties of the estimated energies in the experimental curve, and although most of the neutrons had energies between 100 Mev and 200 Mev, there seems to be one point of valid comparison. This is to note the small number of recoils observed between 80° and 85°. A special search was made for recoils at these angles. While the experimental number shown could be in error by a factor of two or three, it is difficult to see how 10 to 50 times this number, as the theory would require, could be missed.

ANALYSIS OF THE HELIUM DISINTEGRATIONS

There are a limited number of modes of disintegration following a neutron-helium collision. The two prongs could be: (proton, proton); (proton, deuteron); (proton, triton); (deuteron, deuteron); and (deuteron, triton). The incident neutron could also strip off a neutron leaving a low energy He^3 recoil whose track cannot be differentiated in this cloud chamber from that of a He^4 recoil. The calculations of Heidmann predict that the predominant mode will be the one where the neutron strips off a proton, usually leaving the triton with energy in the million volt region. For 200-Mev neutrons all other processes should be negligible, while at 90 Mev, the neutron may cling to the stripped proton forming a (deuteron, triton) disintegration in about 20 percent of the cases. In this latter type the deuteron would continue forward within a cone whose half-width at half-maximum in the laboratory is 8.4°; it would thus carry off most of the energy leaving the triton with less than 1 Mev. The theory further predicts that most of the tritions from the (neutron, proton, triton) disintegration

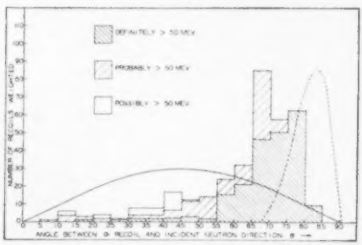

FIG. 6. Angular distribution in laboratory of helium recoils struck by neutrons over 50 Mev. Solid line is curve data should fit if the scattering were isotropic in the center of mass. Dotted curve is prediction of J. Heidmann for neutrons of 90 Mev.

[3] J. Heidmann, Phil. Mag. 41, 444 (1950). I am indebted to Dr. Heidmann for unpublished results of his calculations for neutrons of 200 Mev.

will be emitted isotropically in the laboratory, although the more energetic ones will be concentrated in the forward hemisphere.

Although the individual prongs of the observed helium stars cannot be identified, their angular behavior and general appearance can be discussed in terms of Heidmann's prediction. A triton with energy less than 1 Mev has a range in this cloud chamber of less than 12 centimeters. Many of the (deuteron, triton) or (neutron, proton, triton) stars should thus have one short, heavily ionizing prong, and one considerably thinner and longer track. Stars of this nature were classified as probably due to oxygen, and, as has been shown, all such stars are needed to make the correct ratio between two-prong and three-prong oxygen stars from the water vapor. Among the cases listed as borderline, the lightly ionizing particle was often emitted at large angles to the forward direction, or even into the backward hemisphere. In the majority of cases classified as definitely due to helium, the two prongs of a star show about equal density of ionization.

The angular distribution of prongs from stars listed as definitely due to helium is shown in Fig. 7. Only 12.5 percent go into the backward hemisphere. Of those stars included in this group, there is no tendency for the more heavily ionizing prong to go in the backward direction. This distribution does not seem compatible with the predicted mode (neutron, proton, triton) with most of the tritons emitted nearly isotropically in the laboratory.

If the triton in a (deuteron, triton) disintegration were left with more than 1 Mev, the star would be classified as a possible helium event. All of these have been tested for the momentum balance which this two-body collision must satisfy. Only two stars satisfy conditions within the margin of error of the analyzing apparatus, and one of these at an unfavorable angle is extremely doubtful. We must conclude that not more than 2 percent of the helium stars can be due to a (deuteron, triton) event, with the triton left with greater than 1 Mev in the laboratory.

ABSOLUTE CROSS SECTION

In spite of the poor determination of the absolute number of neutrons, it seems worthwhile to point out the surprisingly low number of helium events observed. Disintegrations are seen in only 5 percent of the pictures, and elastic recoils from neutrons greater than 50 Mev is only 6.5 percent of the pictures. The carbon activation, the number of stars produced in emulsions, and the preliminary calculations of the neutron-proton scattering group would not be compatible with a neutron flux smaller than 2000/cm²/sec. Although the sensitive time of the chamber can be estimated only within wide limits, the cross section for helium disintegration deduced from this experiment cannot be made larger than 18 millibarns, and that for

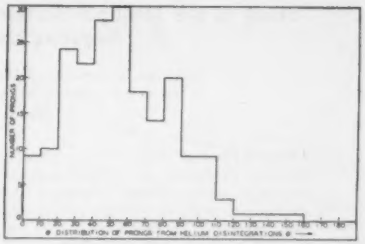

FIG. 7. Angular distribution of prongs from helium stars. Θ is angle between prong and incident neutron direction.

elastic scattering of neutrons greater than 50 Mev, not greater than 14 millibarns. It should further be noted that the number of oxygen stars observed in the helium runs indicates an oxygen disintegration cross section twelve times as large as the total helium cross section. This could be explained if a centimeter pressure of air was inadvertently admitted when the chamber was filled with helium. While this possibility seems remote from this experimenter's standpoint, it cannot be ruled out. However, it is interesting that the number of oxygen stars seen is approximately the same as expected from the estimates of neutron flux, sensitive time, and water vapor pressure.

CONCLUSION

Many of the questions left unanswered in this preliminary work must await better shielding and a strong magnetic field for their solution. Meanwhile it appears that neutrons in the 10- to 30-Mev region scatter almost isotropically from helium, while neutrons above 50 Mev are strongly scattered in the forward direction. There remains an unexplained falling off of neutron scattering at angles less than 20° in the center-of-mass system, leaving the helium recoils emitted at angles between 80° and 90° in the laboratory.

Most of the helium stars appear to have a unique appearance, with two lightly ionizing particles being emitted usually in the forward direction. Disintegration into a (deuteron, triton) seems to have a very low probability. The general appearance of the stars and the angular distribution of the prongs does not agree with the predictions of one theory of the modes of disintegration of helium.

The author owes much to the skilled engineers and instrument makers who produced the elaborate equipment necessary for this experiment. Particular thanks are due Messrs. Arthur Gibson and Eric Chandler. During the course of the experiment the author was supported by a predoctoral fellowship from the Atomic Energy Commission. The advice of Dr. John Tinlot in the final stages of the experiment and thesis preparation is gratefully acknowledged.

Study of the Multiple Scattering of Fast Charged Particles in a Gas. II. (Negative and Positive Beta-Particles)*

GERHART GROETZINGER,† WATTS HUMPHREY, JR.,‡ AND FRED L. RIBE§
Institute for Nuclear Studies, University of Chicago, Chicago, Illinois

(Received September 24, 1951)

The experimental study of the multiple scattering of electrons in a gas has been extended to include electrons of momenta up to 10,200 gauss-cm. The results of these measurements are compared with predictions of various theories of multiple scattering. Furthermore, a parallel investigation of the multiple scattering of positrons has been carried out over the momentum range between 2000 and 9000 gauss-cm. The rms angle of multiple scattering for the positrons is found to be approximately ten percent less than for electrons of the same momentum.

IN a previous publication[1] (to be referred to as I) we described a method for determining the momentum and the multiple scattering of charged particles from their tracks in a "magnetic cloud chamber." Using electrons of momenta $H\rho$ between 2000 and 7000 gauss-cm, originating from a P^{32} source, an experimental scattering law was obtained for their passage through argon of one atmosphere and was compared with the results of various theories of multiple scattering.[2-6] The obtained experimental root-mean-square angle of scattering is represented as a function of $H\rho$ by the upper solid curve in Fig. 1 of the present communication.

The purpose of this investigation is to extend the experimental multiple scattering law to (decay) electrons of higher energies and to determine a similar law for positive beta-particles.

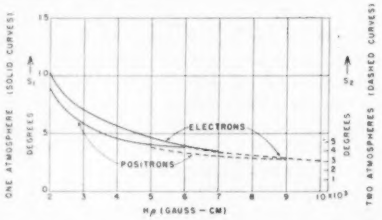

FIG. 1. Root mean angle of multiple scattering for electrons and positrons as a function of $H\rho$. The solid curves, in connection with scales s_1, refer to electrons and positrons in one atmosphere of argon, and the dashed curves in connection with scale s_2, refer to electrons and positrons in two atmospheres of argon. The scales are matched on the basis of the theoretical pressure dependence of multiple scattering.

A comparison of the multiple scattering of electrons and positrons is of interest in view of a recent investigation in which Seliger[7] observed that the ratio of the backscattering coefficients β^- and β^+ for electrons and positrons resulting from beta-decay with a maximum energy of about 0.5 Mev is approximately 1.3 in several media of atomic number between 4 and 82. It follows from theoretical considerations that large angle single scattering for relativistic particles is more pronounced for electrons than for positrons.[8] One might expect that this effect would account for the observed difference in the backscattering but will hardly affect the multiple scattering since tracks displaying large angle deflections are eliminated from considerations. However, Miller[9] remarks that backscattering also results mainly from the "cumulative effects of small angle single scatterings" but obtains nevertheless a theoretical ratio β^- to β^+ of 1.16. Consequently it is possible that a similar difference might occur also for the case of multiple scattering.

The cloud chamber used in this investigation and the method of taking pictures and analyzing the tracks were the same as in I. The determination of the error variance s_E^2 was repeated but, contrary to the procedure employed in the previous investigation, the variances s^2 were corrected individually before they were fitted to a second-order polynomial in $(1/H\rho)^2$. Positrons of momenta between 2000 and 6000 gauss-cm were investigated in one atmosphere of argon with an applied magnetic field of approximately 340 gauss, varying somewhat from exposure to exposure, conditions being similar to the ones in I. For the investigation of the scattering of electrons of momenta between 6000 and 10,200 gauss-cm, and of positrons of momenta between 5000 and 9000 gauss-cm, a magnetic field of approximately 680 gauss, varying somewhat for different exposures, and a pressure of two atmospheres were used. Use of this pressure guaranteed that for the section length of two centimeters in argon used here, the

* Assisted by the joint program of the ONR and AEC.
† Now at the Lewis Laboratory of the NACA, Cleveland, Ohio.
‡ Now at the Chicago Midway Laboratories, Chicago, Illinois.
§ Now at the Los Alamos Scientific Laboratory, Los Alamos, New Mexico.
[1] Groetzinger, Berger, and Ribe, Phys. Rev. **77**, 584 (1950).
[2] W. Bothe, *Handbuch der Physik* (Verlag. Julius Springer, Berlin, 1933), Vol. 22, II, p. 1.
[3] E. J. Williams, Proc. Roy. Soc. (London) **169**, 531 (1939); Phys. Rev. **58**, 292 (1940).
[4] S. Goudsmit and J. L. Saunderson, Phys. Rev. **57**, 24 (1940); Phys. Rev. **58**, 36 (1940).
[5] G. Molière, Z. Naturforsch. **3a**, 78 (1948).
[6] H. S. Snyder and W. T. Scott, Phys. Rev. **76**, 220 (1949).
[7] H. H. Seliger, Phys. Rev. **78**, 491 (1950).
[8] See e.g., N. F. Mott and H. S. W. Massey, *The Theory of Atomic Collisions* (Oxford University Press, New York, 1945), p. 81 ff.
[9] W. Miller, Phys. Rev. **82**, 452 (1951).

condition of multiple scattering was fulfilled even for electrons (or positrons) of the highest energies.

The electrons whose scattering was investigated resulted from the decay of 30-sec Rh^{106} (maximum beta-ray energy = 3.55 Mev[11]) which in turn is a decay product of 1.0-year Ru^{106}.[10]

For the investigation of the scattering of the positrons a source was prepared by bombarding iron with deuterons in the University of Chicago 33-in. cyclotron. The main positron emitter obtained in this way is the 21-minute isomer of Mn^{52} with a maximum energy of 2.66 Mev.[11] The bombarded piece of iron was put into a cylindrical tube extending four centimeters into the chamber and closed inside the chamber by a thin aluminum foil. The source was then used for one to two hours after a bombardment.

The upper dashed curve in Fig. 1 represents in connection with scale s_2 the experimental mean square angle of scattering for electrons of momenta between 6000 and 10,200 gauss-cm in two atmospheres of argon. This curve is based on 54 electrons with momenta fairly evenly distributed over this momentum range. In connection with scale s_1 it represents the root-mean-square angle of scattering in one atmosphere of argon to be expected on the basis of theoretical considerations. Strictly speaking, the two scales s_1 and s_2 should be matched by taking into account the pressure dependence of both factors Q [Eq. (2) of I] and G [Eqs. (3a) to (3c) of I], whose product is equal to the mean-square-scattering angle. However, since the pressure dependence of Q varies from theory to theory and is at most slight, the matching was done by taking into account only the pressure dependence of G, which is the same for all theories. The two lower curves represent the results obtained from an analysis of tracks of 115 positrons with momenta between 2000 and 6000 gauss-cm obtained in one atmosphere of argon and 52 tracks of positrons of momenta between 5000 and 9000 gauss-cm obtained in two atmospheres of argon. In I we claimed an accuracy of 10 percent for our method of obtaining the root-mean-square angle of multiple scattering. It may be noted that the matching of the two pairs of curves (electrons and positrons) in the overlapping momentum range is in agreement with this claim. Arguments based on the matching of these curves necessarily neglect possible systematic errors. Such errors are, however, of little importance in the comparison of electron and positron scattering and the curves obtained for these two cases are sufficiently different from each other to indicate that the rms angle of multiple scattering of electrons is greater by an amount of the order of 10 percent than that of positrons of the same momentum.

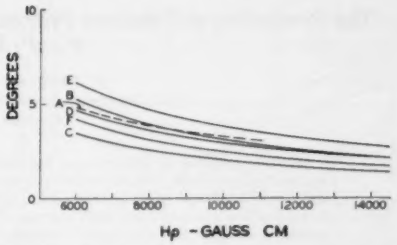

FIG. 2. Comparison of experimental root-mean-square angle with that following from theories of multiple scattering. Curve A: Experimental; curve B: Bothe; curve C: Williams ($\varphi_{max}=(\frac{1}{2}Q)^{\frac{1}{2}}$, $\varphi_{min}=(mc/p)\cdot(Z^{\frac{2}{3}}/137)$); curve D: Williams-Bethe ($\theta_{max}=0.1$ radian, $\theta_{min}=(mc/p)\cdot(Z^{\frac{2}{3}}/181)$; curve E: Goudsmit and Saunderson (Thomas-Fermi potential); curve F: Molière.

The nature of backscattering is sufficiently different from multiple scattering so that it is difficult to make a quantitative comparison of the present results with those of Seliger. It should be noted, however, that the effect is in the same direction and of the same order of magnitude.

In Fig. 2 our experimental results concerning electrons in the range of larger momenta are compared with the results of several theories of multiple scattering. The curves corresponding to the various theories are marked by the same letters as in I. The tendency of the theories to predict a somewhat greater dependence on $H\rho$ than is found experimentally prevails also at these higher momenta.

We are grateful to Messrs. Martin J. Berger and Philip Schwed for valuable discussions.

Note added in proof.—A recent revision of Bothe's theory, in which the factor G has been reduced from 4.125 to 2.74 would move curve b in Fig. 6 of I and Fig. 2 of this communication down somewhat. (Private communication from W. Bothe.)

[10] The source was obtained from the Isotope Division of the AEC in Oak Ridge, Tennessee.

[11] Way, Fano, Scott, and Thew, *Nuclear Data* (National Bureau of Standards, Washington, D. C., 1950).

The Production of Polarized Protons and the Inversion of Energy Levels of the $P_{\frac{1}{2}}-P_{\frac{3}{2}}$ Doublet in Li^{5*}*

M. HEUSINKVELD† AND GEORGE FREIER
Physics Department, University of Minnesota, Minneapolis, Minnesota
(Received September 17, 1951)

Spin-orbit coupling in the scattering of protons by helium is expected to result in polarization of the scattered proton beam. This effect has been established by performing a double scattering experiment, in the form of a polarizer-analyzer arrangement, and measuring the amount of polarization. These data, used in conjunction with the phase shift analysis of the single scattering differential cross-section data, give conclusive evidence that the $P_{\frac{1}{2}}$ and $P_{\frac{3}{2}}$ energy levels in the compound nucleus of Li^{5*} are inverted.

INTRODUCTION

WHEN a proton with spin $\hbar/2$ and a He^4 nucleus with spin 0 collide elastically with an orbital angular momentum of $\hbar$, there are two possible values of the total angular momentum, namely $j=\hbar/2$ and $j=3\hbar/2$. If there is an energy dependent spin orbit coupling involved in the nuclear forces which cause the scattering interaction, it is expected[1-3] that there will be selective scattering of protons; i.e., protons with a given spin orientation will be scattered more or less depending on whether the orientation is parallel or antiparallel to the orbital angular momentum vector with one unit of orbital angular momentum. Consequently an examination of a beam of protons which have been scattered by helium should reveal that this scattered beam is polarized or has more protons with one spin orientation than with the opposite orientation.

Furthermore, if these spin orbit forces are considered in establishing the energy levels of the compound Li^{5*} nucleus, the splitting of the $P_{\frac{1}{2}}$ and $P_{\frac{3}{2}}$ energy levels, if they are separated, will result in a strong interaction of one type when the interacting energy equals the energy of the $P_{\frac{1}{2}}$ level and a strong interaction of another type when the interaction energy equals the energy of the $P_{\frac{3}{2}}$ level which is either a higher or lower energy depending on whether the doublet levels are normal or inverted. The polarization of the protons scattered by the helium nuclei at one of these resonant energies will be opposite in sign to that at the other resonant energy.

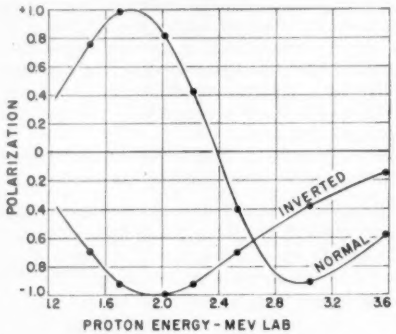

FIG. 1. Expected polarization of protons scattered from He^4 at 90° in the center-of-mass coordinate system as a function of incident proton energy. One curve assumes the normal $P_{\frac{1}{2}}-P_{\frac{3}{2}}$ doublet in Li^{5*} while the other assumes an inverted doublet.

A phase shift analysis of the proton-He^4 elastic scattering data in the energy range of incident protons from 0.95 to 3.58 Mev has been made by Critchfield and Dodder[4] from the experimental differential cross-section scattering data obtained by Freier, Lampi, Sleator, and Williams[5] at the University of Minnesota. The analysis shows that the data can be fitted by assuming that only $S_{\frac{1}{2}}$, $P_{\frac{1}{2}}$, and $P_{\frac{3}{2}}$ waves enter into the scattering interaction in the above energy range. However, the analysis does not establish uniquely the contribution of the $P_{\frac{1}{2}}$ and $P_{\frac{3}{2}}$ waves to the scattering interaction; i.e., two sets of phase shifts are obtained, one corresponding to the case of normal energy levels and the other for the case of inverted energy levels in Li^{5*}.

If the energy levels in Li^5 form a normal doublet, the phase shift analysis implies that both levels are within the above energy range so that it should be possible to polarize a beam of protons in either of two opposite directions in this energy range. If the energy levels are inverted, the phase shift analysis indicates that only the $P_{\frac{3}{2}}$ level is in this energy range and the $P_{\frac{1}{2}}$ level is somewhere above 4 Mev so that only one direction of polarization should take place in the above energy range. The expected polarization of protons scattered from He^4 at 90° in the center-of-mass system of coordinates for the normal and inverted doublets are shown in Fig. 1.

If one measures the polarization with some form of polarizer-analyzer arrangement, it should be possible to determine the order of the energy levels of the $P_{\frac{1}{2}}-P_{\frac{3}{2}}$ doublet in Li^{5*}. A beam of protons with a selected energy can be scattered by helium, and the protons

* This program assisted by the joint program of the ONR and AEC.
† Now at the Radiation Laboratory, Berkeley, California.
[1] F. Bloch, Phys. Rev. **58**, 829 (1949)
[1a] Julian Schwinger, Phys. Rev. **69**, 681 (1946); **73**, 407 (1948).
[2] L. Wolfenstein, Phys. Rev. **75**, 1664 (1949).
[3] M. Hamermesh, Phys. Rev. **75**, 1281 (1949).
[4] C. L. Critchfield and D. C. Dodder, Phys. Rev. **76**, 602 (1949).
[5] Freier, Lampi, Sleator, and Williams, Phys. Rev. **75**, 1345 (1949).

scattered at 90° can be scattered by helium again at some lower energy determined by the mechanics of the scattering process and loss by ionization of the intervening material between the two scattering helium nuclei. If the doublet should be inverted, the second scattering process would favor an azimuthal direction that makes the second scattering similar to the first; while if the doublet should be normal, the opposite azimuthal direction would be favored on the second scattering provided one selects the original laboratory energy of the protons to fall on one side of the cross-over point and the energy of the second scattering to fall on the other.

The variation in azimuthal intensity is given by the differential cross-section relation[6]

$$\sigma(\theta, \phi)=\sigma_{12}[1+P_1(E_1, \theta_1)P_2(E_2, \theta_2)\mathbf{n}_1\cdot\mathbf{n}_2].$$

The quantities $\mathbf{n}_1$ and $\mathbf{n}_2$ are unit vectors representing the planes of the first and second scattering interactions, P_1 and P_2 are the polarizations which would be given to an initially unpolarized beam of protons at the first and second interactions separately, and σ_{12} is the differential cross section which would be obtained for doubly scattered protons if the polarizing of the protons by the first scattering were neglected. This double-scattering differential cross section σ_{12} can be obtained simply as the product of the differential cross sections for the two individual scattering events, i.e.,

$$\sigma_{12}(E_1, \theta_1, E_2, \theta_2)=\sigma_1(E_1, \theta_1)\sigma_2(E_2, \theta_2).$$

Using the notation of Critchfield and Dodder, and considering only the S and P waves, the polarization can be obtained from the scattering amplitudes by the relation $P=A^*\sigma A/A^*A$, where σ here is the Pauli spin matrix and where the scattering amplitude A is understood to contain the spin factors in the correct weight. The calculations can be made most easily by rewriting the original incident beam and scattering amplitude in terms of eigenfunctions with eigenvalues ±1 in the X-direction where the scattering interaction occurs in the $Y-Z$ plane, and then using the spin matrix $\begin{vmatrix}1 & 0\\ 0 & -1\end{vmatrix}$ in the formula for the polarization. The polarization curves of Figs. 2 and 3 were computed from the phase shift data for the $p-He^4$ interaction as given by Critchfield and Dodder,[4] Fig. 2 giving the polarization assuming the existence of the inverted $P_{\frac{1}{2}}-P_{\frac{3}{2}}$ doublet and Fig. 3 giving corresponding curves for the normal doublet.

From these polarization curves and from the formula for the differential cross section given above, the ratio is intensity between the forward double scattering and backward double scattering directions as applied to this experiment is obtained from the relation

$$R=(1+P_1P_2)/(1-P_1P_2),$$

[6] J. V. Lepore, Phys. Rev. **79**, 137 (1950).

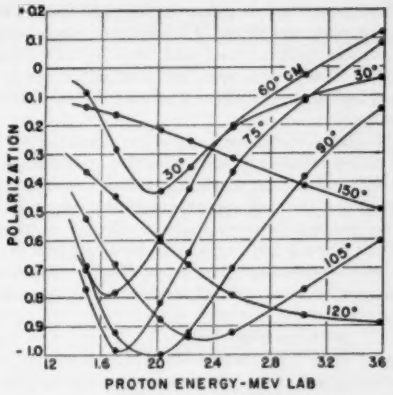

FIG. 2. Expected polarization of protons scattered from He^4 at various center-of-mass angles as a function of incident proton energy. All curves are for the case of in the inverted $P_{\frac{1}{2}}-P_{\frac{3}{2}}$ energy levels in Li^5.

the term $\mathbf{n}_1\cdot\mathbf{n}_2$ being given only the values ±1 for the geometry selected in this experiment.

EXPERIMENTAL APPARATUS AND PROCEDURE

The experimental polarizer-analyzer arrangement is shown in Fig. 4, which is a cross-section diagram of the double scattering chamber used. This chamber provided for double scattering at 90 degrees in the center-of-mass system for each of the two interactions, this angle giving, to a first approximation, the greatest polarization effect because of the maxima of the P waves at 90°. The collimating system between the two large gas volumes defined a beam of protons scattered at 90° in the first interaction, while selection of the protons scattered at 90° in the second interaction was made through analysis of the proton tracks in the nuclear

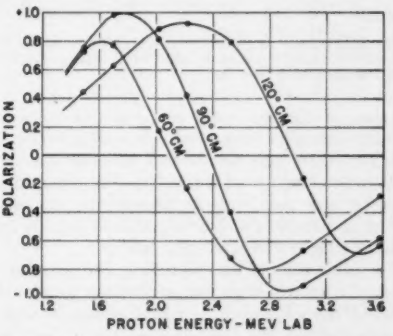

FIG. 3. Expected polarization of protons scattered from He^4 at various center-of-mass angles as a function of incident proton energy. All curves are for the case of the normal $P_{\frac{1}{2}}-P_{\frac{3}{2}}$ energy levels in Li^5.

emulsion plates used for measuring the yield. One nuclear emulsion plate was placed in a position to detect those protons scattered in a backward direction with respect to the incident proton beam, and another was placed in a position to detect those scattered in the forward direction.

The planes of the two scattering interactions were held nearly coplanar by the collimating system between the first and second scattering volumes, so that the expression $\mathbf{n}_1 \cdot \mathbf{n}_2$ took approximately the values ± 1.

The distance between the two effective scattering volumes was selected so that the stopping power of the gas in the chamber gave proper energy separation between the first and second scattering processes.

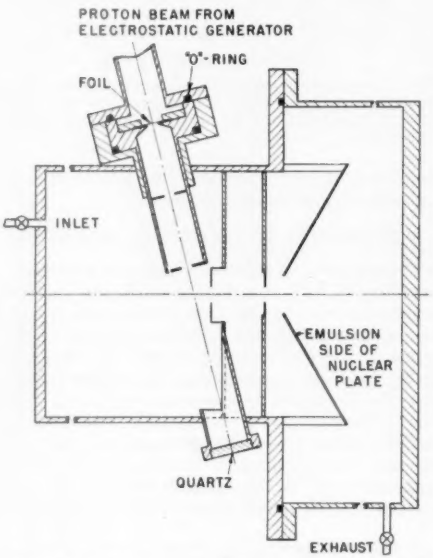

FIG. 4. Schematic diagram of double scattering chamber which uses nuclear emulsion plates as detectors of protons which have been scattered twice from He^4.

Because of the low yield expected, the collimating systems were made to give broad resolution, and nuclear emulsion plates were used so that an integration of the yield over a long period of time could be obtained. The chamber was used with an atmospheric pressure of helium to provide a sufficiently high density of target nuclei for the double scattering process.[7]

For elimination of wall scattering, the chamber was made of relatively large size, so that any protons scattered by the walls would not have enough energy left to pass through the high pressure helium and reach the nuclear emulsion plates. In addition, the plates were so oriented that no protons scattered by the slit edges could reach the emulsion side of the nuclear plates without additional $p-He^4$ collisions.

The atmospheric pressure of the helium was separated from the high vacuum of the electrostatic generator by a combination foil of 0.1-mil nickel and 0.2-mil Nylon placed over a hole $\frac{1}{4}$ inch in diameter but with a bar across its center for greater foil support. With the aid of the $Li^7(p,n)Be^7$ reaction threshold, the foil thickness was found to be 180 kilovolts at an initial proton energy of 2.062 Mev. The first collimating system consisted of the first round hole $\frac{1}{4}$ inch in diameter and the second hole $\frac{5}{16}$ inch in diameter, $3\frac{1}{2}$ inches from the first. An antiscattering slit of $\frac{5}{16}$-inch diameter was placed midway between these two defining slits. The second collimating system consisted of two rectangular slits $\frac{3}{8}$ inch long to provide sufficient intensity after the first scattering, and $\frac{1}{8}$ or $\frac{1}{4}$ inch wide to give sharper resolution in the plane of scattering.

The nuclear emulsion plates, 1 in.$\times$3 in. in size, were held at one end on machined pedestals by spring clips at an angle of 60 degrees with respect to the central ray of the second collimating system. The plates chosen for detection of the protons were special C2 nuclear emulsion plates, made by Ilford, Ltd. In all the exposures made, after insertion of the plates into the chamber and replacement of the cover, the chamber was evacuated to a pressure of the order of 0.1 mm Hg. The helium was then let into the chamber, and the flow through the chamber was set at a rate of approximately six cubic feet per hour.

The relative intensity of the incident proton beam from the electrostatic generator was monitored with a 931-A photomultiplier tube which measured the light produced by the fluorescence of the quartz plate upon proton impact and the light produced by ionization and excitation of the helium. An absolute determination of the number of incident protons was not necessary.

To minimize blackening of plates by the light present in the chamber and to minimize peeling of the emulsions from the glass backing, C2 plates were obtained which contained a yellow screening dye to make the plates less sensitive to violet and ultraviolet light produced by the ionized helium, and with extra plasticizer added to improve the adherence of the emulsion to the glass. Ilford was able to supply these plates most conveniently with emulsions 100 microns thick. The proton tracks were easily visible in these plates, although these tracks may have been somewhat less dense than in the regular C2 plates.

DETAILS OF EXPOSURES

Two types of exposures were made, the first type being made with the emulsion in such a position as to determine the distribution of the singly scattered proton beam as collimated by the second slit system, and the second type being made to measure the intensities of the doubly scattered protons. No anomaly was found

[7] D. C. Dodder, Phys. Rev. **76**, 683 (1949).

in the intensity pattern of the first scattered beam, the resulting distribution on the plates agreeing with that predicted by integrating the cross-section data available over the possible paths permitted by the collimation.

Several exposures were made to measure the comparative densities of the doubly scattered protons. The first was at an initial proton energy of 3.25 Mev, giving a computed proton energy at first scattering of 2.91 Mev. The slits in the second collimating system were $\frac{1}{8}$-inch wide, and a 24-hour continuous exposure was made with an incident proton beam intensity of the order of three microamperes.

A second exposure was made with the same geometry and at 3.50-Mev initial proton energy, giving a proton energy at first scattering of 3.17 Mev, for study of energy-dependent effects.

A third exposure was made at an initial proton energy of 3.25-Mev, but with a slit width of $\frac{1}{4}$ inch for study of resolution-dependent effects.

A background exposure was made by filling the chamber with deuterium. If the incident proton made two collisions with deuterium in such a fashion that it could pass through all collimating slits, it would then have insufficient energy to reach the photographic plates. The complete absence of tracks in the emulsion indicated there was no gas to wall scattering effects.

ANALYSIS OF PLATES

In analyzing the plates we chose to accept only those tracks of protons arriving along paths making an angle of less than 32 degrees with the plane of the plate, this giving equal angles on both sides of the central ray after the second scattering at 76 degrees from the axis of the chamber, or 16 degrees from the plane of the plate. However, because of the considerable statistical change in direction of the protons through multiple small-angle scattering after entering the emulsion, it was decided to place greater reliance on the energy of the protons as indicated by the lengths of the tracks in the emulsion as a criterion in selecting protons which had not been scattered through too large an angle in the second scattering.

The various possible proton paths in this broad-resolution application were traced through, and the energies and angles at which these protons arrived at the plates were then used as the standards of acceptance. The setting of these criteria was not of greatest importance because these same criteria were to be applied for the backward and forward plates alike, and it was only the ratio of the number of tracks and not the absolute number of tracks which was being studied.

The results obtained by counting proton tracks in equivalent strips in the forward and backward plates are given in Table I.

A comparison of the experimental backward to forward ratios with the two possible theoretical values shows that the doublet is inverted. The effect of changing from $\frac{1}{8}$-inch slits to $\frac{1}{4}$-inch slits indicates that the lack

TABLE I. Ratio of proton tracks in equivalent strips in the forward and backward plates.

	No. of tracks on backward plate	No. of tracks on forward plate	Ratio—backward to forward	Theoretical ratio for ideal ray	
				Inverted doublet	Normal doublet
3.25 Mev $\frac{1}{8}$-in. slits	364	191	1.9	2.6	1/20.2
3.25 Mev $\frac{1}{4}$-in. slits	220	156	1.4	2.6	1/20.2
3.50 Mev $\frac{1}{8}$-in. slits	61	33	1.85	1.9	1/6.6

of exact agreement between theoretical and experimental results can be attributed to the broad geometry used in the experiment as described below. The theoretical ratios for an ideal ray are plotted in Fig. 5 for a range of energy values and show that for the normal doublet, the forward plate would have had by far the greater number of tracks in the neighborhood of the energy used. Because of low yield in the 3.50-Mev exposure and consequent poor statistics, no reliable deductions can be made in comparing the ratios at 3.50- and 3.25-Mev initial proton energy.

ERRORS AND CORRECTIONS

Possible sources of error considered were metal-to-gas or gas-to-metal collisions by the protons, generation of free neutrons which might lead to spurious acceptable proton tracks in the emulsions, contamination of the plates before exposure or after exposure and before development, mechanical alignment, helium purity, accuracy of control of energy of the initial proton beam,

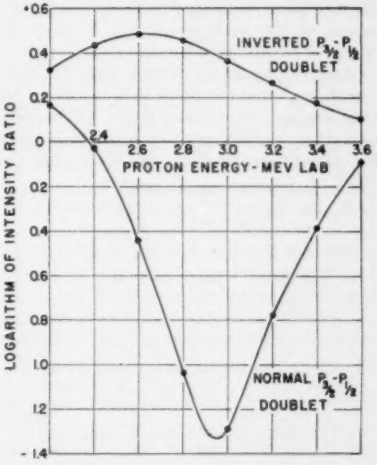

FIG. 5. Expected ratio of intensities on backward plate to forward plate for 90° center-of-mass double scattering of protons by He^4 as a function of incident proton energy before the first scattering.

and the broadness of the resolution in the scattering chamber. None of these except the last were found to have appreciable effect on the experimental ratio of number of proton tracks.

As seen in the results in Table I, however, the broadness of the resolution had a large effect on the correlation between the ratios as found experimentally and the ratios as predicted for the ideal proton path, i.e., the path involving two nuclear scatterings at exactly 90 degrees each in the center-of-mass system of coordinates. A numerical integration was then carried through for the case of incident proton energy of 3.25 Mev and slit width of $\frac{1}{8}$ inch. Factors included were the variation of cross section and energy with angle of scattering and variation of polarization with energy and angle of scattering. This summation gave a ratio in yield at the upper plate to that at the lower plate of 2.2 to 1, rather than the ideal path ratio of 2.6 to 1. Still neglected was the azimuthal variation of the paths of the protons such that the dot products $\mathbf{n}_1 \cdot \mathbf{n}_2$ were not exactly ± 1.

CONCLUSIONS

The theoretical values are also subject to the experimental errors in the data from which the original phase shifts were calculated. With this additional correction, the ratio, as obtained experimentally, is considered to be in a statistical agreement with the ratio as obtained from the phase shift data for the inverted doublet and consequently shows that the $P_{\frac{1}{2}}-P_{\frac{3}{2}}$ doublet in the compound Li^6 nucleus is inverted. Any corrected theoretical ratio for the normal doublet would still be in complete disagreement with the experimental results.

This conclusion is in agreement with Adair's[8] considerations of the inversion of the P states in the mirror nuclei Li^6 and He^6. By assuming that the single level formula of nuclear dispersion theory held in this case, he showed that the phase shift variations for the inverted doublet as calculated by Critchfield and Dodder[4] could be fitted with an appropriate choice of nuclear parameters. He then used these same parameters corrected for the absence of the coulomb field and calculated the $n-\alpha$ total cross sections which were in substantial agreement with the experimental data.

It is expected that differential $p-He^4$ cross-section measurements when extended to proton energies of 5 or 6 Mev would show the presence of the $P_{\frac{1}{2}}$ wave resonance. At this energy the scattered protons would have a polarization opposite in sign to the polarization found in this experiment. An experiment similar to this one would then give a further check on the order of energy levels in Li^{6*}. By selecting the first scattering to take place at the $P_{\frac{3}{2}}$ energy level and the second scattering to take place at the lower $P_{\frac{1}{2}}$ energy level, there should then be a reversal of the backward to forward ratios found in this experiment.

With the development of ion sources capable of high beam intensities and with improvement of electrostatic generator techniques, double process experiments are becoming more feasible. Interactions such as the $p-He^4$ interaction described in this report can be used to polarize the protons in a single scattering process, and the polarized beam produced can be used in other scattering and disintegration experiments in which the angular momenta are of special interest. If there should be strong polarization near the $P_{\frac{1}{2}}$ level resonance of this inverted doublet, the applicability of this experimental device would be extended to higher energy ranges. After the beam has been polarized it can be degraded in energy to any desired value by ionization losses in passing through a material medium without appreciably changing the polarization.

ACKNOWLEDGMENTS

This work was begun by Mr. D. C. Dodder, who made preliminary calculations and suggested the geometry of the chamber to be used to decrease the background to a minimum. We also wish to thank Professor J. H. Williams for his interest and advice and the members of the electrostatic generator group for their cooperation in obtaining the exposures.

This research was materially assisted by the University of Minnesota Technical Research Fund.

[8] R. K. Adair, Phys. Rev. **82**, 750 (1951).

Superconductivity of Vanadium*

AARON WEXLER AND WILLIAM S. CORAK
Westinghouse Research Laboratories, East Pittsburgh, Pennsylvania
(Received September 21, 1951)

The presence of small quantities of oxygen and nitrogen in interstitial positions in the vanadium lattice is found to affect markedly the superconductive properties of the metal. X-ray evidence supports the supposition that these impurities set up internal strains which are known to give rise to properties very similar to those of the hard superconductors. It is suggested that these strains, which, unlike those arising from mechanical work, are not always removable by vacuum heat treatment, are responsible for the difficulties associated with the preparation of samples of the metals exhibiting a reversible B, H curve.

It is shown that the sharp penetration fields for a relatively pure specimen are probably not very different from the equilibrium fields. The transition temperature of vanadium is 5.13°K, $(dH_c/dT)T_c = 436 \pm 20$ oersteds/deg, and the Sommerfeld $\gamma = 15 \times 10^{-4}$ cal/mole deg K^2.

I. INTRODUCTION

THE superconductivity of vanadium is of interest because this metal is one of the so-called hard superconductors whose superconductive properties are highly dependent on the physical and chemical state of the metals. Most specimens of the hard superconductors, which are uranium and the metals of the fourth and fifth transition groups of the periodic table, exhibit appreciable hysteresis in their isothermal B, H curves and three progressively steeper H_c, T curves depending upon whether these are obtained by measurements of critical currents, the magnetic fields which will first penetrate the metal, or the magnetic fields which completely restore normal resistance. In addition, the transition between the superconductive and normal states is not sharp. In contrast with these properties, the mechanically soft metals of the second, third, and fourth groups have practically reversible B, H curves, sharp transitions, and their H_c, T curves are independent of the method of measurement. The work on vanadium reported here is part of a program designed to determine the factors and the mechanisms which are responsible for the properties of the hard superconductors; other superconductors in this classification are also under investigation. Attention to previous work on the hard superconductors titanium,[1] zirconium,[2] hafnium,[2] thorium,[3] vanadium,[4] niobium,[5,6] tantalum,[7] and uranium,[8] may best be drawn by indicating the most recent pertinent papers wherein detailed references to previous work may be found.

The work reported here, when correlated with the results of the investigations of others, indicates that the properties of the hard superconductors outlined above arise from inhomogeneous strains which may be set up in the lattice either by mechanical work or by impurities, particularly carbon, oxygen, and nitrogen, which at low concentrations are known to enter the lattice interstitially. The most striking differences in physical properties between the soft and hard superconductors are the much higher cohesive strengths and mechanical hardness of the latter group. For the purpose of this discussion, the most important corollary of the first factor is the high recrystallization temperatures[9] of hard superconductors. Thus while mechanically produced strains in the soft superconductors are easily removed by an annealing operation (indeed, most of these metals self-anneal at room temperature), quite high temperatures are required for the transition metals. The hardness of these metals increases strongly with mechanical work and especially with increasing content of carbon, nitrogen, and oxygen. From thermodynamic considerations it can be shown[10] that the removal of these contaminants by high vacuum heat treatment is most difficult and, in fact, particularly in the case of oxygen such treatment may increase their concentration through the reaction of the metal with the residual gases in the vacuum. In connection with attempts to remove such contaminants, it is therefore necessary to consider the thermodynamics and kinetics of the reactions involved. This, however, is made difficult by the paucity of data for the thermodynamic stability of alloys containing only a very small fraction of an atomic percent of the interstitial solutes.[11] Metallurgists[12,13] have used the hardness of annealed metals of the fourth, fifth, and sixth transition groups as an index of their content of interstitially located impurities. It seems reasonable to use this same property as a criterion of

* Presented at the Oxford Conference on Low Temperatures, Oxford, England, August 22–28, 1951.
[1] J. G. Daunt and C. V. Heer, Phys. Rev. **76**, 715 (1949).
[2] N. Kurti and F. Simon, Proc. Roy. Soc. (London) **A151**, 610 (1935).
[3] D. Shoenberg, Proc. Cambridge Phil. Soc. **36**, 84 (1940).
[4] A. Wexler and W. S. Corak, Phys. Rev. **79**, 737 (1950).
[5] Cook, Zemansky, and Boorse, Phys. Rev. **80**, 737 (1950).
[6] L. C. Jackson and H. Preston-Thomas, Phil. Mag. **41**, 1284 (1950).
[7] R. T. Webber, Phys. Rev. **72**, 1241 (1947).
[8] B. B. Goodman and D. Shoenberg, Nature **165**, 441 (1950).
[9] F. Seitz, *The Physics of Metals* (McGraw-Hill Book Company, Inc., New York, 1943), Chapter IV.
[10] E. A. Gulbransen and K. F. Andrew, J. Electrochem. Soc. **97**, 396 (1950).
[11] See for example, O. Kubaschewski and E. V. Evans, *Metallurgical Thermochemistry* (Butterworth-Springer, Ltd., London, 1950), pp. 63–65.
[12] A. E. van Arkel, *Reine Metalle* (Julius Springer, Berlin, 1939).
[13] R. I. Jaffee and I. E. Campbell, Trans. Am. Inst. Mech. Engrs. **185**, 646 (1949).

TABLE I. Characteristics of the vanadium samples.

Sample	Length (cm)	Diameter (cm)	Hardness[a] kg/mm²	Residual[c] resistance ratio	Weight % of non-metal impurities Oxygen	Nitrogen	Source
A	2.54	0.55 (max)[b]	65±10	...	0.038	0.021	Battelle Memorial Institute
B	2.54	0.178	...	0.051	...	...	Battelle Memorial Institute
C	2.22	0.357	113±5	0.069	0.044	0.032	General Electric Company
D	2.54	0.278	185±5	0.173	0.075	0.106	Union Carbide and Carbon Corporation
E	2.54	0.276	343±10	0.259	0.15	0.189	Westinghouse Electric Corporation

[a] These measurements all refer to a 1 kg load and were made with a "Tukon" tester, a description of which may be found in *Metals Handbook* (Am. Soc. Metals, Cleveland, Ohio, 1948), pp. 93–105.
[b] The maximum diameter only is noted to give an idea of the size of the specimen, which, consisting of a large number of individual crystals bonded together at isolated points, was necessarily irregular.
[c] The residual resistivity, obtained at 4.90°K by quenching superconductivity with an external magnetic field, relative to the ice point resistivity.

the severity of internal strains. To paraphrase the foregoing, it should be pointed out that in the case of the transition metals which readily accommodate carbon, nitrogen, and oxygen in the interstices between the metal atoms, simple vacuum heat treatment can only remove the internal strains due to cold work but not, in general, those due to the interstitially located foreign atoms which are stable at elevated temperatures. Thus the hardness increment due to increased content of these interstitial impurities is essentially unaffected by simple annealing.

Now it is known[14] that tension applied to a superconductor raises and compression lowers its transition temperature. It has also been shown[15] most clearly that a superconductor inhomogeneously strained by the application of external forces acquires abnormal properties including those which characterize most samples of the hard superconductors. Hence it is clear that mechanical strains and especially interstitially located foreign atoms may be responsible for the departure of the hard superconductors from simple, ideal behavior.

If, indeed, interstitially located atoms are largely responsible for internal strains which confer the characteristic properties of the hard superconductors, then their effect would depend on the crystal structures and atomic volumes of the metals. Supporting evidence for these ideas may be found in the following: The metals of the fifth transition group, V, Nb, and Ta have body-centered cubic structures while of those of the fourth group Ti, Zr, and Hf have hexagonal close-packed structures and Th is face-centered cubic. Thus for a given atomic volume, the largest interstices will be found in the metals of the fourth transition group, and this fact, coupled with the larger atomic volumes of these metals, indicates that the metals of the fourth group should be less affected by interstitial impurities than those of the fifth group. In the light of these remarks, the extreme cases vanadium and thorium may be considered. The room temperature atomic volume of vanadium is 0.42 that of thorium. It is known that mechanically soft thorium is not difficult to prepare and that its hardness is much less affected by nitrogen and oxygen than is that of vanadium, whose hardness is very markedly increased by oxygen and nitrogen absorption. It is therefore significant to note that the only sample of a transition metal superconductor which has been found to display a completely ideal *B*, *H* curve was one of thorium[3] prepared by the thermal decomposition of its iodide,[16] a process which is known to produce a very soft product most free of interstitial impurities.[12] Another sample of thorium[3] investigated by Shoenberg, which showed the properties typical of hard superconductors, was prepared by calcium reduction of the

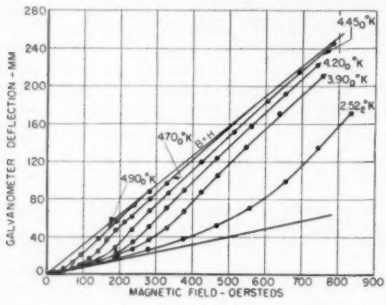

FIG. 1. Magnetic induction in specimen *A*.

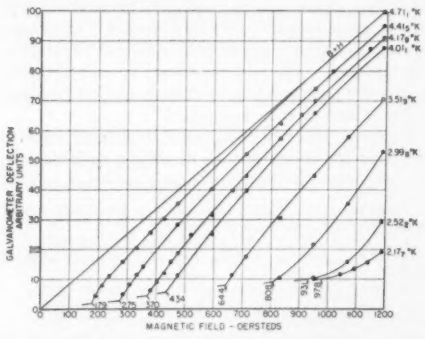

FIG. 2. Magnetic induction in specimen *B*.

[14] C. J. Sizoo and H. Kamerlingh Onnes, Leiden Commun. 180b.
[15] B. Lasarew and A. Galkin, J. Phys. (U.S.S.R.) **8**, 371 (1944).
[16] Private communication from Dr. Shoenberg.

oxide followed by powder metallurgy. This method is known[12] to produce a harder material corresponding to a higher nitrogen, oxygen content. The most extreme case of departure from ideal superconductive behavior was obtained for a very hard sample of vanadium,[17] which gave a $(dH_c/dT)_{T_c}$ of about 4000 oersteds/deg, where H_c is essentially the field at which normal resistance was restored.

The present investigation was undertaken to determine the role of internal strains due to oxygen and nitrogen, as reflected in the mechanical hardness of the metal. It was a further purpose of the work to ascertain the physical significance of the various values of $(dH_c/dT)_{T_c}$ obtained for hard superconductors and in particular to obtain an estimate of this quantity corresponding to that which would be characteristic of a sample exhibiting thermodynamic reversibility in the superconductive transition.

II. CHARACTERISTICS OF THE SPECIMENS STUDIED

The magnetic properties of five specimens of vanadium, obtained from various sources and described in

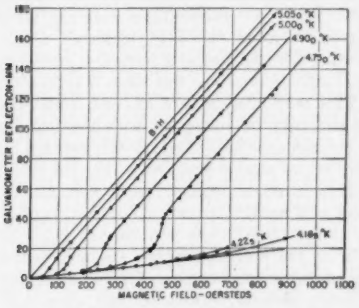

FIG. 3. Magnetic induction in specimen *C*.

Table I, were investigated. Spectrographic analysis of these materials indicated rather similar contents of other metals. The major metallic impurity is less than 0.1 percent iron, while the sum of other metallic impurities is of the order of 0.1 percent. The major differences among the samples are in the nitrogen, oxygen content, and this is seen to be reflected in a rather large range of hardness increasing monotonically with the concentrations of these impurities.

Van Arkel[12] has described the various modes of preparation of vanadium. Sample *A* was grown by the thermal decomposition of vanadium diiodide on a three-mil diameter tungsten filament. The sample consisted of crystals of linear dimensions of the order of 1 mm, the contact between the individual crystals being mechanically weak because of voids. In order to minimize the shape demagnetization effects of such an

[17] Webber, Reynolds, and McGuire, Phys. Rev. **76**, 293 (1949).

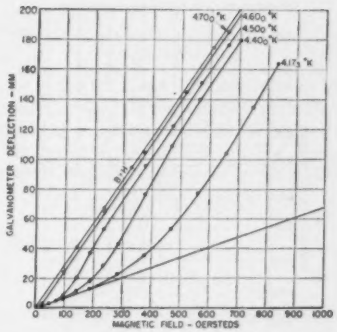

FIG. 4. Magnetic induction in specimen *D*.

array of crystals, this material was swaged down to give a uniform mass from which sample *B* was carefully machined. Sample *C* was obtained from some vanadium prepared by calcium reduction of the pentaoxide. In this particular preparation, the reaction temperature exceeded the melting point which resulted in a melted specimen from which sample *C* was machined. Sample *D* was obtained in a manner similar to that just described; in addition, however, the specimen from which the sample was machined was remelted in a pure argon atmosphere. Sample *E* resulted from the sintering by heat and pressure of fine particles of vanadium prepared by the calcium reduction method. Because of the nature of their preparations, samples *A*, *C*, and *D* were probably free of mechanical strains. Sample *E* was subjected to a high vacuum anneal at 800°C.

The grain sizes of the specimens were determined by metallographic examination. The grain sizes of *C* were in the range 0.2–1 mm; those of *D* were slightly larger. In both cases, the crystal boundaries were almost straight lines and were well defined. The grains of *E* were smaller by about an order of magnitude, and the

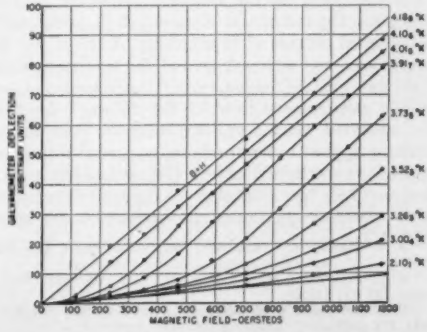

FIG. 5. Magnetic induction in specimen *E*.

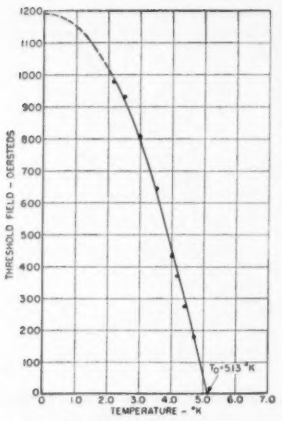

FIG. 6. Threshold fields for superconductive vanadium.

crystal boundaries were very irregular, as would be expected from the method of preparation.

The samples were also studied by x-rays, and all showed the body centered cubic structure. Specimen *A* was found to consist of relatively large single crystals, and the lattice parameter $a_0=3.0282\pm0.0001$A was determined at 30°C. For this material the diffracted beam was very sharp, indicating an unstressed lattice of uniform lattice spacings. As the nitrogen and oxygen content is increased, progressive line broadening is observed, indicative of a stressed lattice, and the lattice parameter increases to 3.0313 ± 0.0006A for *C*, 3.034 ± 0.001A for *D*, and 3.038 ± 0.002A for *E*. These results may account for the diversity of lattice parameters of vanadium recorded in the literature.[12] A similar correlation of lattice parameter and hardness with oxygen and nitrogen content at comparably low concentrations has been reported recently for titanium.[18,19]

III. MEASUREMENTS AND RESULTS

For the study of the magnetic properties of the specimens, the method of Keeley and Mendelssohn[20] was adopted because of its simplicity. A coil of No. 40 copper wire was wrapped around the specimens and, at various constant temperatures,[21] the deflection of the ballistic galvanometer to which the coil was connected was measured when a uniform magnetic field, longitudinally applied to the specimen, was reduced to zero. Applied to a specimen of pure tin (Johnson, Matthey, and Company Lab. No. 2356) of about the same dimensions as the vanadium specimens and machined in the same way, this procedure yielded data of the expected form. A plot of galvanometer deflection *vs* applied field consisted of three straight lines, showing that the magnetic induction B was zero for fields up to the critical field, H_c, i.e., $B=0$ for $0<H<H_c$. In a small field range of the order of 1 percent of H_c, B rose linearly to $B=H$. Above H_c the remanent B was 10 percent H_c when $H=0$, and this accounted for the displacement of the final portion of the curve from the $B=H$ line. The magnetic field was homogeneous and known to ±1 percent. Within these limits, the observed critical field agreed with the data of other workers.[22]

The results for the specimens listed in Table I are shown in Figs. 1–5 in the same sequence as they are tabulated. It was suspected that the fact that the initial field penetration of *A* (Fig. 1) was gradual might have been caused by the demagnetization effects of the irregularly shaped crystals which were bonded together at isolated points. This is confirmed in Fig. 2 which shows that the swaged sample, which was a smooth cylinder, exhibited sharp field penetrations, indicating that the superconductivity of a substantial fraction of the material was destroyed at well-defined magnetic fields. At temperatures near the transition temperature T_c, as the field increased above the penetration field the magnetic induction gradually rose to $B=H$ with no remanent flux when H was reduced to zero. This particular feature has not been observed before and may be connected with the fact that in these specimens the individual crystals were not bonded together on an atomic scale, as is the case with polycrystalline materials obtained from a melt. As would be expected of a material having a distribution of critical fields, as the temperature was lowered below T_c the fraction of the specimen whose superconductivity is destroyed by a small range of field ΔH above the penetration field H_c decreased and eventually the penetration became rather gradual. Arguments will be presented below supporting the hypothesis that the sharp penetration fields, plotted in Fig. 6, probably correspond closely to the equilibrium fields which would be evidenced by a pure, unstrained sample of the metal. The transition temperature may be obtained in several ways. The temperatures corresponding to $B=\frac{1}{2}H_c$ in Fig. 1 extrapolate to $T_c=5.13$°K when $H_c=0$. An identical value of T_c is obtained from the penetration fields for sample *B* as shown in Fig. 6.

The effect of increasing nitrogen and oxygen concentration can be seen in the curves for specimens *C*, *D*, and *E*. Thus for *C* the superconductivity of the specimen was destroyed gradually when the penetration field was exceeded. The penetration fields could be obtained if the sensitivity of the measurements was increased in the low deflection range. These data also yielded $T_c=5.13°$ and $(dH_c/dT)T_c$ was within 10 percent of the value obtained from the data for *B*. Again the decreasing

[18] H. T. Clarke, Jr., Trans. Am. Inst. Mech. Engrs. **185**, 588 (1949).
[19] W. L. Finlay and John A. Snyder, Trans. Am. Inst. Mech. Engrs. **186**, 277 (1950).
[20] T. C. Keeley and K. Mendelssohn, Proc. Roy. Soc. (London) **A154**, 378 (1936).
[21] H. van Dijk and D. Shoenberg, Nature **164**, 151 (1949).
[22] J. G. Daunt and K. Mendelssohn, Proc. Roy. Soc. (London) **A160**, 127 (1937).

slope with which the curve leaves the base line as the temperature is reduced is very evident. Still further increase in nitrogen and oxygen content lowered T_c and exaggerated the features outlined above, as shown in Figs. 4 and 5. For these specimens neither the penetration fields nor those corresponding to the completion of penetration could be obtained with any degree of reliability.

A comparison of our results with those of others,[17,23] on vanadium is somewhat difficult because earlier work was done by methods which essentially measure the resistance of the metals. The rather lower transition temperatures previously reported are probably due to the lower purity of the vanadium specimens used.

Recently questions have been raised[6] concerning the significance of the penetration fields and of the fields corresponding to the completion of penetration. If the characteristics of the hard superconductors are due to inhomogeneous internal strain, then it would appear that the initial sharp penetration fields corresponding to the destruction of superconductivity in an appreciable fraction of a given specimen would be close to the equilibrium fields of a pure specimen. The fact that the field continues to penetrate over a large range of H is expected in view of the internal strain. Confirmation of the significance of the penetration fields may be found in Shoenberg's work on thorium, which showed that the penetration fields of an impure sample were close to the equilibrium fields of a pure sample. While the best way to answer these questions would be to introduce nitrogen and oxygen into the lattice of a pure sample exhibiting a reversible B, H curve, the following arguments may illuminate the situation. It is well known[22,24,25] that the application of thermodynamics to the equilibrium threshold fields—temperature relation enables one to calculate the differences in thermal properties of the metal across the phase boundary. If additional assumptions are made, the thermal properties of the individual phases may be obtained. We are particularly interested in relating $(dH_c/dT)_{T_c}$ to a simple physical property of the metal so that the expected order of magnitude of this derivative may be estimated. For a specimen of zero demagnetization coefficient, the entropy difference is given by

$$\Delta S = S_s - S_n = (VH_c/4\pi)(dH_c/dT) \tag{1}$$

where V is the atomic volume, and the specific heat difference is

$$\Delta C = C_s - C_n = (VT/4\pi)[(dH_c/dT)^2 + (H_c d^2H_c/dT^2)]. \tag{2}$$

It has been pointed out[22] that if the linear term, T, of the specific heat of the normal phase is the Sommerfeld electronic term and if the specific heat of metal in the superconducting state does not contain a term linear in T, then

$$\gamma = (d\Delta S/dT)_{T=0} \tag{3}$$

which, by virtue of (1) may be derived from the equilibrium H_c *vs* T curve. It is to be noted that this method of determining γ involves a double differentiation. On the other hand, if, in addition to the assumptions already made, the following simple law is applicable

$$H_c = H_0[1-(T/T_c)^2] \tag{4}$$

then it has been shown that

$$\gamma = (V/8\pi)(dH_c/dT)^2_{T_c} \tag{5}$$

which involves a single differentiation. Recently Goodman and Mendoza[26] showed that aluminum, cadmium, gallium, and zinc accurately obey Eq. (4) over the whole temperature range and hence used a relation equivalent to Eq. (5) to deduce the corresponding γ values. Taking data from the literature,[22,27,28] we have plotted H *versus* T^2 for mercury, indium, thallium, tin, lead, thorium, and tantalum and find that only in the case of mercury does a straight line accurately fit all of the data. For the other metals, the linearity is

TABLE II. Comparison of γ-values for various metals.

			γ values (cal/mole deg^2) $\times 10^4$		
(1)	(2)	(3)	(4)	(5)	(6)
Element	Atomic volumes[a] (cm^3)	$-(dH_c/dT)_{T_c}$ (oersteds/deg)	$\frac{V}{8\pi}\left(\frac{dH_c}{dT}\right)^2_{T_c}$	$\left(\frac{d\Delta S}{dT}\right)_{T=0}$	Calorimetric
Mercury	13.9	199[b] 197[c]	5.2 5.1	3.8[b] 4.5[d]	···
Indium	15.7	144[d]	3.1	3.5[e] 3.6[d]	3.23[f]
Thallium	17.2	137[e] 139[d]	3.1 3.2	2.8[e] 3.4[d]	···
Tin	16.3	150[b]	3.5	3.5[b] 3.95[e]	4.0[g]
Lead	18.3	212[b]	7.8	7.1[b] 7.0[h]	···
Titanium	10.7	285[e]	···	···	8.3[h]
Zirconium	14.1	230[e]	···	···	6.9[h]
Thorium	19.8	191[i]	6.9	···	···
Vanadium	8.39	436±20	15	···	···
Tantalum	10.9	369±10[h]	14	19[h]	14.1[j]
Uranium	12.5	≷530[e]	···	···	≷34[h]

[a] Atomic volumes were calculated from data given in reference 12 from densities at 20°C, except for Hg for which $V_{-195°C}$ is used.
[b] Reference 22.
[c] Reference 27.
[d] Reference 28.
[e] Estimated from column 6.
[f] J. R. Clement and E. H. Quinnell, Low Temperature Symposium, U. S. Bureau of Standards, March 27-29 (1951).
[g] W. H. Keesom and P. H. van Laer, Physica **5**, 193 (1938).
[h] These data were kindly supplied by Dr. S. Friedberg, Carnegie Institute of Technology, in advance of publication.
[i] Reference 3. From reference 26 it may be inferred that both T_c and $(dH_c/dT)_{T_c}$ for thorium are somewhat higher than the values reported by Shoenberg.
[j] W. H. Keesom and M. Désirant, Physica **8**, 273 (1941).
[k] Reference 8.

[23] W. Meissner and H. Westerhoff, Z. Physik **87**, 206 (1934).
[24] C. J. Gorter and H. Casimir, Physica **1**, 306 (1934).
[25] J. A. Kok, Physica **1**, 1103 (1934).
[26] B. B. Goodman and E. Mendoza, Phil. Mag. **42**, 594 (1951).
[27] Daunt, Horseman, and Mendelssohn, Phil. Mag. **27**, 754 (1939).
[28] A. D. Misener, Proc. Roy. Soc. (London) **A174**, 262 (1940).

quite good in the neighborhood of T_c. As T decreases to 0, the H_c, T^2 curve rises progressively above the line representing the data in the vicinity of T_c. Now it can be shown that in order for (5) to be valid it is only necessary for (4) to represent the data in the vicinity of T_c. Hence it is convenient to obtain the slope of the H_c, T^2 curve at T_c, from which we obtain $(dH_c/dT)_{T_c}=2T_c[dH_c/d(T^2)]_{T_c}$. In Table II are compared γ-values obtained in three ways: by direct calorimetric measurements, from Eq. (3), and from Eq. (5). It will be noted that the values of γ derived from Eq. (5) agree with the calorimetric determinations at least as well as do those obtained from Eq. (3). In particular, the excellent agreement in the case of the hard superconductor tantalum lends support to the applicability of the relation to data which follow the parabolic law (4) accurately only in the vicinity of T_c. The evaluation of γ from data in the range near T_c rather than near 0°K has a further advantage arising from the fact that B, H curves are generally most reversible in the vicinity of T_c, particularly for hard superconductors.† A plot of the penetration fields *versus* T^2 for vanadium specimen B gives a curve rather similar to that of tantalum but with somewhat greater scatter of the points; the value of γ deduced from Eq. (5) is 15×10^{-4} cal/mole deg^2. Since the γ values for the fourth transition group metals do not vary greatly, our value of γ for vanadium in relation to that for tantalum may be taken as a confirmation of the assumption that the penetration fields of Fig. 6 are not too far different from the equilibrium fields that would be characteristic of a pure, unstrained specimen of vanadium. By the same token, it seems clear that the very high critical fields reported for niobium,[6] which imply a $\gamma=375\times10^{-4}$ cal/mole deg^2, are far from the equilibrium fields.[29] Goodman and Shoenberg[8] have reached similar conclusions in evaluating their measurements of the high critical fields of uranium.

CONCLUSIONS

The foregoing indicates that the magnetic properties exhibited by most specimens of the so-called hard superconductors are due to internal strain arising from either mechanical work or interstitially located impurities such as carbon, nitrogen, and oxygen. The very large effects of small concentrations of these impurities on the superconductive properties can be understood on this basis. As shown by Shoenberg's work[3] on thorium, whose structure and large atomic volume reduces the strains introduced by these impurities, a sufficiently pure specimen of a metal in the fourth and fifth transition groups will have a reversible B, H curve, and in general will have properties identical with those of the soft superconductors. It is difficult to correlate our results with Webber's studies[7] on the effect of annealing and gas content on the superconducting properties of tantalum; part of the difficulty may result from the fact that resistance measurements do not necessarily reflect the properties of the bulk material.

From an evaluation of γ in terms of $(dH_c/dT)_{T_c}$, it appears that sharp penetration fields, in the case of those specimens that do not exhibit a reversible B, H transition, are not far different from the equilibrium fields. A direct calorimetric study of vanadium is under way to test these views. It is also planned to correlate the superconductive properties of the hard superconductors with internal friction studies[30] which give direct evidence of the concentrations of interstitial impurities.

ACKNOWLEDGMENTS

We wish to thank our many colleagues who contributed to this work either directly or indirectly. Special thanks are due to Dr. Suzanne Beatty for the x-ray studies, to W. J. Houk for the hardness measurements, to R. L. Anderson for the metallographic work, and to J. W. McWhirter for the residual resistance ratio measurements.

† *Note added in proof.*—The data tabulated in Table II indicate the general validity of (5), which provides a check on the expected magnitude of the equilibrium $(dH_c/dT)_{T_c}$ in terms of the normal electronic specific heat. Since (5) follows from the assumption of (4) as the equilibrium H_c, T relation, then by virtue of (2) the form of $\Delta C=C_s-C_n$ is determined to be a sum of a term linear in T and one cubic in T. Conversely, it has been shown [see G. Preston Burns, Phys. Rev. **76**, 999 (1949)] that if the specific heat of the normal state is given by $C_n=\gamma T+AT^3$ and that of the superconducting state by $C_s=BT^3$, where γ, A, and B are constants, the form of the equilibrium H_c, T relation must be (4).

[29] At the Oxford Conference on Low Temperatures, at which the present paper was read, A. Brown, M. W. Zemansky, and H. A. Boorse reported a calorimetric determination of γ for niobium to be 21.0×10^{-4} cal/mole deg^2, which is in direct support of the conclusion indicated above.

At the same meeting, L. C. Jackson and H. Preston-Thomas reported that niobium, when heated in a high vacuum at 2300°K for 40 hours, exhibited a very appreciable lowering of the initial dH_c/dT as measured both by resistance and magnetic methods. The transition temperature after heat treatment was raised from pre-heat treatment values of 8.35°K for the magnetic method and 8.75°K for the resistance method to a common value of 9.20°K. The mechanical hardness of the metal was observed to decrease greatly as a result of the heat treatment. These results are entirely consistent with the work presented in this paper.

[30] T'ing-Sui Kê, Phys. Rev. **74**, 9 (1948).

Multiple Scattering of Fast Particles in Photographic Emulsions

L. VOYVODIC AND E. PICKUP
Physics Division, National Research Council, Ottawa, Canada
(Received July 9, 1951)

The multiple scattering theory of Williams is applied to photographic emulsion techniques, and the "scattering constant" K, which is commonly used in determining particle energies from mean scattering deflections, is evaluated for various experimental conditions. For fast particles K varies from 19 to 30 for scattering cell lengths between 10 and 10^4 microns of emulsion. The scattering theories of Snyder and Scott and of Molière are also compared with that of Williams. The theories of Molière and Williams agree closely for both photographic emulsions and pure substances when the Molière γ-factor, covering the transition from the classical case to the Born approximation case, is introduced into Williams' theory. For fast particles the theory of Snyder and Scott agrees with the other theories within about 1 percent for most cases for the mean scattering angle between tangents.

A simple formula, based on the theory of Williams with the Molière γ-factor, is derived for K for photographic emulsions, applying over a wide range of velocities and scattering thicknesses within about 1 percent.

The results of a calibration experiment using electron pairs from Be^8 gamma-rays seem to confirm the validity of theoretical values of K in the region $K=22$. The mean gamma-ray energy for 100 electron pairs was found to be 17.4 ± 0.5 Mev, which is in fairly good agreement with an expected mean energy of 16.7 ±0.3 Mev. Results on the energy resolution of the scattering technique, and on the distribution of scattering deflections are also found to be in reasonable agreement with theory.

Finally, comparison is made between theory and other recently published emulsion calibration experiments.

I. INTRODUCTION

THE multiple scattering method has now become widely used for determining the energies of fast, ionizing particles in photographic emulsions, particularly in cosmic-ray investigations. Limited at first to low energy particles using the projection microscope techniques,[1–4] the multiple scattering method was extended to the region of high energy physics by an important advance in technique described by Fowler.[5] A somewhat different scattering technique which is also applicable to high energy particles has been perfected by the Brussels group.[6]

Numerous publications have appeared using Fowler's technique, notably the work of the Bristol group on energies and masses of penetrating shower particles,[5,7] and on neutral meson gamma-rays,[8] whilst the method has also been used in our laboratory[9] and elsewhere. Cosmic-ray studies have also been reported[10,11] using the Brussels experimental method.

The energy-scattering relationship commonly used with Fowler's technique is of the form

$$p\beta=[Kz/\bar{\alpha}(l)]\times(l/100)^{\frac{1}{2}}\ \text{Mev} \qquad (1)$$

where p is the particle momentum in units Mev/c, β its velocity in units of the velocity of light c, z the particle charge, and $\bar{\alpha}(l)$ degrees is the mean projected deflection of the particle over a scattering length of l microns of emulsion. For Ilford G5 emulsions, the numerical value of the "scattering constant" K was given as 32.7 from early grain counting calibrations[5,9] with cosmic-ray protons. From the results of scattering observations in this laboratory, it was felt that this value of K appreciably over-estimated particle energies, at least in some cases.[9]

In order to obtain a direct calibration for K, we have used the emulsion scattering technique as an electron pair spectrometer for the well-known[12] 14- and 17-Mev gamma-rays from Be^8. From a preliminary analysis of the scattering observations, a value of $K=21\pm1$ was reported[13] for the conditions of this experiment. Recently calibration experiments using proton and electrons of known energies have also been reported by Corson,[14] Berger, Lord, and Schein,[15] and Gottstein *et al.*[16]

In this paper we give the results of a theoretical study of emulsion scattering techniques. Theoretical values of the "scattering constant" K, based on Williams' theory[17,18] are presented in convenient graphical form, and an approximate formula is derived, which will be valid under most experimental conditions for photographic emulsions. A detailed description of the analysis and results of the Be^8 gamma-ray calibration experiment is then given. Since the gamma-rays have a fairly simple spectrum it has been possible to check the energy

[1] S. Lattimore, Nature **161**, 518 (1948).
[2] Goldschmidt-Clermont, King, Muirhead, and Ritson, Proc. Phys. Soc. (London) **61**, 183 (1948).
[3] Davies, Lock, and Muirhead, Phil. Mag. **40**, 1250 (1949).
[4] See also method proposed by S. A. Goudsmit and W. T. Scott, (Phys. Rev. **74**, 1537 (1948)), and later note by W. T. Scott (reference 25).
[5] P. H. Fowler, Phil. Mag. **41**, 169 (1950).
[6] V. Goldschmidt-Clermont, Nuovo cimento **7**, 331 (1950).
[7] Camerini, Fowler, Lock, and Muirhead, Phil. Mag. **41**, 413 (1950).
[8] Carlson, Hooper, and King, Phil. Mag. **41**, 701 (1950).
[9] E. Pickup and L. Voyvodic, Phys. Rev. **80**, 89 (1950); 80, 1100 (1950); Can. J. Phys. **29**, 263 (1951).
[10] G. P. S. Occhialini, Nuovo cimento **6**, Supp. 3, 411 (1949).
[11] Dilworth, Goldschmidt-Clermont, Goldsack, and Levy, Phil. Mag. **41**, 1032 (1950).
[12] R. L. Walker and B. D. McDaniel, Phys. Rev. **74**, 315 (1948).
[13] L. Voyvodic and E. Pickup, Phys. Rev. **81**, 471 (1951); **81**, 890 (1951).
[14] D. R. Corson, Phys. Rev. **83**, 217 (1951).
[15] Berger, Lord, and Schein, Phys. Rev. **83**, 850 (1951).
[16] Gottstein, Menon, Mulvey, O'Ceallaigh, and Rochat, Phil. Mag. **42**, 708 (1951); Menon, O'Ceallaigh, and Rochat, Phil. Mag. **42**, 932 (1951).
[17] E. J. Williams, Proc. Roy. Soc. (London) **A169**, 531 (1939).
[18] E. J. Williams, Phys. Rev. **58**, 292 (1940).

resolution as well as the validity of energy determinations from the emulsion scattering technique.

II. SUMMARY OF WILLIAMS' THEORY

Williams' multiple scattering theory was used since it is somewhat simpler mathematically than the later theories of Goudsmit and Saunderson,[19] Molière,[20] and Snyder and Scott,[21] and gives results identical within a few percent, as will be indicated later.

All angles are expressed in units of a natural angle of scattering δ defined[17] by

$$\delta = 2Zze^2(Nt)^{\frac{1}{2}}/p\beta \tag{2}$$

where ze, p, and β are the charge, momentum, and velocity of the scattered particle and Z, t, and N are the atomic number, thickness, and number of atoms per unit volume for the scattering material respectively.

In units of δ, the arithmetic mean projected deflection is given by the statistical relation

$$\bar{\alpha} = 0.80(\log_e M)^{\frac{1}{2}} + 1.45 = 0.80\bar{\alpha}_1 + 1.45 \tag{3}$$

where M measures the average number of collisions experienced by the scattered particle.

The distribution of projected deflections is closely approximated[17] by the probability function $P(\alpha) = G(\alpha) + S(\alpha)$. Here $G(\alpha)$ is a gaussian with arithmetic mean α_m, and $S(\alpha)$ is a single scattering contribution starting at an angle ϕ_2 and equal to π/α^3 for angles greater than ϕ_2, where

$$\alpha_m = (\bar{\alpha} - \pi/\phi_2)/(1 - \pi/2\phi_2^2), \quad \phi_2 = 5.1\bar{\alpha}_1 - 4.0. \tag{4}$$

The transition from multiple to approximately single scattering takes place in the region $\alpha = \alpha_{ms}$, where α_{ms} is the intersection of $G(\alpha)$ and $S(\alpha)$, and is given by

$$\alpha_{ms} = 5.1\alpha_m - 4.0. \tag{5}$$

The distribution functions and ϕ_2, α_{ms} are illustrated in Fig. 7 for the case $M = 21$.

Using a Thomas-Fermi electronic screening field, Williams[17,22] has given two limiting expressions for M, which are designated as M_B (wave-mechanical solution with the Born approximation), and M_{cl} (classical dynamics solution):

$$M_B = 0.64\pi Nlz^2Z^{4/3}\beta^{-2}(\hbar/mc)^2 \quad \text{if} \quad \gamma \ll 1 \tag{6a}$$

$$M_{cl} = 0.20\pi NlZ^{-1}(\hbar^2/me^2)^2 \quad \text{if} \quad \gamma \gg 1 \tag{6b}$$

where $\gamma = zZ/137\beta$, $\hbar$ is Planck's constant divided by 2π, and m is the electronic mass. This factor M corresponds to the factor ν in the theory of Goudsmit and Saunderson, and to Ω_b in Molière's theory. Goldschmidt-Clermont[6] has given an expression in which Molière's factor $(1.13 + 3.76\gamma^2)$, governing the transition from the classical to the Born approximation case, is incorporated into Williams' relation for the mean deflection, using the latter's expression for M_{cl}. Similarly, using M_B, M can be expressed in the form

$$M = M_B/(1 + \gamma^2/0.31) \tag{7}$$

so that $M = M_B$ and M_{cl} for $\gamma \ll 1$ and $\gamma \gg 1$ respectively.

The essential conditions underlying the applicability of the results of Williams' statistical theory are that the average deflection, $\bar{\alpha}\delta$, should be small (an error of a few percent may be involved when $\bar{\alpha}\delta = 10°$), and that M is $\gg 1$. It is only when M is less than about 10 that the results are expected to become appreciably wrong.[17] Molière estimates that there may be an error ~ 1 percent when $\Omega_b \simeq 20$.

An upper limit for the validity of relation (3) is determined by nuclear dimensions. The finite size of the nucleus imposes an upper limit $(\sim \lambda\!\!\!^{-}/b)$ on the permissible Rutherford scattering angle, where $\lambda\!\!\!^{-}$ is the particle's de Broglie wavelength divided by 2π, and b is the radius of the scattering nucleus. For $\lambda\!\!\!^{-}/b \ll \alpha_{ms}$, where α_{ms} is given by (5), the effective value of M becomes independent of scattering thickness, the single scattering tail is eliminated almost completely, and the resultant distribution is practically gaussian with an arithmetic mean α_b, which is given[17] in δ-units by the relation

$$\alpha_b = (19.5 - 3.1\log_{10}Z)^{\frac{1}{2}}. \tag{8}$$

Rossi and Greisen[23] have considered this condition, and thus their results are chiefly applicable to the scattering of very energetic particles by large thicknesses of material.

III. APPLICATION TO EMULSION TECHNIQUES

Because the photographic emulsion consists of a mixture of elements with atomic numbers Z_i, each with N_i atoms per unit volume the resultant mean deflection must be obtained by a summation process from the individual scattering contributions. This is further complicated because of the nature of the expression for the mean deflection, and its dependence on β and t.

For a pure substance, from Eq. (7),

$$\log M = \log(\text{constant} \times tNZ^2) - \log\beta^2 - \log(1 + \gamma^2/0.31)Z^{\frac{1}{2}}. \tag{9}$$

Molière's $\log\Omega_b$ can be expressed in a similar form, and by analogy with his method of summation for mixtures we get

$$\log M = \log(\text{constant} \times t\textstyle\sum_i(N_iZ_i^2)) - \log\beta^2 - \{\textstyle\sum_i N_iZ_i^2 \log Z_i^{\frac{1}{2}}(1 + \gamma_i^2/0.31)\}/\textstyle\sum_i(N_iZ_i^2). \tag{10}$$

In the δ-factor $(NZ^2)^{\frac{1}{2}}$ is replaced by $(\sum_i N_iZ_i^2)^{\frac{1}{2}}$. Thus $\bar{\alpha}$ may be calculated using Eq. (3).

Equation (10) may be written as

$$\log M = \log(\text{constant} \times t\textstyle\sum_i(N_iZ_i^2)) - \log\beta^2 - \log P. \tag{11}$$

[19] S. A. Goudsmit and J. L. Saunderson, Phys. Rev. **57**, 24 (1940).
[20] G. Molière, Z. Naturforsch. **3a**, 78 (1948).
[21] H. S. Snyder and W. T. Scott, Phys. Rev. **76**, 220 (1949).
[22] E. J. Williams, Revs. Modern Phys. **17**, 217 (1945).
[23] B. Rossi and K. Greisen, Revs. Modern Phys. **13**, 241 (1941).

It can be shown graphically that β^2P is closely approximated ($\sim$1 percent) by the relation

$$\beta^2P=11.8(\beta^2+0.31)^{24}$$

for Ilford G5 emulsions, using the data on the components of the emulsion as supplied by the maker. Substituting in Eq. (11) and evaluating the various factors, gives

$$\log M=\log(0.94t/(\beta^2+0.30))=\log M't. \quad (12)$$

Also

$$\delta=1.006t^{\frac{1}{2}}/p\beta \text{ degrees} \quad (13)$$

where the scattering thickness, t (henceforth referred to as cell length) is in microns of emulsion and $p\beta$ is in Mev, and the scattered particle has unit charge.

Substituting (12) and (13) in Eq. (3), we have for singly charged particles,

$$\bar{\alpha}=\frac{10.06}{p\beta}\left(\frac{t}{100}\right)^{\frac{1}{2}}\times\left\{1.45+0.80\left(\log_e\frac{0.94t}{\beta^2+0.30}\right)^{\frac{1}{2}}\right\}\text{degrees} \quad (14)$$

where $\bar{\alpha}$ is the mean angle between successive tangents.

In general $p\beta=\beta^2(E+\mu c^2)$, which reduces to $p\beta\simeq 2E$ for very slow particles and to $p\beta\simeq E$ for extremely relativistic particles, where E is kinetic energy, μc^2 is rest mass energy, and the same symbol β is used[22] for particle velocity and for the dimensionless ratio of particle velocity to the velocity of light c.

A. Theoretical Mean Deflections

The variation of mean deflections with cell length for relativistic, singly charged particles (i.e., $z=1$, $\beta\simeq 1$) in emulsions has been calculated using Eqs. (3), (4), and (12), and the results are shown in Fig. 1. It is expected that the mean deflection $\bar{\alpha}$ as given in Fig. 1 should be valid for cell lengths down to about 15 microns, where $M\simeq 11$. For very large cell lengths ($t\gtrsim 10^4$ microns, $M\gtrsim 10^4$) the correct mean deflection should be the limiting value α_b due to finite nuclear dimensions as given by Eq. (8), or by the corresponding treatment of Rossi and Greisen.[23] The value $\alpha_b=3.81$ units shown in Fig. 1 was derived from (8) using an effective $Z=41$.

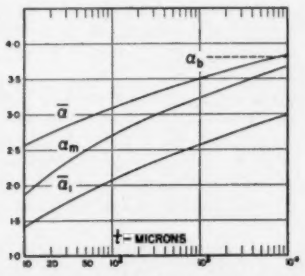

FIG. 1. Theoretical mean deflections, in δ-units, for singly charged relativistic particles traversing t microns of emulsion. $\bar{\alpha}$—arithmetic mean projected deflection; α_m—arithmetic of gaussian $G(\alpha)$; $\bar{\alpha}_1$—$(\log M)^{\frac{1}{2}}$; α_b—limiting deflection due to finite size of nucleus.

[24] It is interesting to note that $11.8(\beta^2+0.31)$ is approximately the same as using the factor $\beta^2(1+\gamma^2/0.31)Z^{\frac{1}{2}}$ in (9) with an effective $Z=41$. This probably arises from the fact that the final mean scattering angle is mainly determined by contributions from the silver and bromine nuclei in the emulsion.

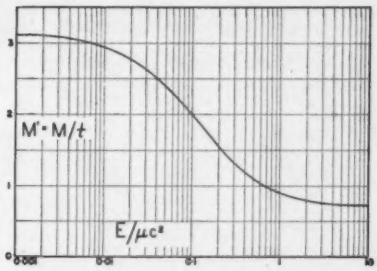

FIG. 2. Variation of M', a measure of the average number of collisions per micron of emulsion, with particle energy E in rest mass units μc^2, for singly charged particles.

The mean deflections for nonrelativistic particles can be obtained by using the results shown in Fig. 1 with the velocity variation of M' as given by Eq. (12), or with the energy variation shown in Fig. 2. Here M' measures the average number of collisions per micron of emulsion, and E is the kinetic energy of the scattered particle whose rest mass energy is μc^2. The data for Fig. 1 are based on the value $M'=0.723$ for $\beta=1$. For a cell length t for nonrelativistic particles, the appropriate mean deflections are those given in Fig. 1 at a cell length of $t\times M'/0.723$ micron.

B. Geometrical Features of Emulsion Techniques

For a continuous track of a particle undergoing multiple scattering in the emulsion, the general scattering theory applies directly if one measures the angles between successive tangents to the projected track at intervals of t microns. In the direct microscope method described by Fowler,[6] and in the projection microscope method of Lattimore,[1] the experimental observations are equivalent to measurements of the angles between successive chords described along the projected track. The relation between the arithmetic mean deflections for chords and tangents depends on the scattering distribution function, but we have used the simple $(2/3)^{\frac{1}{2}}$ relationship. More detailed considerations bearing on this point are given by Scott[25,26] Scott and Snyder,[27] and Snyder.[28]

[25] W. T. Scott, Phys. Rev. **75**, 1763 (1949).
[26] W. T. Scott, Phys. Rev. **76**, 212 (1949).
[27] W. T. Scott and H. S. Snyder, Phys. Rev. **78**, 223 (1950).
[28] H. S. Snyder, Phys. Rev. **83**, 1068 (1951).

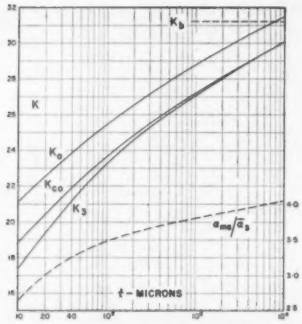

FIG. 3. Theoretical values of the "scattering constant" K for singly charged particles, and Ilford G5 emulsions as a function of cell length t. K_0—no cutoff; K_{co}—cutoff at four times mean; K_3—cutoff at α_{ms} (angle defining transition from multiple to single scattering); K_b—limiting K due to finite size of nucleus. The lower dashed curve shows the cut-off ratio $\alpha_{ms}/\bar{\alpha}_3$ as a function of cell length.

C. Cutoff for Large-Angle Deflections

The principal reason for a cutoff in the experimental scattering distribution is to minimize the effects of the nongaussian single scattering tail. The convenient procedure of cutting off all angles greater than four times the resultant mean has now become standard in emulsion measurements.[2] If we call this resultant $\bar{\alpha}_{co}$, then analogous to Eq. (4) for the gaussian mean deflection α_m, we find the approximate relation

$$\bar{\alpha}_{co}=(\bar{\alpha}-\pi/4\bar{\alpha})/(1-\pi/32\bar{\alpha}^2). \tag{15}$$

Williams[17] has suggested that experimental scattering data be cut off at the angle ϕ_2 as defined by (4), giving a resultant mean deflection $\bar{\alpha}_2$ which is readily calculable. For typical scattering observations on tracks in emulsions this procedure is difficult to apply without ambiguity, whilst a cutoff at the angle α_{ms}, as defined by (5) appears to be a more practical choice. This procedure is less convenient than cutting off at $4\bar{\alpha}_{co}$, but α_{ms} is a more meaningful angle in the general scattering theory, and the resultant distribution truncated at α_{ms} is always close to gaussian. If $\bar{\alpha}_3$ is the resultant mean deflection after all events with scattering angles greater than α_{ms} have been deleted, then

$$\bar{\alpha}_3=(\bar{\alpha}-\pi/\alpha_{ms})/(1-\pi/2\alpha_{ms}^2). \tag{16}$$

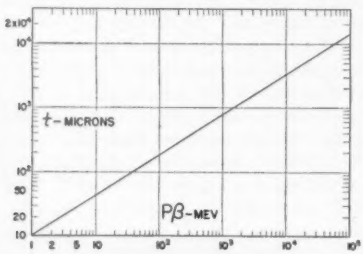

FIG. 4. Relationship between particle "energy" $p\beta$ and cell length t, which is calculated to give a mean deviation of 1.0 microns with Fowler's technique. ($\beta\simeq 1$.)

D. The "Scattering Constant" K

Results of the preceding discussion on multiple scattering theory, geometrical features of emulsion methods, and cut-off procedures are translated here into numerical values for the "scattering constant" K for use with the energy-scattering relationship (1).

(i) For chord angles without experimental cutoff, $K=K_0=10.06\times(2/3)^{\frac{1}{2}}\times\bar{\alpha}=8.21\bar{\alpha}$, where $\bar{\alpha}$ is given by (14). Substituting for $\bar{\alpha}$ we find

$$K_0=11.9\{1+0.837(\log_{10}0.94t/(\beta^2+0.30))^{\frac{1}{2}}\}\times\text{degrees}\times\text{Mev}/(100\text{ microns})^{\frac{1}{2}}. \tag{17}$$

The variation of K_0 with cell length for fast particles ($\beta\simeq 1$) is shown in Fig. 3. Values of K given in Fig. 3 may be somewhat in error due to the $(2/3)^{\frac{1}{2}}$ factor. Very recently Snyder[26] has given the results of more complicated estimates of K (without cutoff) from the distribution for chord angles in the calculations of Snyder and Scott. These give results about 5 percent greater than the corresponding values in Fig. 3.

(ii) For chord angle measurements and a cutoff at $4\bar{\alpha}_{co}$, $K=K_{co}=8.21\bar{\alpha}_{co}$, where $\bar{\alpha}_{co}$ is given by (15). Numerical values of K_{co}, which is equivalent to Fowler's[5] constant k_2, are shown in Fig. 3 for fast particles. For a nonrelativistic particle, the appropriate value of K_{co} is that given in Fig. 3 at cell length $t\times M'/0.723$ micron, where M' is obtained from Fig. 2.

(iii) For chord angle measurements and a cutoff at α_{ms}, which could be used as an alternative to $4\bar{\alpha}_{co}$, $K=K_3=8.21\bar{\alpha}_3$, where $\bar{\alpha}_3$ is given by (16). Numerical values for K_3 and the cutoff ratio $\alpha_{ms}/\bar{\alpha}_3$ are also shown in Fig. 3 for relativistic particles. As for K_{co}, the appropriate values of K_3 and $\alpha_{ms}/\bar{\alpha}_3$ for nonrelativistic particles are those given in Fig. 3 at cell lengths $t\times M'/0.723$ micron.

(iv) For very energetic particles such that cell lengths greater than 10^4 microns are required to obtain measurable deviations, then K_0, K_{co}, and K_3 all approach a limiting value K_b due to finite dimensions of the scattering nuclei. Using the value $\alpha_b=3.81$ units shown in Fig. 1, $K_b=8.21\times 3.81=31.2$ which is also shown in Fig. 3.

(v) For the "tangential" emulsion scattering method[2,3,6] a factor 0.96 ± 0.02 has been given[2] to allow for the departure from exact tangents due to an experimental smoothing procedure adopted in deflection measurements. Hence for this technique the corresponding values of K_0, K_{co}, K_3, and K_b are greater than those given in Fig. 3 by a factor $0.96/(2/3)^{\frac{1}{2}}=1.18\pm 0.02$.

(vi) The effect of inelastic electronic scattering, which has been neglected so far, may be included[17] to a close approximation by replacing Z by $(Z^2+Z)^{\frac{1}{2}}$. This

results in a correction of about 2 percent, which should be added to all values of K in Fig. 3.

(vii) The wide scope of the emulsion scattering technique for fast particle energy determinations is illustrated in Fig. 4. This curve shows the cell length t required in order to obtain a mean deviation $\bar{D}(t)=1.0$ microns using Fowler's technique, for particle energies ranging from 1 Mev to 100 Bev. In conjunction with Fig. 3, this curve is also useful for estimating the appropriate value of K for any particle energy. The numerical data in Fig. 4 were calculated from (1) with values of $K=K_{co}$ from Fig. 3, and the geometrical relation $\bar{\alpha}(t)=(\bar{D}(t)/t)\times 180/\pi$ degrees.[29] The criterion $\bar{D}(t)=1.0$ microns has been found generally to give consistent energy determinations in the absence of severe emulsion distortion, as discussed by Fowler.[5]

IV. COMPARISON BETWEEN THE RESULTS OF DIFFERENT THEORIES

The different scattering theories are based on the same fundamental principles although the theories of

TABLE I. Comparison of results of different theories for scattering of singly charged particles in metal foils.

Scatterer	t (cm)	β^2	$\bar{\alpha}$ (δ-units) Williams	Williams with Molière γ-factor	Molière
Aluminum	0.01	1	3.06	3.06	3.05
Iron	0.002	1	2.99	2.97	2.97
Lead	0.0007	1	2.89	2.70	2.71
	0.015	1	3.45	3.32	3.31
	2.0[a]	0.867	4.14	4.03	4.05
	4.0[a]	0.867	4.18	4.08	4.09

[a] The theoretical angles calculated here are actually greater than the limit imposed by the finite size of the nucleus, according to Eq. (8).

Molière and Snyder and Scott are more rigorous than that of Williams. However, as is indicated below, the results are essentially in agreement.

A graphical comparison of our present calculations (using Figs. 2 and 3) with those of Gottstein *et al.*,[16] based on the exact Molière theory (their Figs. 1 and 2) shows agreement between the values for K_0 within 1 percent over a wide range of β and t. There is similar agreement with the calculations of Goldschmidt-Clermont[6] for photographic emulsions. It may be noted here, however, that the present values for K_{co} differ somewhat from the corresponding values given by Gottstein *et al.* We also give, in Table I, the results of a few calculations for pure substances which show the extent of the agreement between the Williams and Molière theories.

The theory of Snyder and Scott,[21] which applies only to fast particles ($\beta\simeq 1$), cannot be compared so directly as the above two theories. It has been indicated by

[29] See Sec. VI.

TABLE II. Comparison of results of different theories for scattering of fast, singly charged particles in lead and photographic emulsions.

$\bar{\alpha}\times p\beta$ degrees $\times$ Mev ($\bar{\alpha}$ = projected angle between successive tangents)				
Scatterer	t (microns)	Snyder and Scott	Williams	Williams with Molière γ-factor
Emulsion	32	17.0	16.7	16.3
	385	66.3	66.9	66.0
	4330	248	248	246
Lead	107	86.7	86.7	85.4

other authors[16] that the agreement is satisfactory. However, as a check, we have calculated the mean deflection for a number of cases, and compared the results with those given by Williams' theory with and without the Molière γ-factor, for $\beta=1$. The results are given in Table II. The values of Snyder and Scott were obtained graphically making use of the tables issued by these authors, and using their suggested method of summation for mixtures. Cell lengths were chosen so that these tables could be used conveniently. The angles compared are those between successive tangents.

It will be seen that the results are in satisfactory agreement for photographic emulsions, especially for the longer cell lengths. Some values for lead are also included, and the discrepancy noted is mainly due to a combination of a fairly short cell length and the importance of the Molière γ-factor in this case.

V. COMPARISON OF THEORY WITH EXPERIMENTS ON THICK AND THIN FOILS

Experiments on the scattering of fast electrons by thin metallic foils have been made by Lyman *et al.*[30] and by Kulchitsky and Latyshev,[31] and the results in terms of $1/e$ widths for the distribution are shown in Table III together with corresponding theoretical angles. The results are in agreement with theory within

TABLE III. Comparison of experimental and theoretical $1/e$ widths for distribution due to scattering of electrons by thin foils.

Scatterer	t g/cm^2 $\times 10^{-3}$	cm	Energy	$\phi(1/e)$ degrees Williams with Molière γ-factor	Expl.
Lyman *et al*[a]					
Beryllium	257	0.14	15.7 Mev	3.50	3.06
Beryllium	491	0.27		4.73	4.25
Gold	18.7	0.001		2.71	2.58
Gold	37.3	0.002		4.10	3.76
Kulchitsky and Latyshev[b]					
Aluminum	26.6	0.01	2.25 Mev	9.65	9.15
Iron	15.4	0.002		9.55	9.35
Lead	7.9	0.0007		9.2	9.35

[a] See reference 30.
[b] See reference 31.

[30] Lyman, Hanson, Lanzl, and Scott, Phys. Rev. **81**, 309 (1951).
[31] L. A. Kulchitsky and D. G. Latyshev, Phys. Rev. **61**, 254 (1942).

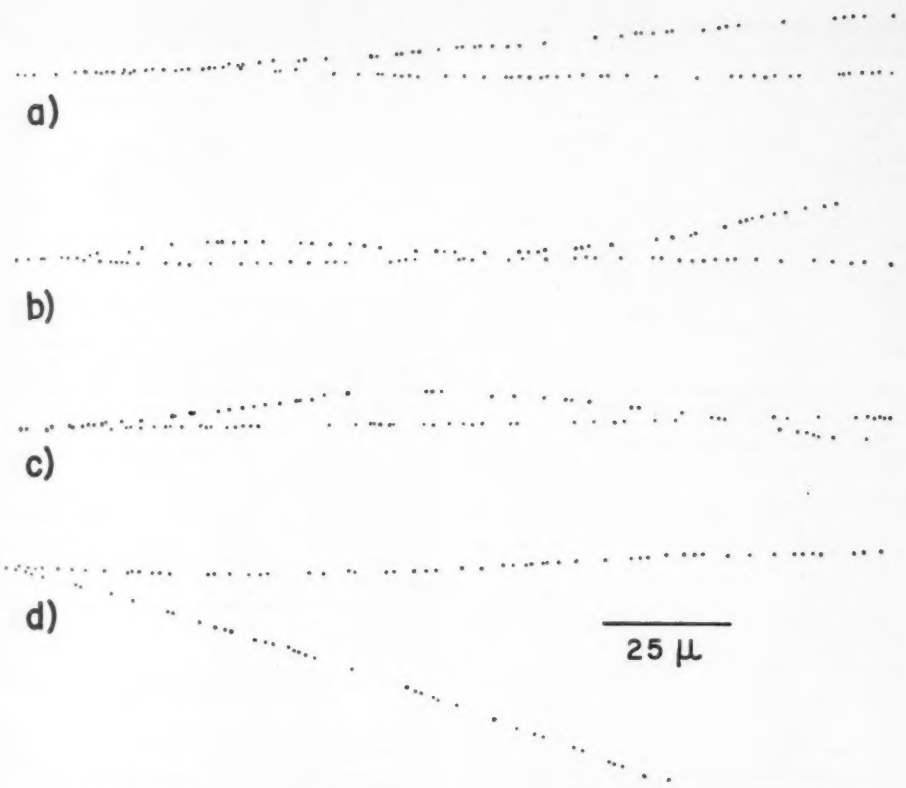

FIG. 5. Projection microscope tracings, showing four typical electron-positron pairs in Ilford G5 emulsion which has been exposed to Be^8 gamma-radiation.

5–10 percent, although in the case of Lyman *et al.* the measured widths are all smaller. The discrepancy between theory and experiment for lead reported by Kulchitsky and Latyshev is largely removed by the inclusion of the Molière γ-factor in the theory, but it must be noted that, for this particular case, $M(\simeq 12)$ and t were small. Earlier experiments[32–34] using a spectrum of electrons with energies in the 5–10 Mev region were reported to give values smaller than theory for lead foils.

Recently Crewe[35] has reported an experiment on the scattering of cosmic-ray μ-mesons (with energies $\sim$184 Mev) by one inch of lead in which the measured mean deflection $\bar{\theta}$ was 3.7 ± 0.4 degrees, to be compared with a theoretical $\theta_b = 5.7$ degrees. In this case the scattering angle is limited by the finite size of the nucleus. Sinha[36] has previously reported a low result for lead. On the other hand experiments made, using cosmic-ray μ-mesons in the energy region 0.5–1 Bev, by Code[37] and Wilson[38] give reasonable agreement with theory within a few percent. Code used a tungsten sheet (3.8 cm) and Wilson used copper (2.0 cm), gold (2.0 cm), and lead (0.3 cm, 1.0 cm), and the results were compared with theoretical ones derived from Williams' equation for the nuclear limiting angle [our Eq. (8)].

Generally, it would appear that the results are in reasonable agreement with theory except perhaps for lead, but further experimental work would seem necessary.

[32] W. A. Fowler and J. R. Oppenheimer, Phys. Rev. **54**, 22 (1938).
[33] Oleson, Chao, Halpern, and Crane, Phys. Rev. **56**, 482 (1939).
[34] C. W. Sheppard and W. A. Fowler, Phys. Rev. **57**, 273 (1939).
[35] A. V. Crewe, Proc. Phys. Soc. (London) **A64**, 660 (1951).
[36] M. S. Sinha, Phys. Rev. **68**, 153 (1945).
[37] F. L. Code, Phys. Rev. **59**, 229 (1941).
[38] J. G. Wilson, Proc. Roy. Soc. (London) **A174**, 73 (1940).

VI. EXPERIMENTAL TEST OF SCATTERING THEORY USING Be^8 GAMMA-RAYS

A. Method

Ilford G5 plates 400 microns in thickness were irradiated with about 10 milliroentgens of Be^8 gamma-radiation from an evaporated lithium target bombarded with a resolved proton beam at about 450-kev proton energy. The plates were aligned approximately parallel to the gamma-ray direction at about 15 cm from the lithium target. Using the normal temperature development method[39] with Elon developer, the plates recorded relativistic particle tracks with a mean grain density of 33 grains per 100 microns, and a mean grain diameter of 0.6 micron. Examples of four typical electron pairs are shown in the projection microscope tracings reproduced in Fig. 5.

Multiple scattering observations were carried out by the method described by Fowler,[8] using a standard Leitz Ortholux binocular microscope. A 90× oil immersion objective was used in conjunction with 6× eyepieces for searching, and 15× compensated eyepieces with calibrated scales for scattering measurements. When a plate was mounted on the mechanical stage of the microscope, the tracks of pair electrons were roughly parallel to the x-axis. It was found from preliminary observations that those pairs which could be followed for about 700 microns along the x-axis under these conditions gave fairly representative events.

In the pairs accepted for gamma-ray energy determinations, the y coordinates of each track were recorded at intervals of 20 scale divisions along the x-axis, where 1 scale division = 0.88 micron for both the x and y coordinate eyepiece scales. The second differences of the y coordinates, $D_n=(y_n-y_{n+1})-(y_{n+1}-y_{n+2})$, measure the deviation between successive chords along a projected track. The mean projected deflection between successive chords at intervals, or cell lengths, t is then $\bar{\alpha}(t)=(\bar{D}/t)\times 180/\pi$ degrees, where $\bar{D}$ is the arithmetic mean of the individual deviations D_n, taken without regard to sign.

The values of $p\beta$ for each track were determined from the energy scattering relation given by Eq. (1), i.e., $p\beta=(K/\bar{\alpha}(t))\times(t/100)^{\frac{1}{2}}$ Mev. Corresponding to experimental cutoffs at α_{ms} and $4\bar{\alpha}_{co}$ for the observed deflection on each track, theoretical values of the "scattering constant" K were taken from the curves for K_3 and K_{co} shown in Fig. 3 to obtain the particle energy for each of these two types of cutoff. After correcting for the effect of inelastic electronic scattering, spurious experimental errors in scattering measurements, and energy losses along the tracks, $p\beta_1+p\beta_2$ was determined for each pair. Since $p\beta=E+mc^2$ for these relativistic electrons, $p\beta_1+p\beta_2$ is also equal to the energy of the gamma-ray responsible for the pair.

[39] Dilworth, Occhialini, and Payne, Nature **162**, 102 (1948).

TABLE IV. Energy determinations on electron pair 15.

Track	Cell length t divs.	No cutoff $\bar{D}$ divs.	Cutoff $\bar{D}_{co}$ divs.	$4\bar{\alpha}_{co}$ $p\beta$ Mev	Cutoff $\bar{D}_3$ divs.	α_{ms} $p\beta$ Mev
1	20	0.46	0.42	7.0	0.42	6.6
	40	0.83	0.74	12.1	0.74	11.6
	60	1.47	1.47	11.6	1.47	11.3
	80	2.05	2.05	13.1	2.05	12.9
2	20	0.89	0.77	3.8	0.72	3.9
	40	1.97	1.78	5.0	1.64	5.3
	60	3.54	3.54	4.8	3.00	5.5
	80	5.50	5.50	4.9	5.50	4.8

B. Examples of Energy Determinations

To illustrate the method of analysis, data for two typical pairs are shown in Tables IV and V, which represent examples of pair production with asymmetric and approximately symmetric energy division.

For each track in the two pairs, the tables show "energy" values $p\beta$ (uncorrected for noise level or ionization losses) for the two types of cutoff at α_{ms} and $4\bar{\alpha}_{co}$ and for cell lengths varying from 20 to 80 divisions. For this range of cell lengths, K_{co} varies from 20.1 to 23.0 and K_3 from 19.0 to 22.5, as obtained from Fig. 3.

C. Noise Level and Energy Losses

At short cell lengths very large corrections are required to obtain the true energy of a particle because of spurious experimental scattering, or noise level,[10, 16] whereas with long cell lengths this correction is small, but the statistical accuracy is usually poor. Thus, because of the importance of noise level corrections, a somewhat complicated choice of cell lengths was adopted for the final energy determinations. The value accepted for the energy $p\beta$ for each track was the mean of two determinations: the first being derived from the minimum cell length t for which $\bar{D}\geqslant 1.0$ divisions, and the second determination from the next longer cell length, i.e., at $t+20$ divisions. A correction of 3 percent was added to each electron energy, based on an estimated mean noise level between 0.15 and 0.2 division

TABLE V. Energy determinations on electron pair 58.

Track	Cell length t divs.	No cutoff $\bar{D}$ divs.	Cutoff $\bar{D}_{co}$ divs.	$4\bar{\alpha}_{co}$ $p\beta$ Mev	Cutoff $\bar{D}_3$ divs.	α_{ms} $p\beta$ Mev
1	20	0.53	0.53	5.5	0.47	5.9
	40	1.08	0.99	9.0	0.92	9.4
	60	1.89	1.89	9.0	1.58	10.4
	80	2.82	2.82	9.6	2.62	10.1
2	20	0.44	0.44	6.7	0.38	7.3
	40	1.10	1.10	8.1	0.96	9.0
	60	1.90	1.90	9.0	1.90	8.7
	80	2.90	2.90	9.3	2.90	9.1

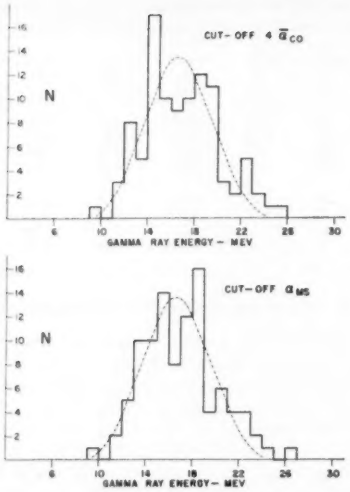

FIG. 6. Gamma-ray energies from 100 electron-positron pairs. The ordinates, N, show the number of events per 1-Mev energy interval. The dashed curve in both cases is the expected distribution for 10 percent statistical probable error in measurement.

and an average deviation $\bar{D}$ about 2.0 divisions using two cell lengths. A further correction of 0.2 Mev was added to each electron pair for energy losses along the track length ($\doteq$1.4 millimeters of emulsion). This may be rather low, although it should be noted that any large energy losses giving noticeable deflections are excluded from the observations.

Applying the procedure described above to the data listed in Table IV, the gamma-ray energy responsible for this electron pair was obtained as 17.6 Mev with an experimental cutoff at $4\bar{a}_{co}$, and 18.2 Mev with a cutoff at α_{ms}. Similarly, for the pair in Table V, the gamma-ray energy was obtained as 18.3 Mev and 19.4 Mev for the two types of cutoff.

D. Statistics

The statistical probable error in each mean deviation $\bar{D}$ is expected to be nearly $50/n^{\frac{1}{2}}$ percent,[2,6] where n is the number of independent deviations. Thus for the pair described in Table V there are 24 independent observations on each track, based on overlapping cells of 40 divisions and a track length of 800 divisions for each electron. This yields a statistical probable error very close to 10 percent of the resultant gamma-ray energy. By taking longer track lengths on the high energy component in cases of extremely asymmetric energy division, an attempt was made to achieve uniform statistics which would yield a 10 percent probable error in total energy for every electron pair.

VII. RESULTS AND CONCLUSIONS OF Be^8 GAMMA-RAY EXPERIMENT

A. Be^8 Gamma-Ray Energies

The results of gamma-ray energy determination for 100 electron-positron pairs are shown in Fig. 6 for the two types of cutoff. The expected distribution for 10 percent probable error (dashed curve) was based on the magnetic pair spectrometer results of Walker and McDaniel,[12] who gave the Be^8 gamma-ray energies at the 440 kev (p,γ)Li resonance as 14.8±0.3 Mev and 17.6±0.2 Mev, with a ratio of 0.5 for the intensity of the lower energy line to the higher energy line, and a natural width of about 2.1 Mev for the 14.8-Mev gamma-ray.

The arithmetic mean quantum energy for the 100 pairs was found, after adding the 2 percent correction for inelastic electronic collisions, to be 17.4±0.5 Mev for both types of cutoff. The probable error of 0.5 Mev is that estimated for statistical uncertainties in scattering data (about 1 percent for the mean of 100 events), and an allowance of 2 percent probable error for corrections due to noise level and energy losses. This experimental mean energy is in fairly good agreement with an expected mean Be^8 gamma-ray energy of 16.7±0.3 Mev, calculated from the results of Walker and McDaniel. We therefore conclude that the present experiment indicates the reliability (within about 5 percent) of the theoretical values for the "scattering constant" K for the cell length region 20 to 70 microns for fast particles, i.e., in the region $K_{co}=21.5$, $K_s=21$.

TABLE VI. Energy division in electron pairs.

$p\beta_1/(p\beta_1+p\beta_2)$	0–0.2	0.2–0.4	0.4–0.6	0.6–0.8	0.8–1.0
No. of events	7	26	28	29	10

B. Resolution of Scattering Technique

The general agreement between the expected distribution and the shapes of the experimental histograms in Fig. 6 indicates that the experimental resolution of energy determinations from our multiple scattering data is very near 10 percent. There is a slight indication of a double humped distribution at about 15 and 18 Mev in both experimental histograms, but these apparent groupings are not considered to be statistically significant. The experimental data shown in Fig. 6 are based on 64 electron pairs due to gamma-radiation emitted in the forward proton direction, and 36 pairs due to radiation emitted at nearly 90° to the direction of the bombarding proton beam. Since the recent magnetic pair spectrometer results of Stearns and McDaniel[40] have indicated that Be^8 gamma-rays are truly isotropic near the 440-kev proton resonance, it was decided not to pursue the possibility of gamma-ray

[40] M. B. Stearns and B. D. McDaniel, Phys. Rev. 82, 299 (1951).

anisotropy which was postulated in our preliminary report[13] on this experiment.

To show that the 100 pairs analyzed are fairly representative pair production events, energy division results are given in Table VI. Here $p\beta_1/(p\beta_1+p\beta_2)$ is the ratio of the energy for the upper track (see Fig. 1) to the total energy for the pair, and the $p\beta$ values are those obtained with a cutoff at α_{ms}. The distribution is seen to fall off for extremely asymmetric energy division, and is roughly constant in the intermediate region. These results are in reasonable agreement with the experimental and theoretical energy division results for 17-Mev gamma-rays given by Delsasso, Fowler, and Lauritsen.[41]

The approximate angular separation (as projected on the x-y plane of the microscope field of view) was also measured for each pair with a simple eyepiece goniometer, with results similar to those given by King[42] for 25-Mev synchrotron x-rays. The distribution of angular separation for the 100 pairs was nearly constant between 0 and 8 degrees, with a rapid decrease at larger angles, resulting in a mean angular separation of 5.0 ± 0.3 degrees. In about 15 cases, both tracks appeared to emerge on the same side with respect to the direction of the original gamma-ray beam, but a more accurate irradiation geometry and goniometer are necessary for reliable data on this effect, which is ascribed to the momentum taken up by the local nucleus in pair production.

C. Distribution of Scattering Deflections

Since the present experiment is based on electron tracks with a wide energy spread, and a different scattering distribution is expected for each electron energy and each cell length, only an approximate test of the distribution in scattering deflections is possible. However, by concentrating on those tracks for which deflections were measured at overlapping cell lengths of 40 scale divisions (35.2 microns), we are able to obtain reasonable statistics for a comparison with theoretical scattering distributions. This cell length for fast particles ($\beta\cong1$) corresponds to a value of $M\sim20-25$.

The approximate distribution function $P(\alpha)=G(\alpha)+S(\alpha)$, which was discussed in Sec. II is shown in Fig. 7 for the case $M=21$. The functions $P(\alpha)$, $G(\alpha)$, and $S(\alpha)$ are plotted here against the projected deflection α expressed in δ-units (bottom scale). An experimental distribution in scattering deflections was obtained from a total of 814 deflections using 24 tracks with electron energies between 8.0 and 9.0 as determined with a cutoff at α_{ms}. These results are also shown in Fig. 7, plotted as the number of deflections per 0.5 scale division interval *versus* the projected deflection, $|D|$ (scale at top). The theoretical curves are normalized to the same total number of deflections, and the abscissas also correspond if the experimental distribution is considered to be equivalent to that for monoenergetic electrons of energy 8.5 Mev.

A comparison of the theoretical and experimental distributions in Fig. 7 indicates that at very small angles the experimental values are too low, which is thought to be due in large part to spurious errors in measurement, or noise level. At larger deflections the two results are felt to be in reasonable agreement, except for an apparent experimental excess over $P(\alpha)$ in the single scattering region beyond α_{ms}. A qualitative examination of Williams' more exact distribution function,[18] as well as some theoretical curves shown by Goldschmidt-Clermont[6] which were based on the theories of Molière and of Snyder and Scott, all indicate a similar excess over the approximate function $P(\alpha)$ in the region of single and plural scattering.

A more direct quantitative test of scattering distributions in the single scattering region may be made by considering the frequency of deflections greater than the cutoffs α_{ms} and $4\bar{\alpha}_{co}$. Since the frequencies, or relative numbers of deflections, depend only on the value of M and not on particle energy, we have analyzed a total of 5000 deflections obtained from overlapping cell lengths of 35.2 microns on 150 tracks whose energies varied from 3 Mev to 15 Mev. In this way, the experimental frequency of deflections greater than α_{ms} was found to be 3.2 percent, and the frequency of deflections greater than $4\bar{\alpha}_{co}$ was 1.1 percent. From the approximate function $S(\alpha)=\pi/\alpha^3$, shown in Fig. 7, the corresponding theoretical frequencies for cutoffs at α_{ms} and $4\bar{\alpha}_{co}$ were calculated to be 2.5 and 1.5 percent for the case $M=21$. Similarly, using the more exact[18] single scattering contribution $S(\alpha)=(\pi/\alpha^3)(1+3\pi\alpha_n^2/\alpha^2)$, the expected frequencies were calculated to be 3.5 and 1.8

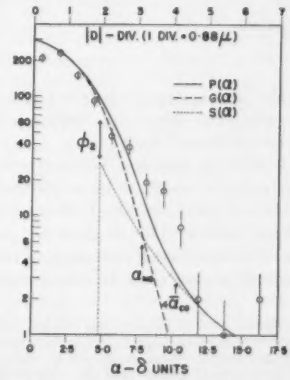

FIG. 7. Distribution of scattering deflections. The theoretical curves show Williams' approximate functions $G(\alpha)$, $S(\alpha)$, and $P(\alpha)=G(\alpha)+S(\alpha)$ for the case $M=21$, plotted against the projected deflection α (bottom scale). The experimental points, with their indicated standard deviations, are plotted against the absolute deflection, $|D|$ (top scale).

[41] Delsasso, Fowler, and Lauritsen, Phys. Rev. **51**, 391 (1937).
[42] D. T. King, Nature **165**, 526 (1950).

percent for the two types of cutoff. Within the uncertainties due to statistics and experimental errors, these results are also considered to indicate approximate agreement between theory and experiment, but experiments with known monoenergetic particles are desirable for more accurate tests of scattering distributions with emulsion techniques.

VIII. GENERAL CONCLUSIONS AND COMPARISON BETWEEN THEORY AND EXPERIMENTS

(1) There appears to be general agreement within about 1 percent for the mean scattering angle (without cutoff) given by the theories of Snyder and Scott,[43] Williams and Molière for the cases where these theories are applicable. The agreement between Williams and Molière is very close when the Molière γ-factor is introduced into Williams' theory.

TABLE VII. Comparison of theoretical and experimental results for K_{co} for the scattering of singly charged particles in Ilford G5 emulsions.

Experiment	β^2	Cell length microns	K_{co} (exp)	K_{co} (theor.)
Gottstein *et al.*[a]				
Positrons 105 Mev	1	200	26.2±0.6	25.3
Positrons 185 Mev	1	400	24.0±0.8	26.4
Protons 336 Mev	0.46	600	29.2±1.0	27.7
Protons and mesons 5–50 Mev	0.14	80	26.1±0.7	25.6
Protons 10–20 Mev	0.02	72	27.5±0.5	25.9
Corson[b]				
Electrons 40–280 Mev	1	not given	26 ±1	
Berger, Lord, and Schein[c]				
Protons 337 Mev	0.46	250	24.4±0.8	26.5
		500	24.5±0.8	27.4
		750	24.6±0.9	28.0
Voyvodic and Pickup[d]				
Electron pairs (Be^8 gamma-rays Mean energy 16.7 Mev)	1	45 (20–70)	21.2±0.7	22.1

[a] See reference 16.
[b] See reference 14.
[c] See reference 15.
[d] See reference 13.

(2) The theoretical results of Williams and Molière can be closely approximated to by a relatively simple equation [(14) or (15)] for Ilford G5 emulsions and singly charged particles, which gives the results to within about 1 percent over a wide range of cell lengths and for different values of β. It may be noted that this accuracy is also within the tolerance with which the emulsion content is given by the maker.

(3) Comparison of theory with the results of metallic foil experiments is not very decisive, and further work would seem necessary. There may be a fairly large discrepancy for the case of lead.

(4) In a Be^8 gamma-ray calibration experiment with G5 emulsions, the mean energy for the two types of experimental cutoff discussed in this paper was found to be 17.4±0.5 Mev in both cases, which is in fairly good agreement with an expected mean energy of 16.7±0.3 Mev. Theoretical "scattering constants" and cell lengths from 20 to 70 microns (average≃45 microns) were used to obtain this experimental result. Expressing the result in terms of the "scattering constant," K_{co} (45 microns)=22.1 from Fig. 3, whereas K_{co} (experimental), using the mean energy value 16.7 Mev, =(16.7/17.4)×22.1=21.2.

(5) Since the present work was completed, several other calibration experiments with singly charged particles of different energies and using G5 emulsions have been published. The results are collected together in Table VII. They are expressed in terms of the "scattering constant" using an experimental cutoff of four times the mean and, for comparison, the corresponding values of K_{co} from the present theory are included. These have all been increased by 2 percent to allow for the effect of inelastic electronic scattering, except for the Be^8 result, where the correction was made in deducing the mean gamma-ray energy.

The results shown in Table VII are in satisfactory agreement with theory within 5–10 percent. The results of the Be^8 gamma-experiment seem to be in fairly good agreement with theory for the smaller values of K, although it would be of interest to check this by measurements using monochromatic electrons with energies of 10–20 Mev. The measurements by Gottstein *et al.* and by Berger, Lord, and Schein on protons do not agree very well. In general it would appear that further experimental work is necessary in order to verify the theory in detail.

(6) Gottstein *et al.* gave measurements of K (without cutoff) for 105-Mev positrons, 185-Mev positrons, and 336-Mev protons, which may be compared with Snyder's recent calculations.[28] The experimental values are 26.7±0.6, 24.9±0.8, and 30.7±1.0 respectively to be compared with values, from Snyder's curve of 27.8, 28.7, and 30.2 respectively. These latter values should probably be increased by about 2 percent to correct for inelastic electronic scattering.

We are much indebted to Dr. B. G. Whitmore (University of Manitoba) for help in connection with Molière's theory and other calculations, and to B. Bigham (Queen's University) for numerical computations.

[43] The agreement here is between the angles essentially as measured between successive tangents. As we have noted, Snyder (reference 28) has recently given values for K (without cutoff), which are about 5 percent greater than the corresponding values in our Fig. 3, calculated using the $(2/3)^{\frac{1}{2}}$ relationship between chord and tangent angles.

Internal Conversion in Pr^{144}, In^{114}, Ba^{137}, and Cd^{110}*

W. C. KELLY
University of Pittsburgh, Pittsburgh, Pennsylvania†
(Received August 20, 1951)

Beta-ray spectrometer measurements have been made of the internal conversion ratio α_K/α_L for four nuclear transitions. Values obtained are: 5.3±0.1 for the 132-kev transition in Pr^{144}; 1.30±0.05, 192 kev, In^{114}; 4.57±0.05, 662 kev, Ba^{137}; and 14±2, 656 kev, Cd^{110}. Tentative assignments of multipolarity are given.

I. INTRODUCTION

FROM measurements of the conversion coefficient for the K shell or the ratio of the K conversion coefficient to the L conversion coefficient, one can, in principle, obtain the multipole order of nuclear transitions and hence the spin and parity changes needed to establish decay schemes. However, the only reliable values of conversion coefficients existent are the values of α_K calculated by Rose *et al.*[1] using exact relativistic wave functions for a wide range of energies, Z values, and multipole orders. Experimental determinations of α_K alone are difficult except when the decay scheme is known to be simple. A few methods have been proposed to obtain α_K for a gamma-ray emitted in a complex decay scheme by utilizing Compton scattering[2] or external conversion.[3] In addition to the experimental difficulty, one faces the possibility that the interpretation of values of α_K may be ambiguous if mixtures of electric 2^l-pole and magnetic 2^{l-1}-pole processes occur in nuclides of low Z.[4] Therefore, one would prefer to measure α_K/α_L and from the ratio to obtain an unambiguous assignment of multipolarity. For the interpretation, the experimentalist will have to await the exact calculation of the L conversion coefficient, which is reported[1] to be under way. Meanwhile, approximate calculations are available for tentative assignments.[5–7]

In this experimental study, beta-ray spectrometer measurements were made of the ratio of α_K/α_L for gamma-rays emitted by the nuclides praseodymium 144, indium 114, barium 137, and cadmium 110.

II. EXPERIMENTAL

Quade and Halliday[8] have described the construction and electron optical properties of the magnetic lens beta-ray spectrometer used in these studies. Additional precautions were taken in the present work to reduce scattering within the chamber and alignment errors. Antiscattering baffles were installed near the source and near the counter. The interior of the spectrometer was covered with a rough coating of ceresin wax. A simple experiment showed that this wax reduces electron scattering by a factor of at least two. It was found necessary to locate the central baffle quite accurately so that the annular aperture at the center of the spectrometer would be uniformly wide. Failure to do this led to a broadening of internal conversion lines.

For this work, a thin-window Geiger counter was developed in which the beta-particles entered at right angles to the axis of the counter. Such a counter has the advantages that both ends of the central wire are accessible for flashing the wire and that the sensitive volume of the counter extends to the window. The counter showed a long term stability, a flat plateau (1.6 percent per 100 volts), and a low background (30 counts/minute). The window had an areal density of 30 $\mu g/cm^2$ and transmitted electrons to energies as low as 5 kev.

Three of the four radioactive materials were available at reasonably high specific activities. Cesium 137, the parent of barium 137, was obtained from Oak Ridge as cesium chloride at an activity of 1.05 mC/ml and with total solids not exceeding 2.4 mg/ml. Cerium 144 was obtained there also as cerium nitrate (3.06 mC/ml and 1.8 mg/ml). Indium 114 was produced in the University of Pittsburgh cyclotron by a $Cd^{114}(d,n)$ reaction and cleanly separated at the radiochemistry laboratory of the Atomic Power Division, Westinghouse Electric Corporation, by H. A. Brightsen. Silver 110, produced at Oak Ridge by neutron bombardment, had a low specific activity (3.97 mC/ml and 150 mg/ml). The thick source resulting from the low specific activity caused difficulty in resolving the cadmium 110 conversion lines. The sources were prepared by depositing a minimal amount of the concentrated radioactive solution upon an aluminum backing of thickness 0.00025 inch. Average areal densities of the sources were obtained by weighing. The areal density of the cerium, indium, and cesium sources was about 0.1 mg/cm^2. That of the silver source was 10 mg/cm^2.

Data were taken automatically.[9] Enough counts were recorded that the statistical error associated with each

* Part of a dissertation submitted in partial fulfillment of the requirements for the degree of Doctor of Philosophy at the University of Pittsburgh.

† Assisted by the joint program of the AEC and ONR and by the Research Corporation.

[1] Rose, Goertzel, Spinrad, Harr, and Strong, Phys. Rev. **83**, 79 (1951).

[2] K. Siegbahn, Proc. Roy. Soc. (London) **188**, 541 (1946).

[3] C. D. Ellis and G. Aston, Proc. Roy. Soc. (London) **129**, 180 (1930).

[4] P. Axel and R. F. Goodrich, Navy Report "Internal conversion data," privately circulated.

[5] M. H. Hebb and E. Nelson, Phys. Rev. **58**, 486 (1940).

[6] N. Tralli and I. S. Lowen, Phys. Rev. **76**, 1541 (1949).

[7] S. D. Drell, Phys. Rev. **75**, 132 (1949).

[8] E. A. Quade and D. Halliday, Rev. Sci. Instr. **19**, 234 (1948).

[9] W. C. Kelly and K. J. Metzgar, Rev. Sci. Instr. **22**, 665 (1951).

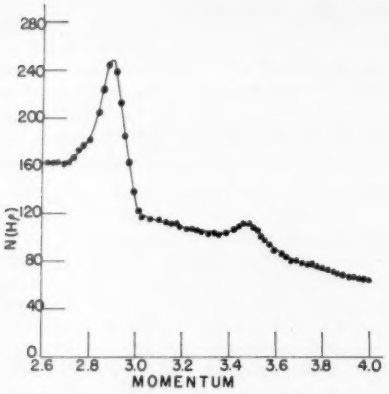

FIG. 1. The electron spectrum of $Ce^{144}-Pr^{144}$ in the region of the conversion peaks of the 132-kev gamma-ray of Pr^{144}. $N(H\rho)$, the number of electrons per unit time per unit momentum interval, is plotted against the electron momentum in arbitrary units.

experimental point did not exceed two percent except where the curves approached the background level.

III. RESULTS

A. Praseodymium 144

A portion of the electron spectrum of cerium 144-praseodymium 144 is shown in Fig. 1. To obtain the conversion peaks of the gamma-ray at 132 kev, it was necessary to subtract the continuous spectrum from the total curve. This was done by making a Fermi plot for cerium and with its help reconstructing the continuous spectrum at the conversion peaks. By subtraction of the continuous spectrum, the conversion peaks of Fig. 2 were obtained. The spread of the K peak is 4 percent. The low energy portion of each line is approximately exponential, a measure of the degradation of the energy of the electrons as they leave the source. In addition to the experimental evidence of Fig. 2, there seems to be theoretical justification[10] for regarding this portion of the curve as exponential. An exponential curve has been fitted to the K peak to extend it to the momentum axis through a region of the total curve where other conversion lines are present. An exponential curve fitted to the L peak extended it to the momentum axis. The correction to the high energy side of the K peak was negligible. The ratio of the areas under the peaks gave $\alpha_K/\alpha_L=5.3\pm0.1$.

The converted gamma-ray must be ascribed to praseodymium 144. Best agreement for the energy of of the gamma-ray is obtained by adding to the energies of the K and L conversion electrons the binding energies for praseodymium. Critical absorption experiments were carried out using aqueous solutions of barium and cesium as absorbers. The absorption data showed conclusively the presence of x-rays which could be either praseodymium $K\alpha$ or neodymium $K\alpha$. Energy considerations make it likely that it is the former. This assignment agrees with that by Emmerich *et al.*[11]

The experiment value of 5.3 ± 0.1 for α_K/α_L indicates an electric quadripole radiation if one uses the non-relativistic calculations of Hebb and Nelson.[5] Their results give the following conversion ratios: E 2^1-pole, 8.4; E_A2^2-pole, 4.5; E 2^3-pole, 1.2. Emmerich *et al.*[11] report an approximate value of 7 for α_K/α_L.

[10] G. E. Owen, private communication.

B. Indium 114

Conversion peaks for the 192-kev gamma-ray of metastable indium 114 are shown in Fig. 3. The spread is 3.3 percent. The contribution of the 2.05-Mev beta-group to the electron intensity at this energy is negligible.

Separation of the two peaks for purposes of planimetry was effected by a method involving successive approximations to the separate curves. First, a gaussian curve[12] was fitted to the high energy side of the K peak. By subtracting this curve from the total curve between the two peaks, one could decide how to continue the L peak in an exponential. The exponential portion of the L peak was then subtracted from the total curve to give a second approximation to the high energy portion of the K peak.

α_K/α_L was found to be 1.30 ± 0.05 and indicates either an electric 2^4-pole or an electric 2^5-pole transition.

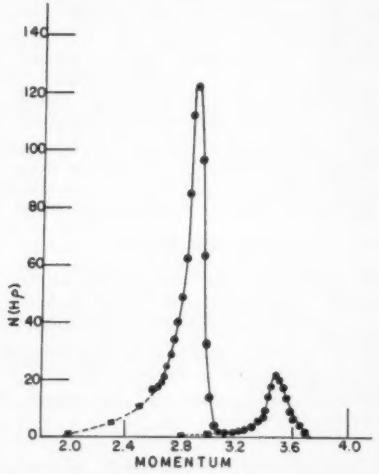

FIG. 2. The conversion electrons of the 132-kev gamma-ray of Pr^{144}. Circles show the experimental points, squares show points on the calculated exponential curves.

[11] Emmerich, John, and Kurbatov, Phys. Rev. **82**, 968 (1951).

[12] The line shape of a magnetic lens spectrometer can be approximated quite well by a skewed gaussian curve. See Van Atta, Warshaw, Chen, and Taimuty, Rev. Sci. Instr. **21**, 985 (1950).

Hebb and Nelson give the following values: E 2^4-pole, 1.7; E 2^5-pole, 0.9. Lawson and Cork[13] report a value of 1.0 ± 0.1 for α_K/α_L. Boehm and Preiswerk[14] give 1.1 ± 0.1, and Steffen[15] reports 1.10 ± 0.05.

C. Barium 137

Figure 4 shows the K and $L-M$ conversion peaks of the 662-kev gamma-ray of metastable barium 137. The spread of the K line is 1.4 percent. A value of 4.57 ± 0.05 is found for α_K/α_{LM} in good agreement with the result $\alpha_K/\alpha_{LM}=4.54$ obtained by Langer.[16] Mitchell and Peacock[17] report the value 4.8 for α_K/α_L, and Osoba[18] finds $\alpha_K/\alpha_L=5.0$. Tentatively, one may assign a multipolarity of electric 2^5 to the transition. It must be emphasized, however, that the nonrelativistic theory may be considerably in error at this energy.

D. Cadium 110

Cadmium 110 is the daughter nucleus by negatron emission of silver 110. The K and $L-M$ conversion peaks of the 656-kev gamma-ray of cadmium 110 have been measured with a line spread of 3.7 percent. The peaks were separated by the procedure referred to above. However, a correction must be applied to the $L-M$ peak to correct for the presence of K conversion electrons due to a gamma-ray of energy 676 kev whose K peak is superimposed (within 2 kev) upon the $L-M$ peak of the 656-kev gamma-ray. The 676-kev line was discovered by Siegbahn[19] in studying the photoelectron spectrum of these radiations in a lead converter. Three lines in the spectrum (676 kev, 705 kev, 759 kev) have about the same photoelectric intensities. Siegbahn concludes that the gamma-intensities are probably about the same upon the assumption that the lines are of the same multipole order. On this basis, the conversion coefficient should be approximately the same, and the K peak of the 706-kev line should approximate that of the 676-kev line. The K peak of the 706-kev line can be readily measured. After applying this plausible, although certainly not rigorous, correction, α_K/α_{LM} was found to be 14 ± 2.

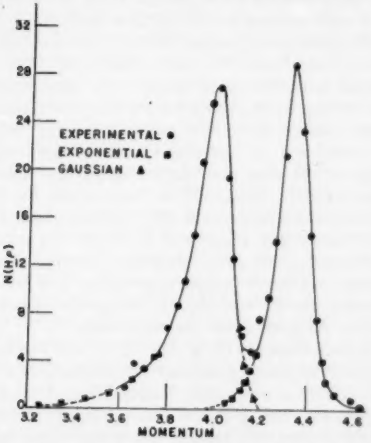

FIG. 3. The conversion electrons of the 192-kev gamma-ray of In^{114}.

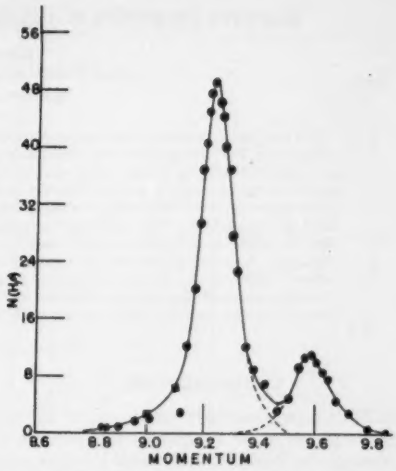

FIG. 4. The conversion electrons of the 662-kev gamma-ray of Ba^{137}. Circles show the experimental points, squares show points on the calculated curves.

This result indicates electric dipole radiation according to the calculations of Hebb and Nelson. However, the difficulties introduced by the source thickness, the approximate nature of the correction for the interfering line, and the nonrelativistic theory used reduce the certainty of the assignment.

By two independent means, Siegbahn[19] has found α_K for this line to be 2.5×10^{-3}. The precise theory shows that this is consistent with either electric or magnetic dipole radiation.

The author would like to acknowledge the support and encouragement given him by Drs. D. Halliday, A. J. Allen, and G. E. Owen. Mr. Kenneth Metzgar assisted with the instrumentation. Mr. Samuel Broder prepared tables of the Fermi function.

[13] J. L. Lawson and J. M. Cork, Phys. Rev. **57**, 982 (1940).
[14] F. Boehm and P. Preiswerk, Helv. Phys. Acta **22**, 331 (1949).
[15] R. M. Steffen, Phys. Rev. **83**, 166 (1951).
[16] L. M. Langer, private communication.
[17] A. C. G. Mitchell and C. L. Peacock, Phys. Rev. **75**, 197 (1949).
[18] J. S. Osoba, Phys. Rev. **76**, 345 (1949).
[19] K. Siegbahn, Phys. Rev. **77**, 233 (1950).

Magnetic Properties of a Hollow Superconducting Lead Sphere *

JULIUS BABISKIN
Naval Research Laboratory, Washington, D. C.
(Received August 20, 1951)

The magnetic hysteresis of a hollow superconducting lead sphere at 4.2°K has been studied by measuring the magnetic field distributions along the equatorial plane with bismuth probes. After cooling in the absence of a magnetic field, the hollow sphere was found to be a perfect magnetic shield in the superconducting state. The magnetic field penetrated into the interior of the sphere when the magnetic field at the surface of the sphere exceeded the threshhold value. Frozen-in fields were observed upon demagnetizing the sphere from the normal state. Upon reversing the applied field, the frozen-in field could be made to vanish, so that the sphere again became a perfect magnetic shield. The magnitude of the applied field necessary to extinguish the frozen-in field was found to be the same independent of the path of approach. The internal frozen-in fields did not change over specified ranges of the applied field, so that the existence of other equilibrium superconducting states are indicated for the hollow sphere. In the intermediate and frozen-in states, 10 to 30 minutes were required for the magnetic field to reach an equilibrium value.

I. INTRODUCTION

PREVIOUS experiments,[1-4] which studied the magnetic properties of superconducting spheres, did not measure the magnetic fields inside a hollow superconducting sphere. The present paper gives the results of an experimental study of the magnetic properties of a hollow lead sphere in the superconducting, intermediate and frozen-in states. This experimental study was performed at the boiling point (~4.2°K) of liquid helium under normal atmospheric pressure by varying the applied field through the magnetic hysteresis cycle. The magneto-resistance of calibrated bismuth probes was used to measure the equatorial magnetic field distributions inside and outside the hollow sphere. Since the magneto-resistance of bismuth exhibits greater sensitivity at higher magnetic fields, it is advantageous to use a superconductor having relatively high critical magnetic fields (H_c). Therefore, lead ($H_c \cong 540$ gauss at 4.2°K) was chosen as the superconductor.

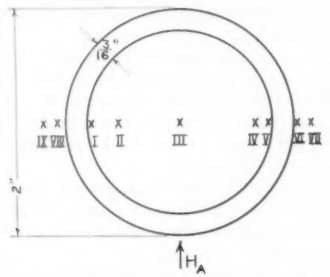

FIG. 1. Cross-sectional view showing positions of the bismuth probes on the equatorial plane of the hollow lead sphere.

II. EXPERIMENTAL METHODS

The bismuth probes were mounted in the fixed positions shown in Fig. 1 and were calibrated in a uniform magnetic field at 4.2°K. Although the magneto-resistance calibration curves for any single bismuth probe were not observed to be reproducible upon cycling from room temperature to 4.2°K. Their shapes were reproducible to form a family of curves. Thus a calibration could be reconstructed to 1 percent from the measurement of a single point on the curve. The probe mounts were then placed on the equatorial plane of the hollow sphere with respect to the applied field (H_A). The magnetic field distributions for the hollow sphere in applied fields below H_c were determined from the graphical extrapolation of normal state measurements using the family of calibration curves. The measured magnetic fields (H_M) as determined from the calibration curves are the absolute values of the average magnetic field over the dimensions of the bismuth probes (0.011 in. diam, 0.16 in. long). When the magnetic field was homogeneous over the dimensions of the probe, the error in H_M was of the order of 1 percent, except for $H_M < 20$ gauss where the effects of thermal electromotive forces become appreciable. For inhomogeneous fields, the error in H_M was greater depending upon the structure of the magnetic field.

The hollow sphere (2 in. o.d., $\frac{3}{16}$ in. wall thickness) was made by welding together two hemispherical lead shells (99.996 percent pure, National Lead Company). The current and potential leads from the internal bismuth probes were brought out of the hollow sphere through a 0.05-in. hole at the pole of the sphere. The effects of the hole have been shown to be minimized there.[3]

The applied magnetic field (H_A) was furnished by a liquid nitrogen-cooled solenoid (16 in. long, 4 in. i.d.), which surrounded the liquid helium flask. H_A was uniform to within 0.2 percent over the volume of the sphere. The over-all error in the measurement of H_A was less than 0.5 percent. Since the solenoid obstructed

* This work is part of a thesis under the direction of Professor M. H. Johnson and submitted in partial fulfillment of the requirements for the M.S. degree at the University of Maryland.

[1] W. J. de Haas and A. Guinau, Physica **3**, 182 and 534 (1936).
[2] K. Mendelssohn and J. Babbitt, Proc. Roy. Soc. (London) **151**, 316 (1935).
[3] A. Shalnikov, J. Phys. U.S.S.R. **6**, 53 (1942).
[4] de Haas, Engelkes, and Guinau, Physica **4**, 494 (1937).

direct observation, a float[5] was used to indicate the liquid helium level.

III. EXPERIMENTAL RESULTS AND DISCUSSION

A. Complete Hysteresis Cycles

The magnetization curves for the interior of the hollow sphere are shown in Fig. 2. In the superconducting state along OA, the hollow sphere was a perfect magnetic shield. Complete reversibility was maintained along OA. The first detectable penetration of the magnetic field into the hollow section of the sphere occurred at A. In the intermediate state along AB, the maxima of the internal magnetic field distributions were at the center of the sphere. The sphere went completely into the normal state at B.

Figure 3 shows a magnetization curve for the exterior of the hollow sphere. The observed slope of OA was 1.45 as compared to the theoretical value of 1.5. This difference can be accounted for on the basis of experimental limitations. H_M became equal to H_c at A and remained equal to H_c along AB.

The magnetization curves in Figs. 2 and 3 were observed to be time-dependent[4,6] both in the intermediate state and along BD, which represents the frozen-in state. All plotted points are equilibrium values of H_M at constant H_A. Along AB, from 30 to 40 minutes were required to reach equilibrium for each increment of H_A. Along BD, the time dependence varied from 30 minutes near B to 10 minutes at $H_A=0$. No time dependence was observed along BD from $H_A=0$ to D. For every time dependent increase or decrease of H_M inside the sphere, there was a simultaneous time-dependent decrease or increase respectively of H_M outside the sphere.

The equilibrium values of H_M outside the sphere along AB in Fig. 3 were equal to H_c. When H_A was given an increment from an equilibrium value along AB, H_M would slightly exceed H_c at first and would then decrease with time until H_M again equaled H_c. Simultaneously, there was a time-dependent increase of H_M inside the sphere, in which the total change was a much larger percentage of the equilibrium value of H_M. This may be interpreted as the resistance of the sphere to the penetration of H_A into the interior, when it is in the intermediate state.

Upon demagnetizing the sphere from the normal state, the initial magnetization OAB was not reversible, as would be the case for an ideal solid sphere. The hollow sphere exhibits magnetic hysteresis in going into the frozen-in state. Frozen-in fields are inherently linked to multiply-connected geometries by London theory.[7] Although the hollow sphere is topologically a singly-connected body, frozen-in fields were observed for the hollow sphere. This suggests the enclosure of non-superconducting regions within the superconducting material, so that the hollow sphere in the frozen-in state may be considered to be a multiply-connected body with respect to the superconducting material.

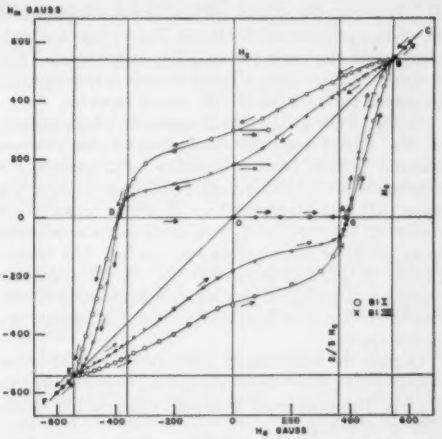

FIG. 2. Magnetization curves for the interior of the hollow sphere. Bi I at the inside edge; Bi III at the center. The magnetization curves for the other internal bismuth probes of Fig. 1 fall within the envelope of the above curves.

The minima of the internal magnetic field distributions in the frozen-in state were at the center of the hollow sphere. In Fig. 2, a relatively large frozen-in field having the same direction of the original H_A was observed at $H_A=0$. Upon reversing H_A, the internal frozen-in field was reduced and finally disappeared at

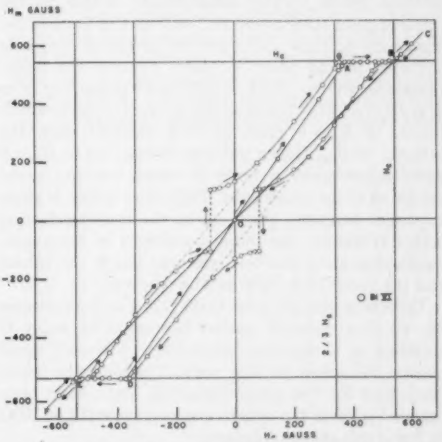

FIG. 3. A magnetization curve for the exterior of the hollow sphere. Bi VI at the outside edge. The magnetization curves for the other external bismuth probes of Fig. 1 were similar to the above curves.

[5] J. Babiskin, Rev. Sci. Instr. **21**, 941 (1950).
[6] W. Tuyn, Leiden Communications No. **198** (1929).
[7] F. London, *Superfluids* (John Wiley & Sons, Inc., New York, 1950), Vol 1, p. 47.

D. The curves for all five internal probes converged at D, where a uniform distribution of $H_M=0$ was observed. Continuing the cycle from D, the intermediate state commences again along DE and the complete symmetric hysteresis cycle $CBDEFEGBC$ can be repeated.

In Fig. 3 along BD, a high degree of inhomogeneity of H_M existed over the dimensions of the external bismuth probes. Since the probes only measure the absolute value of the magnetic field, the reversal of H_M along BD was determined by observing a resistance minimum followed by a continuous increase of resistance until the normal state was reached. The discontinuity in BD has been drawn in at the resistance minimum. The dashed line, which intersects the discontinuity in BD, is an approximation of the average H_M in this region.

Outside the sphere along BD, a frozen-in field in the opposite direction to the original H_A was observed at $H_A=0$. The symmetric hysteresis cycle in Fig. 3 can also be repeated.

B. Restoration of Superconductivity

Upon increasing H_A from $H_A=0$ gauss in Fig. 2, the initial horizontal sections of the branch curves emanating from BD show that the internal frozen-in field was unchanged up to $H_A\cong120$ gauss. This indicates that superconducting currents are induced on the exterior surface of the hollow sphere in the frozen-in state. For $H_A>120$ gauss, the internal frozen-in field was changed and the curves merged into their respective curves in the intermediate state.

Observations were made on branch curves emanating from points along BD other than those at $H_A=0$ in Fig. 2. All these curves exhibited initial horizontal sections which became progressively longer as the starting point approached D. The length of these initial horizontal sections indicates the extent of magnetic shielding in the frozen-in state. Finally, the initial horizontal section of the branch curve emanating from D is DOA, so that the observed internal uniform distribution of $H_M=0$ gauss at D is shielded upon the removal of H_A. Thus a uniform distribution of $H_M=0$ gauss exists again at point O, which was the initial condition of the experiment. The hollow sphere is again a perfect magnetic shield as in the superconducting state. Therefore, the initial conditions of the superconducting state has been restored inside the sphere and the cycle $OABCBDO$ can be repeated.

Upon removing H_A from point D in Fig. 3, the curves for all four external probes converged at point O resulting in a uniform distribution of $H_M=0$ again outside the sphere at that point. Therefore the initial conditions for the superconducting state have been restored outside the sphere and the cycle $OABCBDO$ in Fig. 3 can also be repeated.

The point D occurred at $H_A\cong390$ gauss in Fig. 2 and at $H_A\cong374$ gauss in Fig. 3. Therefore, the restoration of the superconducting state at point O was not simultaneous for the interior and the exterior of the sphere. Some preliminary experiments were performed with a hollow sphere in which the hemispherical shells were poorly welded. In this case, the initial conditions of the superconducting state were restored simultaneously inside and outside the sphere. Upon rewelding the poorly welded hollow sphere, the magnetization curves were in good agreement with those shown in Figs. 2 and 3.

In Fig. 2, a number of minor hysteresis cycles were observed by generating branch curves from the intermediate state along AB by decreasing H_A. These branch curves also exhibited initial horizontal sections, which became progressively shorter as their starting points approached the midpoint of AB. It was found that all the observed branch curves emanating from AB for all the internal bismuth probes converged at D, so that all curves in the upper half of Fig. 2 cross the $H_M=0$ axis at that point. Therefore, all frozen-in fields vanish at D regardless of the path of approach. By symmetry, all curves in the lower half of Fig. 2 cross the $H_M=0$ gauss axis at G. Thus, B, D, E, and G are four focal points into which all the branch curves converged.

Upon approaching the focal points D and G from the frozen-in state, one can branch off either into the initial superconducting state or the intermediate state. It is noted that the initial superconducting state DOA is a bounding horizontal section between the upper and lower halves of Fig. 2 for the initial horizontal sections of the families of branch curves which emanate from the intermediate and frozen-in state. Therefore, the existence of equilibrium superconducting states other than DOA are indicated for the hollow sphere, and DOA can be considered as the limiting case for these states.

C. Magnetic Shielding of Internal Applied Fields

An experiment was performed to determine the effects of a magnetic field applied by a small field coil in the hollow section of the sphere. The magnetic field distribution of the small field coil was first determined in the absence of the hollow sphere. The small field coil was then placed at the center of the hollow sphere and measurements were made on the magnetic field along the equatorial plane.

No measurable magnetic fields due to the small field coil were detected just outside the hollow sphere in the superconducting state, although a maximum magnetic field of about 30 gauss was detected in the same position in the absence of the hollow sphere. For a given current in the small field coil, the magnitude of the internal magnetic field distributions was greater in the presence than in the absence of the hollow sphere. Thus, to the accuracy of the measurements, the exterior of the sphere is completely shielded from magnetic fields applied in the interior of the sphere.

The author wishes to express his appreciation to Dr. R. L. Dolecek and Dr. J. de Launay for having suggested this problem, and to M. C. Steele, Dr. R. T. Webber, and M. F. M. Osborne for profitable suggestions and discussions.

The Range of 18-Mev Protons in Aluminum*

E. L. HUBBARD† AND K. R. MACKENZIE
Physics Department, University of California, Los Angeles, California
(Received June 4, 1951)

The circulating beam of protons in the cyclotron was multiply scattered upward by a strip of Th suspended vertically inside the dee. The energy of the scattered beam was defined by the Th strip and two slits in the magnetic field of the cyclotron. From a plot of the magnetic field along the path of the scattered protons, the mean energy was determined to be 18.00±0.02 Mev. By determining the thickness of Al that stopped half the incident beam, the mean range was found to be 447.0±0.5 mg/cm².

I. INTRODUCTION

THE range-energy curve for protons in Al has been determined experimentally by Parkinson, Herb, Bellamy, and Hudson[1] in the region below 2 Mev, by Bloembergen and van Heerden[2] in the region from 35 to 120 Mev, and by Mather and Segrè at 345 Mev.[3] The theoretical curve has been calculated by Livingston and Bethe[4] up to 13 Mev, and has been extended by Smith[5] up to 10 Bev. The ranges in material other than Al have been calculated by Aron, Hoffman, and Williams.[6] All calculated ranges are mean ranges.

The purpose of this investigation was to obtain an experimental point on the range-energy curve in the region of 18 Mev, the energy of the proton available from the UCLA 41-in. FM cyclotron. Since it is believed that the error in the range values calculated by Smith is about 0.1 percent in this region if the constants used are correct, this accuracy in the experimental measurements was desirable.

II. METHOD

To obtain a monoenergetic beam of protons, the circulating beam of the cyclotron was scattered by a narrow strip of Th suspended vertically inside the dee near the edge where the beam leaves it. The energy of the beam that was scattered upward was defined by the Th strip and two slits in the cyclotron magnetic field at 93 and 170 deg from the Th scatterer. Figure 1 is a plan view of the cyclotron tank showing the position of the Th strip and the slits. The second defining slit S_2 was mounted on the probe that contained the range measuring apparatus. The slits and the "end of the range probe" were located above the median plane of the cyclotron so that they did not interfere with the circulating beam. Approximate focusing of the particles scattered at different horizontal angles was obtained at the 170-deg slit.

Absolute measurements of the magnetic field at points along the path of the scattered protons were made with a nuclear radiofrequency magnetic resonance absorption probe. To determine the energy, an initial direction and energy of the protons leaving the Th strip were assumed, and the trajectory of these particles in the magnetic field was plotted to see if they went through the slits. By plotting trajectories for many energies and initial directions it was possible to determine the energy band that could get through the slits.

Inside the range measuring probe the beam passed through a thin Al foil and struck an Al plate. The thicknesses of the Al foil and plate were adjusted so that part of it penetrated the plate. The protons that penetrated the plate were collected by a second Al plate. The currents collected by either of the Al plates could be measured by an electrometer tube. The thickness of the Al foil could be changed, and the electrometer could be switched from one collecting plate to the other without turning off the cyclotron. The collector that was not being used was grounded. The current collected by each plate was determined for 10 foil thicknesses. A plot of these data gives the foil thickness for which the currents collected by the two plates were equal. This thickness plus the thickness of the first Al plate is the mean range.

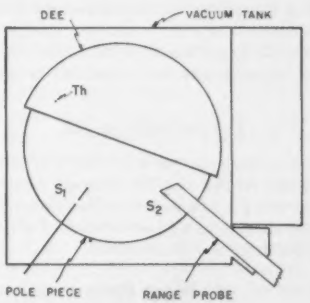

FIG. 1. Plan view of the cyclotron tank showing the location of the Th scatterer and the defining slits S_1 and S_2.

* This research was supported in part by the joint program of the ONR and AEC.
† Now at the Radiation Laboratory, University of California, Berkeley, California.
[1] Parkinson, Herb, Bellamy, and Hudson, Phys. Rev. **52**, 75 (1937).
[2] N. Bloembergen and P. J. van Heerden, Phys. Rev. **83**, 561 (1951).
[3] K. B. Mather and E. Segrè, University of California Radiation Laboratory Report No. 1089 (1951).
[4] M. S. Livingston and H. A. Bethe, Revs. Modern Phys. **9**, 276 (1937).
[5] J. H. Smith, Phys. Rev. **71**, 32 (1947).
[6] Aron, Hoffman, and Williams, Report AECU-663 University of California Radiation Laboratory-121 (1949).

III. APPARATUS AND PROCEDURES

1. Multiple Scattering Deflector

The Th strip that scattered the circulating beam was mounted vertically inside the dee about 15 deg from the edge where the beam leaves it. The strip was 14 mils wide and 2 mils thick. A lead weight was attached to the lower end of the Th strip to make it hang vertically.

The Th strip was placed at a radius of 17.18 in. Because of the radial oscillations of the circulating beam and the loss of energy by multiple scattering in the Th, the deflected beam had an average radius of curvature of 15.8 in. The two defining slits therefore were at a considerably smaller radius than the Th strip.

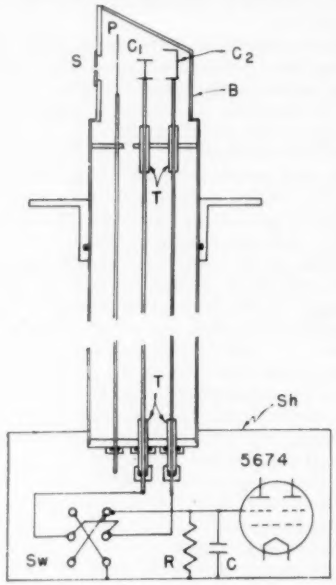

FIG. 2. Range probe and electrometer input circuit.

No appreciable beam was detected behind the last slit when the Th strip was moved out of the circulating beam.

2. First Defining Slit

The first defining slit was a $\frac{1}{8}$-in. vertical slot cut in a sheet of $\frac{1}{8}$-inch Al that was 6 in. long and 2 in. high. The lower edge was $\frac{1}{4}$ in. above the median plane. The outer edge of the slit was located at a radius of 15.74 in. and at 92.94 deg from the Th scatterer.

3. Range Probe

The Al plates (that collected the deflected beam) and the thin Al foils were supported by brass rods that were mounted in a brass tube 3 in. in diameter and 5 ft long. The tube was inserted into the cyclotron tank through a vacuum lock. The collectors and foils were inside a brass box that projected in from the end of the tube above the path of the circulating beam.

A schematic plan view of the range probe is shown in Fig. 2. The probe was mounted in the face plate F of the vacuum lock with a "O" ring seal so that its position could be changed without disturbing the cyclotron vacuum. C_1 and C_2 are the Al collecting plates with the shields that prevent the escape of secondary electrons. The brass rods supporting the collectors were insulated from their supports by Teflon tubes T. The thin foils were mounted on a paddle P. To minimize currents due to ionization of residual gas, the tube was evacuated to the cyclotron pressure through a baffle on the inside end. The rods and insulators were sealed at the outside end of the tube with "O" rings. The brass box B shielded the collectors from the rf, soft x-rays, and stray ions that are present in the tank.

The deflected beam entered the shield box B through a $\frac{1}{4}$-in. hole in the front side. The hole was covered with a 14-mil slit S made from two pieces of brass $\frac{1}{16}$-in. thick. The radius of the outside edge of the slit was 14.52 in. It was at 170.3 deg from the Th scatterer.

The 15,422-gauss magnetic field between the collectors caused some of the slowest protons that penetrated the first collector to miss the second collector. The radius of curvature of protons whose range is 0.1 percent of the range of 18-Mev protons is 2 in. The collectors were spaced $\frac{3}{8}$ in. apart so that the error due to this cause was negligible. The maximum radius of curvature of the secondary electrons knocked out of the collectors by the beam was 0.02 in. The collectors had 0.1-in. Cu shields around the edges to prevent their escape.

The first collecting plate was cut from an extruded rod of 99.995 percent pure Al. It was lapped until a dial indicator showed that the thickness of 66.2 mils was uniform to within 0.05 mil. The edges were made as square as possible and lapped until parallel and flat enough that they reflected light without distortion. The area of both sides was measured with a travelling microscope that could be read to 0.04 mil. The average width was 0.22568 in. It was measured by two observers who agreed to 0.14 mil. The average length measured perpendicular to the width was 0.50494 in. The weight was determined to be 0.3330 ± 0.0001 g with an analytical balance. These data give a thickness of 452.94 ± 0.34 mg/cm^2.

The paddle P contained Al foils of ten different thicknesses between 1 and 7 mils and could be quickly moved in front of the first collector. Using x-rays, Sachs[7] determined that the thickness of the foils was uniform to 1.5 percent. The foils were cut from triangles whose area and weight had been measured. The accuracy of

[7] Donald C. Sachs and J. Reginald Richardson, Phys. Rev. **83**, 834 (1951).

the thickness measurements was limited by the nonuniformity in the thickness of the foils. The estimated limit of error for the foils near the intersection of the straggling curves was 0.1 mg/cm².

4. Position Measurements and Magnetic Field Survey

The position of the slits was determined with an apparatus fitted with radial and azimuthal scales. The estimated rms error in the radius of curvature of the proton trajectories due to play in this apparatus is 0.05 percent. The magnetic field was measured to one part in 5000 along the path by a nuclear magnetic resonance probe using protons in a rubber sample.

The nuclear resonance probe could not be used when the cyclotron tank was evacuated. The magnet current was held constant by a regulator and slow drifts detected by a potentiometer and corrected manually. In this way the field could be held constant to two gauss during any one run. The magnitude of the field was monitored during a run by a pair of flip coils and a fluxmeter. This was necessary, as it was found that although the magnetic field was constant if the current was constant, the value of the field was different for the same magnet current each time the magnet was turned on. One of the flip coils was placed in the fringing field field of the cyclotron outside the vacuum tank. The other was in the field of a permanent Alnico magnet. The two coils were mounted on the same shaft so that they were flipped simultaneously through a definite angle. They were connected in series so that the emf's opposed each other and the fluxmeter read the difference in the number of maxwell turns. The coils and fluxmeter were calibrated with the nuclear absorption probe and could be read to within three gauss.

At four positions near the path, magnetic field readings were taken at several different vertical positions. The median plane field map was corrected to give the field strength at the average height of the deflected beam. The largest vertical correction required was -12 gauss. The magnetic field was three gauss higher when the tank was evacuated than when it was at atmospheric pressure. This correction was added to the field values obtained when the tank was down to air.

5. Determination of Proton Trajectories

The trajectories of the protons leaving the Th strip with a given momentum and initial direction were determined by a graphical method described by Parkins and Crittenden.[8] Points on the trajectory were computed at 10 deg intervals. To make sure that the 10 deg intervals were small enough, one of the trajectories was plotted using 5 deg intervals with no observable difference. The field values used were at the midpoints of the intervals. To further check the method, one trajectory was plotted in both directions and again there was no observable change in the trajectory. The estimated accuracy of the graphical method was 0.01 percent. Therefore the accuracy of the momentum determination was limited by the accuracy of the field values and the positions of the slits and the Th strip.

The lower limit of the momentum of the protons passing through the slits was determined by the trajectory that went through the inside of the Th strip and the second defining at 170 deg slit and the outside of the middle defining slit at 93 deg. The upper limit was determined by the trajectory that went through the outside of the Th strip and the second defining slit and the inside of the middle defining slit.

The trajectory plotting determined the energy of the beam due to the horizontal component of its velocity. The energy due to the vertical component of velocity was 0.011 Mev or 0.06 percent of that due to the horizontal component. The total energy was obtained by adding 0.011 Mev to the value determined graphically.

IV. RESULTS

1. Energy

The maximum and minimum values of the energy W of the protons passing through the slits was calculated from the maximum and minimum values of the momentum using the relativistic equation

$$W=-mc^2+[(mc^2)^2+(BRe)^2]^{\frac{1}{2}}, \qquad (1)$$

where m = rest mass of proton, c = velocity of light, B = magnetic field strength, R = radius of curvature, e = charge of proton, BR = momentum $\times c/e$. Equation (1) is expressed in gaussian units. The values of m, c, and e given by Birge[9] were used. The resulting maximum and minimum values for the energy were 18.037 Mev and 17.965 Mev. The difference between these values is 0.072 Mev or 0.4 percent. The mean value is 18.001 Mev.

Sachs[7] has determined the distribution in energy of the protons that pass through similar slits with an ionization chamber at 210 deg from the second defining slit. He obtained curves that were nearly symmetrical. The symmetry of these curves is consistent with the assumption that the mean energy of the protons was half-way between the extremes calculated from the slit geometry. The width of Sachs' curves at half-maximum was 48 percent of the total width so that 0.2 percent seems like a more reasonable value for the effective energy spread than 0.4 percent.

The total estimated error in the field measurements due to the centering of the pip, frequency measurements, field monitoring, and interpolation for the plotting of the trajectories is 5 gauss or 0.03 percent. The estimate of error in the radius measurement is 0.05 percent. The rms error in $(BR)^2$ or the energy is 0.13 percent or 0.023 Mev.

[8] W. E. Parkins and E. C. Crittenden, J. Appl. Phys. **17**, 447 (1946).

[9] R. T. Birge, Revs. Modern Phys. **13**, 233 (1941).

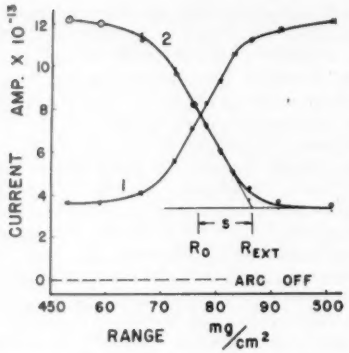

FIG. 3. Straggling curves. Curves 1 and 2 show the currents collected by the first and second Al plates, respectively. The intersection of the two curves determines the mean range R_0.

2. Range

The straggling curves obtained are shown in Fig. 3. The ordinates for curves 1 and 2 are the currents collected by the first and second Al plates, respectively. The abscissa is the thickness of the thin Al foil plus the thickness of the first Al plate. Experimental points on the curve for the second collector are given for two runs. Due to fluctuations in the beam intensity the 2 sets of points do not coincide exactly. The mean range determined by the intersection of the two curves is 476.9 mg/cm².

The current did not go to zero for thicknesses where the shape of the straggling curve indicates that no beam was being collected. Currents of about this magnitude were detected with the first defining slit covered with a $\frac{1}{16}$-inch brass sheet. Since these currents were independent of the Al foil thickness, it was assumed that they were not caused by the scattered beam hitting or entering the shield box around the collectors. Possible sources of this background are ionization of the residual gas in the tube and secondary emission from the collectors caused by general radiation from the circulating beam.

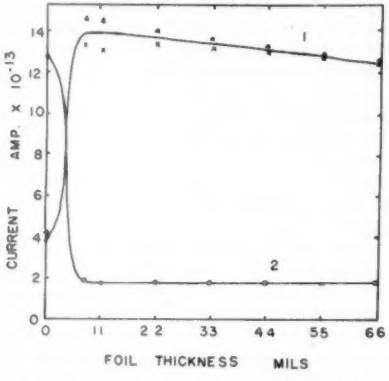

FIG. 4. Straggling curves showing the effect of the low energy component in the beam.

The background on the first collector was 1.5×10^{-13} amp higher than on the second. This difference was subtracted from the current readings on the first collector before plotting Fig. 3, but it is shown in Fig. 4. The extra current on the first collector was attributed to a low energy component in the beam. To show that the subtraction process was justified, a run was made, (Fig. 4) with the thin Al absorbers in front of the first collector replaced by thick absorbers. The first two thicknesses, 452.9 and 500.9 mg/cm², are the smallest and largest thicknesses in Fig. 3. The ratio of beam to background for this run was better than the runs shown in Fig. 3. It is seen in Fig. 4 that the current on the first collector fell off as thicker Al foils were put in front of it while the background on the second collector remained constant. This fall off indicates that there was a low energy component in the beam that should be subtracted from the current on the first collector. The magnitude of the fall off was about the same as the apparent difference in backgrounds on the two collectors. The low energy component in the beam was probably caused by scattering from the slit edges.

The biggest source of error in the range determination is the uncertainty in the amount subtracted from the currents of the first collector. The estimated limit of error due to the subtraction is 0.4 mg/cm² or 0.09 percent. When this error is combined with that of the thickness measurements, a total error of ±0.54 mg/cm² or 0.11 percent in the range measurement is obtained.

The mean square fluctuation of the range, $(R-R_0)_{Av}^2$, was determined from the difference s between the extrapolated range R_{ext} and the mean range R_0 by the equation

$$(R-R_0)_{Av}^2=(2/\pi)s^2. \tag{2}$$

The value obtained was 60.0 (mg/cm²)². The approximate expression

$$(R-R_0)/R \text{ rms}=0.24W^{-0.1}E_0^{-\frac{1}{2}}, \tag{3}$$

where E_0 = rest energy of the proton, and W = ratio of kinetic energy to rest energy, was derived by Wilson[10] for protons in air. When the value given by Eq. (3) is increased by 5 percent to give the range fluctuation in Al, the result is 33.7 (mg/cm²)². If it is assumed that $R\propto E^{1.8}$, an energy spread of 0.2 percent gives a range fluctuation of 3.0 (mg/cm²)². A fluctuation of 23.3 (mg/cm²)² is left unaccounted for. A nonuniformity in the density of the first collector of 1.0 percent would account for this discrepancy. However, runs made with the first collector moved $\frac{1}{32}$ in. so that the beam hit a different part of it gave results identical with those obtained with the collector in its original position.

[10] R. R. Wilson, Phys. Rev. **71**, 385 (1947).

Some of the protons that penetrated the first collector captured an electron in it and emerged as neutral hydrogen atoms. These protons were detected as a positive current on the first collector although they were actually stopped in the second collector. Therefore the measured range was smaller than the actual range. To account for the neutralization effect, 0.1 mg/cm² or 0.02 percent was added to the measured range. This correction was calculated by H. N. Royden from the data of Hall.[11] The corrected mean range is 477.0 mg/cm².

The correction for multiple scattering has not been calculated exactly. If the individual angular deflections are assumed to be small, the measured range must be increased by about 0.2 percent.[2] The calculation is not valid for large deflections that occur near the end of the range.

3. Comparison with Theory

The theoretical curve calculated by Smith[5] and the experimental point with its limits of error are shown in Fig. 5. The experimental point gives a range of 477.0 ±0.5 mg/cm² for a mean energy of 18.00±0.02 Mev. The theoretical curve gives 467.5 mg/cm² for the range of 18.00 Mev protons, differing from the experimental range by two percent. With corrections for multiple scattering the difference is about 2.2 percent.

In his range calculations Smith[5] used the value of 150 ev determined for the average ionization potential of Al by Wilson.[12] Sachs' experiments[7] on the absolute stopping power of Al give 156 ev for the average ionization potential.

Bloembergen and van Heerden[2] find a value of I of 164 volts at 35 Mev with some evidence that it is decreasing as the energy is raised. Mather and Segrè[3] find a value of I of 150±5 ev which agrees with Wilson. A value of 167 ev ($I=12.82$) would fit the present data for 18-Mev protons. This value can be obtained from

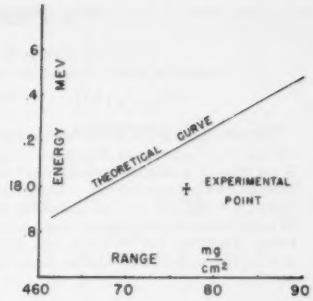

FIG. 5. Theoretical range-energy curve and experimental point.

Wilson's range relation[10]

$$R=\frac{10^{24}E_0W^{1.8}}{NZz^2\ln(4.14\times10^4/I)},$$

and for $I=11.5Z$ this agrees with Smith's calculations. For a given energy the variation of R with I is

$$\delta R/R=(\delta I/I)\ln(4\times10^4/I),$$

and for $\delta R/R=0.02$ (2 percent discrepancy) $\delta I=150\times5.7\times0.02=17$ ev. With corrections for multiple scattering the value of I would be about 170 volts, which is in fair agreement with Bloembergen and van Heerden but differs quite considerably from the values obtained by Sachs,[7] and Mather and Segrè.[3]

ACKNOWLEDGMENTS

The authors wish to thank Dr. J. Reginald Richardson for his many helpful suggestions and continued interest in the project. They are also indebted to the personnel of the Physics Department shop and to the members of the cyclotron crew, especially Steve Plunkett, George Jones, and Donald G. Sachs, for their help in constructing the apparatus and in performing the experiment.

[11] T. Hall, Phys. Rev. **79**, 504 (1950).
[12] R. R. Wilson, Phys. Rev. **60**, 749 (1941).

The Beta-Spectra of P^{32} and P^{33}

ERLING N. JENSEN, R. T. NICHOLS, J. CLEMENT, AND A. POHM
Institute for Atomic Research and Department of Physics, Iowa State College, Ames, Iowa*

(Received August 17, 1951)

The beta-spectrum of P^{32} has been examined with a thin-lens spectrometer. The maximum energy of the 14.3-day beta-activity, as determined from several Kurie plots, was found to be 1.704±0.008 Mev. The Kurie plots gave excellent straight lines from the maximum beta-energy to about 0.26 Mev. In phosphorus samples prepared from neutron irradiated sulfur an additional beta-activity was observed having a maximum energy of 0.26±0.02 Mev and a half-life of 24.8±0.5 days. This low energy beta-group was also observed in phosphorus samples prepared from sulfur and lithium chloride irradiated with x-rays having a maximum energy of 68 Mev. The low energy beta-group was not observed in phosphorus samples prepared from sulfur irradiated with deuterons or phosphorus irradiated with neutrons. The low energy beta-group is ascribed to P^{33}.

I. INTRODUCTION

THE beta-radiations from P^{32} have been examined with various types of spectrometers by a number of investigators.[1] Since the more recent of these investigations have shown that the Kurie plot of the P^{32} spectrum is a good straight line, it was felt that this would be an excellent beta-spectrum with which to check the performance of a thin-lens spectrometer.[2] The initial work on the beta-spectrum of P^{32} was done in December, 1948. Since then the spectrometer has been modified to incorporate ring focusing.[3] In determining the beta-spectrum of P^{32} a low energy beta-component was observed in the Oak Ridge carrier-free samples which has a half-life of 24.8±0.5 days and a maximum beta-energy of 0.26±0.02 Mev. This half-life is appreciably greater than the 14.3-day half-life of the P^{32} beta-component. Preliminary values of these results have been reported in the *Progress Reports in Physics* from the Ames Laboratory at Iowa State College.[4]

During the progress of this investigation Agnew[5] and Warshaw, Chen, and Appleton[6] have reported on the beta-spectrum of P^{32} and observe a distinct excess of electrons in the momentum spectrum below about 300 kev. Agnew[5] states that "the P^{32} was followed for five half-lives with no change in the Fermi plot." Warshaw *et al.*[6] state that "the spectrum has been followed for several half-lives with no change in shape." The data presented in this paper are in disagreement with these results since the half-life of 24.8±0.5 days for the low energy beta-group is appreciably different from the 14.3-day half-life of P^{32}. Our data indicate that there is an observable difference in shape of the beta-spectrum at low energies over a period of one half-life of P^{32}.

The low energy beta-group present in the Oak Ridge carrier-free P^{32} is believed to be due to P^{33}. This assignment is based primarily on the facts that this low energy beta-group is not present in phosphorus irradiated with neutrons or sulfur irradiated with deuterons, but is present in sulfur and lithium chloride irradiated with x-rays, from the Iowa State College synchrotron, having a maximum energy of 68 Mev.

Recently Yaffe and Brown[7] have reported that they have prepared P^{33} by the reaction $P^{32}(n,\gamma)P^{33}$. They found a half-life of 22±5 sec for this activity. Their results are based on the assumption that their target material was pure P^{32}. The data presented in this paper indicate that P^{32} prepared by neutron irradiation of sulfur also contains initially about 2.5 atoms of P^{33} per 100 atoms of P^{32}. Hence, in irradiating P^{32} with neutrons it is possible to form both P^{33} and P^{34}. We have found a half-life of 24.8±0.5 days for P^{33}. Bleuler and Zünti[8] have reported a half-life of 12.4 sec for P^{34}. It seems possible that the activity reported by Yaffe and Brown[7] is that of P^{34} and not P^{33}.

All of the phosphorus samples examined with the thin-lens spectrometer were mounted on thin Formvar-polystyrene films having a surface density of about 40 $\mu g/cm^2$. The G-M counter window was a Formvar film of surface density about 0.3 mg/cm^2. No corrections have been made for the absorption due to the G-M counter window. The resolution of the spectrometer (full width at half-maximum) was about 2.5 percent.

---

* Contribution No. 163 from the Institute for Atomic Research and Department of Physics, Iowa State College, Ames, Iowa. Work was performed in the Ames Laboratory of the AEC.

[1] L. M. Langer and H. C. Price, Jr., Phys. Rev. **76**, 641 (1949); Peacock, Jones, Overman, Plutonium Project Report Mon N-432, 56 (1947); K. Siegbahn, Phys. Rev. **70**, 127 (1946); Nature **153**, 221 (1944); C. M. Witcher, Phys. Rev. **60**, 32 (1941); J. L. Lawson, Phys. Rev. **56**, 131 (1939); E. M. Lyman, Phys. Rev. **51**, 1 (1937).

[2] Jensen, Laslett, and Pratt, Phys. Rev. **75**, 458 (1949).

[3] Pratt, Boley, and Nichols, Rev. Sci. Instr. **22**, 92 (1951); Keller, Koenigsberg, and Paskin, Rev. Sci. Instr. **21**, 713 (1950).

[4] Ames Laboratory of the AEC, *Progress Reports in Physics*, ISC-46, June 16, 1949; ISC-73, March 23, 1950; ISC-104, September 25, 1950; ISC-135, March 15, 1951. The results of a part of this work was reported at the Washington, D. C., meeting of the Am. Phys. Soc., April, 1951; Phys. Rev. **83**, 215 (1951). At the same meeting Sheline, Holtzman, and Fan reported on a P^{33} activity which was formed by gamma-reactions on sulfur and chlorine; Phys. Rev. **83**, 215 (1951).

[5] H. M. Agnew, Phys. Rev. **77**, 655 (1950).

[6] Warshaw, Chen, and Appleton, Phys. Rev. **80**, 288 (1950).

[7] L. Yaffe and F. Brown, Phys. Rev. **82**, 332 (1951).

[8] E. Bleuler and W. Zünti, Helv. Phys. Acta **19**, 137 (1946).

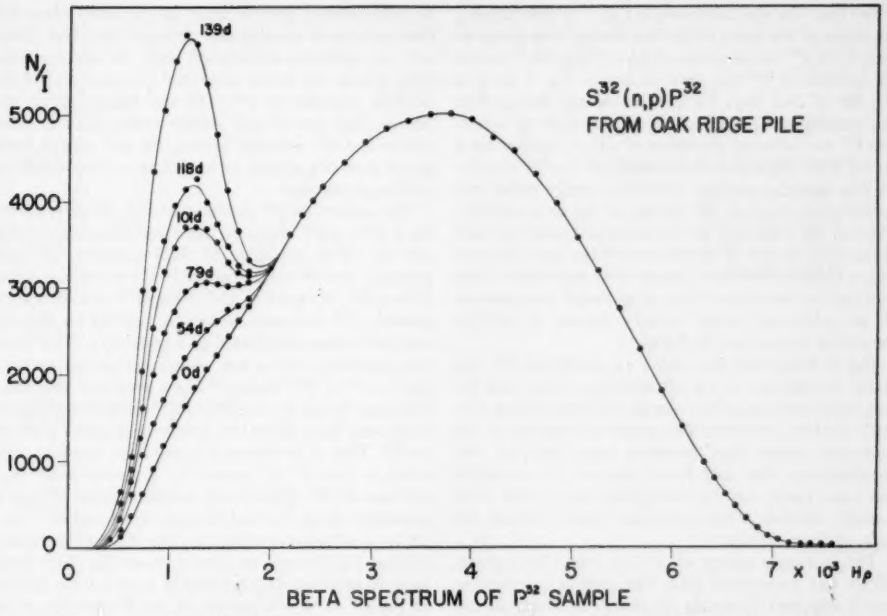

FIG. 1. Beta-spectra of a sample of carrier-free P^{32} obtained at intervals over a period of 139 days. All curves have been normalized at the maximum counting rates of the main beta-group of P^{32}. The ordinate values are for the first spectrum, which is labeled 0 d. N is the number of counts per min and I is the current in the spectrometer coil.

II. BETA-SPECTRUM OF P^{33}

The spectrum of the first sample[9] of carrier-free P^{33}, which was prepared at Oak Ridge about September 15, 1948, was determined as of December 23, 1948. In addition to the main beta-component of P^{32} a weak low energy beta-group was observed having a maximum energy of about 0.26 Mev. The shape of the beta-spectrum was approximately that shown by the curve labeled 101 d in Fig. 1. Several Kurie plots were made of beta-spectra obtained with various sources and all of them gave excellent straight lines from the maximum energy down to about 0.26 Mev. The Kurie plot shown by Agnew[5] is concave toward the energy axis. Our data does not agree with this. The average value of the maximum beta-energy of P^{32}, as determined from several Kurie plots, was found to be 1.704 ± 0.008 Mev and is in good agreement with those determined by other investigators.[1,5,6]

III. THE LOW ENERGY BETA-GROUP

A. Half-Life and Maximum Beta-Energy

The first sample of P^{32} was followed with the spectrometer for 36 days, during which time three additional beta-spectra were obtained. In each succeeding spectrum the low energy beta-group became more prominent in comparison to the P^{32} beta-component.

The second and third samples of carrier-free P^{32} were received directly from Oak Ridge and their initial spectra determined as of July 29, 1949 and April 7, 1950 respectively. The second sample was followed with the spectrometer for 57 days, during which time four beta-spectra were determined. The third sample was followed for 139 days, during which time seven beta-spectra were determined. Six of these spectra are shown in Fig. 1 and have been normalized at the maximum counting rates of the P^{32} beta-spectrum. The ordinates of the graph are applicable to the curve labeled 0 d. The first spectrum and the one determined 54 days later (labeled 0 d and 54 d respectively in Fig. 1) were obtained with one spectrometer source, while the other curves were obtained from a second and somewhat thicker spectrometer source, both of which were prepared from the third sample of carrier-free P^{32}. Samples one and two gave beta-spectra similar to those shown in Fig. 1. In the first beta-spectrum determined on samples two and three the low energy beta-group could not be observed with certainty and could readily be attributed to the effect of a thick source.

The half-life of the low energy beta-group was deter-

[9] We are indebted to Dr. C. W. Sherwin of the University of Illinois for this sample.

mined from the spectra shown in Fig. 1 by determining the ratios of the areas of the low energy beta-group to that of the P^{32} as a function of time. Using 14.3 days as the half-life of P^{32} the data shown in Fig. 1 gives a half-life of 24.2 days for the low energy beta-group. The activity of a portion of the third sample of carrier-free P^{32} was followed by means of a G-M counter for a period of 25 days after it had decayed for 10 months. At this time the activity of the low energy group was estimated to be about 90 percent of the total activity. The half-life was found to be 25.2 days. Another portion of the same sample of carrier-free P^{32} has been followed with a G-M counter for a period of 82 days after it had decayed for 404 days. These data reveal the presence of an additional weak activity having a half-life somewhat longer than 25 days.

The 24.8-day activity, which we ascribe to P^{33}, was about 1.4 percent of the P^{32} activity at the time the first beta-spectrum of the sample was determined. The ratio of these activities was somewhat smaller at the time the sample was removed from the pile, but unfortunately this time is not known. No correction has been made for the absorption due to the G-M counter window. This correction would increase the ratio of the activities.

The maximum energy of the low energy beta-group, which was determined from the various beta-spectra and Kurie plots by noting the energy at which the low energy beta-group became apparent on the respective curves, was found to be 0.26 ± 0.02 Mev. An effort was made to obtain Kurie plots of the low energy beta-group, but these were unsatisfactory due to the thick sources used.

By deflection of the beta-particles in a magnetic field it was found that the low energy beta-group consists of negative electrons. Cloud-chamber pictures obtained with a sample of P^{32} that had decayed for 12 months, at which time it was estimated that the activity of the low energy group was about 96 percent of the total activity, also confirmed the fact that the radiation consists of negative electrons.

There is a possibility that the low energy beta-group could be due to a contaminant that is not sufficiently removed by the chemical purification process of the neutron irradiated sulfur. The first consideration is that of S^{35}. However, the half-life and maximum beta-energy of S^{35} are 87.1 days and 0.166 Mev[10] respectively. This possibility is excluded since these values are not in agreement with those of the low energy beta-group given above. S^{37} is not a possibility since its half-life is only 5.0 min.[10] In fact there is no known beta-activity with a half-life of 24.8 ± 0.5 days and maximum beta-energy of 0.26 ± 0.02 Mev.

If the low energy beta-group is due to a contaminant, the amount of it present in waste products separated from the P^{32} during chemical purification would perhaps be considerably greater than in the carrier-free P^{32}. One such waste fraction was obtained from Oak Ridge and its spectrum determined with the spectrometer. This sample was rather weak, but practically all of the activity was due to P^{32}. The low energy group was present, but not to any greater extent than in other carrier-free P^{32} samples. Hence, the low energy beta-group does not appear to be due to a contaminant in the target material.

The carrier-free P^{32} produced at Oak Ridge is formed by a $S^{32}(n,p)P^{32}$ reaction. Since the isotopes of sulfur are 32 (95.00 percent), 33 (0.74 percent), 34 (4.24 percent), and 36 (0.017 percent)[11] the nuclear reactions $S^{33}(n,p)P^{33}$, $S^{34}(n,p)P^{34}$, and $S^{36}(n,p)P^{36}$ would also be possible. P^{34} is known to have a half-life of 12.4 sec[8] and is therefore eliminated as a possibility. This leaves the possibility of the low energy beta-group as being due to P^{33} or P^{36}. Since S^{36} has a very low abundance the cross section for the $S^{36}(n,p)P^{36}$ reaction would have to be very large if the low energy beta-group were due to P^{36}. This is, of course, a possibility. Another possibility is that P^{32} is formed by a second-order (n,γ) reaction on P^{32}. This is very unlikely unless P^{32} has an extremely large thermal neutron cross section. For a 28 day irradiation of sulfur at a flux of 5×10^{11} neutrons/cm^2/sec the thermal neutron cross section of P^{32} would have to be about 31,000 barns in order for the activity of the P^{33} to be one percent of the P^{32} activity at the end of the irradiation time.

B. Beta-Spectra of P^{32} Prepared by Methods Other than $S(n, p)P$

Radioactive P^{32} can also be prepared by a $P^{31}(n,\gamma)P^{32}$ reaction.[12] Since stable phosphorus consists of a single isotope,[13] P^{32} is the only isotope formed by a (n,γ) reaction. It would be possible to form P^{33} by a second order (n,γ) reaction on P^{32}. If P^{33} were to be detected in the spectrometer by this reaction the cross section for the $P^{32}(n,\gamma)P^{33}$ reaction would have to be very large. For a 14-day irradiation of P^{31} at a flux of 3×10^{13} neutrons/cm^2/sec the thermal neutron cross section of P^{32} would have to be about 980 barns in order for the activity of the P^{33} to be one percent of the P^{32} activity at the end of the irradiation time. The thermal neutron cross section of P^{31} is 0.15 barn.[14]

A sample of P^{32}, prepared by a $P^{31}(n,\gamma)P^{32}$ reaction, was obtained from Oak Ridge. As reported previously[15] this sample appeared to have a low energy beta-group similar to the one observed in the P^{32} samples prepared by neutron irradiation of sulfur. However, the data

[10] Way, Fano, Scott, and Thew, *Nuclear Data* (National Bureau of Standards Circular 499, 1950).

[11] Way, Wood, and Thew, *Nuclear Data* (National Bureau of Standards Circular 499, 1951), Supplement 1.

[12] P. Preiswerk and H. von Halban, Compt. rend. **201**, 722 (1935).

[13] F. W. Aston, *Mass Spectra and Isotopes* (E. Arnold and Company, London, 1942).

[14] H. Pomerance, Oak Ridge National Laboratory-577, 25 (1949) and Oak Ridge National Laboratory-366, 43 (1949).

[15] E. N. Jensen and R. T. Nichols, Phys. Rev. **83**, 215 (1951).

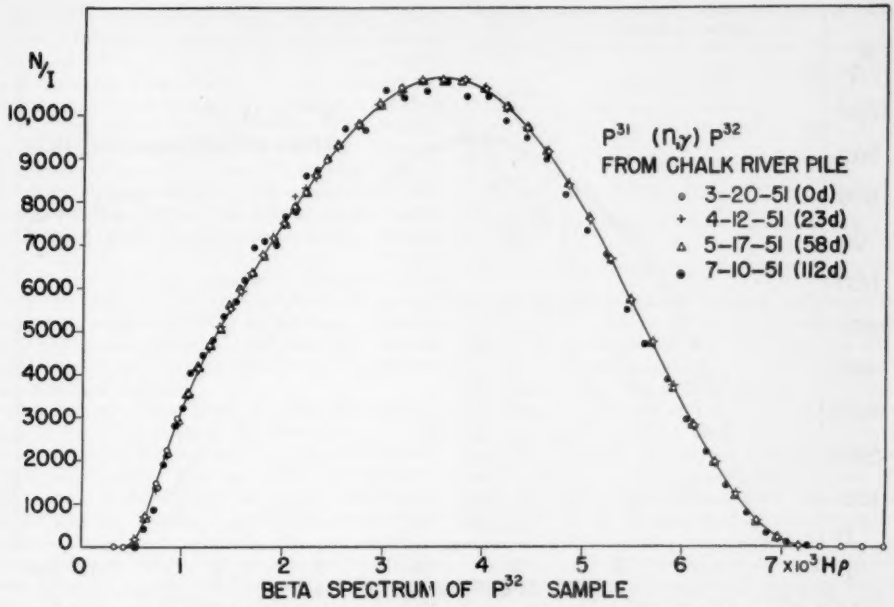

FIG. 2. Beta-ray spectra of P^{32} sample prepared by a $P^{31}(n,\gamma)P^{32}$ reaction. These four spectra were obtained over a period of 112 days. The spectra have been normalized at the maximum counting rates. The ordinates apply to the spectrum determined as of March 20, 1951. The distortion of the spectra at low energies is due to a thick source. The last spectrum was determined 127 days after the sample was removed from the pile. N is the number of counts per min and I is the current in the spectrometer coil.

were not conclusive since the sample had a low specific activity and therefore could not be followed in the spectrometer for a sufficiently long period of time. Two other higher specific activity sources of P^{32}, prepared by a $P^{31}(n,\gamma)P^{32}$ reaction, were obtained, one from Oak Ridge and one from Chalk River. The low energy beta-group was not observed in either one of these samples. The appearance of the low energy beta-group in the first P^{32} sample prepared by a $P^{31}(n,\gamma)P^{32}$ reaction is unexplained.

The Chalk River P^{32} sample was prepared by irradiating red phosphorus for 14 days with a total thermal neutron exposure of 3.65×10^{19} neutrons/cm^2,[16] and was removed from the pile on March 5, 1951. The beta-ray spectra of this sample are shown in Fig. 2, and again are normalized at the maximum counting rates. The ordinates of the graph apply to the data obtained as of March 20, 1951. Since it was of interest to follow the phosphorus sample in the spectrometer for as long a time as possible, the spectrometer source was made quite thick and this accounts for the distortion of the spectra at the lower energies as shown by a spectrum obtained from a thin source of the same sample. The sample was followed with the spectrometer for 112 days during which time four spectra were obtained. The first and last spectra shown in Fig. 2 were obtained 15 days and 127 days respectively after the sample was removed from the Chalk River pile. As can be seen from Fig. 2 all four spectra are essentially identical and there is no evidence of the low energy beta-group observed in the Oak Ridge carrier-free P^{32} prepared by neutron irradiation of sulfur. The spectrum shown in Fig. 2 which was determined as of July 10, 1951 had a maximum N/I value of 43.8.

The second sample of P^{32} prepared by a $P^{31}(n,\gamma)P^{32}$ reaction, which was received from Oak Ridge, was followed with the spectrometer for a period of 47 days during which time three spectra were obtained. The first and last spectra of this sample were obtained 45 days and 92 days respectively after the sample was removed from the pile. As in the case of the Chalk River sample the three spectra were essentially identical and there was no evidence of the low energy beta-group. It is therefore concluded that the low energy beta-group observed in the Oak Ridge carrier-free P^{32}, which is prepared by neutron irradiation of sulfur, is not present in P^{32} samples prepared by a $P^{31}(n,\gamma)P^{32}$ reaction.

[16] K. R. Manning, Chalk River, Ontario, private communication.

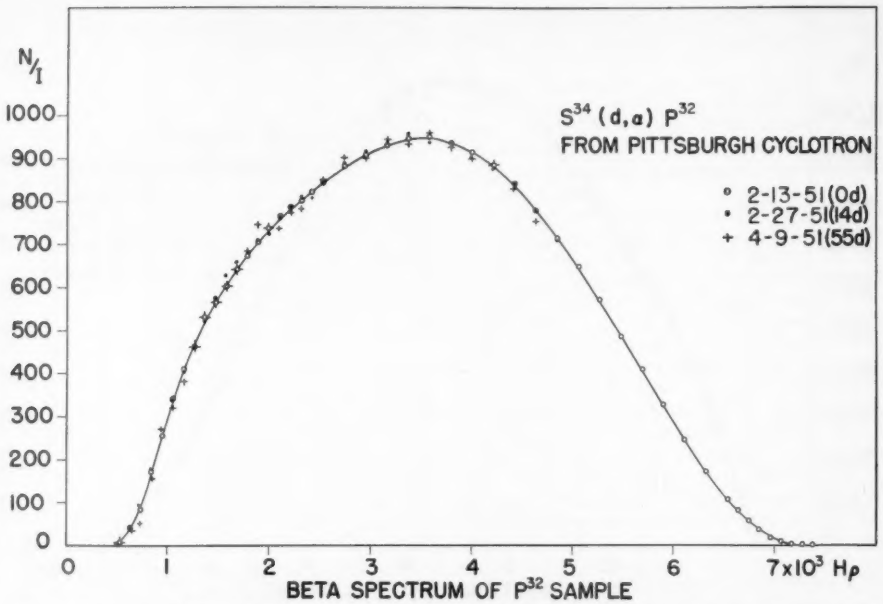

FIG. 3. Beta-spectra of P^{32} sample prepared by a $S^{34}(d,\alpha)P^{32}$ reaction. These three spectra were obtained over a period of 55 days. The spectra have been normalized at the maximum counting rates. The ordinates apply to the spectrum determined as of February 13, 1951. The distortion of the spectra at low energies is due to a thick source. The last spectrum was determined 71 days after the deuteron bombardment. N is the number of counts per min and I is the current in the spectrometer coil.

Since the low energy beta-group is present in P^{32} samples prepared by neutron irradiation of sulfur but is not present in P^{32} samples prepared by neutron irradiation of phosphorus it follows that the low energy beta-group cannot be due to a second-order (n,γ) reaction on P^{32}. If this were the case the low energy beta-group would be much more prominent in the Chalk River sample than in the Oak Ridge P^{32} samples prepared by neutron irradiation of sulfur due to the higher neutron flux of the Chalk River pile. However, it does not rule out the possibility that the low energy beta-group is due to P^{33} or possibly P^{36} as a result of (n,p) reactions on S^{33} and S^{36} respectively.

The isotope P^{32} can also be prepared by a $S^{34}(d,\alpha)P^{32}$ reaction.[17] A sulfur sample was irradiated for two hours with a 16-Mev deuteron beam of approximately 15 μamp[18] at the University of Pittsburgh cyclotron. After receiving the irradiated sulfur a chemical separation of phosphorus was performed on this sample. A description of the chemical procedure is given in Appendix A. The phosphorus sample was then followed in the spectrometer for a period of 55 days during which time three beta-spectra were obtained. These spectra are shown in Fig. 3 and are normalized at the maximum counting rates. The spectrometer source was quite thick and this again accounts for the distortion at the lower energies. The sulfur sample was irradiated with deuterons on January 28, 1951. Hence, the first and last spectra shown in Fig. 3 were obtained 16 days and 71 days respectively after the deuteron bombardment. The ordinates of Fig. 3 apply to the data obtained as of Februrary 13, 1951. From Fig. 3 it is seen that the three spectra are essentially identical and that there is no evidence of the low energy beta-group observed in the Oak Ridge carrier-free samples of P^{32} prepared by neutron irradiation of sulfur.

A (d,α) reaction on all the isotopes of sulfur would form P^{30}, P^{31}, P^{32}, and P^{34}. Since neither P^{30} or P^{34} is formed by this reaction and since P^{32} is the only activity apparent in Fig. 3 it follows that these data are also consistent with the possibility that the low energy beta-group observed in P^{32} samples prepared by neutron irradiation of sulfur is due to P^{33} or possibly P^{36}.

Another method of forming P^{32} is by a (γ,p) reaction on sulfur. This reaction on all the isotopes of sulfur would form P^{31}, P^{32}, P^{33}, and P^{35}. Perlman[19] has reported that at 50 Mev and 100 Mev the (γ,pn) yield on the reaction $Ge^{70}(\gamma,pn)Ga^{68}$ is of the same order as (γ,p)

[17] R. Sagane, Phys. Rev. **50**, 1141 (1936).
[18] A. J. Allen, private communication.
[19] M. L. Perlman, Phys. Rev. **75**, 988 (1949).

yields on five isotopes reported by Perlman and Friedlander.[20] Other (γ,pn) reactions have been reported by Hoffman[21] [$A^{40}(\gamma,pn)Cl^{38}$], Moses[22] [$W^{182}(\gamma,pn)Ta^{180}$], and Katz and Penfold[23] [$S^{32}(\gamma,pn)P^{30}$]. Moses[22] also found that the yield for the (γ,pn) reaction on W^{182} was of the same order as the (γ,p) reaction on W at maximum x-ray energies of 30 Mev and 68 Mev. Hence, in irradiating sulfur with x-rays one would expect to form P^{30}, P^{31}, P^{32}, and P^{34} by (γ,pn) reactions. The radioisotopes expected to be formed by irradiating sulfur with x-rays, and having appreciable half-lives, are those of P^{32} and P^{33}.

Sulfur was irradiated for about 30 hours with x-rays, from the Iowa State College synchrotron, that had a maximum energy of 68 Mev. A phosphorus separation was performed on the irradiated sulfur. The chemical procedure followed in this phosphorus separation is given in Appendix B.

The activity of the synchrotron-produced phosphorus sample was followed for 62 days by means of a G-M counter having a window surface density of 2.3 mg/cm^2. Data were obtained with and without an aluminum absorber of surface density 75 mg/cm^2 between the source and the counter. The aluminum absorber was sufficient to absorb completely electrons having an energy of 0.29 Mev.[24] This completely absorbed the low energy beta-group and therefore only the betas from P^{32} were counted when the absorber was used. In order to obtain the total counting rate due to the P^{32} activity the counting rates of a P^{32} sample, prepared by a $P^{31}(n,\gamma)P^{32}$ reaction, were obtained with and without the same absorber and for the same geometry. The ratio of these two counting rates gave the correction factor by which the counting rates of the synchrotron produced activity, with absorber, were multiplied in order to obtain the total counting rate due to the P^{32} activity. By the method of least squares the half-life of the activity obtained with the absorber was found to be 14.3 days, which is in good agreement with the published values of the half-life[10] of P^{32}. By subtracting from the total activity the counting rates due to the P^{32} activity it was clear that there were two activities present in the synchrotron-produced phosphorus. The half-life of the second activity was found to be 24.6 days.

This is in good agreement with the half-life values of 25.2 and 24.2 days found for the low energy beta-groups in the carrier-free P^{32} prepared by neutron irradiation of sulfur. A previous run on sulfur irradiated with x-rays from the synchrotron gave half-life values of 14.4 days for the P^{32} activity and 25.2 days for the low energy beta-group.

After corrections were applied to the initial experimentally determined activities of P^{32} and the low energy beta-group for the counter window, air absorption, Cellophane covering of the source and self-scattering due to source weight[25] it was found that the initial activity of the low energy beta-group was 45 percent of the total activity. This is about the activity expected for a 30-hr irradiation of sulfur on the assumption that the cross sections for (γ,p) on S^{32} and S^{34} and (γ,np) on S^{34} are all equal. This activity is much larger than the 1.4 percent found in the phosphorus samples prepared by neutron irradiation of sulfur. This is to be expected since the abundances of S^{33} and S^{34} are 0.74 percent and 4.24 percent respectively.

A sample of lithium chloride was also irradiated with the x-rays from the synchrotron at the same time as the sulfur sample was irradiated. The phosphorus separation performed on this sample is given in Appendix B. This phosphorus sample was followed by means of the same G-M counter and in precisely the same manner as the phosphorus sample obtained from the synchrotron irradiation of sulfur. Again two beta-groups were observed. In this case the half-life of the P^{32} activity was determined as 15.2 days while the low energy beta-group was found to have a half-life of 24.7 days. The phosphorus activities are presumably due to the reactions $Cl^{35}(\gamma,2p)P^{33}$, $Cl^{35}(\gamma,n2p)P^{32}$, and $Cl^{37}(\gamma,\alpha)P^{32}$. Again applying the appropriate corrections it was found that the initial activity of the low energy beta-group was 48 percent of the total activity.

TABLE I. Summary of results on phosphorus activities produced by various reactions.

Reaction	Presence of P^{32}	Presence of low energy beta-group	Possible formation of phosphorus isotopes
1. $S(n,p)P$	Yes	Yes	32, 33, 34, 36
2. $P^{31}(n,\gamma)P^{32}$	Yes	No	32
3. $S(d,\alpha)P$	Yes	No	30, 31, 32, 34
4. $S\begin{pmatrix}\gamma,p\\ \gamma,pn\end{pmatrix}P$	Yes	Yes	30, 31, 32, 33, 34, 35
5. $Cl\begin{pmatrix}\gamma,2p\\ \gamma,n2p\\ \gamma,\alpha\end{pmatrix}P$	Yes	Yes	31, 32, 33, 34, 35

C. Discussion

In the experiments described above radioactive phosphorus has been produced by five different reactions. In all of these reactions, except $P^{31}(n,\gamma)P^{32}$, a phosphorus separation was made on the irradiated material before the radiations were examined. Table I gives a summary of the results and the possible isotopes formed by each reaction. The isotopes P^{30} and P^{34} can be eliminated from consideration since their half-lives are 2.18 min[26] and 12.4 sec[5] respectively. The only other isotope, in addition to P^{32}, that is present in all

[20] M. L. Perlman and G. Friedlander, Phys. Rev. **74**, 442 (1948).
[21] M. Hoffman, Phys. Rev. **83**, 215 (1951).
[22] A. J. Moses, Masters thesis, Iowa State College (1950).
[23] L. Katz and A. S. Penfold, Phys. Rev. **81**, 815 (1951).
[24] L. E. Glendenin, Nucleonics **2**, No. 1, 12 (1948).
[25] Engelkemeir, Seiler, Steinberg, and Winsberg, National Nuclear Energy Series **9**, paper 4, 56 (1951).
[26] J. Cichocki and A. Soltan, Compt. rend. **207**, 423 (1938).

three reactions

$$S(n,p)P, \quad S\begin{pmatrix}\gamma,p\\ \gamma,pn\end{pmatrix}P, \quad \text{and} \quad Cl\begin{pmatrix}\gamma,2p\\ \gamma,n2p\\ \gamma,\alpha\end{pmatrix}P$$

in which the low energy beta-group is present is that of P^{32}. Neither P^{35} nor P^{36} is formed in all three of these reactions. It is therefore concluded that the low energy beta-group observed in the carrier-free P^{32} prepared at Oak Ridge, by neutron irradiation of S, is due to P^{33}. The P^{33} is formed by the reaction $S^{33}(n,p)P^{33}$. Our results indicate that P^{33} decays by negatron emission with a maximum beta-energy of 0.26 ± 0.02 Mev and a half-life of 24.8 ± 0.5 days. This half-life value is the mean of the five experimental values. The ratio of the initial activity of P^{33} to P^{32} in carrier-free P^{32} is about 1.4 percent.

Using a maximum beta-energy of 0.26 Mev, a half-life of 24.8 days of an f value of 0.055, obtained from the graphs by Feenberg and Trigg,[27] it is found that P^{33} has a logft value of 5.1. According to Nordheim[28] this is a normal allowed transition. The spin of S^{33} is known to be $\frac{3}{2}$.[29,30] The magnetic moment[30] of S^{33} indicates a $d_{\frac{3}{2}}$ state. According to the nuclear shell model,[31] a regular filling of the levels would give a $d_{\frac{3}{2}}$ state to the P^{33} nucleus. The decay of P^{33} would then be a normal allowed transition in which the orbital momentum is unchanged and with a spin change of zero. For such a transition the values of logft range mostly from 4.8 to 5.5.[28] The experimental value of 5.1 for logft is in good agreement with these values. However, P^{31} is known to have a spin of $\frac{1}{2}$ with a $S_{\frac{1}{2}}$ state. On the basis of the nuclear shell model one would expect P^{33} to have a $S_{\frac{1}{2}}$ state also. The decay of P^{33} would then involve a transition in which the orbital momentum changes by two units with a spin change of one unit. Transitions of this type have logft values[28] mostly in the range 6.5 to 7.5, but with some stragglers. The experimental value of 5.1 for logft is not in agreement with these values. These considerations add confirmation to the $d_{\frac{3}{2}}$ state of P^{33}.

During the early part of the work on the beta-spectrum of P^{32}, when it erroneously appeared that the low energy beta-group was present in P^{31} irradiated with neutrons, it was thought that perhaps the low energy beta-group was due to a daughter product of P^{32}. At this time Dr. L. G. Elliott of Chalk River, Ontario, suggested the possibility of simultaneous emission of two electrons or of two quanta between two states having zero spin and opposite parity. Koenigsberg and Keller[32] have calculated that for the case under consideration here the transition probability of two quanta emission is about 2.2×10^3 times as large as for two electron emission. Also no net coincidence counts were observed, as would be expected for simultaneous emission of two electrons or two quanta, in a P^{32} sample that had decayed for 257 days. To check on the possibility of an isomeric state in sulfur a large batch of carrier-free P^{32} was allowed to decay for 111 days at Oak Ridge. Samples from this batch were obtained when it was first set aside and then 111 days later after the batch had been put through a second chemical purification process which presumably removed any sulfur present. This should have altered the ratio of the activity of the low energy beta-group, to that of P^{32} if there is an isomeric state in sulfur. From the beta-spectra of these samples it was found that the ratio of the activities was not changed due to the second chemical purification. The nuclear shell model[31] indicates that one would not expect to find an isomeric state in sulfur. The fact that the low energy beta-group is not observed in all of the reactions in which P^{32} was observed, even though the samples were followed for many half-lives, eliminates the possibility of the low energy beta-group as being due to a daughter product of P^{32}.

The results of this paper in which the low energy beta-group is ascribed to P^{33} with a maximum beta-energy of 0.26 ± 0.02 Mev and a half-life of 24.8 ± 0.5 days are in disagreement with those reported by Yaffe and Brown[7] in which they give a half-life of 22 ± 5 seconds for P^{33}. Their assignment of P^{33} is based on the assumption that their target material was pure P^{32}. Our results indicate that P^{32} prepared by neutron irradiation of sulfur contains about 2.5 atoms of P^{33} per hundred atoms of P^{32}. It is possible that the activity measured by Yaffe and Brown was that of P^{34} produced by a $P^{33}(n,\gamma)P^{34}$ reaction. The P^{33} would not be observed unless the activity was followed for several half-lives of P^{32}.

Sheline, Holtzman, and Fan[33] have recently reported observing a low energy beta-group in sulfur and chlorine irradiated with the 48-Mev x-ray spectrum of the University of Chicago betatron and also in old Oak Ridge carrier-free P^{32} samples. They also assign the low energy beta-group to P^{33} and give a maximum beta-energy of 0.27 ± 0.02 Mev and a half-life of 25 ± 2 days. Our results are in good agreement with these.

IV. ACKNOWLEDGMENTS

The authors wish to express their appreciation to Dr. L. J. Laslett for many helpful suggestions and his assistance in obtaining part of the data, particularly the determination of the charge of the P^{33} radiation; to Dr. A. F. Voigt and Messrs. L. McIsaac and A. Richardson for the chemical separation performed on the deuteron bombardment of sulfur and preparation of spectrometer sources; to Dr. D. S. Martin, Jr. and Messrs. F. J. Hughes and W. R. Daniels for the chemical

[27] E. Feenberg and G. Trigg, Revs. Modern Phys. **22**, 399 (1950).
[28] L. W. Nordheim, Phys. Rev. **78**, 294 (1950).
[29] C. H. Townes and S. Geschwind, Phys. Rev. **74**, 626 (1948).
[30] Eshbach, Hillger, and Jen, Phys. Rev. **80**, 1106 (1950).
[31] M. G. Mayer, Phys. Rev. **78**, 16 (1950).
[32] E. Koenigsberg and J. M. Keller, private communication. These calculations were made following the theory of R. G. Sachs, Phys. Rev. **57**, 194 (1940).
[33] Sheline, Holtzman, and Fan, Phys. Rev. **83**, 919 (1951).

separations performed on the synchrotron bombardments of sulfur and lithium chloride and the obtaining of the data on these phosphorus samples; to Dr. D. J. Zaffarano and the synchrotron crew for the x-ray irradiation of sulfur and lithium chloride; to Dr. J. M. Keller and Mr. E. Koenigsberg for helpful theoretical discussions on the problem; to Mr. E. Dewell for preparation of some of the spectrometer sources; to Dr. R. Stokes and Mr. M. Hoffman for the cloud-chamber determinations; to Mr. L. Newkirk for making the coincidence measurements; to Messrs. R. E. Kesterson, W. E. Lewis, and J. T. Jones, Jr. for assistance in obtaining part of the data; to Messrs. E. R. Rathbun, Jr. and J. H. Talboy, Jr. for construction of the G-M counters used in the spectrometer; to Dr. A. J. Allen, University of Pittsburgh, for the deuteron irradiation of sulfur and to Messrs. R. K. Sheline, R. B. Holtzman, and Chang-Yun Fan for sending us a copy of their manuscript prior to publication.

The authors are very grateful to Dr. A. F. Rupp, superintendent, Radioisotope Development Department, of the Oak Ridge National Laboratory for his generous cooperation in supplying us with the desired radioactive samples.

A new electronic current control for the thin-lens spectrometer has been designed, constructed and put into operation by Mr. A. Read and for this the authors wish to express their appreciation.

APPENDIX A

The following phosphorus separation[34] was performed on the sulfur irradiated with 16-Mev deuterons. The irradiated sulfur (approximately two grams) was melted in a Pyrex beaker and poured into another beaker containing 15 ml of boiling fuming nitric acid. The mixture was boiled for one hour, after which time the sulfur had settled to the bottom. The supernatant liquid was poured off and boiled again to oxidize any colloidal sulfur and also to remove excess NO_2. When this solution became clear, two mg of $La(NO_3)_3$ were added. This was followed by a careful neutralization with NH_4OH until the precipitation of $La(OH)_3$ was complete. The precipitate was filtered on a medium sintered glass disk and washed with dilute NH_4OH. Following the washing, the precipitate was dissolved with 10 ml of hot 6 *N* HCl and washed with sufficient water to give a final concentration of 0.1 N in HCl. This solution was passed through a Dowex-50 column to replace the metal cations by hydrogen ions. To the effluent one mg of P, as H_3PO_4, was added and the solution evaporated to dryness at 90–100°C. The residue was dissolved in a minimum amount of water and filtered to remove any resin solids. The filtrate was evaporated to near dryness and mounted on a Formvar-polystyrene film.

[34] The chemical procedure for this phosphorus separation was received, by private communication, from J. H. Gillette, superintendent Radioisotope Control Department, Oak Ridge National Laboratory.

APPENDIX B

The separation of phosphorus from sulfur irradiated with x-rays from the Iowa State College synchrotron was essentially a boiling nitric acid extraction described by Cohn[35] and studied by Kenny and Spragg.[36] In addition to this separation it was desirable to remove any trace amounts of other radioisotopes which might have been formed. To accomplish this 10 mg each of cupric, chromic, arsenate, and phosphate ions were added as carriers. The solution was diluted with 3 *N* HCl and saturated with H_2S. After standing for several hours the copper and arsenic sulfides were removed by centrifuging. The supernatant liquid was boiled in order to remove the excess H_2S. HCl was then removed by boiling with H_2SO_4 and the solution was neutralized with NH_3. The chromium was oxidized to chromate with Na_2O_2. The solution was acidified with HCl and $FeCl_3$ solution was added. An excess of NH_3 was added in order to precipitate hydrated $Fe(OH)_3$. This was dried and mounted for counting since the phosphorus was carried in the precipitate as $FePO_4$.

The chemical treatment of the irradiated LiCl was identical with that for the sulfur with the exception that the first step, the nitric acid extraction, was omitted. The rest of the procedure of Kenny and Spragg was used, however, as well as the carrier separation described above.

[35] W. E. Cohn, Clinton Laboratories, MDDC-518 (1946).
[36] A. W. Kenny and W. T. Spragg, AERE-C/R-485 (1950).

The Distribution of Multiplicities of Neutrons Produced by Cosmic-Ray μ-Mesons Captured in Lead*

MARSHALL F. CROUCH† AND ROBERT D. SARD
Washington University, St. Louis, Missouri‡

(Received July 19, 1951)

The nature of the μ-meson capture process in lead has been investigated by studying the number of neutrons emitted by the excited nucleus. Working under 2000 g cm^{-2} of clay and limestone and a 144 g cm^{-2} lead filter, events were studied in which a single charged particle penetrated a triple coincidence telescope and stopped in an 86 g cm^{-2} lead absorber, with one or more delayed coincident neutron counts from an array of ten $B^{10}F_3$ counters in a paraffin moderator placed below the absorber. Events in which more than one G-M tube in any coincidence tray was discharged were rejected. A large paraffin barrier was interposed between the absorber and filter to reduce the sensitivity to neutrons originating above the absorber. The neutron detecting geometry is thought to have had an efficiency sensibly independent of neutron energy up to about 10 Mev. On the basis of 327 delayed neutron coincidences, the mean multiplicity of disintegration neutrons per stopped negative μ-meson was found to be 2.16±0.15, with ±10 percent additional error due to the uncertainty in the strength of the standard neutron source used to determine neutron detecting efficiency. The mean squared multiplicity was found to be 5.2±1.9 on the basis of 3 double-neutron coincidences. On the evaporation model the expected mean multiplicity for 100-Mev excitation energy is about 6, while a calculation based on the $\mu^- + P \rightarrow N + \nu$ hypothesis, using the distribution of excitation energy calculated on the free-particle model, and Weisskopf's statistical theory of the nucleon evaporation process, leads to an expected mean multiplicity of 0.95.

I. INTRODUCTION

IT has been shown by various investigators, using cloud chamber,[1–3] photographic emulsion,[4–6] and crystal counter[9] techniques, that the capture of a negative μ-meson by a nucleus does not lead, in the great majority of cases, to the emission of any charged particles. The nuclear excitation is accordingly presumed to be considerably less than the 107-Mev rest energy of the captured meson. However, it has been observed that the nucleus receives sufficient excitation to emit one or more neutrons,[10,11] and the study described represents an effort to investigate the distribution of nuclear excitations by determining the mean number $\langle m \rangle_{Av}$ of neutrons emitted in the meson capture process in lead. In addition, an attempt has been made to determine the mean squared multiplicity $\langle m^2 \rangle_{Av}$ which gives information about the shape of the distribution function for excitations. The experimental results, based on data obtained underground with a counter telescope, are compared with the theoretical predictions of the values of $\langle m \rangle_{Av}$ and $\langle m^2 \rangle_{Av}$ for two different assumed distributions of excitation energy. The first of these is the case of 100-Mev excitation for each interaction, and the second is the distribution given by a theory developed by Tiomno and Wheeler and by Rosenbluth[12] to account for the observed rarity of charged particles from μ-meson capture. In this theory most of the meson's rest energy is carried away by a neutrino or neutretto, leaving the nucleus with a mean excitation energy of about 10 Mev.

II. APPARATUS

The arrangement of components is indicated in Figs. 1 and 2. There are three trays of Geiger counters designated A, B', and B[13] which are connected as a cosmic-ray coincidence telescope to detect penetrating charged particles. Above the telescope is a lead filter of thickness 144 g cm^{-2}. The entire apparatus was situated in one of the tunnels of the Lemp Brewery cave in St. Louis under about 2000 g cm^{-2} of clay and limestone, in the hope that other charged particles present in the cosmic radiation would thereby be reduced in intensity to the point where events could be ascribed to the μ-meson component alone. It is estimated

* A brief account of this work was presented at the American Physical Society Ohio Section Meeting on November 4, 1950, Phys. Rev. **81**, 134 (1951). This article is a condensation of a dissertation presented to the Graduate Board of Washington University in September, 1950, by one of the authors (M.F.C.) in partial fulfillment of the requirements for the degree of Doctor of Philosophy. The value of $\langle m \rangle_{Av} = 1.90 \pm 0.24$ quoted in the abstract was based on the assumption of zero positive excess of the mesons stopped in the cave. The value arrived at in the present paper, 2.16±0.15, involves the assumption that only 44 percent of the stopped mesons are negative. The value for $\langle m^2 \rangle_{Av}$ quoted in the abstract should have been 5.0±1.8 on the assumption of zero positive excess.

† Now at Case Institute of Technology, Cleveland, Ohio.

‡ Assisted by the joint program of the ONR and AEC.

[1] Cool, Fowler, Street, Fowler, and Sard, Phys. Rev. **75**, 1275 (1949).

[2] W. Y. Chang, Revs. Modern Phys. **21**, 166 (1949).

[3] W. Y. Chang, Phys. Rev. **79**, 205(A) (1950).

[4] Camerini, Muirhead, Powell, and Ritson, Nature **162**, 433 (1948).

[5] Goldschmidt-Clermont, King, Muirhead, and Ritson, Proc. Phys. Soc. (London) **61**, 183 (1948).

[6] D. H. Perkins, Nature **163**, 682 (1949); Phil. Mag. **40**, 601 (1949).

[7] C. Franzinetti, Phil. Mag. **41**, 86 (1950).

[8] E. P. George and J. Evans, Proc. Phys. Soc. (London) **A64**, 193 (1951). These investigators report underground photoplate evidence that in about 10 percent of the capture processes a one-prong star is produced.

[9] H. G. Voorhies and J. C. Street, Phys. Rev. **76**, 1100 (1949).

[10] Sard, Ittner, Conforto, and Crouch, Phys. Rev. **74**, 97 (1948); Sard, Conforto, and Crouch, Phys. Rev. **76**, 1134 (1949).

[11] G. Groetzinger and G. McClure, Phys. Rev. **74**, 341 (1948); Phys. Rev. **75**, 340 (1949).

[12] J. Tiomno and J. A. Wheeler, Revs. Modern Phys. **21**, 153 (1949); M. N. Rosenbluth, Phys. Rev. **75**, 532 (1949). Priority for the $\mu^- + P \rightarrow N + \nu$ hypothesis seems to belong to Sakata and Inoue, Prog. Theor. Phys. **1**, 143 (1946), and B. Pontecorvo, Phys. Rev. **72**, 246 (1947).

[13] Each tray contains five tubes, of 4.97 cm inside diameter and 25.4 cm active length.

that at the depth chosen neutron production by these other charged particles could not introduce an error of more than 5 percent in $\langle m \rangle_{Av}$ and 20 percent in $\langle m^2 \rangle_{Av}$.[14] Below the counter telescope is placed a lead absorber of thickness 86 g cm^{-2} (3 inches), and below it a tray of anticoincidence counters C[15] to permit detection of events in which charged particles that have passed through the telescope stop in the lead absorber. Immediately below the anticoincidence tray *C* is placed a 1500-pound paraffin moderator in which is imbedded an array of ten $B^{10}F_3$ slow neutron counters.[16] Its purpose is to detect disintegration neutrons originating in the absorber that have been slowed down in the paraffin. Finally a paraffin barrier (shown removed in Fig. 1) is interposed between the lead filter and the lead absorber in order to discriminate against neutrons coming from above the absorber, as, for example, from

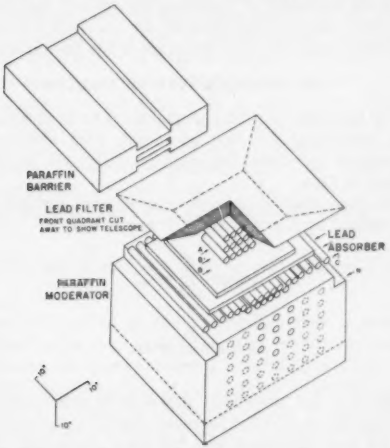

FIG. 1. The experimental arrangement (view from above). For clarity the paraffin barrier is shown removed from the telescope.

nuclear interactions occurring in the filter that produce a number of charged particles and neutrons which discharge counters in the telescope trays and give a (delayed) coincident pulse in the neutron detector (see Fig. 3). Besides decreasing the efficiency with which neutrons from above the absorber are detected, the barrier also increases, by its reflecting action, the efficiency for detecting neutrons from the absorber, and

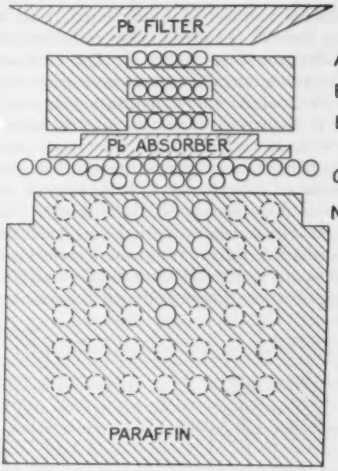

FIG. 2. The experimental arrangement (vertical section).

reduces the contribution to the telescope anticoincidence rate from knock-on electrons and side showers. The lead filter, paraffin barrier, and lead absorber were all mounted on wheeled dollys arranged to run on tracks, so that they could be readily placed in the telescope array or rolled back onto a siding completely out of the telescope cone. This arrangement facilitated control experiments to ascertain the effects of the various layers. For clarity the paraffin barrier in Fig. 1 is shown on the siding rather than in the telescope.

Figure 4 is a simplified block diagram of the circuits used, with amplifier stages, scalers and other details omitted. The signals from trays *A*, *B'*, and *B* are

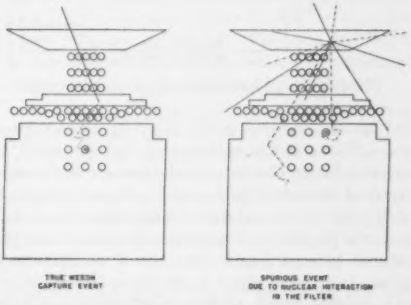

FIG. 3. True meson capture event and spurious event due to interaction in filter. The drawing on the left shows the stopping of a μ-meson with emission of a neutron that enters the paraffin thermalizer. The drawing on the right shows a nuclear interaction in the filter that could be recorded as an **A**:**N** event. Insertion of the paraffin barrier between the filter and absorber and restriction to "single" telescope coincidences greatly reduce the chance of recording such an event.

[14] The recent work of C. Cocconi and V. Cocconi-Tongiorgi [Phys. Rev. 82, 335 (1951)] on the multiple production of neutrons in Pb at various depths under water shows that this estimate is most conservative. They report that 1000 g cm^{-2} is sufficiently deep to bring the neutron shower rate into equilibrium with the penetrating component.

[15] This tray contains 23 tubes, each of 4.97 cm inside diameter and 84.6 cm active length.

[16] The enriched BF_3 was furnished by the Isotopes Division, Atomic Energy Commission, Oak Ridge, Tenn. The counters were made by the N. Wood Counter Laboratory, Chicago, Illinois.

connected to a threefold coincidence circuit with a resolving time of ± 1 μsec. These coincidence events will be designated as events **C**. The four adjacent blocks represent circuits which cause anticoincidence events, denoted **A**, to be recorded whenever no C counter is discharged during an interval from 2 μsec before to 5 μsec after a triple coincidence event **C**. The next circuits, reading from the top of the diagram, record delayed coincidences **C**:**N** between an event **C** and one or more counts **N** in the neutron detecting system, as well as delayed coincidences **A**:**N**. For both these events the neutron count must occur during the interval from 6 to 166 μsec after the **C** event. This long resolving time was chosen to match approximately the

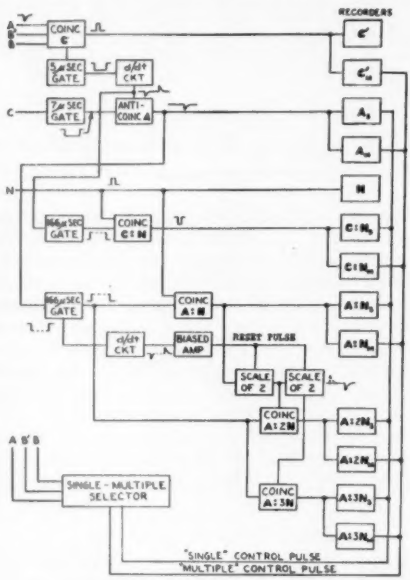

FIG. 4. Simplified functional diagram of the circuits.

mean life of a neutron in the detecting system. Under the conditions of low background that prevailed, the correction for accidental coincidences was always small in spite of the rather long resolving time. By requiring the **N** pulse to be delayed at least 6 μsec from the **C** event, the possibility of spurious events due to shower-produced prompt pulses from the N counters is excluded. As it takes about 5 μsec for a fast neutron to reach thermal speed, no loss in efficiency is entailed. Finally, by means of a scale-of-four reset after each **A**:**N** coincidence gate, anticoincidence events **A** accompanied by two or more and three or more delayed counts in the neutron detector channel are detected, and recorded as **A**:2**N** and **A**:3**N** events. The Single-Multiple selector circuits are provided for the purpose of distinguishing between "single" events in which a single charged particle penetrates the telescope, discharging only one counter in each tray, and "multiple" events in which more than one counter is discharged in any one of the trays and at least one is discharged in each of the two others. It was hoped that by considering rates of "single" events alone a further discrimination against interactions produced by particles other than μ-mesons might be effected. Hence pairs of recorders and associated circuits were provided for each event, to totalize separately cases in which a "single" telescope event is observed and cases in which the telescope event is "multiple." Thus, for example, **A**:**N** events are subdivided into **A**:$\mathbf{N}_s$ and **A**:$\mathbf{N}_m$ events. Each recorder is also connected in parallel with a pen element of a 20-pen Esterline-Angus "Operation Recorder." The chart record from this instrument gave a valuable check on normalcy of operation throughout each run, the extra pens provided being all used to check continuously some aspect of the operation of the equipment.

III. EXPERIMENTAL PROCEDURE

The relations between the quantities to be measured and determined will first be stated, after which the procedures for evaluating each quantity will be considered in turn.

The mean multiplicity and mean squared multiplicity are defined by Eqs. (1) and (2), respectively:

$$\langle m\rangle_{Av}=\sum_{m=0}^{\infty} m a_m, \tag{1}$$

$$\langle m^2\rangle_{Av}=\sum_{m=0}^{\infty} m^2 a_m, \tag{2}$$

where a_m is the probability that a given meson capture process will lead to the emission of exactly m neutrons. If we now introduce the following quantities: M_- = negative meson stopping rate, S = delayed neutron coincidence rate (one or more), D = delayed double neutron coincidence rate (two or more), and ϵ_c neutron detection efficiency (coherent), we can write the following exact expression:

$$S=M_-\sum_{m=1}^{\infty} a_m \sum_{r=1}^{m} \frac{m!}{r!(m-r)!}\epsilon_c^r(1-\epsilon_c)^{m-r}. \tag{3}$$

For small values of ϵ_c Eq. (3) can be represented with sufficient accuracy by the following simplified expression:

$$S=M_-\langle m\rangle_{Av}\epsilon_c. \tag{4}$$

The corresponding approximate expression for the delayed double neutron coincidence rate is

$$D=\tfrac{1}{2}M_-\langle m(m-1)\rangle_{Av}\epsilon_c^2. \tag{5}$$

Equations (4) and (5) can be solved for $\langle m\rangle_{Av}$ and $\langle m^2\rangle_{Av}$ to give the desired expressions for these quantities

in terms of observable rates and neutron detector efficiency, thus:

$$\langle m\rangle_{Av}=S/(M_-\epsilon_c), \tag{6}$$

$$\langle m^2\rangle_{Av}=\langle m\rangle_{Av}+2D/(M_-\epsilon_c^2). \tag{7}$$

The difference between the rates of "single"[17] anticoincidences with and without the Pb absorber was taken to be the meson stopping rate, and 0.44 of this difference was taken to be the negative meson stopping rate. (In spite of the rather high anticoincidence background, which amounts to 50 percent of the effect produced by the absorber and 1.2 percent of the coincidence rate, a telescope geometry similar to ours has been shown by W. L. Kraushaar (Phys. Rev. **76**, 1045, Experiments VIII and II (1949)) to give an apparent meson stopping rate which agrees within $2\frac{1}{2}$ percent with the "best value" obtained using a more elaborate geometry in which the anticoincidence background was held down to 0.5 percent of the coincidence rate.) This factor is that obtained by Wilson[18] for μ-mesons of momentum 4×10^9 ev/c at sea-level; it is these mesons which stop in the absorber under 2000 g cm^{-2} of earth. S and D were taken to be the rates $\mathbf{A}:\mathbf{N}_s$ and $\mathbf{A}:2\mathbf{N}_s$, respectively. The neutron detector efficiency ϵ_c varies somewhat depending upon the particular region of the absorber in which the capture process takes place, so that (4) should actually be written

$$S=M_-\langle m\rangle_{Av}\int d\tau f(x,y,z)\epsilon_c(x,y,z)=M_-\langle m\rangle_{Av}\langle\epsilon_c\rangle_{Av} \tag{8}$$

where $f(x,y,z)d\tau$ is the probability that a meson capture takes place in $d\tau$ at (x,y,z). A rough approximation to the above process of integration was realized by dividing the portion of the absorber in the telescope cone into imaginary blocks $4\frac{1}{2}$ inches square, after which a standard Ra-α-Be source was placed successively at the centers of the top surface, mid-plane, and bottom surface of each block by means of a jig. The Pb absorber was, of course, in place during these measurements. The measured efficiencies with the source at these various positions, corrected as explained below for the coherent counting loss, were taken as the $\epsilon_c(x,y,z)$ in Eq. (8). The values of the weighting factors $f(x,y,z)$ depend upon the angular distribution of the cosmic-ray particles which stop in the absorber, the thickness of absorbing material above the telescope for rays of different directions, and the variation of effective area of the counter telescope with the direction of the incident radiation. Instead of attempting to compute values of $f(x,y,z)$ by evaluating all of these effects, it was decided to use an empirical procedure. It was assumed that the same $f(x,y,z)$ would describe the probability that a given *penetrating* charged particle would pass through the mid-plane of a particular $d\tau$ at (x,y,z), and an experimental determination of these probabilities was made. This was done by removing the absorber and putting small 3 inches$\times3\frac{1}{2}$ inches Geiger counter trays B'' and B''' (two to speed measurements), successively, at points corresponding to the centers of the mid-plane of each block. The coincidence rates $AB'B''B$ and $AB'B'''B$, obtained with an auxiliary dual coincidence unit,[19] properly normalized, were taken as the weighting factors $f(x,y,z)$. Most of the events (90 percent) were found to take place in the center block and those blocks adjacent to it, so that the value found for $\langle\epsilon_c\rangle_{Av}$ was very close to the true values of ϵ_c for most of the individual events. It is true that this efficiency value is an average over the broad spectrum of the Ra-α-Be source, while the spectrum of the neutrons produced in the cosmic-ray interactions is not known. However the neutron detector geometry used (see Figs. 1 and 2) is believed to have an efficiency reasonably independent of incident neutron energy up to about 10 Mev, and the theoretically predicted spectrum of neutrons evaporated from an excited nucleus does not extend to higher energies. Moreover, the measured efficiency and the delayed neutron coincidence rate were found to change by about the same factor when two different neutron detector geometries were tried, so that it seems reasonable to regard the value of efficiency for Ra-α-Be neutrons as applicable to the neutrons being studied.

The neutron detector efficiency as measured directly with a standard source differs from that with which cosmic-ray neutrons are detected because of the coherency requirement imposed by the delayed coincidence circuit. The neutrons are slowed down to thermal speeds in about 5 μsec, and thereafter they have an exponentially decreasing probability of being detected, with a characteristic time, or "mean life," τ, associated with their diffusion and capture. The finite gate length, T, in the delayed coincidence neutron measurements entails a reduction in the efficiency by the factor

$$\epsilon_c/\epsilon_i=1-\exp(-T/\tau). \tag{9}$$

The mean life τ was determined in the following manner. The trailing edge of the 166 μsec gate of the delayed neutron coincidence circuit was made to trigger a second gate associated with a similar coincidence circuit. For coherent neutrons, the ratio of counts in the two gates is

$$[1-\exp(-T_1/\tau)]/[\exp(-T_1/\tau)-\exp(-T_2/\tau)] \tag{10}$$

where T_1 is the stopping time of the first gate, measured from its starting time, and T_2 is the stopping time of the second gate measured from the starting time of the first. Two different sources of coherent neutrons were

[17] It is recognized that a small fraction of the mesons that stop in the absorber are accompanied by a knock-on electron on entering the telescope. Exclusion of these mesons does not introduce any error in $\langle m\rangle_{Av}$ and $\langle m^2\rangle_{Av}$; it only reduces slightly the rate at which data is obtained.

[18] J. G. Wilson, Nuovo cimento **6**, Supplement **3**, 523 (1949).

[19] A. H. Benade and R. D. Sard, Phys. Rev. **76**, 488 (1949).

used. The first was provided by the cosmic radiation: a count in the B' tray placed on the absorber was used to trigger the delayed neutron coincidence gates. The usual **C**:**N** events were of course included here. The high rate of delayed coincidences made it possible to obtain enough counts in about four days' time to give τ to within 5 percent standard error: $\tau=169\pm9$ μsec. The second source was provided by the $Be^9(\alpha,n)C^{12*}$ reaction, in which the excited carbon nucleus emits a γ-ray immediately. The γ-ray was used to trigger the delayed neutron coincidence gates. An old Po-Be source which had decayed to only ~20 neutrons/sec was placed on top of the paraffin moderator on the telescope axis, and the B' tray was centered immediately above the source. The B' tray served to detect γ-rays from the source. The neutron coincidence rate was well above the casual and cosmic-ray rate, the efficiency of B' for the γ-rays being apparently about 0.8 percent. Two days' data sufficed to determine τ as $154\ ^{+9}_{-8}$ μsec.

The coherent neutrons from the Po-Be source have a different spectrum of initial energies from that of the neutrons produced in the cosmic-ray events, but the time required and distance traveled in the slowing down process should differ but little. Indeed, the values of τ obtained from the two methods agree well within the statistical uncertainties, and use of the weighted mean, $162\ ^{+7}_{-6}$ μsec, seems justified. The result, which should depend to some extent on the particular moderator-counter geometry used, is in good agreement with the value of 155±5 μsec found by Cocconi, Tongiorgi, and Widgoff[20] with a similar geometry. Using $T=166$ ±5 μsec for the average gate length over the period in which the multiplicity measurements were made, we find

$$\epsilon_c/\epsilon_i=0.64\pm0.02.$$

This ratio is essentially independent of the position in the absorber at which the neutron originates, so that we can take it outside the integral in (8),

$$\langle\epsilon_c\rangle_{Av}=(\epsilon_c/\epsilon_i)\int d\tau f(x,y,z)\epsilon_i(x,y,z)=(\epsilon_c/\epsilon_i)\langle\epsilon_i\rangle_{Av}. \quad (11)$$

The measurements of $\epsilon_i(x,y,z)$ were made with a 70 μc Ra-α-Be source emitting $(1.69\pm0.17)\times10^3$ neutrons/sec. This figure is based on several recent comparisons of the source with the laboratory's 20-mC Ra-α-Be standard and a recent calibration of the latter by the National Bureau of Standards. The Bureau of Standards, calibration agrees very closely with one made of the same source two years previously by D. J. Hughes at the Argonne National Laboratory. In both cases, the ultimate standard used was the Argonne Laboratory's "Source No. 38," and the uncertainty quoted above represents an estimated 10 percent uncertainty in the flux from this standard. As this uncertainty corresponds to a systematic error which could eventually be corrected for, it will not be mixed with the statistical uncertainties in the computations below. The indicated errors will be simply the statistical standard errors estimated from the number of counts. Numerical integration, using the measured values of $\epsilon_i(x,y,z)$ and $f(x,y,z)$, yields

$$\langle\epsilon_i\rangle_{Av}=2.83 \text{ percent}$$

and, thence,

$$\langle\epsilon_c\rangle_{Av}=(1.81\pm0.06) \text{ percent}.$$

These figures refer to the arrangement of neutron counters shown in Figs. 1 and 2, the ten counters being connected in parallel and the 32 unused holes in the paraffin moderator being filled with close-fitting paraffin plugs ("333100" geometry). Some runs were made in Lemp Cave as well as near sea-level (Crow Hall subbasement, under 0.5 meter reinforced concrete) with an alternative geometry chosen to give high efficiency with some sacrifice of flatness. Seven of the counters were placed in the row of cavities nearest the absorber, with the remaining three counters in the center of the next row ("730000" geometry). For this geometry the measurements gave

$$\langle\epsilon_i\rangle_{Av}=3.87 \text{ percent},$$

whence

$$\langle\epsilon_c\rangle_{Av}=(2.48\pm0.08) \text{ percent}.$$

The "333100" geometry is thought to be essentially "flat" (efficiency independent of energy) over the spectrum of the evaporation neutrons, the situation resembling that in which a plane source of neutrons is immersed in an infinite mass of paraffin and the thermal neutron density is sampled at small equal intervals along a line perpendicular to the plane. It was verified that very few delayed coincidence neutrons are detected by counters placed further below the absorber.

In applying (5), a correction must be made for the fact that the circuits have nonzero resolving time, so that a second **N** pulse can only register an **A**:2**N** event if it occurs at least 7.8 μsec after the first **N** pulse. Calling the resolving time d and expanding in powers of d/τ, we find the correction factor to (5) to be

$$1-\frac{d}{\tau}\frac{1+\exp(-T/\tau)}{1-\exp(-T/\tau)}+\cdots,$$

or 0.90. In (7), ϵ_c^2 will therefore be multiplied by 0.90.

In the cave, several runs were taken without the paraffin barrier in place, in order to determine whether any of the observed neutron events originated in the lead filter. By comparing rates with and without the barrier, and determining by means of the source the factor of change in neutron detector efficiency for neutrons produced in the filter and in the absorber, it was possible to establish that with the barrier in place

[20] Cocconi, Tongiorgi, and Widgoff, Phys. Rev. **79**, 768 (1950).

only a negligible fraction of the **A**:**N**, events observed had their origin in the filter.

Runs were also taken with the absorber removed to determine the background **A**, and **A**:**N**, rates. The delayed coincidence rate **A**:**N**, dropped to essentially zero (2 counts in 118 hours), while the anticoincidence rate **A**, decreased to (0.519 ± 0.009) min^{-1}, indicating an anticoincidence efficiency of at least 98.8 percent.

Since numerous earlier measurements made with cadmium sheaths over the neutron counters in a similar counter array had shown the delayed coincidence rate to drop to zero each time,[10] only one such run was made with this apparatus, verifying that no delayed coincidence counts occurred with cadmium sheaths in place.

IV. TEST PROCEDURE

In general, data were taken during runs of about 20 hours, between which rather thorough equipment checks requiring three or four hours were made. Since the trustworthiness of the data is directly dependent on the degree of thoroughness of the equipment check, some description of this procedure will be given here. These checks apply only to the Lemp Cave data. Data taken at sea level were not checked so systematically, but the results given in Sec. V are based on a series of runs during which the rates were very steady, and the chart records for these runs were checked as described below, so that these data are believed to be reliable.

Each chart was inspected, ordinarily before the start of the next run, and the following matters observed and noted:

1. Steadiness of rates throughout run. 2. Proper association of events (e.g., presence of an **A** pip was verified each time an **A**:**N** pip was observed). 3. Agreement of number of pips for delayed coincidence events with the message register totals. 4. Possible correlation of events with line voltage fluctuations. 5. Possible correlation of delayed coincidence events with the occasional bursts of **N** counts due to insulator leakage. 6. Recording of single events in both single and multiple channels. This effect occurred occasionally because of overlapping of the long gates employed in the thyratron message register circuits, but it was possible to correct for it. In the final data analysis, runs or portions of runs were rejected whenever this inspection showed abnormalities in the run. At the end of each run all rates were computed for the run and plotted on a "rate graph," so that it was possible to tell at a glance whenever one of the rates deviated from the average of the preceding runs.

After this a set of six artificial pulses whose relative times could be adjusted in any manner desired were connected at the counter inputs in such a way as to simulate the occurrence of pulses in the A, B', B, and N channels (3 pulses in the latter). By delaying these suitably with respect to one another it was possible to verify that all circuits were operative and that their resolving times were approximately correct. This was done first using one signal per telescope tray, and then repeated with 4 simulated counter signals (multiple event). Thus every circuit in the apparatus was operationally checked, from preamplifiers to message registers. This check was made without fail every day, since some of the events were so rare (e.g., no count was recorded on **A**:3**N**, during the entire Lemp Cave series of measurements) that it was impossible to detect circuit failure from the cosmic-ray data.

Other checks performed daily without fail were a measurement of neutron detector efficiency with the Ra-α-Be source placed in a standard position at the top of the lead absorber, and a measurement with a Los Alamos-type "precision pulser" of the threshold of the neutron channel amplifier and discriminator.[11] Measurement of these quantities, along with the value of the high voltage applied to the BF_3 counters (2800 volts) and Geiger counters, followed by daily resetting of the controls to correct for any drift of characteristics, resulted in extreme constancy of the efficiency for neutron detection.

Other checks made with a frequency dictated by discretion were measurements of bias and plate voltages in the electronic circuits, measurement of plateaus and pulse heights of Geiger counters, and investigation of any miscellaneous troubles which might be suspected.

Finally calibration of all coincidence circuit resolving times was made at approximate two week intervals using the multiple pulse generators employed in the daily check. The time relation of the six pulses was determined by the settings of six multi-revolution potentiometers, after which an oscilloscope and calibrator were used to translate the settings of the potentiometers into relative time values. As a final step the calibrator was checked against an Army Signal Corps SCR-211 frequency meter.

V. EXPERIMENTAL RESULTS

The rates measured with the normal geometry are given in Table I. Those obtained with the "flat" N detector in the cave (second column) are the basic data of this experiment. The third and fourth columns give the rates obtained using the more efficient neutron detecting geometry, both in the cave and in the subbasement of Crow Hall. The rates are corrected for casual coincidences, computed from the measured individual counting rates and the gate-lengths. This correction is always small, its greatest value being 7 percent, with no correction greater than 0.7 percent in the quantities used to calculate $\langle m\rangle_{Av}$ and $\langle m^2\rangle_{Av}$. The

[11] Atomic Instrument Company Type 204-B (modified) with preamplifier Type 205. The threshold signal level was maintained at 1.2 millivolts. The rise time-decay time setting of the amplifier was 0.2 μsec–0.4 μsec, and examination of the output with a sweep triggered by the counter pulse has shown that the afterpulse due to attached electrons does not get through when this short decay time is used (Cocconi Tongiorgi, Hayakawa, and Widgoff, Rev. Sci. Instr., in press).

TABLE I. Measured rates[a] in principal geometry.[b]

Type of event	Locale		
	Lemp Cave (flat N detector, 333100)	Lemp Cave (efficient N detector, 730000)	Crow Hall (efficient N detector, 730000)
$C^{single}_{multiple}(min^{-1})$	44.01 6.91	44.53 6.98	137.0 15.42
$C:N^{single}_{multiple}(hr^{-1})$	2.28±0.10 0.91±0.06	3.15±0.21 1.31±0.13	14.26±0.28 4.73±0.16
$A^{single}_{multiple}(min^{-1})$	1.50 0.23	1.53 0.23	6.37 0.75
$A:N^{single}_{multiple}(hr^{-1})$	1.03±0.06 0.15±0.02	1.35±0.13 0.18±0.05	7.77±0.20 1.05±0.07
$A:2N^{single}_{multiple}(hr^{-1})$	0.012±0.007 0.012±0.006	0 0.01±0.01	0.41±0.05 0.15±0.03
$A:3N^{single}_{multiple}(hr^{-1})$	0 0.006±0.004	0 0.01±0.01	0.03 ±0.01 0.005±0.005

[a] The neutron coincidence rates are corrected for accidental coincidences.
[b] Pb filter above telescope, paraffin barrier in telescope, Pb absorber in place.

estimated statistical standard deviations are the square roots of the uncorrected numbers of counts divided by the time.

Table II gives the rates used in calculating $\langle m\rangle_{Av}$ and $\langle m^2\rangle_{Av}$ according to (6) and (7). The first, third, and fifth rows correspond to rates listed in the second column of Table I. The other two rows give rates for measurements made with the Pb absorber removed. The first row of Table III gives the result of substituting these figures in (6) and (7), the errors indicated being purely statistical. As explained in Sec. III, the fraction of stoppings corresponding to negative mesons has been taken as 0.44, the coherent neutron detecting efficiency as (1.81±0.06) percent. And in using (7), ϵ_c^2 has been replaced by $0.90\epsilon_c^2$. The value of $\langle m^2\rangle_{Av}-\langle m\rangle_{Av}$ obtained from (7), 3.15±1.84, should be treated with reserve, as it is based on only three counts.

The multiplicity can also be calculated from the data (Table I, third column) obtained with the more efficient neutron detector (730000), with $\epsilon_c=(2.48\pm0.08)$ percent. The result is given in the second row of Table III, errors being stated as in the first row. It is seen to agree very well with that obtained with the geometry thought to be flatter. That is, comparing the two different neutron detecting geometries, the ratio of the rates obtained for Ra-α-Be neutrons is the same, within the statistics, as the ratio of the rates obtained for disintegration neutrons from μ-meson capture in Pb. This can be taken as evidence that the two neutron spectra are similar. During the brief run with the more efficient geometry there were no $\mathbf{A:2N}_s$ events, so that all that can be concluded about $\langle m^2\rangle_{Av}$ on the basis of this run is that it is at least $(2.04\pm0.30)^2$, since in general $\langle m^2\rangle_{Av}>\langle m\rangle_{Av}^2$.

Calculation of $\langle m\rangle_{Av}$ and $\langle m^2\rangle_{Av}$ from the data obtained with only about 240 g cm^{-2} concrete between the Pb filter and the sky (Table I, fourth column, lists some of this data) throws some light on the effect of neutron production in processes other than μ-meson capture on determinations of $\langle m\rangle_{Av}$ and $\langle m^2\rangle_{Av}$. The results are given in the third row of Table III. It is seen that $\langle m\rangle_{Av}$ comes out about 20 percent high. The change in $\langle m^2\rangle_{Av}$ with depth is considerably greater, indicating that in the neutron multiplicity distribution from μ-meson capture there is less of a high multiplicity tail than in the other nuclear interactions that produce $\mathbf{A:N}_s$ events near sea level.

That the separation of "single" telescope events from "multiple" ones has resulted in an increase of the relative contribution of μ-meson capture to the $\mathbf{A:N}$ rate is indicated by two pieces of evidence. Control measurements in the cave made with the paraffin barrier removed show that neutron production in the filter makes no contribution to the $\mathbf{A:N}_s$ rate when the barrier is in place, while some 40 percent of the $\mathbf{A:N}_m$

TABLE II. Rates involved in main multiplicity determination. (Lemp Cave, flat neutron detector, single telescope events.)

Type of event	Counts	Duration (hrs)	Rate, corrected for casuals
$\mathbf{A}_s$ absorber in	29,378	326.15	1.501±0.009 min^{-1}
$\mathbf{A}_s$ absorber out	3683	118.32	0.519±0.009 min^{-1}
$\mathbf{A:N}_s$ absorber in	337	326.15	1.03 ±0.06 hr^{-1}
$\mathbf{A:N}_s$ absorber out	2	118.32	0.016±0.011 hr^{-1}
$\mathbf{A:2N}_s$ absorber in	3	244.79	0.012±0.007 hr^{-1}

rate must be ascribed to interactions in the filter when the barrier is in place. Secondly, in the Crow Hall results, a significant difference is observed in the quantity $\mathbf{A:2N/A:N}$ for "singles" and "multiples." This quantity, which is approximately proportional to the ratio of $\langle m^2\rangle_{Av}$ to $\langle m\rangle_{Av}$ has the value (5.3±0.7) percent for "single" telescope events and (14.3±3.0) percent for the "multiples." Thus, near sea-level the "single" and "multiple" events concern appreciably different distributions of multiplicities.

The experimental result, $\langle m\rangle_{Av}=2.16\pm0.15$, plus possible systematic efficiency error, is not in disagreement with the value 1.4±0.2 reported by Conforto and Sard,[22] since the anticoincidence rate used in their calculation of $\langle m\rangle_{Av}$ was thought to be somewhat higher than the true meson stopping rate. In their experiment, carried out at sea level, a magnetized iron lens designed to focus mesons was used to eliminate the protonic and electronic contributions to $\mathbf{A:N}$.

[22] A. Conforto and R. D. Sard, Phys. Rev. **82**, 335 (1951).

A similar investigation has recently been reported by Groetzinger, Berger, and McClure[23] using a magnetized iron lens to focus mesons and a neutron detecting arrangement somewhat similar to the high efficiency 730000 geometry described above. However, the low counting rate obtained with this arrangement resulted in a lower statistical accuracy, the result being stated as $\langle m\rangle_{Av}=1.96\pm0.72$ (probable error).

Recently, Cocconi and Cocconi-Tongiorgi[14,24] have carried out measurements of the neutron counting rates of various multiplicities (**N**, **2N**, **3N**, $\cdots$) when a Pb block surrounded by a paraffin-BF_3 counter system is held at various depths under water. They did not measure neutrons correlated with charged particles. On the basis of assumptions about the relative frequencies of occurrence and the neutron multiplicity distributions for the various processes giving rise to neutrons, they arrive at $\langle m\rangle_{Av}=2\pm0.5$. The agreement of this published estimate[14] with our more directly measured value can be considered as supporting evidence for the assumptions made by the Cocconi's.

It is noted in passing that comparison of the rates in the second and fourth rows of Table I confirms the previous evidence,[25] obtained at a shallower site, for neutron production in lead by fast μ-mesons. This question will be discussed in detail elsewhere.

VI. THE THEORETICALLY EXPECTED MULTIPLICITIES

Two possible meson-nucleon interactions have been considered. The first is that of the Yukawa particle, which gives all its rest-energy to the proton with which it interacts. The capturing nucleus then receives an excitation energy of about 100 Mev. Fujimoto and Yamaguchi[26] have calculated the disintegration of a capturing silver nucleus in this case. Taking into account the competition between neutron emission and charged particle emission at each step of the reaction, they find that on the average the reaction should lead to the emission of altogether 1.0 protons and 4.7 neutrons. Because of the higher Coulomb barrier in the Tl nucleus, it seems reasonable to expect an average of about 6 neutrons emitted in the reaction studied here. This result is entered in the fourth row of Table III.

The other interaction considered is that in which the encounter of a μ-meson with a nuclear proton results in a neutron and a light "thief" particle. Tiomno and Wheeler as well as Rosenbluth[12] have calculated the distribution function for the excitation energy, treating the nucleus as a confined Fermi gas. The function rises to a peak at about 15-Mev excitation energy and then falls rapidly to zero at about 20 Mev. It is necessary to translate this distribution function for excitation energy into one for number of neutrons emitted. The first step is to assume that proton emission is excluded, and that neutron emission occurs and re-occurs until the residual excitation of the nucleus falls below the binding energy of the last neutron, after which only γ-emission takes place. This assumption seems to be consistent with present knowledge regarding the level widths for possible competing emission processes and, moreover, leads to an upper limit for the predicted neutron multiplicity for a given distribution of initial excitations. In this connection, comparison of the distribution of excitation energy calculated on the "free-particle" model with that calculated by Tiomno and Wheeler[12] on the "dipole" model suggests that the former tends to overestimate the excitation. Thus the following calculation probably errs on the side of generosity in its predictions for $\langle m\rangle_{Av}$ and $\langle m^2\rangle_{Av}$.

The neutron multiplicity distribution is derived from the distribution function of initial excitation energy of the compound nucleus, $f(A;Q_0)$, by means of the function $g(Z,A;Q,\epsilon)$, giving the probability that a nucleus (Z,A) with excitation energy Q emits a neutron of kinetic energy in unit energy interval at ϵ. In effect, the probability of residual excitation in dQ_1 at Q_1 after emission of one neutron is

$$f(A-1;Q_1)dQ_1 = dQ_1\int_{Q_0>BE(Z,A)+Q_1} dQ_0 f(A;Q_0) \times g(Z,A-1;Q_0,Q_0-BE(Z,A)-Q_1), \quad (12)$$

where $Z=81$ for capture in Pb and $BE(Z,A)$ is the binding energy of a neutron in the nucleus (Z,A). The function $g(Z,A;Q,\epsilon)$ is normalized to 1 when integrated with respect to ϵ from $\epsilon=0$ to $\epsilon=Q-BE$. The probability of residual excitation in dQ_2 at Q_2 after

TABLE III. Mean and mean square neutron multiplicity from μ-meson capture in lead.[a]

	$\langle m\rangle_{Av}$	$\langle m^2\rangle_{Av}$
Experimental (Lemp Cave, flat neutron detector, single telescope events)	2.16±0.15	5.3±1.9
Experimental (Lemp Cave, efficient neutron detector, single telescope events)	2.04±0.21	>4.2±0.9
Apparent experimental (Crow Hall, efficient neutron detector, single telescope events)	2.57±0.11	14.8±1.5
Theoretical, for excitation energy of 100 Mev[b]	6	>36
Theoretical, for $\mu^-+P\to N+\nu$, assuming free-particle model for excitation and statistical theory for evaporation	0.95	1.3

[a] The errors indicated for the experimental values are estimated statistical standard errors. They do not include systematic errors such as the estimated ±10 percent uncertainty in the strength of the neutron source used in the efficiency determination.
[b] See reference 26.

[23] Groetzinger, Berger, and McClure, Phys. Rev. **81**, 969 (1951).
[24] G. Cocconi, private communication to R. D. Sard.
[25] R. D. Sard, Phys. Rev. **80**, 134 (1950); Sard, Crouch, Jones, Conforto, and Stearns, Nuovo cimento **8**, 326 (1951).
[26] Y. Fujimoto and Y. Yamaguchi, Prog. Theor. Phys. **4**, 468 (1949); **5**, 787 (1950).

TABLE IV. Neutron binding energies and mass difference energies.

Capturing isotope	Abundance (%)	Tl-Pb mass difference energy[a] (Mev)	B. E. of first neutron[b] (Mev)	B. E. of second neutron[b] (Mev)	B. E. of third neutron[b] (Mev)
Pb^{206}	23.6	1.7	6.23	7.48	6.54
Pb^{207}	22.6	1.5	6.97	6.23	7.48
Pb^{208}	52.3	5.0	3.86	6.97	6.23

[a] See reference 30. [b] See reference 29.

emission of two neutrons is, similarly,

$$f(A-2;Q_2)dQ_2$$

$$=dQ_2\int_{Q_1>BE(Z,A-1)+Q_2} dQ_1 f(A-1;Q_1)$$

$$\times g(Z,A-1;Q_1,Q_1-BE(Z,A-1)-Q_2), \quad (13)$$

and so forth. The probability, a_m, of emitting m neutrons altogether is given by (14) and (15):

$$a_0=\int_{Q_0=0}^{BE(Z,A)} dQ_0 f(A;Q_0), \quad (14)$$

$$a_m=\left(1-\sum_{k=0}^{m-1}a_k\right)\int_{Q_m=0}^{BE(Z,A-m)} dQ_m f(A-m;Q_m). \quad (15)$$

We use for the function g the expression given by Weisskopf[27] in his statistical theory.

$$g(Z,A;Q,\epsilon)=C\epsilon\exp[-(a/\{Q-BE(Z,A)\})^{\frac{1}{2}}\epsilon], \quad (16)$$

the normalization determining C. According to Blatt and Weisskopf,[28] the value of a giving the best agreement with experiment for heavy nuclei is 10 Mev^{-1}. Table IV lists the values we have adopted for the neutron binding energy[29] in the various Tl isotopes, and for the mass difference energy[30] which is needed to build a Tl nucleus from its Pb isobar. This latter energy must be subtracted from Tiomno and Wheeler's Q values to get the true available initial excitation energy Q_0. Table V lists the computed values for the a_m, the integrations indicated in (12), (13), (14), and (15) having been done graphically with a planimeter. The values found for the coefficients a_m seem to be consistent with Wheeler's assertion that on the basis of the charge-exchange reaction emission of 2 neutrons would occur occasionally, whereas 3 would be most rare.[31] Table V also gives the values of $\langle m\rangle_{Av}$ and $\langle m^2\rangle_{Av}$ computed from these a_m. For comparison with the experimental results, these computed values of $\langle m\rangle_{Av}$ and $\langle m^2\rangle_{Av}$ are also entered in the last row of Table III.

VII. CONCLUSIONS

The mean number of disintegration neutrons produced when a Pb nucleus captures a negative μ-meson is found to be 2.16 ± 0.15, with ±10 percent additional systematic error due to the uncertainty in the strength of the standard neutron source used to determine the neutron detecting efficiency.

Despite the poor statistics available for the determination of the mean squared neutron multiplicity (3 events), it is clear that $\langle m^2\rangle_{Av}$ does not greatly exceed $\langle m\rangle^2_{Av}$. This contrasts with the results obtained near sea-level, where $\langle m\rangle_{Av}=2.6\pm0.1$, and $\langle m^2\rangle_{Av}=14.8\pm1.5$, indicating that the neutron multiplicity distribution from μ-meson capture has a considerably less pronounced high multiplicity tail than does the distribution from the other processes occurring at the shallower depth.

TABLE V. Theoretical results, using free-particle model and statistical theory.

Capturing isotope	a_m = probability per capture, of emitting m neutrons				Mean number of neutrons m_{Av}	Mean square number of neutrons m^2_{Av}
	$m=0$	$m=1$	$m=2$	$m=3$		
Pb^{206}	0.199	0.643	0.158	0	0.96	1.28
Pb^{207}	0.128	0.627	0.245	0	1.12	1.61
Pb^{208}	0.245	0.628	0.127	0	0.88	1.14
Average, weighted according to normal abundance	0.207	0.631	0.161	0	0.95	1.28

The result $\langle m\rangle_{Av}=2.16\pm0.15$, clearly rules out the Yukawa-type interaction, and is therefore consistent with the findings of the various investigators who have searched for charged particles associated with negative μ-meson capture. On the other hand, while the general picture of the charge-exchange reaction with its light "thief" particle carrying away most of the rest energy is substantiated, the observed value of $\langle m\rangle_{Av}$ is markedly higher than the value 0.95 predicted on the basis of the free-particle model (for the calculation of the excitation) and the statistical evaporation theory (for the calculation of the neutron emission). A more refined theoretical calculation is needed to decide whether the discrepancy is fundamental, revealing inadequacy of the assumed $\mu^-+P\rightarrow N+\nu$ mechanism, or whether it simply results from the approximations made in the calculation.

VIII. ACKNOWLEDGMENTS

The authors wish to express thanks to Professors H. Primakoff and E. Feenberg for helpful discussions of nuclear reaction theory.

It is also a pleasure to express thanks to Mr. Jen Pu

[27] V. F. Weisskopf, Phys. Rev. **52**, 295 (1937).
[28] J. M. Blatt and V. F. Weisskopf, "The theory of nuclear reactions," Sec. 6A, Massachusetts Institute of Technology Laboratory of Nuclear Science and Engineering Technical Report No. 42, May 1, 1950.
[29] J. A. Harvey, Phys. Rev. **81**, 353 (1951).
[30] R. Gregoire, *Constantes Selectionnées de Physique Nucleaire* (Hermann et Cie., Paris, 1948).
[31] Proceedings of the Echo Lake Cosmic-Ray Symposium, 1949 (ONR). Discussion of paper 7, p. 29.

Cheng for the preparation of some of the Geiger-Müller counters, to Dr. Harold A. Bulger of the Washington University Medical School for the many hours of his time which he contributed in the search for a suitable underground location, to the National Bureau of Standards for calibrating the large Ra-α-Be source, to Mr. Arthur H. Benade for performing a relative calibration of the two Ra-α-Be sources, and to Mr. J. D. Campbell, of the International Shoe Company, for permission to use the Lemp Cave site.

We are very greatly indebted to Mr. John D. Miller for his excellent work in constructing the electronic equipment and for his invaluable help in installing the equipment in the underground location.

PHYSICAL REVIEW VOLUME 85, NUMBER 1 JANUARY 1, 1952

Eigenvalue Problem in Quantum Electrodynamics*

MAURICE NEUMAN
Brookhaven National Laboratory, Upton, Long Island, New York
(Received September 17, 1951)

The eigenvalue problem in quantum electrodynamics is discussed from the point of view of the Fredholm theory of integral equations. Starting with positron theory—the theory of a quantized Dirac field interacting with an external field only—the external potentials are replaced by bare photon fields. To insure causality the photon operators are ordered in time. Certain integral equations for the Fredholm minors constructed on the Feynman kernel are taken to be the equations for the wave functions of n particle systems. An expansion in interaction patterns rather than the coupling constant is indicated. The one particle problem is treated in the first pattern approximation. Procedures proposed by Snyder and Snow and the mass renormalization scheme are discussed in this connection. Finally a purely formal derivation of the Bethe-Salpeter equation for the two-body problem in the lowest pattern approximation is given.

I. INTRODUCTION

SEVERAL new attempts[1,2] have been made recently to deduce from a field theory the equations for a system of two Dirac particles in interaction. The problem has been approached from the point of view of the S matrix[1] and by a formal extension of the theory of Green's functions.[2] The difficulties of a rigorous deduction of these equations have been emphasized by Nambu.[3] Work in this direction has therefore been either purely formal or largely heuristic.

Using arguments of the same character, it is intended to provide in this note additional motivation for the acceptance of certain equations as approximate descriptions of bound systems. The mathematical imagery employed is that of the Fredholm theory of integral equations. Intuition is relied on to extract from it a workable set of equations for one, two, and many body problems.

In brief outline the procedure is the following. We first investigate an electron-positron field subject to an external electromagnetic field only. The integral equation considered is that of a scattering problem with an inhomogeneous term corresponding to the wave function of a free particle in the absence of the external field. The associated homogeneous integral equation may have nontrivial solutions, if certain relations between the energy, the mass and the charge are satisfied. These represent the bound states of the system. The restrictions on the values of the parameters are expressed by the requirement that the Fredholm determinant constructed on the kernel vanish. The wave function of the system is then given by the first Fredholm minor. If for a particular relation between the energy, the mass and the charge the determinant as well as the first minor are identically zero the solution of the equation is given by the second minor, if this quantity does not vanish. The second minor is antisymmetric in its two indices and satisfies the homogeneous equation independently in both. It is therefore the wave function for a two-particle noninteracting system. The external field is now replaced by a quantized electromagnetic field satisfying Maxwell's equations without sources. If a radiation field of such character is to give rise to a causal interaction between charged particles the photon operators must be chronologically ordered[4] and an expectation value relative to a state without photons taken. An expansion in various patterns of interaction, rather then in the coupling constant is then carried out and the effective potentials that arise out of various modes of interaction are isolated. The Bethe-Salpeter equation is obtained in the lowest pattern approximation.

II. ALGEBRAIC PRELIMINARIES

The Fredholm theory in its conventional form is somewhat clumsy for our purpose. Our first task will

* Research carried out under the auspices of the AEC.
[1] H. A. Bethe and E. E. Salpeter, Phys. Rev. **82**, 309 (1951); M. M. Gellman and F. Low, Phys. Rev. **84**, 350 (1951).
[2] J. Schwinger, Proc. Nat. Acad. Sci. **37**, 452 (1951).
[3] Y. Nambu, Prog. Theor. Phys. **5**, 614 (1950).
[4] M. Fiertz, Helv. Phys. Acta **23**, 731 (1950).

therefore be to find operational expressions for the Fredholm minors. The integral equations that they satisfy will then be immediately evident from these representations.

We consider a set of operators $A_1, A_2, \cdots A_n$. Let a typical matrix element of anyone of these be denoted by $\langle x|A|y\rangle$. The symbol A_1A_2 stands for an operator whose matrix element $\langle x|A_1A_2|y\rangle$ is $\langle x|A_1|\tau\rangle\langle\tau|A_2|y\rangle$, where the repeated variable τ is being summed or integrated over. We similarly define a symbol (a cross product) $A_1\times A_2$ with a matrix element

$$\langle x_1x_2|A_1\times A_2|y_1y_2\rangle=\epsilon^{ij}\langle x_1|A_1|y_i\rangle\langle x_2|A_2|y_j\rangle. \quad (1)$$

The letter ϵ^{ij} is here the familiar alternating symbol. Associated with $A_1\times A_2$ is an operator $A_1\times A_2{}^+$ whose matrix element is given by the expression,

$$\langle x_1x_2|A_1\times A_2{}^+|y_1y_2\rangle=\epsilon^{ij}\langle x_i|A_1|y_1\rangle\langle x_j|A_2|y_2\rangle. \quad (2)$$

In general

$$\langle x_1\cdots x_n|A_1\times\cdots\times A_n|y_1\cdots y_n\rangle = \epsilon^{i(1)\cdots i(n)}\langle x_1|A_1|y_{i(1)}\rangle\cdots\langle x_n|A_n|y_{i(n)}\rangle \quad (1')$$

and

$$\langle x_1\cdots x_n|A_1\times\cdots\times A_n{}^+|y_1\cdots y_n| = \epsilon^{i(1)\cdots i(n)}\langle x_{i(1)}|A_1|y_1\rangle\cdots\langle x_{i(n)}|A_n|y_n\rangle. \quad (2')$$

If $A_1=\cdots=A_n=A$ we shall write

$$A_1\times\cdots\times A_n=[A\times]^n.$$

It is readily seen that

$$[A\times]^{n+}=[A\times]^n.$$

We now define scalar operator multiplication into a cross product of two operators. Thus

$$\langle x_1x_2|A\cdot A_1\times A_2|y_1y_2\rangle=\langle x_1|A|\tau\rangle\langle\tau x_2|A_1\times A_2|y_1y_2\rangle, \quad (3)$$

$$\langle x_1x_2|A.A_1\times A_2|y_1y_2\rangle=\langle x_2|A|\tau\rangle\langle x_1\tau|A_1\times A_2|y_1y_2\rangle. \quad (4)$$

Making use of (1) we then obtain

$$A\cdot A_1\times A_2=AA_1\times A_2, \quad (3')$$

$$A.A_1\times A_2=A_1\times AA_2. \quad (4')$$

Scalar postmultiplication is defined for $A_1\times A_2{}^+$:

$$A_1\times A_2{}^+\cdot A=A_1A\times A_2{}^+, \quad (5)$$

$$A_1\times A_2{}^+.A=A_1\times A_2A^+. \quad (6)$$

The extension of these definitions to a cross product of n operators (1′), (2′) is obvious. The Fredholm theory can now be placed in this algebraic framework.

III. OPERATIONAL FORM OF THE FREDHOLM THEORY

The integral equation,

$$\psi=\phi+\lambda K\psi, \quad (7)$$

is solved by

$$\phi=\psi-\lambda[\Delta^{(0)}(\lambda)]^{-1}\Delta^{(1)}(\lambda)\phi, \quad (8)$$

where $\Delta^{(0)}(\lambda)$ is the Fredholm determinant and $\Delta^{(1)}(\lambda)$ the first minor. The operational expressions for these quantities are

$$\Delta^{(0)}(\lambda)=\exp[Tr\log(1-\lambda K)], \quad (9)$$

$$\Delta^{(1)}(\lambda)=[1-\lambda K]^{-1}K\exp[Tr\log(1-\lambda K)]. \quad (10)$$

From these representations one readily infers that

$$Tr\,\Delta^{(1)}(\lambda)=-\Delta^{(0)\prime}(\lambda), \quad (11)$$

$$\Delta^{(1)}(\lambda)=K\Delta^{(0)}(\lambda)+\lambda K\Delta^{(1)}(\lambda) = K\Delta^{(0)}(\lambda)+\lambda\Delta^{(1)}(\lambda)K, \quad (12)$$

where $\Delta^{(0)\prime}(\lambda)$ is the derivative of the determinant with respect to λ. It is seen from (12) that if $\Delta^{(0)}(\lambda)=0$, then $\Delta^{(1)}(\lambda)$ is a solution of the homogeneous equation associated with (7).

The second Fredholm minor may be defined operationally as

$$\Delta^{(2)}(\lambda)=[[1-\lambda K]^{-1}KX]^2\exp[Tr\log(1-\lambda K)]. \quad (13)$$

The well-known properties of this operator

$$Tr\,\Delta^{(2)}(\lambda)=\Delta^{(0)\prime\prime}(\lambda),$$

$$\Delta^{(2)}(\lambda)=K\times\Delta^{(1)}(\lambda)+\lambda K\cdot\Delta^{(2)}(\lambda), \quad (14a)$$

$$\Delta^{(2)}(\lambda)=\Delta^{(1)}(\lambda)\times K+\lambda K.\Delta^{(2)}(\lambda), \quad (14b)$$

$$\Delta^{(2)}(\lambda)=K\times\Delta^{(1)}(\lambda)^+ +\lambda\Delta^{(2)}(\lambda)\cdot K, \quad (15a)$$

$$\Delta^{(2)}(\lambda)=\Delta^{(1)}(\lambda)\times K^2+\lambda\Delta^{(2)}(\lambda).K \quad (15b)$$

are readily deduced with the aid of the formulas given in the previous section.

IV. THE EXTERNAL ELECTROMAGNETIC FIELD

The equation we shall consider is

$$\psi=\psi_0+eK\psi \quad (16)$$

with

$$\langle\alpha x|K|\beta x'\rangle=iS_{\alpha\sigma}F(xx')\gamma_{\sigma\beta}{}^\mu A_\mu(x'). \quad (17)$$

If A_μ is independent of time one readily sees that the boundary conditions incorporated into (16) with $\psi_0=0$ are the correct ones for a bound state. The Fredholm minors constructed on this kernel involve two parameters e and κ. We shall denote them bu $\Delta^{(n)}(e,\kappa)$. These are related to quantities appearing in the S matrix theory by

$$\langle x_1\alpha_1\cdots x_n\alpha_n|\Delta^{(n)}|y_1\beta_1\cdots y_n\beta_n\rangle = \Big[\phi_0,\ T\psi_{\alpha(1)}(x_1)(\bar\psi(y_1)\gamma^\mu)_{\beta(1)}A^\mu(y_1)\cdots \times\psi_{\alpha(n)}(x_n)(\bar\psi(y_n)\gamma^\nu)_{\beta(n)}A^\nu(y_n) \times\exp\Big(-i\int_{-\infty}^{+\infty}H(x')dx'\Big)\phi_0\Big], \quad (18)$$

where ϕ_0 is the vacuum state; $H(x)$, the interaction hamiltonian and T the temporal ordering operator. This

relation was shown[5] to hold for $\Delta^{(0)}$:

$$\Delta^{(0)}(e,\kappa)=(\phi_0, S\phi_0). \tag{19}$$

With the operational representations developed in the previous sections similar relations may be shown to obtain for the higher Fredholm minors. That a quantity constructed on a Feynman kernel is related to one appearing in the solution of an integral equation with retarded boundary conditions is not too surprising. Somewhat similar relations were noticed by Jost and Pais in their treatment of the nonrelativistic problem.[6] Equation (16) with $\psi_0=0$ is equivalent to the conventional formulation of the bound state problem. If A_μ is independent of x_0, Eq. (16) has translational symmetry in time. We may therefore look for solutions of the type $\psi(\mathbf{r})\exp[-ik_0x_0]$. For sufficiently localized potentials it is then seen that $\psi(\mathbf{r})$ has a clear-cut asymptotic behavior. If $k_0^2>\kappa^2$, $\psi(\mathbf{r})\sim\exp[i(k_0^2-\kappa^2)^{\frac{1}{2}}r]$ while if $k_0^2<\kappa^2$, $\psi(\mathbf{r})\sim\exp[-(\kappa^2-k_0^2)^{\frac{1}{2}}r]$. In the first case the potential acts as a source of outgoing waves in the second we have a particle bound by the external field. The existence of these solutions will depend on whether certain relations between k_0^2, κ^2 and e can be satisfied.

In the next sections we shall work with equations that have translational invariance not only in time but also in space. The relations that will have to be satisfied will then involve the effective mass $-k_\mu k_\mu$ the mechanical mass κ^2 and the charge e.

Equation (16) is a well-defined integral equation even if the external potentials do depend on the time. The restrictions on e and κ that are necessary for the existence of a solution of the homogeneous integral equation are expressed by

$$\Delta^{(0)}(e,\kappa)=0. \tag{20}$$

With the parameters so restricted the solution is then given according to (12) by $\langle x|\Delta^{(1)}(e,\kappa)|y\rangle$, since then

$$\Delta^{(1)}(e,\kappa)=eK\Delta^{(1)}(e,\kappa). \tag{21}$$

If this quantity should vanish identically for the particular values of e amd κ we may obtain a solution (according to (14) satisfying the two integral equations,

$$\Delta^{(2)}(e,\kappa)=eK\cdot\Delta^{(2)}(e,\kappa), \tag{22a}$$

$$\Delta^{(2)}(e,\kappa)=eK.\Delta^{(2)}(e,\kappa). \tag{22b}$$

We observe that

$$\langle x_1x_2|\Delta^{(2)}(e,\kappa)|y_1y_2\rangle=-\langle x_2x_1|\Delta^{(2)}(e,\kappa)|y_1y_2\rangle.$$

This quantity may therefore be taken as the wave function for two noninteracting Dirac particles subject to an external electromagnetic field.

V. THE QUANTIZED RADIATION FIELD

Equations (21) and (22) are now taken to hold even if the external field is replaced by photon operators. To introduce the action of a particle on itself or the interaction between particles we order the photon operators in time and take the expectation value of both sides relative to a state in which no photons are present. The photon operators are taken to satisfy Maxwell's equations without sources. Such operators commute among themselves inside a temporally ordered bracket.

We shall treat the simpler equation (21) in some detail. Writing $\psi(x)$ for $\langle x|\Delta^{(1)}(e,\kappa)|y\rangle$ with y fixed we have

$$\psi=e^2K^2\psi. \tag{23}$$

The iteration procedure is now carried out in the following fashion

$$\begin{aligned}\langle\psi\rangle&=e^2\langle K^2\psi\rangle\\&=e^2\langle K^2\rangle\langle\psi\rangle+e^4[\langle K^4\psi\rangle-\langle K^2\rangle\langle K^2\psi\rangle]\\&=e^2\langle K^2\rangle\langle\psi\rangle+e^4[\langle K^4\rangle-\langle K^2\rangle\langle K^2\rangle]\langle\psi\rangle\\&\quad+e^6[\langle K^6\psi\rangle-\langle K^2\rangle\langle K^4\psi\rangle-\langle K^4\rangle\langle K^2\psi\rangle\\&\qquad+\langle K^2\rangle\langle K^2\rangle\langle K^2\psi\rangle]=\cdots.\end{aligned} \tag{24}$$

The bracket $\langle\ \rangle$ denotes here vacuum expectation values as well as ordering of photon operators with respect to time. Retaining the first two terms of this expansion we have

$$\begin{aligned}\langle\psi(x)\rangle=&-ie^2\int S^F(x,\tau)\gamma^\mu S^F(\tau y)\gamma^\mu\\&\times D^F(\tau y)\langle\psi(y)\rangle d\tau dy\\&-e^4\int S^F(x\tau_1)\gamma^\mu S^F(\tau_1\tau_2)\gamma^\nu S^F(\tau_2\tau_3)\gamma^\mu\\&\times S^F(\tau_3 y)\gamma^\nu D^F(\tau_1\tau_3)D^F(\tau_3 y)\langle\psi(y)\rangle d\tau d\tau dy.\end{aligned} \tag{25}$$

The form of the interaction becomes clearer when we go over to the differential equation,

$$\begin{aligned}\left(\gamma\frac{\partial}{\partial x}+\kappa\right)\langle\psi(x)\rangle=&-e^2\int V^{(2)}(xy)\langle\psi(y)\rangle dy\\&-e^4\int V^{(4)}(xy)\langle\psi(y)\rangle dy,\end{aligned}$$

where

$$\begin{aligned}V^{(2)}(xy)&=i\gamma^\mu S^F(xy)\gamma^\mu D^F(xy)\\V^{(4)}(xy)&=\int\gamma^\mu S^F(x\tau_1)\gamma^\nu S^F(\tau_1\tau_2)\gamma^\mu S^F(\tau_2 y)\gamma^\nu\\&\qquad\times D^F(x\tau_2)D^F(\tau_1 y)d\tau.\end{aligned} \tag{26}$$

We have thus isolated the "self-energy potential" acting on the electron due to its interaction with the bare radiation field. Evidently $V^{(2)}$ and $V^{(4)}$ are due to interaction patterns given in Figs. 1(a) and 1(b), respectively. It will be noticed that interactions of the type illustrated in Figs. 1(c) and 1(d) will not appear

[5] M. Neuman, Phys. Rev. **83**, 1258 (1951).
[6] R. Jost and A. Pais, Phys. Rev. **82**, 840 (1951).

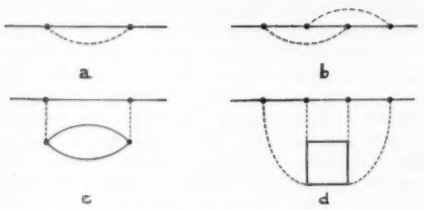

FIG. 1. Interaction patterns for the one-particle problem.

in this formulation. The reason of their absence is the fact that we replaced the external field by a bare photon field satisfying Maxwell's equations without sources. A radiation field of this nature is linear. The virtual photons do not polarize the vacuum and do not scatter each other.

We shall now discuss the self-energy of the electron in the first pattern approximation. Equation (25) is readily seen to have translational symmetry under displacements in space as well as in time. In accordance with the remarks of the previous section we therefore look for relations between the invariant quantity $p_\mu p_\mu$ and the parameters e and κ. More precisely, we try to determine the effective mass of the electron when the particle is subject to a potential arising from the emission and subsequent reabsorption of a single photon. The fourier transform of (25) (retaining only the first term on the right side of this equation) is given by

$$\psi(p)=-4i\alpha(2\pi)^{-3}[p^2+\kappa^2-i\epsilon]^{-1}\phi(p)\psi(p) \quad (27)$$

where

$$\phi(p)=\int_0^1 dx_1\int_0^1 dx_2\delta(x_1+x_2-1)(i\gamma p-\kappa)(i\gamma p x_2+2\kappa)$$
$$\times\int d^4k[k^2+p^2x_1x_2+\kappa^2x_1-i\epsilon]^{-2}. \quad (28)$$

Writing

$$[k^2+p^2x_1x_2+\kappa^2x_1-i\epsilon]^{-2}$$
$$=\int_{\kappa^2}^{\infty} dM 2x_1[k^2+p^2x_1x_2+Mx_1-i\epsilon]^{-3} \quad (29)$$

we immediately obtain

$$[p^2+\kappa^2-i\epsilon]^{-1}\kappa 2\gamma p\psi(p)=[\pi^{-1}\alpha\chi^{(1)}]^{-1}$$
$$\times[1+\pi^{-1}\alpha[\chi^{(0)}-(p^2+\kappa^2)^{-1}p^2\chi^{(1)}]]\psi(p) \quad (30)$$

with

$$\chi^{(0)}=\int_{\kappa^2}^{\infty} dM(p^2)^{-1}\log[(M-i\epsilon)^{-1}(p^2+M-i\epsilon)]$$
$$\underset{\lambda\to\infty}{\approx} \log\lambda+\text{finite terms}, \quad (31a)$$

$$\chi^{(1)}=\chi^{(0)}-(1/2)\int_{\kappa^2}^{\infty} dM(p^2)^{-1}[1-(p^2)^{-1}M$$
$$\times\log[(M-2\epsilon)^{-1}(p^2+M-i\epsilon)]]$$
$$\underset{\lambda\to\infty}{\approx} (3/4)\log\lambda+\text{finite terms}. \quad (31b)$$

In the conventional treatment of the self-energy one replaces $i\gamma p$ in (30) by $-\kappa$ and obtains a linear equation in p^2 with the root

$$\kappa^{-2}p^2=-[1+\pi^{-1}\alpha(\chi^{(0)}-\chi^{(1)})]^{-1}[1+\pi^{-1}\alpha(\chi^{(0)}+\chi^{(1)})]$$
$$\underset{\lambda\to\infty}{\approx} -[1+(4\pi)^{-1}\alpha\log\lambda]^{-1}$$
$$\times[1+(4\pi)^{-1}7\alpha\log\lambda]$$
$$\underset{\lambda\to\infty}{\approx} -[1+(2\pi)^{-1}3\alpha\log\lambda]. \quad (32)$$

The right member of (32) agrees with the expression conventionally given for the self-energy of the electron in the α-approximation. In the pattern approximation, however, neither the replacement nor the expansion are legitimate. It is therefore necessary to iterate (24) which leads to an equation for p^2 of the form,

$$-[p^2+\kappa^2]^{-2}p^2\kappa^2=[\pi^{-1}\alpha\chi^{(1)}]^{-2}$$
$$\times[1+\pi^{-1}\alpha[\chi^{(0)}-(p^2+\kappa^2)^{-1}p^2\chi^{(1)}]]^2. \quad (33)$$

According to the evaluations (31a) and (31b) of $\chi^{(0)}$ and $\chi^{(1)}$ as $\lambda\to\infty$ the left side of 33 approaches a finite value. The roots of (33) become

$$\kappa^{-2}p^2=-(17/2)\pm 4[(17/8)^2-1]^{\frac{1}{2}}. \quad (34)$$

It is clear that the number of roots will increase with the number of photons involved in the interaction. In this treatment of the one-body problem some of the degrees of freedom of the radiation field are apparently transferred to the particle.

No physical significance is of course to be attached to the numbers appearing in Eq. (34). They merely reflect the difficulties that are encountered in an attempt to treat a one-body problem along the same lines as a two-particle system. An electron with a definite mechanical mass could apparently under the influence of its interaction with the vacuum fluctuations of the electromagnetic field assume any one of a large number of experimentally observable masses. This difficulty is by no means peculiar to the quantum theory of fields. Its classical counterpart is the appearance of time derivatives of high order in the equation of motion of an electron interacting with its own radiation field. It has been suggested by Snyder and Snow[7] that ambiguous quantities like $\chi^{(0)}$ and $\chi^{(1)}$ should be subjected to suitable limiting processes and evaluated to yield zero. An examination of (33) shows indeed that the difficulty of multiple roots could be removed in this manner. However, the order of the divergence of an

[7] H. S. Snyder, Phys. Rev. **78**, 95 (1950); Phys. Rev. **79**, 520 (1950); G. Snow and H. S. Snyder, Phys. Rev. **80**, 987 (1950).

expression, even though it can be changed by certain rearrangements, and limiting processes, is a well-defined mathematical concept and the reasons for the appearance of divergent quantities in the particular physical framework on which our theories are based is rather clear. It therefore seems to the author that such forceful methods, even though they formally might solve the problem in this particular case, could hardly be considered as removing the physical difficulty.

The renormalization scheme is an attempt to extract from expressions relating to real processes the terms reflecting the change produced in the inertial properties of the electron due to its interaction with the electromagnetic field. In contrast to the suggestions advanced in reference 7, the order of divergence and the form of various ambiguous quantities is respected and their cancellation after renormalization is noted in each power of the coupling constant. From the point of view outlined in this note that the physical arguments advanced in favor of renormalization may be objected to on the grounds that they disregard the question of transfer of degrees of freedom from the radiation to the matter field and that this aspect should also be taken into account, if the conventional treatment of divergent expressions is being adhered to. One would therefore be inclined to look upon renormalization as a tentative formal prescription, as has been emphasized by many workers in this field, applicable to a class of problems which can be treated in terms of an expansion in powers of the coupling constant, rather than the taking into account of a real physical change that would be produced in the effective mass of the electron if the bare particle were subject to the action of the vacuum fluctuations of the electromagnetic field. Whatever its logical merits, once this rather simple prescription is accepted and a certain computational technique consistently adhered to, finite and unambiguous answers emerge in every power of the coupling constant. It should be quite clear that the class of rearrangements to which the divergent expression are subjected in this scheme are from a purely mathematical point of view no more legitimate than other classes that could easily accomplish the opposite purpose: turn the theory into a completely meaningless array of symbols. Whether one could admit all possible rearrangements of ambiguous expressions and still extract from the theory anything meaningful using sounder physical criteria. as has been attempted in the work cited in reference 7 is an open question. These attempts, however, do emphasize the fact that divergent expressions are indeed ambiguous quantities, and therefore a theory involving them can only be regarded as a tentative prescription, that procedures alternate to the ones that accomplish the isolation of singularities are also possible and are mathematically no less legitimate, and that attempts to resolve the ambiguities on a sounder theoretical basis encounter great difficulties.

We shall now give a purely formal derivation of the Bethe-Salpeter[1] equation in the approximation in which a single photon gives rise to the potentials. The interaction pattern is easily visualized and the symbolic expression corresponding to it is obtained by combining Eqs. (22a) and (22b) and is of the form

$$\Delta^{(2)}=e^2\langle K\cdot K.\rangle\Delta^{(2)}. \tag{35}$$

Denoting the matrix elements of Δ^2 with y_1, and y_2 fixed by

$$\langle x_1x_2|\,\Delta^{(2)}\,|y_1y_2\rangle=\psi_{\alpha(1)\alpha(2)}(x_1x_2)$$

Eq. (35) assumes the explicit form

$$\psi_{\alpha(1)\alpha(2)}(x_1x_2)$$

$$=-ie^2\int[S^F(x_1\tau_1)\gamma^\mu]_{\alpha(1)\beta(1)}[S^F(x_2\tau_2)\gamma^\mu]_{\alpha(2)\beta(2)}$$

$$\times D^F(\tau_1\tau_2)\psi_{\beta(1)\beta(2)}(\tau_1\tau_2)d\tau. \tag{36}$$

The corresponding differential equation is

$$\left(\gamma^{(1)}\frac{\partial}{\partial x_1}+\kappa\right)_1\left(\gamma^{(2)}\frac{\partial}{\partial x_2}+\kappa\right)_2\psi(x_1x_2)$$

$$=-ie^2\gamma^{(1)}\gamma^{(2)}D^F(x_1x_2)\psi(x_1x_2). \tag{37}$$

In (37) $\gamma^{(1)}$ acts and the first, $\gamma^{(2)}$ on the second set of spinor indices of $\psi(x_1x_2)$. These operators therefore commute. Other iterations of Eqs. (22) giving rise to potentials due to a single photon in the field

$$\Delta^{(2)}=e^2\langle K\cdot K^{\cdot}\rangle\Delta^{(2)}, \tag{38a}$$

$$\Delta^{(2)}=e^2\langle K.K.\rangle\Delta^{(2)} \tag{38b}$$

are, of course, also possible. The meaning, consistency, and extensions of these equations to include more complex interaction patterns are currently being investigated.

The author would like to thank Dr. H. S. Snyder for his interest in this work and for many illuminating discussions regarding his views on the divergent aspects of field theory. He is also grateful to Doctors E. J. Kelly, R. Serber, G. Snow, and F. Villars for many stimulating conversations.

Letters to the Editor

PUBLICATION of brief reports of important discoveries in physics may be secured by addressing them to this department. The closing date for this department is five weeks prior to the date of issue. No proof will be sent to the authors. The Board of Editors does not hold itself responsible for the opinions expressed by the correspondents. Communication should not exceed 600 words in length, and should be submitted in duplicate.

The Radiations of RaD

R. C. BANNERMAN AND S. C. CURRAN
Department of Natural Philosophy, The University, Glasgow, Scotland
(Received October 30, 1951)

WITH a view to establishing the decay scheme of RaD,[1] the radiations of this element have been studied using a scintillation spectrometer. A summary of previous work on RaD up to 1949 has been given by Feather,[2] and more recent work has been carried out by Cranberg,[3] Frilley *et al.*,[4] and Butt and Brodie.[5]

The scintillation spectrometer resembles in principle the gas-filled proportional counter, which has previously been applied to the examination of the soft γ- and x-radiations of RaD.[6] However, it has a nearly 100 percent efficiency for the harder γ-rays[2] (37, 42.6, and 46.7 kev), which is a real advantage in view of the very low intensity of these radiations (<3 quanta per 100 disintegrations). If we assume that the main mode of decay consists in the emission of soft β-particles (estimated limiting energy[7,8] between 10 and 40 kev) followed by de-excitation from a 46.7-kev level of RaE, a coincidence system consisting of two scintillation

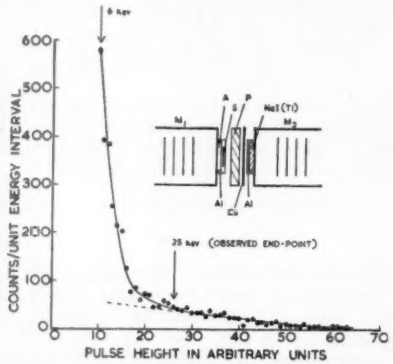

FIG. 1. The primary β-spectrum of RaD, isolated by coincidence with γ-rays of energy >40 kev. Inset: The coincidence arrangement employed in obtaining the primary β-spectrum. M_1, M_2: photomultiplier tubes, E.M.I. type VX 5032. *A*: thin anthracene crystal used as β-particle detector. *S*: separated source of RaD, mounted on Al foil and placed in direct contact with *A*. Al: aluminium reflector surrounding phosphor crystals. *P*: $\frac{1}{4}$-inch sheet of polythene to absorb β-particles from RaE. Cu: 2-mil copper sheet to reduce intensity of *L* x-rays of RaD. NaI(Tl): thin crystal of NaI(Tl) used to detect RaD γ-rays.

spectrometers (Fig. 1, inset) offers a method of isolating and examining the β-particles of the primary spectrum.

A separated source[9] of RaD was used which contained less than 5 percent RaE and RaF contaminant.

The spectrum of pulses from counter M_2 showed some of the known γ-rays of RaD, and the peak corresponding to the radiation of energy 46.7 kev stood out strongly (see Fig. 2 (A)). Careful search for harder radiations,[2] extending up to 140 kev, failed to reveal the presence of such in any significant intensity.

The output from counter M_1 was gated by those pulses from M_2 which corresponded to a γ-ray energy greater than 40 kev, and the resultant distribution analyzed with a single channel kick-sorter. The curve obtained is shown in Fig. 1. The region of the

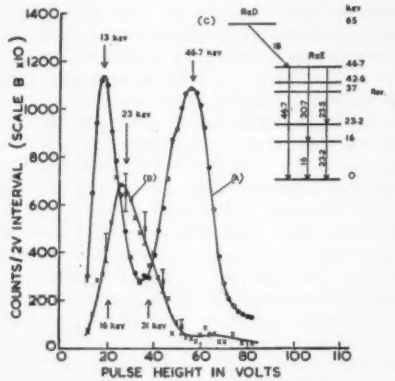

FIG. 2. (A) γ-ray distribution from RaD as observed in either counter of the $\gamma-\gamma$ coincidence arrangement, showing main γ-ray peak at 46.7 kev and x-ray peak at $\sim$13 kev. (B) Pulse height distribution curve of γ-rays producing $\gamma-\gamma$ coincidences. (C) Suggested decay scheme for RaD, showing main transitions involved in $\beta-\gamma$ and $\gamma-\gamma$ coincidences. Other γ-ray transitions are not shown for sake of clarity.

primary β-spectrum from 6 kev to the end point is clearly observed, and the coincidence control eliminates the photoelectron and Auger electron peaks which would otherwise complicate the results. A somewhat intense tail is found, the origin of which is not obvious but which is probably associated with the cosmic radiation and with bremsstrahlung effects from the slight admixture of RaE.

According to the uncorrected energy scale, the end point appears at 25 kev. Calibration was performed with known x- and γ-radiations, and from the observed widths of the peaks for such homogeneous sources it was possible to correct for the energy resolution of the counter. This procedure established that the limiting energy of the β-rays was

$$E_0 = 18 \pm 2 \text{ kev}.$$

This indicates a total disintegration energy of $46.7+18$, i.e., 65 kev approximately, for the transition RaD$\rightarrow$RaE. The form of the spectrum was found to agree, within the rather wide experimental limits of accuracy, with that expected for an allowed β-transition.

Similar work, with the aforementioned system modified to observe $\gamma-\gamma$ coincidences, showed that the γ-rays in coincidence formed a rather broad distribution extending from about 16 kev to just over 30 kev, with a maximum in the region of 23 kev (Fig. 2 (B)).

Further, the integrated spectrum[9] was studied with a split crystal of NaI(Tl), within which a thin source of RaD was held. The form of this curve showed clearly that all the transitions from the level at 46.7 kev were not direct to ground nor of the straightforward cascade type. Indeed it seemed necessary to assume that at least one of the intermediate levels was metastable, with a lifetime greater than 1 μsec, the resolving time of the circuit. Further work aiming at the use of thinner sources is in progress.

The decay scheme which appears to be consistent with previous results on RaD and with our own findings is indicated in Fig. 2 (C). All previously observed γ-rays can be fitted into the

scheme, while those transitions shown account for the $\beta-\gamma$ and $\gamma-\gamma$ coincidence results described above. Either one or both of the 42.6- and 37-kev levels is probably metastable.

[1] Detailed examination, by means of proportional counters of the form of the β-spectrum, is described by Insch, Balfour, and Curran of this Department, in a paper to be published in *The Physical Review*.
[2] N. Feather, Nucleonics **5**, No. 1, 22 (1949).
[3] L. Cranberg, Phys. Rev. **77**, 155 (1950).
[4] Frilley, Gokhale, and Valadares, Compt. rend. **232**, 50 (1951); **232**, 157 (1951).
[5] D. K. Butt and W. D. Brodie, Proc. Phys. Soc. (London) **64**, 791 (1951).
[6] Curran, Angus, and Cockroft, Phil. Mag. **40**, 36 (1949).
[7] *Nuclear Data*, National Bureau of Standards Circular No. 499 (1950).
[8] H. O. W. Richardson and A. Leigh-Smith, Proc. Roy. Soc. (London) **A160**, 454 (1937).
[9] Bannerman, Lewis, and Curran, Phil. Mag. **42**, 1097 (1951).

Information and Thermodynamics

JEROME ROTHSTEIN
Signal Corps Engineering Laboratories, Fort Monmouth, New Jersey
(Received October 9, 1951)

THE connection between information as defined in communication theory and statistical entropy (essentially negative or missing information) has been clarified by the measurement-communication analogy,[1] leading to the following statements which include the second law. Our information about an isolated system can never increase (only by measurement, i.e., interaction with the system, can new information be obtained). Reversible processes conserve information, irreversible ones lose it. Theoretically maximal information, corresponding to a pure state, has zero entropy; minimal information, corresponding to equilibrium, has maximum entropy. If one considers measuring apparatus and system of interest as a compound isolated system, then by the first statement information (obtained by measurement) is amply compensated by entropy increase in the compound system, no measurement is possible for equilibrium between the two parts, and the positive time direction can be taken equally as that corresponding to entropy increase of the compound system or of information increase regarding the system of interest. The last is closer to psychological or subjective time and also corresponds to time measurement (clock is object of interest). Past and future are symmetrical for equilibrium and for the purely mechanical case (zero entropy, pure case; note use of mechanical to include electrical, magnetic, etc., classical or quantal).

Consider now the informational interpretation of the first law and of quantity of heat. The first law can be expressed by mechanical concepts (in the general sense) alone, with quantity of heat then defined by the conservation of energy.[2] The first law asserts the existence of a state energy function, *viz.*: to bring a system adiabatically (i.e., via well-defined mechanical operations) from a definite initial state to a definite final state requires the same amount of mechanical work independently of the sequence of intermediate states. The state function U so defined (energy) is fixed to within an additive constant; for adiabatic change from state 1 to state 2,

$$U_2-U_1=\int_1^2 dW. \tag{1}$$

The quantity of heat given a body going from 1 to 2 over a specific, not necessarily adiabatic, path is now defined by

$$\int_1^2 dQ=(U_2-U_1)-\int_1^2 dW. \tag{2}$$

From an information viewpoint quantity of heat is thus energy transferred in a manner which has eluded mechanical description, about which information is lacking in terms of mechanical categories. Adiabatic changes make (2) vanish and thus for heat to be transferred the path must contain states which cannot be reached adiabatically from the initial state. Applied to (2) in differential form, namely

$$dQ=dU-dW, \tag{3}$$

the existence of adiabatically inaccessible states in the neighborhood of a given state follows. But this is precisely Caratheodory's principle, from which the existence of an integrating denominator for the Pfaffian (3) then follows, and from which in turn absolute temperature and the entropy function can be derived. It is noteworthy that even if the informational or statistical interpretation of entropy were not at hand, the first law with quantity of heat informationally characterized as above would lead to it. For all states adiabatically accessible (equivalent informationally) from a given state would generate a "surface" which would be a member of a one-parameter family. The value of the parameter would be a measure of missing information relative to some standard state; the parameter can be shown to be a function of the entropy only.

To sum up, the laws of thermodynamics can be stated as:

(a) The conservation of energy.

(b) The existence of modes of energy transfer incapable of mechanical description.

In a sense (b) is implied in (a), for (a) without (b) is a mechanical theorem devoid of thermodynamic content.

(c) The third law is true by definition, for in a perfectly ordered state at absolute zero there is no missing information, i.e., the entropy is zero (pure case).

[1] J. Rothstein, Science **114**, 171 (1951) and references cited.
[2] A. Landé, *Handbuch der Physik* (J. Springer, Berlin, 1926), Vol. IX, Chapter IV gives this formulation of the first law and a readable account of Caratheodory's axiomatic formulation of thermodynamics.

Slow Neutron Fission of Am^{242}, Am^{242m}, and Am^{243}*

K. STREET, JR., A. GHIORSO, AND S. G. THOMPSON
Radiation Laboratory and Department of Chemistry, University of California, Berkeley, California
(Received November 19, 1951)

THIS letter is to report the pertinent results of some work which was done at scattered intervals during the years 1947 to 1949 and which may now be published. Independent measurements of the same cross sections by a Canadian team[1] gave somewhat different results.

Shortly after the discovery[2] of Am^{242} in a sample of Am^{241} irradiated with pile neutrons, it became apparent that this nuclide had a large destruction cross section. In a second Am^{241} irradiation of three times the intensity of the first, only 1.4 times as much Am^{242} was formed as determined[3] by counting the beta-particles of Am^{242}. This ratio gave a destruction cross section for Am^{242} of approximately 10^4 barns. (This result is very insensitive to the cross section for the formation of Am^{243} as long as it is much less than 10^4 barns.) That this destruction was at least partially due to neutron capture to form Am^{243} became apparent with the discovery of this nuclide.[3]

When a mass spectrographic analysis of this second americium sample became available in December, 1949, it was possible to estimate the distribution of the destruction cross section of Am^{242} between fission and neutron capture to form Am^{243}. The composition of the americium was shown to be Am^{241} (99 percent), Am^{242} (0.5 percent), and Am^{243} (0.5 percent). From these data one calculates the following approximate cross sections: cross section for the formation of Am^{242}, $\sim$50 barns; neutron capture cross section of Am^{243} to form Am^{244}, $\sim$2000 barns; and total cross section for the destruction of Am^{242}, $\sim$8000 barns. Thus the fission cross section of Am^{242} must be $\sim$6000 barns. The estimate of 2000 barns for the cross section of the reaction $Am^{243}(n, \gamma)Am^{244}$ is somewhat smaller than a previous estimate[3] and is still subject to large errors. The principal uncertainties are in the estimation of the neutron flux.

In 1949 the fissionability of americium samples containing various amounts of the nuclides Am^{242} and Am^{242} was measured with a fission counter[4] in the thermal neutron column of the Argonne heavy water pile. Measurements on americium of the composition given above gave a fission cross section for Am^{242} of

about 6000 barns in agreement with the value obtained above. The measured fissionability was corrected for the Am^{241} present ($\sigma_{fission}$ 3.0 barns).[4,5] The fact that the Am^{243} present contributes a completely negligible amount to the observed fission was demonstrated by measuring an americium sample containing very nearly the same amount of Am^{242} and more than ten times as much Am^{243}. The observed fissionability in this sample was accounted for by the Am^{242} and allows a limit of less than 40 barns to be set on the fission cross section of Am^{243}.

The recent observation of the isomeric transition from the 16-hour Am^{242m} to the ground state[6] makes it seem likely that the Am^{242} observed in these samples came mainly through the formation of Am^{242m} and its subsequent decay to the ground state. Taking the branching of 20 percent given by O'Kelley *et al.*[6] and a cross section of ~300 barns[7] for the formation of Am^{242m}, the apparent cross section for the formation of Am^{242} in long irradiations (i.e., ≫16 hours) is about 60 barns, in fair agreement with that calculated from the isotopic abundances.

Some old measurements from this laboratory on the fissionability of Am^{242m} should be reinterpreted in the light of the isomeric transition to the highly fissionable Am^{242}. In this old work it was found that the fissionability of a sample of Am^{241} containing 50 parts per million of Am^{242m} (the amount of Am^{242m} was determined by counting the Cm^{242} which grew in and has been corrected for 60 percent beta-decay branching)[6] decayed with a 16-hour half-life to the extent of 2.1 percent. Using these data and taking the fission cross section of Am^{241} as 3.0 barns, the fission cross section of Am^{242} as 6000 barns, and the branching decay of Am^{242m} by isomeric transition as 20 percent, one obtains a fission cross section for Am^{242m} of about 2000 barns for thermal column neutrons. Again this value is subject to large errors.

We would like to express our appreciation to W. H. Zinn for the use of facilities at the Argonne National Laboratory for making the fission measurements. We also wish to thank Professor Glenn T. Seaborg for his continued interest and advice.

* This work was performed under the auspices of the AEC.
[1] Hanna, Harvey, Moss, and Tunnicliffe, Phys. Rev. **81**, 893 (1951).
[2] Seaborg, James, and Morgan, National Nuclear Energy Series, Plutonium Project Record, Vol. 14B, *The Transuranium Elements: Research Papers*, Paper No. 22.1 (McGraw-Hill Book Company, Inc., New York, 1949).
[3] Street, Ghiorso, and Seaborg, Phys. Rev. **79**, 530 (1950).
[4] A. Ghiorso and W. C. Bentley, National Nuclear Energy Series, Plutonium Project Record, Vol. 14B, *The Transuranium Elements: Research Papers*, Paper No. 22.29 (McGraw-Hill Book Company, Inc., New York, 1949).
[5] B. B. Cunningham and A. Ghiorso, Phys. Rev. **82**, 558 (1951).
[6] O'Kelley, Barton, Crane, and Perlman, Phys. Rev. **80**, 293 (1950).
[7] Obtained from an observed cross section of 200 barns for the formation of Cm^{242} and 60 percent beta-decay branching of Am^{242m}.

Light Emission from Silicon Carbide

R. W. SILLARS
Metropolitan-Vickers Electrical Company, Manchester, England
(Received November 6, 1951)

THE following observations, made some years ago, seem worth recording in view of the recent paper by Lehovec, Accardo, and Jamgochian.[1]

Various crystals found on silicon carbide "pig" having two roughly parallel plane faces were arranged with a "point" contact on one of the faces and another contact elsewhere on the lump of pig to which the crystal was attached (a large area contact to the crystal itself would presumably have served equally well for the latter). The region of the point contact was viewed through the opposite face, and it was seen that the primary source of light is a very small bright region at the contact, of a color like that of the crystal viewed by transmitted light. If one looks through the face of the crystal to which the point contact is made, however, as indicated in Fig. 1 of reference 1, this primary source of light is always eclipsed by the contact wire itself, and a much less intense light from a much larger volume is seen. This appears to be merely scattered and internally reflected light from the now invisible primary source, and its characteristics are modified by both scattering and absorption.

To make observations of spectral distribution which can be interpreted with any certainty, it seems very desirable to look at the contact region through a different face from that to which contact is made, and to make independent measurements of absorption characteristics between these faces, remembering that some crystals vary considerably from one region to another.

Because of the high refractive index of silicon carbide, the contact must lie almost on a normal to the viewing face, otherwise it cannot be seen directly; also the crystal, if deeply colored, must be very thin. Satisfactory crystals are not common, and it may be preferable to obtain specimens by grinding and polishing.

[1] Lehovec, Accardo, and Jamgochian, Phys. Rev. **83**, 603 (1951).

The Production of Halogen Negative Ions at the Surface of a Thoriated Tungsten Filament*

J. W. TRISCHKA, D. T. F. MARPLE, AND A. WHITE†
Syracuse University, Syracuse, New York
(Received November 9, 1951)

BY directing molecular beams of cesium halides at a hot thoriated W wire we have been able to obtain large percentage yields, as shown in Table I, in the production of some of the halogen negative ions. The percentage yield is defined as the ratio of halogen negative ion current from the activated wire to the cesium positive ion current from the deactivated wire. If the dissociation of the molecule into atoms is complete on the surface, then the Cs ion current is equal to more than 99 percent of the incident, neutral beam current.

Because of the relatively high pressure, of the order of 10^{-6} mm Hg, in the apparatus, electron emission and negative ion yield decreased from maximum values obtained immediately after activation of the wire to stable values which remained constant for long periods of time. Although the cesium positive ion current densities at the hot wire were large, around 5×10^{-4} amp/cm², there was no indication that either electron emission or negative ion yield was affected by prolonged "irradiation" by the beam.

At an early stage in the work negative ions from the activated wire were analyzed with a mass spectrometer and found to be halogen ions. No trace of molecular ions was discovered. For the yield measurements presented here a special electrode arrangement was constructed such that with appropriate potentials all charged particles of one sign leaving the wire could be directed through a system of slits into a collecting cup connected to a galvanometer. The fringing field of a strong permanent magnet located outside the apparatus was used to keep electrons from striking the collector. However, the residual electron current was large enough to prevent measurements of ion yields less than 1 percent.

For wire temperatures in the range from 1200°K to 1500°K no substantial change in negative ion yield was observed. Below 1200°K the ion current dropped sharply to zero. Above 1500°K residual electron currents were too large to permit measurements.

We feel that the negative ions are produced by the process of surface ionization rather than by electron capture in the region outside the hot wire because, (1) the negative ion yield was nearly independent of electron emission from the activated wire, and

TABLE I. Halogen negative ion yields.

Beam material	Maximum yield: percent	Stable yield: percent
CsI	4	2
CsBr	20	11
CsCl	60	30
CsF	<1	—

(2) no negative ions were detected coming from the deactivated wire when it had the same electron emission as the activated wire.

In studies of negative ion formation on pure tungsten surfaces[1] the kinetic theory of reaction rates has been used to interpret the results. According to this theory the ratio of negative ion current to the current of neutral atoms evaporating from the surface is proportional to $e^{(A-\Phi)e/kT}$, where A is the electron affinity of the atom and Φ is the work function of the surface. Hence, much larger halogen negative ion yields would be expected from a thoriated tungsten surface than from a pure tungsten surface at the same temperature. This expectation is in accord with experiments carried out by ourselves and others.[2] According to reference 2, Cl negative ion yields of the order of 0.01 percent are obtained with a pure W surface at very high temperatures. This is to be compared with our value of 60 percent using a thoriated tungsten surface.

The negative ion yields which we find for CsCl, CsBr, and CsI show the trend predicted by the theory, but are in each case much lower than the calculated values. The result for CsF is, of course, completely anomalous.

The theory we have used is considered to be applicable if complete dissociation of the cesium halides occurs on the thoriated W surface and if the accommodation coefficient for the halogen atom is unity. Disagreements between theory and experiment may be interpreted as a failure to satisfy either or both of these assumptions.

* Work assisted by the ONR.
† Present address: Federal Telecommunication Laboratories, Nutley, New Jersey.
[1] H. S. W. Massey, *Negative Ions* (Cambridge University Press, London, 1950).
[2] Davis, Feld, Zabel, and Zacharias, Phys. Rev. **76**, 1076 (1949).

Radioactive Pm^{148} and Pm^{150}

JOHN K. LONG AND M. L. POOL
Ohio State University, Columbus, Ohio
(Received November 21, 1951)

THE 3.7-year activity of Pm^{147}, the 5.3-day activity of Pm^{148}, and the 2-day activity of Pm^{149} are well established.[1] A 2.7-hour activity without a mass assignment has also been attributed to prometheum,[2] and a 27.5-hour activity has recently been assigned to Pm^{151}.[3] The availability of enriched natural isotopes of neodymium in high purity now provides a method for the further study of the prometheum isotopes.

Oxides of enriched neodymium isotopes were supplied by the AEC.[4] Mass analyses and spectroscopic analyses of these samples were also furnished by the supplier. The enriched samples were bombarded with 6-Mev protons. The decay of the products was followed with a Geiger counter and a Wulf electrometer. The sign of the charge of the beta-particles was determined by magnetic deflection. Bombardment of each of the enriched isotopes in turn for three to seven hours disclosed prominent activities of 2.7 hours, 5.3 days, and 48 days. Longer activities were also produced from some of the neodymium isotopes.

As a result of proton bombardment, an activity with a half-life of 48 days was observed in three neodymium samples containing different isotopic abundances. Chemical separation showed that this 48-day activity belonged with the rare earth group.[5] The 5.3-day activity from the reaction $Nd^{148}(p, n)Pm^{148}$ was also observed in these samples. By the use of the 5.3-day activity, the observed intensities of the 48-day activity in the samples were adjusted for small variations in time of bombardment, sample size, and beam strength. With these adjustments, the intensities of the 48-day activity were 0.74, 5.7, and 125, in samples where the percent abundances of Nd^{148} were 1.4, 5.7, and 89.0, respectively. The intensities of the 48-day activity in the three samples could not be matched with the percent abundances of any other neodymium isotope. These intensities indicate that the 48-day activity was formed by a reaction of protons on Nd^{148}. Since the 2-day Pm^{149} was not observed, a (p, γ) reaction on Nd^{148} is regarded as improbable. The 48-day activity may therefore be assigned to Pm^{148}, formed by the reaction $Nd^{148}(p, n)Pm^{148}$.

The 48-day activity is accompanied by negatively charged beta-particles of 1.7 ± 0.1 and 0.6 ± 0.1 Mev, and gamma-radiation of about 0.54 Mev, as shown by absorption measurements of the radiations in aluminum and lead. The total activity and the activity of each of these components have been followed through three half-lives.

The 2.7-hour activity has been observed previously as a result of bombardment of neodymium with protons and deuterons.[2] In the present investigation, it was produced from three neodymium samples containing different isotopic abundances. The observed intensities of the 2.7-hour activity in the samples were adjusted for variations in sample size, bombardment time, and beam strength by the use of the 5.3-day activity. With these adjustments, the intensities of the 2.7-hour activity in the three samples correspond more closely to the concentrations of Nd^{150} in these samples than to the concentrations of any other neodymium isotope. The adjusted intensities of the 2.7-hour activity were 3.8, 7.4, and 20, in samples where the percent abundances of Nd^{150} were 3.9, 5.6, and 94.8, respectively. It was, therefore, concluded that the 2.7-hour activity was formed by a (p, n) or (p, γ) reaction on Nd^{150}.

The 27.5-hour activity of Pm^{151},[3] which, with protons, would be produced by a (p, γ) reaction, was present, if at all, in very low intensity. This observation would indicate that a (p, γ) reaction with 6-Mev protons on Nd^{150} is not a prominent one. The 2.7-hour activity may, therefore, be assigned to Pm^{150} in accordance with the reaction $Nd^{150}(p, n)Pm^{150}$.

The particle radiation associated with the 2.7-hour activity was negative in sign. The beta-end point was observed at 2.4 ± 0.2 Mev by absorption measurements in aluminum.

Grateful acknowledgment is made for an Ohio State University Graduate School Fellowship granted to one of the authors (JKL).

[1] Inghram, Hess, Hayden, and Parker, Phys. Rev. **71**, 743 (1947); G. T. Seaborg and I. Perlman, Revs. Modern Phys. **20**, 623 (1948).
[2] J. D. Kurbatov and M. L. Pool, Phys. Rev. **63**, 463 (1943).
[3] Rutledge, Cork, and Burson, Bull. Am. Phys. Soc. **26**, No. 6, 38 (1951).
[4] Supplied by the Y-12 plant, Carbide and Carbon Chemicals Corporation, through the Isotopes Division, AEC, Oak Ridge, Tennessee.

Connection between $\gamma-\gamma$ and Internal Conversion Angular Correlations

J. W. GARDNER*
Division of Atomic Energy, National Research Council of Canada, Chalk River, Ontario, Canada
(Received November 5, 1951)

FOR angular correlation purposes one may denote two nuclear transitions in cascade by $J_A(l_1)J_B(l_2)J_C$, where the J's are the total angular momenta of the nuclear levels and the l's are the multipole orders of the successive, pure transitions. (Mixed multipole transitions are not discussed in this note.) For cascades involving γ-quanta and/or conversion electrons, the directional correlation function in terms of the angle, θ, between the propagation directions of the emitted particles may be written,

$$I(\theta)\sim\Sigma_k a_k P_k(\cos\theta), \tag{1}$$

with $k=2, 4, \cdots, 2L$, where L cannot exceed the least of l_1, l_2, and J_B. The a_k are, in general, functions of all the J's and l's; they have been tabulated by Lloyd[1] for $\gamma-\gamma$ cascades, and by the present writer[2] for conversion-conversion cascades, subject to certain approximations specified below. Other papers by Hamilton[3] and Falkoff[4] have tabulated the coefficients of $\cos^{2k}\theta$ rather than $P_k(\cos\theta)$ in the $\gamma-\gamma$ correlations. Recent work by Lloyd,[1] and by Rose *et al.*[5] has established a connection between the a_k for a given $\gamma-\gamma$ cascade and the a_k for the same cascade with one or

both γ's replaced by a conversion electron, so that, from the correlation for any one of the cases $\gamma-\gamma$, $\gamma-c$ (or $c-\gamma$), $c-c$, the correlation for the other two cases may be obtained immediately. In general, the factor f_k (Rose's b_ν) by which a_k must be multiplied to allow for the replacement of a γ-quantum by a conversion electron depends on the multipole order l and character (electric or magnetic), on the atomic number Z, and the energy $K(=h\nu/mc^2)$ released by the nuclear transition.[5] However, in the approximation used by Lloyd[1] (ejection of electron from an s-shell by electric multipole transition, treated in the nonrelativistic limit), the Z and K dependence vanishes and the expression for f_k (Lloyd's z_L) becomes,

$$f_k(l)=2l(l+1)/[2l(l+1)-k(k+1)]. \qquad (2)$$

Now Lloyd's approximation is just that used in reference 2, and the point it is desired to make here is the following: By a double application of the approximate f_k (or rather $1/f_k$) to the approximate $c-c$ correlation of reference 2, one arrives at the exact $\gamma-\gamma$ correlation. This is because, as explained by Rose *et al.*,[5] the $\gamma-\gamma$ correlation is independent of Z, K and the multipole character. Thus from (2) above and (18) of reference 2 we have, in the notation of that paper, the following completely general and exact correlation formula for the $\gamma-\gamma$ cascade $J_A(l_1)J_B(l_2)J_C$,

$$I(\theta)\sim\sum_k\left(1-\frac{k(k+1)}{2l_1(l_1+1)}\right)\left(1-\frac{k(k+1)}{2l_2(l_2+1)}\right)\times C_{l_1 0 l_2 0}{}^{k0}C_{l_2 a l_2 0}{}^{k0}W(J_BJ_Akl_1;l_1J_B)\times W(J_BJ_Ckl_2;l_2J_B)P_k(\cos\theta). \qquad (3)$$

(This of course checks with alternative formulas for the same correlation, given elsewhere.[6,7]) Moreover, on dividing Table I of reference 2 by $f_k(l_1)f_k(l_2)$, we have immediately a generic table for all $\gamma-\gamma$ correlations in the physically important case where l_1, l_2 have the lowest values allowed by the angular momentum and parity selection rules. Lloyd's "basic" correlation and numerical tables are derivable, as particular cases, from such a generic table.

A comparison was made in reference 2 between the departure from spherical symmetry in $I(\theta)$ for certain $c-c$ cascades and the corresponding $\gamma-\gamma$ cascades given by Hamilton.[3] The anisotropy, A, was defined as $(I_{\text{greatest}}-I_{\text{least}})/I_{\text{greatest}}$. Such a definition is preferable to one in terms only of $I(\pi)$ and $I(\pi/2)$, which would take no account of the possibility that $I(\theta)$ may have maxima or minima for $\pi>\theta>\pi/2$; thus $\cos^2\theta-\cos^4\theta$ has a maximum at $\theta=3\pi/4$ but is not distinguishable from a spherically symmetric distribution by its values at $\theta=\pi$ and $\pi/2$. It may be objected that our definition takes no account of the width of a peak and so does not distinguish, for example, between a cosine curve and a delta-function, giving $A=1$ for both. However, incorporation of peak-width into the definition of anisotropy would give a formula whose application would be limited not only by its algebraic complexity, but also by the fact that experimentally these angular distributions cannot often be observed with sufficient detail to give a reliable estimate of peak-width. The comparison of A_{c-c} with $A_{\gamma-\gamma}$ was limited to the dipole-dipole tables (Table II of reference 2 and Table I of reference 3) plus a few examples from the quadrupole-dipole tables. For every case tested the result was found $A_{c-c}\geq A_{\gamma-\gamma}$, and in particular no example was found of $A_{\gamma-\gamma}=1$, although there were several of $A_{c-c}=1$. This naturally led one to speculate whether it could be a universal, or at least general rule that the correlation for a cascade involving conversion electrons is stronger than that for the corresponding cascade with conversion electrons replaced by γ-quanta. In other words could it be generally true that, for a given cascade $J_A(l_1)J_B(l_2)J_C$, we have $A_{c-c}\geq A_{c-\gamma}\geq A_{\gamma-\gamma}$?

The question of anisotropy has now been thoroughly investigated for the general angular distributions, $1+a_2P_2(\cos\theta)$ and $1+a_2P_2(\cos\theta)+a_4P_4(\cos\theta)$, by examining algebraically the effect on A of multiplying a_k by some arbitrary factor F_k. The purely algebraic investigation showed that, invariably, the "A" of $1+a_2P_2(\cos\theta)$ is reduced if $|a_2|$ is reduced, and increased if $|a_2|$ is increased. No such general rule was discovered, however, for the $1+a_2P_2(\cos\theta)+a_4P_4(\cos\theta)$ distribution; for example, the reduction of both $|a_2|$ and $|a_4|$ does not necessarily mean a reduction in A, it depends on the relative signs and magnitudes of the a_k and F_k. In physical examples F_k is of course related to f_k; thus it is $(1/f_k)^2$ for converting $I(\theta)_{c-c}$ to the corresponding $I(\theta)_{\gamma-\gamma}$. When f_k is given by Eq. (2) above, a reduction in $|a_k|$ always occurs for the changes $c-c\to c-\gamma\to\gamma-\gamma$; in the exact treatment of Rose *et al.* a reduction usually occurs, the exception being when the substitution $c\to\gamma$ is made in a dipole transition (electric or magnetic) for which $h\nu>mc^2$. The exact treatment also shows that all the F_k approach asymptotically to unity in the high energy limit, so that in this limit there is no distinction between the $c-c$, $c-\gamma$, and $\gamma-\gamma$ angular distributions for the same cascade.

To conclude, then, we may say that $A_{c-c}\geq A_{c-\gamma}\geq A_{\gamma-\gamma}$ is by no means the universal rule one might have expected from the more limited investigation of reference 2. It does, however, apply to all cascades in which one transition is magnetic or electric dipole with $h\nu<mc^2$, and the other transition is also dipole with $h\nu<mc^2$, or is any higher multipole of any energy. For $1+a_2P_2(\cos\theta)+a_4P_4(\cos\theta)$ distributions no general rule can be formulated, although it appears that on the average A is about as often increased as decreased by replacing a conversion electron by a γ-quantum. In view of this it was not thought worthwhile to extend the investigation to more complicated angular distributions, particularly as the algebra here becomes very heavy on account of the numerous alternative analytic expressions for A, depending on the number of maxima and minima in $I(\theta)$, and whether $I(\pi)$ is greater or less than $I(\pi/2)$.

I am indebted to Dr. Lloyd for helpful discussion and a copy of his thesis; also to Dr. Rose and Professor Racah for sending me advance copies of their papers. It is a pleasure to acknowledge the computing assistance rendered by Miss Jean Tucker of this establishment.

[5] N.R.L. Postdoctoral Fellow.
[1] S. P. Lloyd, Phys. Rev. **83**, 716 (1951).
[2] J. W. Gardner, Proc. Phys. Soc. (London) **A62**, 763 (1949).
[3] D. R. Hamilton, Phys. Rev. **58**, 122 (1940).
[4] D. L. Falkoff, Phys. Rev. **82**, 98 (1951).
[5] Rose, Biedenharn, and Arfken, Phys. Rev. **85**, 5 (1952).
[6] Biedenharn, Arfken, and Rose, Phys. Rev. **83**, 586 (1951).
[7] G. Racah, Phys. Rev. **84**, 910 (1951).

Search for Long-Lived Nb^{94}

R. E. Hein,* C. M. Fowler,† and R. H. McFarland†
Kansas State College, Manhattan, Kansas
(Received November 20, 1951)

A 6.6-min activity produced by (n,γ)[1] and (d,p)[2] reactions on niobium has been reported by a number of investigators. This short-lived activity assigned to Nb^{94} emits x-rays[3] which have been characterized as the K-radiation of niobium.[4] Further K, L, and M conversion electron groups, characteristic of niobium, have been observed from a highly converted 41.5-kev x-ray.[5] It is reported[6] that 99.9 percent of the 6.6-min activity decays by the isomeric transition process and the remainder by β^- emission (1.3 Mev) to Mo^{94}. Radiations from a long-lived isomer of Nb^{94} have not been detected and a half-life value of greater than 100 years is indicated on the basis of previous neutron irradiations of niobium.[4]

Since information on the long-lived Nb^{94} is meager, an investigation of this activity seemed desirable. Accordingly, a 500-mg sample of niobium metal was bombarded for 4 months in the Argonne reactor. A spectrographic analysis made by the supplier indicated that less than 0.001 percent each of zirconium, titanium, and iron were present as impurities in the sample. Our own spectrographic studies indicate that tantalum is probably present to a greater extent than 0.001 percent. Hafnium, however, was not detectable spectrographically.

TABLE I. Purification of irradiated niobium.

Purification step	1	2	3	4	5	6
Sp. act. (counts/min/mg)	950	25	11	4	0.7	1

Although the 6.6-min activity was too short to be observed in these laboratories, one or more long-lived activities were present in the irradiated sample. No positrons could be detected in the emitted radiations using standard magnetic deflection techniques. Based on aluminum absorption curves a large part of the activity present could be due to Ta^{182}. This qualitative observation was checked by observing the electron conversion spectrum with a fixed magnetic field camera. Photographs were taken at three different field values, and 30 conversion groups were observed ranging in energy from 30 kev to 415 kev. All but three of these lines matched those reported for Ta^{182}.[7] The remaining three lines, 120±1, 276±2, and 415±4 kev, were initially interpreted as K-conversion lines for a niobium triad ($\gamma=140$, 296, 436 kev). That interpretations based only upon evidence of this type can be erroneous, is seen from the fact that these lines are actually conversion groups arising from the Hf^{181} decay.[8] Corroborative evidence for the statement was provided through the separation of Hf^{181}, macro amounts of niobium, and Ta^{182} in that order from the irradiated niobium on anion exchange resin columns.[9] The activity which preceded the niobium off the column exhibited a delay state of approximately 20 μsec, which again points toward Hf^{181}. On the basis of these experimental results, all of the conversion electron groups observed in the irradiated niobium can be accounted for by Ta^{182} and Hf^{181} activities.

Since a low intensity niobium activity could be masked by the tantalum and hafnium activities, a large sample (220 mg) of the irradiated niobium was decontaminated from these extraneous activities. Six decontamination steps with anion exchange resins reduced the specific activity to a constant value for the niobium. In each step the first fractions off the column (Hf^{181}) and the last fraction (Ta^{182}) were discarded. The specific activity of the niobium after each column separation step is given in Table I. From aluminum absorption curve evidence, the activity still remaining in the niobium is probably Hf^{181}.

On the basis of this investigation a minimum half-life of 5×10^4 years is proposed for Nb^{94}.

* Department of Chemistry.
† Department of Physics.
[1] Sagane, Kojima, Miyamoto, and Ikawa, Proc. Phys.-Math. Soc. Japan 22, 174 (1940).
[2] D. N. Kundu and M. L. Pool, Phys. Rev. 70, 111 (1946).
[3] M. Goldhaber and W. J. Sturm, Phys. Rev. 70, 111 (1946).
[4] M. Goldhaber and C. O. Muehlhause, Phys. Rev. 74, 1248 (1948).
[5] R. L. Caldwell, Phys. Rev. 78, 407 (1950).
[6] W. H. Sullivan, *Trilinear Chart of Nuclear Species* (John Wiley & Sons, Inc., New York, 1949).
[7] Cork, Keller, Rutledge, and Stoddard, Phys. Rev. 78, 95 (1950).
[8] Burson, Blair, Keller, and Wexler, Phys. Rev. 83, 62 (1951).
[9] K. A. Kraus and G. E. Moore, J. Am. Chem. Soc. 73, 9 (1951); 71, 3855 (1949).

The Equation of Motion of the Landé Electron*

PAUL MOLMUD†
Ohio State University, Columbus, Ohio
(Received November 19, 1951)

THE electron, in Landé's modification of classical electrodynamics,[1] is a point mass with an associated charge density function ρ, where

$$\rho=(3ea^2/4\pi)(r^2+a^2)^{-5/2},$$

a is a fundamental length, r is the distance from the point mass, and e the total electronic charge.

The four-force on the electron is given, following Lorentz, by

$$\int \varkappa d\upsilon,$$

where $\varkappa$ is the four-vector of force density due to external and self fields acting upon the charge density, and $d\upsilon$ is an element of three-volume. The region of integration is a sphere of radius R where R increases without limit.

The change of mechanical energy-momentum of the electron between two time intervals is equated to

$$\int \varkappa d\tau,$$

where $d\tau$ is an element of four-volume.

Following Dirac,[2] this volume integral is transformed into a surface integral. Then, using the methods of Dirac,[2] the inversion of infinite series, and Landé's signal law,

$$r^2-c^2t^2+a^2=0,$$

the equation of motion of the electron is obtained as an infinite series:

$$m_0\ddot{z}_\mu=\lim_{R\to\infty}\frac{Q(\alpha+\beta)}{4\pi}\int\int f_{\mu\nu}\dot{z}^\nu(1+R\theta\cos\vartheta)^{\frac{1}{2}}\sin\vartheta d\vartheta d\varphi$$
$$+\frac{eQ\ddot{z}_\mu(\alpha+\beta)^2}{16R\theta(a^2+R^2)^{\frac{1}{2}}}\left[3\ln\left(\frac{1-R\theta}{1+R\theta}\right)+(1+R\theta)^{-1}-(1-R\theta)^{-1}\right]$$
$$+\tfrac{1}{2}(\beta-\alpha)(\alpha+\beta)eQ(R\theta)^{-1}[\dddot{z}_\mu+d\ddot{z}_\mu/ds]$$
$$\times[(1-R\theta)^{-\frac{1}{2}}-(1+R\theta)^{-\frac{1}{2}}]$$

plus terms of higher order in $R\theta$. Here, m_0 is the mechanical rest mass of the electron, z is a positional coordinate in four-space and dots indicate differentiation with respect to proper time, $s(c=1)$, α and β are arbitrary pure numerics such that the effective field of the electron is given as α (advanced field) plus β (retarded field), $f_{\mu\nu}$ is a component of the external field six-vector, θ is the magnitude of the three-acceleration in a coordinate system in which the electron is instantaneously at rest, Q is the total charge enclosed by the sphere of radius R about the point mass,

$$Q=\int 4\pi\rho r^2dr=eR^3(a^2+R^2)^{-\frac{3}{2}},$$

where $Q\approx e$ for $R\gg a$. This series converges, if and only if, $R\theta<1$.

If R is arbitrarily restricted to a finite value, in other words, if the effective radial extension of the charge of the electron is defined as R, then it can be shown that the above series will reduce (under the proper limiting conditions) to the equations of (a) Lorentz-Dirac,[1] (b) Eliezer,[3] and (c) Groenewald.[4]

The conditions to be introduced into the series are: R is finite and much larger than a, $\theta R\ll1$ (quasistationary motion), and $f_{\mu\nu}$ to be of negligible variation over the distance $2R$ (the wavelength of the external field is to be much larger than $2R$, the effective diameter of the electron).

Under these conditions the series assumes the form,

$$m_0\ddot{z}_\mu=(\alpha+\beta)Qf_{\mu\nu}\dot{z}^\nu-\tfrac{1}{2}(\alpha+\beta)^2Qe(R^2+a^2)^{-\frac{1}{2}}\ddot{z}_\mu$$
$$+\tfrac{2}{3}(\beta-\alpha)(\alpha+\beta)eQ(\dddot{z}^2\ddot{z}_\mu+d\ddot{z}_\mu/ds),$$

plus negligible terms of higher order in $R\theta$. Then:

(a) When we define $m=m_0+\frac{1}{2}Qe(R^2+a^2)^{-\frac{1}{2}}$ and allow only retarded fields (i.e., $\alpha=0$, $\beta=1$), the Lorentz-Dirac equation is obtained

$$m\ddot{z}_\mu=Qf_{\mu\nu}\dot{z}^\nu+\tfrac{2}{3}eQ(\dddot{z}^2\ddot{z}_\mu+d\ddot{z}_\mu/ds).$$

(b) By using m as an (a) and taking $\alpha=-\varkappa$ and $\beta=\varkappa+1$, Eliezer's equation results

$$m\ddot{z}_\mu=\tfrac{2}{3}eQ(2\varkappa+1)(\dddot{z}^2\ddot{z}_\mu+d\ddot{z}_\mu/ds)+Qf_{\mu\nu}\dot{z}^\nu.$$

(c) Groenewald's equation was obtained by assuming, first of all, that the charge of the electron is concentrated on its world line and secondly that the self fields are the half-sums of advanced and retarded fields.

To obtain similar results from the above series, Q is replaced by e independently of R, α and β are each equated to $\frac{1}{2}$, and then R is allowed to approach zero as a limit. The resulting equation is

$$m_0\ddot{z}_\mu=ef_{\mu\nu}\dot{z}^\nu-(e^2/2a)\ddot{z}_\mu$$

plus higher order terms.

Groenewald did not introduce any mechanical rest mass, m_0, but set $e^2/2a$ equal to the observed mass of the electron.

* Based upon a PhD dissertation submitted to the Graduate School of Ohio State University.
† Now at Clarkson College of Technology, Potsdam, New York.
[1] A. Landé, Phys. Rev. **76**, 1176 (1949).
[2] P. A. M. Dirac, Proc. Roy. Soc. (London) **A167**, 148 (1938).
[3] C. J. Eliezer, Revs. Modern Phys. **19**, 149 (1947).
[4] H. J. Groenewald, Physica **6**, 115 (1939).

Identification of CO in the Solar Atmosphere*

LEE GOLDBERG, ROBERT R. MCMATH, ORREN C. MOHLER, AND A. KEITH PIERCE
McMath-Hulbert Observatory, University of Michigan, Pontiac, Michigan
(Received November 7, 1951)

RECENTLY, a short section of the solar limb spectrum, extending approximately from λ23,100 to λ23,300, was traced with the high dispersion infrared spectrometer[1] attached to the Snow telescope at the Mount Wilson Observatory. It was noted that over 15 weak lines were conspicuously enhanced in intensity by about a factor of two as compared with their appearance in the spectrum of the center of the disk. Furthermore, the majority of the lines were regularly spaced in a fashion that left no doubt as to their molecular origin. It should be pointed out that enhancement toward the limb is common among solar molecular lines observed in the photographic region of the Fraunhofer spectrum,[2] but that no solar lines of molecular origin have hitherto been noted in the lead-sulfide region of the spectrum.

Investigation of the positions and spacing of the enhanced lines makes it certain that they are members of the positive branch of the 3−1 vibration-rotation band of CO centered at 4207.03 cm^{-1}. The strengthening of the lines toward the limb indicates that they are formed relatively high in the atmosphere where the temperature is about 5000°K. At this temperature the intensity maximum of the CO bands, although relatively flat, occurs at about $J=30$. The observed positions of the solar lines agree to within a few hundredths of a wave number with those calculated for the lines $J=25$ to $J=35$ from the molecular constants recently derived for CO by Rao.[3]

Additional confirmation of the presence of CO in the solar atmosphere has come from an examination of neighboring regions of the spectrum in the infrared atlas,[4] which reveals not only many additional lines of the 3−1 band, but also numerous lines arising from the 2−0 band at 4260.13 cm^{-1} and the 4−2 band at 4154.28 cm^{-1}. In every case, there is precise agreement between the observed and calculated line positions, and for all three bands the only lines observed are those with rotational quantum numbers in the neighborhood of $J=30$. All of the lines in the spectrum of the disk center are very weak; their central absorptions usually do not exceed 5 percent. Also, the line intensities do not appear to differ significantly from one band to the other, which is not surprising inasmuch as the Boltzmann factor is relatively small at solar temperatures.

It should be noted that CO is expected to be one of the most abundant molecules in the solar atmosphere, according to calculations by Russell.[5] Its failure to be observed previously is due only to the location of its electronic bands in the inaccessible ultraviolet.

In view of the presence of the overtone transitions 2−0, 3−1, and 4−2 at 2.3μ, it is to be expected that the corresponding fundamentals 1−0, 2−1, and 3−2 will be very strong. Migeotte has observed indeed the 1−0 band at 4.7μ in the solar spectrum both at Columbus, Ohio,[6] and from the Jungfraujoch.[7] He states, however, that the band originates in the earth's atmosphere and believes that the solar contribution to the band is negligible. He observes further that the band undergoes large and apparently random fluctuations in intensity, the line R_3 varying from 15–50 percent central absorption. Later, the 4.7μ band was observed by Shaw, Chapman, Howard, and Oxholm,[8] also at Columbus, but they found that the central absorption of R_3 was never less than 45 percent over a period of three or four months.

On the basis of observations made at the McMath-Hulbert and Mount Wilson Observatories, it can be stated that the telluric contribution to the 2−0 band, if present, is no greater than the contribution from the center of the solar disk. This result would imply that at least half of the contribution to the 1−0 band is also solar. If so, the 2−1 and 3−2 bands should appear with strength comparable to 1−0, at 2116.75 cm^{-1} and 2090.28 cm^{-1}, respectively. Inspection of the table of wavelengths and of the tracing of the 4.7μ region published by Shaw, *et al.*[8] suggests that some lines of the two difference bands may be present, but they are very much weaker than those of the 1−0 band at 2143.38 cm^{-1}. It would obviously be extremely important to compare tracings of the 4.7μ band made at various points on the solar disk, to determine the existence both of intensity variations and of Doppler shifts resulting from solar rotation.

We wish again to express our appreciation to McGregor Fund for continuing grants-in-aid and to Dr. I. S. Bowen, Director of the Mount Wilson and Palomar Observatories, for the use of the Snow telescope.

* Work supported in part by the ONR.
[1] R. R. McMath and O. C. Mohler, J. Opt. Soc. Am. **39**, 903 (1949).
[2] J.-C. Pecker and R. Peyturaux, Compt. rend. **224**, 1477 (1947).
[3] K. N. Rao, Astrophys. J. **110**, 304 (1949).
[4] Mohler, Pierce, McMath, and Goldberg, *Photometric Atlas of the Near Infrared Solar Spectrum*, λ8465 *to* λ25,242 (University of Michigan Press, Ann Arbor, 1951).
[5] H. N. Russell, Astrophys. J. **79**, 317 (1934).
[6] M. Migeotte, Phys. Rev. **76**, 1108 (1949).
[7] M. Migeotte and L. Neven, Physica **16**, 423 (1950).
[8] Shaw, Chapman, Howard, and Oxholm, Astrophys. J. **113**, 268 (1951).

Far Infrared Transmission of Silicon and Germanium

R. C. LORD
Spectroscopy Laboratory, Massachusetts Institute of Technology, Cambridge 39, Massachusetts
(Received November 6, 1951)

THE infrared transmission spectra of elementary silicon and germanium are of interest because of the remarkable electrical properties of these materials. The temperature-dependence of electrical resistance of germanium, for example, has been interpreted[1,2] as indicating a conduction-band gap resulting from impurity acceptors of approximately 0.01 ev. Study of the absorption of electromagnetic radiation of energies of this magnitude could thus furnish useful evidence for the solid-state theory of the properties of germanium,[3] and perhaps yield more accurate values of the band-gap energies than can be obtained from thermal and electrical measurements.

The infrared transmissions of optically polished samples of silicon and germanium of 2-mm thickness are given in Table I for

TABLE I. Infrared transmission for 2-mm samples of germanium and silicon (uncorrected for reflection losses).

cm^{-1}	T_{Ge}	T_{Si}	cm^{-1}	T_{Ge}	T_{Si}
260	0.12	0.36	540	0.31[a]	0.20
270	0.07	0.37	560	0.33	0.17
280	0.05	0.39	580	0.40	0.18
290	0.05	0.39	600	0.44	0.05
300	0.03	0.38	610	—	0.03[a]
320	0.03	0.37	620	0.47	0.05
340	0.01	0.37	640	0.45	0.27
360	0.01	0.37	660	0.47	0.30
380	0.11	0.37	680	0.47	0.32
400	0.24	0.36	700	0.48	0.36
420	0.15[a]	0.36	720	0.48	0.25
440	0.23	0.36	736	—	0.18[a]
460	0.27	0.37	740	0.47	0.18
480	0.37	0.28	760	0.47	0.19
500	0.34	0.25	780	0.47	0.22
516	—	0.14[a]	800	0.46	0.25
520	0.32	0.20			

[a] Indicates band minimum.

the range 260–800 cm^{-1} (0.03–0.10 ev~40–12 microns). Infrared studies at higher frequencies have already been reported,[4-7] and show that while the spectrum of silicon has considerable structure in the region 800–5000 cm^{-1} (0.10–0.60 ev), germanium, in thin samples, has an approximately constant transmission of about 0.5 independent of thickness. The 0.5 loss is thus presumably the result almost entirely of reflection.

As Table I shows, germanium continues to transmit about 50 percent down to 600 cm^{-1}, and then exhibits a broad, very weak band at 540 cm^{-1} and a sharp, somewhat stronger band at 420 cm^{-1}. The major absorption occurs, however, in a broad band centered at 330 cm^{-1}. Although measurements on the low frequency side of this band extend only to about 250 cm^{-1}, it is already apparent that transmission is significantly higher than at 300 cm^{-1}. The observed increase at low frequency is reminiscent of the effect of instrumental scattered light. We believe it is genuine, however, since suitably thick crystals (>2 cm) of potassium iodide, a satisfactory substance for detection of high frequency scattered light at 250 cm^{-1}, show that instrumental scattered light is less than 5 percent in this region.

If the center of this band is taken as 330 cm^{-1}, the corresponding energy is 0.04 ev. This is a somewhat higher value for the energy gap than that suggested from the temperature-dependence studies[1, 2] and may mean that other bands lie at still lower frequencies, or that the temperature-dependence studies require a more involved interpretation.

It has been reported[8] that appropriate heat treatment of germanium single crystals changes the temperature dependence of resistance to give an energy-gap value of 0.03 ev. In view of the closer concordance of this latter value with the energy of the transmission minimum at 330 cm^{-1}, it is conceivable that the sample on which the data of Table I were obtained had an energy-gap similar to that produced by heat treatment. However, it seems more likely that the band is analogous to the strong absorption in silicon at 610 cm^{-1}, since the other pairs of bands in the spectra have frequency ratios about equal to 610:330, *viz.*, 1120:540 and 756:420. This similarity of the spectra of silicon and germanium is understandable if the bands are ascribed to lattice vibrations for the lattice frequencies of the two substances should differ by a mass factor (72/28)[½] and a factor not much larger than unity, due to difference in lattice binding. This suggestion is compatible with the observation of Keesom and Pearlman[9] that the Debye θ curves as a function of temperature are identical for silicon and germanium apart from a scale factor of 1.8 on both θ and T axes.

Thanks are expressed to Mr. A. H. White and Dr. J. Bardeen of the Bell Telephone Laboratories, Dr. W. C. Dunlap, Jr., of the General Electric Company, and Dr. R. B. Barnes and Dr. W. A. Fraser of American Optical Company for samples of germanium and silicon and for comment on the results here reported. Messrs. R. E. Merrifield and R. W. Walker furnished valuable assistance with the transmission measurements.

[1] G. L. Pearson and W. Schockley, Phys. Rev. **71**, 142 (1947).
[2] C. S. Hung and J. R. Gliessman, Phys. Rev. **79**, 726 (1950).
[3] J. Bardeen, Phys. Rev. **79**, 216 (1950).
[4] M. Becker and H. Y. Fan, Phys. Rev. **76**, 1531 (1949); **77**, 760 (1950); K. Lark-Horovitz and K. W. Meissner, Phys. Rev. **76**, 1530 (1949).
[5] H. B. Briggs, Phys. Rev. **77**, 287 and 727 (1950).
[6] E. Burstein and J. J. Oberly, Phys. Rev. **78**, 642 (1950); Phys. Rev. **82**, 764 (1951).
[7] I. Simon, J. Opt. Soc. Am. **41**, 730 (1951).
[8] W. DeSorbo and W. C. Dunlap, Jr., Phys. Rev. **83**, 875 (1951) (see correction on p. 869).
[9] P. H. Keesom and N. Pearlman, Bull. Am. Phys. Soc. **26**, No. 6, (1951).

Phase Transition of $ND_4D_2PO_4$

B. T. MATTHIAS
Bell Telephone Laboratories, Murray Hill, New Jersey
(Received November 16, 1951)

AMMONIUM dihydrogen phosphate, though isomorphous with KH_2PO_4, does not become ferroelectric. Instead, at 148°K it undergoes a transition which splits the crystal into many small fragments. Below this transition the dielectric constant is small and changes very little with decreasing temperature. It was generally believed that this transition was because of an interaction of the NH_4^+ ions on account of their deviation from a spherical symmetric configuration.[1, 2] However, the magnitude of the anomaly of the specific heat occurring at this transition was much larger than those observed in other ammonia transitions, even though the crystal did not become ferroelectric.

In order to investigate this further, we replaced all the hydrogen by deuterium, making the following crystal; $ND_4D_2PO_4$. The crystals were of the same habit as the corresponding hydrogen salt. Their transition temperature, however, was shifted from 148°K to 242°K, i.e., 94° to higher temperatures.

This result enables us finally to decide whether there is an ammonia transition or not. Replacing H by D in an ammonia transition like that of NH_4Cl, for instance, changes the transition temperature only a few degrees, whereas the ferroelectric Curie point of KD_2PO_4 is about 90° higher than that of KH_2PO_4. The transition in the ammonium salt is therefore believed to be an order-disorder transition of the X_2PO_4 (X=H or D) groups, and the principal effect of the nonspherical symmetric ammonia ion is to prevent the occurrence of a spontaneous polarization, i.e., ferroelectricity.

[1] Baertschi, Matthias, Merz, and Scherrer, Helv. Phys. Acta **18**, 238 (1945).
[2] W. P. Mason, Phys. Rev. **69**, 173 (1946).

Charge-Symmetrical Interaction between Nucleons and Leptons

V. VOTRUBA
Institute for Theoretical Physics, Charles University, Prague, Czechoslovakia
(Received October 22, 1951)

LET us consider the direct interaction between the nucleons and the quantized wave field of leptons, as defined through the Hamiltonian

$$-g\{\psi_P^*\psi_N\cdot\psi_\nu^*\psi_e+\text{c.c.}+\tfrac{1}{2}(\psi_N^*\psi_N-\psi_P^*\psi_P)\cdot\tfrac{1}{2}(\psi_e^*\psi_e-\psi_\nu\psi_\nu^*)\}. \quad (1)$$

The terms in the first row correspond to the usual β-radioactivity. The terms in the second row are just those originally proposed by Oppenheimer and Schwinger[1] (except that we are using the scalar interaction, for simplicity). The expression (1) can be written in a remarkable form, if we accept the Majorana theory for the neutrino (in accordance with the double β-decay).

Thus we suppose $\psi_\nu^\dagger=\psi_\nu=v$ and decompose also $\psi_e=u+iv$ into its real and imaginary parts u and v. Further we put

$$\Psi=\begin{pmatrix}\psi_P\\ \psi_N\end{pmatrix} \quad \text{and} \quad \varphi=\begin{pmatrix}u\\ v\\ w\end{pmatrix}. \quad (2)$$

Then (1) can be written in the form

$$(g/2)\cdot(\Psi^*\boldsymbol{\tau}\Psi)\cdot(\varphi^*\boldsymbol{\xi}\varphi), \quad (1')$$

where $\boldsymbol{\tau}$ is the well-known operator of the isotopic spin of the nucleon and the components of $\boldsymbol{\xi}$ are the matrices

$$\xi_1=\begin{pmatrix}0&0&0\\0&0&i\\0&-i&0\end{pmatrix},\quad \xi_2=\begin{pmatrix}0&0&-i\\0&0&0\\i&0&0\end{pmatrix},\quad \xi_3=\begin{pmatrix}0&i&0\\-i&0&0\\0&0&0\end{pmatrix}. \quad (3)$$

These Hermitian matrices are just the irreducible representation (of rank 3) of the abstract operators satisfying the Duffin-Kemmer relations

$$\xi_i\xi_j\xi_k+\xi_k\xi_j\xi_i=\delta_{ij}\xi_k+\delta_{jk}\xi_i, \quad (4)$$

(i, j, $k=1$, 2, 3). The matrices (3) satisfy further the relations $\xi_1\xi_2-\xi_2\xi_1=i\xi_3$, etc. The charge density of the lepton field can be expressed in the form

$$\rho=(e/2)(\psi_e^\dagger\psi_e-\psi_e\psi_e^\dagger)=e\varphi^\dagger\xi_3\varphi. \quad (5)$$

The vector ξ can be considered as the operator of the isotopic spin of the lepton. Thus the lepton is a particle with isotopic spin 1. Its three charge states (electron, positron, and neutrino) correspond to the three possible eigenvalues $(\mp 1, 0)$ of ξ_3. The three wave functions u, v, w (each of which is a four-component Majorana spinor) themselves form a vector in the space of the isotopic spin.

As is well known,[2] there exists also an irreducible representation of rank four of the three abstract operators satisfying (4). This is given by the Hermitian matrices

$$\xi_1' = \begin{pmatrix} 0 & 0 & 0 & i \\ 0 & 0 & 0 & 0 \\ 0 & 0 & 0 & 0 \\ -i & 0 & 0 & 0 \end{pmatrix}, \quad \xi_2' = \begin{pmatrix} 0 & 0 & 0 & 0 \\ 0 & 0 & 0 & i \\ 0 & 0 & 0 & 0 \\ 0 & -i & 0 & 0 \end{pmatrix}, \quad \xi_3' = \begin{pmatrix} 0 & 0 & 0 & 0 \\ 0 & 0 & 0 & 0 \\ 0 & 0 & 0 & i \\ 0 & 0 & -i & 0 \end{pmatrix}. \tag{6}$$

If we write $\lambda_3 = -i(\xi_2'\xi_1' - \xi_1'\xi_2')$, etc., the matrices λ_I are just reduced in the form

$$\lambda_1 = \begin{pmatrix} \xi_1 & 0 \\ 0 & 0 \end{pmatrix}, \quad \lambda_2 = \begin{pmatrix} -\xi_2 & 0 \\ 0 & 0 \end{pmatrix}, \quad \lambda_3 = \begin{pmatrix} \xi_3 & 0 \\ 0 & 0 \end{pmatrix} \tag{7}$$

and satisfy the relations $\lambda_2\lambda_1 - \lambda_1\lambda_2 = -i\lambda_3$, etc. Thus these λ-matrices can be interpreted as components of the isotopic spin of a particle belonging to (6). This isotopic spin has two values 0 and 1. The particle has four charge states, two charged ones and two different neutral ones. Its wave function φ' has four components (u', v', w', f'), each of which can be, e.g., a Majorana spinor. The first three wave functions u', v', w' form a vector, whereas f' is a scalar (in the isotopic spin-space). The charge density is given by $\rho' = e\varphi'^{\dagger}\lambda_3\varphi'$. Different interactions with nucleons can be defined by writing φ' instead of φ and λ or ξ' instead of ξ in (1).[3]

[1] J. R. Oppenheimer and J. S. Schwinger, Phys. Rev. **56**, 1066 (1939). These authors pointed out that the emission of an electron-positron pair from the nucleus O^{16} could be explained by introducing such a direct (nonelectromagnetic) interaction of protons and/or neutrons with the quantized electron-positron wave field. But they abandoned this possibility in favor of a less radical alternative, which explains the pair as being ejected through the electromagnetic influence of nuclear multipole moments. Recent experiments [Phillips, Cowie, and Heydenburg, Phys. Rev. **83**, 1049 (1951)] show, however, that also the nucleus Be^{8*} can emit a pair, although this nucleus would not be expected to have a similar structure (even parity) to that assumed for O^{16*}. Thus the (electromagnetic) mechanism adopted by Oppenheimer and Schwinger may be actually inoperative, and it is perhaps worth while to consider once again the first possibility.

[2] N. Kemmer, Proc. Cambridge Phil. Soc. **39**, 189 (1943).

[3] The π-mesons (π^+, π^0) can also be considered as the three charge states of a particle with isotopic spin 1 (represented by ξ). Various mass-operators, commutative with the charge-operator ξ_3, can be constructed.

Lifetime of an Excited State of $_{66}Dy^{160}$ and Upper Limits for Some Other Nuclei

F. K. McGowan
Oak Ridge National Laboratory, Oak Ridge, Tennessee
(Received November 16, 1951)

An excited state in $_{66}Dy^{160}$ with a half-life of $(1.8\pm0.2)\times10^{-9}$ sec has been observed with a delayed coincidence scintillation spectrometer using sources of Tb^{160}. The β-decay of Tb^{160} is known to consist of at least two components and is accompanied by a large number of gamma-rays and conversion electrons.[1,2]

The delayed coincidence scintillation spectrometer is similar to that described previously.[2] In many cases the lifetimes of excited nuclear states are too short to be measured and only upper limits can be set.

In the case of Dy^{160}, delayed coincidences were observed by exciting one channel of the delayed coincidence apparatus with 165 to 250 kev nuclear β-rays and the other channel by the L, M, or N internal conversion electrons of the 85-kev transition. The spectrum of the radiation announcing the formation of the metastable state appears to be a β-ray distribution with a maximum energy of about 900 kev and presumably corresponds to the 860 kev β-ray observed in the decay of Tb^{160} from magnetic spectrometer measurements.[1] The L and M internal conversion electrons corresponding to an 85-kev transition were observed in the spectrum of the delayed radiation. No other gamma-rays of higher energy appear in the spectrum of the delayed radiation.

Under favorable conditions a half-life of 5×10^{-10} sec can be detected with the apparatus using anthracene detectors. The observed upper limits of the half-life of some other excited states are listed in Table I.

TABLE I. Upper limits of the half-life of some excited nuclear states.

Nucleus	E_γ	$T_{1/2}$	Radioactive source
$_{53}Te^{128}$	159 kev	$<1.0\times10^{-9}$ sec	Te^{128*}
$_{53}Te^{126}$	35	$<2.0\times10^{-9}$ sec	Te^{126*}
$_{67}Ho^{165}$	95	$<0.8\times10^{-9}$ sec	Dy^{165}
$_{80}Hg^{198}$	411	$<0.4\times10^{-9}$ sec	Au^{198}
$_{81}Tl^{200}$	280	$<0.4\times10^{-9}$ sec	Hg^{200}

[1] Burson, Blair, and Saxon, Phys. Rev. **77**, 403 (1950).
[2] Cork, Branyan, Rutledge, Stoddard, and LeBlanc, Phys. Rev. **78**, 304 (1950).
[3] F. K. McGowan, Phys. Rev. **80**, 923 (1950).

Nuclear Reaction Energies*

D. M. Van Patter, A. Sperduto, P. M. Endt, W. W. Buechner, and H. A. Enge
Physics Department and Laboratory for Nuclear Science and Engineering, Massachusetts Institute of Technology, Cambridge 39, Massachusetts
(Received November 13, 1951)

In a previous publication,[1] the measurements of thirty-eight reaction energies were reported. Since then, the ground-state Q-values of ten additional nuclear reactions have been measured using the 180-degree magnetic spectrograph at MIT. The results are listed in Table I, together with four of the published Q-values that have been revised in the light of new data. Comparison is made with the most recent results of other workers. It may be noted that the reaction energies for the $Mg^{25}(d, p)Mg^{26}$ and $Si^{29}(d, \alpha)Al^{27}$ reactions have not been previously reported by other workers. In the case of the $Si^{29}(d, p)Si^{30}$ and $P^{31}(d, p)P^{32}$ reactions, the reference value is obtained by subtracting a deuteron binding energy of 2.23 Mev from the (n, γ) measurements of Kinsey and his co-workers.[2]

TABLE I. Observed reaction energies.

Reaction	Present Q-value (Mev)	Other Q-value (Mev)
$Ne^{20}(d, p)Ne^{21}$	4.529 ± 0.007	4.54 ± 0.04[a]
$Ne^{22}(d, p)Ne^{23}$	2.964 ± 0.007	2.96[b]
$Na^{23}(p, \alpha)Ne^{20}$	2.372 ± 0.008	2.34 ± 0.04[c]
$Mg^{25}(d, \alpha)Na^{23}$	7.019 ± 0.013	7.24[d]
$Mg^{25}(d, p)Mg^{26}$	8.880 ± 0.012	
$Mg^{26}(d, p)Mg^{27}$	4.207 ± 0.006	4.21 ± 0.10[e]
$Al^{27}(p, \alpha)Mg^{24}$	1.595 ± 0.007	1.585 ± 0.015[e]
$Si^{29}(d, \alpha)Al^{27}$	5.994 ± 0.011	
$Si^{29}(d, p)Si^{30}$	8.388 ± 0.013	8.32 ± 0.05[f]
$P^{31}(p, \alpha)Si^{28}$	1.909 ± 0.010	1.85 ± 0.02[g]
	Revised Q-values	
$Mg^{24}(d, p)Mg^{25}$	5.097 ± 0.007	5.03 ± 0.05[h]
$Si^{30}(d, p)Si^{31}$	4.364 ± 0.007	4.33 ± 0.05[i]
$P^{31}(d, \alpha)Si^{29}$	8.158 ± 0.011	
$P^{31}(d, p)P^{32}$	5.704 ± 0.008	5.71 ± 0.03[f]

[a] R. Middleton and C. T. Tai, Proc. Roy. Soc. (London) **A64**, 801 (1951).
[b] J. Ambrosen and K. M. Bisgaard, Nature **165**, 888 (1950).
[c] J. M. Freeman, Proc. Roy. Soc. (London) **A63**, 668 (1950).
[d] M. S. Livingston and H. A. Bethe, Revs. Modern Phys. **9**, 245 (1937).
[e] Allan, Wilkinson, Burcham, and Curling, Nature **163**, 210 (1949).
[f] See reference 2.
[g] See reference 3.
[h] H. R. Allan and C. A. Wilkinson, Proc. Roy. Soc. (London) **A194**, 131 (1948).
[i] H. T. Motz and R. F. Humphreys, Phys. Rev. **80**, 595 (1950).

TABLE II. Disintegration energy in Mev.

Disintegration	Calculated	Observed
$Na^{24} \rightarrow Mg^{24}$	5.544 ±0.022	5.528[a]
$Mg^{27} \rightarrow Al^{27}$	2.610 ±0.020	2.63 ±0.06[b]
$Al^{28} \rightarrow Si^{28}$	4.647 ±0.020	4.647 ±0.014[c]
$Si^{31} \rightarrow P^{31}$	1.482 ±0.021	1.471 ±0.008[c]

[a] K. Siegbahn, Phys. Rev. **70**, 127 (1946).
[b] Benes, Hedgran, and Hole, Arkiv Mat. Astr. Fys. **A35**, No. 12 (1948).
[c] See reference 5.

The (d, p) reactions of the neon isotopes were investigated, using partially separated isotopic targets deposited on silver sheets. (We are indebted to the Nobel Institute in Stockholm for the preparation of the neon targets.) Attempts to observe the (d, α) reactions of the neon isotopes proved unsuccessful because of the evaporation of neon from the targets when exposed to beam bombardment. In the case of the magnesium isotopes Mg^{25} and Mg^{26}, targets were prepared by allowing a suspension of enriched magnesium dioxide to deposit upon platinum backings. Comparison of the data obtained from these targets with those obtained from a target of natural magnesium permitted the positive identification of the particle groups corresponding to the Mg^{25} and Mg^{26} isotopes. A similar analysis was used for the isotopes Si^{29} and Si^{30}. In this case, the targets were prepared by evaporation of enriched silicon dioxide onto platinum backings. (The enriched samples of magnesium dioxide and silicon dioxide were obtained from the Stable Isotopes Division, AEC, Oak Ridge.) The phosphorus targets consisted of copper phosphate and zinc phosphide evaporated onto platinum backings.

In general, the Q-values reported in Table I are the result of averaging several measurements. However, in the case of the $Ne^{22}(d, p)$, $Na^{23}(p, \alpha)$, $Al^{27}(p, \alpha)$, and $P^{31}(p, \alpha)$ reactions, the value given is based on a single observation. Fortunately, there is sufficient evidence from other sources to indicate that these four measurements may be relied upon.

It is possible to examine the internal consistency of our results using the following closed cycles:

$Al^{27}(d, \alpha)Mg^{25}$	6.694±0.010[1]
$Mg^{24}(d, p)Mg^{25}$	5.097±0.007
$Al^{27}(p, \alpha)Mg^{24}$	1.597±0.009 (calc)
$Al^{27}(p, \alpha)Mg^{24}$	1.595±0.007 (obs)
$Na^{23}(d, \alpha)Ne^{21}$	6.902±0.010[1]
$Ne^{20}(d, p)Ne^{21}$	4.529±0.007
$Na^{23}(p, \alpha)Ne^{20}$	2.372±0.011 (calc)
$Na^{23}(p, \alpha)Ne^{20}$	2.372±0.008 (obs)
$P^{31}(d, \alpha)Si^{29}$	8.158±0.011
$Si^{28}(d, p)Si^{29}$	6.246±0.009[1]
$P^{31}(p, \alpha)Si^{28}$	1.912±0.011 (calc)
$P^{31}(p, \alpha)Si^{28}$	1.909±0.010 (obs)

The $P^{31}(d, \alpha)Si^{29}$ Q-value has been remeasured as 8.158±0.011 Mev compared with the published value of 8.170±0.020 Mev.[1] A confirmation of this new value can be obtained from a comparison of the Q-values of $P^{31}(d, \alpha)$ and $Si^{28}(d, p)$ groups, corresponding to excited states of Si^{29}, leading to a calculated value of 8.157±0.012 Mev. In addition, the new measurement of the $P^{31}(p, \alpha)Si^{28}$ reaction confirms the validity of this revised value. However, the recent value of 1.85±0.02 Mev for the $P^{31}(p, \alpha)Si^{28}$ reaction energy, measured by Freeman and Seed[2] using magnetic analysis, is not in agreement with the present results.

The reaction energies measured in this laboratory now link the masses of nuclei from Ne^{20} to P^{32}. In addition, it is possible to calculate the disintegration energies of Na^{24}, Mg^{27}, Al^{28}, and Si^{31}, by choosing the appropriate reactions.

The disintegration energies listed in Table II were calculated using values[4] of 23.834±0.007 and 1.443±0.002 Mev for the mass differences $(2D^2-He^4)$ and $(2H^1-D^2)$. The agreement with the unpublished results of Motz and Alburger[5] for Al^{28} and Si^{31} is highly satisfactory.

* This work has been supported by the joint program of the ONR and AEC.
[1] Strait, Van Patter, Buechner, and Sperduto, Phys. Rev. **81**, 747 (1951).
[2] B. B. Kinsey (private communication).
[3] J. M. Freeman and J. Seed, Proc. Phys. Soc. (London) **A64**, 314 (1951).
[4] Li, Whaling, Fowler, and Lauritsen, Phys. Rev. **83**, 512 (1951).
[5] H. T. Motz and D. E. Alburger (private communication).

Interactions between Nuclear Spins in Molecules

N. F. RAMSEY AND E. M. PURCELL
Harvard University, Cambridge, Massachusetts
(Received November 9, 1951)

HAHN and Maxwell[1] have recently reported a spin-echo experiment which indicates the existence of an interaction of the form $4J\hbar\mathbf{I}_1\cdot\mathbf{I}_2$ between two protons in dichloroacetaldehyde, with $J/2\pi$ being 0.7 cycle per second. An interaction of this form and magnitude has been difficult to understand. The direct magnetic interaction between the two nuclear spins is not of this form but depends on the relative positions of the two nuclei in such a way that when averaged over all orientations of the molecule it equals zero. Hahn and Maxwell[1] suggest that the magnetic shielding[2] of the nuclear spin magnetic field may modify the spin-spin magnetic interaction in such a way as to prevent its averaging to zero so that an interaction of the desired type is produced. However, they point out that it seems difficult to reconcile the order of magnitude of J to be thus expected with the experimental values.

It is the purpose of this note to point out a mechanism which should give rise to an $\mathbf{I}_1\cdot\mathbf{I}_2$ interaction of the magnitude observed. This mechanism is the magnetic interaction between each nucleus and the electron spin of its own atom together with the exchange coupling of the electron spins with each other. This mechanism can most easily be described for a $^1\Sigma$ diatomic molecule, such as HD. It corresponds to the fact that the magnetic interaction of the one nucleus with the electron of its atom will make the electron of that atom tend to lie more frequently antiparallel to the nuclear spin than parallel to it. On the other hand, the two electron spins in the singlet state must be antiparallel to each other so that the electron of the other atom will tend to lie more frequently parallel to the spin of the first nucleus. However, the electron of that atom magnetically interacts with the second nucleus. The combination of these interactions therefore provides a spin interaction between the two nuclei. In terms of perturbation theory the proposed mechanism corresponds to a second-order perturbation by the higher electronic triplet states of molecules with the perturbing interaction being the magnetic interactions of each nucleus with the electron spins. The reason that electron-spin effects enter here, whereas they are omitted in ordinary magnetic shielding[2] calculations, is that in the present case the magnetic fields from both nuclei vary over the molecule, whereas in the ordinary magnetic shielding case one of the perturbing fields is the externally applied one which is uniform over the molecule and hence affects both electron spins alike.

The effect of the electrons on the interaction of the nuclear spins may be calculated with the following Hamiltonian[3-6] for the molecule

$$\mathcal{H}=\mathcal{H}_1+\mathcal{H}_2+\mathcal{H}_3, \tag{1}$$

where

$$\mathcal{H}_1=\Sigma_k[1/2m_k][(\hbar/i)\nabla_k+(e/c)\Sigma_l\gamma_l\mathbf{I}_l\times\mathbf{r}_{kl}/r_{kl}^3]^2 + V+\mathcal{H}_{LS}+\mathcal{H}_{SS}+\mathcal{H}_{II}$$
$$\mathcal{H}_2=2\beta\Sigma_{kl}\gamma_l[3(\mathbf{S}_k\cdot\mathbf{r}_{kl})(\mathbf{I}_l\cdot\mathbf{r}_{kl})r_{kl}^{-5}-\mathbf{I}_l\cdot\mathbf{S}_k r_{kl}^{-3}] \tag{2}$$
$$\mathcal{H}_3=(16\pi\beta/3)\Sigma_{kl}\gamma_l\delta(\mathbf{r}_k-\mathbf{r}_l)\mathbf{S}_k\cdot\mathbf{I}_l.$$

In the aforementioned, l indicates the lth nucleus with spin $\mathbf{I}_l$ and

k the k'th electron with spin $\mathbf{S}_k$, V is the total electrostatic interaction, and $\mathbf{r}_{kl}$ is the vector $\mathbf{r}_k - \mathbf{r}_l$. $\mathcal{H}_{II}$ corresponds to the direct magnetic interaction of the two nuclei and reduces to zero when averaged over all molecular rotational states. The remaining quantities are defined in the references.[2-4]

With the aforementioned Hamiltonian, the energy of the system can be calculated to second order by perturbation theory. The terms which depend on the products of the spins of the two nuclei then correspond to the various spin-spin interactions. The terms arising from the bracketed quantity in $\mathcal{H}_1$ are analogous to the magnetic shielding terms calculated by Ramsey[2] for uniform magnetic fields and are the ones considered by Hahn and Maxwell[1] and found to produce too small an effect. The terms suggested in the present paper are the second-order perturbation terms arising from $\mathcal{H}_2$ and $\mathcal{H}_3$ and their cross products. The effects of these terms have been calculated approximately for molecular HD with the use of Heitler-London wave functions. The frequency shift arising from second-order perturbations by $\mathcal{H}_2$ was found to be 0.5 $\mathbf{I}_H \cdot \mathbf{I}_D$ cycles per second when averaged over all molecular rotational states, which is small and of the same order of magnitude as the terms considered by Hahn.[1] The cross terms between $\mathcal{H}_2$ and $\mathcal{H}_3$ vanish when averaged over all molecular rotational states. However, the second-order perturbations by $\mathcal{H}_3$ give a frequency shift that is relatively large and approximately equal to 70 $\mathbf{I}_H \cdot \mathbf{I}_D$ cycles per second. It is of interest to note that this term, which is the important one, can be written approximately as $0.46\ \mathbf{I}_H \cdot \mathbf{I}_D \Delta\nu_H \Delta\nu_D / (\Delta E/h)$ where the $\Delta\nu$'s are the atomic hyperfine separations, and ΔE is the separation of the lowest singlet and lowest triplet states in molecular hydrogen.

Although a similar calculation in the case of dichloroacetaldehyde is precluded by the lack of a suitable wave function for the molecule, it is quite reasonable from the foregoing calculation that an effect as large as the observed 0.7 cycle per second should be observed since the exchange coupling of the electrons with each other in the successive bonds lying between the two hydrogens is large. In some substances much larger interactions than the aforementioned could probably be obtained if ΔE were suffiently small.

Experiments to observe this effect in a simple molecule like HD are being planned by the authors. Although such an interaction should also occur in homonuclear molecules such as H_2, it would not be observable in transitions involving no change in molecular rotational state. The authors wish to express their appreciation to Dr. Hahn for sending them an advance copy of the manuscript of his very interesting paper.[5]

[1] E. L. Hahn and D. E. Maxwell, Phys. Rev. **84**, 1246 (1951).
[2] N. F. Ramsey, Phys. Rev. **78**, 699 (1950).
[3] H. A. Bethe, Handbuch der Physik (J. Springer, Berlin, Germany, 1933), Vol. 24/1, p. 386.
[4] A. Abragam and M. H. L. Pryce, Proc. Roy. Soc. (London) **A205**, 136 (1951).
[5] Subsequent to the submission of this letter the authors have studied the recent article of H. S. Gutowsky and C. J. Hoffman [J. Chem. Phys. **19**, 1259 (1951)] in which these authors find multiplet resonance lines with FF's. The mechanism suggested in the present letter should account for a multiplet structure of the observed nature. This mechanism should produce a larger effect than the one considered by Gutowsky, McCall, and Slichter [Phys. Rev. **84**, 590 (1951)] which depends only on electronic orbital contributions arising from $\mathcal{H}_1$ in Eq. (2) above.

Possible Natural Radioactivity of Neodymium*

GEORGE I. MULHOLLAND AND TRUMAN P. KOHMAN
Department of Chemistry, Carnegie Institute of Technology, Pittsburgh, Pennsylvania
(Received November 13, 1951)

A NUMBER of investigators have looked for natural radioactivity in neodymium.[1-12] All agree that alpha-activity is absent, and most either reported no beta-activity or ascribed the observed activity to common radioactive impurities. However, Libby,[7] who used by far the most sensitive detection method, reported a beta-radiation of maximum energy of about 11 kev and specific activity about 60–120 disintegrations per second per gram. That this activity is truly characteristic of neodymium has been in doubt because Libby did not repurify or fractionate his samples from all other elements to constant specific activity. Takvorian[9] reported inability to detect activity in neodymium, but an inspection of his data shows that his sensitivity was grossly inadequate. A reference by Broda[11] to the unpublished work of Jha (1949) gives no data but implies confirmation of Libby's findings. A recent report by Curran, Dixon, and Wilson[12] states that Libby's data are probably wrong and that the maximum beta-energy may greatly exceed 11 kev. The implication is that radiation attributable to the element was observed, but no indication of the level of activity or degree of chemical purification is given.

One of us[13] has pointed out that Nd^{150} appears to be outside the limits of beta-stability for even-even nuclides, and suggested the possible identification of the radiations found by Libby with those of Nd^{150}. This would imply the natural occurrence of Pm^{150} in equilibrium with Nd^{150} in rare earth minerals, a relatively long lifetime for the daughter being required to explain the absence of hard radiations in Libby's samples. An alternate possibility suggested, that Nd^{140} is long-lived and occurs naturally, has been eliminated by the subsequent finding[14] that Nd^{140} has a 3.3-day half-life with a 2-minute daughter emitting energetic radiations. The determination[15] that Pm^{148} undergoes electron-capture decay to Nd^{148} removes the possibility[16] that the latter is unstable.

Our measurements were made with a proportional counter accommodating internally solid samples 1650 cm² in area, filled with 68-cm argon and 8-cm ethylene. About 10 percent of the sample is obscured by three longitudinal rods which support the wire from one end so that samples can be inserted from the other end. It is used as a crude spectrometer for low energy radiations by varying the external amplifier gain so as to obtain bias curves. An energy calibration was obtained from the sharp cutoff of the manganese K x-rays of Fe^{55} (6 kev), and the highest gain used corresponds to a bias level of 0.3 kev on the energy scale. By combined absorption and bias-curve measurements of the K Auger electrons from this transition (5 kev), we have verified that electrons of a very few kev energy are counted with apparent high efficiency and no reduction in energy. The background has been reduced to about 32 counts per minute by shielding with a ring of Geiger counters in anticoincidence, 2 inches of hot-rolled steel, and 3 inches of lead. Since Libby observed 10 counts per minute from an area of 193 cm² at 14 percent geometry, we would expect 270 counts/min from our 1650 cm² at 45 percent geometry if his data were correct, the sample thickness being immaterial for such low energy radiations.

Commercial 99 percent pure neodymium oxide (Lindsay Light and Chemical Company, Chicago) was twice purified in a cation exchange column (Dowex 50) 80 cm long, with very slow citrate elution, scavenged by barium sulfate and zirconium iodate precipitations, precipitated as oxalate, and ignited. A 15-gram layer of the resulting oxide spread uniformly on a copper sheet gave a counting rate about 4 per minute above background at the lowest bias. The bias curves showed that practically all of the excess radiations were more energetic than 11 kev. Moreover, the sensitivity of the copper-lined counter to external gamma-radiation (Co^{60}) is increased about 11 percent by the Nd_2O_3 coating, which just about accounts for the excess observed, since most of the residual background is presumably due to gamma-radiation. No growth of activity was observed in two months. We conclude that not more than 1 count/min of either soft or hard radiation is contributed by the neodymium. Accordingly, the maximum specific beta-activity is 0.003 disintegration per second per gram of element, corresponding to a minimum half-life of 2×10^{18} years for Nd^{150}.

In spite of the negative results of this experiment we feel that it is still likely that Nd^{150} is unstable but with a highly forbidden decay and very long lifetime. In the discussion of the limits of beta-stability,[13] Nd^{150} and Ca^{48} were given similar special mention as being apparently outside of the stability region, and another

letter[17] cites evidence that Ca^{48} is indeed unstable but with an extremely long lifetime. Nordheim[18] has pointed out that odd-odd nuclides frequently have large nuclear spins, and this may well be the case for Pm^{180}. Nd^{180} could probably decay only to the ground state of Pm^{180}, and the large spin change would make this transition highly forbidden as must be the case for Ca^{48}.

Although we did not look specifically for alpha-activity, our measurements set an upper limit of 0.02 alphas per second per gram of neodymium, about one-fifteenth of the previous limit set by Bestenreiner and Broda.[10]

* This work has been supported by the AEC. Fe^{58} and Co^{60} were obtained from the Isotopes Division of the AEC.

[1] W. F. Libby and W. M. Latimer, J. Am. Chem. Soc. **55**, 433 (1933).
[2] M. Curie and S. Takvorian, Compt. rend. **196**, 923 (1933).
[3] Hevesy, Pahl, and Hosemann, Z. Physik **83**, 43 (1933).
[4] W. Yeh, Compt. rend. **197**, 142 (1933).
[5] L. Rolla and L. Mazza, Atti. accad. nazl. Lincei **18**, 472 (1933).
[6] G. v. Hevesy and M. Pahl, Z. physik. Chem. **A169**, 147 (1934).
[7] W. F. Libby, Phys. Rev. **45**, 845; **46**, 196 (1934).
[8] Mazza, Bracci, and Guerri, Gazz. chim. ital. **65**, 993 (1935).
[9] S. Takvorian, Ann. chim. **20**, 113 (1945).
[10] F. Bestenreiner and E. Broda, Nature **164**, 658 (1949).
[11] E. Broda, *Advances in Radiochemistry* (Cambridge University Press, London, 1950), p. 35.
[12] Curran, Dixon, and Wilson, Phys. Rev. **84**, 151 (1951).
[13] T. P. Kohman, Phys. Rev. **73**, 16 (1948).
[14] G. Wilkinson and H. G. Hicks, Phys. Rev. **75**, 1687 (1949).
[15] F. D. S. Butement, Nature **167**, 400 (1951).
[16] N. E. Ballou, Phys. Rev. **73**, 630 (1948).
[17] J. W. Jones and T. P. Kohman, Phys. Rev. (to be published).
[18] L. W. Nordheim, Argonne National Laboratory Report 4626, Part II (1951); Revs. Modern Phys. (to be published).

The Hyperfine Structure Anomaly of the Rb Isotopes*

S. A. Ochs and P. Kusch
Columbia University, New York, New York
(Received November 20, 1951)

EFFECTS arising from the distribution of the nuclear magnetic moment over a finite volume lead to a discrepancy in the ratios of the hfs splittings of Rb^{85} and Rb^{87}, as measured directly[1] and as calculated from the ratio of the nuclear moments, if the nuclei are assumed to be point dipoles.[2] As the effect depends strongly on the relative distribution of the spin and orbital magnetic moments within the nuclear volume of each isotope, it presents a critical test of a nuclear model and accurate knowledge of its magnitude affords a valuable guide to theoretical investigation. The magnitude of this anomaly has been explained with some success by considering the nuclei in question to consist of a single nucleon moving in the field of a nuclear core of no intrinsic angular momentum.[3,4]

Bitter, using his own results[5] and data obtained by Millman and Kusch,[1] showed that

$$\Delta=\frac{(\Delta\nu^{87}/\Delta\nu^{85})_{obs}-(\Delta\nu^{87}/\Delta\nu^{85})_{calc}}{(\Delta\nu^{87}/\Delta\nu^{85})_{calc}},$$

is (0.33 ± 0.05) percent. The recent direct measurement by Yasaitis and Smaller[6] of the ratio $\mu(Rb^{87})/\mu(Rb^{85})$ is of much greater accuracy (one part in 250,000) than either the previous moment ratio or the previous ratio of the hfs splittings. It became worthwhile, therefore, to redetermine the $\Delta\nu$ ratio to a precision comparable to that of the moment ratio and to obtain Δ to a high degree of precision.

We have used a previously described[6] atomic beam method to determine $\Delta\nu$ from a measurement of some of the lines $\Delta m_I=\pm1$, $\Delta m_J=0$ in the hfs spectrum of the Rb isotopes. Those transitions were chosen which give rise to doublets ($m_J=\pm1/2$) whose mean frequencies attain maximum values at characteristic values of x, where $x\equiv(g_J-g_I)\mu_0H/h\Delta\nu$. $Rb^{87}(I=3/2)$ has one such doublet, while $Rb^{85}(I=5/2)$ has two. Within a small range of x, bracketing the value for maximum frequency, the line frequencies are almost field independent. The measured doublet separation ($2g_I\mu_0H/h$) and approximate values of g_J/g_I and $\Delta\nu$ then suffice for the determination of x, which, together with the measured mean frequency, yields a value of $\Delta\nu$ whose accuracy is limited only by the precision of the frequency measurements. Of the two maxima in the Rb^{85} spectrum one (m_F: $0\leftrightarrow1$) occurs at an x of 5.8284 and the other (m_F: $-1\leftrightarrow-2$) at an x of 1.9250. The first of these, therefore, corresponds to a larger doublet separation and yields a more precise value of x. In addition for the doublet (m_F: $0\leftrightarrow-1$), the frequency at values of x close to that at the maximum mean frequency is much less field dependent than the frequency of the doublet (m_F: $-1\leftrightarrow-2$) near its maximum mean frequency. Thus, the doublet (m_F: $0\leftrightarrow-1$) is much better suited for an accurate determination of $\Delta\nu(Rb^{85})$ and was used in this experiment.

Our results are

$$\Delta\nu(Rb^{85})=3035.730\pm0.005\text{ Mc/sec}$$
$$\Delta\nu(Rb^{87})=6834.681\pm0.010\text{ Mc/sec}.$$

Measurements taken for the transition (m_F: $-1\leftrightarrow-2$) gave

$$\Delta\nu(Rb^{85})=3035.745\pm0.025\text{ Mc/sec},$$

which compares favorably with the forestated value. The ratio

$$\Delta\nu^{87}/\Delta\nu^{85}=2.251413\pm0.000005,$$

together with the result of Yasaitis and Smaller,[6] yields

$$\Delta=(0.3501\pm0.0006)\text{ percent}.$$

Bohr and Weisskopf[3] found the best agreement between the experimentally determined value of Δ and that predicted from their rather crude nuclear model by choosing for g_S and g_L the g-values of the odd proton. They thus calculated $\Delta=0.29$ percent. Bohr subsequently studied a model in which he assumed the individual nucleons to move in an asymmetric average field[7] and used it to recalculate the hfs anomaly in greater detail.[4] Neglecting the contribution of the nuclear core to the angular momentum and making special assumptions about the couplings between the various angular momentum vectors, he found $\Delta=0.26$ percent. The increase in the experimental value of Δ here reported as compared to the earlier results, and the decrease in the value calculated by Bohr on the basis of a refined nuclear model, lead to a rather large discrepancy between Δ_{obs} and Δ_{calc}. It is clear that a more detailed theoretical analysis is required to predict a value of Δ in good agreement with and comparable in uncertainty to Δ_{obs}.

* This research supported in part by the ONR.

[1] S. Millman and P. Kusch, Phys. Rev. **58**, 438 (1940).
[2] F. Bitter, Phys. Rev. **75**, 1326 (1949).
[3] A. Bohr and V. F. Weisskopf, Phys. Rev. **77**, 94 (1950).
[4] A. Bohr, Phys. Rev. **81**, 331 (1951).
[5] E. Yasaitis and B. Smaller, Phys. Rev. **82**, 750 (1951).
[6] P. Kusch and H. Taub, Phys. Rev. **75**, 1477 (1949).
[7] A. Bohr, Phys. Rev. **81**, 134 (1951).

Condition for Radiation from a Solar Plasma

J. Feinstein
National Bureau of Standards, Washington, D. C.
(Received November 21, 1951)

RECENT attempts to account for the bursts of radiofrequency electromagnetic radiation received from the sun have employed the mechanism of wave growth in a uniform plasma of infinite extent for the conversion of the kinetic energy of moving streams into the time varying fields of a space charge wave. The existence of a Poynting flux vector within the infinite oscillating plasma has then been taken as the criterion for the escape of radiation.[1] It is the purpose of this note to point out that while a model which is infinite in extent is undoubtedly satisfactory for the determination of the bands within which wave amplification can occur in the interior of a finite sized plasma, one cannot justify the use of a point value of the Poynting vector within a uniform infinite plasma as a criterion for the reception of radiation at a point exterior to, and far removed from, the actual oscillating plasma.

Instead, to formulate such a criterion, one must follow the usual procedure of integrating the inhomogeneous wave equation. For a harmonic time variation, the Hertz vector takes the form:[2]

$$\mathbf{\Pi}(\mathbf{r},t)=\frac{ie^{-i\omega t}}{4\pi\omega\epsilon}\int_{v'}\mathbf{J}(\mathbf{r}')\frac{\exp(ik|\mathbf{r}-\mathbf{r}'|)}{|\mathbf{r}-\mathbf{r}'|}dv(\mathbf{r}'),\tag{1}$$

where the source of the field, $\mathbf{J}$, is the oscillating plasma current. For a traveling space charge wave possessing a propagation constant $\mathbf{\Gamma}$, and assumed for simplicity to build up and decay at the same rate, one may set

$$\mathbf{J}(\mathbf{r}')=\mathbf{J}_0\exp(-|\mathbf{b}\cdot\mathbf{r}'|+i\mathbf{\Gamma}\cdot\mathbf{r}').\tag{2}$$

At distances far from the current distribution, the electric component of the radiation field then takes the form:

$$\mathbf{E}(\mathbf{r},t)=\frac{i\omega\mu_0}{4\pi}\cdot\frac{\mathbf{J}_0\times\mathbf{r}}{|\mathbf{r}|^2}e^{ik|\mathbf{r}|-i\omega t}\times\int_{v'}\exp\left[-|\mathbf{b}\cdot\mathbf{r}'|+\frac{ik(\mathbf{r}\cdot\mathbf{r}')}{|\mathbf{r}|}+i\mathbf{\Gamma}\cdot\mathbf{r}'\right]dv(\mathbf{r}').\tag{3}$$

First, it is evident that the existence of a component of $\mathbf{J}_0$ transverse to the plasma propagation vector $\mathbf{\Gamma}$, the condition for the existence of a Poynting vector in the uniform infinite model, is not relevant. Instead the field depends essentially upon the value of the phase integral taken over the volume occupied by the oscillating current. It is primarily the magnitude of $\mathbf{b}$ with respect to $\mathbf{\Gamma}$ and k which determines the net value of this integral. Thus we may conclude that coupling of energy from an oscillating plasma into a radiation field is dependent upon the existence of rapid spatial changes in the amplitude of the current distribution of the plasma. This is, of course, precisely the requirement for an element to act as an antenna. It arises through the necessity of preventing phase cancellation of the radiation effects of current elements separated by half a wavelength.

For evaluation purposes the volume integral in (3) may be reduced to the product of three one-dimensional integrals. Utilizing the fact that $|\mathbf{\Gamma}|\gg k$ for stream speeds which are small compared to the velocity of light, if $|\mathbf{b}|\ll|\mathbf{\Gamma}|$, and if further the plasma may be considered to decay with cylindrical symmetry in planes perpendicular to the propagation direction $\mathbf{\Gamma}$, one obtains

$$\int_v\simeq(\mathbf{b}\cdot\mathbf{\Gamma})/k^2|\mathbf{\Gamma}|^2.\tag{4}$$

It may be noted that this result is consistent with the view expressed in an earlier paper[3] regarding the efficacy of rapid spatial changes in the production of a radiation field. At that time, however, the author considered this mechanism complementary to those associated with the production of a Poynting flux in an infinite model. The present analysis indicates it is the only possibility.

[1] V. A. Bailey, Phys. Rev. **83**, 439 (1951); **78**, 428 (1950); J. A. Roberts, Phys. Rev. **76**, 340 (1949).
[2] J. A. Stratton, *Electromagnetic Theory* (McGraw-Hill Book Company, Inc., New York, 1941), p. 431.
[3] J. Feinstein and H. K. Sen, Phys. Rev. **83**, 405 (1951).

The Decay Series $Nd^{140}-Pr^{140}-Ce^{140*}$

CHARLES I. BROWNE,† JOHN O. RASMUSSEN, JOSEPH P. SURLS, AND DONALD F. MARTIN
Radiation Laboratory and Department of Chemistry, University of California, Berkeley, California
(Received October 29, 1951)

THE nuclide $_{60}Nd^{140}$ has been previously reported[1] as a 3.3-day K-capture, and its daughter $_{59}Pr^{140}$, as a 3.4-minute K-capture and β^+ emitter, with a β^+ energy, determined by aluminum absorption methods, of 2.4 Mev. We have prepared Nd^{140} by a bombardment of 300 mg of praseodymium oxide with 19-Mev deuterons on the Crocker 60-inch cyclotron followed by chemical separations by citrate elution from a Dowex-50 cation exchange resin column at 83°C.[2] The decay chain was studied on a double focusing beta-ray spectrometer, a bent crystal x-ray spectrometer, and a scintillation crystal gamma-spectrometer.

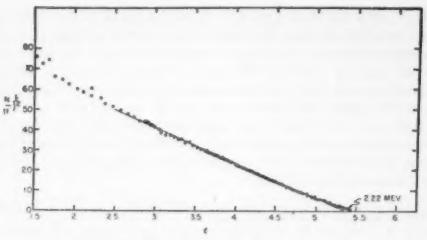

FIG. 1. Fermi plot Pr^{140} β^+ spectrum.

The Bethe and Bacher approximation was used to calculate the Fermi function employed in a Fermi plot of the Pr^{140} positron spectrum, which exhibited good linearity with an end-point energy of 2.23±0.02 Mev (Fig. 1). The data do not exclude the possibility of a low abundance lower energy (~1 Mev) component. The ϵ^- spectrum was investigated up to $H\rho$ values corresponding to an electron energy of 1 Mev, and showed only one discernible line, at 28.9±0.5 kev, which we interpret as electrons from Auger conversion of K-shell vacancies, in either praseodymium or cerium, or both, as the resolution of the line does not permit this distinction.

The gamma-ray spectrum showed no lines in addition to K x-ray, annihilation radiation, and Compton radiation, in intensity as high as 10 percent of that of the K x-rays; there was a meager indication of radiation of energy 1–1.2 Mev. The x-ray spectrum (Fig. 2) showed only the $K_{\alpha_1\alpha_2}$ (unresolved) and $K\beta_1$ x-rays of both praseodymium and cerium, in the following intensity ratios:

$$PrK\alpha_{1,2}:CeK\alpha_{1,2}:PrK\beta_1:CeK\beta_1=100:50:28:11.$$

Since no sources of origin of K x-rays other than electron capture could be detected, we attribute all observed x-rays to that source, from which, if we consider only K-capture, we calculate the K/β^+ ratio in Pr^{140} to be 1.0±0.1.

The value of ft of the Pr^{140} decay was calculated from the theoretical values of Feenberg and Trigg[3] for $(f_+ + f_k)$ to be 2×10^4, which leads to the conclusion that the transition is allowed, and if we take the total angular momentum of Ce^{140} as 0, the ΔI must be, by Gamow-Teller selection rules, unity. The ratio f_k/f_+ is given by Feenberg and Trigg to be 1.0, in good agreement with the value for K/β^+ given previously. If L capture is taken into consideration, the experimental value for K/β^+ in Pr^{140} is changed somewhat. An internally consistent solution based upon Rose's[4] theoretical L/K-capture ratios, our data, and theoretical values for f_k leads to the conclusion that Nd^{140} decays 26 percent by L-capture and 74 percent by K-capture; that Pr^{140} decays 58 percent by β^+ emission, 37 percent by K-capture, and 5 percent

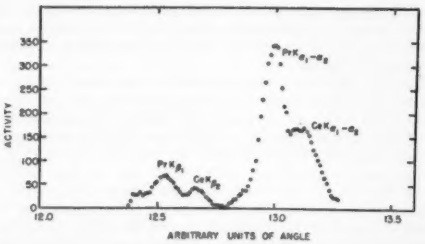

FIG. 2. X-ray spectrum.

by L-capture; that the ratio of β^+/K in Pr^{140} is $\sim 1.6/1$, and that the decay energy of Nd^{140} is 105 ± 40 kev.

The ground state of Ce^{140} is very probably S_0, so that the state of Pr^{140}, by Nordheim's[5] rule that $\Delta L=0$ for an allowed transition, must be S_1. Both the odd nucleons in Pr^{140} fall into the shell $50<N\leqq 82$, with possible states, by the Mayer model, of $g_{7/2}$, $d_{3/2}$, $d_{1/2}$, $s_{1/2}$, and $h_{11/2}$. Since the total angular momentum is low, Nordheim's[5] rule 9 should apply to Pr^{140}, leading to six possible combinations of these states as describing the odd neutron and the odd proton. However, the total angular momentum of Pr^{141} is known to be 5/2, and that of $_{56}Ba^{137}$ as 3/2, suggesting the probable choice of $d_{3/2}$ as the state of the proton, and $d_{3/2}$ as that of the neutron, which is one of the combinations admitted by Nordheim's rule. If, then, the angular momenta couple antiparallel, as Nordheim implies, the resulting over-all state of Pr^{140} would be S_1, in agreement with the conclusion reached earlier.

We have also integrated the β^+ and ϵ^- spectra, and find a ratio of β^+/ϵ^- of approximately 50, leading to a K/ϵ^- ratio of 100. Such a value leads to a very high figure (0.99) for the mean K fluorescent yield at $Z=58$ and 59. Considering that an error of a factor of 10 (a very high estimate indeed) because of self-absorption, backscattering, etc., in the ϵ^- spectrum would reduce the value of W_K to 0.90, it seems likely that W_K in this region is at least 0.90.

We wish to express our appreciation to Professors G. T. Seaborg and I. Perlman, and Drs. S. G. Thompson and R. M. Diamond for their continued interest and advice.

* This work was performed under the auspices of the AEC.
† Major, United States Air Force; USAF Institute of Technology, Dayton, Ohio.
[1] G. Wilkinson and H. G. Hicks, Phys. Rev. **75**, 1687 (1949).
[2] Thompson, Ghioso, and Seaborg, Phys. Rev. **80**, 782 (1950).
[3] E. Feenberg and G. Trigg, Revs. Modern Phys. **22**, 399 (1950).
[4] M. E. Rose and J. L. Jackson, Phys. Rev. **76**, 1540 (1949).
[5] L. W. Nordheim, Phys. Rev. **78**, 294 (1950).

Quadrupole Radiation in nD Capture

N. AUSTERN*
Cornell University, Ithaca, New York
(Received November 13, 1951)

THAT thermal neutrons are captured by deuterons, appears to be largely a consequence of the existence of nuclear interaction currents ("exchange" currents), and may provide a measure of those currents.[1,2] The very small size of the capture cross section makes it essential to investigate the competing electric quadrupole process. Although an earlier estimate[1] showed this process to be of approximately equal importance with the magnetic one, it is the purpose of the present note to report that the quadrupole contribution is actually completely negligible. The capture must therefore proceed entirely by the emission of magnetic dipole radiation, and may be exclusively a result of the presence of interaction currents.

The earlier crude estimate of the importance of the quadrupole process was obtained in the usual manner, by computing the square of the ratio of the interaction operators. In the electric operator e^2/mc^2 was used for the displacement of the proton charge. After correction for the 4 percent probability of triton ^4D state, the ratio came out to be unity. A more elaborate calculation seemed to be improper, the three-body wave functions being so nearly unknown that any numerical result would be of slight significance. It has since been found that the numerical value of the quadrupole contribution is actually so very small that even an unreliable calculation shows it to be negligible.

The calculation is based upon the evaluation of the dimensionless ratio,

$$|R|^2=\frac{\langle|(^1S,\ (\mathbf{u}\cdot\boldsymbol{\rho}_3)(\boldsymbol{\kappa}\cdot\boldsymbol{\rho}_3)^4D)|^2\rangle_{\Omega_R}}{(e^2/mc^2)^4\langle(^1S,\ ^4S)\rangle_{\Omega_R}(^1D,\ ^4D)}. \tag{1}$$

Here ^4S is the continuum wave function and ^4D the ground-state wave function, while $\boldsymbol{\rho}_3$ is the separation of the proton from the center of mass of the nucleus, and $\mathbf{u}$ and $\boldsymbol{\kappa}$ are the unit polarization and propagation vectors of the light wave. The angular brackets enclosing the matrix elements indicate averaging over continuum spin states. The earlier estimate is obtained if $|R|$ is replaced by unity. Actually, $|R|^2$ is of the order of 10^{-6}. Most of the discrepancy comes in the angular integration in the numerator of $|R|^2$, part from the spin sum, and part because the root mean square proton coordinate is only about half e^2/mc^2.

The ^4D functions of Pease and Feshbach[2] were employed for this calculation. For ^4S the following form was chosen (unnormalized)

$$\psi_{^4S}=(r_{13}-r_{23})\exp[-\tfrac{1}{2}a(r_{13}+r_{23}+r_{21})]\times\{\chi_1^m(23)\chi^\mu(1)+\chi_1^m(13)\chi^\mu(2)\}. \tag{2}$$

Particles 1, 2, and 3 are the two neutrons and the proton, respectively. The function χ_1^m is the triplet spin function of its arguments, while χ^μ is the single particle spin function of its argument. The ground state damping parameter of Avery and Adams[4] was arbitrarily chosen for the parameter a. This $\psi_{^4S}$ exhibits the major properties of the state it is intended to describe, but is certainly wrong in its details. That the function is written as if the state were bound is, however, satisfactory for the present application. It is also exactly correct to use product spin functions in the present application, as this device incorporates the correct relative amplitudes of the quartet continuum states.

There is yet another quadrupole nD capture transition. The deuteron ^3D wave gives the continuum nD system some ^3D part, even at zero energy. From this the system can then make an electric quadrupole transition to the triton ^3S ground state. The resulting capture cross section is again negligibly small.

With the elimination of electric quadrupole transitions as important contributors to nD capture, it becomes more likely that the entire capture cross section must be attributed to interaction currents. Capture into an antisymmetric ^3S wave part of the triton ground state now provides the only competing process. (It is interesting that if nuclear forces are invariant against rotations in isotopic spin space, then there can be no such antisymmetric admixture.) Although the earlier interaction moment estimate only led to about half the observed cross section, a revised estimate is in good agreement with the corresponding portion of the similar calculation by Roth, and is in as good agreement with the measured value as can be expected.

I am grateful to A. M. L. Messiah for a conversation which prompted this calculation, and for his mention of the possible role of a continuum ^3D state. I am grateful for the opportunity to have read Roth's thesis.

* AEC Postdoctoral Fellow.
[1] N. Austern, Phys. Rev. **83**, 672 (1951).
[2] B. Roth, Ph.D. thesis (Cornell University, Ithaca, New York, 1951).
[3] R. Pease and H. Feshbach, Phys. Rev. **81**, 142 (1951); also private communications from Dr. Pease.
[4] R. Avery and E. N. Adams, Phys. Rev. **75**, 1106 (1949).

Absence of Spontaneous Emission of Neutrons from Samarium

S. D. CHATTERJEE AND R. N. OLCOTT
National Bureau of Standards, Washington, D. C.
(Received November 8, 1951)

YAGODA and Kaplan[1] claim to have detected spontaneous emission of neutrons from samarium, corresponding to a half-life of $\sim 10^{16}$ years. Their experiments were carried out with 200-micron Ilford C2 plates, loaded with B^{10} and Li^6 nuclei, the source of neutrons being 18.6 g of Sm_2O_3, which could be used either in the form of powder or a pellet.

In view of the far-reaching consequences of such a process, it was considered worthwhile to repeat their experiment with a much larger quantity of samarium, using a different method for the detection of neutrons.

The source consisted of samarium oxalate in the form of powder, with a samarium-content of 782 g. Spectrochemical analysis re-

vealed that the sample was completely free from Be and B. It contained, however, traces of Mg, Al, and Si, which might contribute to some (α, n) reaction, in addition to traces of Mn, Cu, Bi, Eu, Gd, and Pb. On account of the unusually high absorption cross section[2] of natural samarium for slow neutrons (10,600 barns for $E_n = 0.025$ ev), the powder was evenly distributed into twelve thin-walled boron-free glass-tube-containers. Furthermore, the powder was compressed into sticks with the help of a little absolute alcohol, which was subsequently evaporated away.

The detector of neutrons consisted of one or more proportional counters, filled with B^{10} enriched BF_3, containing 96 percent B^{10} to a pressure of 45 cm Hg. Each counter was 2.5 cm in diameter and 45 cm long; the cathode was a brass cylinder with wall-thickness 0.8 mm and the central tungsten wire (2 mil) was supported by glass insulators.

During the investigation, two different experimental arrangements were set up. In the first arrangement, depicted in Fig. 1,

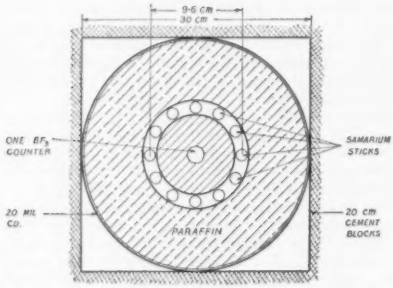

FIG. 1. Single BF_3 proportional counter arrangement for the detection of slow neutrons

only one BF_3 proportional counter was placed centrally along the axis of a paraffin cylinder, 50 cm long and 30 cm in diameter. Twelve samarium sticks were placed symmetrically in a cylindrical annular ring, surrounding the proportional counter. The efficiency of the arrangement for neutron-detection was experimentally determined by putting a standard neutron source of 0.5 mg (Ra+Be) in a fixed position in the middle of the annular ring and recording the neutron-counts, above the background, per minute. When the samarium sticks were removed from their places, the efficiency was 0.37 percent; it diminished to 0.28 percent when the sticks were replaced, indicating strong absorption of slow neutrons in samarium.

The efficiency for the detection of slow neutrons was considerably enhanced by adopting the arrangement depicted in Fig. 2, where the samarium sticks were placed near the axis of the paraffin cylinder and surrounded by a concentric row of six BF_3 proportional counters connected in parallel. With the standard neutron source of 0.5 mg (Ra+Be) kept at the center of the paraffin cylinder, the efficiency of the second arrangement for the detection of neutrons, was 4.8 percent, when the Sm sticks were absent. The efficiency diminished to 3.3 percent when the Sm sticks were present.

No evidence about the spontaneous emission of neutrons from samarium could be obtained in either of the experiments cited previously. On the other hand, the presence of samarium slightly lowered the average background count of the BF_3 proportional counters, indicating the absorption of cosmic-ray neutrons or local neutron-flux within the paraffin cylinder.

The emission of neutrons from samarium, as reported by Yagoda and Kaplan, may be attributed to one of the following causes, none of which appears to be *a priori* feasible:

(1) Presence of Be, B, Al, and other light elements with a large cross section for (α, n) reaction. Yagoda and Kaplan, however, showed by calculation that the necessary degree of contamination was improbable in their sample.

(2) Spontaneous fission of Sm. This process is extremely unlikely, particularly when judged in the light of theoretical calculations made by Bohr and Wheeler[3] and Flügge,[4] regarding the spontaneous fission process in uranium and the neighboring nuclei.

(3) Alpha-decay of Sm leads to an excited state of Nd, followed by a neutron emission.

The α-activity of Sm has been ascribed to the isotope Sm^{147} by Rasmussen, Reynolds, Thompson, and Ghiorso.[5] The decay product is then

$$_{62}Sm^{147} \xrightarrow{\alpha} {}_{60}Nd^{143}.$$

Now, the 83rd neutron is very loosely bound, the binding energy being about 2 Mev less than the average value of neutron binding energies. It might be not more than 4–5 Mev, compared with the average value of 6–7 Mev. So, if the α-decay of Sm^{147} would lead to an excited state of Nd^{143}, with an excitation-energy of this order of magnitude, the α-decay could be followed by a neutron emission, in analogy with the "delayed neutron emission" of some fission-product nuclei. The only identified "delayed neutron emitters" are $_{56}Ba^{139}$ and $_{38}Sr^{89}$, the neutron emission following the β^- decays of $_{55}Cs^{139}$ and $_{37}Rb^{89}$, respectively. It may be noted that $_{56}Ba^{139}$ and $_{38}Sr^{89}$ have only one neutron more than the closed-shell-configuration numbers 82 and 50.

On the other hand, it is hardly probable that the Sm^{147} nucleus should not rather undergo α-transformation to the ground state of Nd^{143}, with a decay energy >6 Mev, than to the assumed excited state with the observed α-energy of 2.2 Mev, even if there were angular momentum selection rules, which would favor the lower energy transition. According to Gamow, these selection rules cannot be strong enough to overcome the very strong energy dependence of the α-transition probabilities.

Furthermore, one should expect lower lying excited states of Nd^{143} to exist with angular momenta, which would comply with the angular momentum selection rules as well.

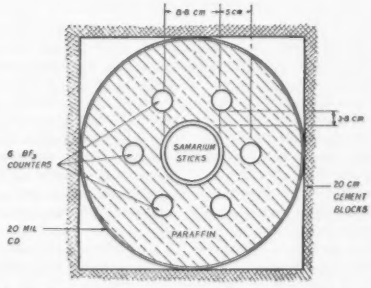

FIG. 2. Multiple BF_3 proportional counter arrangement for the detection of slow neutrons.

We are grateful to Dr. L. F. Curtiss, Chief, Neutron Measurement Laboratory, for his valuable suggestions and also for permitting us to carry out this investigation in his laboratory. One of us (S.D.C.) wishes to thank Professor J. H. D. Jensen of the Heidelberg University for helpful discussions.

[1] H. Yagoda and N. Kaplan, Phys. Rev. **76**, 702 (1949).
[2] *Nuclear Data*, National Bureau of Standards Circular 499, 182 (1950).
[3] N. Bohr and J. Wheeler, Phys. Rev. **56**, 426 (1939).
[4] W. Bothe and S. Flügge, *Nuclear Physics and Cosmic Rays*, FIAT Rev. (Office of Military Government for Germany, Field Information Agencies Technical. Printed under direction of Dieterich'she Verlegsbuchhnadlung, Inhaber W. Klemm, Wiesbaden, Germany, 1948), p. 218.
[5] Rasmussen, Reynolds, Thompson, and Ghiorso, Phys. Rev. **80**, 475 (1950).

Bipolar Expansion of Coulombic Potentials. Addenda*

ROBERT J. BUEHLER AND JOSEPH O. HIRSCHFELDER
University of Wisconsin Naval Research Laboratory, Madison, Wisconsin
(Received November 9, 1951)

IN our recent article[1] the general formula for $Bn_1, n_2{}^{|m|}(r_1, r_2; R)$ was not given in Region II where $|r_1-r_2| \leq R \leq r_1+r_2$. Instead, Table I gave the coefficients to be used for all those cases where n_1 and n_2 are equal to 3 or less. By using r_2' as the independent variable in the integrations indicated in Eq. (34) and expanding the integrands in powers of r_2', it was possible to obtain the following general expression for $Bn_1, n_2{}^{|m|}(r_1, r_2; R)$ in Region II.

$$Bn_1, n_2{}^{|m|}(r_1, r_2; R) = Hn_1, n_2{}^{|m|} \sum_{j=0}^{2n_2} \sum_{w=0}^{n_2-|m|} \sum_{v=0}^{n_1-|m|} K(j)^{|m|} W n_2{}^{|m|}(w) S n_1{}^{|m|}(v) X n_1(\beta).$$

Here $\beta = j+v+w$ and

$$Hn_1, n_2{}^{|m|} = \left(\frac{2n_2+1}{2}\right) \frac{(n_2-|m|)!(n_1-|m|)!(-1)^{n_2-|m|}}{(n_2+|m|)!(n_1+|m|)!2^{n_1+n_2}R}.$$

$$K(j)^{|m|} = \frac{(-1)^j(|m|)!}{j!} \sum_{k=k_1}^{|m|} \frac{(-1)^k(2k)!}{k!(2k-j)!(m-k)!} \left(\frac{R^2+r_2^2}{2Rr_2}\right)^{2k}.$$

$k_1 = j/2$ or $(j+1)/2$.

$$Wn_2{}^{|m|}(w) = \frac{(-1)^w}{w!} \sum_{q=0}^{q_2} \frac{(-1)^q(2n_2-2q)![(R^2+r_2^2)/2Rr_2]^{n_2-|m|-2q}}{(n_2-q)!(n_2-|m|-2q-w)!q!}.$$

$q_2 = \frac{1}{2}(n_2-|m|-w)$ or $\frac{1}{2}(n_2-|m|-w-1)$.

$$Sn_1{}^{|m|}(v) = \left(\frac{2R}{r_2}\right)^{n_1-|m|} \left(\frac{R^2+r_2^2}{4R^2}\right)^{p} \sum_{p=p_1}^{n_1-|m|-v} \frac{(-1)^{n_1-|m|-v-p}(2|m|+2v+2p)![(R^2-r_2^2)/4R^2]^p}{(n_1-|m|-v-p)!(p+2v-n_1+|m|)!p!(m+v+p)!}$$

$p_1 = n_1-|m|-2v$ when $v \leq \frac{1}{2}(n_1-|m|)$ or $\frac{1}{2}(n_1-|m|-1)$; otherwise $p_1 = 0$.

$$Xn_1(\beta) = \left(\frac{r_2}{r_1}\right)^{n_1-\beta} \left(\frac{r_1^2}{R^2+r_2^2}\right)^{\beta} \left\{\frac{1}{2\beta+2}\left[1-\left(\frac{R-r_2}{r_1}\right)^{2\beta+2}\right] + \frac{1}{2\beta+1-2n_1}\left[-1+\left(\frac{R+r_2}{r_1}\right)^{2\beta+1-2n_1}\right]\right\}.$$

The running summation variables only assume integer values so that the choice of k_1, q_2, and p_1 is unique.

The authors would like to thank George Gioumousis for checking these formulas.

* This work was carried out under a contract between the United States Navy Bureau of Ordnance and the University of Wisconsin.
[1] R. J. Buehler and J. O. Hirschfelder, Phys. Rev. **83**, 628 (1951).

Disintegration of the Ground-State Sr^{85} and Metastable Energy Level of 514 Kev in Rb^{85}

W. S. EMMERICH AND J. D. KURBATOV
Ohio State University, Columbus, Ohio
(Received November 13, 1951)

IT is accepted that the disintegration of the ground state of strontium 85 to rubidium 85 takes place by orbital electron capture of 65 days half-life followed by emission of a gamma-ray of 513 kev.[1] Electrons have also been found.[2] The radiations of strontium 85 were reinvestigated in an effort to compare excited states in Rb^{85} observed in disintegration of Sr^{85} and Kr^{85}.

Strontium 85 was produced by deuteron bombardment of spectroscopically pure rubidium and was separated from the latter without addition of carrier. Adsorption procedure was employed for the separation. An analysis of the radiations emitted by the

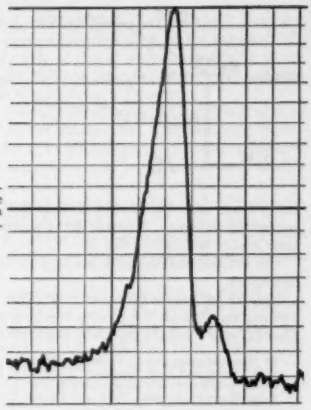

FIG. 1. Internal conversion electrons of the 514-kev gamma-ray in the Sr^{85} disintegration.

65-day period showed that electrons, x-rays, and gamma-rays are present. The electrons were measured by spectrometers and found to consist of internal conversion electrons corresponding to a 514+3-kev gamma-transition. An energy determination of this gamma-ray from photoelectrons with a lead radiator agreed with the aforementioned value. In the region from 120 to 200 kev, where an energy level of Rb^{85} was reported from the disintegration of Kr^{85}, neither internal conversion nor photoelectrons were observed. The limit of measurement extended to 0.5 percent of monochromatic electronic intensity of the 514-kev transition.

For the 514-kev transition, the internal conversion coefficient in the *K*-shell was found to be 0.7 percent from comparative measurements with the well-known gamma-transition in the decay of Cs^{137}.[3] This internal conversion was determined using a spectrometer with sources prepared, from Sr^{85} and Cs^{137}, suitable for measurement of internal conversion electrons and photoelectrons at the same geometry. Comparison of the intensity ratios yielded the foregoing value of the experimental conversion coefficient after a correction had been applied for difference in radiator efficiency because of difference in gamma-ray energies. An alternate method consisted of measuring the ratio of electrons to gamma-rays in a calibrated Geiger counter. In this measurement, a correction was made for Compton electrons and *L*-shell conversion electrons as found with a spectrometer. The ratio of *K*- to *L*-shell conversion was obtained, as shown in Fig. 1, from photographic plates in a permanent magnet spectrograph. From these data, the *K* to *L* ratio is estimated to be 12±3. The internal conversion tables of Rose *et al.*[4] give $\beta_2 = 6.6\times10^{-3}$ and $\alpha_2 = 8.2\times10^{-3}$ for 514 kev in rubidium as the two closest values to the experimental results of 7×10^{-3}. Using a conventional coincidence counter with a resolving time of ~one microsecond, the only coincidences observed could be traced to electrons in coincidence with ~one percent of the total number of x-rays, because of internal conversion. No coincidences were observed between x-rays and gamma-rays, indicating that the 514-kev level has a measurable lifetime.

In order to determine whether orbital electron capture takes place directly to the ground state of Rb^{85}, a relative intensity measurement of x-rays and gamma-rays was made. For this purpose, the counter efficiency for x-rays of rubidium was determined from the coincidences between electrons and x-rays as mentioned in the previous paragraph. For the particular counter used, the ratio of x-ray to gamma-ray efficiency was thus found to be 3.6±0.4, whereas the actual counting rate showed a ratio of x-rays to gamma-rays of 3.8, from which it can be concluded that disintegration directly to the ground state and to excited

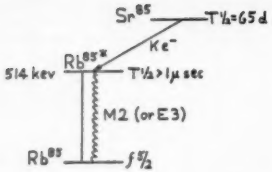

FIG. 2. Decay scheme for the ground state of Sr^{85}.

states other than the 514-kev level in Rb^{85} does not occur with appreciable intensity. A partial decay scheme of Sr^{85} summarizing these results is shown in Fig. 2.

The authors wish to thank Major J. E. Duval for the chemical separation.

Support by grants from the Ohio State University Research Foundation through the Graduate School and from the O. S. U. Development Fund are gratefully acknowledged by the authors.

[1] M. Ter-Pogossian and F. T. Porter, Phys. Rev. **81**, 1057 (1951).
[2] L. S. Cheng and J. D. Kurbatov, Phys. Rev. **79**, 237 (1950).
[3] M. A. Waggoner, Phys. Rev. **82**, 906 (1951).
[4] Rose, Goertzel, Spinrad, Harr, and Strong, Phys. Rev. **83**, 79 (1951).

Studies on the Linearity of a Scintillation Gamma-Ray Spectrometer

V. O. ERIKSEN AND G. JENSSEN
Joint Establishment for Nuclear Energy Research, Kjeller, Norway
(Received November 13, 1951)

THE linearity between pulse-height and absorbed energy in NaI(Tl) crystal has been carefully investigated during the last two years. Johanson[1] has reported a linear relationship in the region 0.4–6 Mev. Pringle and Standil[2] have found that the relationship is not strictly linear in the region 0.05–0.4 Mev. We have made some measurements in the region 0.05–0.5 Mev, and are finding a linear relationship in this region.

A single-crystal scintillation spectrometer has been used. One clear NaI(Tl) crystal, supplied from Harshaw Chemical Company, 20 mm thick and 30 mm in diameter was employed in conjunction with an EMI-5311 photomultiplier tube. Mirrors of thin mica coated with silver or aluminium to ensure high reflection were used. Just a slight oxidation of the mirrors caused considerable variation in the peak widths.

The crystal was kept in a glass tube cemented on to the surroundings of the photocathode and filled with paraffin. The crystal had been carefully polished with flannel or velvet in a dry atmosphere. The paraffin was dried with metallic Na.

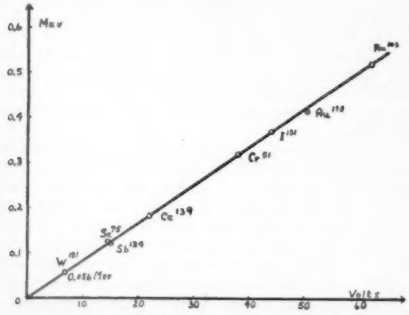

FIG. 1. Pulse-height as a function of gamma-ray energy.

The amplifier was type 1008 delivered by Cole, Ltd. No preamplifier or cathode-follower was used. A ten-channel pulse-height analyzer was used for the pulse-height analysis. The stability of the apparatus was very good; for the high voltage it was better than ±0.5 per thousand.

The counter was surrounded by a 5-cm-thick shield of lead.

Nuclides with 7 different gamma-rays in the region 0.1–0.5 Mev were used.[3] The activity of the sources varied between 10^{-3}–10^{-9} curie. The collimated rays had an angular width of about 5°.

Figure 1 shows the linearity between pulse-height and energy of the various gamma-rays.

[1] S. A. E. Johanson, Arkiv Fysik, B2 (1950).
[2] Pringle and Standil, Phys. Rev. **80**, 762 (1950).
[3] Gamma-ray energies are according to *Nuclear Data* (National Bureau of Standards Circular 499, 1950).

Heat Capacity and Lattice Defects of Silver Chloride

KOICHI KOBAYASHI
Chemical Institute, Faculty of Science, Tohoku University, Sendai, Japan
(Received October 25, 1951)

THE magnitude of the heat of activation for the formation of lattice defects in AgCl crystal, ΔH, has hitherto been in doubt. Previously, I had measured the heat capacity of AgCl from room temperature to 500°C to calculate the thermodynamic relations on some chemical reaction[1] and found an abnormal increase in the heat capacity curve in the vicinity of the melting point.

Berry[2] has concluded that the defects in AgBr crystal are of Frenkel type. I assume that Frenkel defects may dominate in AgCl by analogy with the result on the lattice behavior of AgBr and by consideration of the ionic conductivity measurements on AgCl, in spite of Mitchell's conclusion.[3]

If the concentration of the Frenkel defect, n/N, is expressed by the equation,

$$n/N = C\exp(-\Delta H/2RT), \tag{1}$$

the excess heat capacity ΔC_p per mole should be given by

$$\Delta C_p = [C(\Delta H)^2/2RT^2]\exp(-\Delta H/2RT). \tag{2}$$

So, ΔH may be obtained by the relation between $\log(T^2\Delta C_p)$ and $1/T$. For the heat capacity contributed by the perfect lattice of AgCl, I assume

$$C_p = 11.21 + 6.57\times10^{-3}T - 3.2\times10^{-6}T^2 \text{ cal/mole} \quad (T: °\text{K}), \tag{3}$$

which was obtained by extrapolation of the heat capacity data in the range 300–400°K, as given in the previous paper.[1] ΔC_p was estimated as the deviation from the expression (3) of the measured heat capacity which was shown in Table II of the previous paper.[1] Figure 1 shows a plot of $\log(T^2\Delta C_p)$ *versus* $1/T$ in the range 600–724°K, indicating that the resultant points fall well on a straight line in the range from 600 to 700°K and deviate upwards above this. The slope of this straight line determines ΔH to be 35,200 cal/mole. This value is 20 percent larger than that for AgBr derived by Teltow.[4] The contribution of C_p of the perfect lattice to ΔH is quite sensitive, and a variation of 0.1 cal/mole (6 percent in ΔC_p) at 700°K corresponds to 1 kcal in ΔH, but by this treatment the plot at 600°K deviates from the linear relation.

From this ΔH we may estimate n/N at any temperature. We find n/N to be 7.5×10^{-3} at 724°K, 4.3×10^{-4} at 600°K, and 1.6×10^{-10} (4×10^{12} per cc) at 300°K. The integrated value of the excess enthalpy at 724°K is 220 cal/mole and the corresponding entropy is 0.31 eu. The value of C in Eq. (1) is obtained as 1.08×10^{2}; on the other hand, C for AgBr is estimated as 1.6×10^{4} from the work of Christy and Lawson.[5] The fact that C is exceedingly large seems to indicate that the defects in silver halide are of the Schottky type, but I shall not discuss this problem further.

The deviation of the plots above 700°K from the linear relation seems to be associated with an increase in ΔH, or a small con-

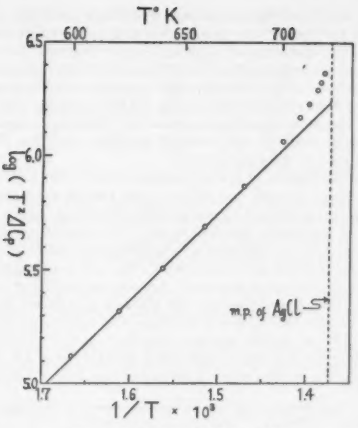

FIG. 1. Plots of $\log(T^2\Delta C_p)$ vs $1/T$.

centration of Schottky defects. If the curve is resolved into two lines, the upper component may be used to estimate the concentration of the pairs of vacant sites associated with the Schottky defect. If we assume that the concentration of Frenkel defects in AgCl obeys the relation (1) with $\Delta H = 35{,}200$ cal/mole and that the mutual interaction between the defects of both types is very small, we obtain 36 cal/mole as the excess enthalpy associated with Schottky defects. This appears to suggest that the magnitudes of ΔH for both types of defect are nearly equal and that Schottky defects are present to an extent of 20 percent of the total at 724°K.

I wish to express my sincere thanks to Professor F. Ishikawa and Assistant Professor I. Higuchi for their guidance and to Professor F. Seitz for his encouragement.

[1] K. Kobayashi, Sci. Repts. Research Inst., Tohoku University, Series I **34**, 112 (1950).
[2] C. R. Berry, Phys. Rev. **82**, 422 (1951).
[3] J. W. Mitchell, Phil. Mag. **40**, 667 (1949).
[4] J. Teltow, Ann. Physik **5**, 63 (1949).
[5] R. W. Christy and A. W. Lawson, J. Chem. Phys. **19**, 517 (1951).

Measurements of Some *K*-Shell Internal Conversion Coefficients

F. K. McGowan
Oak Ridge National Laboratory, Oak Ridge, Tennessee
(Received November 16, 1951)

K-SHELL internal conversion coefficients of four γ-rays in neighboring nuclei have been measured with a NaI scintillation spectrometer. In three cases it is possible to classify the transitions and assign angular momenta to the nuclear states.

A NaI scintillation detector 1.5 inches in diameter and 1 inch long has an intrinsic efficiency of unity for γ-radiation less than 100 kev. Thus, it is possible under favorable circumstances to obtain *K*-shell internal conversion coefficients of γ-rays by measuring the intensity ratio of the *K* x-ray to γ-ray provided the appropriate corrections are made for fluorescent yield, effective detection efficiency, and escape peak intensity.

A typical spectrum of the *K* x-ray and the 85-kev γ-ray following the β^--decay of Tm^{170} is shown in Fig. 1. The solid curve represent the line shapes (Gaussian) into which the pulse-height distribution has been resolved. The peak at 23.9 kev is the escape peak whose energy is the difference between the energy of the *K* x-ray from the source and the *K* x-ray of iodine. The peaks at 52.5 and 85 kev correspond to the full energy of the *K* x-ray and the γ-ray from the source being dissipated in the detector. The corresponding escape peak of the 85-kev γ-radiation is in the high energy edge of the 52.5-kev line; the escape peak intensity for 85-kev γ-radiation is only about 6.5 percent.

The escape peak intensity relative to the total intensity of γ-radiation incident on the detector has been measured experimentally for γ-radiation at 8 different energies distributed between 41.6 and 73 kev. The measured escape intensities agree reasonably well with computed escape intensities for a collimated beam of γ-radiation entering a semi-infinite crystal of NaI normal to its plane surface. The ratio of the *K* x-ray to γ-ray intensity is obtained from the areas of the Gaussian components. Results for the experimental *K*-shell internal conversion coefficients are tabulated in Table I.

Only an upper limit is indicated for $\alpha_{exp}{}^K$ in the case of Ho^{166} because there are several other γ-rays at higher energies which, if there is any internal conversion of these in the *K*-shell, will contribute to the observed *K* x-ray intensity. In the case of Dy^{159} the ratio of the *K* x-ray to γ-ray intensity was measured in coincidence with a 200-kev γ-ray preceding the 85-kev transition.

Although relativistic *K*-shell internal conversion coefficients for $E_\gamma < 150$ kev are not yet available, there is a method for obtaining extrapolated values of the coefficients at low energies. The ratio of the relativistic coefficients[1] to the nonrelativistic coefficients[2] is plotted for $E_\gamma \geq 150$ kev, and the ratio is extrapolated to one at zero electron energy.[3] Low energy *K*-shell conversion coefficients for electric radiation are obtained by multiplying the nonrelativistic values by a correction factor from the ratio plot. Similarly, for magnetic radiation, extrapolated coefficients are obtained by multiplying the extrapolated coefficient for electric radiation by a correction factor from a plot of β_{L-1}/α_L extrapolated to zero electron energy. To check this extrapolation procedure there are some low energy relativistic conversion coefficients for electric dipole, quadrupole, and magnetic dipole for $Z = 29$, 49, 84, and 92 obtained by Reitz.[4] A comparison shows that the extrapolated values agree with Reitz's results for $E_\gamma = 70$ kev to within 15

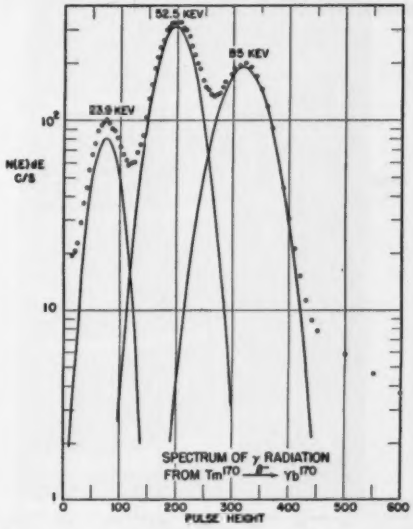

FIG. 1. Spectrum of the γ-radiation from $Tm^{170} \xrightarrow{\beta^-} Yb^{170}$.

TABLE I. Experimental and theoretical K-shell conversion coefficients.

Nucleus	E_γ, kev	$T_{1/2}$, sec	$\alpha_{exp}{}^K$	$(\alpha_2{}^K)_{extrap}$
$_{66}Dy^{160}$	85	1.8×10^{-9}	1.65 ± 0.2	1.75
$_{67}Ho^{165}$	95	$<.8\times10^{-9}$	$\leqslant 2.9$	1.40
$_{68}Er^{166}$	81	1.7×10^{-9}	$1.9^{\circ}\pm0.3$	1.94
$_{70}Yb^{170}$	85	1.6×10^{-9}	$1.5\ \pm0.2$	1.65

percent which justifies the foregoing procedure at least for electric dipole, quadrupole, and magnetic dipole.

The extrapolated K-shell conversion coefficients for electric quadrupole radiation are listed in Table I. Corresponding values for electric dipole and magnetic dipole radiation are about 4 times smaller and 3.5 to 7 times larger than $\alpha_2{}^K$, respectively.

In the case of Dy^{160}, Er^{166}, and Yb^{170}, the isomeric transitions are to the ground state in even-even nuclei which presumably have spin zero and therefore only pure multipole radiation is possible. Thus, these transitions are of the $E2$ type and the spin of the excited state is two.

[1] Rose, Goertzel, Spinrad, Harr, and Strong, Phys. Rev. **83**, 79 (1951).
[2] M. H. Hebb and E. Nelson, Phys. Rev. **58**, 486 (1940).
[3] P. Axel and R. F. Goodrich, Office of Naval Research Report (unpublished).
[4] J. R. Reitz, Phys. Rev. **77**, 10 (1950).

Classification of the γ-Radiation of Hf^{177}

F. K. McGowan, E. D. Klema, and P. R. Bell
Oak Ridge National Laboratory, Oak Ridge, Tennessee
(Received November 16, 1951)

THREE γ-rays of Hf^{177} following the β^--decay of Lu^{177} are classified, and the angular momentum and relative parity of the nuclear states are assigned by measurements of the directional angular correlation of successive gamma-quanta and the K-shell internal conversion coefficients.

The 6.7 day Lu^{177} β^--activity is known to decay by three beta-groups to Hf^{177}.[1] The lowest energy beta-group leads to an excited state in Hf^{177} followed by two γ-rays in cascade with energies 206 and 112 kev.

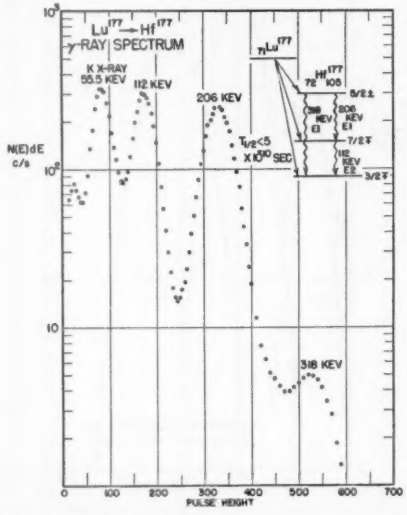

FIG. 1. Spectrum of the γ-radiation following the β^--decay of Lu^{177}.

The half-life of the excited state at 112 kev above the ground state is $T_{\frac{1}{2}}<5\times10^{-10}$ sec as measured with a delayed coincidence scintillation spectrometer using anthracene detectors. The γ-ray spectrum has been examined with a NaI scintillation spectrometer and is shown in Fig. 1. The spectrum was taken at such a geometry that the 318-kev peak is due to the 318-kev crossover transition alone. The peaks have been resolved into Gaussian components and the intensity of the crossover transition from the 318-kev excited state is (4.5 ± 0.5) percent.

Since the lifetime of the intermediate state at 112 kev is sufficiently small, the 206- and 112-kev γ-ray cascade appeared to be an ideal case in which to investigate the directional angular correlation of successive gamma-quanta. The angular correlation, measured with a coincidence scintillation spectrometer using NaI detectors, is found to be anisotropic. The γ-rays entering in the angular correlation measurement are selected according to their energy. One detector selects the 206-kev γ-radiation and the other detector the 112-kev γ-radiation. The coincidence resolving time is 10^{-7} sec and the angular resolution is $\pm12.7°$. Under these conditions the true coincidence rate is of the order of 2.5 counts/sec while the random rate is 8 percent of this. Figure 2 shows the

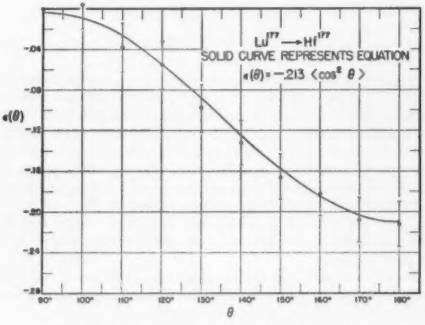

FIG. 2. Directional angular correlation of the 206- and 112-kev γ-ray cascade from Hf^{177}.

observed angular distribution. The ordinate represents

$$\epsilon(\theta)=[n(\theta)-n(\tfrac{1}{2}\pi)]/n(\tfrac{1}{2}\pi)=W(\theta)-1, \qquad (1)$$

where

$$W(\theta)=1+\sum_{i=1}^{n} a_{2i}\cos^{2i}\theta.$$

The solid curve represents $\epsilon(\theta)=-0.213\cos^2\theta$, where $\cos^2\theta$ has been averaged over the finite angular resolution of the apparatus. $W(\theta)=1-0.213\cos^2\theta$ is characteristic of a dipole-quadrupole cascade with angular momenta $5/2\to7/2\to3/2$ for the three states in order of decreasing excitation energy. Other dipole→quadrupole combinations with the correct magnitude ($a_2=-0.21\pm0.02$) of the anisotropy may be excluded either on the basis of the observed shape of the angular correlation distribution or from the requirement that the ground state be restricted to $J\leq3/2$.[2] The measured contribution of the 318-kev transition by a Compton scattering between the two detectors is 0.01 percent of the true coincidence rate.

By measuring the intensity ratio of the K x-ray to the γ-ray in coincidence with the other γ-ray of the cascade, one obtains the K-shell internal conversion coefficient of each γ-ray in the cascade. The observed intensity ratio must be corrected for fluorescent yield,[3] escape peak intensity, fraction of the detected γ-rays appearing in the full energy peak, and effective detection efficiency. These are tabulated in Table I. The experimental error for $\alpha^K(206)$ is rather large because there is the additional interference from back-scattered photons by the Compton process from one detector

TABLE I. Experimental results and correction factors.

E_γ	Observed intensity ratio	Fluorescent yield W_K	Escape peak intensity for x-ray	Detected γ-rays in full energy peak	Detection efficiency ratio $\epsilon_\gamma/\epsilon_x$	α^K_{exp}
112 kev	0.69	0.937	0.15	0.98	0.95	0.81 ±0.08
206	0.046	0.937	0.15	0.92	0.80	0.042±0.015

to the other. Some measurements were taken with a Pb-Cd diaphragm between the detectors to reduce the back-scattering. Typical coincidence counting rates at the peaks in the measurement of $\alpha^K(112)$ are 30 counts/sec while the random rate is 0.5 percent of this.

The experimental and theoretical internal conversion coefficients[4] are compared in Table II. From the internal conversion

TABLE II. Experimental and theoretical internal conversion coefficients.

E_γ	α^K_{exp}	$\alpha_1{}^K$	$\alpha_2{}^K$	$\beta_1{}^K$
112 kev	0.81 ±0.08	0.22	0.80	2.8
206	0.042±0.015	0.045	0.153	0.52

coefficient data one concludes that the 206- and 112-kev transitions are of the $E1$ and $E2$ type, respectively. It appears that both the internal conversion and the directional angular correlation data are consistent with the interpretation that both transitions are pure multipoles.

A proposed level scheme for Hf^{177} is shown in Fig. 1. Mayer's strong spin orbit coupling shell model[5] would predict either a $p_{\frac{1}{2}}$ or $f_{\frac{7}{2}}$ orbit for Hf^{177} with $N=105$. Although relative parities are indicated in Fig. 1, the shell model predicts the ground state to be odd parity. In this case the parities of the excited states would be odd and even in order of increasing excitation energy. The even parity for the state at 318 kev is in contradiction to the shell model, which would predict odd parity orbits except for $i_{13/2}$ orbits for N odd between 83 and 125. The occurrence of two $E1$ transitions is also in contradiction to the shell model. The $E1$ crossover transition of 318 kev should compete favorably with the 206-kev transition, but the observed intensity ratio is 80 times smaller than the theoretical estimates from transition probability-energy relations.[6] Thus, one should use the estimates for transition probabilities between states in a given nucleus with extreme caution for estimating intensities of crossover transitions.

[1] D. G. Douglas, Phys. Rev. **75**, 1960 (1949).
[2] E. Rasmussen, Naturwiss. **23**, 69 (1935).
[3] Steffen, Huber, and Humbel, Helv. Phys. Acta **22**, 167 (1949).
[4] Rose, Goertzel, Spinrad, Harr, and Strong, Phys. Rev. **83**, 79 (1951).
[5] Maria G. Mayer, Phys. Rev. **78**, 16 (1950).
[6] P. Axel and S. M. Dancoff, Phys. Rev. **76**, 892 (1949); V. F. Weisskopf, Phys. Rev. **83**, 1073 (1951).

The Isomeric Transition in Ge^{77}*

ALLAN C. G. MITCHELL AND ALAN B. SMITH
Indiana University, Bloomington, Indiana
(Received November 5, 1951)

THE nucleus Ge^{77} decays to As^{77} *via* a beta-ray transition of 12-hour half-life and also by a beta-ray transition of 59-sec half-life. The isomeric states, 59-sec and 12-hour, occur in the parent nucleus. Ge^{77} has 45 neutrons and, according to the older version of the shell model, the two states responsible for the isomeric transition should have configurations $p_{1/2}$ and $g_{9/2}$. Recent considerations[1] show, however, that for 3, 5, 7 neutrons beyond neutron number $N=38$ the states may be $G_{7/2}$ and $p_{1/2}$.

The present work stems from an investigation of the spectrum of the 12-hour Ge^{77} which is nearing completion in the laboratory, and will be published shortly. The spectrum of the 12-hour Ge^{77} is complicated, but we have shown that the highest energy beta-ray group has an end-point energy of 2.2 Mev and leads to an excited state of As^{77} 0.263 Mev above the ground state. The energy of the 12-hour Ge^{77} is therefore 2.46 Mev above the ground state of As^{77}. Arnold and Sugarman[2] have excited the 59-sec isomeric state and measured the beta-ray end point by absorption. They obtain an energy of 2.8 Mev. One would, therefore, expect the isomeric states to have a difference in energy of approximately 0.34 Mev.

In the present experiment a piece of germanium metal was bombarded for 1.5 minutes with slow neutrons from the cyclotron. It was then examined with the help of a scintillation spectrometer by the photographic method of Hofstadter and McIntyre.[3] Figure 1 shows pictures of the envelope of the oscillograph traces taken with a Polaroid Land Camera. The exposure time of each picture was one minute and the procedure was such that the exposure of each picture was started 2 minutes after the start of the previous picture. An inspection of Fig. 1 shows that the radiation decays with a half-life of about 1 minute. The energy of the gamma-ray, obtained by measuring the height of the pulse envelope and comparing this with the 0.661 gamma-ray of Cs^{137}, is 380±20 kev. This is in good agreement with the energy of the transition as determined by the previously mentioned absorption and spectrometric work.

From these experiments and those on the decay of the 12-hour Ge^{77} it is possible to obtain the configurations of the two states of Ge^{77}. The upper state (59-sec) is $p_{1/2}$, since it goes to the ground state of $As^{77}(p_{3/2})$ with the emission of a beta-particle for which $\log ft=4.8$. The lower state (12 hr) goes *via* a beta-transition to an excited state of As^{77}. This transition shows a $\log ft=7.6$ and has an allowed shape. The first excited state of As^{77} is probably $f_{5/2}$.

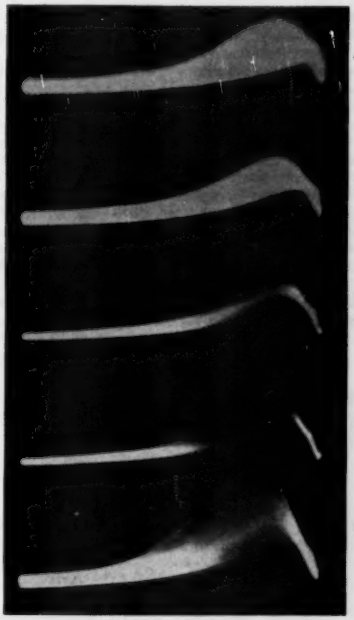

FIG. 1. Isomeric state of Ge^{77} (from top to bottom): A—bombardment +0.5 min; B—bombardment +2.5 min; C—bombardment +4.5 min; D—bombardment +6.5 min; and E—Cs^{137} for calibration.

If the ground state of Ge^{77} were $g_{9/2}$, the beta-ray spectrum would have a forbidden shape ($\Delta j = \pm 2$, yes) and a larger value of logft. If the ground state of Ge^{77} is $G_{7/2}$ the spectral shape and value of logft are consistent with a transition of the type $\Delta j = \pm 1$, yes. In addition, one can get an approximate idea of the half-life for gamma-ray emission by using the emperical formula of Goldhaber and Sunyar.[1] For a transition $\Delta I = 4$ ($p_{1/2}$ to $g_{9/2}$) one obtains 3×10^4 sec and for $\Delta I = 3$ ($p_{1/2}$ to $G_{7/2}$) one obtains <1 sec for the half-life. The value $\Delta I = 3$ will allow the gamma-ray transition to compete with the 59-sec beta-decay whereas the transition $\Delta I = 4$ would make the gamma-ray transition extremely weak. From these two lines of evidence it is concluded that the ground state of Ge^{77} has the configuration $G_{7/2}$ and that the isomeric state ($p_{1/2}$) lies 380 kev above it.

* Supported by the joint program of the ONR and AEC.
[1] M. Goldhaber and A. W. Sunyar, Phys. Rev. **83**, 906 (1951).
[2] J. R. Arnold and N. Sugarman, J. Chem. Phys. **15**, 703 (1947).
[3] R. Hofstadter and J. A. McIntyre, Phys. Rev. **80**, 631 (1950).

Ions of Mass 19 from Water

FRANCIS J. NORTON
General Electric Research Laboratory, Schenectady, New York
(Received November 8, 1951)

A RECENT paper[1] has shown that in the mass spectrometric determination of the HOD^+ ion of mass 19 present in ordinary water, high H_2O pressures can yield spurious mass 19 ions, presumably H_3O^+, from the collision of H_2O^+ ions with H_2O molecules.

I have found that excess H_2 when present with water also yields much H_3O^+ in the mass spectrometer, and that the shape of its ionization probability function, as ionizing voltage is changed, is entirely different from the ionization curve for HOD^+.

Figure 1 shows the magnitude of the ratio peak 19/peak 18. Curve (a) represents increasing amounts of water alone. Curve (b) is for similar amounts of water with added hydrogen, from a mixture of 98.2 percent H_2 and 1.8 percent H_2O, and shows how greatly the added H_2 increases peak 19. All these measurements were made at an ionizing voltage of 70 and an accelerating voltage of 2000.

Figure 2 gives variation of peak height, or positive ion current, as ionizing voltage is changed. Curve (1) is peak 19, HOD^+ from a mixture of about 50 percent H_2O and 50 percent D_2O. Curve (2) is peak 19, H_3O^+ from the mixture of H_2 and H_2O. The ion current at the maximum for H_3O^+ was 1.9×10^{-13} amps, and for HOD^+, 1.1×10^{-11} amps.

The ionizing efficiency curve (1) is normal and like that for H_2O^+ and for D_2O^+. Curve (2) for H_3O^+ is very unusual for ionizing efficiency, having a sharp maximum at 19 volts. It resembles excitation curves and leads to the suggestion that perhaps

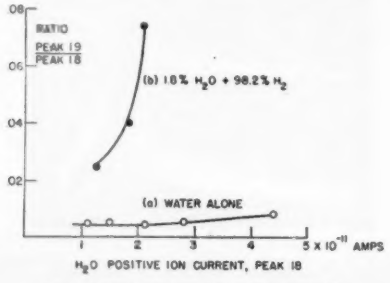

FIG. 1. Formation of ions of mass 19 by excess H_2.

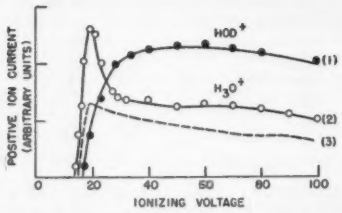

FIG. 2. Ionizing efficiency curves for H_3O^+ and HOD^+.

there is first excitation and then ionization of a complex on second electron impact.

Niira[2] discussed H_2O excitation by electron impact, showing that excited H_2O molecules dissociate to the H atom and the OH radical in the excited $^2\Sigma^+$ state. The latter then makes a transition to the $^2\Pi$ ground state, emitting ultraviolet bands. Some of these OH radicals, according to Niira, rotate at abnormally high speeds corresponding to a temperature of 8000°K. This same paper gives the excitation curve, according to Hayakawa,[3] to the $^2\Sigma^+$ state. This has a maximum near 20 volts and bears a marked resemblance to the ionizing efficiency curve for the H_3O^+ ion. Its shape is indicated by curve (3), Fig. 2.

The suggested process for formation of this ion then becomes: (1) Formation of an excited H_2O molecule which dissociates to give the OH radical. A portion decays to the ground state, but another part in the presence of H_2 can form the complex OH_3 in some unspecified state. (2) Electron impact then forms OH_3^+ from this. The ionizing efficiency curve for H_3O^+ might be considered a superposition of the excitation and ionization processes.

A practical test for distinguishing between the ions H_3O^+ and HOD^+ is to measure the ratio of mass 19 positive ion current at 20 volts ionizing potential to that at 70 volts. For H_3O^+ the ratio is 2.0; for HOD^+ the ratio is 0.45.

[1] Washburn, Berry, and Hall, Symposium on Mass Spectroscopy, Natl. Bur. Standards, Washington, D. C., Sept. 6–8, 1951. (To be published in a bound volume of symposium papers.)
[2] Kazuo Niira, J. Phys. Soc., Japan **4**, 230 (1949).
[3] G. Hayakawa, Proc. Phys.-Math. Soc., Japan **26**, 78 (1944).

Experimentally Derived Configurational Coordinate Curves for Phosphors

CLIFFORD C. KLICK
Crystal Branch, Metallurgy Division, Naval Research Laboratory, Washington, D. C.
(Received November 12, 1951)

RECENTLY Williams[1] has attempted to put configurational coordinate curves on a quantitative basis by computing them for the system KCl:Tl from fundamental properties of the ions involved. In this letter another technique will be described for evaluating these curves using experimental results as primary data.

The assumptions made here concerning the configurational coordinate curves are as follows:

(1) The curves are parabolic.

(2) The variation in energy of the system about its equilibrium position in either the ground or excited state is small compared with the energy band width in the corresponding absorption or emission band.

(3) Transitions are made to parts of the parabolic configurational coordinate curves which can be represented closely by a straight line.

(4) The system acts as a harmonic oscillator so that its energy levels and spatial distribution can be computed in the usual way. The population of the states is given by a Boltzmann distribution.

(5) The probability of a transition between the configurational coordinate curves is independent of position along the portions of the curves which lie within the experimental range.

Materials to which these assumptions apply will have Gaussian emission and absorption bands at low temperatures. This is observed in the emission of tungstate phosphors[2] and in the absorption of *F*-centers and thallium in alkali halides. Furthermore, the relative change in band width with temperature follows the form given in Fig. 1 where the curves are normalized at 300°K. The points for the absorption of KCl:Tl[3] and the emission of $MgWO_4$[2] and Zn_2SiO_4:Mn[3,4] follow the curves reasonably well and indicate vibrational frequencies of normal values.

Let the ground and excited states be represented as in Fig. 2 with force constants k_g and k_e, respectively, and let all quantities be given in cgs units. The absorption energy at the center of the band is given by

$$U_{abs}=U_0+\tfrac{1}{2}k_eX_0^2, \tag{1}$$

and the energy of emission at the peak is

$$U_{emis}=U_0-\tfrac{1}{2}k_gX_0^2. \tag{2}$$

From the relative change in width of the absorption band with temperature, the classical frequency of the system in its ground state can be evaluated as discussed previously. This frequency is given by

$$\nu_g=(1/2\pi)(k_g/M_g)^{\frac{1}{2}}, \tag{3}$$

where M_g is the effective mass of the vibrating system in its ground state. A similar equation, with subscripts e, can be applied to emission data. The band width in ergs, ΔE_A, of the low temperature absorption curve measured at the half-maximum points can be expressed as

$$\Delta E_A=1.905\times10^{-12}k_eX_0(\nu_g/k_g)^{\frac{1}{2}}, \tag{4}$$

and the band width of the emission curve at low temperature is given by a similar equation with the subscripts e and g interchanged. The ground and excited state curves intersect at some energy W above the minimum of the excited state curve which can be computed from measurements on luminescence efficiency or decay rate. From Eqs. (1) and (2) W is given by

$$W=\frac{k_gk_eX_0[k_eX_0+k_gX_0-2(k_gk_eX_0^2-2k_gU_0-2k_eU_0)^{\frac{1}{2}}]+2k_eU_0(k_g-k_e)}{2(k_g-k_e)^2}. \tag{5}$$

TABLE I. Configurational coordinate constants for KCl:Tl.

Configurational coordinate constant	Theoretically derived values	Experimentally derived values
k_g	27×10^4	26.5×10^4
k_e	10.3×10^4	8.2×10^4
U_0	8.1×10^{-12}	7.7×10^{-12}
X_0	0.36×10^{-8}	0.28×10^{-8}

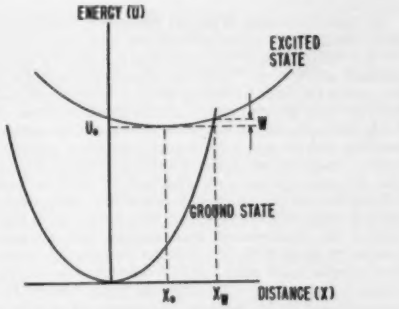

FIG. 2. Schematic configurational coordinate plot.

The complete determination of the configurational coordinate curves requires that the six constants k_g, k_e, X_0, U_0, M_g, and M_e be evaluated from a possible seven pieces of data. If M_g and M_e are assigned values, only four constants need be evaluated.

In order to compare the configurational coordinate curves determined in this way with those computed by Williams, the equations have been solved for KCl:Tl assuming the absorption energy peak to be at 2475A,[5] the emission peak at 2980A,[5] the vibrational frequency in the ground state (see Fig. 1) as 4×10^{12} sec^{-1}, and the width of the low temperature absorption band to be 0.108 electron volts.[3]

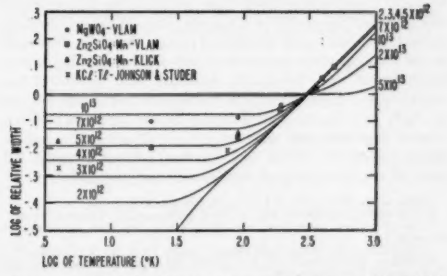

FIG. 1. Plot of the logarithm of the computed relative width at half-maximum of emission or absorption curves as a function of the logarithm of the temperature for various frequencies of vibration. Curves are normalized at 300°K.

It is further assumed with Williams[6] that only a single mode of vibration is important and that this corresponds to a synchronous and radial motion of the chlorine ions surrounding the thallium ion. The results of this analysis are given in Table I.

The agreement is surprising in view of the radically different approaches to the determination of the configurational coordinate curves and indicates, first, that the assumption of a single, radial vibratory mode produces results in agreement with experiment and, second, that the method described here may be used in the case of simple systems to evaluate configurational coordinates from experimental data.

[1] F. E. Williams, J. Chem. Phys. **19**, 457 (1951).
[2] C. C. Vlam, Physica **15**, 609 (1949).
[3] P. D. Johnson and F. J. Studer, Phys. Rev. **82**, 976 (1951).
[4] C. C. Klick and J. H. Schulman, J. Opt. Soc. Am. **40**, 509 (1950).
[5] W. von Meyern, Z. Physik **61**, 321 (1930).
[6] F. E. Williams, Phys. Rev. **82**, 281 (1951).

Protons and Deuterons from Li^6+T Reactions

T. P. PEPPER, K. W. ALLEN,* E. ALMQVIST, AND J. T. DEWAN†
Atomic Energy Project, National Research Council of Canada, Chalk River, Ontario, Canada
(Received November 9, 1951)

THE interaction of tritons with Li^6 may lead to the following exothermic reactions:[1]

$$Li^6+T=Li^7+D^2+0.988\ \text{Mev} \tag{1}$$
$$Li^{7*}+D^2+0.509\ \text{Mev} \tag{2}$$

$$Li^3+H^1+0.800\ \text{Mev} \quad (3)$$
$$Be^9+n+16.04\ \text{Mev} \quad (4)$$
$$Be^{8*}+n+<16.004\ \text{Mev} \quad (5)$$
$$He^4+He^4+n+16.100\ \text{Mev} \quad (6)$$
$$He^3+He^4+15.23\ \text{Mev}. \quad (7)$$

This letter discusses the first three reactions and describes the experimental technique used to study the low energy proton and deuteron groups in the presence of the α-particle continuum from reactions (4) to (7).

Hydrogen containing 10 percent tritium was used in the Chalk River 200-kv high tension set[2] and the mass three component, T^+ and HHH^+ ions, of the beam, was magnetically selected to bombard a Li^6F target.[3] The charged particles emitted at 90° to the beam were deflected through 90° in a homogeneous magnetic field, and were detected using a ZnS Ag-activated screen with an RCA 5819 photomultiplier. The photomultiplier pulses were amplified and fed into a 30-channel pulse-height analyzer.[4] The value of magnetic field which selected the deuterons from reaction (1) also allowed α-particles and He^3-particles from the $Li^6(p,\alpha)He^3$ reaction produced by the HHH^+ component of the beam to strike the ZnS screen. It so happens that under the conditions of the experiment all these particles have the same momentum to charge ratio, and therefore the same $H\rho$, but as they have energies in the ratio 1:2:2.67, different pulse heights were obtained. Figure 1 shows the deuterons clearly resolved from the α-particles and the He^3-particles. The corresponding pulse heights are in the ratio 1:2.1:2.9. Additional measurements have shown that, for a given magnetic field, the pulse heights from doubly and singly charged α-particles are in the same ratio as their energies, i.e., 4:1. Therefore the light output of ZnS appears to be proportional to the particle energy and to be the same for deuterons and α-particles. By combining the magnetic selection with the pulse-height measurements it is possible to distinguish, among deuterons, singly charged and doubly charged α-particles. Furthermore, protons can be recognized in the presence of doubly charged α-particles of the same $H\rho$, and therefore the same energy, by covering the ZnS screen with an Al foil to stop the α-particles.

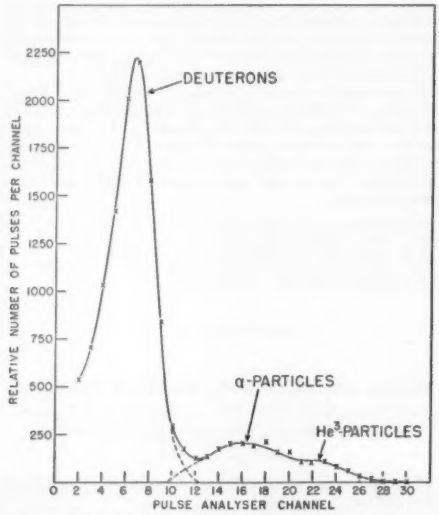

FIG. 1. The pulse-height distribution from an Ag-activated ZnS screen produced by different particles having the same value of $H\rho$. The energies are: deuteron 0.866 Mev, α-particle 1.74 Mev, and He^3-particles 2.32 Mev.

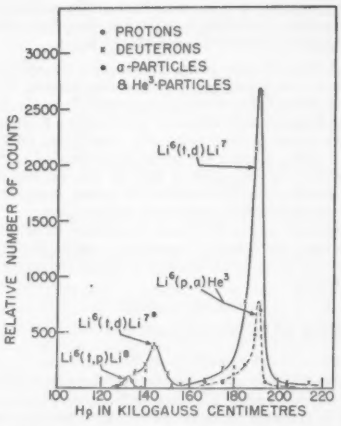

FIG. 2. Protons and deuterons from Li^6+T reactions observed at 90° to a 240-kev triton beam. The dashed curve represents He^3 and α-particles produced by 80-kev protons (HHH^+ ions) on Li^6. The relative intensities of the groups were obtained by correcting the areas under the peaks for variation of resolution of the magnet with $H\rho$.

The momentum distributions of the deuterons and the protons from the first three reactions are shown in Fig. 2. The two more intense groups of particles are the deuterons from reactions (1) and (2) corresponding to the formation of Li^7 in the ground state and in the well-known 479-kev excited state.[5] The least intense group consists of protons from reaction (3). The broken curve is the group of α-particles and He^3-particles from the $Li^6(p,\alpha)He^3$ reaction. At the low proton bombarding energy used, these particles are not resolved and appear as a single group which, within the accuracy of the measurements, coincides with the deuteron group from reaction (1). This fortuitous coincidence permits a rather precise determination of the Q value of reaction (1) in terms of the accurately known Q value, 4.016±0.004 Mev of the $Li^6(p,\alpha)He^3$ reaction.[6,7] Using the latter Q and allowing for an oil layer on the target having a measured thickness equivalent to 5×10^{-3} cm of air the Q for the $Li^6(t,d)Li^7$ reaction is 0.982 ±0.007 Mev. The Q of reaction (2) is therefore 0.503±0.007 Mev. Using this value and the measured separation of the groups from reactions (2) and (3) the Q of the $Li^7(t,p)Li^9$ reaction is computed to be 0.784±0.015 Mev. These Q values are consistent with those calculated from reaction cycles using the data of Li *et al.*[6]

The total yields of the different reactions are not known as the measurements have been made at one angle only. However, reaction (1) accounts for about 54 percent of all the disintegrations emitting particles at 90° to the beam, reaction (2) for about 14 percent, and reaction (3) for about 2 percent. Assuming that most of the disintegrations produced at 240 kev bombarding energy result from S wave tritons, the deuterons must be emitted isotropically, and conservation of parity requires that they be emitted in P, F, etc., waves. The potential barrier penetrabilities for P-wave deuterons from reactions (1) and (2) are in the ratio of approximately 4:1, which indicates that, without a barrier, Li^7 and Li^{7*} would be produced with about equal probability.

* Now at the University of Liverpool, Liverpool, England.
† Now with Schlumberger Well Surveying Corporation, Houston, Texas.
‡ The Q values have been calculated using the data compiled in reference 4.
[2] Allen, Almqvist, Dewan, and Pepper, Can. J. Phys. (to be published).
[3] Lithium, 99.4 percent Li^6, 0.6 percent Li^7, kindly provided by the U. S. Atomic Energy Project.
[4] Moody, Battell, Howell, and Taplin, Rev. Sci. Instr. **V22**, 551 (1951).
[5] Brown, Snyder, Fowler, and Lauritsen, Phys. Rev. **82**, 159 (1951).
[6] Li, Whaling, Fowler, and Lauritsen, Phys. Rev. **83**, 512 (1951).
[7] Collins, McKenzie, and Ramm, Nature **167**, 682 (1951).

Decay of the π-Meson*†

M. RUDERMAN
Radiation Laboratory, Physics Department, University of California, Berkeley, California
(Received November 21, 1951)

THE decay of the charged π-meson through virtual nucleon pairs and the annihilation of a pair with the creation of a neutrino and an electron or μ-meson is permitted by the accepted couplings between these particles.[1] Conservation of angular momentum and parity together with Furry's theorem[2] forbid the decay for most choices of the meson field and the β-decay coupling. The forbiddenness is independent of perturbation theory.[3] Assuming the π to be a pseudoscalar meson at rest in order that the final spinor pair have the same transformation properties under reflection and rotation as the π, the β-coupling must be $\alpha_1\alpha_2\alpha_3$ or $\alpha_1\alpha_2\alpha_3\alpha_4$. Therefore, only the axial vector or pseudoscalar β-decay theories can lead to the pseudoscalar $\pi\rightarrow e, \nu$ decay.[4]

If electrons and π-mesons are similarly coupled to nucleons, a pseudoscalar matrix element in β-decay leads to an electron decay five times as often as a μ-decay. For axial vector it has been shown[1] that the matrix element involves

$$1-[(p_\nu)^2/E_\nu E_{e,\mu}].$$

$\pi\rightarrow\mu, \nu$ is then 10^4 times as probable as $\pi\rightarrow e, \nu$. Any mixture of scalar, vector, axial vector, and tensor is not in contradiction with experiment.[5]

The decay of the pseudoscalar π into a photon and electron (or a μ-meson) and a neutrino is not limited by such rigid selection rules. For axial vector β-decay this mode is more probable than $\pi\rightarrow e, \nu$ because of the latter's singularly small matrix element. The emission of a photon by the π^+ or the electron in Figs. (1b) and (1d) does not alter any of the selection rules forbidding the nonradiative decay. Only the graph of Fig. (1c) can contribute. For vector β-decay and direct meson coupling the matrix element for $\pi\rightarrow e+\nu+\gamma$ a photon of momentum $\mathbf{k}$ and polarization $\mathbf{e}$ is

$$-i\Sigma\int\frac{d^4p}{(2\pi)^4}\frac{4\pi e g g_\beta}{(4m_\pi E_\gamma)^{\frac{1}{2}}}$$
$$\times\mathrm{Spur}\left(\gamma_5\frac{1}{\mathbf{p}-M}\mathbf{e}\frac{1}{\mathbf{p}-\mathbf{k}-M}\gamma_\mu\frac{1}{\mathbf{p}-\mathbf{q}-M}\right)\cdot\langle\psi_e{}^+\gamma_\mu\psi_\nu\rangle \quad (1)$$

$\mathbf{q}$ is the meson 4-vector. The decay rate is

$$\tau^{-1}=(e^2/4\pi)(g^2/4\pi)(m_\pi/M)^2(g_\beta{}^2m_\pi{}^5)(2/15\pi^3)$$
$$=4\times10^5g^2\ \mathrm{sec}^{-1} \quad (2)$$

for

$$g_\beta=10^{-49}\ \mathrm{erg\ cm}^3.$$

The lifetime is between 6×10^{-4} and 6×10^{-5} sec, corresponding to a g^2 of 4 or 40. Gradient coupling gives a divergent matrix element for (1), spoiling the equivalence theorem. Tensor β-decay diverges for both couplings. Conservation of angular momentum and parity still forbid a decay through scalar β-decay.

For axial vector β-coupling the emission of a photon by the electron as in Fig. (1b) is expected to be more probable than emission by the heavy nucleon or π. (Emission from the π does not alter the very small matrix element associated with the β-decay.) If the μ and electron are assumed to have the same axial vector coupling with nucleons, the ratio $(\pi\rightarrow e+\nu+\gamma):(\pi\rightarrow\mu+\nu)$ is again independent of the perturbation treatment of the meson field and the divergent integrals arising in the separate calculation of each lifetime. The ratio of the probability for radiative $\pi-e$ decay to nonradiative $\pi-\mu$ decay is

$$(e^2/4\pi)(3.1)=5.7\times10^{-3}. \quad (3)$$

A symmetrical coupling scheme with axial vector coupling predicts one nonradiative electron decay and over 10 radiative electron decays for every 10^6 $\pi-\mu$ decays. The ambiguities arising from the divergences and the pseudoscalar direct coupling constant preclude conclusions for vector and tensor β-coupling.

I wish to thank Professor R. P. Feynman for helpful discussion.

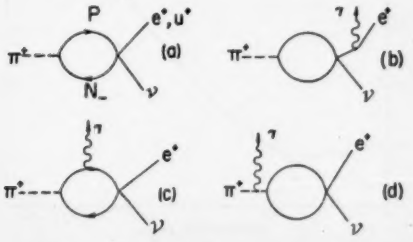

FIG. 1. Feynman's diagrams contributing to charged π decay.

* Work initiated at the California Institute of Technology, Pasadena, California.
† This work was performed under the auspices of the AEC.
[1] M. Ruderman and R. Finkelstein, Phys. Rev. **76**, 1458 (1949).
[2] W. H. Furry, Phys. Rev. **51**, 125 (1937).
[3] If Furry's theorem forbids the Feynman graph of Fig. (1a), it will also forbid all more complex graphs. Except for the original meson line, for every meson emitted from a closed loop, one is also absorbed so that the "evenness" or "oddness" of the matrix element is unchanged. For exact cancellation of graphs with an odd number of "even" operators it is necessary to assume that the square of the coupling constant between neutral mesons and protons is equal to that between neutrals and neutrons. All of the forbidden cases of reference (1) except scalar mesons with gradient coupling and vector β-decay vanish to all orders.
[4] If one adopts the spinor reflection rule of Yang and Tiomno, Phys. Rev. **79**, 496 (1950), their interactions (12) and (13) are the appropriate ones. Referring the β-decay labeling to the proton-neutron coupling our results are independent of the μ, e, and ν inversion property.
[5] H. L. Friedman and J. Rainwater, Phys. Rev. **82**, 334 (1951).

Some Comments on the Mechanism of Fission

GLENN T. SEABORG
Department of Chemistry and Radiation Laboratory, University of California, Berkeley, California
(Received November 20, 1951)

A NUMBER of spontaneous fission rates are now known,[1-4] and a study of the relation of these to Z and A should make it possible to come to a better understanding of this process, which in turn should lead to a better understanding of the slow neutron fission mechanism as well. A number of spontaneous fission rates are summarized in Table I.

Our attempts to correlate these rates with the existing theoretical expectations[5,6] have not been successful, and therefore it seems worthwhile to attempt to study the data from the point of view of finding their empirical relationship.

Figure 1 shows a plot of the logarithm of the "half-life" for spontaneous fission *versus* the fissionability parameter, Z^2/A, and leads to some very interesting conclusions. The points for the even-even nuclides, with some exceptions, seem to indicate that the rate for this nuclear type depends exponentially in a simple way on the parameter Z^2/A. It is tempting to assume that

TABLE I. Summary of spontaneous fission rates.

Nuclide	Fissions/gram/hour	Half-life (years)	References
Th^{230}	$\leqslant 1.4$	$\geqslant 1.5\times10^{17}$	1
Th^{232}	0.15	1.4×10^{18}	1
	1.2	1.7×10^{17}	2
Pa^{231}	$\leqslant 20$	$\geqslant 10^{16}$	1
U^{233}	$\leqslant 25{,}000$	$\geqslant 8\times10^{13}$	1
U^{235}	<0.7	$>3\times10^{17}$	1
U^{236}	<30	$>7\times10^{15}$	1
U^{238}	1.2	1.9×10^{17}	1
U^{238}	24.8 ± 0.9	8.0×10^{15}	3, 1
Np^{237}	$\leqslant 5$	$\geqslant 4\times10^{16}$	1
Np^{239}	$\leqslant 40{,}000$	$\geqslant 5\times10^{12}$	1
Pu^{238}	5.1×10^4	5.4×10^{10}	1
Pu^{239}	36	5.5×10^{15}	1
Am^{241}	$\leqslant 14{,}000$	$\geqslant 1.4\times10^{13}$	1
Cm^{242}	2.7×10^{10}	7.2×10^6	4

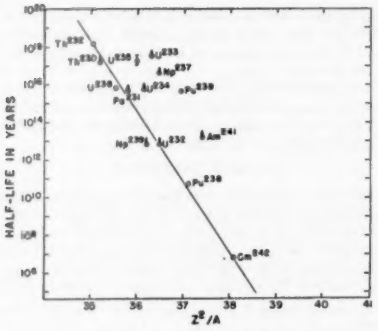

FIG. 1. Plot of spontaneous fission rates (⌀ signifies lower limit to half-life).

the rate of spontaneous fission is controlled by a Boltzmann, type factor in which the required activation energy for fission depends on Z^2/A; the form of the plot would suggest that this might be a linear dependence with a negative coefficient for Z^2/A. However, another type such as an inverse dependence on Z^2/A in the exponential term also fits nearly as well over the range of data plotted. In any case it is interesting to note that extrapolation of the line in Fig. 1 to the region of instantaneous rate of spontaneous fission (that is, half-life of order of 10^{-20} seconds) gives a value of about 47 for Z^2/A, which corresponds with the predicted limiting value[1] for Z^2/A.

The data seem also to indicate that on the average for a given value of Z^2/A, the rate is greater for an even-even nuclide than one with an odd number of nucleons. Since Z^2/A is a representation of Z^2/r^3, where r is the nuclear radius, the slower rates for the odd-nucleon nuclides may be related to their expected larger radii; on this basis the largest departure of an odd-nucleon nuclide from the line in Fig. 1 corresponds to the order of one percent larger radius than for the "hypothetical" corresponding even-even nuclide. On this picture an important contributing factor to the slower rates may result from the lower zero-point energy of the modes of vibration which lead to fission associated with the nuclei with the larger radii.

Similar considerations may be useful in interpreting some of the results from the study of slow neutron fission probabilities. The slow neutron fission probabilities of the even-even nuclides in the transuranium region seem to be lower than expected on the simple theory.[1] For example, a nucleus like Cm^{243} has a slow neutron fission cross section of less than 5 barns[7] in spite of the fact that the critical fission energy of the intermediate Cm^{242} is of the order of 4 Mev, much less than the estimated 6 Mev of neutron binding energy. It is possible that the time for fission is lengthened for such an odd-nucleon intermediate nucleus to the point where the (n, γ) reaction is able to compete more successfully than is the case for even-odd nuclides like U^{235}, Pu^{239}, etc., where the intermediate fissioning nuclei are of the even-even type.

The effect of an odd nucleon in slowing the fission process may also explain the photofission results of Koch, McElhinney, and Gasteiger[8] who found, for example, higher effective energetic thresholds for U^{235}, U^{233}, and Pu^{239} than for U^{238}, contrary to expectations from existing theory.[5,6]

It will be interesting to see whether even-even nuclei with abnormally small nuclear radii due to closed sub-shells will have especially high rates of spontaneous fission. Thus, a nucleus such as 100^{248} which would have two closed sub-shells on the Mayer picture,[9] 100 protons and 148 neutrons, might be expected to exhibit such an abnormally high rate. Similarly, the large slow neutron fission cross section[7] of a nuclide like Am^{242} might be connected with the sub-shell of 148 neutrons in the intermediate Am^{243}.

The above considerations may make it possible to predict with a fair degree of confidence, especially for the even-even nuclides, the spontaneous fission rates for undiscovered nuclides and hence make it possible to plan experiments more intelligently for their detection.

It is a pleasure to acknowledge helpful discussions with K. Street, Jr., A. Ghiorso, J. O. Rasmussen, and I. Perlman.

[1] Chamberlain, Farwell, Jungerman, Segrè, and Wiegand, quoted by E. Segrè in AEC Declassified Document, LADC-975 (May 8, 1951).
[2] H. Pose, Z. Physik **121**, 293 (1943).
[3] G. Scharff-Goldhaber and G. S. Klaiber, Phys. Rev. **70**, 229 (1946).
[4] Hanna, Harvey, Moss, and Tunnicliffe, Phys. Rev. **81**, 466 (1951).
[5] N. Bohr and J. A. Wheeler, Phys. Rev. **56**, 426 (1939).
[6] S. Frankel and N. Metropolis, Phys. Rev. **72**, 914 (1947).
[7] Hanna, Harvey, Moss, and Tunnicliffe, Phys. Rev. **81**, 893 (1951).
[8] Koch, McElhinney, and Gasteiger, Phys. Rev. **77**, 329 (1950).
[9] M. G. Mayer, Phys. Rev. **75**, 1969 (1949).

The Melting Pressure of He^3

B. WEINSTOCK, B. M. ABRAHAM, AND D. W. OSBORNE
Argonne National Laboratory, Chicago, Illinois
(Received November 13, 1951)

THE previously reported measurements[1] on the melting pressure of He^3 between 1.51° and 1.02°K have been extended to 0.16°K. The lower temperatures were obtained by adiabatic demagnetization of ferric ammonium alum, which surrounded the capillary (0.16 mm i.d. cupro-nickel) containing the He^3. In order to enhance the thermal contact between the capillary and the salt, copper vanes were soldered to the capillary, and the salt chamber was filled with He^4 to a pressure of one atmosphere at liquid nitrogen temperature. The He^3 apparatus external to the cryostat was the same as in the earlier measurements.

The melting pressures were again obtained by the blocked capillary technique. Magnetic temperature measurements were made with a ballistic galvanometer and a secondary coil around the salt as described elsewhere.[2] Corrections were made for the difference between the magnetic and thermodynamic temperatures on the basis of the results of Kurti, Simon, and Squire.[3]

The results of all the measurements are shown in Fig. 1. The solid circles represent the previous results,[1] obtained with the capillary immersed directly in the He^4 bath, and the open circles represent the present results, obtained with the capillary im-

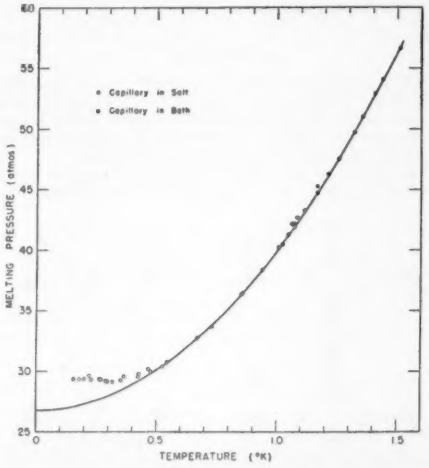

FIG. 1. Melting pressure of He^3.

mersed in the paramagnetic salt. From 0.5° to 1.5°K the data are represented by the equation,

$$P = 26.8 + 13.17^2 \text{ atmos},$$

which is shown as a solid line in the figure. Below 0.5°K the experimentally determined pressures rapidly approach a constant value of 29.3 atmos.

If the horizontal portion of the observed melting curve is correct, the entropy difference between liquid and solid becomes zero near 0.5°K, which implies a transition in the liquid near this temperature. However, another possible explanation is that below 0.5°K the thermal contact between the capillary and the salt may become so poor that no part of the capillary is cooled below 0.44°K, at which temperature the melting pressure from the equation is 29.3 atmos. Further experiments are planned in which an attempt will be made to improve the thermal contact between the salt and the capillary.

It is clear that the melting pressure at absolute zero is positive, and therefore that the liquid is the stable condensed phase of He^3 at absolute zero.

[1] Osborne, Abraham, and Weinstock, Phys. Rev. **82**, 263 (1951).
[2] R. A. Hull, *Report of Cambridge Conference on Low Temperatures* (Phys. Soc., London, 1947), p. 72.
[3] A. H. Cooke, Proc. Phys. Soc. (London) **A62**, 269 (1949).

Nuclear Interactions of the Decay Products of a Neutral *V*-Particle*

HERBERT BRIDGE, HANS COURANT, AND BRUNO ROSSI
Physics Department and Laboratory for Nuclear Science and Engineering, Massachusetts Institute of Technology, Cambridge, Massachusetts
(Received November 12, 1951)

IN a series of pictures taken with a large multiple-plate cloud chamber at 10,600 feet, we have observed several decays of neutral *V*-particles. In one such event, both charged secondaries from the *V*-particle decay interact in one of the 0.25-inch lead plates, each producing a low energy star.

Two of the three views of this event are reproduced in Fig. 1. Analysis of the three views shows that the electron track between the second and third plates below the point of decay is unrelated to the decay event.

There is very little doubt that both secondary particles actually undergo nuclear interactions. The event takes place entirely within the well-illuminated region of the cloud chamber. Stereoscopic analysis shows that, in each case, the tracks of the incident particle and of the secondary products intersect at one point. Moreover, the right-hand particle scatters 20° in the plate, and the left-hand particle appears to lose a large amount of energy, becoming heavily ionizing after the traversal.

From recent work[1] it appears fairly certain that either there are two different kinds of V^0-particles with the decay schemes:

$$V^0 \rightarrow (\text{proton}) + (\text{negative meson}), \quad (1)$$
$$V^0 \rightarrow (\text{positive meson}) + (\text{negative meson}); \quad (2)$$

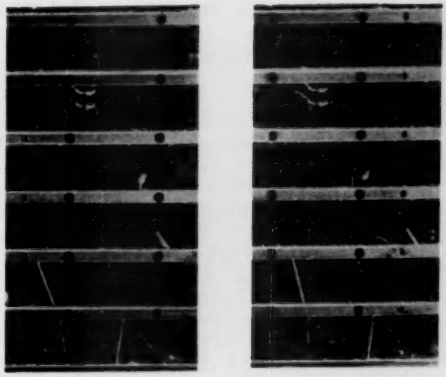

(a) (b)

FIG. 1. Stereoscopic cloud-chamber pictures of a V^0-particle decay.

or that the V^0-particle has two alternate disintegration schemes:

$$V^0 \rightarrow (\text{proton}) + (\text{negative meson}) + (\text{neutral meson}), \quad (3)$$
$$V^0 \rightarrow (\text{neutron}) + (\text{negative meson}) + (\text{positive meson}). \quad (4)$$

Under the assumption of a two-body decay, one can decide between the disintegration schemes (1) and (2) from a knowledge of the momenta of the two secondary particles and of the angle enclosed by their trajectories. In our picture, the angle is 19° and the observed scattering corresponds for both particles to momenta of the order of 500 Mev/*c*. However, the determination of the momenta is not sufficiently precise to permit discrimination between processes (1) and (2). All that can be said is that if the event is of the type (1), the meson is a π-meson rather than a μ-meson, and that if the event is of the type (2), both particles are π-mesons. This is so, of course, because π-mesons (as well as protons) have cross sections for nuclear interactions of the order of the geometrical cross sections of the nuclei; whereas the cross sections for nuclear interactions of μ-mesons are exceedingly small. For the same reason, one can conclude that if the V^0-particle disintegrates according to schemes (3) or (4), the mesons involved must be of the π-variety.

Lastly, it should be pointed out that the disintegration scheme recently suggested by T. D. Lee,[2] $V^0 \rightarrow (\text{proton}) + (\mu^-\text{-meson}) + (\text{neutrino})$, could not explain the observed event.

* This work was supported in part by the joint program of the ONR and AEC.
[1] Armenteros, Barker, Butler, Cachon, and Chapman, Nature **167**, 501 (1951); Thompson, Cohn, and Flum, Phys. Rev. **83**, 175 (1951); Leighton, Wanlass, and Alford, Phys. Rev. **83**, 843 (1951).
[2] As reported by W. B. Fretter, Phys. Rev. **83**, 1053 (1951).

Proceedings of the American Physical Society

Minutes of the 1951 Fall Meeting of The Ohio Section at Antioch College, Yellow Springs, Ohio

THE regular Fall meeting of The Ohio Section of the American Physical Society convened at Antioch College, in Yellow Springs, Ohio, on November 10, 1951. Fifty members were present. Abstracts of three contributed papers follow. These papers were followed by a discussion on Physics in General Eduction. Papers were presented in the order indicated: *Physics, a Part of General Education at Harvard*, by G. E. Owen of Antioch College; *The Course in Physical Science as General Education at Denison*, by Edward M. Collins of Denison University; *The Course of General Education in Physics and Astronomy at Ohio State University*, by C. E. Hesthal of Ohio State University; and, *Physics in General Education*, by D. W. Bowman, of Bowling Green State University.

The only item of business transacted had to do with the appointment of a Program Committee to be charged with the duty of preparing and arranging programs and meeting places.

Leon E. Smith, *Secretary, Ohio Section,*
Denison University,
Granville, Ohio

Vibrational Analysis of Chain Molecules. W. Edward Deeds, *Ohio State University.*—By an extension of a method originally developed by Lagrange, it is relatively easy to solve the classical vibration problem for any chain type molecule which consists of repeating units. The kinetic energy function is considerably simplified if a separate coordinate system satisfying the Eckart conditions is used for each characteristic group of atoms. Application of suitable boundary conditions for chain molecules of finite size leads to expressions for the discrete normal frequencies of vibration. The vibration-rotation bands occur in related sets with intensities which can be calculated in a straightforward manner. The calculated intensities are very helpful in the assignment of the observed band sets, the assignment of the observed bands within a set, and the determination of the end conditions for the chain. The observed vibrational frequencies can be plotted in such a way as to give graphical solutions to the vibrational secular determinant. Comparison of these experimental curves with the corresponding theoretical ones makes it easy to determine the important force constants.

On the Energy Levels of the S^{32} Nucleus.* G. R. Grove† and John N. Cooper, *Ohio State University.*—The observed energy levels of the compound nucleus S^{32} resulting from proton capture[1] in P^{31} have been related to predictions of the Wilson spherical shell nuclear model,[2] which suggests levels given by

$$E_{n,j}=0.387[(n-1)(n+2)]^{\frac{1}{3}}+1.44(Z^4A)^{-\frac{1}{3}}j(j+1)\ \text{Mev}.$$

The absolute values of the observed levels of S^{32} are difficult to know accurately, but the relative spacings of the levels are reliably known. It was found that the 17 observed levels can be roughly accounted for with n's of 28, 29, 30, and 31, and low j's. The j's are not always successive; for $n=30$, levels may be assigned to $j=0$, 1, 2, 3, 5, and 6, but none seems to correspond to $j=4$. For several of the levels the predicted and observed energies differ by considerably more than can be explained by experimental errors.

* Assisted by the AEC through a contract with the Ohio State University Research Foundation.
† Formerly AEC Predoctoral Fellow; now at Mound Laboratory, Miamisburg, Ohio.
[1] G. R. Grove and J. N. Cooper, Phys. Rev. **82**, 505 (1951).
[2] H. A. Wilson, Phys. Rev. **77**, 516 (1950).

A Curved Quartz Crystal X-Ray Spectrometer. John E. Edwards, *Ohio University.*—A quartz crystal is cut to utilize the 310 and 110 planes for diffraction of x-rays by transmission. The crystal, 0.2 mm thick, is curved to a radius of 15 inches with an effective area variable to 3 cm width and 1.3 cm height. An adjustable slit with attached ionization chamber and FP-54 tube is moved along the focal circle on an arm attached to a shaft at the center of the focal circle. The slit is maintained perpendicular to the x-ray beam by a device similar to that used by Marimer *et al.*[1] Since the sharpest focus of the diffracted beam is obtained at the point on the focal circle, the crystal was cut at such an angle that all spectra up to 2A could be formed within 9° of this point. X-rays up to 0.4A can be diffracted from the 310 planes with the sharpest focus in the region of 0.1A, while x-rays from 0.4A to 2A may be diffracted from the 110 planes with the sharpest focus near 1A. Profiles of the $WL_{\gamma 1}$ line will be shown to illustrate the effect of slit width and crystal opening on the width and intensity of the line. A full width at half-maximum of 1.12 X.U. has been obtained thus far in comparison with 1.01 X.U. obtained by Williams[2] with a double crystal spectrometer.

[1] Marimer, Blaser, Preiswerk, and Scherrer, Helv. Phys. Acta **22** (No. 4) 155–63 (1949).
[2] Williams, Phys. Rev. **45**, 71 (1934).

THE AMERICAN INSTITUTE OF PHYSICS

INCORPORATED

57 East 55 Street New York 22, N.Y.

MEMBER SOCIETIES:

American Physical Society
Karl K. Darrow, *Secretary*, Columbia University, New York 27, New York

Optical Society of America
Arthur C. Hardy, *Secretary*, Massachusetts Institute of Technology, Cambridge 39, Massachusetts

Acoustical Society of America
Wallace Waterfall, *Secretary*, 57 East 55th Street, New York 22, New York

Society of Rheology
G. J. Dienes, *Secretary*, Brookhaven National Laboratory, Upton, Long Island, New York

American Association of Physics Teachers
R. F. Paton, *Secretary*, University of Illinois, Urbana, Illinois

AFFILIATED SOCIETIES:

American Crystallographic Association
Electron Microscopy Society of America
Physical Society of Pittsburgh
Physics Club of Chicago
Physics Club of Philadelphia
Cleveland Physics Society
Physics Club of the Lehigh Valley

ASSOCIATES:

Over seventy-five leading industrial enterprises and other institutions which contribute to the support of the Institute.

JOURNALS:

The Physical Review
S. A. Goudsmit, *Editor*, Brookhaven National Laboratory, Upton, Long Island, New York

Reviews of Modern Physics
L. W. Bruner, *Editor*, University of Minnesota, Minneapolis, Minnesota

Journal of the Optical Society of America
Wallace R. Brode, *Editor*, National Bureau of Standards, Washington 25, D. C.

The Journal of the Acoustical Society of America
Floyd A. Firestone, *Editor*, 57 East 55th Street, New York 22, New York

American Journal of Physics
Thomas Hall Osgood, *Editor*, Michigan State College, East Lansing, Michigan

The Review of Scientific Instruments
Gaylord P. Harnwell, *Editor*, Randal Morgan Laboratory of Physics, University of Pennsylvania, Philadelphia, Pennsylvania

The Journal of Chemical Physics
Joseph E. Mayer, *Editor*, Institute for Nuclear Studies, University of Chicago, Chicago, Illinois

Journal of Applied Physics
Elmer Hutchisson, *Editor*, Case Institute of Technology, Cleveland 6, Ohio

Physics Today
Gaylord P. Harnwell, *Editorial Director*; [illegible], *Managing Editor*; American Institute of Physics, 57 East 55th Street, New York 22, New York

OFFICERS

George B. Pegram, *Chairman*
Columbia University

George R. Harrison, *Chairman*
Massachusetts Institute of Technology

GOVERNING BOARD

J. W. Beams
C. Paul Boner
Wallace R. Brode
W. F. Fair, Jr.
S. A. Goudsmit
G. P. Harnwell
George R. Harrison
F. V. Hunt
Rudolph Kingslake
Paul Kirkpatrick
F. W. Loomis
J. R. Oppenheimer
George B. Pegram
I. I. Rabi
Duane Roller
Harold K. Schilling
Frederick Seitz
Francis G. Slack
John C. Stehman

Consultant on Printing
Melvin Loos

ADMINISTRATIVE STAFF

Henry A. Barton, *Director*
Wallace Waterfall, *Executive Secretary*
Thurston Vosburgh, *Advertising Manager*
Ruth F. Bevans, *Publication Manager*
Betty H. Goodfriend, *Assistant Secretary*
Eileen B. Neuschel, *Circulation Manager*
Kathryn Smith, *Assistant Treasurer*

THE American Institute of Physics was founded in 1931 as a federation of leading societies in the field of Physics. It combines into one operating agency those functions on behalf of physics which can best be done for the societies jointly. Its purpose is the advancement and diffusion of physics and its applications to human welfare. To this end it operates for itself or the Societies the publication journals listed on this page; promotes unity and effectiveness of effort among all who are interested in physics; renders various direct services to physicists and the public; and cooperates with governmental agencies, national associations, educational institutions, technical industries, and others in such manner as to make the opportunities and fulfill the responsibilities of physics to as productive and constructive human activity

THE PHYSICAL REVIEW

Adiabatic Thermal Changes in Nuclear
Internal Conversion Angular Distribution
Note on the Adiabatic Demagnetization
Range Straggling of a Monoenergetic Group
Rotational Magnetic Moments of Gases
On the Critical State of Normal Helium
Nuclear Magnetic Moment and Hyperfine
Motion of an Electron in a Perturbed Field
Cross Section for the Radiation Capture
Polarization of Scattered Quanta
Theory of Molecular Spectra and
Superposition of Configurations in the
Louis C. Glasser, Mortimer
Pressure Effects of Argon and Helium
Magnetic Susceptibility of Uranium
High Energy Neutron Collisions with
Study of the Multiple Scattering of
Production of Polarized Protons and
Superconductivity of Vanadium
Multiple Scattering of Fast Electrons in
Internal Conversion in Sm^{149}, Ir^{191}, Pa^{231}, and
Magnetic Properties of a Nickel-Copper
Range of 18-Mev Protons in Aluminum
Beta-Spectra of P^{32} and Ca^{45}
Distribution of Radiolead in Human
Eigenvalue Problem in Quantum Mechanics
Letters to the Editor:
Radiations of Ra_E
Information and Communication
Slow Neutron Fission of Lead
Light Emission from Silicon Crystals
Production of Electron Showers
Radioactive Pairs and Parity
Connection between γ- and β-Ray Spectra
Search for Long-Lived Mesotron
Equation of Motion of the Lamb
Identification of CO in the Solar
Far-Infrared Transmission of
Phase T-matrices of $Rh^{103}+p$, $Pd^{105}+p$
Charge-Symmetrical Interactions
Lifetime of an Excited State of
Nuclear Reaction Energies
D. R.
Interactions between Neutrons and
Possible Natural Radioactivity of
Hyperfine Structure Anomaly in
Condition for Radiation from a
Decay Series Ra^{226}-Pb^{210}-Cu^{63}
Ca
Quadrupole Radiation in α-Decay
Absence of Gamma-Ray Emission
Bipolar Expansion of Coulomb
Disintegration of the Gamma-Ray
Studies on the Linearity of a
Heat Capacity and Lattice
Measurements of Some K-Shell
Classification of the γ-Rays
Isomeric Transition in Co^{58}
Loss of Mass 19 from Wood
Experimentally Derived Cross
Protons and Deuterons from
Decay of the π^0-Meson
Some Comments on the
Washing Processes of Ra^{E}
Nuclear Interactions of the
Proceedings of the American Physical
Minutes of the 1951 Fall